EMERGING INFECTIOUS DISEASES®

U.S. CENTERS FOR DISEASE CONTROL AND PREVENTION

Vectorborne Diseases

June 2025

Sarah Hunter (1883–1967), *Jar-shaped Basket*, 1910. Willow, bulrush; coiled (3 rods), 4 15/16 in × 7 5/16 in/12.5 cm × 18.5 cm. Open access image from Cleveland Museum of Art, Cleveland, Ohio, USA.

EMERGING INFECTIOUS DISEASES®

Emerging Infectious Diseases is published monthly by the Centers for Disease Control and Prevention, 1600 Clifton Rd NE, Mailstop H16-2, Atlanta, GA 30329-4018, USA. Telephone 404-639-1960; email eideditor@cdc.gov

EMERGING INFECTIOUS DISEASES®

Vectorborne Diseases **June 2025**

On the Cover

Sarah Hunter (1883–1967), *Jar-shaped Basket*, 1910. Willow, bulrush; coiled (3 rods), 4 15/16 in × 7 5/16 in/12.5 cm × 18.5 cm. Open access image from Cleveland Museum of Art, Cleveland, Ohio, USA.

About the Cover p. 1271

Synopses

Research

Dispatches

EMERGING INFECTIOUS DISEASES®
June 2025

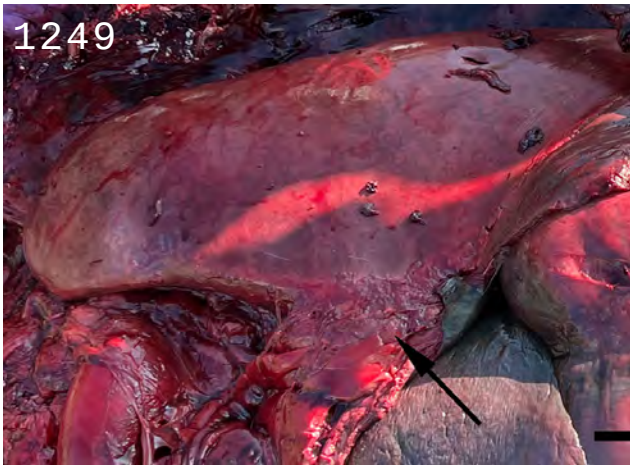

EMERGING INFECTIOUS DISEASES®
June 2025

Research Letters

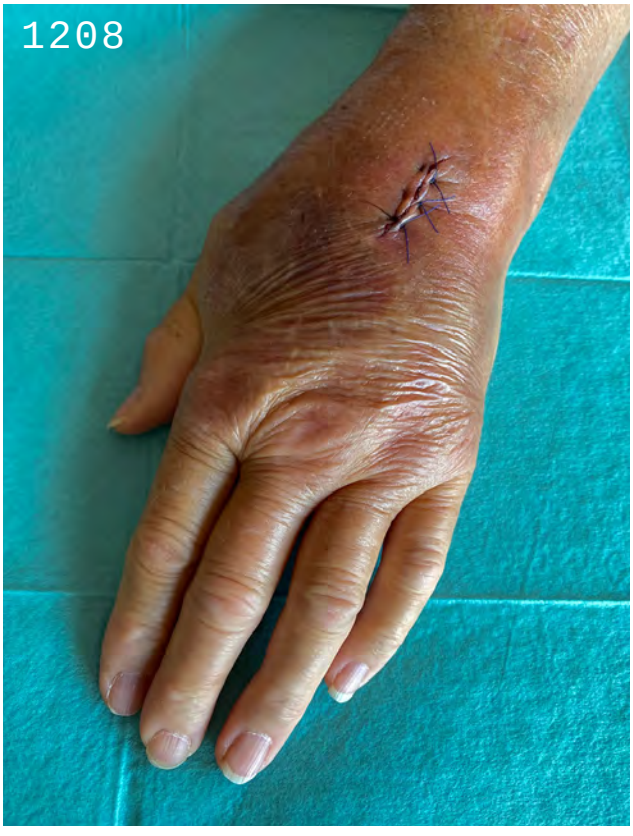

Comment Letter

About the Cover

Etymologia

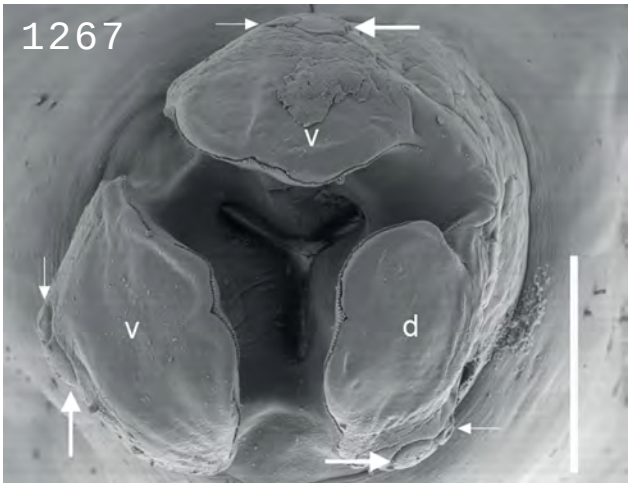

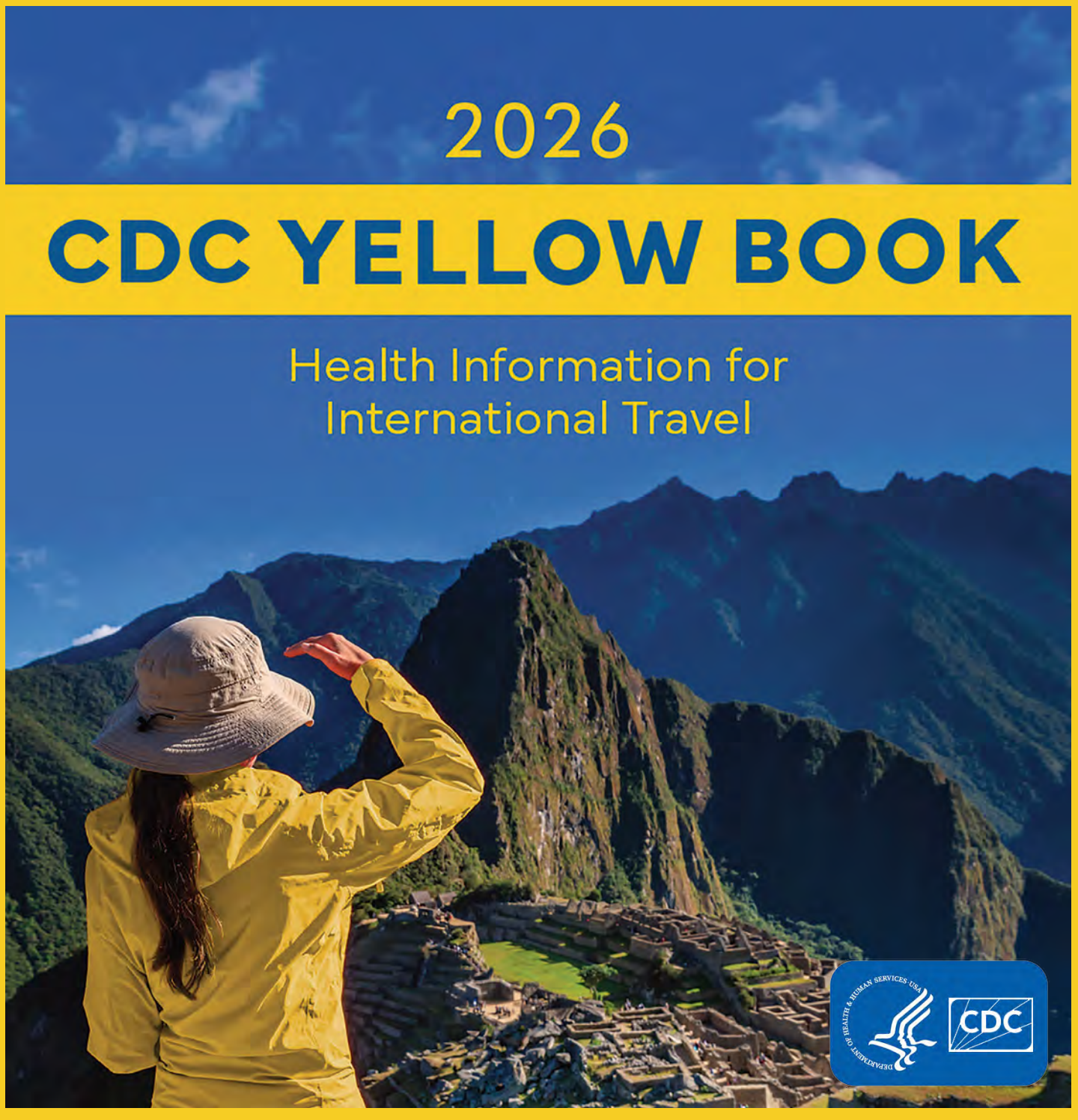

Launch of CDC Yellow Book 2026– A Trusted Travel Medicine Resource

CDC is pleased to announce the launch of the **CDC Yellow Book 2026**. The CDC Yellow Book is a resource containing the U.S. government's travel medicine recommendations and has been trusted by the travel medicine community for over 50 years. Healthcare professionals can use the print and digital versions to find the most up-to-date travel medicine information to better serve their patients' healthcare needs.

The CDC Yellow Book is available online now at www.cdc.gov/yellowbook and in print starting in June 2025 through Oxford University Press and other major online booksellers.

Clinical Manifestations, Risk Factors, and Disease Burden of Rickettsiosis, Cambodia, 2007–2020

Gerard C. Kelly, Agus Rachmat, Long Khanh Tran, Chonthida Supaprom, Hip Phireak, Satharath Prom, Heng Sopheab, Nora Cleary, Michael von Fricken, Christina M. Farris, Andrew G. Letizia

In support of improving patient care, this activity has been planned and implemented by Medscape, LLC and Emerging Infectious Diseases. Medscape, LLC is jointly accredited with commendation by the Accreditation Council for Continuing Medical Education (ACCME), the Accreditation Council for Pharmacy Education (ACPE), and the American Nurses Credentialing Center (ANCC), to provide continuing education for the healthcare team.

Medscape, LLC designates this Journal-based CME activity for a maximum of 1.00 ***AMA PRA Category 1 Credit(s)™***. Physicians should claim only the credit commensurate with the extent of their participation in the activity.

Successful completion of this CME activity, which includes participation in the evaluation component, enables the participant to earn up to 1.0 MOC points in the American Board of Internal Medicine's (ABIM) Maintenance of Certification (MOC) program. Participants will earn MOC points equivalent to the amount of CME credits claimed for the activity. It is the CME activity provider's responsibility to submit participant completion information to ACCME for the purpose of granting ABIM MOC credit.

All other clinicians completing this activity will be issued a certificate of participation. To participate in this journal CME activity: (1) review the learning objectives and author disclosures; (2) study the education content; (3) take the post-test with a 75% minimum passing score and complete the evaluation at https://www.medscape.org/qna/processor/74364?showStandAlone=true&src=prt_jcme_eid_mscpedu; and (4) view/print certificate. For CME questions, see page 1274.

NOTE: It is the policy of Medscape Education to avoid the mention of brand names or specific manufacturers in accredited educational activities. However, trade and manufacturer names in this activity are provided in an effort to provide clarity. The use of brand or manufacturer names should not be viewed as an endorsement by Medscape of any specific product or manufacturer.

Release date: May 27, 2025; Expiration date: May 27, 2026

Learning Objectives

Upon completion of this activity, participants will be able to:

- Analyze the prevalence of rickettsial infection in the current study of patients with acute undifferentiated febrile illness
- Distinguish the most common form of rickettsial infection in the current study
- Assess risk factors for rickettsial infection in the current study
- Evaluate symptoms associated with rickettsial infection in the current study

CME Editor

Jill Russell, BA, Technical Writer/Editor, Emerging Infectious Diseases. *Disclosure: Jill Russell, BA, has no relevant financial relationships.*

CME Author

Charles P. Vega, MD, Health Sciences Clinical Professor of Family Medicine, University of California, Irvine School of Medicine, Irvine, California. *Disclosure: Charles P. Vega, MD, has the following relevant financial relationships: served as a consultant or advisor for Boehringer Ingelheim Pharmaceuticals, Inc.; Exact Sciences Corporation.*

Authors

Gerard C. Kelly, PhD; Agus Rachmat, BSc; Long Khanh Tran, PhD; Chonthida Supaprom, MSc; Hip Phireak, BSc; Satharath Prom, MD; Heng Sopheab, MD, PhD; Nora Cleary, MPH; Michael von Fricken, PhD; Christina M. Farris, PhD; Andrew G. Letizia, MD.

During 2007–2020, we conducted a cross-sectional prevalence study among patients with acute undifferentiated febrile illness to describe the burden and long-term epidemiology of rickettsioses in Cambodia. Serum samples were collected from 10,243 participants, along with epidemiologic data, information on clinical symptoms, demographic characteristics, and risk factors. A total of 802 (7.8%) participants met the definition for acute rickettsial infection after ruling out malaria, influenza, dengue, and chikungunya; 557 (5.4%) cases were typhus, 154 (1.5%) spotted fever, and 136 (1.3%) scrub typhus. Overall seroprevalence was 18.1% (1,857/10,243). Increased age, residence in urban settings, and recent travel to forests were significantly associated with rickettsial infection. Symptoms significantly associated with infection included rash, vomiting, and skin lesions. Our results confirm the underlying burden of rickettsioses and associated risk factors in Cambodia and highlight the need for accessible diagnostics and clinical guidance that consider rickettsioses when treating persons with acute undifferentiated febrile illness.

Rickettsioses are vectorborne bacterial infections caused by obligate, intracellular, gram-negative coccobacilli belonging to the genera *Rickettsia* and *Orientia*, which are transmitted to humans through arthropods such as ticks, fleas, mites, and lice (*1*–*4*). Transmission occurs globally and is influenced by varying factors, such as vector populations, ecology, and human activities (*5*–*7*).

The 3 main rickettsioses groups are typhus group (TG), consisting of endemic murine typhus (*Rickettsia typhi*) and the rarely occurring epidemic typhus (*R. prowazekii*); spotted fever group (SFG), consisting of multiple *Rickettsia* species (e.g., *R. rickettsii, R. conorii, R. felis)*; and the scrub typhus group (STG) (e.g., *Orientia tsutsugamushi*) (*2*,*8*). Infection is associated with a broad range of symptoms, often including an acute nonspecific febrile illness accompanied by headache, myalgia, nausea, and rash (*9*–*11*). In scrub typhus and tickborne SFG infections, an eschar at the bite site might also be observed (*9*,*10*). Although most symptomatic infections lead to mild or moderate illness, some cases can be severe and life-threatening if left untreated (*11*–*14*).

Throughout Southeast Asia, rickettsioses are a leading cause of acute febrile illness and disproportionately affect poorer communities (*1*,*10*,*15*,*16*). Despite being readily treatable with antibiotic therapy, particularly during the early course of infection, rickettsioses often remain underdiagnosed and subsequently undertreated (*1*,*10*,*13*,*17*). A lack of appropriate point-of-care diagnostics and the often nonspecific clinical manifestations associated with infection further complicate definitive diagnosis (*1*,*14*,*17*–*19*). The substantial public health concerns associated with rickettsioses (*1*,*20*–*22*) reflect the need to elucidate the true burden of disease and the associated population risk profile to support effective clinical management and public health responses.

In Cambodia, as part of a long-term health facility–based disease surveillance initiative established in 2006 by the Royal Cambodian Ministry of Health, standardized laboratory testing procedures were conducted on healthcare-seeking patients with acute undifferentiated febrile illness (AUFI) (*23*–*25*). Aims of this passive surveillance included using AUFI seroprevalence surveillance data to describe the burden and long-term epidemiology of rickettsioses among AUFI patients in Cambodia.

Methods

Study Site Selection, Design, and Participant Enrollment

We conducted a cross-sectional prevalence study among participants with AUFI symptoms at selected health facilities throughout Cambodia during January 2007–December 2020. The Cambodian Ministry of Health selected 28 health facilities from 9 provinces located within 4 terrestrial ecoregions (*26*) to represent a diversity of geographic locations throughout the country. Those facilities included 3 rural provincial hospitals and 14 rural health centers, together with 11 urban health centers primarily located around the capital, Phnom Penh (Figure 1). We collected data continuously throughout the course of the study during both the dry season (November–April) and wet season (May–October). We used terrestrial ecoregions, defined as standardized large land areas classified by distinct biogeographic

Author affiliations: Culmen International, LLC, Alexandria, Virginia, USA (G.C. Kelly, L.K. Tran); AC Investment Co, contractor for NAMRU INDO PACIFIC, Phnom Penh, Cambodia (A. Rachmat, C. Supaprom, H. Phireak); Oxford University Clinical Research Unit, Jakarta, Indonesia (A. Rachmat); Cambodia Ministry of National Defense Department of Health, Phnom Penh (S. Prom); Cambodia National Institute of Public Health, Phnom Penh (H. Sopheab); University of Florida College of Public Health and Health Professions, Gainesville, Florida, USA (N. Cleary, M. von Fricken); US Naval Medical Research Command Viral and Rickettsial Diseases Department, Silver Spring, Maryland, USA (C.M Farris); US Naval Medical Research Unit INDO PACIFIC, Singapore (A.G. Letizia)

DOI: https://doi.org/10.3201/eid3106.241752

groups of species and ecosystems, to describe ecologic zones (*26*).

In this study, we defined AUFI as acute onset of fever lasting ≥24 hours but <10 days where, even after comprehensive clinical history and physical examination, a distinct etiology could not be identified as previously described (*24*,*25*,*27*). Persons >2 years of age experiencing AUFI symptoms with an oral or tympanic temperature >38°C or axillary temperature >37.5°C were eligible. As part of the AUFI surveillance initiative, patients who tested negative for influenza (by nasal swab or rapid test), malaria (by microscopy or rapid test), dengue (by rapid test or laboratory-confirmed diagnosis, including PCR or serologic assay), or chikungunya (by PCR, serologic assay, or both), as previously described (*23*–*25*,*28*), were tested for rickettsioses. Patients positive for 1 of those more common etiologies were not evaluated for rickettsioses.

We asked eligible patients to complete a questionnaire to capture demographic information such as gender, employment status, residential address, and contact details. As part of an acute-stage sampling phase, participants underwent a medical history and physical examination, and blood samples were collected for laboratory testing. An acute clinical assessment questionnaire (Appendix Figure 1, https://wwwnc.cdc.gov/EID/article/31/6/24-1752-App1.pdf) was also completed that detailed travel history or any time spent working in forested areas in the previous 2 months before assessment. Participants were asked to return 14–30 days later to complete a follow-up medical examination and provide a convalescent blood sample for laboratory analysis. If participants did not return for their scheduled convalescent visit, study-associated healthcare staff visited the participant's place of residence to conduct follow-up assessment and specimen collection.

Laboratory Analysis

After collection, we labeled blood samples and sent them to Phnom Penh for processing. Serum was separated from the whole blood specimen, aliquoted into prelabeled cryovials, and stored at –70°C or in liquid nitrogen. We performed rickettsioses antibody testing on serum samples using IgG in-house ELISAs developed by the Naval Medical Research Center (Silver Spring, Maryland, USA). The assays targeted antibodies against specific rickettsial antigens of the typhus group (*R. typhi*, Wilmington strain), scrub typhus group (*O. tsutsugamushi*, Gilliam, Kato, and Karp strains), and spotted fever group (*R. conorii*),

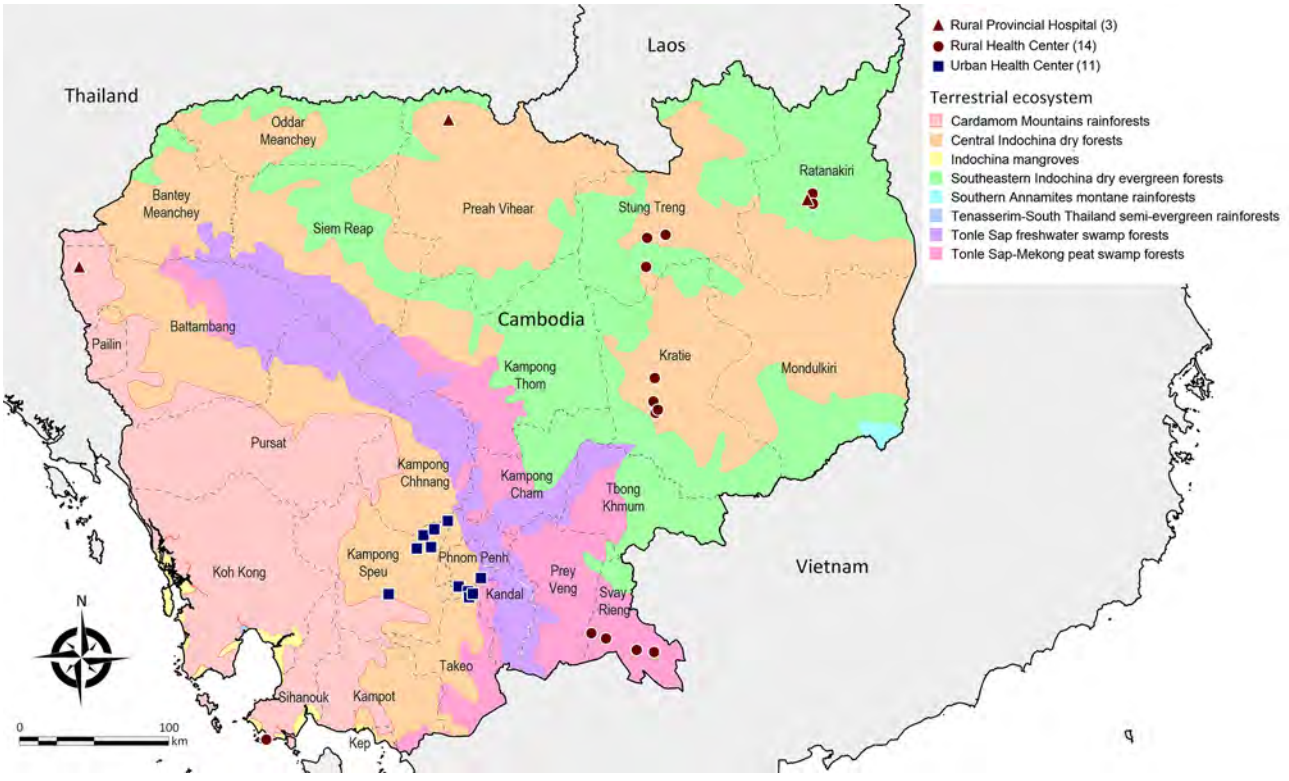

Figure 1. Study site locations of urban and rural health facilities included in cross-sectional prevalence study of clinical manifestations, risk factors, and disease burden of rickettsiosis, Cambodia, 2007–2020, overlayed on top of terrestrial ecoregions of Cambodia.

as previously described (*25*,*29*–*31*). Positive and negative controls for each assay were derived from pooled serum samples collected from participants in the Cambodia AUFI surveillance initiative with net optical density (OD) values of <0.2 (negative) and >1.0 (positive). For initial screening, we tested convalescent samples at 1:100 dilution and scored them as positive if they yielded a net OD of ≥0.5 for any of the 3 antigen preparations. All screen-positive serum samples were titrated at 4 dilutions of 1:100, 1:400, 1:1,600, and 1:6,400. We considered samples positive when the cumulative net OD value for the 4 dilutions was ≥1,000. Titers for the positive samples were determined to be the inverse of the highest dilution that gave a net OD of >0.2. Samples that achieved an OD of >0.5 at screening but failed to be confirmed by titration were reported as negative for all later analyses. We then paired convalescent samples identified as IgG-positive with their corresponding acute serum samples and retested to identify a positive rickettsial infection.

Definition of a Positive Rickettsial Infection

In this study, we defined a positive rickettsial infection as either a 4-fold increase in titer from acute to convalescent sample or a result change of negative in the acute sample to positive in the convalescent sample, considered indicative of seroconversion. We defined previous exposure (seroprevalence) as any participant with a seropositive result in either the acute or convalescent sample, regardless of seroconversion.

Data Management and Statistical Analysis

We matched and double-entered data into Access (Microsoft, https://www.microsoft.com) and performed statistical analysis using R version 4.3.0 (The R Project for Statistical Computing, https://www.r-project.org). We used the Pearson χ^2 test to analyze frequency of categorical variables and generalized linear models for binomial regression analysis to calculate odds ratios (ORs) and 95% CIs to measure the association between rickettsioses and recorded symptoms, demographics, and environmental characteristics. We also analyzed potential interactions between key variables including urban or rural status and terrestrial ecosystems.

Ethical Clearance and Consent

We obtained written informed consent from eligible participants ≥18 years of age or the parent/legal guardian of eligible nonadult participants <18 years of age. Ethics approval was obtained by the Kingdom of Cambodia's National Ethics Committee for Health Research (208 NECHR) and the United States Naval Medical Research Center (NAMRU2.2012.0001), in compliance with all applicable federal regulations governing the protection of human subjects.

Results

We enrolled a total of 42,221 participants during 2007–2020, of whom 29,982 (71.0%) provided paired acute-convalescent blood samples (Figure 2). In accordance with the study testing protocol, we tested 10,243 (34.2%) paired samples for rickettsioses after seeing the results of rapid and laboratory testing; we did not test 9,340 (31.1%) participants because they tested positive for influenza, malaria, dengue, or chikungunya (Figure 2). We did not test the remaining 10,399 (34.7%) participants because of supply limitations and logistical challenges experienced during the study, as well as because of host country operational priorities, including no participants being tested for rickettsioses in 2009 because of a reallocation of resources to address the swine influenza pandemic. Participants tested for rickettsioses were 2–90 years of age; the mean age was 24.2 (SD 17.3) years. The median number of tested participants per year was 512 (mean 787.9 [SD 619.6]) (Appendix Table 1).

We identified a total of 847 rickettsial infections among 802 (7.8%) participants during the study. Of those infections, most belonged to the TG (65.8%, n = 557), followed by the SFG (18.2%, n = 154), and STG (16.0%, n = 136) (Table 1). We detected co-infections with multiple rickettsioses in 44 (0.4%) of the 10,243 tested participants, including 1 participant who tested positive for all 3 rickettsial groups (Appendix Table 2). We recorded significant positive associations between TG and STG (OR 2.36 [95% CI 1.34–3.88]), SFG and TG (OR 2.50 [95% CI 1.49–3.97]), and STG and SFG (OR 6.13 [95% CI 3.06–11.1]) infections (Appendix Table 3). Among the 10,243 participants tested, 1,857 (18.1%) recorded a positive result in either the acute or convalescent sample, indicative of rickettsioses exposure, including 1,068 (10.4%) recording positive exposures to TG, 596 (5.8%) to SFG, and 451 (4.4%) to STG.

We identified a significant association between year and number of rickettsial infections detected over the 14-year study period (p<0.001). Most rickettsial infections were detected during 2016–2019 (70.7%, n = 567); the highest number of cases (n = 227) and proportion of positive tests by year (13.3%) occurred in 2018 (Figure 3).

Most rickettsial infections were detected among study participants >15 years of age (83.3%, n = 684), which had a recorded test positivity percentage of

11.2% (684/6,132); percentage of test positivity in participants ≤15 years of age (14.7%, n = 118) was 2.9% (118/4,111) (Table 2; Appendix Tables 4, 5). The highest overall percentages of positivity for rickettsial infections were recorded among participants ≥46 years (14.7%, 216/1,468) and 36–45 (14.2%, 156/1,096) years of age (Appendix Figure 2). In participants who reported travel to the forest, 14.8% (406/2,735) tested positive, whereas 12.0% (165/1,375) of participants who reported travel outside their home region tested positive. Similarly, high test-positivity percentages for TG infections were recorded within those categories; 11.9% (326/2,735) of participants who reported traveling to the forest tested positive for TG infections, and 9.0% (124/1,371) of participants who reported travel outside their home regions tested positive. A strong positive association was observed among participants testing positive for TG and traveling to the forest (OR 4.26 [95% CI 3.58–5.08]).

All persons in age groups >15 years had significantly higher odds of infection than did participants <15 years of age; persons in the 36–45-year age group had the highest likelihood (OR 4.17 [95% CI 3.14–5.54]), followed by the ≥46-year group (OR 4.02 [95% CI 3.07–5.26), the 16–25-year age group (OR 3.68 [95% CI 2.79–4.86), and the 26–35-year age group (OR 3.06 [95% CI 2.30–4.06]) (Table 3). In addition to age and forest exposure (OR 1.87 [95% CI 1.52–2.30]); other risk factors included participants testing positive in health facilities located in Central Indochina dry forest (OR 3.68 [95% CI 2.51–5.60]) and Tonle Sap-Mekong peat swamp forest ecoregions (OR 1.74 [95% CI 1.03–2.98]), and urban areas (OR 1.95 [95% CI 1.29–2.99). In addition to education, significant negative

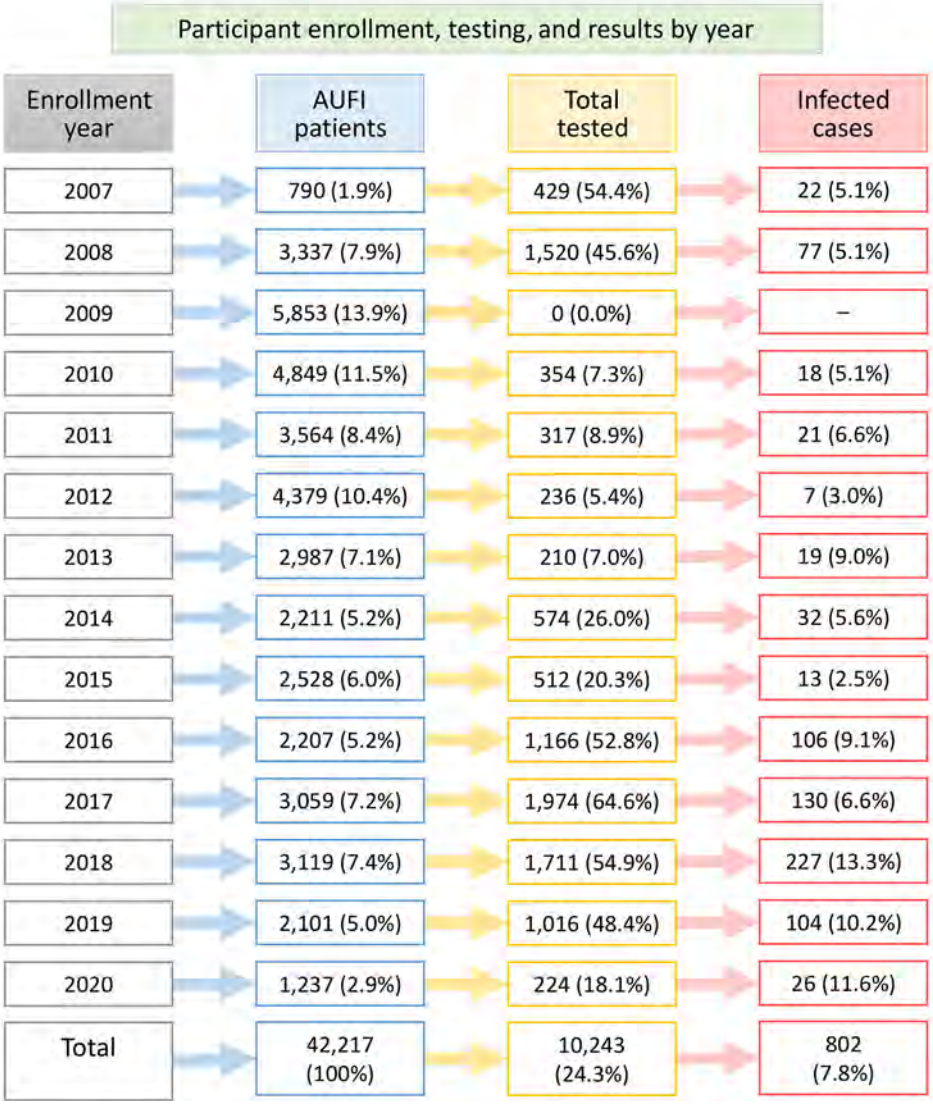

Figure 2. Flowchart of patients enrolled in rickettsioses cross-sectional prevalence study of clinical manifestations, risk factors, and disease burden of rickettsiosis, Cambodia, 2007–2020. Columns indicate percentage of total AUFI patents (blue), percentage of participants tested for rickettsioses (yellow), and percentage of infected persons detected per year (red). No testing was conducted in 2009. AUFI, acute undifferentiated febrile illness.

Table 1. Rickettsial infections detected by type and diagnostic method among patients with acute undifferentiated febrile illness tested for rickettsioses at health facilities as part of study of rickettsiosis in Cambodia, 2007–2020*

Group	Result	Diagnostic method, no. (%) patients		
		4-fold increase	Seroconversion	Seroconversion or 4-fold increase
STG	Negative	10,211 (99.7)	10,139 (99.0)	10,107 (98.7)
	Positive	32 (0.3)	104 (1.0)	136 (1.3)
TG	Negative	10,176 (99.3)	9,753 (95.2)	9,686 (94.6)
	Positive	67 (0.7)	490 (4.8)	557 (5.4)
SFG	Negative	10,221 (99.8)	10,111 (98.7)	10,089 (98.5)
	Positive	22 (0.2)	132 (1.3)	154 (1.5)

*SFG, spotted fever group; STG, scrub typhus group; TG, typhus group.

associations were recorded among employed participants (OR 0.69 [95% CI 0.50–0.94). We did not observe any significant association between rickettsial infection and gender, general travel, or season (wet or dry) in this study (Appendix Table 6).

Positive symptom associations included rash (adjusted OR [aOR] 2.21 [95% CI 1.63–2.97]), vomiting (aOR 1.64 [95% CI 1.29–2.07]), and skin lesions (aOR 1.63 [95% CI 1.25–2.12]) (Table 4). Among participants tested for rickettsioses, 23.1% (129/559) of persons with skin lesions and 22.8% (76/334) of persons with rash tested positive for a rickettsial infection (Table 4).

Discussion

Using laboratory-level diagnostics and associated patient and community level variables, this study provides a unique opportunity to describe the variable burden and characteristics of rickettsial infection in Cambodia over a 14-year period. The overall rickettsioses test-positivity percentage of 7.8% observed in this study demonstrates a notable burden of disease among febrile patients seeking treatment who had tested negative for influenza, malaria, dengue, and chikungunya. Similarly, the positive detection of antibodies in 18.1% of all tested participants suggests a significant level

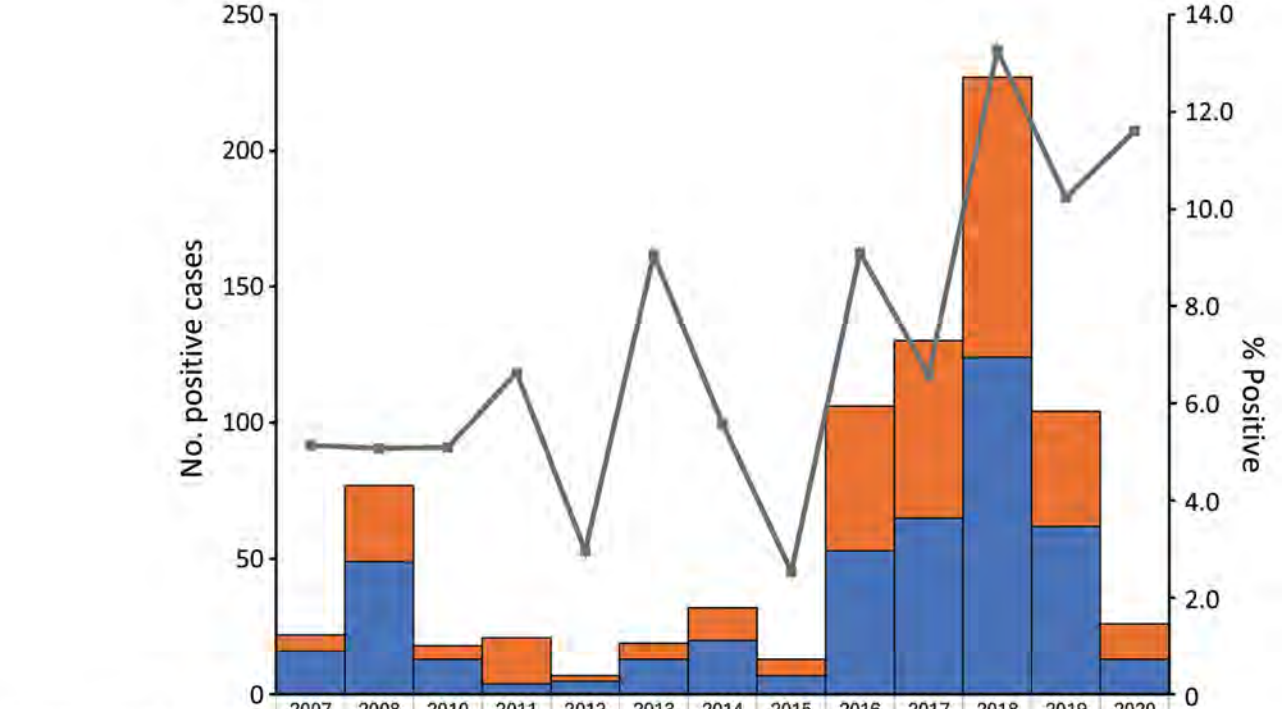

	2007	2008	2010	2011	2012	2013	2014	2015	2016	2017	2018	2019	2020
Total tested	429	1,520	354	317	236	210	574	512	1,166	1,974	1,711	1,016	224
Infected cases (p<0.001)	22	77	18	21	7	19	32	13	106	130	227	104	26
Dry season cases	6	28	5	17	2	6	12	6	53	65	103	42	13
Wet season cases	16	49	13	4	5	13	20	7	53	65	124	62	13
% Positive	5.1%	5.1%	5.1%	6.6%	3.0%	9.0%	5.6%	2.5%	9.1%	6.6%	13.3%	10.2%	11.6%

Figure 3. Detected rickettsial infections by year and season and yearly percentage of rickettsioses-positive patients with acute undifferentiated febrile illness in cross-sectional prevalence study of clinical manifestations, risk factors, and disease burden of rickettsiosis, Cambodia, 2007–2020. p values determined using the Pearson χ^2 test. The year 2009 is omitted because no testing was conducted.

of exposure to rickettsioses among the population of Cambodia. Wide variances in rickettsioses seroprevalence proportions are noted in the literature (5%–30%); differences are often explained by geography, study design, targeted population immunological profiles, diagnostic approaches used, and thresholds or clinical definitions applied, likely contributing to this wide range (*10*,*32*). However, this study recorded a higher prevalence of TG cases (5.4%) than STG cases (1.3%), in contrast to previous studies from adjacent countries such as Thailand (9.0% TG vs. 9.8% STG), Vietnam (3.7% TG vs. 26.4% STG), and Laos (9.6% TG vs. 14.8% STG) (*33*–*35*). Of note, the prevalence of confirmed STG cases (1.3%) and overall STG seroprevalence (4.4%) in this study were lower than that observed in studies referenced from neighboring countries but are similar to those reported for similar AUFI studies in Cambodia (*36*). The discordance might relate to vector dynamics, disease reservoirs, or differences among target population risk profiles across studies, which will require further research to confirm the causative factors driving these variances.

Although we did not compare the prevalence of rickettsioses to influenza, malaria, dengue, and chikungunya, our results indicated that almost 1 in 10 cases of AUFI in this study were likely caused by rickettsiosis (after those more common etiologies had been ruled out). Given rickettsial infections are known to be chronically underdiagnosed, those findings highlight a clear need for accessible point-

Table 2. Characteristics of study participants and seroprevalence of rickettsial infection by type among patients with acute undifferentiated febrile illness tested for rickettsioses at health facilities as part of study of rickettsiosis in Cambodia, 2007–2020*

Category	Total tested, no. (%)‡	Negative, no. (%)†	Positive, no. (%)†			
			STG	TG	SFG	All rickettsiae
Participants	10,243 (100)	9,441 (92.1)	136 (1.3)	557 (5.4)	154 (1.5)	802 (7.8)
Age group, y						
≤15	4,111 (40.1)	3,993 (97.1)	28 (0.7)	74 (1.8)	22 (0.5)	118 (2.9)
16–25	1,805 (17.6)	1,637 (90.7)	36 (2.0)	107 (5.9)	38 (2.1)	168 (9.3)
26–35	1,763 (17.2)	1,619 (91.8)	17 (1.0)	97 (5.5)	36 (2.0)	144 (8.2)
36–45	1,096 (10.7)	940 (85.8)	13 (1.2)	120 (10.9)	32 (2.9)	156 (14.2)
≥46	1,468 (14.3)	1,252 (85.3)	42 (2.9)	159 (10.8)	26 (1.8)	216 (14.7)
Sex						
F	4,936 (48.2)	4,601 (93.2)	68 (1.4)	221 (4.5)	62 (1.3)	335 (6.8)
M	5,307 (51.8)	4,840 (91.2)	68 (1.3)	336 (6.3)	92 (1.7)	467 (8.8)
Education	6,182 (60.4)	5,653 (91.4)	91 (1.5)	376 (6.1)	86 (1.4)	529 (8.6)
Lower primary school	2,224 (21.7)	2,062 (92.7)	29 (1.3)	110 (4.9)	38 (1.7)	162 (7.3)
Primary school	938 (9.2)	875 (93.3)	6 (0.6)	40 (4.3)	19 (2.0)	63 (6.7)
Lower secondary school	816 (8.0)	770 (94.4)	10 (1.2)	29 (3.6)	11 (1.3)	46 (5.6)
High school	83 (0.8)	81 (97.6)	0 (0)	2 (2.4)	0 (0)	2 (2.4)
Diploma or university						
Employment status						
Unemployed	8,907 (87.0)	8,164 (91.7)	115 (1.3)	521 (5.8)	149 (1.7)	743 (8.3)
Employed	1,336 (13.0)	1,277 (95.6)	21 (1.6)	36 (2.7)	5 (0.4)	59 (4.4)
Season						
Dry, Nov–Apr	4,497 (43.9)	4,139 (92.0)	49 (1.1)	251 (5.6)	78 (1.7)	358 (8.0)
Wet, May–Oct	5,746 (56.1)	5,302 (92.3)	87 (1.5)	306 (5.3)	76 (1.3)	444 (7.7)
Area						
Rural	5,331 (52.0)	4,875 (91.4)	67 (1.3)	330 (6.2)	70 (1.3)	456 (8.6)
Urban	4,912 (48.0)	4,566 (93.0)	69 (1.4)	227 (4.6)	84 (1.7)	346 (7.0)
Had traveled						
No	8,872 (86.6)	8,235 (92.8)	115 (1.3)	433 (4.9)	121 (1.4)	637 (7.2%)
Yes	1,371 (13.4)	1,206 (88.0)	21 (1.5)	124 (9.0)	33 (2.4)	165 (12.0%)
Traveled to forest						
No	7,508 (73.3)	7,112 (94.7)	97 (1.3)	231 (3.1)	100 (1.3)	396 (5.3)
Yes	2,735 (26.7)	2,329 (85.2)	39 (1.4)	326 (11.9)	54 (2.0)	406 (14.8)
Terrestrial ecosystem						
Southeastern Indochina dry evergreen forests	869 (8.5)	840 (96.7)	7 (0.8)	10 (1.2)	13 (1.5)	29 (3.3)
Cardamom Mountains rain forests	292 (2.8)	287 (98.3)	2 (0.7)	3 (1.0)	1 (0.3)	5 (1.7)
Central Indochina dry forests	6,791 (66.3)	6,135 (90.3)	95 (1.4)	482 (7.1)	114 (1.7)	656 (9.7)
Tonle Sap-Mekong peat swamp forests	2,291 (22.4)	2,179 (95.1)	32 (1.4)	62 (2.7)	26 (1.1)	112 (4.9)
Antibiotic use in past 30 d						
No	9,736 (95.0)	8,979 (92.2)	129 (1.3)	523 (5.4)	149 (1.5)	757 (7.8)
Yes	507 (5.0)	462 (91.1)	7 (1.4)	34 (6.7)	5 (1.0)	45 (8.9)

*SFG, spotted fever group; STG, scrub typhus group; TG, typhus group.
†Percentages of participants by category.
‡Percentages of total participants.

of-care diagnostics and effective surveillance. Similarly, strengthening awareness and education among healthcare providers and ensuring appropriate antibiotic treatments are available is critical to addressing rickettsiosis in Cambodia.

The number of positive cases detected over time was shown to differ in this study; yearly test positivity percentages ranged from 2.5% in 2015 to 11.6% in 2020, illustrating variable transmission dynamics. Such longitudinal variability indicates a need to incorporate effective surveillance into routine health system practice to adequately monitor transmission and identify potential disease outbreaks. Challenges associated with early diagnosis, variable transmission rates, and the potential for serious and life-threatening illness, when paired with exposure and infection rates observed in this study, highlight the public health impact of rickettsioses in Cambodia. The final 3 years of the study recorded the 3 highest test-positivity percentages recorded over the 14-year study period, which also saw positivity percentages for rickettsial DNA as high as 36% in ectoparasites collected in southern Cambodia (*37*), indicating a potential resurgence of rickettsial infections in recent years. That period was immediately before lockdowns associated with the COVID-19 pandemic and might not be reflective of current patterns, warranting the investigation of contemporary epidemiologic data.

Table 3. Association between key participant characteristics and rickettsial infection among patients with acute undifferentiated febrile illness who tested positive for rickettsioses as part of study of rickettsiosis in Cambodia, 2007–2020*

Characteristic	OR (95% CI)	p value
Year	1.04 (1.02–1.07)	0.001
Age group, y		
≤15	Referent	
16–25	3.68 (2.79–4.86)	<0.001
26–35	3.06 (2.30–4.06)	<0.001
36–45	4.17 (3.14–5.54)	<0.001
≥46	4.02 (3.07–5.26)	<0.001
Sex		
F	Referent	
M	1.16 (0.99–1.36)	0.072
Education		
Lower primary school	Referent	
Primary school	0.77 (0.63–0.95)	0.014
Lower secondary school	0.70 (0.52–0.94)	0.019
High school	0.56 (0.39–0.77)	<0.001
Diploma or university	0.23 (0.04–0.77)	0.047
Employment status		
Unemployed	Referent	
Employed	0.69 (0.50–0.94)	0.022
Season		
Dry, Nov–Apr	Referent	
Wet, May–Oct	0.97 (0.84–1.13)	0.7
Area		
Rural	Referent	
Urban	1.95 (1.29–2.99)	0.002
Terrestrial ecosystem		
Southeastern Indochina dry evergreen forests	Referent	
Cardamom Mountains rain forests	0.90 (0.30–2.21)	0.8
Central Indochina dry forests	3.68 (2.51–5.60)	<0.001
Tonle Sap-Mekong peat swamp forests	1.74 (1.03–2.98)	0.041
Influence of rural/urban setting within terrestrial ecosystem†		
Urban/Cardamom Mountains rain forests		
Urban/Central Indochina dry forests	0.52 (0.32–0.85)	0.009
Urban/Tonle Sap-Mekong peat swamp forests		
Had traveled		
No	Referent	
Yes	0.79 (0.62–1.01)	0.061
Traveled to forest		
No	Referent	
Yes	1.87 (1.52–2.30)	<0.001
Antibiotic use in past 30 d		
No	Referent	
Yes	1.02 (0.72–1.41)	>0.9

*Determined by generalized linear model for binomial regression. OR, odds ratio.
†Reference group is rural location (data not listed) for respective urban ecosystems.

Consistent with previous studies from neighboring countries, including Thailand, Laos, and Malaysia (*33*,*38*,*39*), our findings demonstrated a significant association between increasing age and rickettsial infection. Higher case rates among adults than in children suggests potential increased exposure among participants >15 years of age to environmental settings favorable to the vectors and vector hosts known to transmit rickettsial bacteria, likely because of occupational or lifestyle activities. This study also identified a negative association between rickettsial infection and participants with formal employment and higher levels of education, consistent with findings from previous studies within the region examining those sociodemographic variables (*33*,*38*). Of note, we observed similar proportions of STG seroprevalence and infection between urban and rural participants in this study. Given the high percentage of the labor force engaged in the agricultural sector (32%), particularly rice production, together with Cambodia's relatively small size and good transport network (*40*), those findings warrant further detailed investigation into the effects of occupational exposure and risk stratification on STG infection.

In addition to age across all 3 main rickettsioses groups, we identified significant associations between SFG infection and urban settings, as well as associations between infection and travel to forests and associations between the Central Indochina dry forests and Tonle Sap-Mekong peat swamp forest

Table 4. Association between reported symptoms and rickettsial infection among patients with acute undifferentiated febrile illness who tested positive for rickettsioses as part of study of rickettsiosis in Cambodia, 2007–2020*

		Rickettsial infection						
		Total, n =	Negative,	Positive,	Unadjusted†		Adjusted‡	
Symptom	Present	10,243	n = 9,441	n = 802	OR (95% CI)	p value	OR (95% CI)	p value
Fever	Yes	10,243	9,441 (92.2)	802 (7.8)				
Malaise	No	3,373	3,204 (95.0)	169 (5.0)	Referent		Referent	
	Yes	6,870	6,237 (90.8)	633 (9.2)	1.92 (1.62–2.30)	<0.001	0.76 (0.60–0.96)	0.019
Chills	No	4,475	4,260 (95.2)	215 (4.8)	Referent		Referent	
	Yes	5,768	5,181 (89.8)	587 (10.2)	2.24 (1.91–2.64)	<0.001	1.39 (1.16–1.68)	<0.001
Joint pain	No	7,359	6,921 (94.1)	438 (5.9)	Referent		Referent	
	Yes	2,884	2,520 (87.4)	364 (12.6)	2.28 (1.97–2.64)	<0.001	1.15 (0.95–1.38)	0.2
Nausea	No	7,594	7,104 (93.6)	490 (6.4)	Referent		Referent	
	Yes	2,649	2,337 (88.2)	312 (11.8)	1.94 (1.67–2.25)	<0.001	0.79 (0.62–1.00)	0.056
Vomit	No	8,347	7,820 (93.7)	527 (6.3)	Referent		Referent	
	Yes	1,896	1,621 (85.5)	275 (14.5)	2.52 (2.15–2.94)	<0.001	1.64 (1.29–2.07)	<0.001
Abdominal	No	9,083	8,349 (91.9)	734 (8.1)	Referent		Referent	
cramps	Yes	1,160	1,092 (94.1)	68 (5.9)	0.71 (0.54–0.91)	0.008	0.77 (0.55–1.04)	0.10
Diarrhea	No	9,813	9,048 (92.2)	765 (7.8)	Referent		Referent	
	Yes	430	393 (91.4)	37 (8.6)	1.11 (0.78–1.55)	0.5	1.57 (1.02–2.38)	0.036
Bloody stool	No	10,203	9,403 (92.2)	800 (7.8)	Referent		Referent	
	Yes	40	38 (95.0)	2 (5.0)	0.62 (0.10–2.02)	0.5	0.52 (0.08–1.87)	0.4
Cough	No	3,362	3,099 (92.2)	263 (7.8)	Referent		Referent	
	Yes	6,881	6,342 (92.2)	539 (7.8)	0.86–1.17	>0.9	0.95 (0.77–1.18)	0.7
Headache	No	1,615	1,566 (97.0)	49 (3.0)	Referent		Referent	
	Yes	8,628	7,875 (91.3)	753 (8.7)	3.06 (2.30–4.15)	<0.001	1.47 (1.07–2.07)	0.020
Sore throat	No	4,348	4,040 (92.9)	308 (7.1)	Referent		Referent	
	Yes	5,895	5,401 (91.6)	494 (8.4)	1.20 (1.04–1.39)	0.016	0.99 (0.81–1.21)	>0.9
Muscle aches	No	6,223	5,944 (95.5)	279 (4.5)	Referent		Referent	
	Yes	4,020	3,497 (87.0)	523 (13.0)	3.19 (2.74–3.71)	<0.001	1.39 (1.12–1.74)	0.004
Shortness of	No	9,430	8,681 (92.1)	749 (7.9)	Referent		Referent	
breath	Yes	813	760 (93.5)	53 (6.5)	0.81 (0.60–1.07)	0.15	0.84 (0.62–1.13)	0.3
Rash	No	9,909	9,183 (92.7)	726 (7.3)	Referent		Referent	
	Yes	334	258 (77.3)	76 (22.7)	3.73 (2.84–4.84)	<0.001	2.21 (1.63–2.97)	<0.001
Lesion	No	9,684	9,011 (93.1)	673 (6.9)	Referent		Referent	
	Yes	559	430 (76.9)	129 (23.1)	4.02 (3.24–4.95)	<0.001	1.63 (1.25–2.12)	<0.001
Seizure	No	10,172	9,375 (92.2)	797 (7.8)	Referent		Referent	
	Yes	71	66 (93.0)	5 (7.0)	0.89 (0.31–2.01)	0.8	1.00 (0.34–2.35)	>0.9
Other symptoms	No	9,670	8,881 (91.8)	789 (8.2)	Referent		Referent	
	Yes	573	560 (97.7)	13 (2.3)	0.26 (0.14–0.44)	<0.001	0.36 (0.19–0.60)	<0.001

*Values are no. (%) except as indicated. OR, odds ratio.
†Unadjusted generalized linear model for binomial regression.
‡Generalized linear model for binomial regression adjusted by age, gender, and enrollment year.

ecoregions with TG infection. Those findings suggest lifestyle and occupational and environmental exposure, such as living in high-density residencies or engaging in forest-based and forest-fringe–based informal occupations (such as agriculture, logging, and animal trapping), are all associated with an increased risk for specific types of infection. Providers should have a higher index of suspicion for rickettsial infection if those risk factors are present. We also found no significant difference in association between wet and dry seasons in this study, indicating that rickettsial infections should be considered as a potential etiology regardless of season.

In this study, we sought to elucidate the burden of rickettsial disease in Cambodia after ruling out more common pathogens. Consistent with other studies, significant symptoms associated with rickettsial infections observed after multivariable analysis consisted of rash, vomiting, skin lesions, headache, diarrhea, chills, and muscle aches (*10*,*19*,*41*,*42*). Despite those associations, the nonspecific nature of those symptoms is common to many febrile illnesses, emphasizing the challenges associated with the clinical diagnosis of rickettsioses, particularly in the absence of specific laboratory diagnostics (*3*,*10*,*19*). Of note, we observed a high proportion of specific gastrointestinal symptoms among infected participants. Previous research highlights a higher propensity for the misdiagnosis of rickettsial infections if gastrointestinal symptoms are prominent or no skin rash is present (*10*,*19*). Therefore, providers should not exclude rickettsioses from the differential diagnosis in the setting of vomiting or diarrhea and could consider empiric therapy if proper diagnostics are not available. The overlap in the identified symptom associations of rickettsioses with other

well-known febrile illnesses in the region, such as dengue and malaria, together with relatively high proportions of rickettsial infection identified among participants tested in this study, highlights the overlapping nonspecific clinical manifestations likely seen by frontline healthcare providers. The substantial risk of underdiagnosing rickettsioses supports the development of a point-of-care diagnostic that can be used in low-resource settings.

The first limitation of this study is its reliance on deidentified passive surveillance data collected from symptomatic patients seeking care for AUFI; persons with asymptomatic and mildly symptomatic rickettsial infections might have been missed, because those patients would not seek care. Similarly, only AUFI patients who tested negative for influenza, malaria, dengue, and chikungunya were tested for rickettsioses, meaning rickettsial-infected patients co-infected with any of those diseases could have been missed in this study because of selection bias. Testing proportions might also have been influenced by seasonal factors; 19.7% of AUFI patients were tested for rickettsioses during the wet season compared with 32.1% in the dry season, possibly because of higher positivity proportions for other diseases during the wet season or seasonal dynamics of the vectors. Those factors might have led to underestimating the true prevalence of rickettsioses. Also, because most study site facilities were located within the Central Indochina dry forests and Tonle Sap-Mekong peat swamp forests ecoregions, the potential for bias associated with the uneven distribution of sites should be considered when interpreting the terrestrial ecoregion analyses. The collection of additional patient level data (such as occupation and specific participant interactions with domestic or agricultural animals), as well as household level information (such as number of persons residing in the household) and the expansion of data collection to all ecoregion types in Cambodia, should be incorporated into future surveillance efforts to fill additional knowledge gaps identified by this effort.

This long-term surveillance study has documented the rate of rickettsial infections among AUFI patients in Cambodia as ≈8% once more common etiologies were ruled out; seroprevalence was 18%. Clinical and epidemiologic risk factors identified over the 14-year study period associated with rickettsial infection, in addition to fever, include rash, skin lesions, and vomiting, as well as age, residence in urban settings, and recent travel to forests. Given the complex diagnostic challenges, clinical prognosis, and disease burden identified in this study, point-of-care diagnostics for resource-limited settings are needed. In the meantime, providers with clinical suspicion could consider empiric therapy. Additional surveillance and research are needed to better define transmission dynamics, the associated risk profiles of populations most at risk, the specific rickettsial pathogens responsible for disease (i.e., species specific molecular and serologic assays), and the influence of environmental and economic changes to inform appropriate public health interventions. Our results add to our overall understanding and awareness of rickettsioses in Cambodia and make a strong case for deploying diagnostic tools for detecting TG, SFG, and STG rickettsiae in clinical settings.

Acknowledgments

We thank our Cambodian Department of Health and Ministry of National Defense colleagues, together with Provincial Health Department and local health facility personnel involved in this multiyear study, for their sustained support and cooperation. We also thank our field research and Naval Medical Research Unit Indo Pacific laboratory teams for their long-term service and contribution. In addition, we thank Allen Richards for his guidance and assistance throughout the study.

This work was funded through work unit nos. P0150_20_N2_01, P0150_19_NA_01.01, and P0150_18_NA_03.01 as a component of the Armed Forces Health Surveillance Branch Global Emerging Infections Surveillance program.

About the Author

Dr. Kelly is a senior epidemiologist with Culmen International specializing in infectious disease surveillance and spatial epidemiology. His current research focuses on the surveillance of vectorborne diseases throughout the Indo-Pacific region.

References

1. Salje J, Weitzel T, Newton PN, Varghese GM, Day N. Rickettsial infections: a blind spot in our view of neglected tropical diseases. PLoS Negl Trop Dis. 2021;15:e0009353. https://doi.org/10.1371/journal.pntd.0009353
2. Ngamprasertchai T, Hanboonkunupakarn B, Piyaphanee W. Rickettsiosis in Southeast Asia: summary for international travellers during the COVID-19 pandemic. Trop Med Infect Dis. 2022;7:18. https://doi.org/10.3390/tropicalmed7020018
3. Premaratna R. Rickettsial illnesses, a leading cause of acute febrile illness. Clin Med (Lond). 2022;22:2–5. https://doi.org/10.7861/clinmed.2021-0790
4. Azad AF, Beard CB. Rickettsial pathogens and their arthropod vectors. Emerg Infect Dis. 1998;4:179–86. https://doi.org/10.3201/eid0402.980205
5. Derne B, Weinstein P, Musso D, Lau C. Distribution of rickettsioses in Oceania: past patterns and implications for the future. Acta Trop. 2015;143:121–33.
6. Piotrowski M, Rymaszewska A. Expansion of tick-borne rickettsioses in the world. Microorganisms. 2020;8:1906. https://doi.org/10.3390/microorganisms8121906
7. Zhang Y-Y, Sun Y-Q, Chen J-J, Teng A-Y, Wang T, Li H, et al. Mapping the global distribution of spotted fever group rickettsiae: a systematic review with modelling analysis. Lancet Digit Health. 2023;5:e5–15. https://doi.org/10.1016/S2589-7500(22)00212-6
8. Jensenius M, Fournier PE, Raoult D, Raoult D. Rickettsioses and the international traveler. Clin Infect Dis. 2004;39:1493–9. https://doi.org/10.1086/425365
9. Walker DH. Rickettsial diseases in travelers. Travel Med Infect Dis. 2003;1:35–40. https://doi.org/10.1016/S1477-8939(03)00025-5
10. Aung AK, Spelman DW, Murray RJ, Graves S. Rickettsial infections in Southeast Asia: implications for local populace and febrile returned travelers. Am J Trop Med Hyg. 2014;91:451–60. https://doi.org/10.4269/ajtmh.14-0191
11. Cowan G. Rickettsial diseases: the typhus group of fevers—a review. Postgrad Med J. 2000;76:269–72. https://doi.org/10.1136/pmj.76.895.269
12. Walker DH, Ismail N. Emerging and re-emerging rickettsioses: endothelial cell infection and early disease events. Nat Rev Microbiol. 2008;6:375–86.
13. Suputtamongkol Y, Suttinont C, Niwatayakul K, Hoontrakul S, Limpaiboon R, Chierakul W, et al. Epidemiology and clinical aspects of rickettsioses in Thailand. Ann N Y Acad Sci. 2009;1166:172–9. https://doi.org/10.1111/j.1749-6632.2009.04514.x
14. Xu G, Walker DH, Jupiter D, Melby PC, Arcari CM. A review of the global epidemiology of scrub typhus. PLoS Negl Trop Dis. 2017;11:e0006062. https://doi.org/10.1371/journal.pntd.0006062
15. Yuhana MY, Hanboonkunupakarn B, Tanganuchitcharnchai A, Sujariyakul P, Sonthayanon P, Chotivanich K, et al. Rickettsial infections are neglected causes of acute febrile illness in Teluk Intan, Peninsular Malaysia. Trop Med Infect Dis. 2022;7:77. https://doi.org/10.3390/tropicalmed7050077
16. Acestor N, Cooksey R, Newton PN, Ménard D, Guerin PJ, Nakagawa J, et al. Mapping the aetiology of non-malarial febrile illness in Southeast Asia through a systematic review—terra incognita impairing treatment policies. PLoS One. 2012;7:e44269. https://doi.org/10.1371/journal.pone.0044269
17. Kamath V, Ganguly S, Bhatia JK, Himabindu R. Rickettsial infections: past and present perspectives. APIK Journal of Internal Medicine. 2020;8:4–10. https://doi.org/10.4103/AJIM.AJIM_22_19
18. Blanton LS. The rickettsioses: a practical update. Infect Dis Clin North Am. 2019;33:213–29. https://doi.org/10.1016/j.idc.2018.10.010
19. Hendershot EF, Sexton DJ. Scrub typhus and rickettsial diseases in international travelers: a review. Curr Infect Dis Rep. 2009;11:66–72. https://doi.org/10.1007/s11908-009-0010-x
20. van Eekeren LE, de Vries SG, Wagenaar JFP, Spijker R, Grobusch MP, Goorhuis A. Under-diagnosis of rickettsial disease in clinical practice: a systematic review. Travel Med Infect Dis. 2018;26:7–15.
21. Vohra RF, Walker DH, Blanton LS. Analysis of health-care charges in murine typhus: need for improved clinical recognition and diagnostics for acute disease. Am J Trop Med Hyg. 2018;98:1594–8. https://doi.org/10.4269/ajtmh.17-0411
22. Drexler NA, Traeger MS, McQuiston JH, Williams V, Hamilton C, Regan JJ. Medical and indirect costs associated with a Rocky Mountain spotted fever epidemic in Arizona, 2002–2011. Am J Trop Med Hyg. 2015;93:549–51. https://doi.org/10.4269/ajtmh.15-0104
23. Rachmat A, Kelly GC, Hontz RD, Supaprom C, Heang V, Hip P, et al. Clinical and epidemiologic evaluation of a 2020 chikungunya outbreak in Cambodia. BMC Infect Dis. 2022;22:949.
24. Rachmat A, Kelly GC, Tran LK, Christy N, Supaprom C, Heang V, et al. Clinical presentation, risk factors, and comparison of laboratory diagnostics for seasonal influenza virus among Cambodians from 2007 to 2020. Open Forum Infect Dis. 2024;11:ofae062. https://doi.org/10.1093/ofid/ofae062
25. Kasper MR, Blair PJ, Touch S, Sokhal B, Yasuda CY, Williams M, et al. Infectious etiologies of acute febrile illness among patients seeking health care in south-central Cambodia. Am J Trop Med Hyg. 2012;86:246–53. https://doi.org/10.4269/ajtmh.2012.11-0409
26. Olson DM, Dinerstein E, Wikramanayake ED, Burgess ND, Powell GVN, Underwood EC, et al. Terrestrial ecoregions of the world: a new map of life on earth: a new global map of terrestrial ecoregions provides an innovative tool for conserving biodiversity. Bioscience. 2001;51:933–8. https://doi.org/10.1641/0006-3568(2001)051[0933:TEOTWA]2.0.CO;2
27. Mørch K, Manoharan A, Chandy S, Chacko N, Alvarez-Uria G, Patil S, et al. Acute undifferentiated fever in India: a multicentre study of aetiology and diagnostic accuracy. BMC Infect Dis. 2017;17:665. https://doi.org/10.1186/s12879-017-2764-3
28. Blair PJ, Wierzba TF, Touch S, Vonthanak S, Xu X, Garten RJ, et al. Influenza epidemiology and characterization of influenza viruses in patients seeking treatment for acute fever in Cambodia. Epidemiol Infect. 2010;138:199–209. https://doi.org/10.1017/S095026880999063X
29. Graf PCF, Chretien J-P, Ung L, Gaydos JC, Richards AL. Prevalence of seropositivity to spotted fever group rickettsiae and *Anaplasma phagocytophilum* in a large, demographically diverse US sample. Clin Infect Dis. 2008;46:70–7. https://doi.org/10.1086/524018
30. Richards AL, Soeatmadji DW, Widodo MA, Sardjono TW, Yanuwiadi B, Hernowati TE, et al. Seroepidemiologic evidence for murine and scrub typhus in Malang, Indonesia. Am J Trop Med Hyg. 1997;57:91–5.
31. Jiang J, Myers TE, Rozmajzl PJ, Graf PCF, Chretien J-P, Gaydos JC, et al. Seroconversions to rickettsiae in US military personnel in South Korea. Emerg Infect Dis. 2015;21:1073–4. https://doi.org/10.3201/eid2106.141487

32. Bonell A, Lubell Y, Newton PN, Crump JA, Paris DH. Estimating the burden of scrub typhus: a systematic review. PLoS Negl Trop Dis. 2017;11:e0005838. https://doi.org/10.1371/journal.pntd.0005838
33. Chaisiri K, Tanganuchitcharnchai A, Kritiyakan A, Thinphovong C, Tanita M, Morand S, et al. Risk factors analysis for neglected human rickettsioses in rural communities in Nan province, Thailand: a community-based observational study along a landscape gradient. PLoS Negl Trop Dis. 2022;16:e0010256. https://doi.org/10.1371/journal.pntd.0010256
34. Trung NV, Hoi LT, Hoa TM, Huong DT, Huyen MT, Tien VQ, et al. Systematic surveillance of rickettsial diseases in 27 hospitals from 26 provinces throughout Vietnam. Trop Med Infect Dis. 2022;7:88. https://doi.org/10.3390/tropicalmed7060088
35. Phongmany S, Rolain JM, Phetsouvanh R, Blacksell SD, Soukkhaseum V, Rasachack B, et al. Rickettsial infections and fever, Vientiane, Laos. Emerg Infect Dis. 2006;12:256–62. https://doi.org/10.3201/eid1202.050900
36. Chheng K, Carter MJ, Emary K, Chanpheaktra N, Moore CE, Stoesser N, et al. A prospective study of the causes of febrile illness requiring hospitalization in children in Cambodia. PLoS One. 2013;8:e60634. https://doi.org/10.1371/journal.pone.0060634
37. Prasetyo DB, Fiorenzano JM, Nop D, Noch N, Huot B, Mom S, et al. Molecular detection of *Rickettsia* species in ectoparasites collected from two southern provinces of Cambodia. PLoS Negl Trop Dis. 2024;18:e0012544. https://doi.org/10.1371/journal.pntd.0012544
38. Vallée J, Thaojaikong T, Moore CE, Phetsouvanh R, Richards AL, Souris M, et al. Contrasting spatial distribution and risk factors for past infection with scrub typhus and murine typhus in Vientiane City, Lao PDR. PLoS Negl Trop Dis. 2010;4:e909. https://doi.org/10.1371/journal.pntd.0000909
39. Tay ST, Ho TM, Rohani MY, Devi S. Antibodies to *Orientia tsutsugamushi*, *Rickettsia typhi* and spotted fever group rickettsiae among febrile patients in rural areas of Malaysia. Trans R Soc Trop Med Hyg. 2000;94:280–4. https://doi.org/10.1016/S0035-9203(00)90322-5
40. Asian Development Bank. Cambodia agriculture, natural resources, and rural development sector assessment, strategy, and road map. Manila (Philippines): The Bank; 2021.
41. PicKard AL, McDaniel P, Miller RS, Uthaimongkol N, Buathong N, Murray CK, et al. A study of febrile illnesses on the Thai-Myanmar border: predictive factors of rickettsioses. Southeast Asian J Trop Med Public Health. 2004;35:657–63.
42. Mahajan SK. Rickettsial diseases. J Assoc Physicians India. 2012;60:37–44.

Address for correspondence: Andrew G. Letizia, Naval Medical Research Unit Indo Pacific, 285 Sudan Rd 757965, Singapore; email: andrew.g.letizia.mil@health.mil

etymologia revisited

Petri Dish

[pe'tre 'dish]

The Petri dish is named after the German inventor and bacteriologist Julius Richard Petri (1852–1921). In 1887, as an assistant to fellow German physician and pioneering microbiologist Robert Koch (1843–1910), Petri published a paper titled "A minor modification of the plating technique of Koch." This seemingly modest improvement (a slightly larger glass lid), Petri explained, reduced contamination from airborne germs in comparison with Koch's bell jar.

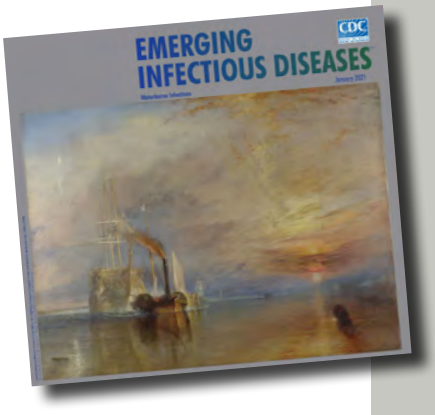

Originally published in January 2021

References:

1. Central Sheet for Bacteriology and Parasite Science [in German]. Biodiversity Heritage Library. Volume 1, 1887 [cited 2020 Aug 25]. https://www.biodiversitylibrary.org/item/210666#page/313/mode/1up
2. Petri JR. A minor modification of the plating technique of Koch [in German]. Cent für Bacteriol und Parasitenkd. 1887;1:279–80.
3. Shama G. The "Petri" dish: a case of simultaneous invention in bacteriology. Endeavour. 2019;43:11–6. DOIExternal
4. The big story: the Petri dish. The Biomedical Scientist. Institute of Biomedical Science [cited 2020 Aug 25]. https://thebiomedicalscientist.net/science/big-story-petri-dish

https//wwwnc.cdc.gov/eid/article/27/1/et-2701_article

Multicenter Retrospective Study of *Spiroplasma ixodetis* Infantile Cataract in 8 Countries in Europe

Luc Van Os, Nathalie Cassoux, Symira Cholidis, Pascal Dureau, Navid Farassat, Fabienne Catherine Fierz, Ebba Ghyczy, Elena-Cristina Nitulescu, Eva Stifter, Marie-José Tassignon, Anne Le Flèche-Matéos,[1] Birgit Lorenz,[1] for the *Spiroplasma* Infantile Cataract Group[2]

In support of improving patient care, this activity has been planned and implemented by Medscape, LLC and Emerging Infectious Diseases. Medscape, LLC is jointly accredited with commendation by the Accreditation Council for Continuing Medical Education (ACCME), the Accreditation Council for Pharmacy Education (ACPE), and the American Nurses Credentialing Center (ANCC), to provide continuing education for the healthcare team.

Medscape, LLC designates this Journal-based CME activity for a maximum of 1.00 ***AMA PRA Category 1 Credit(s)™***. Physicians should claim only the credit commensurate with the extent of their participation in the activity.

Successful completion of this CME activity, which includes participation in the evaluation component, enables the participant to earn up to 1.0 MOC points in the American Board of Internal Medicine's (ABIM) Maintenance of Certification (MOC) program. Participants will earn MOC points equivalent to the amount of CME credits claimed for the activity. It is the CME activity provider's responsibility to submit participant completion information to ACCME for the purpose of granting ABIM MOC credit.

All other clinicians completing this activity will be issued a certificate of participation. To participate in this journal CME activity: (1) review the learning objectives and author disclosures; (2) study the education content; (3) take the post-test with a 75% minimum passing score and complete the evaluation at https://www.medscape.org/qna/processor/74428?showStandAlone=true&src=prt_jcme_eid_mscpedu; and (4) view/print certificate. For CME questions, see page 1275.

NOTE: It is the policy of Medscape Education to avoid the mention of brand names or specific manufacturers in accredited educational activities. However, trade and manufacturer names in this activity are provided in an effort to provide clarity. The use of brand or manufacturer names should not be viewed as an endorsement by Medscape of any specific product or manufacturer.

Release date: May 28, 2025; Expiration date: May 28, 2026

Learning Objectives

Upon completion of this activity, participants will be able to:

- Assess the microbiology of infections with *Spiroplasma*
- Distinguish the prevalence of anterior uveitis in infant infections with *Spiroplasma*
- Evaluate other ocular characteristics of infant infections with *Spiroplasma*
- Compare different diagnostic techniques for *Spiroplasma* among infants

CME Editor

Bryce Simons, MPH, Technical Writer/Editor, Emerging Infectious Diseases. *Disclosure: Bryce Simons, MPH, has no relevant financial relationships.*

CME Author

Charles P. Vega, MD, Health Sciences Clinical Professor of Family Medicine, University of California, Irvine School of Medicine, Irvine, California. *Disclosure: Charles P. Vega, MD, has the following relevant financial relationships: served as consultant or advisor for Boehringer Ingelheim; GlaxoSmithKline.*

Authors

Luc Van Os, MD; Nathalie Cassoux, MD, PhD; Symira Cholidis, MD; Pascal Dureau, MD, PhD; Navid Farassat, MD, PhD; Fabienne Catherine Fierz, MD; Ebba Ghyczy, MD; Elena-Cristina Nitulescu, MD; Eva Stifter, MD, MBA; Marie-José Tassignon, MD, PhD ; Anne Le Flèche-Matéos, PhD; Birgit Lorenz, MD, PhD.

Spiroplasma ixodetis has been reported to cause the rare combination of cataract and uveitis in infants. Through a retrospective analysis of available literature and additional unpublished cases, we identified 28 eyes from 18 infants from 8 countries in Europe with cataracts and intraocular inflammation. The cataracts were bilateral in 55.6%, unilateral in 44.4%, and progressive in 46.4% of patients. Granulomatous anterior uveitis was found in all infants. Presence of *S. ixodetis* was supported by PCR (positive in 89.3% of eyes tested), transmission electron microscopy (positive in 90% of eyes tested), or culture of aspirated lens material (positive in 87.5% of eyes tested). Treatment with macrolide antimicrobial drugs, corticosteroids, and lensectomy appeared to be effective. Two patients had a recurrence of the uveitis after lens extraction and needed prolonged treatment. To increase awareness of *S. ixodetis*, we suggest its inclusion with the organisms of the TORCH acronym.

Infantile cataracts are rare diseases, with an incidence varying from 6.3 to 136 per 100,000 births (*1*–*5*). The etiology is diverse, including genetic disorders, metabolic diseases, or ocular infections. Intrauterine infectious causes are referred to by the TORCH acronym: toxoplasmosis, other infectious pathogens (such as HIV, syphilis, parvovirus B19/fifth disease, varicella/chickenpox, and Zika), rubella, cytomegalovirus, and herpes viruses (*6*,*7*).

Uveitis in children is even rarer; a recent study reported an incidence of 0.69/100,000 person-years in children from South Korea 0–6 years of age (*8*). Furthermore, uveitis manifests only exceptionally in the first months after birth. In a retrospective study performed in Finland, no child <1 year of age had uveitis (*9*). A study from India reported 15 cases of neonatal uveitis out of a population of 1,450 premature infants. All those cases were of infectious etiology, with toxoplasma, rubella, cytomegalovirus, varicella zoster, *Mycobacterium tuberculosis*, other bacteria, and fungi as the causative organisms (*10*), illustrating that neonatal uveitis is usually infectious in nature and causative organisms are similar to those causing cataracts. Diagnostic tests are readily available for the most common of those pathogens, making diagnosis relatively straightforward.

In 2002, the first case of unilateral infantile cataracts with anterior uveitis caused by *Spiroplasma ixodetis* was published (*11*). In this article, we provide a review of the cases published before 2024 and evaluate an additional series of unpublished cases from different centers in Europe. We aim to describe a phenotype characterizing *Spiroplasma*-related cataracts and uveitis in infants through a review of the available literature and the newly published cases. In addition, we describe diagnostic steps and effective treatment options.

Methods and Materials

After confirmation of a *S. ixodetis* diagnosis in a child from Romania and treated in Antwerp, Belgium, L.V.O. and M.T. contacted the authors of previously published cases and asked if they had encountered new patients since case publication. We also reached out to other centers that contacted the authors of the published cases for assistance in diagnosis and treatment of *S. ixodetis* in their patients. The resulting study group was named the *Spiroplasma* Infantile Cataract Group.

After initial contact through email, the group held a virtual meeting on June 1, 2023, to discuss the setup of the study and article. We determined patients were eligible for inclusion when cataracts were diagnosed and ≥1 of 3 diagnostic tests (16S RNA PCR, transmission electron microscopy [TEM], or culture) confirmed the presence of *S. ixodetis* in 1 or both eyes. Each center provided anonymized case reports for their cases with identifying parameters as limited as possible. We included patients through July 14, 2023. We combined the information from the new cases with information available from published cases (*12*–*16*). We then made separate tables summarizing the demographic data, diagnostic approach, and characteristics of the cataracts; the aspects of the uveitis; and the treatment details for each included case (Appendix 1 Tables 1, 2, https://wwwnc.cdc.gov/EID/

Author affiliations: University Hospital Antwerp, Edegem, Belgium (L. Van Os, M. Tassignon); University of Antwerp, Antwerp, Belgium (L. Van Os, M.-J. Tassignon); Institut Curie, Paris, France (N. Cassoux); Université Paris Descartes, Paris (N. Cassoux); Oslo University Hospital, Oslo, Norway (S. Cholidis); Rothschild Foundation Hospital, Paris (P. Dureau); Medical Center–University of Freiburg, Freiburg, Germany (N. Farassat); University Hospital Zurich, Zurich, Switzerland (F.C. Fierz); Cantonal Hospital Winterthur, Winterthur, Switzerland (F.C. Fierz); Amsterdam University Medical Centers, Amsterdam, the Netherlands (E. Ghyczy); Emergency Children's Hospital Marie Sklodowska Curie, Bucharest, Romania (E.-C. Nitulescu); Medical University of Vienna, Vienna, Austria (E. Stifter); Institut Pasteur, Paris (A. Le Fleche-Matéos); Justus Liebig University Giessen, Giessen, Germany (B. Lorenz)

DOI: https://doi.org/10.3201/eid3106.240954

[1]These senior authors contributed equally to this article.

[2]Additional members of the *Spiroplasma* Infantile Cataract Group who contributed data are listed at the end of this article.

article/31/6/24-0954-App1.xlsx). We filled in the information on active cases after the tables were created on the basis of published reports.

Our study aim was 3-fold: first, to specify the characteristics of the clinical manifestations regarding the uveitis and the cataracts; second, to evaluate the different diagnostic modalities; and third, to compare the different treatment regimens used in the included cases. This research adhered to the tenets of the Declaration of Helsinki. Informed consent was obtained from the parents or guardians of every patient. The Ethical Committee of the Antwerp University Hospital considered this work exempt from formal review because of the observational nature of the research.

Results

In addition to the 7 cases published to date (*11*–*14*), we have included information on 3 patients reported as 2 poster presentations (*15*,*16*) and 8 new patients. We have included a total of 18 children and 28 eyes from 8 countries in Europe (Germany, n = 6; France, n = 5; Austria, n = 2; Luxembourg, n = 1; the Netherlands, n = 1; Norway, n = 1; Romania, n = 1; and Switzerland, n = 1). Since finalization of this study, 1 additional case was published outside of this study group, reporting a similar clinical manifestation of uveitis, progressive cataracts, and ocular hypertension (*17*).

We created a list of the clinical manifestations of *S. ixodetis* infection in the cases reported in this study (Table). In addition, we summarized the characteristics and demographics of the previously published cases and additional descriptions and figures of each (Appendix 1 Tables 1, 2; Appendix 2, https://wwwnc.cdc.gov/EID/article/31/6/24-0954-App2.pdf).

We found anterior uveitis in all patients (Figure 1, panel A). Anterior uveitis is classified as granulomatous or nongranulomatous depending on the clinical manifestation and does not refer to any histological aspects. A granulomatous uveitis is characterized by the presence of large endothelial precipitates or iris nodules. Of the 28 eyes from 18 patients included in the study, we found large endothelial precipitates in 25 (89.3%) eyes of 16 (88.9%) patients and iris nodules in 10 (35.7%) eyes of 8 (44.4%) patients. In patient 9, the uveitis affected only 1 eye, whereas the cataracts were bilateral, although less pronounced in the eye without uveitis (Figure 1, panel B). Patient 6 had vitreous infiltration, snowballs (cell aggregates in the vitreous), and some peripheral necrotic retinal infiltrates, and patient 10 demonstrated a clinical manifestation of endophthalmitis. Those patients' clinical manifestations demonstrate uveitis can extend to the posterior segment. Patient 14 had unilateral cataracts with uveitis but bilateral macular scarring without a documented presence of posterior segment inflammation and a negative workup for other infectious causes. The relation of those scars to the inflammation is not clear.

Posterior synechiae were found in all eyes with uveitis (96.4%) and were often extensive, possibly leading to complete pupillary seclusion. In 14 (50%) eyes from 9 (50%) patients, a pupillary membrane was found. Both synechiae and pupillary membranes can lead to angle closure and a secondary increase of intraocular pressure (IOP), leading to an enlarged corneal diameter, which was seen in patients 5, 7, and 8. Twelve (42.8%) eyes from 9 (50%) patients had an increased IOP. Four (14.3%) eyes from 4 (22.2%)

Table. Common clinical manifestations documented in multicenter retrospective study of *Spiroplasma ixodetis* infantile cataract in 8 countries in Europe that should prompt the clinician to consider a diagnosis of *S. ixodetis*–related infantile cataract with uveitis*

Clinical manifestation in eyes (%)	Characteristics (%)	Additional comments
Lens opacity (100), can be highly asymmetric	Bilateral (55.6)	NA
	Unilateral (44.4)	NA
	Progressive over time (46.4)	NA
	White lens opacity (35.7)	NA
	Abnormal lens anatomy (25)	Fibrous plaque, fibrovascular membranes, improperly formed lens
Anterior uveitis (96.4), can be highly asymmetric	Extensive posterior synechiae (96.4)	May lead to the full seclusion of the pupil and increased intraocular pressure with enlarged corneal diameter
	Large endothelial precipitates (89.3)	Peculiar shape over the entire surface of the cornea
	Dilated immature iris vessels (71.4)	Can be adherent to the anterior lens capsule or to a pupillary membrane
	Pupillary membranes (50)	NA
	Involvement of the posterior segment (14.3)	Inflammation, retinal scars
Elevated intraocular pressure (42.8)	Preoperative (14.3)	NA
	Postoperative (25)	NA
	Pre and postoperative (3.6)	NA
	Requiring glaucoma surgery (14.3)	NA

*We defined elevated intraocular pressure as the need for treatment for increased eye pressure on the basis of the treating physicians clinical judgement. NA, not applicable.

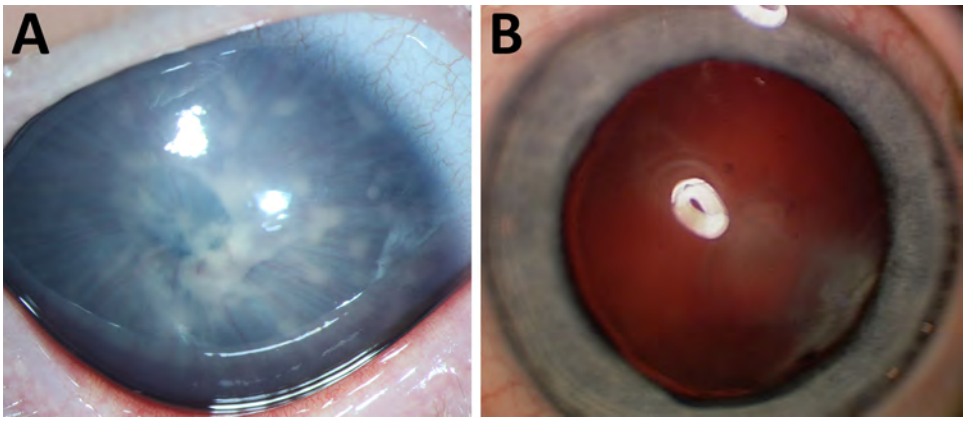

Figure 1. Spectrum of *Spiroplasma* spp.–caused eye disease documented in a multicenter retrospective study of *Spiroplasma ixodetis* infantile cataract in 8 countries in Europe. The study included a total of 18 children and 28 eyes. A) Preoperative image of patient 15, showing extensive endothelial precipitates and cataract and iris vascularization extending to the lens. B) Mild cataract in the left eye of patient 9 without apparent uveitis.

patients had increased IOP before cataract surgery, and increased IOP developed in 7 (25%) eyes from 6 (33.3%) patients after the initial cataract surgery. One (3.6%) eye from 1 (6.3%) patient had increased IOP before and after cataract surgery. Two patients (patients 8 and 18) had 1 eye with increased IOP before surgery and developed increased IOP in the other eye after surgery.

Of the 12 eyes with ocular hypertension, 4 needed glaucoma surgery (14.3% of all eyes): patient 8 (right eye) underwent a trabeculotomy, patient 14 (right eye) received a glaucoma drainage device, and patient 16 (left eye) underwent trabeculectomy with mitomycin C. Patient 18 (left eye) underwent cyclophotocoagulation because of severe scarring of the trabecular meshwork and continued to require topical IOP lowering medication. Furthermore, 20 (71.4%) eyes from 14 (77.8%) patients demonstrated severely dilated iris vessels adherent to the lens (Appendix 1 Tables 1, 2).

Eight (44.4%) infants had unilateral cataracts, of whom 1 showed bilateral macular scars without the presence of uveitis. Bilateral cataracts manifested in 10 (55.6%) infants; patient 9 was affected by cataracts in both eyes but uveitis only in the right eye.

The cataracts were variable in clinical manifestation. In 10 (35.7%) eyes, the cataracts manifested as a white cataract within the first weeks of life. In 13 (46.4%) eyes, we found the cataracts got denser during the first months of life, as described previously (*11*). No progression was reported in 5 (17.9%) eyes.

Abnormal lens anatomy was found in 7 (25%) eyes from 5 (27.8%) patients. The abnormal anatomy found included fibrotic subcapsular membranes (patients 8 and 14), persistent fibrovascular membranes (patient 17), small and deformed lens (patients 8 and 15), and lens subluxation (patient 18).

There is currently no standardized technique to diagnose *Spiroplasma* infection. 16S-rRNA PCR was performed on lens fiber material from the patients reported in this study. The PCR testing generated a positive result in 25 (89.3%) eyes. We created a phylogenetic tree with the 16S sequences (Figure 2); the available sequences were uploaded to the GenBank database. TEM was performed on lens material in 10 eyes from 7 patients and identified *Spiroplasma* spp. within lens fibers in 9 (90%) of the eyes tested. Culture was attempted on lens material of 8 eyes from 6 patients and *S. ixodetis* was cultured from 7 (87.5%) of those eyes (*14*).

Of the 18 patients, 77.8% received topical corticosteroids before surgery, and all patients had topical corticosteroids in the postoperative period. In addition, 5 (27.8%) patients received systemic steroids to control the ocular inflammation. Systemic antimicrobial treatment was used in 17 (94.4%) patients. In 16 (88.9%) patients, the antimicrobial drug was a macrolide (erythromycin, azithromycin, clarithromycin, or josamycin). The remaining patient (patient 5) received a systemic antimicrobial drug, but we could not determine which type.

Discussion

We describe 28 eyes in 18 infants from 8 countries in Europe that had cataracts and intraocular inflammation caused by *S. ixodetis*. Three modes of diagnosis were used: 16S-rRNA PCR on aspirated lens tissue, TEM on lens tissue, and culture on aspirated lens material (Mycoplasma A7 agar medium [ELITechGroup]). All 3 tests seemed equally likely to generate a positive result in the affected eyes. PCR was positive in 89.3% of eyes (all eyes were tested), TEM was positive in 90% of 10 eyes tested, and culture was positive in 87.5% of 8 eyes where culture was attempted. The positive cultures are an additional requirement of Koch's postulates to confirm *S. ixodetis* as the cause of this clinical entity. Lens tissue was obtained by simple aspiration with either a

syringe or a vitrector. Patients from cases 9 and 10 demonstrate that PCR can be negative but TEM can still confirm the diagnosis; therefore, we recommend using each of the available diagnostic paths in cases with a high clinical suspicion.

In several of the patients, aqueous humor samples were analyzed by 16S-rRNA PCR. This testing yielded a positive result only for case 11, in which the aqueous humor sample was obtained after lensectomy and could have been contaminated with *Spiroplasma* spp. DNA from inside the lens. *Spiroplasma* spp. most likely cannot survive in the eye outside of the lens and needs the presence of cells for survival. The refreshing of the aqueous humor within the eye could play an additional role in the absence of positive PCR results. This potential role highlights the need to perform PCR on lens tissue obtained during cataract surgery to confirm the diagnosis.

Cataracts were bilateral in 55.6%, unilateral in 44.4%, and progressive in 46.4% of patients. All patients had a granulomatous uveitis in ≥1 eye, with thick endothelial precipitates scattered over the entire endothelium. Similar deposits were seen on the iris. The uveitis can be highly asymmetric. Diagnosis of a very limited uveitis in a newborn can be challenging and could easily remain unnoticed.

In the left eye of patient 9, no uveitis was found, and the cataract was very limited, although it was progressive over time. PCR and TEM results were positive in the eye with uveitis (right eye) but negative in the left eye. This positivity might indicate the load of *Spiroplasma* spp. was lower in the eye with

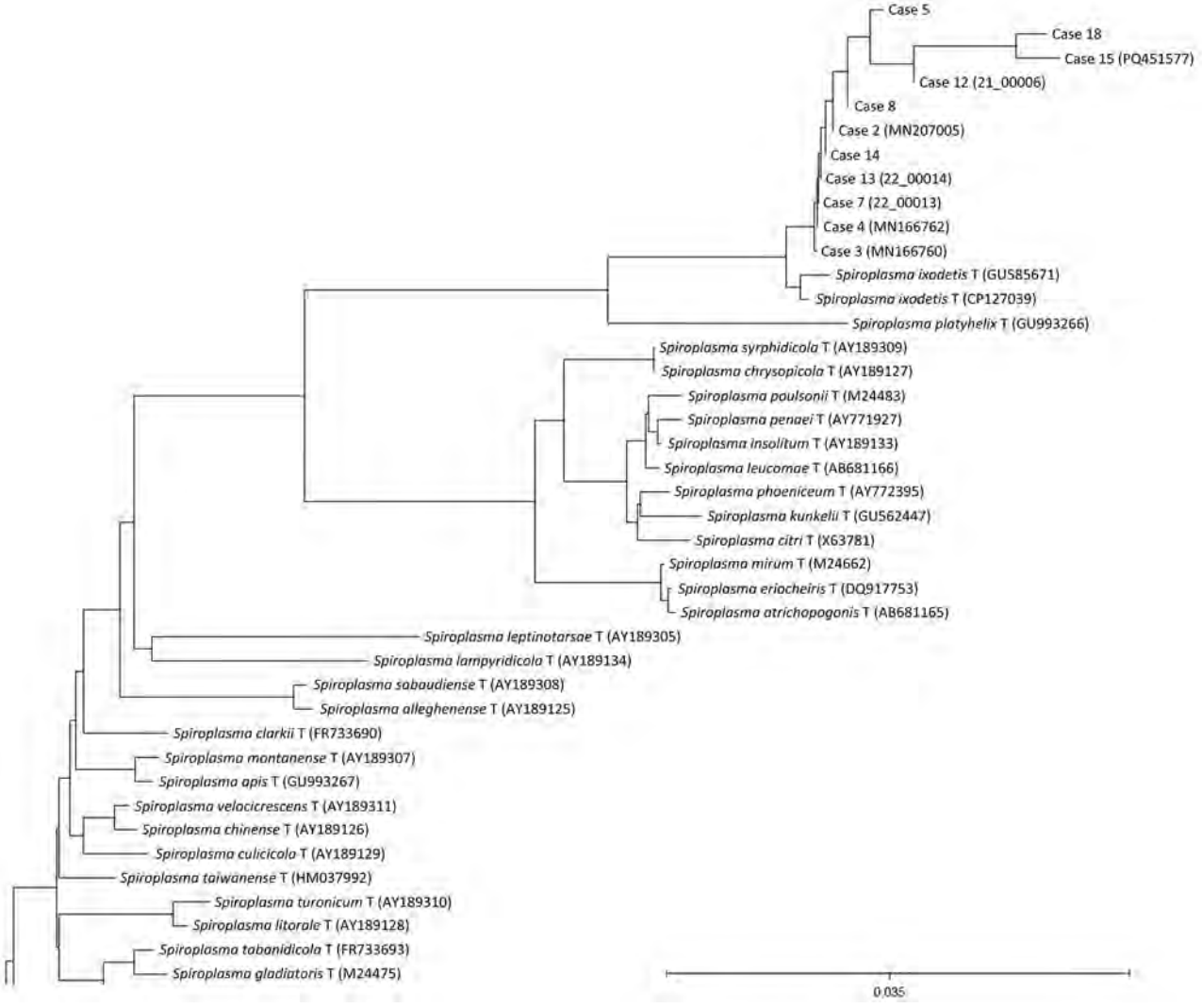

Figure 2. Neighbor-joining unrooted tree based on *rrs* gene sequences recovered from a multicenter retrospective study of *Spiroplasma ixodetis* infantile cataract in 8 countries in Europe. The study included a total of 18 children and 28 eyes. Numbers in parentheses are GenBank accession numbers. Scale bar represents substitutions per nucleotide position.

mild cataract and no detectable uveitis and that the inoculum of *Spiroplasma* spp. has a role in the pathophysiology. Furthermore, the examinations are conducted on only a portion of the removed lens tissue, which can leave the *Spiroplasma* spp. undetected. The presence of minor lens changes could disturb the normal metabolism of the lens, causing the cataracts to progress further over time. This progression possibly happens in the absence of the *Spiroplasma* spp. that triggered the cascade. The cataract with negative PCR result illustrates that *Spiroplasma* spp. could cause an isolated mild cataract without signs of inflammation and may escape detection by PCR and TEM.

Cataract progression was seen in 46.4% (n = 13) eyes before surgery, even after reducing inflammation, as previously described (*11*,*16*). Several factors could be involved in this progression, and they are not mutually exclusive. Topical steroids, when used for several months, can cause progression of cataracts, as can the ongoing anterior chamber inflammation. The clinical picture of cataracts in those cases does not fit the manifestation of a purely corticosteroid-induced cataract, and cataract was documented before the start of steroids in most cases. Extensive fibrosis of the lens capsule was noted in 3 patients (patients 8, 14, and 17), and the lens was deformed in 3 patients (patients 8, 15, and 18) with abnormal or absent zonules. This finding might indicate that the infection with *Spiroplasma* spp. can interfere with normal lens development. Progression of the cataract might be because of poor penetration of the antimicrobial in the lens material, enabling *Spiroplasma* spp. to trigger the capsular lens epithelial cells to transform into fibroblasts and lose their transparency.

The timing of surgery for infants with cataracts is critical to avoid amblyopia. A balance between early surgery to improve visual prognosis and reduction of inflammation before surgery needs to be sought. We recommend starting a systemic antimicrobial drug treatment as soon as *Spiroplasma* spp. is suspected and adding an antiinflammatory treatment guided by the amount of intraocular inflammation. In this review, treatment regimens varied between patients, but most received a perioperative systemic macrolide antimicrobial in combination with topical or systemic steroids. The inflammation resolved rapidly once treatment was started. The patient in case 3 did not receive systemic antimicrobial drugs, only topical tobramycin in the first postoperative month. In that patient, there were no recurrences in the 18 months after surgery. The lens removal could be part of the treatment because it is possible *Spiroplasma* spp. cannot survive in the eye after lens removal.

Intraocular lens (IOL) implantation is considered controversial both in young children and in eyes with inflammation. In patients 8 and 10, an IOL was implanted after the bag-in-the-lens technique. In our experience implanting the lens, we saw very little postoperative inflammation in patients with uveitis, even at a young age (*18*,*19*). However, the threshold for implantation of an IOL in those children should be very high, no classic in-the-bag approach should be used, and aphakia is preferred when there is any doubt regarding activity of inflammation.

Reactivation of uveitis has not been reported in any of the previously published cases. However, 2 of the patients reported in this article suffered a reoccurrence after initial control of the inflammation. Those relapses were treated with a combination of a repeated course of systemic macrolide antimicrobials and a low dose of topical steroids, which was slowly tapered.

A strength of this study is that we provide additional information on many newborns with *Spiroplasma*-induced cataracts and uveitis in a multicentric cooperation. This additional information adds to the known information on the topic, therefore strengthening the generalizability of the data.

A limitation of this study is that we cannot give a clear mechanism of the infection with *Spiroplasma* spp., but our findings could serve as a basis for further research to enlighten this process. A standardization of the diagnostic approach can make diagnosis easier and will help in giving those children the appropriate treatment.

The genus *Spiroplasma* belongs to the class Mollicutes, which contains only bacteria without a cell wall. *Spiroplasma* spp. can be found on plants, in insects, or crustaceans (*20*). *Spiroplasma* spp. are symbionts of ticks and are transmitted vertically from the female tick to her eggs (*21*). *S. ixodetis* was first described in Western blacklegged ticks (*Ixodes pacificus*) in Oregon, USA (*22*), and has since been identified in other tick species, such as *I. ricinus* and *Dermacentor marginatus* (*23*). Several studies have found a heterogeneous geographic distribution of the presence of *Spiroplasma* spp. in harvested ticks (*24*–*26*).

Spiroplasma spp. is not generally considered a human pathogen, but several reports of human disease caused by *Spiroplasma* spp. have been documented (*11*–*15*,*27*–*30*). The first reported human infection with *Spiroplasma* spp. in a premature child with unilateral cataract and uveitis occurred within a prospective study examining lens material from a series of infant cataracts that were not hereditary in origin (*11*). Since then, further cases of coincident

progressive cataract and granulomatous uveitis because of infection with *Spiroplasma* spp. in neonates have been published (*12*–*17*). We identified a small number of reports on systemic infections with *Spiroplasma* spp. occurring in immunocompromised patients (*27*,*29*,*30*). One case in an elderly woman (*28*) led to the suggestion of advanced age as a possible cause of relative immunosuppression. In addition, 1 report identified *Spiroplasma* spp. in a series of persistent root canal infections (*31*).

A derivative of a related species, *S. mirum*, known as suckling mouse cataract agent (SMCA), has been used in experimental eye models. In those models, injection of SMCA into the brain of newborn rodents caused inflammatory eye disease, microphthalmia, and structural defects of cornea, lens, and retina. In adult animals, no disease could be induced (*32*–*34*). Those findings confirm the preference for the eye as a target organ and agree with the reports of uveitis and cataracts in newborns caused by *S. ixodetis*.

The exact mode of infection in the patients reviewed in this article is unclear. In the first published case and in cases 9 and 10, a maternal infectious disease was noted during the pregnancy. In patient 9, a *Mycoplasma* infection was suspected. *Mycoplasma* also belongs to the class Mollicutes and therefore could have been a misdiagnosis of an infection with a relative of *Spiroplasma* spp. In patients 8 and 11, there was a positive history of a tick bite during the pregnancy, as well as a wasp sting in case 11. That history demonstrates 2 possible modes of maternal infection: either community-acquired or by an arthropod vector (most likely a tick), but other modes of infection could still be possible. Those modes of infection may not be mutually exclusive and could lead to a possibly asymptomatic or mild maternal infection.

Because infection is possibly transplacental (*11*), both eyes would be equally likely to be affected. However, of note, the manifestations ranged from unilateral cases (44.4%) to asymmetric and bilateral cases (55.6%) in both cataracts and uveitis. We also found a case of a child from a diamniotic, dichorionic twin in which the sibling was unaffected (patient 18) (Appendix 2).

Because *S. ixodetis* can be cultured from lens tissue of affected infants and positive PCR results are similarly found in the lens tissue itself, *S. ixodetis* might be contained inside the lens, within the barrier formed by the lens capsule. TEM clearly shows the intracellular location within lens fibers (*11*,*16*). This containment could mean *S. ixodetis* was already present before the closure of the lens vesicle (*35*), as described previously (*36*). However, in animal studies (*32*–*34*), pathological changes in the lens are seen in rabbits inoculated with SMCA within 48 hours of birth, which indicates SMCA can penetrate the lens capsule of an immature lens after birth. Research on the involvement of *S. mirum* in transmissible spongiform encephalopathies has shown *Spiroplasma* spp. use curli-like fibers to drill into the cell wall (*37*). There may be a similar pathway enabling *S. ixodetis* to perforate the lens capsule. Because *Spiroplasma* spp. have been proven to cause cataracts in both newborn humans (*11*–*17*) and newborn animals (*32*–*34*), it is possible the ability to invade the lens is limited to a certain period, probably related to the immaturity and thickness of the lens capsule at the time of infection (*35*). Both pathways of infection, either before closure of the lens vesicle or by penetration of the immature capsule, are not mutually exclusive.

Factors such as timing of the infection, genetic susceptibility, the inoculum of *S. ixodetis*, host immune responses, or differences in the local microenvironment could influence the development and severity of the disease. To better study those factors and further characterize the disease, we are setting up a prospective study with a standardized diagnostic and treatment approach. This prospective study might generate more robust data on the performance of the different diagnostic modalities and can help in developing a targeted quantitative PCR, which would make diagnosis easier.

Because of the rarity of these manifestations, we suggest considering *S. ixodetis* along with the organisms implied in the TORCH acronym in the diagnostic workup of cataracts and uveitis in infants. Analysis of lens material with 16S-rRNA PCR, culture, and TEM is crucial to confirm the diagnosis.

Additional members of *Spiroplasma* Infantile Cataract Group who contributed data: Monika Andrassi-Darida, Andreea Ciubotaru, Margot Denier, Eugen Domann, Christina Gerth-Kahlert, Nils Olav Hermansen, Can Imirzalioglu, Frank Imkamp, Melanie Jäger, Wolf Alexander Lagrèze, Fabienne Lomprez, Anne-Claude Madkaud, Gerd Magdowski, Gilles Martin, Alexandre Matet, Veerle Matheeussen, Rotraud Saurenmann, Christian Schultz, Annerose Serr, Anne Regine Skogen, H. Stevie Tan, Robin van Houdt, Jarne M van Hatte, Franziska Zucol.

About the Author

Dr. Van Os is as an ophthalmologist at the Antwerp University Hospital. His interests include pediatric cataract and uveitis.

References

1. Bermejo E, Martínez-Frías ML. Congenital eye malformations: clinical-epidemiological analysis of 1,124,654 consecutive births in Spain. Am J Med Genet. 1998;75:497–504. https://doi.org/10.1002/(SICI)1096-8628(19980217)75:5<497::AID-AJMG8>3.0.CO;2-K
2. Abrahamsson M, Magnusson G, Sjöström A, Popovic Z, Sjöstrand J. The occurrence of congenital cataract in western Sweden. Acta Ophthalmol Scand. 1999;77:578–80. https://doi.org/10.1034/j.1600-0420.1999.770520.x
3. Haargaard B, Wohlfahrt J, Fledelius HC, Rosenberg T, Melbye M. Incidence and cumulative risk of childhood cataract in a cohort of 2.6 million Danish children. Invest Ophthalmol Vis Sci. 2004;45:1316–20. https://doi.org/10.1167/iovs.03-0635
4. SanGiovanni JP, Chew EY, Reed GF, Remaley NA, Bateman JB, Sugimoto TA, et al. Infantile cataract in the collaborative perinatal project: prevalence and risk factors. Arch Ophthalmol. 2002;120:1559–65. https://doi.org/10.1001/archopht.120.11.1559
5. Rahi JS, Dezateux C; British Congenital Cataract Interest Group. Measuring and interpreting the incidence of congenital ocular anomalies: lessons from a national study of congenital cataract in the UK. Invest Ophthalmol Vis Sci. 2001;42:1444–8.
6. Nahmias AJ, Walls KW, Stewart JA, Herrmann KL, Flynt WJ. The ToRCH complex-perinatal infections associated with toxoplasma and rubella, cytomegol- and herpes simplex viruses. Pediatr Res. 1971;5:405–6. https://doi.org/10.1203/00006450-197108000-00144
7. Schwartz DA. The origins and emergence of Zika virus, the newest TORCH infection: what's old is new again. Arch Pathol Lab Med. 2017;141:18–25. https://doi.org/10.5858/arpa.2016-0429-ED
8. Kim BH, Chang IB, Lee S, Oh BL, Hong IH. Incidence and prevalence of pediatric noninfectious uveitis in Korea: a population-based study. J Korean Med Sci. 2022;37:e344. https://doi.org/10.3346/jkms.2022.37.e344
9. Siiskonen M, Hirn I, Pesälä R, Hautala T, Ohtonen P, Hautala N. Prevalence, incidence and epidemiology of childhood uveitis. Acta Ophthalmol. 2021;99:e160–3. https://doi.org/10.1111/aos.14535
10. Jayadev C, Vinekar A, Bauer N, Mangalesh S, Mahendradas P, Kemmanu V, et al. Look what else we found—clinically significant abnormalities detected during routine ROP screening. Indian J Ophthalmol. 2015;63:373–7. https://doi.org/10.4103/0301-4738.159859
11. Lorenz B, Schroeder J, Reischl U. First evidence of an endogenous *Spiroplasma* sp. infection in humans manifesting as unilateral cataract associated with anterior uveitis in a premature baby. Graefes Arch Clin Exp Ophthalmol. 2002;240:348–53. https://doi.org/10.1007/s00417-002-0453-3
12. Matet A, Le Flèche-Matéos A, Doz F, Dureau P, Cassoux N. Ocular *Spiroplasma ixodetis* in newborns, France. Emerg Infect Dis. 2020;26:340–4. https://doi.org/10.3201/eid2602.191097
13. Farassat N, Reich M, Serr A, Küchlin S, Erwemi M, Auw-Hädrich C, et al. *Spiroplasma* species as a rare cause of congenital cataract and uveitis: a case series. BMC Ophthalmol. 2021;21:434. https://doi.org/10.1186/s12886-021-02201-0
14. Martin GC, Denier M, Le Flèche-Matéos A. Spiroplasma-induced uveitis mimicking congenital glaucoma in a newborn. Ophthalmology. 2023;130:255. https://doi.org/10.1016/j.ophtha.2022.06.007
15. Stifter E, Moser E, Mitteregger D, et al. Pediatric cataract, anterior uveitis, and dilatative cardiomyopathy associated with *Spiroplasma* sp. Infection. Poster presented at: 2nd World Congress of Paediatric Ophthalmology and Strabismus; Milan, Italy; 2012 Sep 7–9.
16. Lorenz B, Andrassi-Darida M, Jäger M, Magdowski G, Imirzalioglu C. Secondary infantile cataract associated with presumed intrauterine infection. Poster presented at: 36th Annual Meeting of the European Paediatric Ophthalmological Society; Bad Nauheim, Germany; 2010 Sep 20–Oct 2. Poster P17.
17. Van Haecke H, Roels D, Nerinckx F, Schaballie H, Schelstraete P, Vandekerckhove L, et al. *Spiroplasma* infection as a cause of severe congenital keratouveitis, cataract and glaucoma. BMC Ophthalmol. 2024;24:217. https://doi.org/10.1186/s12886-024-03480-z
18. Tassignon MJ, De Veuster I, Godts D, Kosec D, Van den Dooren K, Gobin L. Bag-in-the-lens intraocular lens implantation in the pediatric eye. J Cataract Refract Surg. 2007;33:611–7. https://doi.org/10.1016/j.jcrs.2006.12.016
19. Van Looveren J, Ní Dhubhghaill S, Godts D, Bakker E, De Veuster I, Mathysen DGP, et al. Pediatric bag-in-the-lens intraocular lens implantation: long-term follow-up. J Cataract Refract Surg. 2015;41:1685–92. https://doi.org/10.1016/j.jcrs.2014.12.057
20. Regassa LB, Gasparich GE. Spiroplasmas: evolutionary relationships and biodiversity. Front Biosci. 2006;11:2983–3002. https://doi.org/10.2741/2027
21. Bell-Sakyi L, Palomar AM, Kazimirova M. Isolation and propagation of a *Spiroplasma* sp. from Slovakian *Ixodes ricinus* ticks in *Ixodes* spp. cell lines. Ticks Tick Borne Dis. 2015;6:601–6. https://doi.org/10.1016/j.ttbdis.2015.05.002
22. Tully JG, Rose DL, Yunker CE, Carle P, Bové JM, Williamson DL, et al. *Spiroplasma ixodetis* sp. nov., a new species from *Ixodes pacificus* ticks collected in Oregon. Int J Syst Bacteriol. 1995;45:23–8. https://doi.org/10.1099/00207713-45-1-23
23. Palomar AM, Premchand-Branker S, Alberdi P, Belova OA, Moniuszko-Malinowska A, Kahl O, et al. Isolation of known and potentially pathogenic tick-borne microorganisms from European ixodid ticks using tick cell lines. Ticks Tick Borne Dis. 2019;10:628–38. https://doi.org/10.1016/j.ttbdis.2019.02.008
24. Lernout T, De Regge N, Tersago K, Fonville M, Suin V, Sprong H. Prevalence of pathogens in ticks collected from humans through citizen science in Belgium. Parasit Vectors. 2019;12:550. https://doi.org/10.1186/s13071-019-3806-z
25. Olsthoorn F, Sprong H, Fonville M, Rocchi M, Medlock J, Gilbert L, et al. Occurrence of tick-borne pathogens in questing *Ixodes ricinus* ticks from Wester Ross, Northwest Scotland. Parasit Vectors. 2021;14:430. https://doi.org/10.1186/s13071-021-04946-5
26. Krawczyk AI, Röttjers L, Fonville M, Takumi K, Takken W, Faust K, et al. Quantitative microbial population study reveals geographical differences in bacterial symbionts of *Ixodes ricinus*. Microbiome. 2022;10:120. https://doi.org/10.1186/s40168-022-01276-1
27. Aquilino A, Masiá M, López P, Galiana AJ, Tovar J, Andrés M, et al. First human systemic infection caused by *Spiroplasma*. J Clin Microbiol. 2015;53:719–21. https://doi.org/10.1128/JCM.02841-14
28. Eimer J, Fernström L, Rohlén L, Grankvist A, Loo K, Nyman E, et al. *Spiroplasma ixodetis* infections in immunocompetent and immunocompromised patients after tick exposure, Sweden. Emerg Infect Dis. 2022;28:1681–5. https://doi.org/10.3201/eid2808.212524
29. Mueller NJ, Tini GM, Weber A, Gaspert A, Husmann L, Bloemberg G, et al. Hepatitis from *Spiroplasma* sp. in an

immunocompromised patient. Am J Transplant. 2015;15:2511–6. https://doi.org/10.1111/ajt.13254
30. Etienne N, Bret L, Le Brun C, Lecuyer H, Moraly J, Lanternier F, et al. Disseminated *Spiroplasma apis* infection in patient with agammaglobulineamia, France. Emerg Infect Dis. 2018;24:2382–6. https://doi.org/10.3201/eid2412.180567
31. Murad CF, Sassone LM, Faveri M, Hirata R Jr, Figueiredo L, Feres M. Microbial diversity in persistent root canal infections investigated by checkerboard DNA-DNA hybridization. J Endod. 2014;40:899–906. https://doi.org/10.1016/j.joen.2014.02.010
32. Kirchhoff H, Heitmann J, Trautwein G. Pathogenicity of *Spiroplasma* sp. strain SMCA in rabbits: clinical, microbiological, and histological aspects. Infect Immun. 1981;33:292–6. https://doi.org/10.1128/iai.33.1.292-296.1981
33. Clark HF. Rat cataract induced by suckling mouse cataract agent. Am J Ophthalmol. 1969;68:304–8. https://doi.org/10.1016/0002-9394(69)94074-4
34. Kirchhoff H, Kuwabara T, Barile MF. Pathogenicity of *Spiroplasma* sp. strain SMCA in Syrian hamsters: clinical, microbiological, and histological aspects. Infect Immun. 1981;31:445–52. https://doi.org/10.1128/iai.31.1.445-452.1981
35. Danysh BP, Duncan MK. The lens capsule. Exp Eye Res. 2009;88:151–64. https://doi.org/10.1016/j.exer.2008.08.002
36. Karkinen-Jääskeläinen M, Saxén L, Vaheri A, Leinikki P. Rubella cataract in vitro: sensitive period of the developing human lens. J Exp Med. 1975;141:1238–48. https://doi.org/10.1084/jem.141.6.1238
37. Bastian FO. The case for involvement of *Spiroplasma* in the pathogenesis of transmissible spongiform encephalopathies. J Neuropathol Exp Neurol. 2014;73:104–14. https://doi.org/10.1097/NEN.0000000000000033

Address for correspondence: Luc Van Os, Antwerp University Hospital, Drie Eikenstraat 655, 2650 Edegem, Belgium; email: luc.vanos@uza.be

Genomic Surveillance of Climate-Amplified Cholera Outbreak, Malawi, 2022–2023

Lucious Chabuka,[1] Wonderful T. Choga,[1] Carla N. Mavian,[1] Monika Moir,[1] Christian Morgenstern,[1] Houriiyah Tegaly, Abhinav Sharma, Eduan Wilkinson, Yeshnee Naidoo, Rhys Inward, Samir Bhatt, G.R. William Wint, Kamran Khan, Isaac I. Bogoch, Moritz U.G. Kraemer, José Lourenço, Cheryl Baxter, Massimiliano Tagliamonte, Marco Salemi, Richard J. Lessells, Collins Mitambo, Ronald Chitatanga, Joseph Bitilinyu-Bango, Mabvuto Chiwaula, Yollamu Chavula, Mphatso Bukhu, Happy Manda, Moses Chitenje, Innocent Malolo, Alex Mwanyongo, Bernard Mvula, Mirrium Nyenje, Tulio de Oliveira, Mathew Kagoli

In the aftermath of 2 extreme weather events in 2022, Malawi experienced a severe cholera outbreak; 59,325 cases and 1,774 deaths were reported by March 31, 2024. We generated 49 *Vibrio cholerae* full genomes from isolates collected during December 2022–March 2023. Phylogenetic and phylogeographic methods confirmed that the Malawi outbreak strains originated from Pakistan's 2022 cholera outbreak. That finding aligns with substantial travel between the 2 countries. The estimated most recent ancestor of this lineage was from June–August 2022, coinciding with Pakistan's floods and cholera surge. Our analysis indicates that major floods in Malawi contributed to the outbreak; reproduction numbers peaked in late December 2022. We conclude that extreme weather events and humanitarian crises in Malawi created conditions conducive to the spread of cholera, and population displacement likely contributed to transmission to susceptible populations in areas relatively unaffected by cholera for more than a decade.

Cholera is an acute diarrheal disease caused by ingestion of food or water contaminated with the bacterium *Vibrio cholerae* (*1*). Since mid-2021, the seventh cholera pandemic, associated with the *V. cholerae* O1 El Tor biotype, has been on an acute upsurge. Several large outbreaks have occurred in endemic and nonendemic countries; countries in Africa were particularly heavily affected (*2*). Those outbreaks have been driven by multiple factors, including extreme weather events, humanitarian crises, overlapping health emergencies (particularly during the COVID-19 pandemic), and consequently overstretched health systems (*3*,*4*).

In Malawi, cholera was first reported in 1973 and has been endemic since 1998. Annual increases in incidence occur during the rainy season (November–May, average temperature 30°C–35°C), particularly in the southern part of the country (*5*). During 2022–2024, Malawi experienced a widespread cholera outbreak that persisted throughout the dry season (May–November, average temperature 13°C); 59,325 cases and 1,774 deaths were reported as of March 31,

Author affiliations: Centre for Epidemic Control and Innovation, School of Data Science and Computational Thinking, Stellenbosch University, Stellenbosch, South Africa (L. Chabuka, W.T. Choga, M. Moir, H. Tegally, E. Wilkinson, Y. Naidoo, C. Baxter, T. de Oliveira); Public Health Institute of Malawi, Lilongwe, Malawi (L. Chabuka, C. Mitambo, R. Chitatanga, J. Bitilinyu- Bango, M. Chiwaula, Y. Chavula, M. Bukhu, H. Manda, M. Chitenje, I. Malolo, A. Mwanyongo, B. Mvula, M. Nyenje, M. Kagoli); University of Florida Emerging Pathogens Institute, Gainesville, Florida, USA (C.N. Mavian, M. Tagliamonte, M. Salemi); Imperial College London, London, UK (C. Morgenstern, S. Bhatt); South African Medical Research Council Centre for Tuberculosis Research, Cape Town, South Africa (A. Sharma); University of Oxford, Oxford, UK (R. Inward, G.R. William Wint, M.U.G. Kraemer); Copenhagen University, Copenhagen, Denmark (S. Bhatt); Environmental Research Group Oxford, Oxford (G.R. William Wint); BlueDot, Toronto, Ontario, Canada (K. Khan); University of Toronto, Toronto (K. Khan, I.I. Bogoch); Pandemic Sciences Institute, University of Oxford, Oxford (M.U.G. Kraemer); Biosystems and Integrative Sciences Institute at University of Lisbon, Lisbon, Portugal (J. Lourenço); Kwazulu-Natal Research and Innovation Sequencing Platform, Durban, South Africa (R.J. Lessells, T. de Oliveira)

DOI: https://doi.org/10.3201/eid3106.240930

[1]These authors contributed equally to this article.

2024 (*6*). The outbreak in Malawi unfolded amidst a global surge in cholera outbreaks, intensifying the scarcity of vaccines, tests, and treatments (*7*). Several other countries in southeastern Africa, in particular Mozambique, South Africa, Tanzania, Zambia, and Zimbabwe, were experiencing outbreaks concomitant with the outbreak in Malawi (*7*).

Previous genomic analysis has revealed cholera epidemics in Africa to be associated with transcontinental transmission of *V. cholerae* O1 El Tor sublineages from Asia, followed by regional cross-border spread within Africa (*8*,*9*). To explore the origin and drivers of the 2022–2023 Malawi cholera outbreak, the Public Health Institute of Malawi (PHIM) partnered with the Centre for Epidemic Response and Innovation (CERI), a specialized genomics facility of the Africa Centres for Disease Control and Prevention and World Health Organization Regional Office for Africa (AFRO) (*10*), to perform in-country genomic sequencing of *V. cholerae*. Using phylogenetic and phylogeographic methods alongside epidemiologic modeling that incorporates flooding and vaccination data, we investigated the genomic epidemiology of the cholera outbreak in Malawi, while delving into its climate-amplified implications.

Methods

Ethics, Sample Selection, Culture, and DNA Extraction

To investigate the origin of the current cholera outbreak in Malawi, the Public Health Institute of Malawi, supported by CERI and the Climate Amplified Diseases and Epidemics (CLIMADE) program, performed onsite genomic sequencing of local isolates. Isolates were anonymized and did not contain any personal identifiers. The Stellenbosch University Health Research Ethics Committee approved the CLIMADE initiative (BES-2023-24266). The Public Health Institute of Malawi and Ministry of Health National Health Sciences Research Committee approved this study.

We collected fecal samples from patients with cholera symptoms who sought care in district and central hospitals. We used rapid diagnostic tests (RDTs) to identify the presence of *V. cholerae* and then performed culture on all samples that were RDT positive. We performed drug susceptibility testing on all positive cultures. We sent all positive culture plates to the National Genomic Sequencing Reference Laboratory for DNA extraction; we used the QIAamp DNA Mini Kit 51304 (QIAGEN, https://www.qiagen.com) for extraction and Qubit High Sensitivity DNA kit Q32854 (Thermo Fisher Scientific, https://www.thermofisher.com) on Qubit 4 for quantification. We obtained DNA extracts from 70 *V. cholerae* isolates from samples collected during December 2022–February 2023 from the Southern, Central, and Northern Regions of Malawi. We extracted demographic, clinical, and diagnostic data from the routine cholera surveillance system.

Sequencing

We prepared libraries using the Illumina DNA library preparation kit and Nextera CD indexes (Illumina, https://www.illumina.com), according to the manufacturer's protocol. We performed whole-genome sequencing using the NextSeq 1000 instrument with P2 (300) cycle kit reagents (Illumina). We have deposited the genomic sequences into the National Center for Biotechnology Information Sequence Read Archive (BioProject no. PRJNA967700).

Assembly and High-Quality Single-Nucleotide Polymorphism Calling

We obtained full genomes and single-nucleotide polymorphism (SNP) alignments with our CholeraSeq pipeline (https://github.com/CERI-KRISP/CholeraSeq). In brief, we assessed read quality and trimmed all residual adaptors with fastp (*11*) and used Snippy version 4.6.0 (https://github.com/tseemann/snippy) to perform reference-based assembly against the N16961 strain (GenBank accession nos. NZ_CP028827.1, NZ_CP028828.1) before assembly. We set FreeBayes variant calling thresholds (E. Garrison, G. Marth, unpub. data, https://arxiv.org/abs/1207.3907) as ≥10× for site coverage, >60 for mapping quality, and ≥90% for base concordance. We merged individual vcf files using bctfools version 1.15 (*12*). We ran core genome alignment through fastBaps version 1.0.8 (*13*) before recombination screening with Gubbins version 3.2.1 (*14*). We manipulated FASTA files with seqkit version 2.0.0 (*15*) and the Biostrings R package version 2.58 (https://bioconductor.org/packages/release/bioc/html/Biostrings.html). We extracted parsimony informative sites from consensus genome alignments in MEGAX version 10.0.3 (*16*). We downloaded all available *V. cholerae* whole-genome sequencing experiments from the National Center for Biotechnology Information Short Read Archive and the European Nucleotide Archive. We assembled paired-end reads and called SNPs using the same methodology applied to the newly sequenced Malawi strains.

Phylogenetic Inference with Worldwide Cholera Dataset

We inferred a maximum-likelihood phylogenetic tree from the parsimony informative sites using IQ-TREE (*17*) to investigate the genetic relationship of

the Malawi outbreak to that of other strains from around the world (sampled during 1957–2023; N = 2,778) (Appendix 1 Table 1, https://wwwnc.cdc.gov/EID/article/31/6/24-0930-App1.xlsx). The reference set included 1,160 sequences from Africa, 898 from the Americas, 693 from Asia, 26 from Europe, and 1 from Oceania. We determined phylogenetic signal using a likelihood mapping test in IQ-TREE (*17*). We used Treetime (*18*) to obtain a maximum-likelihood tree scaled in time employing a standard mutation rate of 0.0179 substitutions/SNP site/year, as estimated by phylodynamic inference, after rerooting the tree by oldest tip.

Phylodynamic Inference

We investigated the phylogenetic relationships of the 49 new clinical strains from Malawi with strains within a monophyletic multicountry clade containing 31 strains collected in 2022 from Pakistan, 49 publicly available strains from the same outbreak in Malawi (*19*), 114 strains collected from South Africa in 2023 (*20*), and 20 strains collected from Zimbabwe in 2023 (*21*) (Appendix 1 Table 2). We determined phylogenetic signal using the likelihood mapping test in IQ-TREE (*17*) and estimated temporal signal by plotting the root-to-tip divergence using TempEst (*22*). We used the Bayesian framework to infer a posterior distribution of trees and estimate the time of the most recent common ancestor (tMRCA) of the sampled sequences. We considered different molecular clock models (strict or uncorrelated relaxed molecular clock) and demographic priors (constant or Bayesian Skygrid) (*23*). We used BEASTX version 10.5.0-β5 (*24*) to run Markov chain Monte Carlo samplers for 500 million generations, sampling every 50,000 generations, which was sufficient to achieve mixing of the Markov chain as evaluated by effective sampling size >200 for all parameter estimates under a given model. We performed hypothesis testing for best molecular clock, demographic model, by obtaining marginal likelihood estimates via path sampling and stepping-stone methods for each model to be compared, then calculating the Bayes factor (BF). BF is the ratio of the of the null (H_0) and the alternative hypothesis (H_A) marginal likelihood estimation s (*25*), where *ln*BF<0 indicates support for H_0; *ln*BF<2, negligible difference; 2<*ln*BF<6, strong support for H_A; and *ln*BF>6, decisive support for H_A[46] (Appendix 2 Table 1, https://wwwnc.cdc.gov/EID/article/31/6/24-0930-App2.pdf). We estimated the mutation rate at 0.0179 substitutions/SNP site/year, which is in line with previous rates for cholera (*26*,*27*). We obtained the maximum clade credibility (MCC) tree from the posterior distribution of trees using optimal burn-in with TreeAnnotator (https://beast.community/programs). We manipulated the MCC phylogeny in R using the package ggtree as described (*28*) for publishing purposes. We inferred the geographic origin of the epidemic in Malawi using discrete trait model with asymmetric transition (migration) and Bayesian stochastic search variable selection, enforcing the best molecular clock and demographic model (uncorrelated relaxed molecular clock and Bayesian Skygrid) in BEASTX. BF values of 3–20 indicate positive evidence, values of 20–150 indicate strong evidence, and values >150 indicate very strong evidence (*29*,*30*) (Appendix 2 Table 2). We investigated cholera movement across Malawi, South Africa, and Zimbabwe by ancestral state reconstruction using continuous traits with the migration extension of TreeTime (*18*). We used a custom Python script to estimate dates of exchange events. We mapped results using the R packages maptools, raster, rgdal, and sf (The R Project for Statistical Computing, https://www.r-project.org). XML, MCC tree, ML phylogeny, and Treetime migration files are available at https://github.com/cmavian/cholera_Malawi_2022-2023.

We used the WebPlotDigitizer tool (https://apps.automeris.io/wpd) to extract data from a WHO report on cholera in the Africa region (https://iris.who.int/bitstream/handle/10665/366745/AFRO%20Cholera%20Bulletin.06.pdf). The report provided daily information on cholera cases and deaths within Malawi until April 4, 2023.

Estimation of Time Varying Reproduction Number

We inferred the instantaneous reproduction number over time (R_t), at the national level, for Malawi using a semimechanistic Bayesian framework described in Bhatt et al. (*31*). To estimate the model, we used the epidemia package in R (https://imperialcollegelondon.github.io/epidemia), which enables us to estimate the effects of flooding and vaccinations as covariates. The estimate of R_t is based on daily national case counts, flooding, and vaccination data. We report the mean R_t estimate and 95% credible interval (CrI), a comparison of the observed and fitted case counts, and the effect sizes of our covariates (Appendix 2).

To check for robustness of our results, we estimated R_t with both flooding and vaccinations, only flooding, and with no covariates. We also confirmed that the estimation of R_t without any covariates is consistent with that of EpiEstim (*32*), which is an alternative implementation of a branching process model in R. Our R_t estimates were more stable because of the weekly random walk we used instead of daily data.

Flooding Data and Processing

We obtained real-time or near–real-time flooding data by remotely sensed Earth observation imagery (*33*).

Three sources are the Sentinels in Europe (*34*), the US National Aeronautics and Space Administration LANCE MODIS NRT global flood product (MCDWD) product using images generated from the Moderate Resolution Imaging Spectroradiometer instrument (https://www.earthdata.nasa.gov/global-flood-product), and Flood version 1.0 (*35*) using images generated from the Visible Infrared Imaging Radiometer Suite instrument available at the RealEarth website (https://floods.ssec.wisc.edu) and associated archives (https://jpssflood.gmu.edu). Sentinels in Europe are generally used to provide data for emergency response rather than long-term archives; MCDWD provided a long-term time series through 2022; and Flood provides ongoing daily and 5-day composites, which were downloaded for all of 2022 and then until April 13, 2023. Image values distinguish normal open water (value ≤99) from flood water, for which values ≥100 represent percentage flooding plus 100. The 5-day composite is the maximum value recorded during the period. The files are in simple tiled geotiff format; 2 tiles are required to cover the whole of Malawi, which must be combined and cropped before analysis.

International Passenger Flight Data

We evaluated travel data generated from the International Air Transport Association (*36*) to quantify passenger volumes originating from international airports and arriving in Malawi. International Air Transport Association data account for ≈90% of passenger travel itineraries on commercial flights, excluding transportation via unscheduled charter flights; the remaining data are modeled using market intelligence.

Results

Overview of the Cholera Outbreak in Malawi

Before 2022, Malawi had experienced major cholera outbreaks in 1998–1999, 2001–2002, and 2008–2009 (*5*,*7*) (Figure 1). On March 3, 2022, Malawi declared a cholera outbreak after a confirmed case (symptom onset February 25, 2022) was found in Machinga District after Tropical Storm Ana (January 2022) and Cyclone Gombe (March 2022) caused severe flooding with resulting displacement of populations with low immunity to cholera and limited access to clean water and sanitation (*7*). Initially confined to flood-affected areas, the outbreak spread to central and northern regions by August 2022 (*7*). At the initiation of this study, 58,577 confirmed cases and 1,756 deaths were reported (Table; Figure 1). Given the consistent high case-fatality rate (>3%) and continued spread, the Malawi government declared a public health emergency on December 5, 2022. From December on, cases surged again affecting all regions,

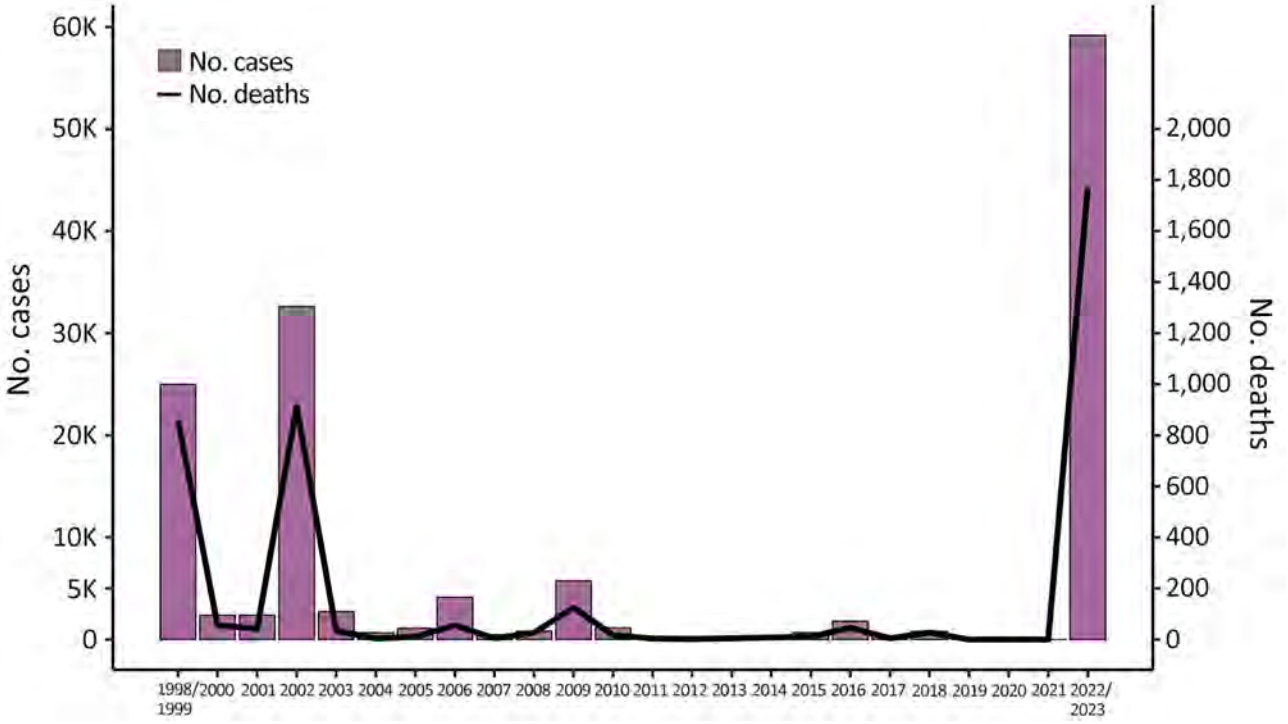

Figure 1. Cumulative case counts and deaths from cholera in Malawi by year, 1998–2023. Outbreaks occurred in 1998–1999, 2001–2002, 2008–2009, and 2022–2023. Scales for the y-axes differ substantially to underscore patterns but do not permit direct comparisons.

Table. Epidemiologic characteristics of cholera outbreak by region, Malawi, 2022–2023

Region	No. samples sequenced	No. cases	No. deaths
Northern	5	4,373	94
Central	18	23,274	750
Southern	44	30,930	912

including Blantyre and Lilongwe, the country's 2 largest cities (*7*). We obtained 70 *V. cholerae* isolates from stool samples collected during December 2022–March 2023. A total of 67 from the southern (n = 44), central (n = 18) and northern (n = 5) regions were processed into libraries (Table). From these 67 isolates, we generated 49 high-quality, near-complete *V. cholerae* genomes (Appendix 2 Figure 1).

Global Origin and Timing of 2022–2023 Cholera Outbreak

We constructed a time-scaled maximum-likelihood phylogeny based on high-quality SNPs of the 49 genomes from Malawi obtained in this study, 40 publicly available genomes (that passed quality filter) from the same outbreak (*19*), and 2,689 worldwide genomes (Figure 2). The genomes of the Malawi strains from this study clustered within a well-supported monophyletic clade (bootstrap >90%) together with the previously reported genomes from the same outbreak (*19*), denoting AFR15 introduction (*20*) (Figure 2). Those strains did not cluster with historical strains obtained from previous outbreaks within Malawi, which would indicate a new single introduction of cholera into the country. Instead, they were closely related to isolates from the 2022 outbreak in Pakistan (*37*) that clustered at the base of the clade, suggesting that the Malawi outbreak may have been caused by a strain introduction from Pakistan. However, we cannot reject that another unsampled country may have been involved in the origin of the Malawi cholera strain. The outbreak in Pakistan began in January 2022 and recorded >335,000 suspected cholera cases during January 15, 2022–March 15, 2023 (*38*). Phylogeographic analyses confirmed movement of cholera from Pakistan into Malawi (BF = 180.7) (Appendix 2 Table 3). The maximum clade credibility tree estimated tMRCA of the Malawi strains to be July 4, 2022 and determined a 95% highest posterior density (HPD) interval of June 11–August 6 (Figure 3). The tMRCA shared between Pakistan and Malawi outbreaks was June 4, 2022 (95% HPD interval of March 24–July 1, 2022), which suggests that the Malawi outbreak may have resulted from a long-range transmission event from Pakistan as early as March 2022, a close estimate to the beginning of the outbreak (*7*). Because the spread of cholera in Africa is associated with human movement (*9*), we queried the passenger volumes originating from international airports and arriving in Malawi (Figure 4). We found that Malawi was well connected to Pakistan by large numbers of air passengers traveling between them during the first half of 2022 (Figure 4).

Cholera Transmission across Malawi and Africa

Next, we explored the spread of cholera within Malawi. Our phylogeographic analysis supported a single source introduction into Malawi with consequent spread within the country and confirmed epidemiologic reports indicating that the outbreak expanded from southern regions, initially affected by flooding, to the northern and central parts of the country (Figure 5). The analysis showed evidence of dispersal from multiple hubs, including Machinga Blantyre, and Lilongwe, in the epidemic acceleration phase (Figure 5). Introduction of cholera from Malawi into South Africa occurred through multiple transmission events (Figure 5). Phylogeographic analyses strongly

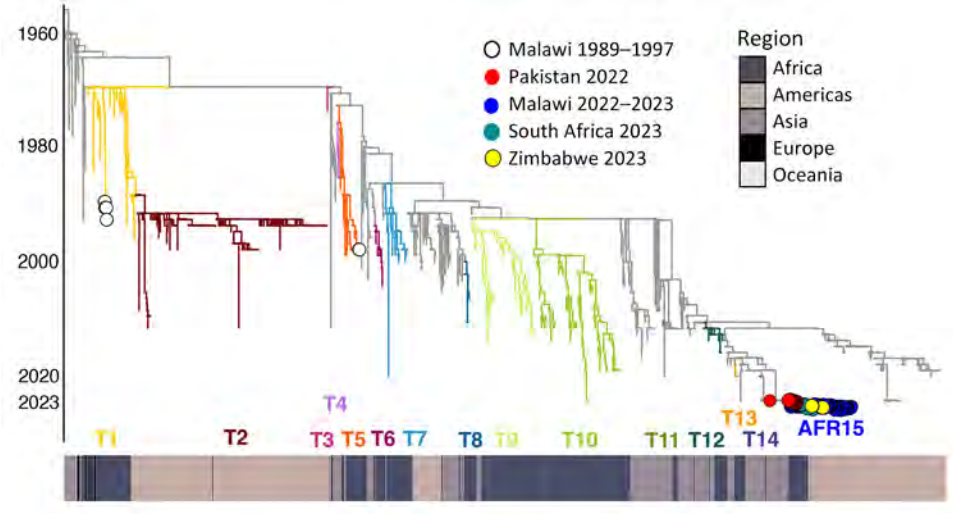

Figure 2. Phylogenetic history of cholera outbreaks within Malawi shown as part of a time-scaled maximum likelihood global phylogeny of 2,778 cholera genomes. Clade branches are colored by the previous 12 introduction events involving Africa (T1–T14 and AFR15) as described by Weill et al. (*9*). We denote the clade containing the genomes from the 2022–2023 outbreaks in Malawi, South Africa, and Zimbabwe as the AFR15 lineage. Heat map below the tree shows continent of sample origin.

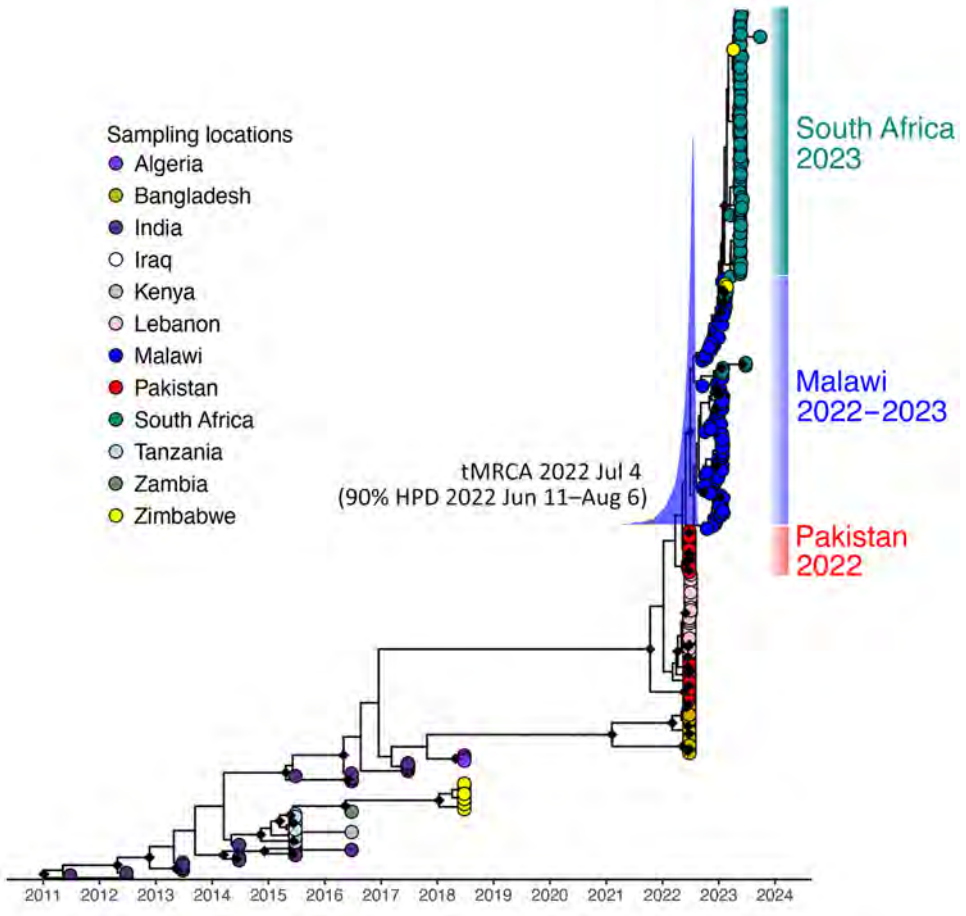

Figure 3. Maximum clade credibility phylogeny depicting the clade containing genomes from the 2022–2023 outbreak in Malawi (n = 89, sampled December 10, 2022–February 2023) with a basal clade of genomes sequenced from Pakistan in 2022. tMRCA estimate is shown. The blue curve shows posterior distribution of tMRCA. Black diamonds at nodes indicate posterior probability >0.9. HPD, highest posterior density; tMRCA, time to most recent common ancestor.

suggested that cholera spread into South Africa from Malawi (BF = 50,222) on multiple separate introductions (Appendix 2 Table 3). The substantial flow of air passengers between Malawi and South Africa underscores the strong connectivity between the countries (Figure 4). After the introduction in South Africa, cholera futher spread into Zimbabwe from South Africa (BF = 25,109) on ≥2 separate occasions (Figure 5). Our analysis was limited by the sampling date range (September 2022–September 2023) and thus might not provide accurate insights into the dispersal patterns during the early phase of the outbreak.

Effect of Severe Flooding in Malawi

Because the 2022 Pakistan cholera outbreak was exacerbated by major floods during June–October 2022 (*39*), we next examined the Malawi outbreak in light of the extreme weather events that occurred in 2022 (Figure 6, panel A; Appendix 2 Figure 2). The outbreak started after Tropical Storm Ana (January 28, 2022), which caused widespread flooding and damage in southern Malawi and left >200,000 persons displaced, many in emergency camps without adequate access to safe water and sanitation (*7*). Soon after the start of the outbreak, Cyclone Gombe caused further flooding (as measured by area flooded) and heavy damage across southern Malawi, including many areas already affected by Tropical Storm Ana (Appendix 2 Figure 2). The interval of the introduction of cholera into Malawi (95% HPD March 2022–August 2022) correlates with the beginning of the reported cases for the current cholera outbreak in the country (Figure 6, panel A; Appendix 2 Figure 2) and overlaps with flooding in Pakistan that exacerbated the ongoing cholera outbreak in that country. Initial floods in Malawi did not seem to correlate with amplification of cases, suggesting that the introduction was followed only by low circulation restricted to the flood-affected areas in the southern region (Appendix 2 Figure 2). Floods that occurred during the normal rainy season in late November 2022 likely intensified transmission; cases surged particularly in Blantyre and Lilongwe, the 2 main urban centers (Appendix 2 Figure 2) (*7*). The rapid surge of cases was likely spurred on by the extreme flooding events causing a lack of access to safe drinking water, poor sanitation and hygiene, and displacement of a vulnerable population (Figure 6) (*7*). Because we did not have genomes from the early phase of the outbreak in our

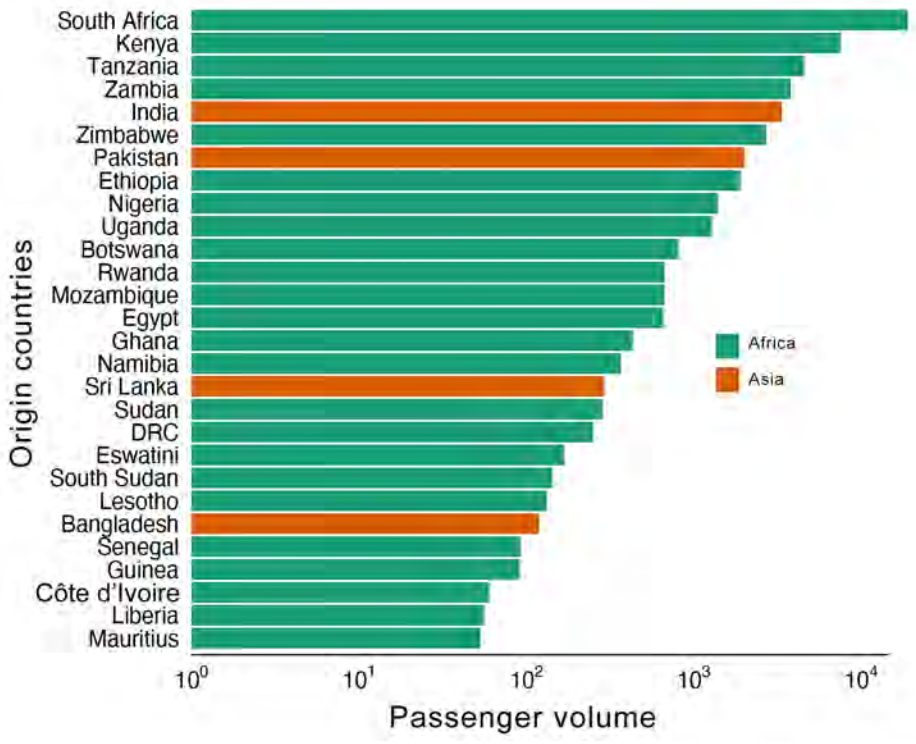

Figure 4. Number of passengers arriving by air travel into Malawi, by country of origin, January–June 2022. DRC, Democratic Republic of the Congo.

study and because the introduction interval was relatively wide, spanning several months, we must consider an alternative hypothesis: the initial floods may have led to low-level circulation of endemic cholera strains, initiating the outbreak in Malawi. Subsequently, during the dry season, the introduction of the strain from Pakistan occurred with minimal transmission until later floods permitted the amplified transmission of a potentially more transmissible strain.

We estimated that R_t from daily case data increased after November 28, 2022, to a maximum of 1.619 on December 29, 2022, before starting to decline in early January 2023; it was consistently <1 from mid-February 2023 and at 0.704 at the end of the study period (Figure 6, panel B). Flooding (Figure 6, panel A) was positively associated with R_t (0.262 [95% CrI 0.003–0.509]) (Appendix 2 Figure 3, panel D).

Two oral cholera vaccination campaigns have been conducted since the onset of the outbreak; a total of 2,825,229 doses were administered by December 2, 2022, covering 96.8% of the population residing in communities with high risk and burden of cholera (*7*). We estimated a negative association between the vaccination campaigns and R_t (−0.320 [90% CrI −0.638 to −0.013]) (Appendix 2 Figure 3, panel D) but note that the association is only significant at a 90% CrI. Our results were robust to a varying level of the initial susceptible population (S_0), which is important because the initial vaccination campaign in early 2022 may have reduced the S_0 further than the S_0 we used as our baseline, and we do not know about any prior immunity in the community caused by previous outbreaks (Appendix 2 Figure 3).

Discussion

In this genomic analysis, we provide evidence of a link between the recent large cholera outbreaks in Pakistan and Malawi, consistent with previous genomic analyses revealing the importance of long-range *V. cholerae* transmission events between Asia and Africa (*8*,*9*). However, we cannot rule out that another unsampled country could be the origin of both the Malawi and Pakistan outbreaks. Our main findings support another recent analysis of the Malawi outbreak (*19*), which was linked to the strains previously identified in Asia, and another report of cases from South Africa in 2023 epidemiologically linked to Malawi (*20*). The extreme weather events and humanitarian crises in Malawi provided a suitable environment for the amplified spread of *V. cholerae*, and the subsequent movement of large numbers of persons may have enabled its spread to susceptible populations in areas relatively unaffected by cholera for more than a decade.

The relatively narrow sampling date range for this genomic analysis meant that we cannot confidently differentiate whether the introduction of *V. cholerae* was responsible for initiating the outbreak or if it only contributed to the later expansion of the outbreak through

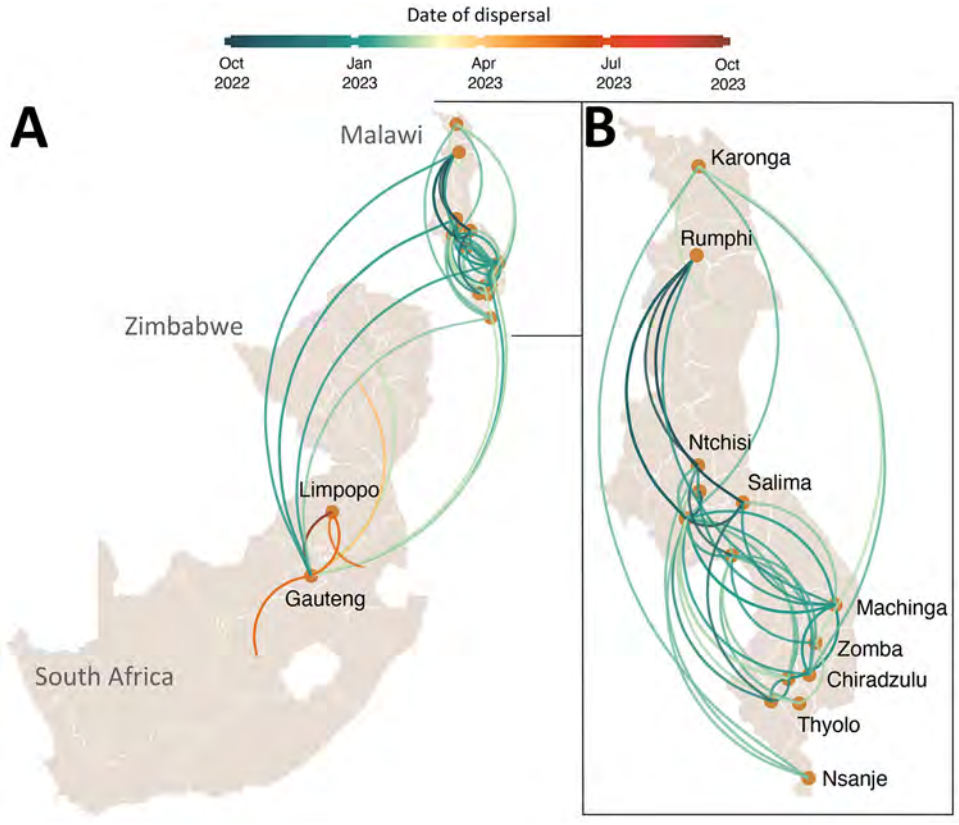

Figure 5. Spatiotemporal reconstruction of the spread of cholera in Malawi, South Africa, and Zimbabwe (A) and within Malawi (B) during the 2022–2023 outbreak. Circles represent nodes of the maximum likelihood phylogeny, and curved lines denote the links between nodes. Line colors indicates inferred time of occurrence. Directionality of spread is counterclockwise along each curve.

multiple transmission chains. Further sequencing of isolates from earlier stages of the outbreak could elucidate the initial dynamics, emphasizing the criticality of controlling cholera outbreaks and preventing introductions during the dry season to prevent escalation during subsequent flooding seasons. We are also working with partners in other heavily affected countries in Africa to conduct genomic sequencing of

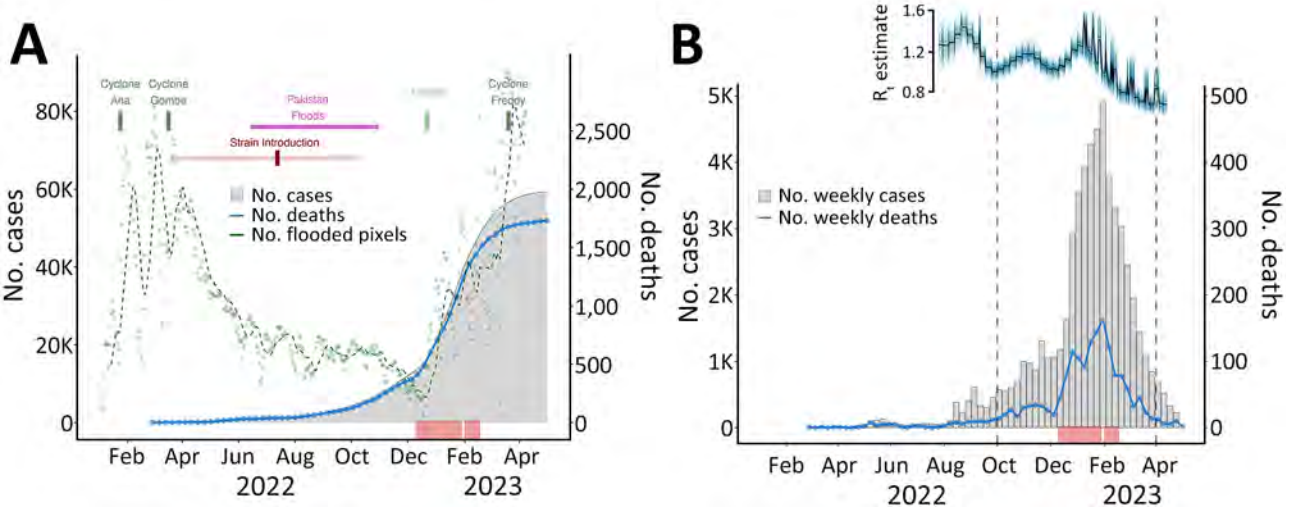

Figure 6. Relationships between confirmed cholera cases and cholera outbreak dynamics in Malawi during the 2022–2023 outbreak. A) Cyclones and flooding events affecting Malawi are shown. Green dots represent flooding conditions across Malawi as the daily number of pixels detected from remotely sensed satellite imagery; dashed green line indicates the moving average. Dark red mark indicates inferred time of introduction of a Pakistan strain into Malawi; the lighter shaded line indicates the 95% highest posterior density interval for the time estimate. B) Weekly number of newly confirmed cholera cases and deaths in Malawi during February 2022–April 2023. Estimation of R_t and association with other variables is shown above the case data for September 2022–April 2023 with plots of posterior distributions, median (black), and sample paths (blue). In both plots, red rug plot below charts indicates temporal distribution of cases sequenced in our study. R_t, time-varying reproduction number.

V. cholerae isolates, which will help with understanding the extent of cross-border regional transmission at different phases of the outbreak.

We modeled R_t over the course of the outbreak, incorporating satellite data to assess the effect of flooding on cholera transmission, which is particularly important in studying a waterborne disease like cholera. A substantial positive association between flooding and reproduction numbers explained the sustained high case numbers in January. The decline after February 2023 was likely caused by a successful vaccination campaign, infection-acquired immunity, and depletion of susceptible persons. Our model, based on national case data, lacked precise vaccination rollout details, which limited its accuracy. Future research should use spatially disaggregated data to better assess the effects of flooding and vaccination on cholera dynamics. Overall, our study highlights the need for coordinated global and regional cholera prevention and control efforts and the importance of heightened awareness, data sharing, and preparedness whenever outbreaks occur in any part of the world (*40*).

This article was preprinted at https://www.medrxiv.org/content/10.1101/2023.08.22.23294324v1.

With permission from the Public Health Institute of Malawi, raw reads of the isolates that were successfully sequenced have been made publicly available and deposited in the National Center for Biotechnology Information Short Read Archive (BioProject PRJNA967700).

Centre for Epidemic Response and Innovation and the CLIMADE program are supported by grants from the Rockefeller Foundation (no. HTH 017), the SAMRC South African mRNA Vaccine Consortium, the South African Department of Science and Innovation, and by Medical Research Foundation (no. MRF-RG-ICCH-2022-100069). S.B. and C.M. acknowledge funding from the MRC Centre for Global Infectious Disease Analysis (reference no. MR/X020258/1), funded by the UK Medical Research Council. This UK-funded award is carried out in the frame of the Global Health EDCTP3 Joint Undertaking. S.B. is funded by the National Institute for Health and Care Research (NIHR) Health Protection Research Unit in Modelling and Health Economics, a partnership between UK Health Security Agency, Imperial College London, and London School of Hygiene & Tropical Medicine (grant code NIHR200908); the Novo Nordisk Foundation via the Novo Nordisk Young Investigator Award (no. NNF20OC0059309); and the Danish National Research Foundation (no. DNRF160). S.B. acknowledges support from the Eric and Wendy Schmidt Fund For Strategic Innovation via the Schmidt Polymath Award (no. G-22-63345) , which also supports C.M. The views expressed are those of the authors and not necessarily those of the NIHR, UK Health Security Agency, or the UK Department of Health and Social Care. The funders of the study had no role in study design, data collection, data analysis, data interpretation, or writing of the report.

About the Author

Dr. Chabuka is a dedicated medical scientist at the Public Health Institute of Malawi and a PhD fellow at Stellenbosch University. His research focuses on infectious diseases, including COVID-19, cholera, malaria, and arbovirus-related illnesses. His primary research interest is leveraging next-generation sequencing technologies to track pathogen evolution, antimicrobial resistance, and outbreak dynamics.

References

1. Kanungo S, Azman AS, Ramamurthy T, Deen J, Dutta S. Cholera. Lancet. 2022;399:1429–40. https://doi.org/10.1016/S0140-6736(22)00330-0
2. World Health Organization. Outbreaks and other emergencies bulletin, week 30: 24–30 July 2023. 2023 [cited 2025 Feb 24]. https://www.afro.who.int/health-topics/disease-outbreaks/outbreaks-and-other-emergencies-updates
3. World Health Organization. Disease outbreak news; cholera—global situation. 2022 Dec 16 [cited 2025 Feb 24]. https://www.who.int/emergencies/disease-outbreak-news/item/2022-DON426
4. World Health Organization. Disease outbreak news; cholera—global situation. 2023 Feb 11. [cited 2025 Feb 24]. https://www.who.int/emergencies/disease-outbreak-news/item/2023-DON437
5. Msyamboza KP, Kagoli M, M'bang'ombe M, Chipeta S, Masuku HD. Cholera outbreaks in Malawi in 1998–2012: social and cultural challenges in prevention and control. J Infect Dev Ctries. 2014;8:720–6. https://doi.org/10.3855/jidc.3506
6. World Health Organization African Region. Weekly regional cholera bulletin. 2024 Apr 1 [cited 2025 Feb 24]. https://iris.who.int/bitstream/handle/10665/376526/AFRO%20Cholera%20Bulletin.58.pdf
7. World Health Organization. Disease outbreak news: cholera—Malawi. 2023 Feb 9 [cited 2025 Feb 24]. https://www.who.int/emergencies/disease-outbreak-news/item/2022-DON435
8. Mutreja A, Kim DW, Thomson NR, Connor TR, Lee JH, Kariuki S, et al. Evidence for several waves of global transmission in the seventh cholera pandemic. Nature. 2011;477:462–5. https://doi.org/10.1038/nature10392
9. Weill FX, Domman D, Njamkepo E, Tarr C, Rauzier J, Fawal N, et al. Genomic history of the seventh pandemic of cholera in Africa. Science. 2017;358:785–9. https://doi.org/10.1126/science.aad5901
10. Inzaule SC, Tessema SK, Kebede Y, Ogwell Ouma AE, Nkengasong JN. Genomic-informed pathogen surveillance in Africa: opportunities and challenges. Lancet Infect Dis. 2021;21:e281–9. https://doi.org/10.1016/S1473-3099(20)30939-7
11. Chen S, Zhou Y, Chen Y, Gu J. fastp: an ultra-fast all-in-one FASTQ preprocessor. Bioinformatics. 2018;34:i884–90. https://doi.org/10.1093/bioinformatics/bty560

12. Li H. A statistical framework for SNP calling, mutation discovery, association mapping and population genetical parameter estimation from sequencing data. Bioinformatics. 2011;27:2987–93. https://doi.org/10.1093/bioinformatics/btr509
13. Tonkin-Hill G, Lees JA, Bentley SD, Frost SDW, Corander J. Fast hierarchical Bayesian analysis of population structure. Nucleic Acids Res. 2019;47:5539–49. https://doi.org/10.1093/nar/gkz361
14. Croucher NJ, Page AJ, Connor TR, Delaney AJ, Keane JA, Bentley SD, et al. Rapid phylogenetic analysis of large samples of recombinant bacterial whole genome sequences using Gubbins. Nucleic Acids Res. 2015;43:e15. https://doi.org/10.1093/nar/gku1196
15. Shen W, Le S, Li Y, Hu F. SeqKit: a cross-platform and ultrafast toolkit for FASTA/Q file manipulation. PLoS One. 2016;11:e0163962. https://doi.org/10.1371/journal.pone.0163962
16. Kumar S, Stecher G, Li M, Knyaz C, Tamura K. MEGA X: Molecular Evolutionary Genetics Analysis across computing platforms. Mol Biol Evol. 2018;35:1547–9. https://doi.org/10.1093/molbev/msy096
17. Nguyen LT, Schmidt HA, von Haeseler A, Minh BQ. IQ-TREE: a fast and effective stochastic algorithm for estimating maximum-likelihood phylogenies. Mol Biol Evol. 2015;32:268–74. https://doi.org/10.1093/molbev/msu300
18. Sagulenko P, Puller V, Neher RA. TreeTime: maximum-likelihood phylodynamic analysis. Virus Evol. 2018;4:vex042. https://doi.org/10.1093/ve/vex042
19. Chaguza C, Chibwe I, Chaima D, Musicha P, Ndeketa L, Kasambara W, et al. Genomic insights into the 2022–2023 *Vibrio cholerae* outbreak in Malawi. Nat Commun. 2024;15:6291.
20. Smith AM, Sekwadi P, Erasmus LK, Lee CC, Stroika SG, Ndzabandzaba S, et al. Imported cholera cases, South Africa, 2023. Emerg Infect Dis. 2023;29:1687–90. https://doi.org/10.3201/eid2908.230750
21. Olatunji G, Kokori E, Moradeyo A, Olatunji D, Ajibola F, Otolorin O, et al. A perspective on the 2023 cholera outbreaks in Zimbabwe: implications, response strategies, and policy recommendations. J Epidemiol Glob Health. 2024;14:243–8. https://doi.org/10.1007/s44197-023-00165-6
22. Rambaut A, Lam TT, Max Carvalho L, Pybus OG. Exploring the temporal structure of heterochronous sequences using TempEst (formerly Path-O-Gen). Virus Evol. 2016;2:vew007. https://doi.org/10.1093/ve/vew007
23. Gill MS, Lemey P, Faria NR, Rambaut A, Shapiro B, Suchard MA. Improving Bayesian population dynamics inference: a coalescent-based model for multiple loci. Mol Biol Evol. 2013;30:713–24. https://doi.org/10.1093/molbev/mss265
24. Suchard MA, Lemey P, Baele G, Ayres DL, Drummond AJ, Rambaut A. Bayesian phylogenetic and phylodynamic data integration using BEAST 1.10. Virus Evol. 2018;4:vey016. https://doi.org/10.1093/ve/vey016
25. Baele G, Li WL, Drummond AJ, Suchard MA, Lemey P. Accurate model selection of relaxed molecular clocks in bayesian phylogenetics. Mol Biol Evol. 2013;30:239–43. https://doi.org/10.1093/molbev/mss243
26. Mavian C, Paisie TK, Alam MT, Browne C, Beau De Rochars VM, Nembrini S, et al. Toxigenic Vibrio cholerae evolution and establishment of reservoirsin aquatic ecosystems. Proceedings of the National Academy of Sciences. 2020:201918763.
27. Mavian C, Tagliamonte M, Alam M, Sakib SN, Cash M, Moir M, et al. Ancestral origin and dissemination dynamic of reemerging toxigenic *Vibrio cholerae*, Haiti. Emerg Infect Dis. 2023;29:2072–82. https://doi.org/10.3201/eid2910.230554
28. Yu GC, Smith DK, Zhu HC, Guan Y, Lam TTY. GGTREE: an R package for visualization and annotation of phylogenetic trees with their covariates and other associated data. Methods Ecol Evol. 2017;8:28–36. https://doi.org/10.1111/2041-210X.12628
29. Bielejec F, Rambaut A, Suchard MA, Lemey P. SPREAD: spatial phylogenetic reconstruction of evolutionary dynamics. Bioinformatics. 2011;27:2910–2. https://doi.org/10.1093/bioinformatics/btr481
30. Kass RE Raftery AE. Bayes factors. J Am Stat Assoc. 1995; 90:773–95. https://doi.org/10.1080/01621459.1995.10476572
31. Bhatt S, Ferguson N, Flaxman S, Gandy A, Mishra S, Scott JA. Semi-mechanistic Bayesian modelling of COVID-19 with renewal processes. J R Stat Soc Ser A Stat Soc. 2023;186:601–15. https://doi.org/10.1093/jrsssa/qnad030
32. Cori A, Ferguson NM, Fraser C, Cauchemez S. A new framework and software to estimate time-varying reproduction numbers during epidemics. Am J Epidemiol. 2013;178:1505–12. https://doi.org/10.1093/aje/kwt133
33. Cartalis C, Feidas H, Glezakou M, Proedrou M, Chrysoulakis N. Use of earth observation in support of environmental impact assessments: prospects and trends. Environ Sci Policy. 2000;3:287–94.
34. Tarpanelli A, Mondini AC, Camici S. Effectiveness of Sentinel-1 and Sentinel-2 for flood detection assessment in Europe. Nat Hazards Earth Syst Sci. 2022;22:2473–89. https://doi.org/10.5194/nhess-22-2473-2022
35. Li S, Sun D, Goldberg MD, Sjoberg B, Santek D, Hoffman JP, et al. Automatic near real-time flood detection using Suomi-NPP/VIIRS data. Remote Sens Environ. 2018;204:672–89.
36. Turner B. International Air Transport Association (IATA). In: Turner B, editor. The statesman's yearbook 2008: the politics, cultures and economies of the world. London: Palgrave Macmillan UK; 2007. p. 48.
37. Sim EM, Martinez E, Blackwell GA, Pham D, Millan G, Graham RMA, et al. Genomes of *Vibrio cholerae* O1 serotype Ogawa associated with current cholera activity in Pakistan. Microbiol Resour Announc. 2023;12:e0088722. https://doi.org/10.1128/mra.00887-22
38. World Health Organization Eastern Mediterranean Region. Epidemic and pandemic-prone diseases: acute watery diarrhoea/cholera updates (16–31 March 2023). 2023 [cited 2025 Feb 24]. https://www.emro.who.int/pandemic-epidemic-diseases/cholera/acute-watery-diarrhoeacholera-updates-1631-march-2023.html
39. Jamil H, Liaqat A, Lareeb I, Tariq W, Jaykumar V, Kumar L, et al. Monsoon and cholera outbreaks in Pakistan: a public health concern during a climate catastrophe. IJS Global Health. 2023;6:e105. https://doi.org/10.1097/GH9.0000000000000105
40. Global Task Force on Cholera Control. Ending cholera: a global roadmap to 2030. 2017 [cited https://www.gtfcc.org/wp-content/uploads/2019/10/gtfcc-ending-cholera-a-global-roadmap-to-2030.pdf

Address for correspondence: Carla N. Mavian, University of Florida—Emerging Pathogens Institute, 2055 Mowry Rd , Gainesville, FL 32610 USA; email: cmavian@ufl.edu; Tulio de Olivera, JC Smuts building, School for Data Science and Computational Thinking, Stellenbosch University, Stellenbosch, South Africa; email: tulio@sun.ac.za

Genesis and Spread of Novel Highly Pathogenic Avian Influenza A(H5N1) Clade 2.3.4.4b Virus Genotype EA-2023-DG Reassortant, Western Europe

Steven Van Borm, Ann Kathrin Ahrens, Claudia Bachofen, Ashley C. Banyard, Cathrine Arnason Bøe, François-Xavier Briand, Zuzana Dirbakova, Marc Engelsma, Alice Fusaro, Evelien Germeraad, Britt Gjerset, Béatrice Grasland, Frank Harders, Pierre Hostyn, Ari Kauppinen, Bénédicte Lambrecht, Benjamin C. Mollett, Isabella Monne, Alexander Nagy, Anne Pohlmann, Daniel Polzer, Scott M. Reid, Sandra Revilla-Fernandez, Mieke Steensels, Michaela Stätter, Edyta Swieton, Niina Tammiranta, Michele Wyler, Bianca Zecchin, Siamak Zohari, Simon Dellicour

In Europe, highly pathogenic avian influenza (HPAI) virus circulates in avian wildlife, undergoing frequent reassortment, sporadic introductions in domestic birds, and spillover to mammals. An H5N1 clade 2.3.4.4b reassortant, EA-2023-DG, affecting wild and domestic birds was detected in western Europe in November 2023. Six of its RNA segments came from the EA-2021-AB genotype, but the polymerase basic 2 and polymerase acidic segments originated from low pathogenicity avian influenza viruses. Discrete phylogeographic analyses of concatenated genomes and single polymerase basic 2 and polymerase acidic segments suggested reassortment in summer 2023 near the southwestern Baltic Sea. Subsequent continuous phylogeographic analysis of all concatenated EA-2023-DG genomes highlighted circulation in northwestern Europe until June 2024 and long-distance dispersal toward France, Norway, England, Slovakia, Switzerland, and Austria. Those results illustrate the value of phylodynamic approaches to investigate emergence of novel avian influenza virus variants, trace their subsequent dispersal history, and provide vital clues for informing outbreak prevention and intervention policies.

Author affiliations: Avian Virology and Immunology Unit, Sciensano, Brussels, Belgium (S. Van Borm, P. Hostyn, B. Lambrecht, M. Steensels); Institute of Diagnostic Virology, Friedrich Loeffler Institut, Greifswald-Insel Riems, Germany (A.K. Ahrens, A. Pohlmann); Institute of Virology and Immunology, Federal Department of Home Affairs, Mittelhäusern, Switzerland (C. Bachofen, M. Wyler); World Organisation for Animal Health/Food and Agriculture Organization of the United Nations International Reference Laboratory for Avian Influenza and Newcastle Disease, Animal and Plant Health Agency-Weybridge, Addlestone, UK (A.C. Banyard, B.C. Mollett, S.M. Reid); Norwegian Veterinary Institute, Ås, Norway (C. Arnason Bøe, B. Gjerset); Agence Nationale de Sécurité Sanitaire de l'alimentation, de l'environnement et du travail, Ploufragan-Plouzané-Niort, France (F.-X. Briand, B. Grasland); State Veterinary Institute Department of Animal Health, Zvolen, Slovakia (D. Dirbakova); Wageningen Bioveterinary Research Department of Virology, Lelystad, the Netherlands (M. Engelsma, E. Germeraad, F. Harders); European Reference Laboratory for Avian Influenza and Newcastle Disease, Istituto Zooprofilattico Sperimentale delle Venezie, Padua, Italy (A. Fusaro, I. Monne, B. Zecchin); Finnish Food Authority, Helsinki, Finland (A. Kauppinen, N. Tammiranta); Department of Molecular Biology, State Veterinary Institute Prague, Praha, Czech Republic (A. Nagy); Austrian Agency for Health and Food Safety, Institute for Veterinary Disease Control, Mödling, Austria (D. Polzer, S. Revilla-Fernandez, M. Stätter); National Veterinary Research Institute Department of Research Support, Puławy, Poland (E. Swieton); Swedish Veterinary Agency Department of Microbiology, Uppsala, Sweden (S. Zohari); Spatial Epidemiology Lab (SpELL), Université Libre de Bruxelles, Brussels, Belgium (S. Dellicour); Laboratory for Clinical and Epidemiological Virology, Department of Microbiology, Immunology and Transplantation, Rega Institute, KU Leuven, Leuven, Belgium (S. Dellicour); Interuniversity Institute of Bioinformatics in Brussels, Université Libre de Bruxelles, Vrije Universiteit Brussel, Brussels (S. Dellicour)

DOI: https://doi.org/10.3201/eid3106.241870

Since 2016, Europe has experienced periodic introductions of clade 2.3.4.4b highly pathogenic avian influenza (HPAI) subtype H5 viruses via wild migratory bird movements and sporadic spillover events to poultry, which have resulted in several outbreaks affecting wildlife and poultry (*1*). In 2021, the typically seasonal epidemiologic cycle changed, and HPAI viruses became enzootic in Europe (*2*). The hemagglutinin (HA) gene of HPAI clade 2.3.4.4 viruses (*3*) showed rapid wild bird–mediated expansion, including global spread (*4*), and rapid evolution in all affected geographic areas (*5*–*7*). After 2021, increased HPAI incidence in Europe resulted in greater genetic diversity and in the evolution of new genotypes by frequent reassortment events. By 2022, the continued circulation of HPAI viruses led to numerous poultry outbreaks, affected an increasing number of wild bird species, and led to frequent reassortment, making assessment of the epidemiologic situation difficult (*2*). Sporadic infection of mammals is observed, including the unexpected spread to cattle in North America and cases of human infection (*8*,*9*), and is sometimes associated with adaptive mutations for viral replication in mammalian cells. Those observations stress the zoonotic risk associated with this particular HPAI virus (HPAIV) clade and the need for surveillance efforts, including whole-genome sequencing.

By the end of 2023, continued circulation and frequent reassortment events resulted in the co-circulation of 11 H5Nx HPAIV genotypes in Europe, 7 of which emerged during the fall of 2023 (*10*,*11*). One of those novel reassortants was assigned genotype EA-2023-DG, according to the standardized avian influenza virus (AIV) genotyping nomenclature in Europe (*2*). EA-2023-DG was first reported in Germany in November 2023 and shared most of its genomic segments with the contemporary dominating genotype EA-2021-AB but also gained polymerase basic protein (PB) 2 and polymerase acidic protein (PA) segments from low pathogenicity avian influenza viruses circulating in western Europe (*10*). Using all available EA-2023-DG genotype complete genome sequences, we conducted recombination and discrete as well as continuous phylogeographic analyses to investigate the emergence and subsequent dispersal dynamic of this genotype.

Methods

Data Selection and Genotyping

The European Union Reference Laboratory, national reference laboratories, and some other partners perform sequencing analyses of the complete genome of HPAI H5Nx viruses detected through ongoing surveillance programs. All sequences are deposited in the GISAID EpiFlu database (http://www.gisaid.org). Partners perform genotyping on the basis of the phylogenetic tree topology, using previously described methods (*2*). During November 1, 2023–June 25, 2024, genotyping identified a total of 54 virus genomes as belonging to genotype EA-2023-DG. We extracted publicly available complete genomes comprising 8 segments from GISAID EpiFlu on January 15, 2025, resulting in a dataset consisting of all 54 identified EA-2023-DG genomes associated with exact temporal and spatial sampling metadata (Appendix 1 Table 1, https://wwwnc.cdc.gov/EID/article/31/6/24-1870-App1.pdf). The earliest publicly available EA-2023-DG genome, A/*Gallus_gallus*/Belgium/11307_0002/2023 (GISAID EpiFlu accession no. EPI_ISL_18607170), was sequenced from a chicken sample collected in Belgium on November 30, 2023. We used that strain as the reference strain for genotype EA-2023-DG in this study.

Investigation of Geographic Origin of Reassortant EA-2023-DG Genotype

To retrieve a selection of the most homologous sequences to each of the EA-2023-DG viral genome segments, we conducted a search in GISAID EpiFlu on May 27, 2024. For each of the genome segments of reference strain A/*Gallus_gallus*/Belgium/11307_0002/2023, we identified the 500 sequences with highest nucleotide homology and downloaded the sequences of all 8 gene segments of those genomes along with any available metadata (Appendix 2, https://wwwnc.cdc.gov/EID/article/31/6/24-1870-App2.xlsx). The accompanying metadata included sampling location and precise collection date.

We used MAFFT 7.453 (*12*) to align sequences. Because genotyping identified EA-2023-DG as a reassortant containing the PB1, HA, nucleoprotein (NP), neuraminidase (NA), matrix protein (MP), and nonstructural (NS) protein segments from EA-2021-AB–like viruses, as well as PB2 and PA segments of other circulating AIVs, we assembled 3 distinct datasets. One dataset was an alignment concatenating the 6 nonrecombinant segments, PB1, HA, NP, NA, MP, and NS, of all 54 EA-2023-DG samples and the 500 most homologous H5N1 virus samples found for those 6 segments. We removed duplicates from the 6 segment searches by using a custom Python script (Python Software Foundation, https://www.python.org), resulting in a total dataset of 958 samples. The second and third datasets, 1 for PA and 1 for PB2, used a distinct PA or PB2 alignment from all 54

EA-2023-DG samples and the 500 most homologous samples for the corresponding segment.

Because the initial concatenated alignment was computationally too large to conduct Bayesian phylogeographic inference, we conducted a preliminary maximum-likelihood phylogenetic inference in IQTREE 1.6.12 (*13*), using default settings and the best-fitting substitution model identified by ModelFinder (*14*). We used that preliminary phylogenetic inference to restrict the alignment to a large monophyletic clade of 225 samples containing the 54 EA-2023-DG samples. Thus, that phylogeny-guided downsampling reflects the evolutionary history of the larger set of 958 samples.

To assess the presence of a recombination signal within the resulting PB1-HA-NP-NA-MP-NS concatenated alignment of those 6 segments, we performed the Φ test (*15*) implemented in the SplitsTree 4.14.8 program (*16*), which confirmed the occurrence of past recombination events ($p<0.001$). We then used the RDP4 program (*17*) to identify recombinant samples: we identified and discarded 41 recombinants within the set of background samples, which resulted in a PB1-HA-NP-NA-MP-NS concatenated alignment of 184 samples. We performed a new Φ test on that final alignment and confirmed the absence of a remaining recombination signal.

We conducted a discrete phylogeographic analysis based on each of the 3 alignments (PA, PB2, and recombinant-free PB1-HA-NP-NA-MP-NS) to reconstruct the transition history of viral lineages among countries and investigate the country from which EA-2023-DG genotype emerged. For those analyses, the selection of countries as discrete locations was imposed by the lack of higher sampling precision for most publicly available background sequences retrieved from GISAID EpiFlu. We performed the discrete phylogeographic analyses by using the discrete diffusion model (*18*) implemented in the BEAST 1.10 software package (*19*), specifying a GTR+Γ (general time-reversible with a gamma-distributed rate heterogeneity) nucleotide substitution model (*20*), a relaxed molecular clock with an underlying log-normal distribution to model branch-specific evolutionary rates (*21*), and a skygrid coalescent model for the tree prior (*22*). We ran the PA analysis for 300 Markov chain Monte Carlo (MCMC) iterations, the PB2 analysis for 500 MCMC iterations, and the concatenated analyses for 210 million MCMC iterations and sampled posterior trees every 100,000 iterations. We assessed the MCMC convergence and mixing by using the Tracer 1.7 program (*23*), checking that all estimated parameters were associated with an effective sample size value >200. After discarding the initial 10% of sampled posterior trees as burn-in, we retrieved and annotated the maximum clade credibility (MCC) tree by using TreeAnnotator 1.10 (*19*) and eventually plotted the tree in R (The R Project for Statistical Computing, https://www.r-project.org) by using a custom script (https://github.com/sdellicour/ea-2023-dg_emergence).

Reconstruction of Reassortant EA-2023-DG Dissemination History

To reconstruct the spread of the EA-2023-DG genotype after the reassortment event at its genesis, we performed a continuous phylogeographic reconstruction on the basis of the concatenated alignment of all 8 genomic segments of the 54 EA-2023-DG genomes available on January 15, 2025. We then aligned sequences again using MAFFT 7.453 (*12*) and performed the Φ test (*15*) in SplitsTree (*16*) to confirm the absence of a recombination signal within the concatenated alignment made of EA-2023-DG genomic sequences. The availability of precise sampling coordinates for all considered samples in this alignment made a spatially explicit phylogeographic reconstruction possible. We performed that continuous phylogeographic reconstruction by using the relaxed random walk model (*24*,*25*) in BEAST version 1.10 (*19*). As with the discrete approach, the continuous phylogeographic approach involves a joint inference of both the phylogenetic tree representing the evolutionary relationships between sampled sequences, and the locations, in this case the geographic coordinates (latitude and longitude) of unsampled common ancestors (*26*). Specifically, we used a gamma distribution to model the among-branch heterogeneity in diffusion velocity, and modeled branch-specific evolutionary rates according to a relaxed molecular clock with an underlying log-normal distribution and the nucleotide substitution process according to a GTR+Γ parameterization. As for the tree prior, we specified a flexible skygrid model (*22*). We ran the MCMC for 250 million iterations, sampling posterior trees every 100,000 iterations, and eventually discarded the first 25 million sampled trees as burn-in. We used Tracer 1.7.2 to assess the MCMC convergence and mixing properties and ensure that estimated parameters were all associated with an effective sample size >200. We used TreeAnnotator version 1.10 to identify and annotate the MCC tree and R functions in the SERAPHIM package (*27*,*28*) to extract the spatiotemporal information embedded within the 1,000 trees sampled from the post–burn-in posterior distribution and to estimate the weighted diffusion coefficient (*29*) associated with the spread of the EA-2023-DG genotype.

Results

Epidemiologic Findings

Our analysis showed that the EA-2023-DG genotype was initially detected in a sample from a swan found dead on a Baltic Sea island in Finland on November 1, 2023 (GISAID accession no. EPI_ISL_19409779) (Figure 1; Appendix 1 Table 1). Then, on November 17, 2023, the EA-2023-DG genotype emerged in a hobby farm near the North Sea coast in northern Germany that had a mixed population of 52 chickens, 3 turkeys, and 11 ducks (Appendix 1 Table 1). EA-2023-DG subsequently spread to a total of 11 countries, and 54 cases were detected (Appendix 1 Table 2). The most affected countries included Germany, Sweden, and Poland. Germany was most affected, with cases in 13 poultry farms, 8 wild birds, 1 captive bird, and 1 wild mammal (red fox). Sweden experienced cases on 1 poultry farm and in 11 wild birds, and Poland had 5 poultry and 3 wild bird cases. Affected poultry were among the Phasianidae family (n = 21), which includes chickens (*Gallus gallus*) and turkeys (*Meleagris gallopavo*), and the Anatidae family (n = 1), which includes geese and ducks. Domestic poultry were only infected in Germany, Poland, Sweden, and Belgium. Captive animals included 1 captive barn owl (Tytonidae family, *Tyto alba*) and 1 black necked swan (Anatidae family, *Cygnus melancoryphus*) in a zoo. Wild birds, all found dead during passive surveillance efforts, included birds from the Anatidae (n = 24), Accipitridae (n = 3), Falconidae (n = 1), Strigidae (n = 1), Gruidae (n = 1), and Ardeidae (n = 1) families (Appendix 1 Table 1). A single mammal sample from a red fox (*Vulpes vulpes*) from the Hamburg district of Germany was EA-2023-DG positive. The most recent (June 25, 2024) occurrence was a wild goose sample in Germany.

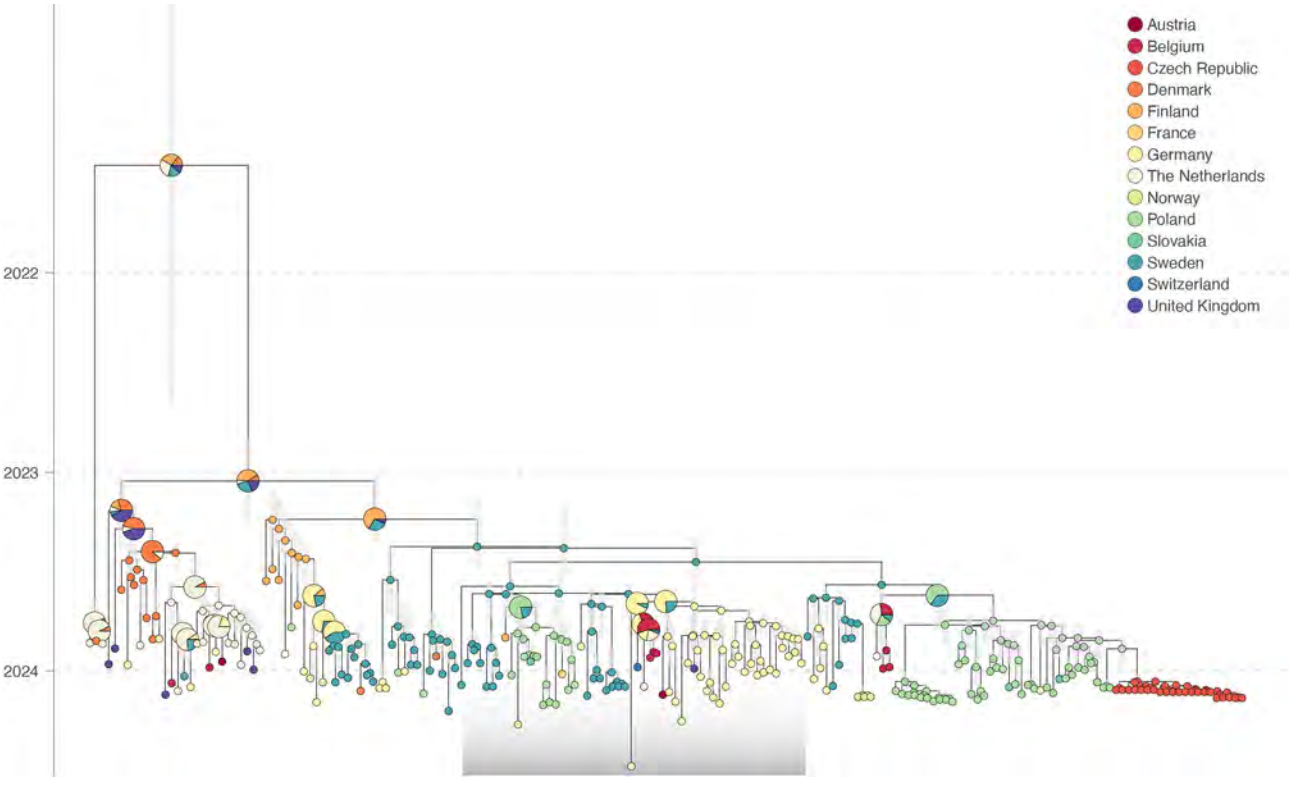

Figure 1. Discrete phylogeographic analysis from study of genesis and spread of novel highly pathogenic avian influenza A(H5N1) clade 2.3.4.4b virus genotype EA-2023-DG reassortant, western Europe. The maximum clade credibility (MCC) tree was obtained from discrete phylogeographic inference based on the analysis of the PB1-HA-NP-NA-MP-NS (polymerase basic 1, hemagglutinin, nucleoprotein, neuraminidase, matrix protein, nonstructural protein) concatenated alignment of EA-2023-DG samples and selected EA-2021-AB reference sequences sourced from GISAID EpiFlu (http://www.gisaid.org). Vertical gray shaded bars reflect the 95% highest posterior density interval associated with each internal node age estimate; internal nodes are colored according to their inferred location, and tip nodes are colored according to their sampling location. For the internal nodes, when a single location could not be inferred with a posterior probability >0.95, we used a pie chart to display the posterior probabilities associated with inferred locations with a posterior probability of ≥0.05. The gray transparent box highlights the position of the EA-2023-DG clade. The discrete phylogeographic reconstruction based on the analysis of the polymerase basic 2 and polymerase acidic segments are available as supplementary information (Appendix 1 Figures 1, 2, https://wwwnc.cdc.gov/EID/article/31/6/24-1870-App1.pdf).

Genesis of AIV Genotype EA-2023-DG in Western Europe

The discrete phylogeographic analyses conducted on the recombinant-free PB1-HA-NP-NA-MP-NS concatenated alignment and the PB2 and PA alignments confirmed the monophyletic nature of the EA-2023-DG clade (Figure 1; Appendix 1 Figures 1, 2). The analysis based on the PB1-HA-NP-NA-MP-NS concatenated alignment inferred the origin of the EA-2023-DG clade at the end of July 2023 (July 22, 2023; 95% highest posterior density [HPD] interval June 10–August 27, 2023) in Sweden with a posterior probability >0.99 (Figure 1). The analyses of the PB2 and PA segments, inferred its origin in Germany (posterior probability = 0.99); the PB2 analysis inferred its origin on January 6, 2023 (95% HPD September 17, 2022–April 20, 2023), and the PA analysis inferred its origin on June 30, 2023 (95% HPD April 14–September 24, 2023) (Appendix 1 Figures 1, 2).

Outcomes of discrete phylogeographic inference are known to be notably affected by sampling bias (*30*). Thus, the discrepancy between the country of origin inferred from the discrete phylogeographic analyses conducted for the recombinant-free PB1-HA-NP-NA-MP-NS concatenated alignment on the one hand and on the PB2 and PA alignments on the other could arise from the heterogeneous sampling of closely related sequences in the different countries within the study area. However, those results overall indicated that EA-2023-DG emerged during the spring and summer of 2023 in the southwestern Baltic Sea region. The continuous phylogeographic analysis further confirms the emergence of the reassortant genotype in this region and time frame (Figure 2).

Spread History and Dynamics of EA-2023-DG

Our continuous phylogeographic analysis using concatenated EA-2023-DG sequences for all 8 segments confirmed that the ancestral node of this clade traces back to the southwestern Baltic Sea shores of Sweden, Germany, and Denmark (Figure 2, panel B). Although the most ancestral nodes of the MCC tree are inferred in northern Germany (Figure 2, panel C), the uncertainty associated with the Bayesian phylogeographic inference (shaded 80% HDP polygons) highlights a potential area of origin that is relatively large and corresponds to the larger southwestern Baltic Sea area, which aligns with the results of the discrete phylogeographic reconstructions. Our continuous phylogeographical analysis dates the most ancestral node of the EA-2023-DG clade as August 2, 2023 (95% HPD July 16–September 7, 2023), also aligning with the discrete phylogenetic analyses (Figure 2, panel A). The continuous phylogeographic analysis indicated that after its emergence, lineages of the EA-2023-DG genotype further spread in Germany and Poland, toward the Netherlands, and to southern Sweden and southern Finland before November 2023. Its lineages then reached Belgium, England, Slovakia, and Switzerland during November and December 2023. By June 2024, EA-2023-DG spread as far north as the island of Åland in south Finland; as far south as Lyon, France; as far east as Slovakia; and as far west as England (Figure 2, panels B–F). Overall, the virus predominantly circulated in Germany, Sweden, and Poland, with only occasional detections in other countries in Europe.

Discussion

The ongoing panzootic caused predominantly by clade 2.3.4.4b HPAIVs is notorious for its diversifying evolution, including frequent reassortment events that result in an ever-changing range of circulating genotypes (*2*,*6*). Reassortment events represent crucial shifts in virus evolution that can affect host range, pathogenicity, and other epidemiologically relevant aspects of the virus phenotype; thus, understanding the dynamics behind the emergence and spread of such novel reassortants is critical. Combining complete avian influenza genomes and exact spatial and temporal sampling data enables detailed reconstruction of virus dispersal during an outbreak (*31*) and identification of reassortment events (*2*).

In this study, we analyzed all available full-genome sequences of novel reassortant HPAIV H5N1 genotype EA-2023-DG, which emerged in 2023 in western Europe (*10*), to reconstruct its genesis and dispersal dynamics. We traced its origin to the southwestern Baltic Sea area in the spring and summer of 2023. More precisely, most of the genome (i.e., PB1, HA, NP, NA, MP, and NS segments) originated from the dominant EA-2021-AB genotype, and the most recent common ancestor of those EA-2023-DG genomic segments likely emerged in or close to Sweden during summer 2023. As for the PA and PB2 segments, we inferred their origin in Germany, meaning that they could have originated from low pathogenicity avian influenza viruses circulating in Germany during winter and spring 2023, as suggested by others merely on the basis of sequence similarity (*10*). Overall, our results point toward a local reassortment event that occurred in the southwestern Baltic Sea area, which is in line with the first occurrence of the genotype in southern Finland.

Of note, our phylogeographic reconstructions of the genesis of EA-2023-DG agree with the AIV

introduction risk prediction on the basis of wild bird migration data and AIV occurrences by the EFSA Bird Flu Radar Tool (*32*). Those predictions indicated high introduction risk near the southwestern Baltic Sea along the shores of Germany, Denmark, and Sweden for the week fitting the time to most recent common ancestor (tMRCA) of the EA-2023-DG clade (August 7–13, 2023). In addition, the population density and ringing recapture data of species from the Anatidae family associated with the most distant translocations of EA-2023-DG and captured in Germany and Denmark around the week of the tMRCA according to the Migration Mapping Tool, Bird Flu Radar Tool (*32*), do not contradict the viral lineage movements we reconstructed here. Those observations confirm the continued involvement of an increasing spectrum of wild bird species in the epidemiology of HPAIV.

The spectrum of bird families affected by EA-2023-DG, including Phasianidae, Anatidae, Accipitridae, Falconidae, Strigidae, Tytonidae, Gruidae, and Ardeidae, aligns largely to the host spectrum of genotype EA-2021-AB that donated most of the genome (*2*). A single dead fox was found infected in the core area of EA-2023-DG circulation in northern

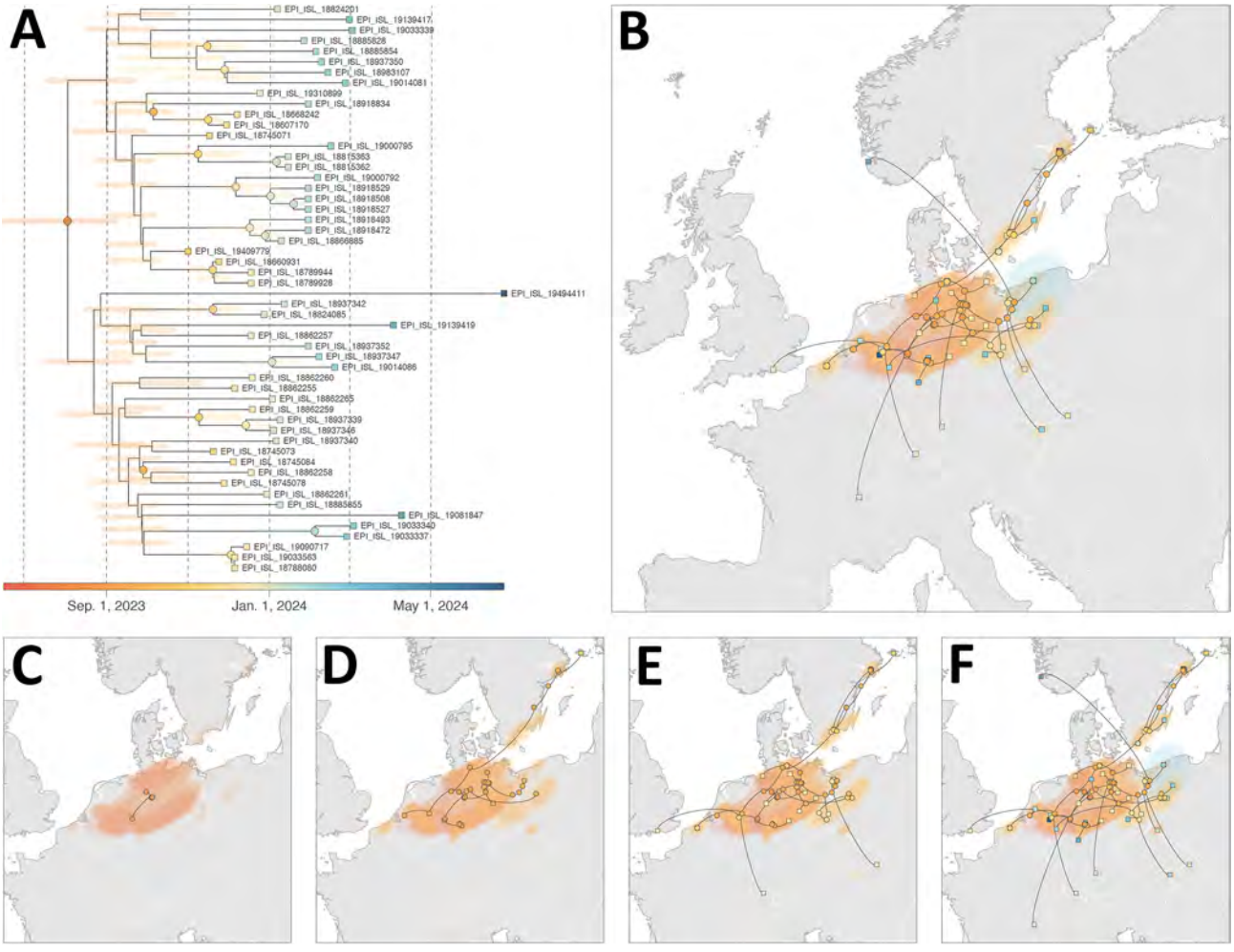

Figure 2. Continuous phylogeographic analysis from study of genesis and spread of novel highly pathogenic avian influenza A(H5N1) clade 2.3.4.4b virus genotype EA-2023-DG reassortant, western Europe. A) Time-scaled maximum clade credibility treeretrieved and annotated from the continuous phylogeographic inference based on analysis of 54 publicly available complete EA-2023-DG genomes and associated sampling metadata from GISAID EpiFlu (http://www.gisaid.org). The tree shows horizontal shaded bars reflecting the 95% highest posterior density (HPD) associated with each internal node age estimate. The tree and HPD estimates are based on 1,000 trees sampled from the posterior distribution of trees and are colored according to time of occurrence; internal nodes are displayed as dots and tip nodes are displayed as squares. Dotted vertical lines correspond to 2-month intervals beginning July 1, 2023. B–F) Phylogeographic reconstruction of EA-2023-DG viral lineages across western Europe. We mapped the MCC tree and 80% HPD regions reflecting the uncertainty related to the Bayesian phylogeographic inference as of June 25, 2024 (B), and for other time points: C) September 1, 2023; D) November 1, 2023; E) January 1, 2024; and F) June 25, 2024. On the maps, the dispersal direction of viral lineages is indicated by the edge curvature in a counterclockwise direction.

Germany, confirming the role of wild carnivores as dead-end hosts of HPAIV clade 2.3.4.4b (*5*). Because of the reassortment event, we could not include ancestral DG precursor genomes in the detailed whole-genome–based phylogeographic reconstruction, resulting in a substantial spatial uncertainty covering the western Baltic Sea shores and North Sea coast of Germany. Another factor that might have contributed to the temporal and spatial uncertainty in our predictions is the lack of standardized surveillance approaches between countries, especially for wildlife surveillance. Our spatially explicit phylogeographic reconstruction highlights continued circulation with a focus in Germany, Poland, and Sweden and sporadic occurrences as far north as central Sweden, as far south as central France, as far west as England, and as far east as Slovakia.

During its period of circulation, EA-2023-DG became the second most frequent (54 cases) genotype in the countries it affected, but EA-2021-AB remained the dominant genotype with 84 reported cases. Other prevalent genotypes were EA-2023-DB (32 cases), EA-2024-DI (26 cases), EA-2022-BB (16 cases), EA-2021-I (14 cases), and EA-2023-DA (13 cases) (*33*,*34*). Ten additional genotypes circulated at lower frequency (<10 cases), reflecting the known diversification potential of H5N1 clade 2.3.4.4b viruses (*2*).

In vivo experiments following up on the emergence of HPAIV H5N1 in cattle in the United States (*35*), and its subsequent spillover to other mammals, including cats (*35*) and exposed humans (*36*), used an EA-2023-DG genotype virus as a model of contemporary circulating viruses in Europe. Those studies indicated that these viruses efficiently replicate in bovine mammary tissue and can produce adaptive mutations (PB2 E627K) during replication (*37*). Those findings underscore the value of phenotypic characterization of currently circulating H5Nx clade 2.3.4.4b viruses, including the newly emerged EA-2023-DG genotype, because the zoonotic potential of the viruses can evolve, driven and shaped by epidemiologic events that could increase the likelihood of spillover to mammals and subsequent adaptation. In response to HPAIV reassortment promiscuity resulting in fast evolution and diversification (*2*,*6*), efficient livestock and wildlife surveillance programs including a viral genomic characterization are essential.

In conclusion, although gaps in surveillance data will always exist, we demonstrated that viral genomic data collected from surveillance programs combined with precise spatial and temporal metadata can enable a comprehensive investigation of the genesis of novel AIV reassortants and of their spread dynamics. In addition to viral genetic characterization, such as adaptive mutations and genotyping, these parameters provide vital clues for informing outbreak prevention and intervention policies.

Acknowledgments

We thank K. De Geest for data curation, and all staff and organizations involved in surveillance activities in the affected countries, including L. Palumbo and the French Biodiversity Agency and I. Mertens and the Federal Agency for the Safety of the Food Chain, Brussels. We also gratefully acknowledge the authors of originating and submitting laboratories for sequences from GISAID's EpiFlu Database used in this research (Appendix 2, https://wwwnc.cdc.gov/EID/article/31/6/24-1870-App2.xlsx).

Influenza A virus genomic sequences used in this study are available in the GISAID EpiFlu database (accession numbers listed in Appendix 1 Table 1; Appendix 2). R scripts related to the preparation and visualization of discrete and continuous phylogeographic analyses are available along with the associated input files at https://github.com/sdellicour/ea-2023-dg_emergence.

Support was provided by the European Commission within the framework of the activities foreseen by the European Union Reference Laboratory for Avian Influenza and Newcastle Disease under grant agreement no. SI2.870510, as well as by the Belgian Federal Public Service Health, Food Chain Safety and Environment under grant agreement no. RT 23/01 FLUCART 1. Support by the European Union under the Horizon Europe programme grant agreement KAPPA-FLU no. 101084171 is also acknowledged. A.P. and A.K.A. acknowledge support by the German Federal Ministry of Education and Research within the project 'PREPMEDVET' grant no. 13N15449. A.C.B., S.R., and B.M. were partially funded by the UK Department for the Environment, Food and Rural Affairs (Defra) and the devolved Scottish and Welsh governments under grant nos. SV3032, SV3400, and SE2227. S.D. acknowledges support from the Fonds National de la Recherche Scientifique (F.R.S.-FNRS, Belgium; grant no. F.4515.22), from the Research Foundation—Flanders (Fonds voor Wetenschappelijk Onderzoek — Vlaanderen, FWO, Belgium; grant no. G098321N), and from the European Union Horizon 2020 projects MOOD (grant agreement no. 874850) and LEAPS (grant agreement no. 101094685). Views and opinions expressed are however those of the author(s) only and do not necessarily reflect those of the European Union or REA. Neither the European Union nor the granting authority can be held responsible for them.

Author contributions: S.V.B.: conceptualization, investigation, formal analysis, methodology, supervision, data curation, writing original draft, writing review, and editing. S.D.: conceptualization, investigation, formal analysis, methodology, visualization, supervision, writing original draft, writing review, and editing. A.K.A., C.B., A.C.B., C.A.B., F.B., Z.D., M.E., A.F., E.G., B.Gj., B.Gr., P.H., A.K., B.L., B.C.M., I.M., A.N., A.P., D.P., S.M.R., S.R., M.Ste., M.Stä., E.S., N.T., M.W., B.Z., S.Z.: investigation, resources, data curation, methodology, writing review, and editing.

About the Author

Dr. Van Borm is a senior scientist at the Avian Virology and Immunology Unit of Sciensano, Brussels, Belgium. His research interests include molecular diagnostics, characterization, and evolution of livestock viruses including avian influenza and Newcastle disease virus.

References

1. Verhagen JH, Fouchier RAM, Lewis N. Highly pathogenic avian influenza viruses at the wild-domestic bird interface in Europe: future directions for research and surveillance. Viruses. 2021;13:212. https://doi.org/10.3390/v13020212
2. Fusaro A, Zecchin B, Giussani E, Palumbo E, Agüero-García M, Bachofen C, et al. High pathogenic avian influenza A(H5) viruses of clade 2.3.4.4b in Europe—why trends of virus evolution are more difficult to predict. Virus Evol. 2024;10:veae027. https://doi.org/10.1093/ve/veae027
3. Smith GJD, Donis RO; World Health Organization/ World Organisation for Animal Health/Food and Agriculture Organization (WHO/OIE/FAO) H5 Evolution Working Group. Nomenclature updates resulting from the evolution of avian influenza A(H5) virus clades 2.1.3.2a, 2.2.1, and 2.3.4 during 2013–2014. Influenza Other Respir Viruses. 2015;9:271–6. https://doi.org/10.1111/irv.12324
4. Antigua KJC, Choi W-S, Baek YH, Song M-S. The emergence and decennary distribution of clade 2.3.4.4 HPAI H5Nx. Microorganisms. 2019;7:156. https://doi.org/10.3390/microorganisms7060156
5. Graziosi G, Lupini C, Catelli E, Carnaccini S. Highly pathogenic avian influenza (HPAI) H5 clade 2.3.4.4b virus infection in birds and mammals. Animals (Basel). 2024;14:1372. https://doi.org/10.3390/ani14091372
6. Kandeil A, Patton C, Jones JC, Jeevan T, Harrington WN, Trifkovic S, et al. Rapid evolution of A(H5N1) influenza viruses after intercontinental spread to North America. Nat Commun. 2023;14:3082. https://doi.org/10.1038/s41467-023-38415-7
7. Lee D-H, Criado MF, Swayne DE. Pathobiological origins and evolutionary history of highly pathogenic avian influenza viruses. Cold Spring Harb Perspect Med. 2021;11:a038679. https://doi.org/10.1101/cshperspect.a038679
8. Peacock T, Moncla L, Dudas G, VanInsberghe D, Sukhova K, Lloyd-Smith JO, et al. The global H5N1 influenza panzootic in mammals. Nature. 2025;637:304–13. https://doi.org/10.1038/s41586-024-08054-z
9. Webby RJ, Uyeki TM. An update on highly pathogenic avian influenza A(H5N1) virus, clade 2.3.4.4b. J Infect Dis. 2024;230:533–42. https://doi.org/10.1093/infdis/jiae379
10. Ahrens AK, Pohlmann A, Grund C, Harder T, Beer M. Novel genotypes of highly pathogenic avian influenza H5N1 clade 2.3.4.4b viruses, Germany, November 2023. Emerg Infect Dis. 2024;30:1737–9. https://doi.org/10.3201/eid3008.240103
11. Adlhoch C, Fusaro A, Gonzales JL, Kuiken T, Mirinavičiūtė G, Niqueux É, et al.; European Food Safety Authority; European Centre for Disease Prevention and Control; European Union Reference Laboratory for Avian Influenza. Avian influenza overview September–December 2023. EFSA J. 2023;21:e8539.
12. Katoh K, Standley DM. MAFFT multiple sequence alignment software version 7: improvements in performance and usability. Mol Biol Evol. 2013;30:772–80. https://doi.org/10.1093/molbev/mst010
13. Nguyen L-T, Schmidt HA, von Haeseler A, Minh BQ. IQ-TREE: a fast and effective stochastic algorithm for estimating maximum-likelihood phylogenies. Mol Biol Evol. 2015;32:268–74. https://doi.org/10.1093/molbev/msu300
14. Kalyaanamoorthy S, Minh BQ, Wong TKF, von Haeseler A, Jermiin LS. ModelFinder: fast model selection for accurate phylogenetic estimates. Nat Methods. 2017;14:587–9. https://doi.org/10.1038/nmeth.4285
15. Bruen TC, Philippe H, Bryant D. A simple and robust statistical test for detecting the presence of recombination. Genetics. 2006;172:2665–81. https://doi.org/10.1534/genetics.105.048975
16. Huson DH. SplitsTree: analyzing and visualizing evolutionary data. Bioinformatics. 1998;14:68–73. https://doi.org/10.1093/bioinformatics/14.1.68
17. Martin DP, Murrell B, Golden M, Khoosal A, Muhire B. RDP4: detection and analysis of recombination patterns in virus genomes. Virus Evol. 2015;1:vev003. https://doi.org/10.1093/ve/vev003
18. Lemey P, Rambaut A, Drummond AJ, Suchard MA. Bayesian phylogeography finds its roots. PLOS Comput Biol. 2009;5:e1000520. https://doi.org/10.1371/journal.pcbi.1000520
19. Suchard MA, Lemey P, Baele G, Ayres DL, Drummond AJ, Rambaut A. Bayesian phylogenetic and phylodynamic data integration using BEAST 1.10. 1. Virus Evol. 2018;4:vey016. https://doi.org/10.1093/ve/vey016
20. Goldman N, Yang Z. A codon-based model of nucleotide substitution for protein-coding DNA sequences. Mol Biol Evol. 1994;11:725–36.
21. Drummond AJ, Ho SYW, Phillips MJ, Rambaut A. Relaxed phylogenetics and dating with confidence. PLoS Biol. 2006;4:e88. https://doi.org/10.1371/journal.pbio.0040088
22. Gill MS, Lemey P, Faria NR, Rambaut A, Shapiro B, Suchard MA. Improving Bayesian population dynamics inference: a coalescent-based model for multiple loci. Mol Biol Evol. 2013;30:713–24. https://doi.org/10.1093/molbev/mss265
23. Rambaut A, Drummond AJ, Xie D, Baele G, Suchard MA. Posterior summarization in Bayesian phylogenetics using Tracer 1.7. Syst Biol. 2018;67:901–4. https://doi.org/10.1093/sysbio/syy032
24. Lemey P, Rambaut A, Welch JJ, Suchard MA. Phylogeography takes a relaxed random walk in continuous space and time. Mol Biol Evol. 2010;27:1877–85. https://doi.org/10.1093/molbev/msq067
25. Pybus OG, Suchard MA, Lemey P, Bernardin FJ, Rambaut A, Crawford FW, et al. Unifying the spatial epidemiology and molecular evolution of emerging epidemics. Proc Natl Acad Sci U S A. 2012;109:15066–71. https://doi.org/10.1073/pnas.1206598109

26. Dellicour S, Gill MS, Faria NR, Rambaut A, Pybus OG, Suchard MA, et al. Relax, keep walking—a practical guide to continuous phylogeographic inference with BEAST. Mol Biol Evol. 2021;38:3486–93. https://doi.org/10.1093/molbev/msab031
27. Dellicour S, Rose R, Pybus OG. Explaining the geographic spread of emerging epidemics: a framework for comparing viral phylogenies and environmental landscape data. BMC Bioinformatics. 2016;17:82. https://doi.org/10.1186/s12859-016-0924-x
28. Dellicour S, Rose R, Faria NR, Lemey P, Pybus OG. SERAPHIM: studying environmental rasters and phylogenetically informed movements. Bioinformatics. 2016;32:3204–6. https://doi.org/10.1093/bioinformatics/btw384
29. Trovão NS, Suchard MA, Baele G, Gilbert M, Lemey P. Bayesian inference reveals host-specific contributions to the epidemic expansion of influenza A H5N1. Mol Biol Evol. 2015;32:3264–75. https://doi.org/10.1093/molbev/msv185
30. Layan M, Dacheux L, Lemey P, Brunker K, Ma L, Troupin C, et al. Uncovering the endemic circulation of rabies in Cambodia. Mol Ecol. 2023;32:5140–55. https://doi.org/10.1111/mec.17087
31. Van Borm S, Boseret G, Dellicour S, Steensels M, Roupie V, Vandenbussche F, et al. Combined phylogeographic analyses and epidemiologic contact tracing to characterize atypically pathogenic avian influenza (H3N1) epidemic, Belgium, 2019. Emerg Infect Dis. 2023;29:351–9. https://doi.org/10.3201/eid2902.220765
32. Gargallo G, Davies JG, Faverjon C, Kampichler C, Baillie SR, Cameron A, et al. Development of a prototype early warning system for avian influenza in the EU based on risk-mapping. EFSA Support Publ. 2022;19:7762E. https://doi.org/10.2903/sp.efsa.2022.EN-7762
33. European Food Safety Authority; European Centre for Disease Prevention and Control; European Union Reference Laboratory for Avian Influenza; Fusaro A, Gonzales JL, Kuiken T, Mirinavičiūtė G, Niqueux É, Ståhl K, et al. Avian influenza overview December 2023–March 2024. EFSA J. 2024;22:e8754. https://doi.org/10.2903/j.efsa.2024.8754
34. European Food Safety Authority; European Centre for Disease Prevention and Control; European Union Reference Laboratory for Avian Influenza; Alexakis L, Fusaro A, Kuiken T, Mirinavičiūtė G, Ståhl K, Staubach C, et al. Avian influenza overview March–June 2024. EFSA J. 2024;22:e8930. https://doi.org/10.2903/j.efsa.2024.8930
35. Burrough ER, Magstadt DR, Petersen B, Timmermans SJ, Gauger PC, Zhang J, et al. Highly pathogenic avian influenza A(H5N1) clade 2.3.4.4b virus infection in domestic dairy cattle and cats, United States, 2024. Emerg Infect Dis. 2024;30:1335–43. https://doi.org/10.3201/eid3007.240508
36. Garg S, Reed C, Davis CT, Uyeki TM, Behravesh CB, Kniss K, et al. Outbreak of highly pathogenic avian influenza A(H5N1) viruses in U.S. dairy cattle and detection of two human cases—United States, 2024. MMWR Morb Mortal Wkly Rep. 2024;73:501–5. https://doi.org/10.15585/mmwr.mm7321e1
37. Halwe NJ, Cool K, Breithaupt A, Schön J, Trujillo JD, Nooruzzaman M, et al. H5N1 clade 2.3.4.4b dynamics in experimentally infected calves and cows. Nature. 2025;637:903–12. https://doi.org/0.1038/s41586-024-08063-y

Address for correspondence: Steven Van Borm, Sciensano, Avian Virology and Immunology, Groeselenberg 99, B1180 Ukkel, Brussels B1180, Belgium; email:steven.vanborm@sciensano.be

Characterization of Adult and Pediatric Healthcare-Associated and Community-Associated *Clostridioides difficile* Infections, Canada, 2015–2022

Tim Du, Anada Silva, Kelly B. Choi, Cassandra Lybeck, George R. Golding, Romeo Hizon, Sean Ahmed, Nicole Anderson, Suzanne Bakai-Anderson, Blanda Chow, Ian Davis, Meghan Engbretson, Gerald A. Evans, Charles Frenette, Matthew Garrod, Jennie Johnstone, Kevin C. Katz, Pamela Kibsey, Joanne M. Langley, Jenine Leal, Jenna Leamon, Bonita E. Lee, Diane Lee, Yves Longtin, Dominik Mertz, Jessica Minion, Ericka Oates, Michelle Science, Jocelyn A. Srigley, Kathryn N. Suh, Nisha Thampi, Reena Titoria, Kristen Versluys, Alice Wong, Jeannette L. Comeau, Susy S. Hota

We investigated epidemiologic and molecular characteristics of healthcare-associated (HA) and community-associated (CA) *Clostridioides difficile* infection (CDI) among adult and pediatric patients in Canadian Nosocomial Infection Surveillance Program hospitals during 2015–2022. Of 30,824 reported CDI cases, 94.9% (29,250/30,824) were among adult (73.2% HA; 26.8% CA) and 5.1% (1,574/30,824) pediatric (77.6% HA; 22.4% CA) patients. During the study period, adult HA CDI rates decreased by 19.9% and CA CDI rates remained stable; pediatric HA CDI rates decreased by 29.6% and CA CDI decreased by 58.3%. Ribotype (RT) 106 was most common among both groups and replaced RT027 as the predominant strain type. RT027 was most associated with adult patients, HA acquisition, severe CDI, and severe outcomes. Moxifloxacin resistance was higher in adult than pediatric cases; clindamycin and rifampin resistance rates were similar between groups. Continued national surveillance is integral to understanding the epidemiology of adult and pediatric CDI in Canada and informing prevention efforts.

Clostridioides difficile, a gram-positive, spore-forming anaerobe, is the leading cause of healthcare-associated (HA) diarrhea in high-income countries (*1*). Disease manifestations can range from asymptomatic colonization to pseudomembranous colitis, toxic megacolon, and death (*2*). In the past 2 decades, *C. difficile* has become a major public health concern; the Public Health Agency of Canada and the US Centers for Disease Control and Prevention declared it an urgent health threat in 2019 (*3*,*4*). Healthcare

Author affiliations: National Microbiology Laboratory, Winnipeg, Manitoba, Canada (T. Du, G.R. Golding, R. Hizon, S. Ahmed); Public Health Agency of Canada, Ottawa, Ontario, Canada (A. Silva, K.B. Choi, C. Lybeck, D. Lee); Alberta Health Services, Calgary, Alberta, Canada (N. Anderson, B. Chow, J. Leal, E. Oates); Hamilton Health Sciences, Hamilton, Ontario, Canada (S. Bakai-Anderson, D. Mertz); Queen Elizabeth II Health Sciences Centre, Halifax, Nova Scotia, Canada (I. Davis); Children's Hospital of Eastern Ontario, Ottawa (M. Engbretson, N. Thampi); Kingston Health Sciences Centre, Kingston, Ontario, Canada (G.A. Evans); McGill University Health Centre, Montreal, Quebec, Canada (C. Frenette); Fraser Health Authority, Vancouver, British Columbia, Canada (M. Garrod); Sinai Health, Toronto, Ontario, Canada (J. Johnstone); North York General Hospital, Toronto (K.C. Katz); Royal Jubilee Hospital, Victoria, British Columbia, Canada (P. Kibsey); IWK Health Centre, Halifax (J.M. Langley); Western Health Authority, Corner Brook, Newfoundland, Canada (J. Leamon); Stollery Children's Hospital, Edmonton, Alberta, Canada (B.E. Lee); Jewish General Hospital, Montreal (Y. Longtin); Regina General Hospital, Regina, Saskatchewan, Canada (J. Minion); The Hospital for Sick Children, Toronto (M. Science); BC Children's & Women's Hospitals, Vancouver (J.A. Srigley); The Ottawa Hospital, Ottawa (K.N. Suh); Provincial Health Services Authority, Vancouver (R. Titoria); Interior Health Authority, Kelowna, British Columbia, Canada (K. Versluys); Royal University Hospital, Saskatoon, Saskatchewan, Canada (A. Wong); Dalhousie University, Halifax (J.L. Comeau); University Health Network, Toronto (S.S. Hota)

DOI: https://doi.org/10.3201/eid3106.250182

costs for treating *C. difficile* infection (CDI) are substantial, and recurrent episodes further complicate case management (*5*,*6*).

Although some countries have reported increased incidence of HA or community-associated (CA) CDI, the paucity of global data primarily focuses on CDI in adult rather than pediatric populations (*7*,*8*). Studies suggest that pediatric CDI is more likely to be community-associated and have rapid onset and shorter and less complicated infections, whereas illness in adults is characterized by more complicated and severe disease, increased recurrence rates because of more underlying conditions, and risk for infection with hypervirulent strain NAP1/027/BI (*9*,*10*).

Here, we contrast findings of adult and pediatric HA and CA CDI identified in a multicenter study in Canada evaluating incidence, patient characteristics, outcomes, ribotype (RT) prevalence, and antimicrobial resistance during 2015–2022. We also evaluate associations between predominant *C. difficile* RTs and all-cause and CDI-attributable deaths.

Methods

Data Sources and Collection

Hospitals participating in the Canadian Nosocomial Infection Surveillance Program (CNISP) have conducted prospective surveillance for HA CDI in hospitalized patients in Canada since 2007 and CA CDI since 2015. By 2022, CNISP encompassed a network of 88 acute-care hospitals across 10 provinces and 1 territory, representing 35% of all acute-care beds in Canada (*11*). We analyzed data collected during 2015–2022 from adult, pediatric, and mixed (adult and pediatric) hospitals. Stool samples, severity indicators, and outcomes were collected during a 2-month targeted surveillance period (March–April) each year for adult patients and year-round for pediatric patients. We included adult and pediatric patients from mixed hospitals in age-specific CDI rate calculations if age-specific denominators were available. Data were collected through the Canadian Network for Public Health Intelligence platform; we verified clinical and laboratory surveillance data to ensure accuracy, as previously described (*12*).

Case Definition

We used previously described case definitions for primary CDI (*13*). We defined HA CDI as laboratory confirmation of CDI accompanied by compatible clinical symptoms developing ≥72 hours after admission, or <72 hours after admission if the patient had a previous hospital admission and was discharged within the previous 4 weeks. We defined CA CDI as onset of CDI symptoms <72 hours after admission with no history of hospitalization or healthcare exposure, including outpatient healthcare exposures, within the previous 12 weeks.

A severe CDI case was an albumin level <30 g/L, leukocyte count ≥15×10^9/L, or both. Severe outcomes were CDI-attributable admission to an intensive care unit (ICU), colectomy, or death ≤30 days after first *C. difficile*–positive specimen, where CDI was the cause of or contributed to death. All deaths were reviewed by an infectious disease physician or medical microbiologist to determine whether deaths were CDI-attributable, as defined in our published protocol (*14*).

Laboratory Methods

Hospitals sent stool samples to the National Microbiology Laboratory (NML; Winnipeg, MB, Canada) for *C. difficile* isolation and molecular characterization. We performed *C. difficile* isolation by using an ethanol shock treatment, then selection on *C. difficile* Moxalactam Norfloxacin agar (Oxoid, https://www.oxoid.com) (*15*,*16*). We prepared DNA for PCR analysis and ribotyping by using InstaGene Matrix (Bio-Rad Laboratories, https://www.bio-rad.com) (*16*). We performed multiplex PCR targeting toxin A (*tcdA*), toxin B (*tcdB*), binary toxin (*cdtB*), negative regulator of toxin production (*tcdC*), and triose phosphate isomerase (*tpi*) housekeeping genes (*17*). We performed capillary gel electrophoresis–based ribotyping and RT assignment as previously described (*18*,*19*).

We used Etest strips (bioMérieux, https://www.biomerieux.com) to perform susceptibility testing for metronidazole, clindamycin, vancomycin, rifampin, moxifloxacin, and tigecycline, as previously described (*16*,*20*). We interpreted antimicrobial resistance in accordance with published guidelines (*20*).

Statistical Analysis

We calculated HA CDI incidence rates as number of cases per 10,000 patient-days and CA CDI incidence rates as number of cases per 1,000 patient admissions. We conducted a sensitivity analysis, restricting our analysis to hospitals participating in the entire 8-year surveillance period. We used the Cochran-Armitage test for categorical variables and the Mann-Kendall test for continuous variables to assess statistically significant trends over time for patient characteristics and outcome results. To compare characteristics between adult and pediatric patients, we used χ^2 test for categorical variables and Student *t*-test or Wilcoxon rank-sum test for continuous variables. Denominators for individual case characteristics

vary because we excluded missing or unknown values from the analysis.

We used multivariable logistic regression to model factors associated with select CDI strains (RT027 and RT106) and a severe CDI outcome and adjusted for a priori–selected confounders of age group, sex, severe CDI, and CDI case type (i.e., HA vs. CA). We used 2-tailed statistical tests and considered $p \leq 0.05$ significant. We performed all analyses in R version 4.3.0 (The R Project for Statistical Computing, https://www.r-project.org).

Results

The study encompassed 30,824 inpatient cases of primary CDI from CNISP during 2015–2022. Adult CDI accounted for 94.9% (n = 29,250) and pediatric CDI for 5.1% (n = 1,574) of cases. Among adult patients, HA CDI accounted for 73% (n = 21,405) and CA CDI for 27% (n = 7,845) of cases. Among pediatric patients, HA CDI accounted for 78% (n = 1,222) and CA CDI for 22% (n = 352) of cases. Hospital participation varied by age group and case type throughout the study period (Appendix 1 Table 1, https://wwwnc.cdc.gov/EID/article/31/6/25-0182-App1.pdf).

During 2015–2022, adult HA CDI rates decreased by 19.9%, from 4.83 to 3.87 cases/10,000 patient-days (p = 0.006), whereas CA CDI rates remained stable, ranging from 1.39 to 1.75 cases/1,000 admissions. Pediatric HA CDI rates decreased by 29.6%, from 4.52 to 3.18 cases/10,000 patient-days (p = 0.003), and CA CDI rates decreased by 58.3%, from 0.84 to 0.35 cases/1,000 admissions (p = 0.0133) (Figure 1).

Regionally, adult HA CDI rates decreased significantly in the central (27.4%; p = 0.003) and western (20.8%; p = 0.003) regions of Canada, but rates increased by 34% in the eastern region (p = 0.0478) (Figure 2). Pediatric HA CDI rates significantly decreased by 54.7% (p = 0.0065) in the western region, but central and eastern region rates fluctuated. Pediatric CA CDI rates decreased significantly by 65.3% (p = 0.0178) in the western region, but eastern region rates fluctuated from 0.19 to 0.58 cases/1,000 admissions after an

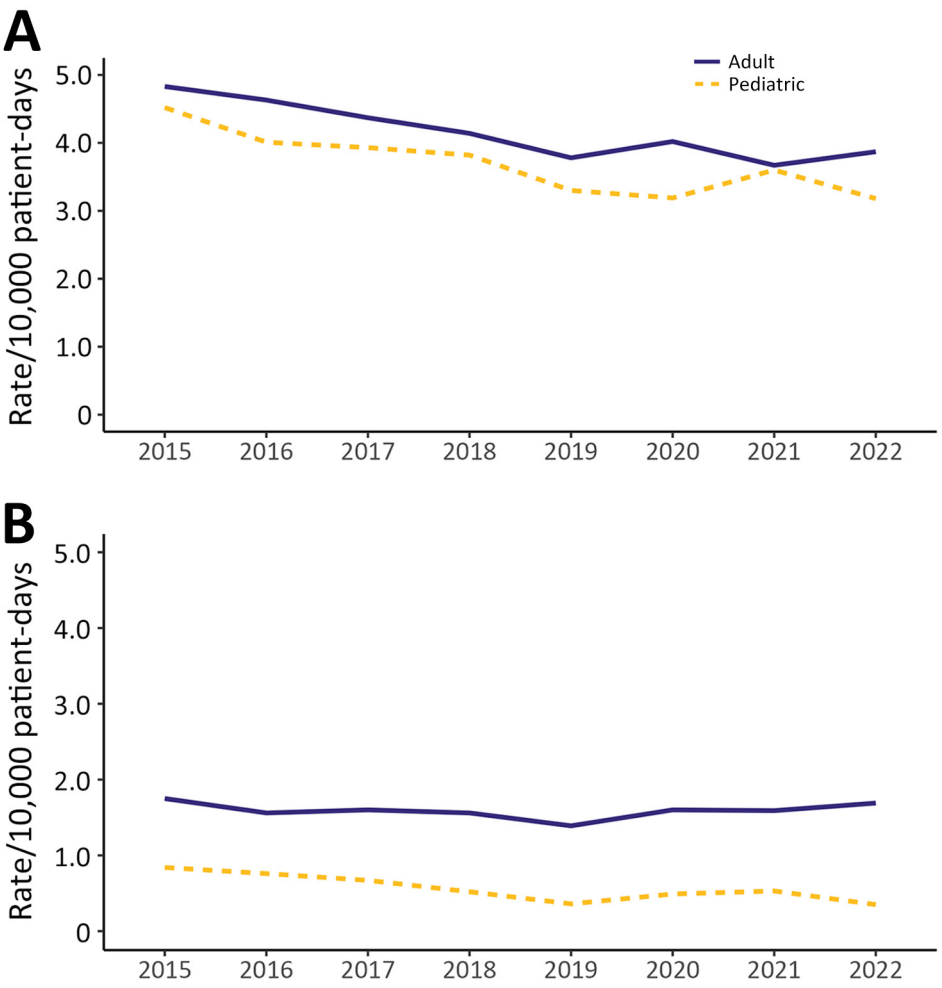

Figure 1. National adult and pediatric healthcare-associated and community-associated *Clostridioides difficile* infection (CDI) rates, Canada, 2015–2022. A) Healthcare-associated CDI; B) community-associated CDI.

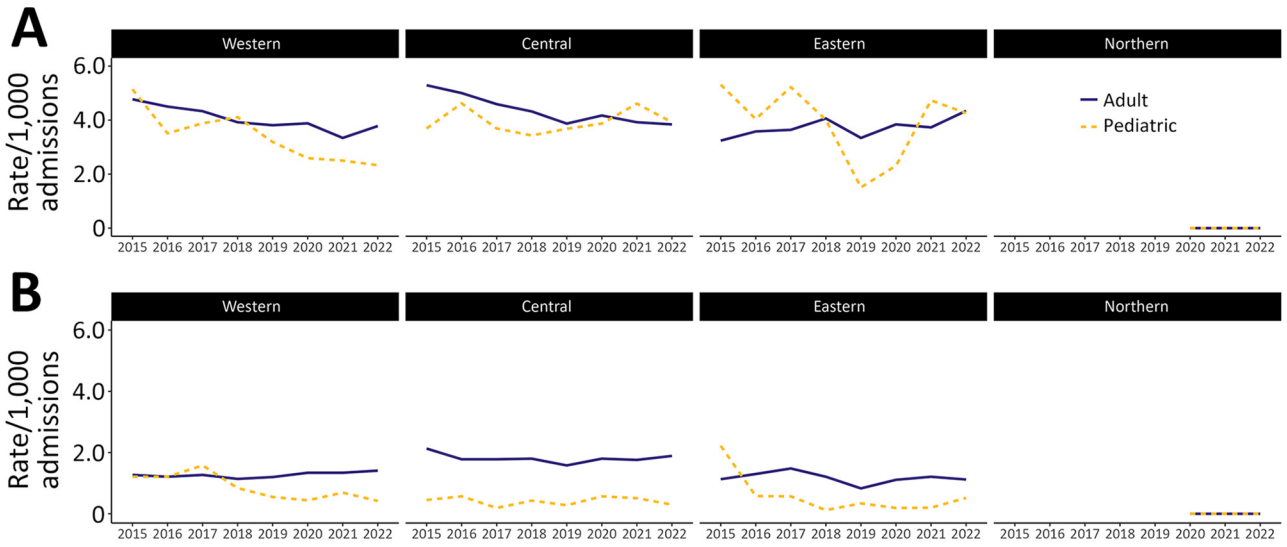

Figure 2. Regional adult and pediatric healthcare-associated and community-associated *Clostridioides difficile* infection (CDI) rates, Canada, 2015–2022. A) Healthcare-associated CDI; B) community-associated CDI. Western region includes British Columbia, Alberta, Saskatchewan, and Manitoba; Central region includes Ontario and Quebec; Eastern region includes Nova Scotia, New Brunswick, Prince Edward Island, and Newfoundland and Labrador. Northern region is Nunavut. The Northern region has reported 0 cases of CDI since they started conducting surveillance in 2020.

initial decrease from 2.22 cases/1,000 admissions in 2015. Sensitivity analyses that restricted analysis to hospitals participating for the entire study period by region for adult and pediatric surveillance and those that conducted both HA and CA CDI surveillance yielded no statistically significant differences (data not shown).

Clinical Manifestations

We aggregated patient characteristics and outcomes by age group (adult and pediatric) and case type (Tables 1, 2). For HA CDI, fewer pediatric than adult patients were female (45% vs. 49%; p = 0.024), but differences between pediatric and adult CA CDI were not statistically significant for female sex (49% vs. 55%; p = 0.07). Adults with HA CDI were significantly older than adults with CA CDI (70 [interquartile range (IQR) 59–81] vs. 67 [IQR 54–78] years; p<0.0001). Pediatric patients with CA CDI were older than those with HA CDI (10 [IQR 3–13] vs. 7 [IQR 4–15] years; p=0.0007). For HA CDI, the median days from admission to infection were longer in adult (10 [IQR 5–21] days) than pediatric patients (7 [IQR 2–15] days) (p<0.001). Adult patients experienced significantly longer hospital stays for HA CDI than did pediatric patients (15 [IQR 9–24] vs. 9 [IQR 5–18] days for HA CDI, 7 [IQR 4–13] vs. 5 [IQR 2–8] days for CA CDI; p<0.001 for both). Regardless of acquisition type, metronidazole was the drug most used to treat CDI among pediatric patients and vancomycin was most common among adult patients. Fecal microbiota transplantation referral was uncommon among adult and pediatric patients.

Ribotyping Analysis

Of 30,824 cases with linked epidemiologic data, NML successfully characterized 4,622 (3,560 adult, 1,062 pediatric) samples that met study criteria. Of 3,560 adult samples analyzed, 74.7% (2,659/3,560) were HA CDI and 25.3% (901/3,560) were CA CDI, and we identified 241 unique RTs.

The most common adult RTs were RT106 (11.9% HA, 13.2% CA), RT027 (13.2% HA, 5.9% CA), RT014 (9.1% HA, 8.0% CA), RT020 (6.7% HA, 8.4% CA), and RT002 (5.8% HA, 5.3% CA) (Figure 3). The 20 most common adult CDI RTs accounted for 73.9% of isolates tested (Appendix 1 Figure 1). Among adult CDI cases, RT027 rates decreased from 21.9% in 2015 to 3.2% in 2022 (p = 0.003). RT106 rates fluctuated over the study period but increased overall from 7.1% in 2015 to 15.8% in 2022. During 2015–2022, RT106 replaced RT027 as the predominant strain type and had an overall combined prevalence of 12.2% (434/3,560).

Of 1,062 pediatric samples analyzed, 834 (78.5%) were HA CDI and 228 (21.5%) were CA CDI, and we identified 145 unique RTs. The most common RTs among pediatric CDI cases were RT106 (17.0% HA, 13.2% CA), RT020 (8.2% HA, 11.4% CA), RT014 (7.9% HA, 9.2% CA), RT056 (4.4% HA, 4.0% CA), and RT002 (4.4% HA, 3.1% CA) (Figure 4). The 20

Table 1. Characteristics of adult and pediatric healthcare-associated *Clostridioides difficile* infections, Canada, 2015–2022*

Characteristics	Overall, n = 22,627	Adult cases, n = 21,405	Pediatric cases, n = 1,222	p value†
Median age, y (IQR)	69 (56–80)	70 (59–81)	7 (3–13)	
Sex				**0.024**
F	10,994/22,625 (49)	10,445/21,404 (49)	549/1,221 (45)	
M	11,631/22,625 (51)	10,959/21,404 (51)	672/1,221 (55)	
Median days from admission to infection (IQR)	10 (4–21)	10 (5–21)	7 (2–15)	**<0.001**
Median length of stay, d (IQR)	14 (7–23)	15 (9–24)	9 (5–18)	**<0.001**
Treatment				NA
Metronidazole	6,377/18,907 (34)	5,818/17,947 (32)	559/960 (58)	
Vancomycin	10,876/18,907 (58)	10,588/17,947 (59)	288/960 (30)	
Metronidazole and vancomycin	982/18,907 (5.2)	957/17,947 (5.3)	25/960 (2.6)	
Fidaxomicin	22/18,907 (0.1)	22/17,947 (0.1)	0/960 (0)	
Other	186/18,907 (1.0)	170/17,947 (0.9)	16/960 (1.7)	
No treatment	464/18,907 (2.5)	392/17,947 (2.2)	72/960 (7.5)	
FMT referral	17/9,825 (0.2)	17/9,318 (0.2)	0/507 (0)	>0.9
30-day outcomes‡				
Loop ileostomy§	14/2,413 (0.6)	14/1,816 (0.8)	0/597 (0)	**0.028**
All-cause mortality	416/4,429 (9.4)	399/3,454 (12)	17/975 (1.7)	**<0.001**
Severe outcome¶	205/4,232 (4.8)	180/3,270 (5.5)	25/962 (2.6)	**<0.001**
ICU admission for CDI complications	73/4,448 (1.6)	61/3,477 (1.8)	12/971 (1.2)	0.3
Colectomy	62/4,296 (1.4)	50/3,329 (1.5)	12/967 (1.2)	0.5
CDI-attributable death	99/405 (24)	98/388 (25)	1/17 (5.9)	0.084
CDI recurrence#				
Recurrence	223/2,709 (8.2)	205/2,514 (8.2)	18/195 (9.2)	0.6
Median days from primary infection to recurrence (IQR)	29 (21–40)	29 (21–41)	26 (22–30)	0.4
Recurrence length of stay, d (IQR)	10 (6–19)	10 (6–16)	30 (30–30)	0.2
Recurrence FMT referral	0/81	0/79	0/2	NA
Recurrence loop ileostomy	1/81 (1.2)	1/78 (1.3)	0/3	>0.9
Recurrence all-cause mortality	16/189 (8.5)	16/177 (9.0)	0/12	0.6
Recurrence severe outcome¶	8/186 (4.3)	8/174 (4.6)	0/12	>0.9
ICU admission for recurrent CDI complications	3/198 (1.5)	3/185 (1.6)	0/13	>0.9
Recurrence-attributable death	5/16 (31)	5/16 (31)	0	NA
Recurrence colectomy	1/196 (0.5)	1/183 (0.5)	0/13	>0.9

*Values are no. cases/no. in category (%) except as indicated. Denominators for individual case characteristic vary because missing or unknown values were excluded from the analysis. Bold font indicates statistical significance. CDI, *C. difficile* infection; FMT, fecal microbiota transplant; ICU, intensive care unit; IQR, interquartile range; NA, not applicable.
†p value determined by Wilcoxon rank-sum test, Fisher exact test, or Pearson χ^2 test.
‡Outcome data were collected during March–April of each calendar year for adult patients and year-round for pediatric patients.
§Loop ileostomy added in 2018.
¶Severe outcome was defined as CDI-attributable admission to an intensive care unit, colectomy, or death within 30 d of positive *C. difficile* specimen where CDI was the cause of death or contributed to death.
#Adult and pediatric cases identified during March–April of each calendar year were followed prospectively for 8 weeks for recurrence.

most prevalent pediatric RTs accounted for 74.6% of isolates tested (Appendix 1 Figure 2). RT106 rates increased from 13.3% in 2015 to 16.8% in 2021 and decreased to 8.8% in 2022 (p = 0.02). In contrast to adult cases, RT027 prevalence was lower in pediatric cases (average 3.2%) and fluctuated throughout the study period.

Prevalence of livestock-associated strains RT078 and RT126 averaged 2.8% (range 1.8%–5.8%) among adult CDI cases. Among pediatric CDI cases, those strains averaged 2.1% (range 1.1%–3.8%) (Appendix 1 Table 2).

Clinical Outcomes

Of the 30,824 cases analyzed, 19.1% (n = 5,902) had outcome data available for adult (n = 4,715) and pediatric (n = 1,265) patients. Overall, the 30-day all-cause mortality rate was 10.6% (494/4,655) for adult patients, and 26.8% (128/477) of those deaths were directly or indirectly attributable to CDI. HA CDI comprised most adult all-cause (80.8%; 399/494) and CDI-attributable (76.6%; 98/128) deaths. We noted no major differences in adult CDI-attributable death by sex or older age (data not shown). In contrast, 1.4% (17/1,247) of pediatric CDI patients died of any cause at 30 days, and only 1 death was CDI-attributable and was HA CDI. We noted no statistically significant differences in all-cause death by age group (1 to <2 years of age: 2.9% [4/139]; 2 to <12 years of age: 1.2% [8/676]; 12 to <18 years of age: 1.2% [5/432]; p = 0.3) (data not shown).

Comparing acquisition types, pediatric patients had significantly lower all-cause mortality rates than adult patients for HA CDI (1.7% vs. 12%; p<0.001) and CA CDI (0 vs. 7.9%; p<0.001) (Tables 1, 2). We observed no significant differences in ICU admission resulting from CDI complications between adult and pediatric patients for either acquisition type.

Of 5,686 cases with available data, 5.4% (242/4,454) of adult cases and 2.8% (34/1,232) of pediatric cases had a severe CDI-related outcome ≤30 days after the first *C. difficile*–positive specimen. More adult than pediatric patients experienced a severe outcome for HA CDI (12% vs. 1.7%; p<0.001), but we noted no statistically significant difference for CA CDI (5.2% adult vs. 3.3% pediatric; p = 0.2) (Tables 1, 2).

Compared with patients with non-RT027 CDI, patients with RT027 had adjusted odds of 2.15 (95% CI 1.63–2.90; p<0.0001) times higher for severe CDI and of 1.93 (95% CI 1.31–2.90; p = 0.0005) times higher for CDI-related severe outcome (Table 3). In addition, RT027 patients had much higher odds of being adult than pediatric and of having HA rather than CA CDI. In contrast, RT106 strains were less likely to be associated with adult cases, but we found no evidence of association with severe CDI outcomes compared with non-RT106 strains.

CDI Recurrence

Rates of recurrent CDI within 8 weeks of the first positive specimen were similar in adult (7.9%) and pediatric (7.2%) patients (p = 0.6). Median time from primary infection to recurrence was 29 (IQR 22–40) days, and we noted no major difference between adult and pediatric patients (data not shown). We noted no statistically significant differences in recurrence by age group (Tables 1, 2); however, pediatric recurrence was significantly higher for HA CDI (9.2%; 18/195) than CA CDI (2.4%; 2/84) (p = 0.04), and adult recurrence was similar, 8.2% (205/2,514) for HA and 7.4% (79/1,065) for CA (p = 0.5) (data not shown). Among cases with recurrent outcome data (n = 247), 9 (3.6%) had severe outcomes; all were adult patients.

Antimicrobial Susceptibility

We conducted antimicrobial resistance testing for isolates collected during 2015–2022 (Appendix 2 Tables

Table 2. Characteristics of adult and pediatric community-associated *Clostridioides difficile* infections, Canada, 2015–2022*

Characteristics	Overall, n = 8,197	Adult cases, n = 7,845	Pediatric cases, n = 352	p value†
Median age, y (IQR)	66 (52–78)	67 (54–79)	10 (4–15)	
Sex				
F	4,525/8,197 (55)	4,351/7,845 (55)	174/352 (49)	0.070
M	3,672/8,197 (45)	3,494/7,845 (45)	178/352 (51)	
Median length of stay, d (IQR)	7 (4, 12)	7 (4, 13)	5 (2, 8)	**<0.001**
Treatment				NA
Metronidazole	2,264/7,497 (30)	2,100/7,225 (29)	164/272 (60)	
Vancomycin	4,515/7,497 (60)	4,441/7,225 (61)	74/272 (27)	
Metronidazole and vancomycin	448/7,497 (6.0)	436/7,225 (6.0)	12/272 (4.4)	
Fidaxomicin	7/7,497 (<0.1)	7/7,225 (<0.1)	0/272	
Other	72/7,497 (1.0)	72/7,225 (1.0)	0/272	
No treatment	191/7,497 (2.5)	169/7,225 (2.3)	22/272 (8.1)	
FMT referral	13/4,360 (0.3)	13/4,228 (0.3)	0/132	>0.9
30-day outcomes‡				
Loop ileostomy§	8/874 (0.9)	8/730 (1.1)	0/144	0.4
All-cause mortality	5/1,473 (6.4)	95/1,201 (7.9)	0/272	**<0.001**
Severe outcome¶	71/1,454 (4.9)	62/1,184 (5.2)	9/270 (3.3)	0.2
ICU admission for CDI complications	27/1,482 (1.8)	22/1,203 (1.8)	5/279 (1.8)	>0.9
Colectomy	23/1,470 (1.6)	19/1,193 (1.6)	4/277 (1.4)	>0.9
CDI-attributable death	30/89 (34)	30/89 (34)	0	NA
CDI recurrence#				
Recurrence	81/1,149 (7.0)	79/1,065 (7.4)	2/84 (2.4)	0.083
Median days from primary infection to recurrence (IQR)	29 (23–38)	29 (23–38)	36 (36–36)	0.5
Recurrence length of stay, d (IQR)	9 (5, 17)	9 (5, 17)	NA	NA
Recurrence FMT referral	0/35	0/34	0/1	NA
Recurrence loop ileostomy	0/37	0/36	0/1	NA
Recurrence all-cause mortality	3/67 (4.5)	3/66 (4.5)	0/1	>0.9
Recurrence severe outcome¶	1/61 (1.6)	1/61 (1.6)	0	NA
ICU admission for recurrent CDI complications	0/69	0/69	0	NA
Recurrence-attributable death	1/2 (50)	1/2 (50)	0	NA
Recurrence colectomy	0/68	0/67	0/1	NA

*Values are no. cases/no. in category (%) except as indicated. Denominators for individual case characteristic vary because missing or unknown values were excluded from the analysis. Bold font indicates statistical significance. CDI, *C. difficile* infection; FMT, fecal microbiota transplant; ICU, intensive care unit; IQR, interquartile range; NA, not applicable.
†p value determined by Wilcoxon rank-sum test, Fisher exact test, or Pearson χ^2 test.
‡Outcome data was collected during March–April of each calendar year for adult patients and year-round for pediatric patients.
§Loop ileostomy added in 2018.
¶Severe outcome was defined as CDI-attributable admission to an intensive care unit, colectomy, or death within 30 d of positive *C. difficile* specimen where CDI was the cause of death or contributed to death.
#Adult and pediatric cases identified during March–April of each calendar year were followed prospectively for 8 weeks for recurrence.

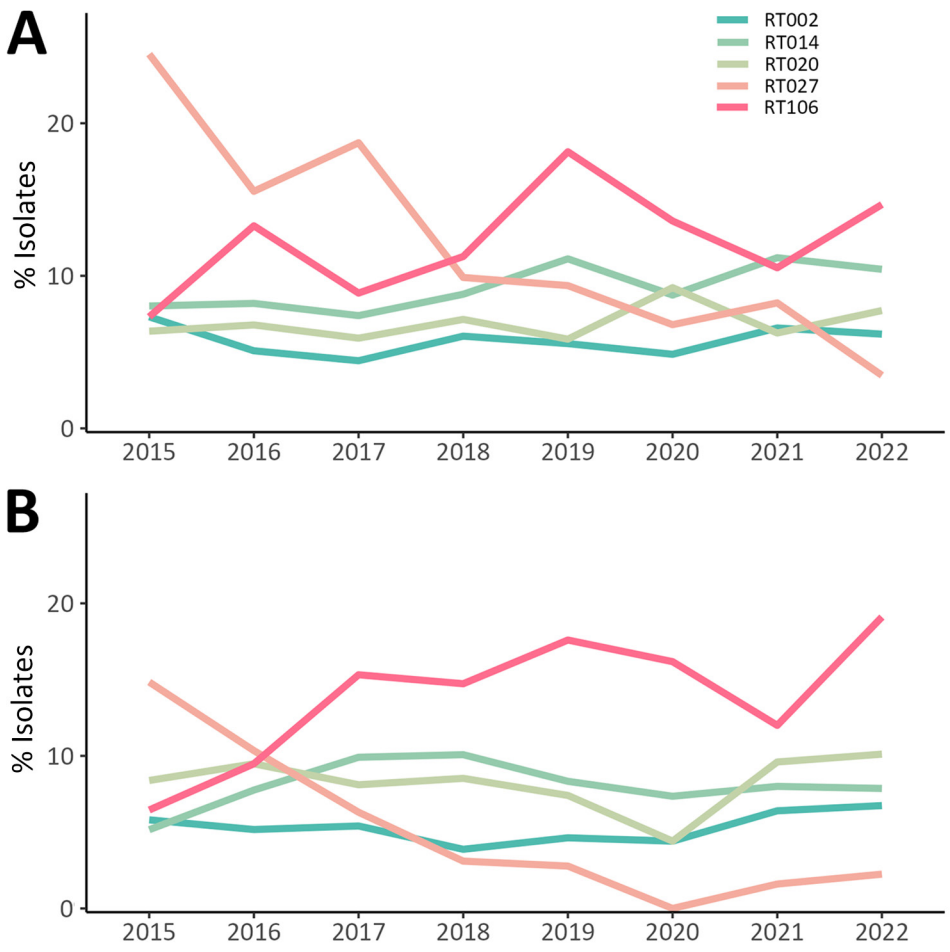

Figure 3. Percentages of 5 most common ribotypes detected among isolates in a characterization of adult healthcare-associated and community-associated *Clostridioides difficile* infection (CDI), Canada, 2015–2022. A) Healthcare-associated CDI rates; B) community-associated CDI rates. RT, ribotype.

1, 2, https://wwwnc.cdc.gov/EID/article/31/6/25-0182-App2.xlsx). Among HA CDI during the study years, 18.0% of adult and 5.8% of pediatric cases were moxifloxacin resistant, 27.7% of adult and 24.0% of pediatric cases were clindamycin resistant, and 1.6% of adult and 1.7% of pediatric cases were rifampin resistant. For CA CDI, 10.7% of adult and 7.9% of pediatric cases were moxifloxacin resistant, 28.4% of adult and 23.7% of pediatric cases were clindamycin resistant, and 1.3% of adult and no pediatric cases were rifampin resistant. Overall moxifloxacin resistance was higher in adult (16.2%) than pediatric (6.2%) populations. Of note, from 2015 to 2022, moxifloxacin resistance decreased by 27.3% for adult HA CDI and 14.2% for adult CA CDI. Despite variability in clindamycin resistance (range 8.8%–50.4%) during the study period, overall resistance was 27.9% for adult and 23.9% for pediatric cases.

Among the isolates examined, RT027 accounted for 55.0% (316/575) of adult and 24.2% (16/66) of pediatric moxifloxacin-resistant isolates. Among RT027 samples, 78.2% (316/404) of adult and 47.1% (16/34) of pediatric isolates were moxifloxacin resistant. Among moxifloxacin-resistant RT027, all pediatric (n = 16) and 97.5% (308/316) of adult samples had MICs ≥32 μg/mL. In contrast, RT106, the most prevalent (13.1%) pediatric strain type and second most prevalent (12.2%) adult strain type, accounted for 16.7% (11/66) of pediatric and 6.6% (38/575) adult moxifloxacin-resistant isolates. Overall, fluoroquinolone resistance in RT106 isolates was much lower in adult (8.8%, 38/434) and pediatric (6.4%, 11/172) populations.

Of note, multidrug resistance was more common among tested RT027 strains. Of 231 (206 adult, 25 pediatric) isolates resistant to both moxifloxacin and clindamycin, 37.2% (n = 86; 83 adult, 3 pediatric) were RT027. Of 31 (29 adult, 2 pediatric) isolates resistant to moxifloxacin, clindamycin, and rifampin, 51.6% (n = 16) were RT027. In contrast, no RT106 isolates exhibited resistance to moxifloxacin, clindamycin, and rifampin.

One RT012 isolate from a 2018 pediatric HA CDI case was metronidazole resistant (MIC 48 μg/mL), and 2 adult cases were vancomycin intermediate

resistant: an RT002 HA CDI case in 2019 (MIC 6 μg/mL) and an RT126 CA CDI case in 2021 (MIC 12 μg/mL). Treatment and outcome data were not available for the metronidazole-resistant case. For the 2 adult vancomycin intermediate resistant cases, both were treated with vancomycin and had no severe outcomes, indicated treatment failure, or reported recurrence. We did not observe tigecycline resistance in any cases during the study period.

Discussion

We analyzed 8 years of CDI surveillance data from adult and pediatric inpatients from acute care hospitals in Canada. Nationally, HA CDI rates declined by 19.9% in adult and 29.6% in pediatric inpatients and CA CDI rates declined by 58.3% among pediatric inpatients. Epidemiologic and molecular characterization of CDI in adult and pediatric populations revealed more severe 30-day outcomes among adult than pediatric patients and that RT106 was the predominant ribotype in both populations.

Decreasing national adult and pediatric HA CDI rates coincided with global declines in CDI, including in the United States (*21*,*22*). One study reported the annual rate of pediatric CDI-associated hospitalization in the United States increased from 7.24 to 12.8/10,000 hospitalizations during 1997–2006 (*23*), and another reported a doubling in annual incidence among 22 pediatric hospitals in a multicenter study during 2001–2006 (*24*). A more recent estimate showed the overall CDI burden in the United States decreased 24% from 2011 to 2017, after adjusting for testing method (*22*). The decreases in pediatric HA CDI rates we report during 2015–2022 are a reversal from trends reported by CNISP from 2007–2011 (*25*), and adult HA CDI rates continued the decline trends observed during 2011–2016 (*19*). Although the reasons for declining incidence in Canada are not fully elucidated, enhanced infection control and antimicrobial stewardship measures might have contributed (*26*,*27*). Declines in RT027 and changes in testing methodology and criteria might have further contributed to decreased CDI rates (*28*).

The nondecreasing trends in adult CA CDI incidence during 2015–2022 could be attributed to the increase in adult CA CDI during the COVID-19

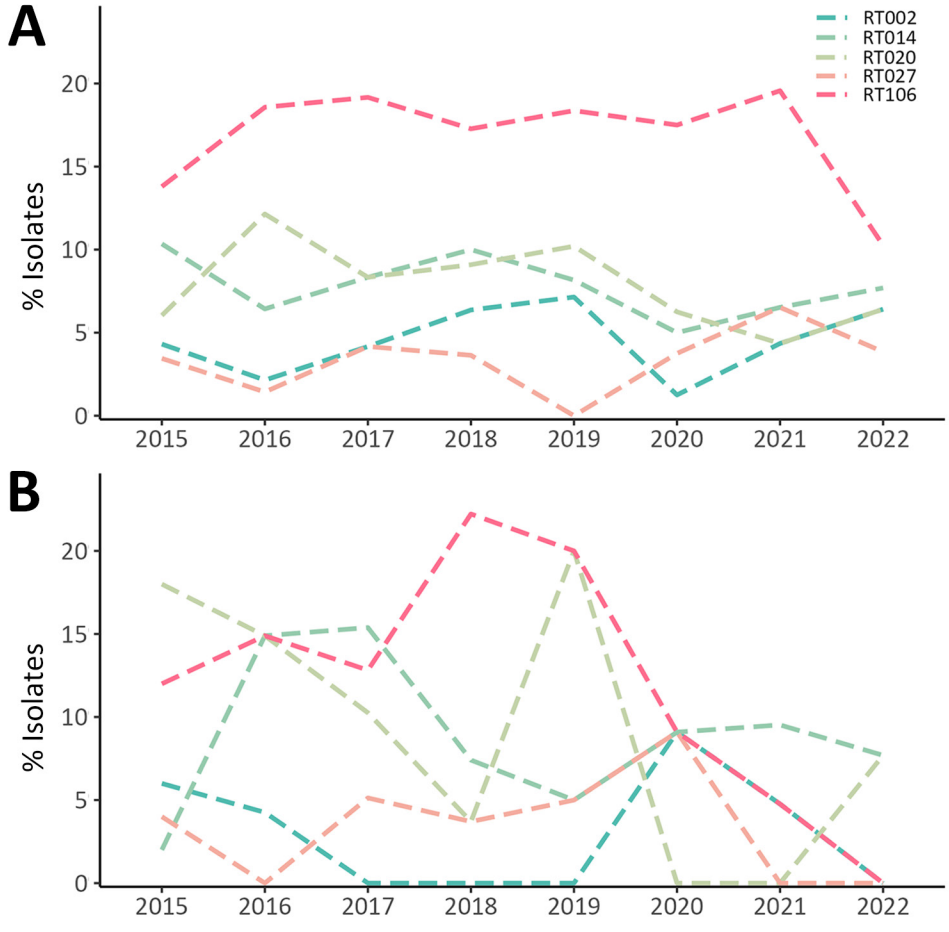

Figure 4. Percentages of 5 most common RTs detected among isolates in a characterization of pediatric healthcare-associated and community-associated *Clostridioides difficile* infection (CDI), Canada, 2015–2022. A) Healthcare-associated CDI rates; B) community-associated CDI rates. RT, ribotype.

Table 3. Multivariate regression modeling of epidemiologic factors in characterization of adult and pediatric healthcare-associated and community-associated *Clostridioides difficile* infections, Canada, 2015–2022*

Characteristics	Univariable analysis		Multivariable analysis	
	Odds ratio (95% CI)	p value	Odds ratio (95% CI)	p value
RT027 (n = 438) vs. non-RT027 (n = 4,184) strains				
Age group				
Adult	**3.87 (2.75–5.63)**	**<0.0001**	**3.42 (2.35–5.18)**	**<0.0001**
Pediatric	Referent		Referent	
Sex				
F	Referent		Referent	
M	0.97 (0.79–1.17)	0.720	0.97 (0.79–1.20)	0.970
CDI case type				
Community-associated	Referent		Referent	
Healthcare-associated	**2.16 (1.65–2.89)**	**<0.0001**	**2.18 (1.64–2.95)**	**<0.0001**
Severe CDI†	**2.24 (1.71–2.99)**	**<0.0001**	**2.15 (1.63–2.90)**	**<0.0001**
Severe outcome‡	**2.27 (1.56–3.24)**	**<0.0001**	**1.93 (1.31–2.90)**	**0.0005**
RT106 (n = 606) vs. non-RT106 (n = 4,016) strains				
Age group				
Adult	**0.72 (0.59–0.87)**	**0.0007**	**0.71 (0.58–0.88)**	**0.002**
Pediatric	Referent		Referent	
Sex				
F	Referent		Referent	
M	0.905 (0.76–1.07)	0.251	0.89 (0.74–1.07)	0.208
CDI case type				
Community-associated	Referent		Referent	
Healthcare-associated	0.99 (0.81–1.21)	0.921	1.01 (0.82–1.25)	0.936
Severe CDI†	0.83 (0.69–1.01)	0.0621	0.87 (0.72 – 1.06)	0.168
Severe outcome‡	0.76 (0.41–1.17)	0.233	0.80 (0.50 – 1.24)	0.345

*Bold font indicates statistical significance. CDI, *C. difficile* infection.
†Severe CDI defined as albumin level <30 g/L, leukocyte count >15 × 10^9 cells/L, or both.
‡Severe outcome was defined as CDI-attributable admission to an intensive care unit, colectomy, or death within 30 d of first positive *C. difficile* specimen where CDI was the cause of death or contributed to death.

pandemic period (2019–2022), after our previous report of declining incidence during 2015–2019 (*17*). In agreement with previous findings, our study showed that adult CA CDI patients were more likely to be younger and female compared with HA CDI patients (*29*–*31*). In contrast, pediatric CA CDI patients were more likely to be older, and we noted no differences in sex. Although age group–specific data on CA CDI incidence is sparse, population-based estimates in the United States increased during 2012–2017 (*32*). Data from Europe reported a 2018–2020 mean CA CDI hospital incidence of 1.35 cases/1,000 patient admissions (*33*), but those data were not stratified by age group. The decreases in pediatric CDI rates we report coincide with other reported decreases among hospitalized pediatric patients from 49 US pediatric tertiary care centers without distinction of acquisition type (*34*). A single-center study in Taiwan reported an overall 2013–2019 pediatric CA CDI incidence rate of 0.564 cases/1,000 patient admissions, although that rate increased substantially from the 2007–2012 period (*35*).

Molecular analysis of CDI isolates in Canada revealed a dynamic and heterogeneous RT population and that RT106 predominated in both adult and pediatric patients. RT106, first identified in the United Kingdom in 1999 (*36*), is now found worldwide and is among the most prevalent strains in the United States (*37*). Reports of enhanced spore-producing and biofilm-forming capabilities of RT106 suggest adaptive advantages that might enable greater persistence in the environment and hospital settings, possibly leading to increased infection and recurrence rates (*36*–*39*).

RT027 prevalence in Canada decreased substantially among adults and remained relatively low in pediatrics inpatients. Parallel decreases in RT027 prevalence have been observed in North America, the United Kingdom, and elsewhere (*1*,*32*,*40*–*42*). Despite a decrease in prevalence, multivariable analysis revealed that patients infected with RT027 were more likely to be adults with HA CDI, who also experienced more severe CDI-related ICU admission, colectomy, or death.

Livestock-associated *C. difficile* RT078 and RT126, notable from a One Health perspective, have demonstrated increased virulence, disease severity, and epidemic potential in several countries in Europe (*43*,*44*) but appear to be uncommon in hospitalized CDI patients in Canada. Overall, adult RT078 and RT126 prevalence was 2.8% and pediatric prevalence was 2.1%, a small increase from previously reported data (*13*).

Antimicrobial susceptibility testing suggested that resistance in *C. difficile* is lower in Canada than

in the United States or globally (*8*). The percentage of tested isolates resistant to moxifloxacin (2%–87%), clindamycin (15%–97%), and metronidazole (0.1−18.3%) were previously reported (*8*,*45*). Stratified by case type, HA and CA CDI isolates revealed no major differences in resistance for either adult or pediatric populations, except for moxifloxacin. Adult moxifloxacin resistance was 16.5% for HA CDI and 10.0% for CA CDI. Moxifloxacin resistance was lower in the pediatric population; 5.7% of HA and 7.7% CA CDI isolates exhibited resistance. Most strikingly, among RT027 isolates characterized, moxifloxacin resistance decreased from 92.1% to 9.1% in adult and from 66.7% to 0 in pediatric populations during 2015–2022. The exceptionally high percentage of tested RT027 moxifloxacin-resistant isolates recorded at the beginning of our study parallels rates observed in the United States, where 98% resistance was recorded (*46*). Similarly, our findings are consistent with a previously published study from North America that found RT027 strains are more likely to be resistant to multiple drugs, including clindamycin, moxifloxacin, and rifampin (*47*). The lower resistance observed in our diverse RT population is consistent with the suggestion that RT heterogeneity is inversely correlated with antimicrobial resistance, as measured by cumulative resistance scores (*48*,*49*).

The first limitation of our study is that hospitals self-select whether to participate in both HA and CA CDI surveillance; participation varied over time, which might have influenced comparisons between patients and observed temporal trends. Thus, we conducted sensitivity analyses restricted to hospitals that conducted both HA and CA CDI surveillance and to hospitals that participated in all 8 years of the study period, and results of those analyses were not significantly different from the full analyses. Second, although CDI diagnostic testing methods were collected throughout the study period, data completeness was not consistent from year to year, limiting the inferences we could make regarding the effect of CDI diagnostic testing methods on adult and pediatric rates over time. Third, for CA CDI surveillance, we captured data from patients admitted to a CNISP hospital and requiring medical intervention for CDI symptoms or other underlying conditions. The features and outcomes of those patients might not be relevant to patients with CA CDI who do not require hospital care. Fourth, isolates and outcome data were only collected for adults during a 2-month targeted period and might not represent the epidemiologic and molecular characteristics across the full year. Finally, although a qualified physician determined the cause of death in CDI patients, attribution of death is difficult and could be subjective.

In conclusion, rates of adult and pediatric HA CDI in Canada declined during 2015–2022, coinciding with decreased prevalence of RT027 and increased prevalence of RT106. We noted major decreases in antimicrobial resistance to moxifloxacin in both adult HA and CA CDI populations, concordant with an overall decrease in prevalence of RT027. Despite declining rates, CDI continues to be a major health burden in Canada. To ensure continued success in combatting this global health threat, robust national surveillance and infection prevention and control programs are integral to clarifying CDI epidemiology, investigation, and control.

Acknowledgments

We gratefully acknowledge the physicians, epidemiologists, infection control practitioners, and laboratory staff at each participating hospital for their contributions.

This work was supported by the Public Health Agency of Canada.

Canadian Nosocomial Infection Surveillance Program hospitals provided expertise in the development of protocols in addition to collection and analysis epidemiologic data and laboratory isolates. National Microbiology Laboratory staff and epidemiologists from Public Health Agency of Canada were responsible for the conception, analysis, interpretation, drafting, and revision of the paper.

About the Author

Mr. Du is a biologist with the Public Health Agency of Canada in Winnipeg at the National Microbiology Laboratory. His primary research interests include the epidemiology of *Clostridioides difficile* in addition to antimicrobial resistance in hospital acquired infections.

References

1. Katz KC, Golding GR, Choi KB, Pelude L, Amaratunga KR, Taljaard M, et al.; Canadian Nosocomial Infection Surveillance Program. The evolving epidemiology of *Clostridium difficile* infection in Canadian hospitals during a postepidemic period (2009–2015). CMAJ. 2018;190:E758–65. https://doi.org/10.1503/cmaj.180013
2. Rupnik M, Wilcox MH, Gerding DN. *Clostridium difficile* infection: new developments in epidemiology and pathogenesis. Nat Rev Microbiol. 2009;7:526–36. https://doi.org/10.1038/nrmicro2164
3. Canadian Antimicrobial Resistance Surveillance System (CARSS). Pan-Canadian action plan on antimicrobial resistance. Ottowa (ON): Public Health Agency of Canada; 2023.

4. Centers for Disease Control and Prevention. Antibiotic resistance threats in the United States, 2019. Atlanta: The Centers; 2019.
5. Bouza E. Consequences of *Clostridium difficile* infection: understanding the healthcare burden. Clin Microbiol Infect. 2012;18:5–12. https://doi.org/10.1111/1469-0691.12064
6. Levy AR, Szabo SM, Lozano-Ortega G, Lloyd-Smith E, Leung V, Lawrence R, et al. Incidence and costs of *Clostridium difficile* infections in Canada. Open Forum Infect Dis. 2015;2:ofv076. https://doi.org/10.1093/ofid/ofv076
7. Eng L, Collins DA, Alene KA, Bory S, Theng Y, Vann P, et al. *Clostridioides* (*Clostridium*) *difficile* infection in hospitalized adult patients in Cambodia. Microbiol Spectr. 2025;13:e0274724. https://doi.org/10.1128/spectrum.02747-24
8. Zhao H, Nickle DC, Zeng Z, Law PYT, Wilcox MH, Chen L, et al. Global landscape of *Clostridioides difficile* phylogeography, antibiotic susceptibility, and toxin polymorphisms by post-hoc whole-genome sequencing from the MODIFY I/II studies. Infect Dis Ther. 2021;10:853–70. https://doi.org/10.1007/s40121-021-00426-6
9. McFarland LV, Ozen M, Dinleyici EC, Goh S. Comparison of pediatric and adult antibiotic-associated diarrhea and *Clostridium difficile* infections. World J Gastroenterol. 2016;22:3078–104. https://doi.org/10.3748/wjg.v22.i11.3078
10. Silva A, Du T, Choi KB, Pelude L, Golding GR, Hizon R, et al.; CNISP C. difficile working group. Epidemiology of primary and recurrent healthcare-associated and community-associated pediatric *Clostridioides difficile* infection in Canada, 2015–2020. J Pediatric Infect Dis Soc. 2023;12:222–5. https://doi.org/10.1093/jpids/piad003
11. Canadian Nosocomial Infection Surveillance Program. Health infobase: Canadian Nosocomial Infection Surveillance Program, 2024 [cited 2025 Dec 12]. https://health-infobase.canada.ca/cnisp/index.html
12. Canadian Nosocomial Infection Surveillance Program. Healthcare-associated infections and antimicrobial resistance in Canadian acute care hospitals, 2018–2022. Can Commun Dis Rep. 2024;50:179–96. https://doi.org/10.14745/ccdr.v50i06a02
13. Canadian Nosocomial Infection Surveillance. Healthcare-associated infections and antimicrobial resistance in Canadian acute care hospitals, 2014–2018. Can Commun Dis Rep. 2020;46:99–112. https://doi.org/10.14745/ccdr.v46i05a01
14. Infection Prevention and Control Canada. CNISP protocols & publications, 2024 [cited 2025 Jan 13]. https://ipac-canada.org/cnisp-publications
15. Miller M, Gravel D, Mulvey M, Taylor G, Boyd D, Simor A, et al. Health care-associated *Clostridium difficile* infection in Canada: patient age and infecting strain type are highly predictive of severe outcome and mortality. Clin Infect Dis. 2010;50:194–201. https://doi.org/10.1086/649213
16. Lynch T, Chong P, Zhang J, Hizon R, Du T, Graham MR, et al.; Canadian Nosocomial Infection Surveillance Program (CNISP). Characterization of a stable, metronidazole-resistant *Clostridium difficile* clinical isolate. PLoS One. 2013;8:e53757. https://doi.org/10.1371/journal.pone.0053757
17. Du T, Choi KB, Silva A, Golding GR, Pelude L, Hizon R, et al. Characterization of healthcare-associated and community-associated *Clostridioides difficile* infections among adults, Canada, 2015–2019. Emerg Infect Dis. 2022;28:1128–36. https://doi.org/10.3201/eid2806.212262
18. Fawley WN, Knetsch CW, MacCannell DR, Harmanus C, Du T, Mulvey MR, et al. Development and validation of an internationally-standardized, high-resolution capillary gel-based electrophoresis PCR-ribotyping protocol for *Clostridium difficile*. PLoS One. 2015;10:e0118150. https://doi.org/10.1371/journal.pone.0118150
19. Xia Y, Tunis MC, Frenette C, Katz K, Amaratunga K, Rhodenizer Rose SR, et al. Epidemiology of *Clostridioides difficile* infection in Canada: a six-year review to support vaccine decision-making. Can Commun Dis Rep. 2019;45:191–211. https://doi.org/10.14745/ccdr.v45i78a04
20. Clinical and Laboratory Standards Institute. Performance standards for antimicrobial susceptibility testing of anaerobic bacteria, 9th edition (M11). Wayne (PA): The Institute; 2018.
21. Ho J, Wong SH, Doddangoudar VC, Boost MV, Tse G, Ip M. Regional differences in temporal incidence of *Clostridium difficile* infection: a systematic review and meta-analysis. Am J Infect Control. 2020;48:89–94. https://doi.org/10.1016/j.ajic.2019.07.005
22. Guh AY, Mu Y, Winston LG, Johnston H, Olson D, Farley MM, et al.; Emerging Infections Program Clostridioides difficile Infection Working Group. Trends in U.S. burden of *Clostridioides difficile* infection and outcomes. N Engl J Med. 2020;382:1320–30. https://doi.org/10.1056/NEJMoa1910215
23. Zilberberg MD, Tillotson GS, McDonald C. *Clostridium difficile* infections among hospitalized children, United States, 1997–2006. Emerg Infect Dis. 2010;16:604–9. https://doi.org/10.3201/eid1604.090680
24. Kim J, Smathers SA, Prasad P, Leckerman KH, Coffin S, Zaoutis T. Epidemiological features of *Clostridium difficile*–associated disease among inpatients at children's hospitals in the United States, 2001–2006. Pediatrics. 2008;122:1266–70. https://doi.org/10.1542/peds.2008-0469
25. Le Saux N, Gravel D, Mulvey M, Moore D, Langley JM, Richardson S, et al.; Canadian Nosocomial Infection Surveillance Program. Healthcare-associated *Clostridium difficile* infections and strain diversity in pediatric hospitals in the Canadian Nosocomial Infection Surveillance Program, 2007–2011. J Pediatric Infect Dis Soc. 2015;4:e151–4. https://doi.org/10.1093/jpids/piv011
26. Silva A, Du T, Choi KB, Pelude L, Golding GR, Hizon R, et al.; CNISP C. difficile working group. Epidemiology of primary and recurrent healthcare-associated and community-associated pediatric *Clostridioides difficile* infection in Canada, 2015–2020. J Pediatric Infect Dis Soc. 2023;12:222–5. https://doi.org/10.1093/jpids/piad003
27. Pereira JA, McGeer A, Tomovici A, Selmani A, Chit A. Incidence and economic burden of *Clostridioides difficile* infection in Ontario: a retrospective population-based study. CMAJ Open. 2020;8:E16–25. https://doi.org/10.9778/cmajo.20190018
28. Bogaty C, Lévesque S, Garenc C, Frenette C, Bolduc D, Galarneau LA, et al.; Quebec Clostridium difficile Infection Surveillance Program (QCISP). Trends in the use of laboratory tests for the diagnosis of *Clostridium difficile* infection and association with incidence rates in Quebec, Canada, 2010–2014. Am J Infect Control. 2017;45:964–8. https://doi.org/10.1016/j.ajic.2017.04.002
29. Kotila SM, Mentula S, Ollgren J, Virolainen-Julkunen A, Lyytikäinen O. Community- and healthcare-associated *Clostridium difficile* infections, Finland, 2008–2013. Emerg Infect Dis. 2016;22:1747–53. https://doi.org/10.3201/eid2210.151492
30. Tan XQ, Verrall AJ, Jureen R, Riley TV, Collins DA, Lin RT, et al. The emergence of community-onset *Clostridium difficile* infection in a tertiary hospital in Singapore: a cause

for concern. Int J Antimicrob Agents. 2014;43:47–51. https://doi.org/10.1016/j.ijantimicag.2013.09.011
31. Fellmeth G, Yarlagadda S, Iyer S. Epidemiology of community-onset *Clostridium difficile* infection in a community in the South of England. J Infect Public Health. 2010;3:118–23. https://doi.org/10.1016/j.jiph.2010.07.002
32. Centers for Disease Control and Prevention. 2018 Annual report for the Emerging Infections Program for *Clostridioides difficile* infection. Atlanta: The Centers; 2019.
33. European Centre for Disease Prevention and Control. *Clostridioides difficile* infections annual epidemiological report for 2019–2020. Stockholm; The Centre: 2024.
34. Edwards PT, Thurm CW, Hall M, Busing JD, Kahn SA, Kellermayer R, et al. *Clostridioides difficile* infection in hospitalized pediatric patients: comparisons of epidemiology, testing, and treatment from 2013 to 2019. J Pediatr. 2023;252:111–116.e1. https://doi.org/10.1016/j.jpeds.2022.08.030
35. Chien M-M, Chang M-H, Chang K-C, Ni Y-H, Wu J-F. The incidence of *Clostridium difficile* infection in children with and without inflammatory bowel diseases: a single-center study in Taiwan from 2006 to 2019. J Formos Med Assoc. 2025;124:253–7. https://doi.org/10.1016/j.jfma.2024.04.006
36. Stubbs SLJ, Brazier JS, O'Neill GL, Duerden BI. PCR targeted to the 16S-23S rRNA gene intergenic spacer region of *Clostridium difficile* and construction of a library consisting of 116 different PCR ribotypes. J Clin Microbiol. 1999;37:461–3. https://doi.org/10.1128/JCM.37.2.461-463.1999
37. Carlson TJ, Blasingame D, Gonzales-Luna AJ, Alnezary F, Garey KW. *Clostridioides difficile* ribotype 106: a systematic review of the antimicrobial susceptibility, genetics, and clinical outcomes of this common worldwide strain. Anaerobe. 2020;62:102142. https://doi.org/10.1016/j.anaerobe.2019.102142
38. Roxas BAP, Roxas JL, Claus-Walker R, Harishankar A, Mansoor A, Anwar F, et al. Phylogenomic analysis of *Clostridioides difficile* ribotype 106 strains reveals novel genetic islands and emergent phenotypes. Sci Rep. 2020;10:22135. https://doi.org/10.1038/s41598-020-79123-2
39. Suárez-Bode L, Barrón R, Pérez JL, Mena A. Increasing prevalence of the epidemic ribotype 106 in healthcare facility-associated and community-associated *Clostridioides difficile* infection. Anaerobe. 2019;55:124–9. https://doi.org/10.1016/j.anaerobe.2018.12.002
40. Jassem AN, Prystajecky N, Marra F, Kibsey P, Tan K, Umlandt P, et al. Characterization of *Clostridium difficile* strains in British Columbia, Canada: a shift from NAP1 majority (2008) to novel strain types (2013) in one region. Can J Infect Dis Med Microbiol. 2016;2016:8207418. https://doi.org/10.1155/2016/8207418
41. Karlowsky JA, Zhanel GG, Hammond GW, Rubinstein E, Wylie J, Du T, et al. Multidrug-resistant North American pulsotype 2 *Clostridium difficile* was the predominant toxigenic hospital-acquired strain in the province of Manitoba, Canada, in 2006-2007. J Med Microbiol. 2012;61:693–700. https://doi.org/10.1099/jmm.0.041053-0
42. Public Health England. *Clostridium difficile* Ribotyping Network (CDRN) for England and Northern Ireland, 2015–2018. London: Public Health England; 2019.
43. Keessen EC, Harmanus C, Dohmen W, Lipman LJA, Kuijper EJ. *Clostridium difficile* infection associated with pig farms. Emerg Infect Dis. 2013;19:1032–4. https://doi.org/10.3201/eid1906.121645
44. Knetsch CW, Kumar N, Forster SC, Connor TR, Browne HP, Harmanus C, et al. Zoonotic transfer of *Clostridium difficile* harboring antimicrobial resistance between farm animals and humans. J Clin Microbiol. 2018;56:e01384-17. https://doi.org/10.1128/JCM.01384-17
45. Peng Z, Jin D, Kim HB, Stratton CW, Wu B, Tang YW, et al. Update on antimicrobial resistance in *Clostridium difficile*: resistance mechanisms and antimicrobial susceptibility testing. J Clin Microbiol. 2017;55:1998–2008. https://doi.org/10.1128/JCM.02250-16
46. Wieczorkiewicz JT, Lopansri BK, Cheknis A, Osmolski JR, Hecht DW, Gerding DN, et al. Fluoroquinolone and macrolide exposure predict *Clostridium difficile* infection with the highly fluoroquinolone- and macrolide-resistant epidemic *C. difficile* strain BI/NAP1/027. Antimicrob Agents Chemother. 2015;60:418–23. https://doi.org/10.1128/AAC.01820-15
47. Tenover FC, Tickler IA, Persing DH. Antimicrobial-resistant strains of *Clostridium difficile* from North America. Antimicrob Agents Chemother. 2012;56:2929–32. https://doi.org/10.1128/AAC.00220-12
48. Freeman J, Vernon J, Morris K, Nicholson S, Todhunter S, Longshaw C, et al.; Pan-European Longitudinal Surveillance of Antibiotic Resistance among Prevalent Clostridium difficile Ribotypes' Study Group. Pan-European longitudinal surveillance of antibiotic resistance among prevalent *Clostridium difficile* ribotypes. Clin Microbiol Infect. 2015;21:248.e9–16. https://doi.org/10.1016/j.cmi.2014.09.017
49. Freeman J, Vernon J, Pilling S, Morris K, Nicolson S, Shearman S, et al.; Pan-European Longitudinal Surveillance of Antibiotic Resistance among Prevalent *Clostridium difficile* Ribotypes' Study Group. Five-year pan-European, longitudinal surveillance of *Clostridium difficile* ribotype prevalence and antimicrobial resistance: the extended ClosER study. Eur J Clin Microbiol Infect Dis. 2020;39:169–77. https://doi.org/10.1007/s10096-019-03708-7

Address for correspondence: Tim Du, Surveillance, Reference and Science Directorate of the National Microbiology Laboratory Branch, One Health Division, Antimicrobial Resistance and Nosocomial Infections National Microbiology Laboratory, 1015 Arlington St, Winnipeg, MB R3E 3R2, Canada; email: tim.du@phac-aspc.gc.ca

Prospective Multicenter Surveillance of Non–*H. pylori Helicobacter* Infections during Medical Checkups, Japan

Kengo Tokunaga,[1] Emiko Rimbara,[1] Toshihisa Tsukadaira, Katsuhiro Mabe, Koji Yahara, Hidekazu Suzuki, Tadashi Shimoyama, Mitsushige Sugimoto, Tadayoshi Okimoto, Hidenori Matsui, Masato Suzuki, Keigo Shibayama, Hiroyoshi Ota, Kazunari Murakami, Mototsugu Kato

To evaluate non–*H. pylori Helicobacter* (NHPH) infections in Japan, we enrolled 673 consecutive patients who underwent gastric endoscopy during annual medical checkups at 4 hospitals during April 2022–February 2023. We collected intragastric fluid and serum samples to detect NHPH infection by PCR and serologic tests. The prevalence of NHPH was 3% (20/673); 70% (14/20) of patients were infected with *H. suis* and 30% (6/20) with non–*H. suis* NHPH species. All 14 *H. suis*–infected patients were men and had a history of pork offal ingestion. Among non–*H. suis* NHPH-infected patients, 50% (3/6) owned pet cats, whereas only 22% (145/667) of other patients owned cats. Endoscopic evaluation revealed marbled crack-like gastritis was present in 93% (13/14) of *H. suis*–infected patients, a significantly higher prevalence than for *H. pylori*–infected (28.6%) and *H. pylori* eradication therapy (27.6%) groups. Pork offal ingestion and having pet cats increase risk for *Helicobacter* spp. infections.

Non–*H. pylori Helicobacter* (NHPH) species are helical corkscrew-like bacteria; *Helicobacter* spp. have been reported since the 1980s to infect the human stomach (*1*). In humans, NHPH infection causes gastric diseases, such as peptic ulcers, chronic gastritis, gastric cancer, and gastric mucosa-associated lymphoid tissue (MALT) lymphoma (*2*–*5*). Although *H. suis* is the most common NHPH species that infects the human stomach (*4*,*6*,*7*), its pathogenicity remains unclear because isolation has not previously been feasible. The recent successful isolation of *H. suis* from patients with gastric disease demonstrated *H. suis* pathogenicity in the human stomach (*8*), ushering in a new stage of NHPH research.

NHPH infection rates have mostly been analyzed in patients with specific gastric-related diseases (*2*–*5*,*9*–*12*). Most studies have used gastric biopsy to detect NHPH infection, making it difficult from an ethical standpoint to investigate NHPH infection in asymptomatic persons. Recent studies have shown the usefulness of gastric juice samples for *H. pylori* diagnoses (*13*,*14*), and we recently developed a method to detect NHPH infections by using gastric juice samples (*15*,*16*) without performing a biopsy. In addition, we developed a highly sensitive serologic diagnostic method for *H. suis* infection in humans (*15*,*16*). We conducted a multicenter survey of NHPH infection among patients who underwent gastric endoscopy during medical checkups in Japan by using those methods. We evaluated NHPH infection rates and regional differences, identified bacterial species, and determined associations between NHPH stomach infections, demographics, and endoscopic findings.

Author affiliations: Kyorin University School of Medicine, Tokyo, Japan (K. Tokunaga); National Institute of Infectious Diseases, Tokyo (E. Rimbara, K. Yahara, H. Matsui, M. Suzuki); Kenwakai Hospital, Iida, Japan (T. Tsukadaira); Mabe Goryokaku Gastrointestinal Endoscopy Clinic, Hakodate, Japan (K. Mabe); Tokai University School of Medicine, Isehara, Japan (H. Suzuki); Aomori General Health Examination Center, Aomori, Japan (T. Shimoyama); Oita University, Oita, Japan (M. Sugimoto, K. Murakami); Oita Prefectural Hospital, Oita (T. Okimoto); Nagoya University Graduate School of Medicine, Nagoya, Japan (K. Shibayama); Shinshu University School of Medicine, Matsumoto, Japan (H. Ota); Public Interest Foundation Hokkaido Cancer Society, Sapporo, Japan (M. Kato)

DOI: https://doi.org/10.3201/eid3106.241315

[1]These authors contributed equally to this article.

Materials and Methods

Ethics

We explained the study to all participants and obtained written informed consent from each. The study was approved by the Ethics Committees of Kyorin University Hospital, Junpukai Health Maintenance Center (Kurashiki, Japan), Kenwakai Hospital, and Hokkaido Cancer Society (approval no. 810, project no. R03-052-52) and registered with the University Hospital Medical Information Network, Clinical Trials Registry (UMIN registration no. UMIN000054538).

Study Design, Inclusion Criteria, and Sample Collection

We enrolled consecutive patients who underwent an upper endoscopy during annual medical checkups at 4 hospitals in Japan during April 2022–February 2023. Hospital A is in Hokkaido, hospital B is in Tokyo, hospital C is in Nagano, and hospital D is in Okayama. We excluded patients who underwent gastrectomy. We collected gastric washes (intragastric fluid) and serum samples from all patients to test for NHPH infection by PCR (fluids) and for *H. suis* by ELISA (serum samples). We collected the following clinical information: age; sex; endoscopic findings; and histories of *H. pylori* infection, *H. pylori* eradication therapy, pork offal ingestion, and pet ownership. We assessed the endoscopic grade of gastric mucosal atrophy by using the Kimura and Takemoto classification (*17*). To verify the endoscopic characteristics of NHPH infection, we confirmed the presence or absence of white-marbled appearance (*18*) and crack-like mucosa (*11*). We defined white-marbled appearance as a mottled mucosa with a white mesh pattern from the gastric antrum to the angulus (Figure 1, panel A; Appendix Figure 1, https://wwwnc.cdc.gov/EID/article/31/6/24-1315-App1.pdf) and crack-like mucosa as a mesh pattern composed of faded, depressed, and varying width lines on a coarse surface from the gastric antrum to angulus (Figure 1, panel B; Appendix Figure 1). Although both appearances are similar to atrophy, they have a white mesh; however, the crack-like mucosa appearance also has depressions in the white mesh. We defined a white-marbled with crack-like mucosa appearance as marbled crack-like (MARC) gastritis. In NHPH-infected patients, we also examined the presence and location of nodular gastritis from the antrum to angulus (Figure 1, panel C), spotty redness from the antrum to the body (Figure 1, panel D), and the regular arrangement of collecting venules (RAC; Figure 1, panel E) (*19*). We defined endoscopic findings as normal if no atrophic gastritis, peptic ulcers, gastric cancer, nodular gastritis, white-marble appearance, or crack-like mucosal gastritis were present.

We divided *H. pylori* infections into the following 3 groups: infected with *H. pylori* (*H. pylori* infection group), history of *H. pylori* infection treated with eradication therapy (posteradication group), and no history of *H. pylori* infection (no *H. pylori* infection group). Diagnosis of *H. pylori* infection was confirmed by endoscopy physicians (K.T., K.M., T.K., and M.K.) with >10 years of experience in diagnosing *H. pylori* infection, according to results of a urea breath test, serum *H. pylori* antibody test, fecal antigen test, rapid urease test, histologic studies, and endoscopic observation, according to the Kyoto classification of gastritis (*20*). The posteradication group also included patients with no history of *H. pylori* eradication but with an endoscopically suspected history of *H. pylori* infection, according to the Kyoto classification of gastritis.

NHPH Detection by PCR and ELISA

We detected NHPH infection by PCR of DNA extracted from intragastric fluid collected during endoscopic examination. We centrifuged 1 mL of intragastric fluid and collected the precipitates for DNA extraction by using the DNeasy Blood and Tissue Kit (QIAGEN, https://www.qiagen.com). We performed PCR by using NHPH species–specific primers targeting 16S rRNA and *H. suis*–specific primers targeting the *hsvA* gene, as previously described (*8*). We determined the samples to be *H. suis* positive by using both PCR primer sets. However, if PCR targeting 16S rRNA for NHPH species was positive and PCR targeting *hsvA* was negative, we identified those samples as non–*H. suis* NHPH positive.

We measured serum *H. suis* antibody titers as previously described (*15*,*16*). In brief, we determined *H. suis* antibody titers by using ELISA and calculated the cutoff index (COI) value as the ratio of the absorbance of the sample to the absorbance of the positive control, both at 450 nm. We deemed the samples as positive when COI values were >1.

Statistics

We examined associations between clinical characteristics of patients and the specific status of *Helicobacter* infection (i.e., infection by *H. suis*, non–*H. suis* NHPH, or *H. pylori*, as well as after *H. pylori* eradication and absence of *Helicobacter* infection without eradication therapy) by using the Fisher exact test for discrete characteristics and Wilcoxon rank-sum test for continuous characteristics. We also examined the association between specific hospitals and *Helicobacter* infection status by using the Fisher exact test.

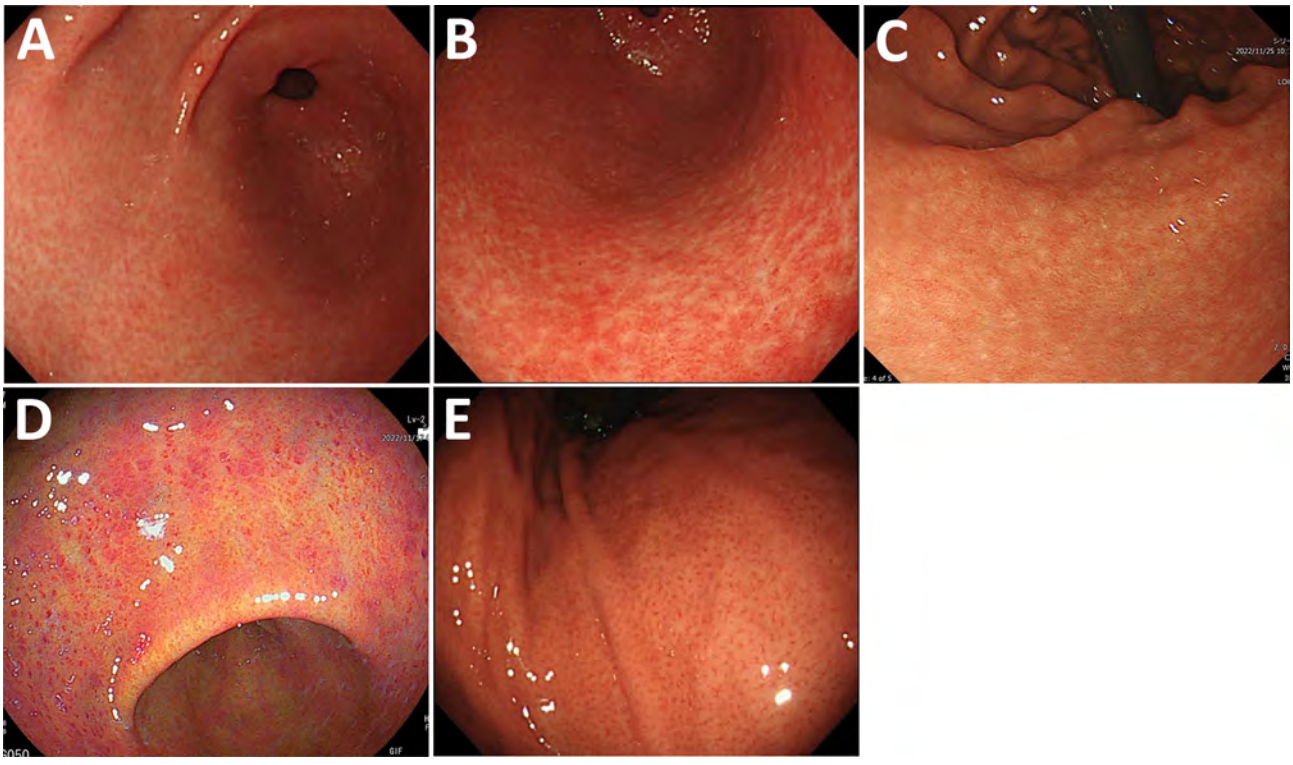

Figure 1. Representative endoscopic images of gastritis types observed in study of non–*H. pylori Helicobacter* infections, Japan, 2022. A) White marbled appearance. A white mesh pattern composed of shallow depressions that looks like white marble from the gastric antrum to the angle. White light imaging (WLI). B) Crack-like mucosa. A mesh pattern composed of faded and depressed lines with varied widths on coarse surfaces (WLI). C) Nodular gastritis. Compared with nodular gastritis caused by *H. pylori* infection, nodules that are shorter and appear as white spots are also considered nodular gastritis (WLI). D) Spotty redness, includes findings similar to those of *H. pylori* infection in the gastric body and the antrum (linked-color imaging). E) Regular arrangement of collecting venules. Microvessels with starfish-like appearance are observed as minute red points in the gastric lower body (WLI).

We evaluated differences in age and *H. suis* ELISA titers between groups by using the Kruskal-Wallis test. We used SPSS Statistics 29 (IBM, https://www.ibm.com) and R version 4.3.2 (The R Project for Statistical Computing, https://www.r-project.org) for statistical analyses and set statistical significance at $p<0.05$.

Results

Prevalence of NHPH Infection

Five patients were excluded from the analysis; 2 at hospital B and 1 at hospital D underwent remnant gastrectomy, and intragastric fluid or serum could not be obtained from 2 other patients at hospital B. We included 673 participants in the study: 100 at hospital A, 198 at hospital B, 199 at hospital C, and 179 at hospital D. The median patient age was 55 (range 29–91) years; 57.6% were male and 42.4% female (Table 1).

Intragastric fluid from all patients was tested for NHPH infection. NHPH infections were found in 3% (20/673) of patients; *H. suis* infection was found in 70% (14/20) and non–*H. suis* NHPH infections in 30% (6/20) of those patients. Among the 20 patients, 15 were in the no *H. pylori* infection group, 3 in the *H. pylori* infection group, and 2 in the posteradication group. Diagnoses of the 3 NHPH-positive patients in the *H. pylori* infection group were made by using either the urea breath test, serum *H. pylori* antibody test, or endoscopic findings. However, we found those patients to be *H. pylori* negative by PCR targeting the *H. pylori*–specific region of the 16S rRNA gene (*21*). Therefore, those 3 patients were considered to be false positives for *H. pylori* because of their NHPH infection. The 2 NHPH-positive patients in the posteradication group had no history of *H. pylori* eradication; 1 of those patients was *H. pylori* negative by serologic and histologic analyses, and both showed *H. pylori*–negative status by PCR. Therefore, both patients were placed in the posteradication group according to endoscopic observations of NHPH infection and Kyoto classification of gastritis. After detecting NHPH species in intragastric fluid by PCR, patients were recategorized as follows: no *Helicobacter* infection, n = 378; posteradication, n = 254; *H. pylori* infection, n = 21;

H. suis infection, n = 14; and non–*H. suis* NHPH infection, n = 6. The proportion of patients with *H. suis* infections was significantly higher in hospital C than in the other hospitals ($p<10^{-5}$) (Table 2).

Comparison of Clinical Characteristics among Groups

We compared clinical characteristics of patients in each of the recategorized groups (Table 3). The *H. suis* infection group consisted entirely of men (100%), which differed from the combined 4 groups not infected with *H. suis* (57% men; p = 0.0005) (Figure 2, panel A). When compared with the non–*H. suis* NHPH infection group (66.7%), the percentage of atrophic gastritis was 100% in the *H. suis* (p = 0.04) and *H. pylori* (p = 0.04) infection groups and 97.6% in the posteradication group (p = 0.01) (Table 3). The percentage of nodular gastritis was 42.9% for *H. suis*, 50.0% for non–*H. suis* NHPH, and 19.0% for *H. pylori* infection groups (p = 0.2 overall). The overall percentage of nodular gastritis among those 3 groups was 32%, which was significantly higher than that in the no *Helicobacter* infection (0%; p<0.0001) and posteradication (2.8%; p<0.0001) groups. In addition, a white marbled appearance (*18*) was observed in 78.6% and crack-like mucosa (*11*) in 85.7% of the *H. suis* infection group, indicating endoscopic characteristics of *H. suis* infection. The percentage of patients with at least 1 of the 2 endoscopic characteristics of NHPH infection was 92.9% (13/14) among the *H. suis*–infected patients, which was significantly higher than that among *H. pylori*–infected (28.6% [6/21]; p = 0.0003) and post-eradication (27.6% [70/254]; p<0.0001) groups.

The atrophic grade of patients with *H. suis* infection was mostly C-2, and no patient had an atrophic grade greater than C-2. Among *H. pylori*–infected patients, most had atrophic grades of C-2; however, some had O-1 (4.8%) and O-2 (9.5%) grades (Table 3; Figure 2, panel B).

Among the non–*H. suis* NHPH-infected patients, 50% (3/6) had a history of owning cats, which was higher than the 22% (145/667) observed among the other patients in the study. However, the difference was not statistically significant (p = 0.12) because of the small sample size of non–*H. suis* NHPH-infected patients (Figure 2, panel C). All (14/14) *H. suis*–infected patients had a pork offal ingestion history, a

Table 1. Characteristics of patients in study of non–*H. pylori Helicobacter* infections, Japan, 2022*

Characteristics	Total, n = 673	Hospital			
		A, n = 100	B, n = 198	C, n = 199	D, n = 176
Median age, y (range)	55 (29–91)	64 (43–88)	61 (29–91)	52 (31–77)	51 (34–77)
Sex					
M	390 (57.9)	47 (47.0)	119 (60.1)	111 (55.8)	113 (64.2)
F	283 (42.1)	53 (53.0)	79 (39.9)	88 (44.2)	63 (35.8)
Endoscopic findings					
Normal	322 (47.8)	56 (56.0)	114 (57.6)	73 (36.7)	79 (44.9)
Atrophic gastritis	340 (50.5)	41 (41.0)	80 (40.4)	125 (62.8)	94 (53.4)
Peptic ulcer	5 (0.7)	0	2 (1.0)	0	3 (1.7)
Gastric cancer	7 (1.0)	0	1 (0.5)	0	6 (3.4)
Nodular gastritis	20 (3.0)	1 (1.0)	1 (0.5)	8 (4.0)	10 (5.7)
White marble appearance	80 (11.9)	0	9 (4.5)	31 (15.6)	40 (22.7)
Crack-like mucosa	67 (10.0)	0	4 (2.0)	62 (31.2)	1 (0.6)
Atrophic grading†					
C-0	333 (49.5)	59 (59.0)	118 (59.6)	74 (37.2)	82 (46.6)
C-1	133 (19.8)	5 (5.0)	14 (7.1)	90 (45.2)	24(13.6)
C-2	116 (17.2)	15 (15.0)	30 (15.2)	35 (17.6)	36 (20.5)
C-3	37 (5.5)	11 (11.0)	7 (3.5)	0	19 (10.8)
O-1	22 (3.3)	6 (6.0)	9 (4.5)	0	7 (4.0)
O-2	21 (3.1)	2 (2.0)	11 (5.6)	0	8 (4.5)
O-3	11 (1.6)	2 (2.0)	9 (4.5)	0	0
Pets					
No history	208 (30.9)	33 (33.0)	89 (44.9)	47 (23.6)	39 (22.2)
Dog	354 (52.6)	48 (48.0)	85 (42.9)	110 (55.3)	111 (63.1)
Cat	148 (22.0)	29 (29.0)	26 (13.1)	46 (23.1)	47 (26.7)
Pork offal ingestion					
No history	275 (40.9)	11 (11.0)	121 (61.1)	29 (14.6)	114 (64.8)
Sometimes	347 (51.6)	78 (78.0)	75 (37.9)	154 (77.4)	40 (22.7)
Often	51 (7.6)	11 (11.0)	2 (1.0)	16 (8.0)	22 (12.5)
Infection status					
H. pylori infection	24 (3.6)	7 (7.0)	3 (1.5)	6 (3.0)	8 (4.5)
Posteradication‡	256 (38.0)	35 (35.0)	72 (36.4)	61 (30.7)	88 (50.0)
No *H. pylori* infection	393 (58.4)	58 (58.0)	123 (62.1)	132 (66.3)	80 (45.5)

*Values are no. (%) except as indicated. Hospital A is in Hokkaido, B is in Tokyo, C is in Nagano, and D is in Okayama.
†C-0, no atrophy; C-1 and C-2, mild atrophy; C-3 and O-1, moderate atrophy; and O-2 and O-3, severe atrophy.
‡Patients who had previous *H. pylori* eradication therapy.

Table 2. Infection status of patients in 4 hospitals in study of NHPH infections, Japan, 2022*

Infection status	No. (%) patients				
		Hospital†			
	Total, n = 673	A, n = 100	B, n = 198	C, n = 199	D, n = 176
No *Helicobacter* infection	378 (56.2)	57 (57.0)	121 (61.1)	121 (60.8)	79 (44.9)
Posteradication‡	254 (37.7)	35 (35.0)	72 (36.4)	59 (29.6)	88 (50.0)
H. pylori infection	21 (3.1)	6 (6.0)	2 (1.0)	5 (2.5)	8 (4.5)
H. suis infection	14 (2.1)	0	1 (0.5)	13 (6.5)	0
Non–*H. suis* NHPH infection	6 (0.9)	2 (2.0)	2 (1.0)	1 (0.5)	1 (0.6)

*NHPH, non–*Helicobacter pylori Helicobacter*.
†Hospital A is in Hokkaido, B is in Tokyo, C is in Nagano, and D is in Okayama.
‡Patients who had previous *H. pylori* eradication therapy.

proportion that was significantly higher than that in the combined 4 groups not infected with *H. suis* (384/659; p = 0.0006) (Figure 2, panel D).

Endoscopic Characteristics of Patients with NHPH Infection

We determined the type and site of gastritis and the presence or absence of RAC in the 20 NHPH-infected patients (Appendix Table). In each patient, gastritis was observed from the glandular border around the angulus to the pyloric antrum (Figure 1; Appendix Figure 1). Endoscopic gastritis results differed by NHPH species. The percentages of MARC gastritis were significantly different between the *H. suis*–infected (92.9% [13/14]) and non–*H. suis* NHPH–infected (33.3% [2/6]) groups (p = 0.014), whereas spotty redness was observed at similar rates in the *H. suis*–infected (35.7% [5/14]) and non–*H. suis* NHPH–infected (50.0% [3/6]) groups (p = 0.6). Gastritis of the pyloric canal was found in 50.0% (7/14) of the *H. suis* infection group, whereas it was absent in 83.3% (5/6) of the non–*H. suis* NHPH infection group, although the difference was not statistically significant (p = 0.3). RAC was absent in 1 patient who had petechial erythema spread over the entire gastric body.

Table 3. Comparison of clinical characteristics between groups stratified by gastric *Helicobacter* species infection status in study of NHPH infections, Japan, 2022*

Characteristics	Gastric *Helicobacter* species infection status				
	No *Helicobacter* infection	*H. pylori* infection	Posteradication	Non–*H. suis* NHPH infection	*H. suis* infection
Total no. patients	378	21	254	6	14
Median age, y (range)	53 (29–84)	61 (35–88)	57 (30–84)	65 (44–91)	50 (35–66)
Sex					
M	224 (59.3)	10 (47.6)	139 (54.5)	3 (50.0)	14 (100.0)
F	154 (40.7)	11 (52.4)	115 (45.3)	3 (50.0)	0
Endoscopic findings					
Normal	317 (83.9)	0	5 (2.0)	0	0
Atrophic gastritis	53 (14.0)	21 (100.0)	248 (97.6)	4 (66.7)	14 (100)
Peptic ulcer	0	2 (9.5)	2 (0.8)	1 (16.7)	0
Gastric cancer	2 (0.5)	2 (9.5)	3 (1.2)	0	0
Nodular gastritis	0	4 (19.0)	7 (2.8)	3 (50.0)	6 (42.9)
White marble appearance	15 (4.0)	4 (19.0)	49 (19.3)	1 (16.7)	11 (78.6)
Crack-like mucosa	29 (7.7)	3 (14.3)	22 (8.7)	1 (16.7)	12 (85.7)
White marble appearance or crack-like mucosa	40 (10.6)	6 (28.6)	70 (27.6)	2 (33.3)	13 (92.9)
Atrophic grading†					
C-0	325 (86.0)	0	6 (2.4)	2 (33.3)	0
C-1	47 (12.4)	2 (9.5)	80 (31.5)	0	4 (28.6)
C-2	5 (1.3)	10 (47.6)	88 (34.6)	3 (50.0)	10 (71.4)
C-3	0	6 (28.6)	31 (12.2)	0	0
O-1	0	1 (4.8)	21 (8.3)	0	0
O-2	0	2 (9.5)	18 (7.1)	1 (16.7)	0
O-3	1 (0.3)	0	10 (3.9)	0	0
Pets					
No history	128 (33.9)	3 (14.3)	71 (28.0)	2 (33.3)	4 (28.6)
Dog	189 (50.0)	11 (52.4)	145 (57.1)	1 (16.7)	8 (57.1)
Cat	75 (19.8)	9 (42.9)	58 (22.8)	3 (50.0)	3 (21.4)
Pork offal ingestion					
No history	147 (38.9)	6 (28.6)	119 (46.9)	3 (50.0)	0
Sometimes	206 (54.5)	14 (66.7)	113 (44.5)	2 (33.3)	12 (85.7)
Often	25 (6.6)	1 (4.8)	22 (8.7)	1 (16.7)	2 (14.3)

*Values are no. (%) except as indicated. NHPH, non–*Helicobacter pylori Helicobacter*.
†C-0, no atrophy; C-1 and C-2, mild atrophy; C-3 and O-1, moderate atrophy; and O-2 and O-3, severe atrophy.

H. suis ELISA

The COI for the *H. suis* ELISA was significantly higher for the *H. suis* infection group than for the other groups (Figure 3). All patients in the *H. suis* infection group were considered *H. suis* positive according to *H. suis* ELISA criteria (*16*). In the non–*H. suis* NHPH infection group, 1 (16.7%) patient was *H. suis* positive and 5 (83.3%) were *H. suis* negative, according to ELISA. We determined that 28.6% (6/21) of patients in the *H. pylori* infection, 7.1% (18/254) in the posteradication, and 3.4% (13/378) in the no *Helicobacter* infection groups were *H. suis* positive, according to *H. suis* ELISA. Among the 13 *H. suis*–positive patients in the no *Helicobacter* infection group, atrophic gastritis was found in 3 patients, suggesting the possibility of previous *H. suis* infection or false-negative results by PCR of intragastric fluid.

Discussion

In this study of consecutive patients who underwent gastric endoscopy during medical checkups in Japan, the NHPH infection rate was 3%. NHPH infection rates of 0.25%–6.1% have been reported previously (*2*–*5*,*9*–*11*), indicating that rates among healthy persons are not much lower than among patients with gastric diseases. A 10-year study on NHPH infection

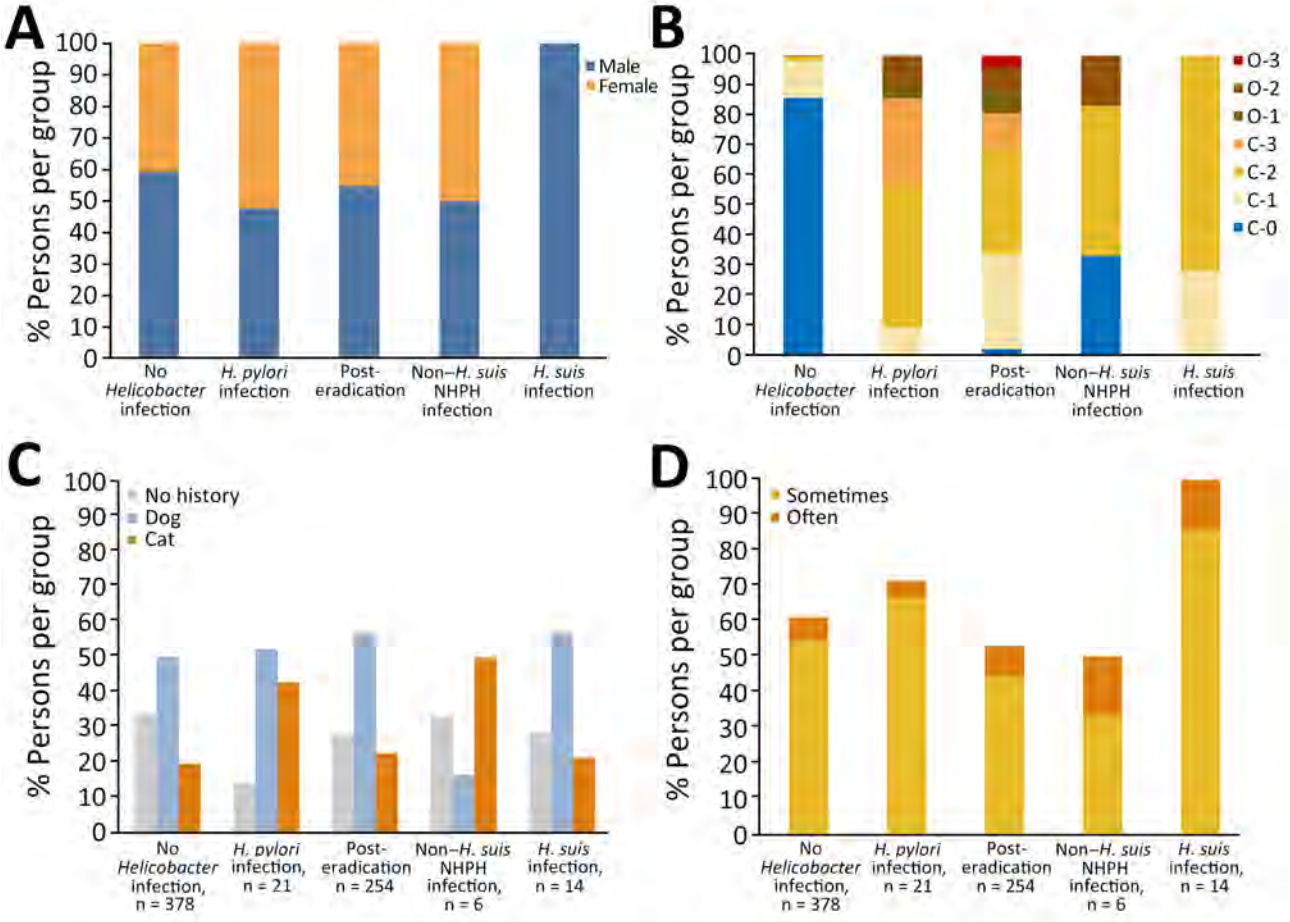

Figure 2. Comparison of patient groups stratified by gastric *Helicobacter* infection status in study of NHPH infections, Japan, 2022. A) Percentage of men and women in each group. All patients in the *H. suis* infection group were men. Prevalence of the male sex was significantly higher in the *H. suis* infection group than in the no *Helicobacter* infection (59.3%), *H. pylori* infection (47.6%), posteradication (54.7%), and non–*H. suis* NHPH infection (50.0%) groups. B) Percentages of patients categorized by each atrophic grade were compared between groups stratified by gastric *Helicobacter* infection status. In the *H. suis* infected group, 71.4% were C-2, with no higher grade of atrophy. C-0, no atrophy; C-1 and C-2, mild atrophy; C-3 and O-1, moderate atrophy; O-2 and O-3, severe atrophy. C) Percentages of patients who had no history of pets or who had a history of having pet dogs or cats. No significant differences were observed between the groups, although the proportion of patients with pet cats appeared higher (50%) in the non–*H. suis* NHPH infection group than in the no *Helicobacter* infection (19.8%) and *H. suis* infection (21.4%) groups. D) Patients in each infection group were subdivided into those who sometimes or those who often ingested pork offal. All patients in the *H. suis* infection group had a history of pork offal ingestion. Prevalence of patients with any history of pork offal ingestion was significantly higher in the *H. suis* infection group (100%) than in the no *Helicobacter* infection (61.1%; p = 0.0014), posteradication (53.1%; p = 0.0003), and non–*H. suis* NHPH infection (50.0%; p = 0.0175) groups. NHPH, non–*H. pylori Helicobacter*.

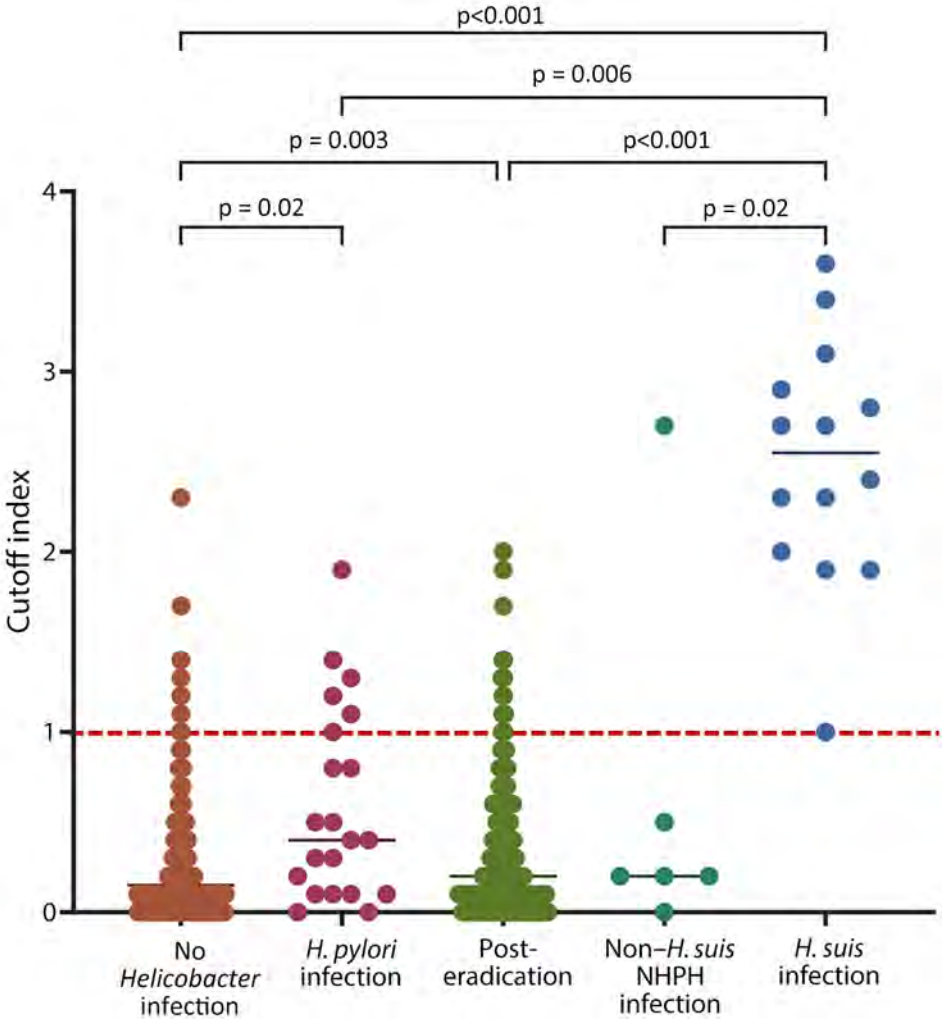

Figure 3. *Helicobacter suis* antibody titers according to gastric *Helicobacter* infection status in study of NHPH infections, Japan, 2022. Antibodies were measured by using ELISA. Gastric *Helicobacter* infection status was categorized into 5 groups. Horizontal lines within each group indicate the median value for that group. Red dotted line indicates the threshold for diagnosing *H. suis* infection, as previously described (*16*). p value comparisons are indicated above the groups. NHPH, non–*H. pylori Helicobacter*.

rates in a single institution in Japan showed the infection rate increased from 1.3% to 3.35% (30 of 896 patients) in the last 2 years and 4 months of the study period because of increased recognition of characteristic endoscopic findings (*11*). Therefore, NHPH infections might be missed in many patients with gastric diseases. In our survey, the *H. pylori* infection rate was 3.6%, and 38% of patients had a history of *H. pylori* infection. The estimated *H. pylori* infection rate in persons born in Japan in 1968 was reported to be 37.5% (*22*). Considering the median age (55 years) of the patients in our study, our sample represents a major section of the population in Japan.

Gastric NHPH species have been found in patients with gastric diseases by using culture tests, including *H. suis* (*8*), which also infects pigs and monkeys, and *H. ailrurogastricus* (*23*), *H. felis* (*24*), and *H. bizzozeronii* (*25*,*26*), which infect cats and dogs. Other species that infect dogs and cats, such as *H. heilmannii* and *H. salomonis*, have also been detected by PCR in patients with gastric diseases (*2*–*5*,*9*–*12*). *H. suis* is the most prevalent NHPH species infecting humans in Japan and other countries, whereas other species infecting dogs and cats have also been detected in most studies (*2*–*5*,*9*–*12*). In this study, *H. suis* was the most prevalent NHPH species (14/20), consistent with previous reports in Japan (*4*,*11*).

All patients infected with *H. suis* in this study were men. The percentage of men in the group infected with non–*H. suis* NHPH species was 50%, similar (57.8%) to that in the entire tested study population. Other studies have also demonstrated a high prevalence of *H. suis* infections among men (*11*). Future studies should investigate the difference in prevalence of *H. suis* infection between men and women by focusing on aspects such as the transmission route of infection. The natural hosts of *H. suis* are pigs and monkeys, and pork meat is suspected to be a carrier of *H. suis* infection to humans. In this study, a relationship between the history of pork offal ingestion

and *H. suis* infection was strongly suggested. Because a history of pork offal ingestion was found in only 40% of the no *Helicobacter* infection group, it was not always a risk factor for *H. suis* infection. However, hospital C, which had the highest percentage of *H. suis* infections, is located in an area where pork and pork offal are commonly eaten. A survey held in Japan in 2008 showed by using PCR that 74% of slaughtered sows were infected with *Helicobacter* spp. (*27*); however, updated surveys are needed to identify the current prevalence of *H. suis* infection in pigs.

Among NHPH-infected patients, 6 were infected with non–*H. suis* NHPH species. The non–*H. suis* NHPH species that infect dogs and cats are *H. felis*, *H. bizzozeronii*, *H. heilmannii*, *H. ailirogastricus*, *H. cynogastricus*, *H. baculiformis*, and *H. salomonis*. A survey of NHPH infections in dogs and cats in Japan indicated that 34.7% of dogs and 50% of cats were infected with NHPH species (*28*,*29*). Compared with other groups, 50% of patients infected with non–*H. suis* NHPH species had pet cats. Because not all patients had pets, pets might not be the only risk factor for non–*H. suis* NHPH infection. Multiple reports have suggested that non–*H. suis* NHPH species are transmitted from dogs and cats to humans (*23*–*26*), and studies demonstrating the genetic identity between strains from humans and pets will be needed to confirm that transmission. Species identification was not possible in this study because of the small number of bacterial cells in the samples. Further analysis using culture tests will be needed to identify non–*H. suis* NHPH species infecting humans.

No mixed infections of NHPH and *H. pylori* were observed; very low prevalences of mixed infections have been previously reported (*7*,*30*). Because NHPH infection was not observed in the posteradication group, *H. pylori* infection history might prevent NHPH infection, although further investigation is needed to clarify this possibility. Alternatively, NHPH might have also been eradicated by *H. pylori* eradication treatment. This study was conducted with patients who had undergone health checks in Japan; therefore, a substantial proportion of study participants had a history of *H. pylori* eradication therapy. Further analysis of a population with no history of *H. pylori i*nfection will be needed to clarify whether *H. pylori* infection prevents NHPH infection.

After we developed serologic tests for *H. suis* infection (*16*), we compared those results with PCR results. Serologic tests for *H. suis* infection revealed high detection sensitivity. Some patients in the no *Helicobacter* infection group tested positive in serologic tests for *H. suis* infection, and some of those patients had atrophic gastritis. Serologic tests will be useful to confirm PCR results and might help to detect overlooked *H. suis* infections. The serologic test for *H. suis* infection had low reactivity with the serum samples obtained from non–*H. suis* NHPH–infected patients. PCR remains the standard method for detecting NHPH infection, and a diagnostic method for non–*H. suis* NHPH infection is required. Some *H. pylori*–infected patients and patients with a history of *H. pylori* eradication showed positive serologic test results for *H. suis* infection, possibly because of cross-reactivity between *H. pylori* and NHPH species or NHPH infection might have been overlooked by PCR because of extremely low bacterial counts. Alternatively, the patients might have had a history of NHPH infection. Various possibilities exist; therefore, interviews regarding *H. pylori* eradication history are critical for accurately diagnosing NHPH infection by PCR and serologic tests. In addition to diagnostic testing, recognizing endoscopic characteristics of NHPH gastritis is essential. NHPH gastritis is antrum predominant and causes milder atrophy than *H. pylori* gastritis (*2*).

In this study, 94.1% (16/17) of patients with NHPH gastritis without *H. pylori* infection had RAC in the gastric corpus and had a Kimura-Takemoto classification of C-2 or lower, indicating that NHPH gastritis was localized within the angulus-antrum region and rarely extended to the gastric corpus (indicated by the presence of RAC). In addition, endoscopic gastritis of the pyloric canal was not observed in 60.0% of patients, suggesting that NHPH gastritis progresses from the angulus to the antrum, which differs from *H. pylori* gastritis, in which atrophy progresses from the antrum to the gastric body (Appendix Figure 2). In *H. pylori* gastritis, the incidence of gastric cancer increases as atrophy extends to the gastric body (*31*); however, in NHPH gastritis, atrophy does not extend to the gastric body, suggesting that gastric cancer might be less common. Because all asymptomatic NHPH-infected patients had MARC gastritis, nodular gastritis, or spotty redness similar to endoscopic gastritis, epidemiologic studies can determine whether NHPH gastritis is an etiopathogenic agent of gastric MALT lymphoma and peptic ulcers.

We found endoscopic characteristics of NHPH infection (i.e., MARC gastritis) in 93% of the *H. suis*–infected patients, which was more frequent than for *H. pylori*-infected patients (29%) and patients in the posteradication group (28%). Those findings were not observed in the non–*H. suis* NHPH group. Endoscopists should suspect NHPH infection, especially from *H. suis*, when NHPH-specific endoscopic characteristics

are found in *H. pylori*–negative patients. Nodular gastritis was found in 42.9% (6/14) of the *H. suis*–infected group, similar to the rate in the non–*H. suis* NHPH infected group (50.0%), and was more frequent than in *H. pylori*–infected patients (19.0%), although the difference was not significant. Differences in the pathogenesis and endoscopic findings between *H. suis* and non–*H. suis* NHPH infections might become more apparent as the number of patients increases.

The first limitation of our study is that the study population was highly health conscious and had a large number of patients who had undergone *H. pylori* eradication therapy. Because a difference in the prevalence of *H. suis* infection was detected among the study areas, the population background must have had a substantial influence on the prevalence of NHPH species. Continued surveys targeting other areas in Japan and other countries can provide comprehensive information to elucidate the prevalence of NHPH infections. Second, because the participants underwent medical checkups, the age of the target group was relatively high; very few young persons were in the study population. Although endoscopy cannot be performed at all ages, a study using serologic testing for *H. suis* infection might be useful to determine *H. suis* infection status in young persons.

In conclusion, the prevalence of NHPH infection in patients who underwent gastric endoscopy during medical checkups in Japan was 3.0%, similar to that of *H. pylori* infection (3.1%). Whether all NHPH-infected patients need to receive an eradication regimen remains controversial, as does the contribution of NHPH infections to gastric MALT lymphoma and peptic ulcers. In regions with decreasing rates of *H. pylori* infections, it is crucial to differentiate NHPH infections. Our findings provide critical information on the prevalence and endoscopic characteristics of NHPH infections in Japan. NHPH infections are zoonotic. Our findings that pork offal ingestion is a risk factor for *H. suis* infections and having pet cats increases risk for non–*H. suis* NHPH infection can help prevent gastric *Helicobacter* diseases.

This work was supported by the Japanese Society for *Helicobacter* Research, Japan Agency for Medical Research and Development (AMED grant nos. 23fk0108678 and 24ym0126140 to E.R.), Health Labour Sciences Research Grant (grant no. 21HA1005 to K.S., no. 24HA1002 to E.R.), and Ministry of Education, Culture, Sports, Science and Technology/Japan Society for the Promotion of Science KAKENHI program (grant no. 20K08365 to K.T., no. 23H02636 to E.R., and no. 24K11176 to K.T.). The authors declare no conflict of interest.

About the Author

Dr. Tokunaga is a professor in public health at Kyorin University School of Medicine in Japan. His main interests focus on gastric diseases, gastric *Helicobacter* infections, and preventive medicine.

References

1. Dent JC, McNulty CA, Uff JC, Wilkinson SP, Gear MW. Spiral organisms in the gastric antrum. Lancet. 1987;330:96. https://doi.org/10.1016/S0140-6736(87)92754-1
2. Stolte M, Kroher G, Meining A, Morgner A, Bayerdörffer E, Bethke B. A comparison of *Helicobacter pylori* and *H. heilmannii* gastritis. A matched control study involving 404 patients. Scand J Gastroenterol. 1997;32:28–33. https://doi.org/10.3109/00365529709025059
3. Morgner A, Lehn N, Andersen LP, Thiede C, Bennedsen M, Trebesius K, et al. *Helicobacter heilmannii*–associated primary gastric low-grade MALT lymphoma: complete remission after curing the infection. Gastroenterology. 2000;118:821–8. https://doi.org/10.1016/S0016-5085(00)70167-3
4. Nakamura M, Øverby A, Michimae H, Matsui H, Takahashi S, Mabe K, et al. PCR analysis and specific immunohistochemistry revealing a high prevalence of non-*Helicobacter pylori* Helicobacters in *Helicobacter pylori*-negative gastric disease patients in Japan: high susceptibility to an Hp eradication regimen. Helicobacter. 2020;25:e12700. https://doi.org/10.1111/hel.12700
5. Kadota H, Yuge R, Miyamoto R, Otani R, Takigawa H, Hayashi R, et al. Investigation of endoscopic findings in nine cases of *Helicobacter suis*–infected gastritis complicated by gastric mucosa-associated lymphoid tissue lymphoma. Helicobacter. 2022;27:e12887. https://doi.org/10.1111/hel.12887
6. Haesebrouck F, Pasmans F, Flahou B, Chiers K, Baele M, Meyns T, et al. Gastric helicobacters in domestic animals and nonhuman primates and their significance for human health. Clin Microbiol Rev. 2009;22:202–23. https://doi.org/10.1128/CMR.00041-08
7. De Groote D, Van Doorn LJ, Van den Bulck K, Vandamme P, Vieth M, Stolte M, et al. Detection of non-pylori *Helicobacter* species in "*Helicobacter heilmannii*"–infected humans. Helicobacter. 2005;10:398–406. https://doi.org/10.1111/j.1523-5378.2005.00347.x
8. Rimbara E, Suzuki M, Matsui H, Nakamura M, Morimoto M, Sasakawa C, et al. Isolation and characterization of *Helicobacter suis* from human stomach. Proc Natl Acad Sci USA. 2021;118:e2026337118. https://doi.org/10.1073/pnas.2026337118
9. Heilmann KL, Borchard F. Gastritis due to spiral shaped bacteria other than *Helicobacter pylori*: clinical, histological, and ultrastructural findings. Gut. 1991;32:137–40. https://doi.org/10.1136/gut.32.2.137
10. Okiyama Y, Matsuzawa K, Hidaka E, Sano K, Akamatsu T, Ota H. *Helicobacter heilmannii* infection: clinical, endoscopic and histopathological features in Japanese patients. Pathol Int. 2005;55:398–404. https://doi.org/10.1111/j.1440-1827.2005.01844.x
11. Tsukadaira T, Hayashi S, Ota H, Kobayashi N, Sekiguchi Y, Kodaira H, et al. Prevalence, clinical features, and esophagogastroduodenoscopy (EGD) findings of non-*Helicobacter pylori Helicobacter* infection: a study of 50 cases at a single facility in Japan. Helicobacter. 2021;26:e12811. https://doi.org/10.1111/hel.12811

12. Taillieu E, De Witte C, De Schepper H, Van Moerkercke W, Rutten S, Michiels S, et al. Clinical significance and impact of gastric non-*Helicobacter pylori Helicobacter* species in gastric disease. Aliment Pharmacol Ther. 2023;57:1432–44. https://doi.org/10.1111/apt.17488
13. Rimbara E, Tamura R, Tanuma M, Noguchi N, Kawai T, Sasatsu M. Evaluation of clarithromycin resistance in *Helicobacter pylori* obtained from culture isolates, gastric juice, and feces. Helicobacter. 2009;14:156–7. https://doi.org/10.1111/j.1523-5378.2009.00663.x
14. Tsuda M, Watanabe Y, Oikawa R, Watanabe R, Higashino M, Kubo K, et al. Clinical evaluation of a novel molecular diagnosis kit for detecting *Helicobacter pylori* and clarithromycin-resistant using intragastric fluid. Helicobacter. 2022;27:e12933. https://doi.org/10.1111/hel.12933
15. Matsui H, Suzuki M, Aoki S, Shibayama K, Tokunaga K, Suzuki H, et al. Protocol for detecting *Helicobacter suis* infection in gastric biopsies and serum by PCR and ELISA. STAR Protoc. 2023;4:102556. https://doi.org/10.1016/j.xpro.2023.102556
16. Matsui H, Rimbara E, Suzuki M, Tokunaga K, Suzuki H, Sano M, et al. Development of serological assays to identify *Helicobacter suis* and *H. pylori* infections. iScience. 2023;26:106522. https://doi.org/10.1016/j.isci.2023.106522
17. Kimura K, Takemoto T. An endoscopic recognition of the atrophic border and its significance in chronic gastritis. Endoscopy. 1969;1:87–97. https://doi.org/10.1055/s-0028-1098086
18. Shiratori S, Mabe K, Yoshii S, Takakuwa Y, Sato M, Nakamura M, et al. Two cases of chronic gastritis with non-*Helicobacter pylori Helicobacter* infection. Intern Med. 2016;55:1865–9. https://doi.org/10.2169/internalmedicine.55.5891
19. Yagi K, Nakamura A, Sekine A. Characteristic endoscopic and magnified endoscopic findings in the normal stomach without *Helicobacter pylori* infection. J Gastroenterol Hepatol. 2002;17:39–45. https://doi.org/10.1046/j.1440-1746.2002.02665.x
20. Haruma K, Kato M, Inoue K, Murakami K, Kamada T, editors. Kyoto classification of gastritis. Tokyo: Nihon Medical Center; 2017.
21. Okuda M, Osaki T, Kikuchi S, Ueda J, Lin Y, Yonezawa H, et al. Evaluation of a stool antigen test using a mAb for native catalase for diagnosis of *Helicobacter pylori* infection in children and adults. J Med Microbiol. 2014;63:1621–5. https://doi.org/10.1099/jmm.0.077370-0
22. Wang C, Nishiyama T, Kikuchi S, Inoue M, Sawada N, Tsugane S, et al. Changing trends in the prevalence of *H. pylori* infection in Japan (1908–2003): a systematic review and meta-regression analysis of 170,752 individuals. Sci Rep. 2017;7:15491. https://doi.org/10.1038/s41598-017-15490-7
23. Sano M, Rimbara E, Suzuki M, Matsui H, Hirai M, Aoki S, et al. *Helicobacter ailurogastricus* in patient with multiple refractory gastric ulcers, Japan. Emerg Infect Dis. 2023;29:833–5. https://doi.org/10.3201/eid2904.221807
24. Wüppenhorst N, von Loewenich F, Hobmaier B, Vetter-Knoll M, Mohadjer S, Kist M. Culture of a gastric non-*Helicobacter pylori Helicobacter* from the stomach of a 14-year-old girl. Helicobacter. 2013;18:1–5. https://doi.org/10.1111/j.1523-5378.2012.00990.x
25. Jalava K, On SL, Harrington CS, Andersen LP, Hänninen ML, Vandamme P. A cultured strain of "*Helicobacter heilmannii*," a human gastric pathogen, identified as *H. bizzozeronii*: evidence for zoonotic potential of *Helicobacter*. Emerg Infect Dis. 2001;7:1036–8. https://doi.org/10.3201/eid0706.010622
26. Kivistö R, Linros J, Rossi M, Rautelin H, Hänninen ML. Characterization of multiple *Helicobacter bizzozeronii* isolates from a Finnish patient with severe dyspeptic symptoms and chronic active gastritis. Helicobacter. 2010;15:58–66. https://doi.org/10.1111/j.1523-5378.2009.00730.x
27. Kikuchi M, Iwaya O, Endo H, Sigeta F, Une M, Osaka S, et al. The presence of *Helicobacter* infection in sows. Nippon Juishikai Zasshi. 2004;57:310–2. https://doi.org/10.12935/jvma1951.57.310
28. Kubota-Aizawa S, Ohno K, Kanemoto H, Nakashima K, Fukushima K, Uchida K, et al. Epidemiological study on feline gastric *Helicobacter* spp. in Japan. J Vet Med Sci. 2017;79:876–80. https://doi.org/10.1292/jvms.16-0567
29. Kubota-Aizawa S, Ohno K, Fukushima K, Kanemoto H, Nakashima K, Uchida K, et al. Epidemiological study of gastric *Helicobacter* spp. in dogs with gastrointestinal disease in Japan and diversity of *Helicobacter heilmannii* sensu stricto. Vet J. 2017;225:56–62. https://doi.org/10.1016/j.tvjl.2017.04.004
30. Liu J, He L, Haesebrouck F, Gong Y, Flahou B, Cao Q, et al. Prevalence of coinfection with gastric non-*Helicobacter pylori Helicobacter* (NHPH) species in *Helicobacter pylori*-infected patients suffering from gastric disease in Beijing, China. Helicobacter. 2015;20:284–90. https://doi.org/10.1111/hel.12201
31. Uemura N, Okamoto S, Yamamoto S, Matsumura N, Yamaguchi S, Yamakido M, et al. *Helicobacter pylori* infection and the development of gastric cancer. N Engl J Med. 2001;345:784–9. https://doi.org/10.1056/NEJMoa001999

Addresses for correspondence: Emiko Rimbara, Department of Bacteriology II, National Institute of Infectious Diseases; 4-7-1 Gakuen, Musashimurayama-shi, Tokyo 208-0011, Japan; email: rimbara@niid.go.jp; and Kengo Tokunaga, Department of Preventive Medicine, Kyorin University School of Medicine, 6-20-2 Shinkawa, Mitaka-shi, Tokyo 181-8611, Japan; email: kentoku@ks.kyorin-u.ac.jp

Safety and Immunogenicity of Poultry Vaccine for Protecting Critically Endangered Avian Species against Highly Pathogenic Avian Influenza Virus, United States

Todd E. Katzner, Ashleigh V. Blackford, Mary Donahue, Samantha E.J. Gibbs, Julianna Lenoch, Michael Martin, Tonie E. Rocke, J. Jeffrey Root, Darrel Styles, Sunny Cooper, Kristin Dean, Zachary Dvornicky-Raymond, Dominique Keller, Carlos Sanchez, Brett Dunlap, Thomas Grier, Michael P. Jones, Gregory Nitzel, Erin Patrick, Maureen Purcell, Aaron J. Specht, David L. Suarez

In 2023, an outbreak of highly pathogenic avian influenza occurred among critically endangered California condors (*Gymnogyps californianus*), and ≥21 died. We evaluated safety, immunogenicity, vaccination strategies, and correlates of antibody response of an influenza vaccine for poultry in black vultures (*Coragyps atratus*) and then California condors. We noted differences in antibody titers between vaccinated and unvaccinated birds (vultures $p \leq 0.004$; condors $p \leq 0.02$) but no adverse effects of vaccination. All vaccinated vultures and 80% of vaccinated condors showed maximum measured antibody response within the published range associated with survival of vaccinated and virally challenged chickens. We noted weak evidence of higher antibody responses for birds given two 0.5-mL vaccines versus those given one 1-mL vaccine but no correlation between antibody titers and sex for either species or between antibody titers and bone lead concentrations in vultures. Our results prompted initiation of a vaccination program for condors that could reduce spread of this disease among highly threatened species.

Emerging infectious diseases are a growing threat to global biodiversity and particularly to endangered species (*1*). Since 2020, highly pathogenic avian influenza (HPAI) virus (HPAIV) of the goose/Guangdong/1996 (GS/GD/96) lineage, specifically influenza A(H5N1) clade 2.3.4.4b, has caused a panzootic in poultry and wild birds (*2*,*3*) and subsequent spillover into some wild mammals (*4*). Birds, especially those in the orders Anseriformes and Charadriiformes, can be infected with

Author affiliations: US Geological Survey, Forest and Rangeland Ecosystem Science Center, Boise, Idaho, USA (T.E. Katzner, M. Purcell); US Fish and Wildlife Service, California Condor Recovery Program, Vero Beach, Florida, USA (A.V. Blackford); US Department of Agriculture, Animal and Plant Health Inspection Service (APHIS) Veterinary Services, Minneapolis, Minnesota, USA (M. Donahue); US Fish and Wildlife Service, National Wildlife Refuge System, Wildlife Health Office, Chiefland, Florida, USA (S.E.J. Gibbs); US Department of Agriculture, APHIS Wildlife Services, National Wildlife Disease Program, Fort Collins, Colorado, USA (J. Lenoch); North Carolina Department of Agriculture and Consumer Services, Raleigh, North Carolina, USA (M. Martin); US Geological Survey, National Wildlife Health Center, Madison, Wisconsin, USA (T.E. Rocke); US Department of Agriculture, APHIS Wildlife Services, National Wildlife Research Center, Fort Collins (J.J. Root); US Department of Agriculture, APHIS Veterinary Services, Riverdale, Maryland, USA (D. Styles); Carolina Raptor Center, Huntersville, North Carolina, USA (S. Cooper, K. Dean); San Diego Zoo Wildlife Alliance, San Diego, California, USA (Z. Dvornicky-Raymond); Los Angeles Zoo and Botanical Garden, Los Angeles, California, USA (D. Keller); Oregon Zoo, Portland, Oregon, USA (C. Sanchez); US Department of Agriculture, APHIS Wildlife Services, Madison, Tennessee, USA (B. Dunlap); Purdue University School of Health Sciences, West Lafayette, Indiana, USA (T. Grier, A.J. Specht); American Eagle Foundation, Kodak, Tennessee, USA (M.P. Jones); Zoetis, Inc., Kalamazoo, Michigan, USA (G. Nitzel); US Department of Agriculture, APHIS Wildlife Services, Knoxville, Tennessee, USA (E. Patrick); US Department of Agriculture, Southeast Poultry Research Laboratory, Agricultural Research Service, Athens, Georgia, USA (D.L. Suarez)

DOI: https://doi.org/10.3201/eid3106.241558

avian influenza viruses, with or without showing clinical signs, and can shed high quantities of virus (*5*), enabling widespread dispersion. HPAIV infections from the current H5N1 lineage were first detected in wild birds in the United States in January 2022 (*6*). In addition, deaths among many wild bird species infected with H5N1 HPAIV appear to have contributed to deaths among predatory and scavenging mammals and birds that consume carcasses of infected animals (*6*–*8*).

One of the highest profile wildlife species known to be affected by HPAI in North America is the California condor (*Gymnogyps californianus*) (Figure 1, panel A). California condors are critically endangered, and only ≈560 birds exist in 5 geographically dispersed wild subpopulations and in captivity (*9*). Exposure to lead, an immunosuppressant that also lethally poisons avian scavengers, has been the most critical factor limiting growth and recovery of condor populations, and the continued existence of this species is largely the result of ongoing field-based and captive conservation efforts that began in the 1970s (*10*). In 2023, the subpopulation of condors that occupies northern Arizona and southern Utah experienced an HPAI outbreak during which ≥21 birds (≈18% of the subpopulation) died; other subpopulations were not affected (*9*,*11*).

Considering the conservation consequences of that outbreak, vaccination was evaluated as a potential means to reduce illness, death, and virus transmission or shedding (*12*). Vaccines for HPAIV have been used for decades in some countries where the virus is endemic in poultry or where a high likelihood of virus transmission exists in the environment (*13*). However, we found no data on vaccination of condors against avian influenza, although captive studies of other species, including raptors, demonstrated antibody responses (*14*) and a protective immune response (*15*) from administration of an influenza subtype H5N2 vaccine.

For critically endangered species, evaluating the potential risk from vaccination by first conducting trials on surrogate species is appropriate (*16*). Black vultures (*Coragyps atratus*) (Figure 1, panel B) are a good surrogate for California condors because they are susceptible to HPAIV infection (*8*), are co-familial and abundant, and are readily available for study because they are sometimes lethally controlled as a nuisance species (*17*). We evaluated safety, immunogenicity, vaccination regimens, and correlates of antibody response for a conditionally licensed influenza subtype H5N1 vaccine designed for poultry, first in black vultures as a surrogate species, and then in California condors. Our specific objectives were to determine the safety and immunogenicity of the vaccine in vultures and, if warranted by those results, subsequently in condors; to compare the typical prime-boost vaccination regimen used for poultry to a single-vaccination regimen that could be more feasible for wild birds; and to evaluate 2 correlates of antibody response of vultures, sex and lead exposure.

Figure 1. Photographs of avian species tested in study of safety and immunogenicity of poultry vaccine for protecting critically endangered avian species from highly pathogenic avian influenza virus, United States. A) California condor (*Gymnogyps californianus*), whose infection with highly pathogenic avian influenza virus was the motivation for this research. B) Black vulture (*Coragryps atratus*), closely related species used as a surrogate for condors in this research. Photo credits: panel A, US Fish and Wildlife Service public domain; panel B, Todd E. Katzner.

Materials and Methods

Vaccines

For our trials, we used an H5N1 subtype, reverse genetics-derived, inactivated vaccine that includes genes from the gyrfalcon/2014 virus, avian influenza vaccine (1057.R1 serial 590088) (rgH5N1) (Zoetis, Inc., https://www.zoetis.com), as previously described (*18*). The US Department of Agriculture (USDA) (*19*), the US Fish and Wildlife Service (USFWS), the North Carolina Department of Agriculture, and the North Carolina Wildlife Resources Commission specifically authorized use of that conditionally licensed vaccine for vultures, and numerous state and federal agencies subsequently approved its use in condors (Appendix Table 1, https://wwwnc.cdc.gov/EID/article/31/6/24-1558-App1.pdf).

Lead Exposure of Vultures

We evaluated lead exposure of vultures by measuring bone lead concentrations with a portable x-ray fluorescence (XRF) device (*20*) 66 days after they were removed from the wild and 53 days after the start of the vaccine trial. An XRF device measures backscatter radiation signals to noninvasively infer lead density in bone, a technique used for years in humans and recently adapted for use with birds of prey (*21*,*22*). We placed the XRF device against the leg (tarsometatarsus) of the living bird, where it measured spectra that were then interpreted as lead concentrations (*21*). Bone lead measurements are typically considered indicative of cumulative or long-term exposure to lead, whereas blood measurements are indicative of more recent, acute, exposure (*23*). Because all condors in the study were captive and fed untainted food, we did not evaluate their bone lead.

Study Design

We randomly assigned 28 vultures to 1 of 3 treatment groups (Appendix). We vaccinated 1 group of 10 vultures (4 male, 6 female) with a prime-boost (2-vaccine) regimen typically used for poultry, in which 0.5 mL is given on day 0 and again on day 21. We gave another group of 10 vultures (all female) a 1-vaccine regimen of 1.0 mL on day 0. A third group of 8 vultures (1 male, 7 female) remained unvaccinated to serve as a control group.

We administered vaccine subcutaneously between the shoulder blades because that location is near the standard subcutaneous vaccine site used for poultry (back of the neck) and because it avoids the cervical and other air sacs along the back. We did not use a sham vaccine (e.g., saline) on control birds. Experienced wildlife husbandry professionals monitored all birds daily for signs of lethargy, reduction of food intake, and other potential indicators of an adverse vaccine reaction. They also visually evaluated the vaccine site 3 days after each vaccination. We collected blood samples from all vultures 1 day before and 10, 21, 31, and 42 days after the initial vaccination. We used 42 days postvaccination (dpv) as the experimental endpoint because that is the standard for vaccine experiments in poultry (*18*), and because of challenges in keeping vultures in captivity.

We used a similar design for the condor trial, giving the 2-vaccine regimen to 10 birds and the 1-vaccine regimen to 10 birds and using 5 unvaccinated birds as controls (Appendix). However, because condors are highly endangered and no single facility holds large numbers, we made several modifications to the design of the trial to reduce risk and stress to birds. Specifically, because birds are held at multiple different locations, we identified 10 birds at the Los Angeles Zoo and Botanical Gardens (LAZ) (2 male, 6 female) and San Diego Zoo Wildlife Alliance (SDZ) (1 male, 1 female) for the prime-boost regimen, 10 at SDZ (4 male, 2 female) and Oregon Zoo (ORZ) (2 male, 2 female) for the single-vaccine regimen, and 5 at ORZ (3 male, 2 female) as controls. We staged implementation of the trial and vaccinated 3 condors in each regimen group first, then vaccinated the remaining condors in that group only after confirming that the first birds had no apparent short-term negative effects, as described for vultures. For condors, we administered the vaccine in the inguinal region to avoid the cervical air sacs, which are larger than those found in vultures. Finally, because of concerns for potential problems caused by frequent handling of these critically endangered birds, we conducted blood draws for serologic analyses less frequently than for vultures, at 0, 21, and 42 dpv.

Laboratory Analyses

We evaluated vaccine-induced antibody formation for all birds by using both an ELISA, AI MultiS-Screen Ab Test (IDEXX Laboratories, https://www.idexx.com), to detect antibodies to the nucleoprotein of influenza A viruses and a hemagglutination inhibition (HI) assay (*24*). We also evaluated blood chemistry for vultures at 31 dpv (Appendix).

Data Analyses

We used HI titers to statistically compare the antibody response among treatment groups. We inferred potential conservation value of vaccinating condors by comparing HI titers obtained in our study to a

prior study that established correlates of vaccine protection by linking postvaccination HI titers to survival of domestic chickens (*Gallus gallus domesticus*) in a viral challenge (*18*). Chickens given the same vaccine used in our study had antibody titers ranging from 16 to 1,024, and 100% survived infection with the virus (*18*). Thus, to interpret the conservation value of the vaccines, we conservatively assumed that an antibody titer of ≥16 was responsive to vaccination and that a titer of ≥32 likely provided adequate protection against death. We considered HI titers ≤8 as nonresponsive and likely nonprotective.

We used a Wilcoxon test to compare antibody titers for vaccinated and unvaccinated birds using wilcox.test in R (The R Project for Statistical Computing, https://www.r-project.org). We used Kruskal-Wallis tests (kruskal.test) with Dunn's test (package dunn.test) of multiple comparisons in R to evaluate differences in antibody titers and in blood chemistry for birds given 0, 1, or 2 vaccinations. We used another Wilcoxon test to test for sex-specific differences in antibody responses to vaccination for the subset of groups in which both sexes were represented. We generated effect estimates for both the Kruskal-Wallis and Wilcoxon tests (*25*). Finally, because lead can suppress immune response to vaccination, we used a Pearson correlation (corr.test in R) to evaluate HI titers of vultures as a function of bone lead concentration. In all cases, we considered $p<0.05$ indicative of differences between groups.

Results

Vaccine Safety

Vaccinated vultures showed no adverse effects, and we detected no changes in behavior or food intake. We did detect small (≈5 mm) and temporary nodules at the injection site on 2 vultures after the first round of vaccination. Blood chemistry of vaccinated vultures was generally unremarkable (Appendix Table 2). No condors vaccinated in this trial showed adverse behavioral or physical effects linked to vaccination.

Vaccine Immunogenicity in Vultures

Of the 28 vultures, 27 had negative ELISA results at the start of the study; 1 bird had a positive ELISA result before vaccination, indicating prior exposure to an avian influenza A virus (Appendix Table 3). We detected a positive HI antibody response in all 20 vaccinated vultures at some point during the 42-day trial and in none of the control (unvaccinated) birds (Table 1; Figure 2, panel A; Appendix Table 3). Statistical tests suggested that HI titers were different, and higher, for vaccinated birds than for unvaccinated birds starting at 21 days after the first vaccination: at 10 dpv, Wilcoxon rank-sum value (W) = 81 ($p = 0.962$); at 21 dpv, $W = 28$ ($p = 0.004$); at 31 dpv, $W = 4$ ($p<0.001$); at 42 dpv, $W = 8$ ($p<0.001$). Outcomes of statistical tests were similar when we excluded the 1 bird previously exposed to an influenza A virus (Appendix).

Of 20 vaccinated birds, 19 (95%) had titers ≥32 on ≥1 postvaccination blood draw. The exception was 1 of the birds in the 1-vaccine group; its highest titer was 16 on day 42. The bird with presumed prior influenza A virus exposure was in the 2-vaccine group and appeared to have a faster and generally stronger antibody response to vaccination than the other birds (Appendix Table 3). At 10 dpv, 2 (10%) birds had titers ≥16; at 21 dpv, 13 (65%) birds had titers above that level, 19 (95%) did at 31 dpv, and 18 (90%) did at 42 dpv.

All vaccinated vultures also tested positive for an antibody response by ELISA at some point over the 42-day trial. At 42 dpv, 1 bird that received the 2-vaccine regimen and 1 bird that received the 1-vaccine regimen had negative ELISA results; HI titers measured at the same time were 0 for the bird in the 2-vaccine group and 256 for the bird in the 1-vaccine group.

Vaccine Immunogenicity in Condors

We detected a positive HI antibody response in 16 (80%) of the 20 vaccinated condors at some point during the 42-day trial and in none of the control (unvaccinated) birds (Table 1; Figure 2, panel B; Appendix Table 4). Of the 4 nonresponsive but immunized birds, 1 that received the 1-vaccine regimen had an HI titer of 0; the other 3 birds, 2 from the 1-vaccine group and 1 from the 2-vaccine group, had HI titers of 8. Two of the birds that showed no antibody response from the 1-vaccine group were only tested for HI antibodies at 21 dpv and not at 42 dpv. Statistical tests suggested higher HI titers at both blood draws for vaccinated birds relative to unvaccinated birds: at 21 dpv, $W = 17.5$ ($p = 0.020$); at 42 dpv, $W = 12.5$ ($p = 0.017$) (note that at 42 dpv, HI data were available for only 6 birds in the 1-vaccine group). Nine (45%) of 20 vaccinated birds had HI titers ≥32 on ≥1 of the postvaccination blood draws. At 21 dpv, 10 (50%) birds had an HI titer ≥16, and 4 of those also were ≥32. At 42 dpv, 10 (62.5%) of 16 birds had an antibody response of ≥16, and 6 of those also were ≥32.

Of the 20 vaccinated condors, 18 (90%) also tested positive for an antibody response by ELISA at some point over the 42-day trial. At 21 dpv, 9 birds

Table 1. Hemagglutination inhibition antibody titers in surrogate and target species in a study of safety and immunogenicity of poultry vaccine for protecting critically endangered avian species from highly pathogenic avian influenza virus, United States*

Time, dpv	HI titer [SD] (range) per vaccine regimen			χ^2	p value	η^2	Intergroup difference (p value)		
	None, n = 8	1-vaccine, n = 10	2-vaccine, n = 10				None–1 vaccine	None–2 vaccines	1–2 vaccines
Black vultures (*Coragryps atratus*)									
10	0 [0.7] (0–2)	0 [5.1] (0–16)	0 [81.0] (0–256)	0.01	0.994	−0.08	NA	NA	NA
21	0	32 [96.8] (0–256)	16 [82.9] (0–256)	9.65	0.008	0.31	−3.09 (**0.006**)	−2.019 (0.130)	1.13 (0.774)
31	0	96 [75.6] (0–256)	64 [40.5] (32–128)	16.01	<0.001	0.56	−3.50 (**0.001**)	−3.55 (**0.001**)	−0.06 (1.00)
42	0	64 [73.6] (0–256)	128 [180.5] (0–512)	16.26	<0.001	0.57	−2.71 (**0.020**)	−3.99 (**<0.001**)	−1.35 (0.528)
California condors (*Gymnogyps californianus*)									
21	0	16 [19.3] (0–64)	4 [11.0] (0–32)	7.49	0.024	0.25	−2.72 (**0.020**)	−1.59 (0.334)	1.38 (0.501)
42†	0	12 [7.9] (0–16)	32 [20.3] (0–64)	7.42	0.025	0.25	−1.40 (0.484)	−2.71 (**0.0203**)	−1.23 (0.656)

*Bold text indicates statistical significance. Birds were vaccinated with a 1057.R1 serial 590088 Avian Influenza Vaccine, H5N1 subtype, reverse genetics-derived, inactivated vaccine. See main text for details on the vaccine and vaccination regimens. Titers were compared by using Kruskal-Wallis test reporting a χ^2, a p value, and an effect estimate (η^2); degrees of freedom = 2 in all tests and, when different, a Dunn's multiple comparison (reporting a Z statistic and a p value). dpv, days postvaccination; HI, hemagglutination inhibition; NA, no difference detected so multiple comparison not relevant. †For day 42, HI titers are only available for 6 condors given a single vaccination.

given the 1-vaccine regimen and 4 given the 2-vaccine regimen had a positive ELISA result. At 42 dpv, four 1-vaccine regimen birds and seven 2-vaccine regimen birds had positive ELISA test results. The 2 birds with a negative ELISA were both in the 2-vaccine group, and both had HI titers of 16 at day 21 and of 0 at day 42.

Response to Vaccine Regimen

We detected statistically relevant differences between vultures that were vaccinated and those that were not but not between vultures that received the different vaccination regimens (Table 1). The mean maximum HI titer (188.8) of vultures that received the 2-vaccine regimen trended higher compared with birds that received the 1-vaccine regimen (mean maximum = 126.4). At 21 dpv, 80% of the birds in the 1-vaccine group and 50% in 2-vaccine group had titers ≥32. At 32 dpv, 80% of the birds in the 1-vaccine group and 100% in the 2-vaccine group had titers ≥32. At 42 dpv, 70% of the birds in the 1-vaccine group and 90% in the 2-vaccine group had titers ≥32.

For condors, we detected statistically relevant differences between vaccinated and unvaccinated birds, but not between those given the different vaccine regimens (Table 1). Despite that finding, at 21 dpv, only 1 of the 2-vaccine regimen birds had an HI titer ≥32, and 4 had titers ≥16; three birds in the 1-vaccine group had titers ≥32 and 6 had titers ≥16. At 42 dpv, of the birds in the 2-vaccine group, 6 had titers ≥32, and 7 had titers ≥16; of the birds given the 1-vaccine regimen, 0 had titers ≥32 and 3 had titers ≥16 (note that HI data are only available for 6 birds in the 1-vaccine group at 42 dpv). In the 2-vaccine group, only 1 bird was deemed nonresponsive over the course of the trial (titer was 8); in the 1-vaccine group, 3 birds met that criterion (titers were 0, 8, and 8).

Correlates of Antibody Response

We detected no sex-related differences in antibody response for vultures given the 2-vaccine regimen (Table 2) or condors given either regimen (Table 3). Although the sex ratio of our sample group was not even, for vultures, the maximum antibody response in each group was always highest for female birds. That did not appear to be the case for condors.

We did not detect a relationship between bone lead concentrations and antibody response of vultures at any time postvaccination. The absolute value of the correlation coefficients tended to be low, ranging from 0.1 to 0.5, and the tests indicated no evidence of correlations (p>0.05) (Appendix Table 5). However, 7 of the 8 correlation coefficients were negative, and the strongest antibody responses tended to be in the vultures with the lowest bone lead concentrations (Appendix Figure).

Discussion

Many types of HPAIV vaccines have been developed (*26*), including inactivated whole virus vaccines, subunit vaccines, and live vectored viral vaccines (*27*). Risk analysis for this vaccination trial included consideration of the potential to stimulate a protective immune response, legal availability of the vaccine, and the antigenic relatedness of vaccines to a potential field challenge. That approach led us to select the inactivated adjuvanted reverse genetics vaccine for this trial because it safely stimulated immune responses in multiple avian species and because it has ≈95.6% amino acid similarity to the currently circulating H5N1 2.3.4.4b virus isolates.

Although nearly all birds of both species responded immunologically to the vaccine, the generally stronger short-term antibody responses of black vultures compared with California condors are notable. Interspecific differences are not surprising because

vaccines developed for one species can have unexpected effects in other species and related species can have substantially different responses to vaccination (*28*). Despite those differences, maximum HI titers of vultures given a 2-vaccine regimen were similar to those reported for domestic fowl given a similar vaccination regimen (i.e., vulture maximum titers were 32–512, chicken titers at 42 dpv were 16–1,024) (18). Similarly, maximum titers of condors given a 2-vaccine regimen were 8–64, and all but 1 titer was within the lower end of the range reported for chickens.

Work with endangered species presents many hurdles and often precludes the possibility of testing the effectiveness of a vaccine with a viral challenge (*29*). Furthermore, because of the dramatic impacts of HPAI on wild condors, we conducted the trials rapidly and in an extremely urgent context. Together with biosafety considerations, those issues made it impractical to conduct a logistically difficult viral challenge for the vultures or to evaluate longer-term immune response. However, we can draw inference from prior work with this vaccine. As we noted, 100% of chickens given this same vaccine responded with similar antibody levels and survived a viral challenge at 42 dpv (*18*). Given the similarity of those responses, had a viral challenge at 42 dpv had been feasible, we reason that most if not all vultures, and perhaps condors, would likely have survived.

The vaccine we evaluated was developed for prime-boost (2-vaccine) application. However, because trapping and handling can stress condors, we evaluated a 1-vaccine regimen as an alternative to the originally designed regimen. Despite the lack of a statistical difference between antibody responses associated with the 2 regimens, qualitative evaluation suggested that antibody responses were weaker and dissipated more rapidly for the birds that received the 1-vaccine regimen. Thus, we suspect that if birds were given a viral challenge, birds that received prime and boost vaccinations would have been more effectively protected than those vaccinated once. However, because our study ended at 42 dpv, we could not evaluate the potential for differences in waning immunity (*30*) between the 2 vaccine strategies.

Our failure to detect a statistical effect of either sex or bone lead concentration on antibody response might have been because of the small sample sizes and skewed sex ratios in our trials. Trends in the data suggested that if our sample size had been larger and the sex ratios more even, we might have detected differences in responses between sexes. Likewise, in the case of the response to bone lead concentrations, the statistical approach we used might not have uncovered difficult-to-detect patterns. We noted that, regardless of vaccine regimen, the birds with the strongest antibody response were also those with the lowest bone lead level. Therefore, subsequent trials might evaluate the presence of threshold-type effects in those responses.

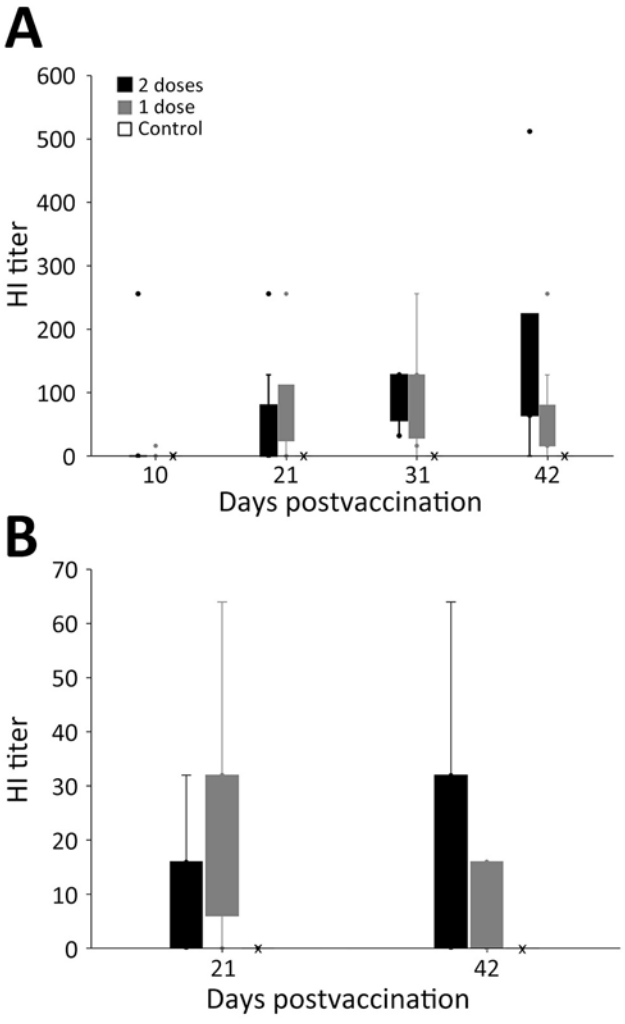

Figure 2. Hemagglutination inhibition (HI) titers in a study of safety and immunogenicity of poultry vaccine for protecting critically endangered avian species from highly pathogenic avian influenza virus, United States. A) Titers for 28 black vultures (*Coragryps atratus*); B) titers for 25 California condors (*Gymnogyps californianus*). Birds were included in 1 of 3 highly pathogenic avian influenza vaccine trial groups comprised of 10 birds given two 0.5-mL vaccinations at days 0 and 21, another 10 birds given a single 1-mL vaccination at day 0, and 8 vultures and 5 condors that were unvaccinated negative controls. Vaccinated animals were given a 1057.R1 serial 590088 avian influenza accine, H5N1 subtype, reverse genetics-derived, inactivated vaccine (see main text for details on the vaccine). For vultures, postvaccination blood draws were conducted at 10, 21, 31, and 42 days after first vaccination; for condors, blood draws were on days 21 and 42. Box tops and bottoms show quartiles, whiskers are 95% CI, dots outliers; X indicates 0 values for control groups.

Table 2. Antibody titers and bone lead levels in black vultures (*Coragryps atratus*) in a trial to evaluate safety and immunogenicity of poultry vaccine for protecting a critically endangered avian species from highly pathogenic avian influenza virus, United States*

		10 dpv		21 dpv		31 dpv		42 dpv	
Birds	Mean lead	Mean HI [SD]	Median HI (range)	Mean HI [SD]	Median HI (range)	Mean HI [SD]	Median HI (range)	Mean HI [SD]	Median HI (range)
Sex									
F, n = 6	22.76	43 [104]	0 (0–256)	80 [99]	48 (0–256)	101 [46]	128 (32–128)	235 [218]	128 (64–512)
M, n = 4	18.67	0	0	8 [16]	0 (0–32)	56 [16]	64 (32–64)	96 [64]	128 (0–128)
W		14		15		12		6.5	
p value		0.54		0.56		1.00		0.25	
R		0.37		0.39		0.35		0.25	

*Antibody titers (as determined by hemagglutination inhibition) and mean bone lead levels (as determined by XRF), organized by sex for black vultures given a 1057.R1 serial 590088 avian influenza vaccine, H5N1 subtype, reverse genetics-derived, inactivated vaccine (see main text for details on the vaccine). Only vultures given a 2-vaccine regimen were considered; those given a 1-vaccine regimen were all female. Titers were compared between sexes at each timepoint with a Wilcoxon rank-sum test (*W*), a p value (p), and an effect estimate (*R*). dpv, days postvaccination; HI, hemagglutination inhibition.

Given the virulence and spread of the currently circulating HPAIV, vaccination of threatened and endangered wild birds could be a potential tool to mitigate losses from this disease. Vaccination may be particularly relevant when the resiliency of populations has decreased to the extent that naturally occurring illness and death from disease could impair the species' long-term persistence. Despite the potential value of that approach, negative consequences of vaccination are possible, and this trial and implementation in the condor program are unique within the United States. Given the importance of economic considerations associated with poultry farming, close coordination with the USDA and many other federal and state agencies was essential to receive authorization to implement these vaccination trials. However, the outcomes from these trials were positive enough, and the threat from HPAIV so great, that the USFWS subsequently decided to initiate a vaccination program for the California Condor Recovery Program (*11*). By October 2024, a total of 207 condors had received ≥1 vaccination (*30*).

Species-specific variations in physiological response to vaccination are characteristic problems associated with vaccination programs for wildlife (*31*). Despite such variations, evidence suggests that vaccination strategies that reach <50% of an affected wildlife population can still be effective at staving off extinction (*32*,*33*). Those trends, together with results of our work, suggest several next steps for protecting endangered wildlife, whether condors or other species, from infectious diseases. Vaccination of the at-risk population of the target species can begin once safety, immunogenicity, and vaccination regimens have been established and some correlate of protection established, either from published work with other species or from direct challenge trials. Critical next steps include monitoring vaccine effectiveness in field settings and demographic modeling to understand the most effective strategy for vaccination of wild animals. Specifically, given the challenges inherent in vaccinating wild animals, using life history traits of the species in question, together with population modeling, can confirm the

Table 3. Antibody titers for California condors (*Gymnogyps californianus*) in a study of the safety and immunogenicity of poultry vaccine for protecting critically endangered avian species from highly pathogenic avian influenza virus, United States*

	21 dpv		42 dpv	
Vaccine regimen	Mean HI [SD]	Median HI (range)	Mean HI [SD]	Median HI (range)
1-vaccine†				
Sex				
F, n = 7	32 [23]	24 (16–64)	16 [0]	16 (16–16)
M, n = 3	11 [12]	8 (0–32)	6 [8]	4 (0–16)
W	20.5		7	
p value	0.08		0.21	
R	0.45		0.26	
2-vaccine				
Sex				
F, n = 4	8 [8]	8 (0–16)	21 [24]	16 (0–64)
M, n = 6	11 [18]	0 (0–32)	32 [0]	32 (32–32)
W	11		6	
p value	1.00		0.32	
R	0.33		0.24	

*Antibody titers were determined by hemagglutination inhibition organized by sex for California condors given a 1057.R1 serial 590088 Avian Influenza Vaccine, H5N1 subtype, reverse genetics-derived, inactivated vaccine (see main text for details on the vaccine and vaccination regimen). HI titers were measured only at 21 and 42 dpv. Titers were compared between sexes at each timepoint with a Wilcoxon rank-sum test (*W*), a p value (p), and an effect estimate (*R*). dpv, days postvaccination; HI, hemagglutination inhibition.
†For day 42 , HI titers are only available for 2 female and 4 male condors given a single vaccination.

costs and benefits of vaccination in relation to its risks and, thus, can help identify vaccination strategies that can stabilize populations and enable them to recover. Relevant vaccination strategies might involve varying the time of year (especially relative to reproductive seasons and seasonal variation in survivorship), age classes, and proportion of the population that is vaccinated.

In summary, we evaluated safety, immunogenicity, vaccination regimens, and correlates of antibody response for a conditionally licensed influenza subtype H5N1 vaccine designed for poultry in black vultures and California condors. Our work suggests that the use of licensed vaccines can be a realistic strategy to aid in conservation of condors and potentially other species facing similar threats, especially those with small and highly threatened populations.

Acknowledgments

This effort was aided by the contributions of a huge number of people and organizations across the United States, too many to name here. Special thanks to the staff at the Carolina Raptor Center, Los Angeles Zoo and Botanical Garden, San Diego Zoo Wildlife Alliance, and Oregon Zoo, without whom these trials would not have been possible. Likewise, we thank the staff at the many different administrative units and laboratories at the US Department of Agriculture (USDA) and the US Fish and Wildlife Service (USFWS) whose cooperation were essential to these efforts. We thank Ricky Zoller, Mark Harden, and Suzanne DeBlois for assisting with laboratory analyses. Three anonymous reviewers and Allen Herbst provided helpful feedback to improve the manuscript. We thank the many state and federal permitting agencies who moved with unprecedented speed to quickly provide permits and authorizations to support this work. David White and his staff at the USDA Center for Veterinary Biologics were essential in getting vaccine to trial participants. Zoetis, Inc. (https://www.zoetis.com) freely contributed vaccines and expertise to this study.

HI titers and ELISA data from this study are available online from the US Geological Survey (USGS) (*34*).

Funding was provided by the USGS, the USFWS, the USDA, and the Carolina Raptor Center. Any use of trade, firm, or product names is for descriptive purposes only and does not imply endorsement by the US government. All opinions expressed in this paper are the authors and do not necessarily reflect the policies and views of the USDA. The findings and conclusions in this article are those of the authors and do not necessarily represent the views of the US Fish and Wildlife Service. This paper has been peer reviewed and approved for publication consistent with USGS Fundamental Science Practices (https://pubs.usgs.gov/circ/1367).

D.L.S. was part of the team that constructed the vaccine used in this study. G.N. is an employee at Zoetis, the company that developed and conditionally licensed that vaccine, and that donated vaccine for use in this study. The authors declare that they have no additional potential conflicts of interest.

Author contributions: D.L.S., A.V.B., M.D., S.E.J.G., T.E.K., J.L., M.M., G.N., M.P., T.R., J.J.R., A.S., D.S., and D.W. designed the study. S.C., B.D., K.D., Z.D.-R., S.E.J.G., T.G., M.P.J., D.K., T.E.K., M.M., E.P., C.S., and D.L.S. collected data. T.E.K. performed data analysis and wrote the initial draft. All authors contributed to revisions.

About the Author

Dr. Katzner is a research wildlife biologist at the USGS, Forest and Rangeland Ecosystem Science Center in Boise, Idaho, USA. His research interests focus on birds of prey, renewable energy, and conservation biology.

References

1. McCallum H. Disease and the dynamics of extinction. Philos Trans R Soc Lond B Biol Sci. 2012;367:2828–39. https://doi.org/10.1098/rstb.2012.0224
2. United Nations Food and Agricultural Organization. EMPRES-i global animal disease information system [cited 2023 June 27]. https://empres-i.apps.fao.org/diseases
3. World Organisation for Animal Health. World animal health information system [cited 2023 May 24]. https://wahis.woah.org
4. Plaza PI, Gamarra-Toledo V, Euguí JR, Lambertucci SA. Recent changes in patterns of mammal infection with highly pathogenic avian influenza A(H5N1) virus worldwide. Emerg Infect Dis. 2024;30:444–52. https://doi.org/10.3201/eid3003.231098
5. Wille M. Ecology and evolution of avian influenza A viruses in wild birds. In: Tibayrenc M, editor. Genetics and evolution of infectious diseases, 3rd edition. London: Elsevier; 2024. p. 863–98.
6. US Department of Agriculture. Detections of highly pathogenic avian influenza in wild birds, 2024 [cited 2024 Aug 5]. https://www.aphis.usda.gov/livestock-poultry-disease/avian/avian-influenza/hpai-detections/wild-birds
7. European Food Safety Authority; European Centre for Disease Prevention and Control; European Union Reference Laboratory for Avian Influenza; Fusaro A, Gonzales JL, Kuiken T, Mirinavičiūtė G, Niqueux É, Ståhl K, et al. Avian influenza overview December 2023–March 2024. EFSA J. 2024;22:e8754. https://doi.org/10.2903/j.efsa.2024.8754
8. US Department of Agriculture. Detections of highly pathogenic avian influenza in mammals [cited 2024 Aug 5]. https://www.aphis.usda.gov/livestock-poultry-disease/avian/avian-influenza/hpai-detections/mammals
9. US Fish and Wildlife Service California Condor Recovery Program. 2023 annual population status. Ventura (CA): The Service; 2024.

10. Finkelstein M, Kuspa Z, Snyder NF, Schmitt NJ. California condor (*Gymnogyps californianus*), version 1.0. In: Rodewald PG, editor. Birds of the world. Ithaca (NY): Cornell Lab of Ornithology; 2024.
11. US Fish and Wildlife Service California Condor Recovery Program. California condors & HPAI update, 2024 [cited 2024 June 28]. https://www.fws.gov/program/california-condor-recovery/southwest-california-condor-flock-hpai-information-updates-2023
12. Swayne DE, Kapczynski DR. Vaccines and vaccination for avian influenza in poultry. In: Swayne DE, editor. Animal influenza, 2nd ed. Ames (IA): Wiley-Blackwell; 2017. p. 378–438.
13. World Organisation for Animal Health. Policy brief. Avian influenza vaccination: why it should not be a barrier to safe trade [cited 2025 Feb 5]. https://www.woah.org/en/avian-influenza-vaccination-why-it-should-not-be-a-barrier-to-safe-trade
14. Furger M, Hoop R, Steinmetz H, Eulenberger U, Hatt JM. Humoral immune response to avian influenza vaccination over a six-month period in different species of captive wild birds. Avian Dis. 2008;52:222–8. https://doi.org/10.1637/8111-091707-Reg.1
15. Lierz M, Hafez HM, Klopfleisch R, Lüschow D, Prusas C, Teifke JP, et al. Protection and virus shedding of falcons vaccinated against highly pathogenic avian influenza A virus (H5N1). Emerg Infect Dis. 2007;13:1667–74. https://doi.org/10.3201/eid1311.070705
16. Jarvi SI, Lieberman MM, Hofmeister E, Nerurkar VR, Wong T, Weeks-Levy C. Protective efficacy of a recombinant subunit West Nile virus vaccine in domestic geese (*Anser anser*). Vaccine. 2008;26:5338–44. https://doi.org/10.1016/j.vaccine.2008.08.011
17. Zimmerman GS, Millsap BA, Avery ML, Sauer JR, Runge MC, Richkus KD. Allowable take of black vultures in the eastern United States. J Wildl Manage. 2019;83:272–82. https://doi.org/10.1002/jwmg.21608
18. Spackman E, Suarez DL, Lee CW, Pantin-Jackwood MJ, Lee SA, Youk S, et al. Efficacy of inactivated and RNA particle vaccines against a North American clade 2.3.4.4b H5 highly pathogenic avian influenza virus in chickens. Vaccine. 2023;41:7369–76. https://doi.org/10.1016/j.vaccine.2023.10.070
19. US Department of Agriculture. USDA takes action to help protect endangered California condors from highly pathogenic avian influenza, 2023 May 16 [cited 2025 Feb 5]. https://www.aphis.usda.gov/aphis/newsroom/stakeholder-info/SA_By_Date/SA-2023/ca-condor-hpai
20. Specht AJ, Parish CN, Wallens EK, Watson RT, Nie LH, Weisskopf MG. Feasibility of a portable x-ray fluorescence device for bone lead measurements of condor bones. Sci Total Environ. 2018;615:398–403. https://doi.org/10.1016/j.scitotenv.2017.09.123
21. Hampton JO, Specht AJ, Pay JM, Pokras MA, Bengsen AJ. Portable x-ray fluorescence for bone lead measurements of Australian eagles. Sci Total Environ. 2021;789:147998. https://doi.org/10.1016/j.scitotenv.2021.147998
22. Specht AJ, Hoover C, Grier T. Portable x-ray fluorescence for bone lead measurement: current approaches and future directions. Curr Environ Health Rep. 2024;11:443–51. https://doi.org/10.1007/s40572-024-00450-x
23. Slabe VA, Anderson JT, Millsap BA, Cooper JL, Harmata AR, Restani M, et al. Demographic implications of lead poisoning for eagles across North America. Science. 2022;375:779–82. https://doi.org/10.1126/science.abj3068
24. Spackman E, Sitaras I. Hemagglutination inhibition assay. In: Spackman E, editor. Animal influenza virus. Methods in molecular biology. New York (NY): Humana; 2020. p. 2123.
25. Tomczak M, Tomczak E. The need to report effect size estimates revisited. An overview of some recommended measures of effect size. Trends Sport Sci. 2014;1:19–25.
26. Suarez DL, Pantin-Jackwood MJ. Recombinant viral-vectored vaccines for the control of avian influenza in poultry. Vet Microbiol. 2017;206:144–51. https://doi.org/10.1016/j.vetmic.2016.11.025
27. Swayne DE, Pavade G, Hamilton K, Vallat B, Miyagishima K. Assessment of national strategies for control of high-pathogenicity avian influenza and low-pathogenicity notifiable avian influenza in poultry, with emphasis on vaccines and vaccination. Rev Sci Tech. 2011;30:839–70. https://doi.org/10.20506/rst.30.3.2081
28. Curlee JF Jr. Cross-species vaccination in wild and exotic animals. Adv Vet Med. 1999;41:551–6. https://doi.org/10.1016/s0065-3519(99)80041-x
29. Gulland FM, Barbieri M, Cleaveland S, Gilbert M, Hall AJ, Rocke TE. Vaccination of endangered wildlife as a conservation tool: hindsights and new horizons in the pandemic era. Biol Conserv. 2024;300:110842. https://doi.org/10.1016/j.biocon.2024.110842
30. US Fish and Wildlife Service. Final California condor HPAI incident command report [cited 2025 Apr 12]. https://www.fws.gov/story/2024-10/final-california-condor-hpai-incident-command-report
31. Barnett KM, Civitello DJ. Ecological and evolutionary challenges for wildlife vaccination. Trends Parasitol. 2020;36:970–8. https://doi.org/10.1016/j.pt.2020.08.006
32. Haydon DT, Randall DA, Matthews L, Knobel DL, Tallents LA, Gravenor MB, et al. Low-coverage vaccination strategies for the conservation of endangered species. Nature. 2006;443:692–5. https://doi.org/10.1038/nature05177
33. Gilbert M, Sulikhan N, Uphyrkina O, Goncharuk M, Kerley L, Castro EH, et al. Distemper, extinction, and vaccination of the Amur tiger. Proc Natl Acad Sci U S A. 2020; 117:31954–62. https://doi.org/10.1073/pnas.2000153117
34. Katzner TE. California condor and black vulture highly pathogenic avian influenza vaccine trial: U.S. Geological Survey data release. 2025 [cited 2025 Apr 14]. https://doi.org/10.5066/P137ULU7

Address for correspondence: Todd E. Katzner, US Geological Survey, Forest and Rangeland Ecosystem Science Center, 230 N Collins Rd, Boise, ID 83702, USA; email: tkatzner@usgs.gov

Diagnostic Accuracy of 3 Mpox Lateral Flow Assays for Antigen Detection, Democratic Republic of the Congo and United Kingdom

Elie Ishara-Nshombo,[1] Anushri Somasundaran,[1] Alessandra Romero-Ramirez, Konstantina Kontogianni, Daniel Mukadi-Bamuleka, Marithé Mukoka-Ntumba, Emile Muhindo-Milonde, Hugues Mirimo-Nguee, Jacob Parkes, Yusra Hussain, Susan Gould, Christopher T. Williams, Dominic Wooding, Juvenal Nkeramahame, Mikaela Watson, Hayley E. Hardwick, Malcolm G. Semple, John Kenneth Baillie, Jake Dunning, ISARIC 4C Investigators,[2] Thomas E. Fletcher, Thomas Edwards, Devy M. Emperador, Hugo Kavunga-Membo,[1] Ana Isabel Cubas-Atienzar[1]

The ongoing outbreaks of mpox highlight the urgent need for a rapid and low-cost diagnostic test to accurately detect and control this emerging disease. We estimated the analytical sensitivity using viral culture of the monkeypox virus clade IIb lineage B1 and clinical diagnostic performance of 3 antigen detection rapid diagnostic tests (Ag-RDT) by using skin swab samples and upper-respiratory swab samples from mpox patients in the Democratic Republic of the Congo and the United Kingdom. The analytical limit of detection was 1.0×10^4 plaque-forming units/mL, fulfilling World Health Organization recommendations. Specificity of the 3 Ag-RDTs was 100%, but sensitivity was estimated at 0.00%–15.79% using skin samples and 0.00% using respiratory samples. None of the 3 Ag-RDTs reached the World Health Organization's target clinical sensitivity, and we do not recommend them as diagnostic or screening tools for suspected mpox cases. Accurate Ag-RDTs for mpox diagnosis remain urgently needed.

Mpox is a zoonotic disease caused by monkeypox virus (MPXV), which belongs to the *Orthopoxvirus* genus, Poxviridae family; it has 2 major clades: clade I, which is subdivided into subclade Ia and Ib; and clade II, which is subdivided into subclade IIa and IIb (*1*). Historically, mpox was endemic to Central and West Africa. In May 2022, the number of mpox cases increased in a surge that included rapid expansion in nonendemic countries; it was declared the first mpox public health emergency of international concern (PHEIC) by the World Health Organization (WHO) (*2*). Since then, >100,000 cases of mpox and >200 deaths have been described in >120 countries not previously considered mpox endemic. The number of infections during the 20th Century has already been surpassed by the number of cases that occurred after the 2022 outbreak caused by clade II (*3*). On August 14, 2024, a second mpox PHEIC was declared by WHO after the substantial increase in mpox cases in the Democratic Republic of the Congo (DRC) and neighboring countries (*4*). In 2024, DRC, where mpox was first identified in 1970, reported the highest number of suspected cases globally, >27,000, and 800 deaths (*5*).

Author affiliations: Rodolphe Mérieux Laboratory, Institut National de Recherche Biomédicale, Kinshasa, Democratic Republic of the Congo (E. Ishara-Nshombo, D. Mukadi-Bamuleka, M. Mukoka-Ntumba, E. Muhindo-Milonde, H. Mirimo-Nguee, H. Kavunga-Membo); Liverpool School of Tropical Medicine, Liverpool, UK (A. Somasundaran, A. Romero-Ramirez, K. Kontogianni, J. Parkes, Y. Hussain, S. Gould, C.T. Williams, D. Wooding, T.E. Fletcher, T. Edwards, A. Cubas-Atienzar); Royal Liverpool University Hospital NHS Foundation Trust, Liverpool (S. Gould, T.E. Fletcher); Foundation for Innovative New Diagnostics, Geneva, Switzerland (J. Nkeramahame, M. Watson, D.M. Emperador); University of Liverpool, Liverpool (H.E. Hardwick, M.G. Semple); University of Edinburgh, Edinburgh, Scotland, UK (J.K. Baillie); Pandemic Sciences Institute, University of Oxford, Oxford, UK (J. Dunning); Royal Free London NHS Foundation Trust, London, UK (J. Dunning)

DOI: https://doi.org/10.3201/eid3106.250166

[1]These authors contributed equally to this article.

[2]Members of ISARIC 4C investigator group are listed at the end of this article.

In the United Kingdom, most cases before 2022 were associated with travel from mpox-endemic countries. During August 2018–September 2021, a total of 7 mpox cases were identified in the United Kingdom (4 imported cases and 3 secondary cases) (*6*). The discovery of the first mpox case of the 2022 global outbreak in the United Kingdom was on May 7, 2022, in a person who traveled from Nigeria; as of June 8, 2022, a total of 336 cases had been laboratory confirmed, a number that rose to 3,732 by the end of 2022. On October 30, 2024, the first clade Ib mpox case was confirmed in the United Kingdom; 3 further household contact cases were confirmed (*7*). Those were the first locally transmitted clade Ib mpox cases in the WHO European Region and the first outside Africa since a PHEIC was declared for a second time in August 2024 (*4*).

To confirm a clinical diagnosis, WHO advises testing for MPXV as soon as possible in persons who fit the suspected case definition. Laboratory-based real-time PCR is the primary method used for MPXV detection. Laboratory-based PCR testing requires costly equipment, up-front DNA extraction, and skilled personnel, which might only be available in specialized laboratories, making rapid detection of cases during outbreaks more challenging. In contrast, rapid diagnostic tests (RDTs) are low cost, equipment free, easy to use, and suitable to use at the point of care (POC); results are available within 20 minutes (*8*). The value of antigen-detecting RDTs (Ag-RDTs) in rapidly detecting infected persons and enabling isolation and management of patients has been proven for many viral diseases, notably during the COVID-19 pandemic (*9*).

The global increase in mpox cases after the 2022 PHEIC and the subsequent PHEIC 15 months later brought to light the increased demand for decentralized POC diagnostics for this highly infectious virus and highlighted the urgent need for Ag-RDTs for MPXV as a priority. This increased demand has resulted in the availability of dozens of Ag-RDTs in the market. As of January 2024, >69 Ag-RDTs for MPXV were in varying stages of development, of which >35 had received CE marking for in vitro diagnostics (IVD) (required for devices sold in Europe) and were commercially available (*10*). Despite the increased number of Ag-RDTs for MPXV, clinical evaluation data are still lacking (*11*). To ensure reliable and accurate performance of Ag-RDTs, diagnostic evaluation studies across multiple, independent sites are required to generate evidence of their effectiveness to guide implementation.

The aim of this study was to evaluate the diagnostic performance of 3 Ag-RDT brands at detecting MPXV antigens: FlowFlex Monkeypox Virus Antigen Rapid Test (ACON Biotech [Hangzhou] Co., Ltd., https://www.aconbio.com), Ecotest Monkeypox Antigen Rapid Test (Assure Tech [Hangzhou] Co., Ltd., https://www.assuretech-product.com), and Standard Q Monkeypox Ag Test (SD Biosensor, https://www.sdbiosensor.com). We used skin lesion swab samples and upper respiratory tract swab samples from patients in DRC and the United Kingdom, 2 countries with different MPXV epidemiologic characteristics and clades (clade I [DRC] and clade II [United Kingdom]). We evaluated the Ag-RDTs in prospectively collected samples in DRC and retrospectively in the United Kingdom.

Materials and Methods

Study Settings and Participants

In DRC, persons ≥2 years of age suspected to have mpox according to the WHO case definition (*12*) were eligible to participate in the study. Ethical approval was obtained by DRC's National Ethics and Health Committee (Comité National d'Ethique et de la Santé [CNES], reference 452/CNES/BN/PMMF/2023). Recruitment took place during January–December 2023 in Maniema Province through home visits of eligible persons. Paired skin samples and upper respiratory specimens were collected from all recruited participants (n = 68) by trained heathcare workers and placed in 3 mL of noninactivating virus transport medium (VTM) for viral preservation. The Ag-RDTs could not be tested at the POC because of health and safety restrictions; all VTM samples were transported in cool boxes (2°C–8°C) to the Institut National de Recherche Biomédicale (INRB) Biosafety Level 2 laboratories in Lubutu for processing according to national guidance for MPXV testing. All VTM tubes were processed within 4 hours for MPXV Ag-RDT testing and quantitative PCR (qPCR).

In the United Kingdom, we used retrospectively collected skin samples (n = 30) and upper respiratory samples (n = 23 [1 nasopharyngeal, 22 oropharyngeal]) in universal transport media (UTM) (Copan, https://www.copangroup.com) from a cohort of 16 adult patients positive for mpox by PCR from the Royal Liverpool University Hospital, Sheffield Teaching Hospital NHS Foundation Trust, and Royal Free London Hospital for this study. Patients were recruited during the last 2 outbreaks of mpox in the United Kingdom in 2018 and 2022. Trained healthcare workers collected all swab samples. Patients gave consent under the WHO ISARIC Clinical Characterization Collaboration Protocol for severe emerging infections (ISRCTN66726260).

Ethical approval was obtained from the National Research Ethics Service and the Health Research Authority (IRAS ID:126600, REC 13/SC/0149).

Mpox diagnosis was confirmed by the UK Health Security Agency using qPCR before enrollment in the study. In addition to samples from mpox-positive patients, to fulfill the minimum number of negative swab specimens for mpox diagnostic evaluations recommended by the US Food and Drug Administration (*13*), we used a set of 32 leftover nasopharyngeal samples in UTM from previous COVID-19 studies (*14*) as mpox negative controls. The samples were collected under the Facilitating Accelerated Clinical Validation of Novel diagnostics for COVID-19 (FALCON), and ethical approval was obtained from the National Research Ethics Service and the Health Research Authority (IRAS ID:28422, REC: 121 20/WA/0169). All samples were aliquots stored at –80°C and thawed for the first time for this study. Samples were processed and tested at the Biosafety Level 3 laboratories of the Liverpool School of Tropical Medicine (LSTM) as previously described (*14*).

MPXV Ag-RDT Testing

We selected the Ag-RDTs evaluated in this study after an expression of interest launched by FIND (https://www.finddx.org) and a scoring process based on defined criteria. We evaluated 3 Ag-RDTs: FlowFlex Monkeypox Virus Antigen Rapid Test, Ecotest Monkeypox Antigen Rapid Test, and Standard Q Monkeypox Ag Test. The 3 RDTs are based on immunochromatography and show the presence of MPXV A29L antigen using colloidal gold for visualization. Flowflex and Ecotest were commercially available, whereas Standard Q was for research use only at the time of evaluation. All test brands can be used with skin lesion samples. In addition, Flowflex can be used with serum, plasma, and upper respiratory samples; Standard Q can be used in serum, plasma, and whole-blood samples; and Ecotest can be used in upper respiratory samples.

We performed tests in INRB Biosafety Level 2 laboratories in DRC and in LSTM Biosafety Level 3 laboratories in the United Kingdom. In brief, we added the specified amount of VTM or UTM confirmed by the manufacturers (200 µL for Flowflex and Ecotest and 300 µL for Standard Q) into the extraction buffer and then added the number of drops of the extraction buffer specified in the instructions for use into the sample well (4 drops for Flowflex and Standard Q and 3 drops for Ecotest). We read tests and interpreted them visually after 15–30 minutes according to the instructions. Two independent technicians read the results; a third technician acted as a tiebreaker in case of discrepant results.

Reference MPXV qPCR Test

At both sites, we extracted DNA and performed MPXV qPCR using the same UTM or VTM tube used for the 3 Ag-RDT tests. At INRB, we extracted DNA from a 300-µL aliquot of sample by using the Natch 16S automated platform with the Nucleic Acid Extraction-Purification Kit (both Sansure Biotech, https://www.sansureglobal.com), according to the instructions for use. At LSTM, we extracted DNA from 200 µL of UTM using the QiAamp96 Virus Qiacube HT kit (QIAGEN, https://www.qiagen.com), according to the instructions for use.

We used the same MPXV qPCR reference test in both sites for evaluating index tests (Monkeypox Virus Nucleic Acid Diagnostic Kit; Sansure Biotech). We carried out qPCR by using a MA-1620Q qPCR thermocycler (Sansure Biotech) at INRB and a QuantStudio 5 (Thermo Fisher Scientific, https://www.thermofisher.com) at LSTM. We considered a qPCR result with a cycle threshold (Ct) ≤40 MPXV positive according to instructions for use. We used this qPCR kit as the reference test because it has been successfully demonstrated to detect MPXV clades I, IIa, and IIb (*15*), is CE marked for commercial use, and has demonstrated higher diagnostic accuracy than the mpox Centers for Disease Control and Prevention laboratory–based qPCR (*16*).

Analytical Limit of Detection of Ag-RDTs

We cultured mpox viral stock of a MPXV strain from clade II, subclade IIb, lineage B.1 (Slovenia_MPXV–1_2022) obtained from the European Virus Archive Global (https://www.european-virus-archive.com) in Vero E6 cells (ECACC 85020206) in Dulbecco's Modified Eagle Medium plus 10% fetal bovine serum and 1% penicillin/streptomycin solution to generate the MPXV stock. We serially diluted a fresh aliquot 10-fold using UTM to produce concentrations from 5.0×10^4 to 5.0×10^0 PFU/mL. We defined the limit of detection (LOD) as the lowest concentration at which all 3 replicates were positive. Once the LOD was achieved, half dilutions were tested above and below the LOD. We performed Ag-RDT testing to calculate the LOD and quantified the viral copy numbers per mL (copies/mL) of the serial dilutions, as previously described (*14*,*16*).

Statistical Analysis

To assess the diagnostic accuracy of Ag-RDTs in patients with suspected mpox, we calculated point

estimates of sensitivity and specificity for each Ag-RDT on the basis of results of the reference MPXV qPCR assay from the same VTM or UTM tube used for the Ag-RDT. We derived the 95% CI for each point estimate on the basis of Wilson's score method. To compare performance of the Ag-RDTs at different Ct values, we stratified point estimates of sensitivity by Ct value of the reference test. We used 2-tailed Fisher exact test and χ^2 test to determine nonrandom associations between categorical variables. We assessed differences between the Ct values (expressed as mean ±SD) in sample groups using the paired Student *t* test. Statistical significance was set at <0.05. We performed statistical analysis using R version 4.5.0 (R Foundation for Statistical Computing, https://ww.r-project.org) and GraphPad Prism version 9.1.0 (GraphPad Software, Inc., https://www.graphpad.com).

Results

Clinical Evaluation

In DRC, 34/68 (50%) of mpox patients were men (Table 1). The median time from onset of symptoms was 4 (range 1–34) days. The most prevalent symptoms were fever (91%), skin lesions (100%), influenza-like symptoms (75%), headaches (54%), and cough (50%). In the United Kingdom, 16/16 (100%) mpox patients were men; mean age was 35.1 (range 24–58) years. The median time from onset of symptoms was 8 (range 0–11) days. The most common symptoms were skin lesions (100%), skin rashes (87.5%), and fever (68.8%).

In DRC, 19/68 (28%) skin samples and 14/68 (21%) upper-respiratory samples from persons suspected of having mpox tested positive using the Sansure qPCR. Flowflex and Ecotest Ag-RDTs detected MPXV antigens in 3/19 MPXV-positive skin samples, resulting in a clinical sensitivity of 15.79% (95% CI 5.52%–37.57%), whereas Standard Q detected MPXV antigens in 2/19 samples, resulting in a clinical sensitivity of 10.53% (95% CI 2.94%–31.39%). The Ag-RDT Flowflex was more sensitive when detecting MPXV antigen in skin samples with Ct ≤20 than those with Ct values ≥33 (p = 0.008); however, this difference was not observed with the other Ag-RDT brands. None of the Ag-RDT brands detected MPXV antigen in upper respiratory samples, resulting in 0% (95% CI 0%–23.2%) sensitivity. The clinical specificity was 100% (95% CI 92.73%–100%) for each of the Ag-RDTs in both sample types (Table 2).

In the United Kingdom, 16/23 upper-respiratory samples (69.56%) and 27/30 skin samples (90%) from mpox-positive patients were positive by Sansure qPCR. All 32 upper respiratory samples analyzed from the COVID-19 cohort tested negative for MPXV as expected. No positive results were obtained when testing either respiratory or skin swab samples

Table 1. Clinical characteristics of recruited mpox patients in study of diagnostic accuracy of 3 mpox lateral flow assays for antigen detection, Democratic Republic of the Congo and United Kingdom*

Characteristic	Democratic Republic of the Congo, n = 68	United Kingdom, n = 16
Mean age (range), y	17 (2–47)	35.1 (24–58)
Sex		
M	34 (50)	16 (100)
F	34 (50)	0
Time from symptom onset, d		
Median (interquartile range)	4 (3–7)	8 (4.25–12.75)
0–3	32 (47)	1 (6.25)
4–7	22 (32)	6 (37.5)
≥8	14 (21)	9 (56.25)
Symptoms		
Skin lesions	68 (100)	16 (100)
Fever	62 (91)	11 (68.75)
Influenza-like symptoms	51 (75)	4 (25)
Skin rashes	0	14 (87.5)
Headache	37 (54)	4 (25)
Cough	34 (50)	1 (6.25)
Sore throat	25 (37)	4 (25)
Nausea	20 (29)	0
Abdominal pain	19 (28)	0
Chest pain	14 (21)	0
Vomiting	6 (9)	0
Diarrhea	5 (7)	1 (6.25)
Painful Urination	4 (6)	0
Eye discharge	3 (4)	0
Redness of eyes	2 (3)	0

*Values are no. (%) except as indicated.

Table 2. Clinical diagnostic accuracy parameters of 3 MPXV antigen-detecting rapid diagnostic tests from 68 suspected mpox case-patients, the Democratic Republic of the Congo*

	Skin lesion swab samples, n = 68			Upper respiratory tract swab samples, n = 68		
Category	Ecotest	Flowflex	Standard Q	Ecotest	Flowflex	Standard Q
True positive	3	3	2	0	0	0
True negative	49	49	49	54	54	54
False positive	0	0	0	0	0	0
False negative	16	16	17	14	14	14
Specificity, % (95% CI)	100 (92.7–100)	100 (92.7–100)	100 (92.7–100)	100 (93.4–100)	100 (93.4–100)	100 (93.4–100)
Sensitivity, % (95% CI)	15.79 (5.5–37.6)	15.79 (5.5–37.6)	10.53 (2.9–31.4)	0 (0.0–23.2)	0 (0.0–23.2)	0 (0.0–23.2)
PPV, % (95% CI)	100 (29.2–100)	100 (29.2–100)	100 (15.8–100)	NA	NA	NA
NPV, % (95% CI)	75.38 (71.6–78.8)	75.38 (71.6–78.8)	74.24 (71.2–77.1)	79.41 (68.4–87.3)	79.41 (68.4–87.3)	79.41 (68.4–87.3)
Sensitivity by Ct, % (95% CI)						
Ct ≤20	0 (0.0–79.4), n = 1	100 (20.7–100), n = 1	0 (0.0–79.4), n = 1	NA	NA	NA
Ct ≤25	14.29 (2.6–51.3), n = 7	28.57 (8.2–64.1), n = 7	14.29 (2.6–51.3), n = 7	0 (0.0–79.4), n = 1	0 (0.0–79.4), n = 1	0 (0.0–79.4), n = 1
Ct ≤33	27.27 (9.8–56.7), n = 11	27.27 (9.8–56.7), n = 11	18.18 (5.1–47.7), n = 11	0 (0.0–39.0), n = 6	0 (0.0–39.0), n = 6	0 (0.0–39.0), n = 6
Ct ≤40	15.79 (5.5–37.6), n = 19	15.79 (5.5–37.6), n = 19	10.53 (2.9–31.4), n = 19	0 (0.0–21.5), n = 14	0 (0.0–21.5), n = 14	0 (0.0–21.5), n = 14

*Tests evaluated: Ecotest, Ecotest Monkeypox Antigen Rapid Test (Assure Tech [Hangzhou] Co., Ltd., https://www.assuretech-product.com); Flowflex, FlowFlex Monkeypox Virus Antigen Rapid Test (ACON Biotech [Hangzhou] Co., Ltd., https://www.aconbio.com); Standard Q, Standard Q Monkeypox Ag Test (SD Biosensor, https://www.sdbiosensor.com). Ct, cycle threshold; MPXV, monkeypox virus; NA, not available; NPV, negative predictive value; PPV, positive predictive value.

regardless of the Ag-RDT brand used (0%, 95% CI 0%–20.59%). The specificity was 100% (95% CI 90.97%–100%) for the 3 Ag-RDT brands on both sample types (Table 3).

The difference in sensitivity in MPXV Ag-RDTs was lower when testing upper-respiratory samples than in skin samples (p = 0.007). We assessed the comparison of the Ct values and noted a difference in Ct values between upper-respiratory and skin sample groups (p=0.042) from DRC but not from the United Kingdom (Figure 1). The mean Ct value of upper-respiratory samples in DRC was 30.7 (±4.79) and mean Ct value for skin samples was 26.63 (±6.87), whereas in the United Kingdom mean Ct value for respiratory samples was 27.2 (±2.34) and for skin was 28.83 (±6.88). We found no difference in sensitivity between the 3 Ag-RDT brands and between countries. We also analyzed test results by onset of symptoms (Figure 2) but observed no difference in Ag-RDT results by symptom onset group.

Table 3. Clinical diagnostic accuracy parameters of 3 MPXV antigen-detecting rapid diagnostic tests using retrospectively collected samples from 16 mpox patients and 32 COVID–19 patients, United Kingdom*

	Skin lesion swab samples, n = 30			Upper respiratory tract swab samples, n = 55		
Category	Ecotest	Flowflex	Standard Q	Ecotest	Flowflex	Standard Q
True positive	0	0	0	0	0	0
True negative	3	3	3	39	39	39
False positive	0	0	0	0	0	0
False negative	27	27	27	16	16	16
Specificity, % (95% CI)	100 (29.2–100)	100 (29.2–100)	100 (29.2–100)	100 (90.9–100)	100 (90.9–100)	100 (90.9–100)
Sensitivity, % (95% CI)	0 (0.0–12.7)	0 (0.0–12.7)	0 (0.0–12.7)	0 (0.0–20.6)	0 (0.0–20.6)	0 (0.0–20.6)
PPV, % (95% CI)	NA	NA	NA	NA	NA	NA
NPV, % (95% CI)	10.00 (3.5–25.6)	10.00 (3.5–25.6)	10.00 (3.5–25.6)	70.9 (57.9–81.2)	70.9 (57.9–81.2)	70.9 (57.9–81.2)
Sensitivity by Ct, % (95% CI)						
Ct ≤20	0 (0.0–84.2), n = 2	0 (0.0–84.2), n = 2	0 (0.0–84.2), n = 2	NA	NA	NA
Ct ≤25	0 (0.0–36.9), n = 8	0 (0.0–36.9), n = 8	0 (0.0–36.9), n = 8	0 (0.0–60.2), n = 4	0 (0.0–60.2), n = 4	0 (0.0–60.2), n = 4
Ct ≤33	0 (0.0–19.5), n = 17	0 (0.0–19.5), n = 17	0 (0.0–19.5), n = 17	0 (0.0–28.5), n = 11	0 (0.0–28.5), n = 11	0 (0.0–28.5), n = 11
Ct ≤40	0 (0.0–12.7), n = 27	0 (0.0–12.7), n = 27	0 (0.0–12.7), n = 27	0 (0.0–20.6), n = 16	0 (0.0–20.6), n = 16	0 (0.0–20.6), n = 16

*Tests evaluated: Ecotest, Ecotest Monkeypox Antigen Rapid Test (Assure Tech [Hangzhou] Co., Ltd., https://www.assuretech-product.com); Flowflex, FlowFlex Monkeypox Virus Antigen Rapid Test (ACON Biotech [Hangzhou] Co., Ltd., https://www.aconbio.com); Standard Q, Standard Q Monkeypox Ag Test (SD Biosensor, https://www.sdbiosensor.com). Ct, cycle threshold; MPXV, monkeypox virus; NA, not available; NPV, negative predictive value; PPV, positive predictive value.

Analytical Evaluation

Using the viral stock, all Ag-RDT brands were positive at 5.0 × 10^4 PFU/mL, 2.5 × 10^4 PFU/mL, and 1.0 × 10^4 PFU/mL. The LOD of all the Ag-RDT brands using the MPXV viral culture was determined to be 1.0 × 10^4 PFU/mL (1.3 × 10^5 copies/mL). All concentrations tested below the LOD were negative in all instances.

Discussion

After the recent PHEIC, WHO issued an urgent call to accelerate availability of POC diagnostics for mpox (*17*). The lack of validation data for MPXV Ag-RDTs represents a large gap in the diagnostics landscape that has slowed down rapid, effective responses to new outbreaks and ongoing endemic transmission (*18*). The primary aim of this study was to evaluate the diagnostic accuracy of 3 Ag-RDT brands (Flowflex, Ecotest, and Standard Q) in DRC and the United Kingdom.

WHO's target product profile (TPP) for MPXV Ag-RDTs recommends minimal clinical sensitivity of 80% and specificity of 97% (*19*). Specificity was fulfilled by the 3 Ag-RDTs evaluated in both countries, but sensitivity was extremely low (0%–15.79%), making the tests unsuitable for diagnostic or screening use. Evaluation data on Ag-RDT for MPXV are very limited. A previous study reported detection of MPXV antigens using the Ag-RDT Tetracore Orthopox BioThreat (https://tetracore.com) in 5 of 6 tested MPXV-positive samples with low Ct values (Ct 15–22) (*20*). In addition to the limited number of samples, this assay required sonication for swab material and dry ice/ethanol bath freezing followed by pestle grinding, making it unsuitable for POC use. Another study using an Orthopoxvirus Ag-RDT prototype failed to detect MPXV antigens among 80 MPXV qPCR-positive clinical samples in Belgium (*21*). That study suggested that the failure to detect MPXV antigen in swab samples could be caused by inhibition by the inactivating components of the VTM, which can cause protein denaturation. In this study, we used noninactivating swab transport medium in both sites and different types of medium (VTM in the DRC and UTM in the United Kingdom); clinical sensitivity was not improved. Studies on Ag-RDTs for SARS-CoV-2 comparing the use of dry swabs with Amies, VTM, and UTM have documented false-positive results because of nonspecific electrostatic interactions between the antibodies in the assay (*22*,*23*), a decreased LOD because of a dilution effect (*23*), or no changes in sensitivity or specificity depending on the Ag-RDT brand (*23*). The use of different types of swab transport medium should be investigated to optimize performance of Ag-RDT for mpox while preserving the virus for transport and storage.

Investigations of the analytical sensitivity of these Ag-RDTs gave an LOD of 1.0 × 10^4 pfu/mL, being more sensitive than previous analytical evaluations of Ag-RDTs for MPXV. The Orthopoxvirus Ag-RDT prototype had an LOD of 3.0 × 10^5 PFU/mL (*21*), and the commercially available Tetracore Orthopox BioThreat had an LOD of 1.5 × 10^6 PFU/mL after sonication (*20*). The recommended analytical LOD in the WHO TPP is at 10^6 PFU/mL, being fulfilled by the 3 brands of Ag-RDTs evaluated here and the previously published study on the Orthopoxvirus Ag-RDT prototype (*21*), suggesting that laboratory sensitivity using the PFU/mL measurement does not align with clinical sensitivity in the field.

The use of LOD using viral isolates is often used as a proxy before having the test evaluated using clinical specimens; however, in this study and others (*21*), the correlation between analytical and clinical sensitivity for MPXV has been shown to be very poor, yielding lower sensitivity than expected among clinical samples. The reason for this variability in antigen detection sensitivity between mpox clinical samples and mpox viral isolates is still uncertain and needs further investigation, as does the quantity and type of accessible antigen in clinical samples. In addition, the targeted antigen of the Ag-RDTs evaluated in this study was

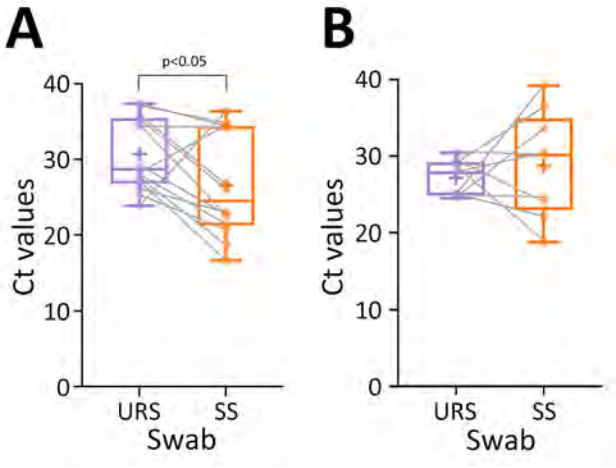

Figure 1. Boxplots of Ct values from paired URS and SS tested by Sansure quantitative PCR in study of diagnostic accuracy of 3 mpox lateral flow assays for antigen detection, Democratic Republic of the Congo (DRC) and United Kingdom. A) DRC, n = 14; B) United Kingdom, n = 9. Horizontal lines within boxes indicate medians, box tops and bottoms indicate interquartile range, and whiskers indicate maximum and minimum values. Ct values were significantly higher (p<0.05) in the URS group than in the SS group in the DRC cohort. Ct, cycle threshold; SS, skin lesion samples; URS, upper respiratory specimens.

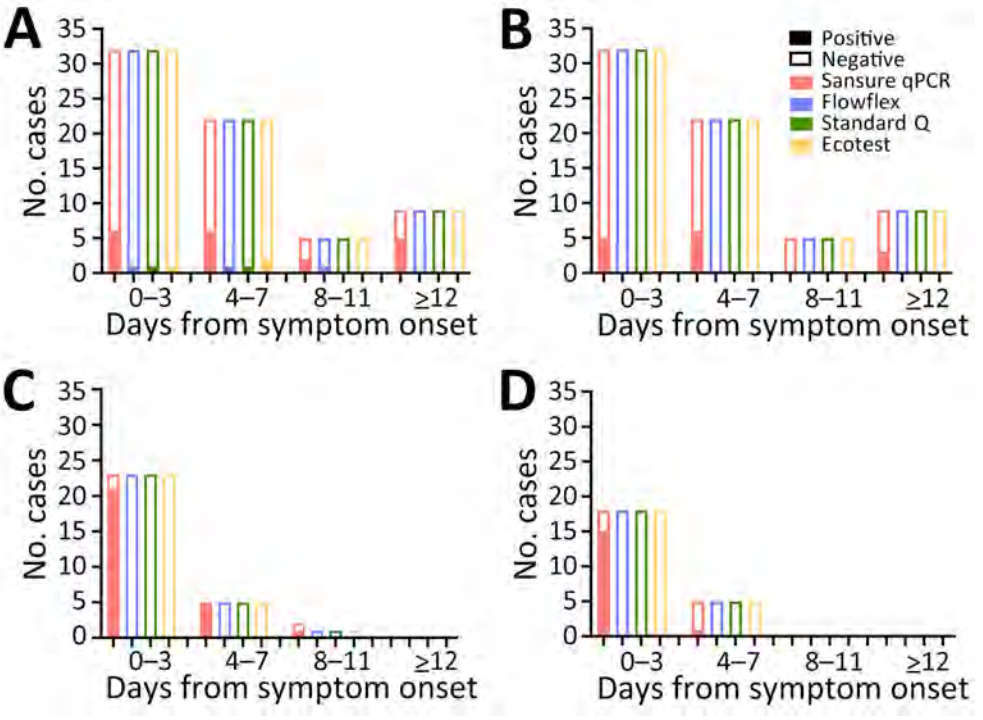

Figure 2. Number of positive and negative results by test and by days from symptom onset in study of diagnostic accuracy of 3 mpox lateral flow assays for antigen detection, Democratic Republic of the Congo (DRC) and United Kingdom. A) Skin lesion swab samples in DRC; B) upper respiratory swab samples in DRC; C) skin swab samples in the United Kingdom; D) upper respiratory swab samples in the United Kingdom. Rapid diagnostic tests evaluated: Ecotest, Ecotest Monkeypox Antigen Rapid Test (Assure Tech [Hangzhou] Co., Ltd., https://www.assuretech-product.com); Flowflex, FlowFlex Monkeypox Virus Antigen Rapid Test (ACON Biotech [Hangzhou] Co., Ltd., https://www.aconbio.com); Standard Q, Standard Q Monkeypox Ag Test (SD Biosensor, https://www.sdbiosensor.com). Sansure qPCR (Monkeypox Virus Nucleic Acid Diagnostic Kit; Sansure Biotech, https://www.sansureglobal.com) was used to evaluate results of the rapid diagnostic tests.

MPXV A29L. Target antigens for other Ag-RDT brands include A29L, A35R, A5L, B6R, E8L, H3, and M1R (*10*). The antigen A27L (homologous of MPXV A29L in vaccinia virus) has previously been suggested to be a good candidate because it is conserved and abundant within the virion; however, the Ag-RDTS targeting this antigen in this study and reported elsewhere (*21*) did not yield acceptable sensitivity. This finding highlights the need for further evaluations using clinical samples with Ag-RDTs that target different antigen types. Currently, manufacturers of ≥3 Ag-RDT brands in the market have disclosed the use of MPXV A29L as antigen target (Hangzhou Testsea Biotechnology, Guangdong Wesail Biotech, and Nanjing Synthgene Medical Technology).

Flowflex and Ecotest are designed to be used with upper-respiratory samples; however, none of the Ag-RDTs detected MPXV antigens in those samples, suggesting that using this sample type for antigen detection is not appropriate. Diagnostic evaluation studies using PCR found lower positivity rates in respiratory samples than in skin samples (*24*), which might be attributed to lower viral titer levels (*25*) or earlier clearance in this sample type (*26*), which is exacerbated by the lower sensitivity of the Ag-RDTs evaluated here.

Major limitations of this study were that testing could not be done at the POC in DRC (because samples had to be transported to the designated laboratory) and that retrospective frozen samples were used in the United Kingdom. The effect of testing delay and of sample storage and freeze-thawing on Ag-RDT results has not been studied with MPXV. Studies on SARS-CoV-2 Ag-RDTs noted a decline in test-line intensity (not false-negative results) after storage periods of 24 hours to >7 days at 2°C–8°C (*27*–*30*). Results of Ag-RDT testing for SARS-CoV-2 did not find a significant difference between 101 datasets that involved fresh specimens and 23 freeze-thawed specimens (*31*). However, MPXV is a larger DNA virus, whereas SARS-CoV-2 is a smaller RNA virus; thus, the 2 are not directly comparable. The use of retrospective frozen and refrigerated samples is accepted for production of clinical diagnostic data (*13*), and the WHO TPP recommends that MPXV Ag-RDTs be compatible with samples that have been refrigerated or frozen with use of preservation media for quality control, repeats, or follow-up testing (*19*).

In conclusion, the results of this study raise considerable doubts on the suitability of Ag-RDT for mpox surveillance and diagnosis because of their poor clinical sensitivity among suspected mpox cases. Recommendations for future mpox Ag-RDT evaluations should include brands that detect different MPXV antigens and evaluation of different swab preservation mediums.

This article was published as a preprint at https://www.medrxiv.org/content/10.1101/2024.11.07.24316894v1.

Members of ISARIC 4C: Mike Beadsworth, Ingeborg Welters, Lance Turtle, Jane Minton, Karl Ward, Elinor Moore, Elaine Hardy, Mark Nelson, David Brealey, Ashley Price, Brian Angus, Graham Cooke, and Oliver Koch.

Acknowledgments

We thank the FIND team dedicated to managing and supervising this study: Emmanuel Agogo, Audrey Albertini, Daniel G. Bausch, Berra Erkosar, Susan Logoose, Michael Otieno, and Aurelia Vessiere. In the Democratic Republic of the Congo, we thank all the participants who volunteered for this study. We also thank all the staff at Lubutu General Referral Hospital, especially Jean Meniko, Fiston Kaleba, Berthon Okoma, Naomie Koho, Emmanuel Matengano, and Justin Kapela, for their contribution to the success of this study. We would also like to thank Patrick Karungu for his work in entering the source data into the electronic database. In the United Kingdom, we thank the ISARIC 4C investigators (https://isaric4c.net/about/authors), all the Clinical Research Network research nurses, and clinical research fellows for supporting us with the sample collection and recruitment. We thank the CONDOR steering group: A. Joy Allen, Julian Braybrook, Richard Body, Peter Buckle, Eloise Cook, Paul Dark, Kerrie Davis, Gail Hayward, Adam Gordon, Anna Halstead, Charlotte Harden, Colette Inkson, Naoko Jones, William Jones, Dan Lasserson, Joseph Lee, Clare Lendrem, Andrew Lewington, Mary Logan, Massimo Micocci, Brian Nicholson, Rafael Perera-Salazar, Graham Prestwich, D. Ashley Price, Charles Reynard, Beverley Riley, John Simpson, Valerie Tate, Philip Turner, Mark Wilcox, and Melody Zhifang.

The raw data for this evaluation are available from the corresponding authors upon reasonable request.

This work was funded as part of FIND's work as coconvener of the diagnostics pillar of the Pandemic Threats Programme, who received funds from the Germany (Federal Ministry of Economic Cooperation and Development) and Canada governments. ISARIC4C was funded from the National Institute for Health Research (NIHR) (award CO-CIN-01), the UK Medical Research Council (grant MC_PC_19059), the NIHR for Health Research Health Protection Research Unit (HPRU) in Emerging and Zoonotic Infections (in partnership with the University of Liverpool), the United Kingdom Health Security Agency (UKHSA), LSTM and the University of Oxford) (NIHR award 200907), the Wellcome Trust and Department for International Development (215091/Z/18/Z), Bill and Melinda Gates Foundation (OPP1209135), and the Liverpool Experimental Cancer Medicine Centre (grant reference C18616/A25153). The FALCON study was funded by the NIHR, Asthma United Kingdom, and the British Lung Foundation.

The study was planned and designed by A.I.C.-A., J.D., D.M.E., H.K.-M., E.I.-N., D.M.E., and D.M.-B. Laboratory work was performed by A.S., J.P., Y.H., D.W., K.K., C.T.W., A.R.-R., and E.M.-M. under the supervision of A.I.C.-A., T.E., E.I.-N., and H.K.-M. Data analysis and interpretation were conducted by A.S., A.R.-R., A.I.C.-A., M.W., and E.I.-N. A.I.C.-A. and E.I.-N. drafted the initial manuscript. The funding was obtained by A.I.C.-A., H.K.-M., M.G.S., J.K.B., and J.D. Study oversight was provided by A.I.C.-A. and H.K.-M. All authors reviewed and approved the final manuscript.

About the Author

Dr. Ishara-Nshombo is a scientist and project manager at the Institut National de Recherche Biomédicale in the Democratic Republic of the Congo. His work focuses on epidemiologic surveillance of emerging diseases at the human–animal interface. Dr. Somasundaran works in diagnostic research at Liverpool School of Tropical Medicine Centre for Drugs and Diagnostics in the United Kingdom. Her primary research interests are public health and improving disease detection.

References

1. World Health Organization. Mpox. 2024 [cited 2025 Mar 16]. https://www.who.int/news-room/fact-sheets/detail/mpox
2. Sah R, Padhi BK, Siddiq A, Abdelaal A, Reda A, Ismail Lashin B, et al. Public health emergency of international concern declared by the World Health Organization for monkeypox. Glob Secur Health Sci Policy. 2022;7:51–6. https://doi.org/10.1080/23779497.2022.2124185
3. World Health Organization. Global mpox trends [cited 2024 Oct 15]. https://worldhealthorg.shinyapps.io/mpx_global
4. World Health Organization. WHO Director-General declares mpox outbreak a public health emergency of international concern [cited 2024 Oct 9]. https://www.who.int/news/item/14-08-2024-who-director-general-declares-mpox-outbreak-a-public-health-emergency-of-international-concern
5. Breman JG, Kalisa-Ruti, Steniowski MV, Zanotto E, Gromyko AI, Arita I. Human monkeypox, 1970-79. Bull World Health Organ. 1980;58:165–82.
6. Gov.UK. Mpox outbreak: epidemiological overview, 6 February 2025 [cited 2025 Mar 16]. https://www.gov.uk/government/publications/monkeypox-outbreak-epidemiological-overview/mpox-outbreak-epidemiological-overview-6-february-2025
7. Gov.UK. Confirmed cases of mpox clade Ib in United Kingdom [cited 2025 Mar 16]. https://www.gov.uk/guidance/confirmed-cases-of-mpox-clade-ib-in-united-kingdom
8. Land KJ, Boeras DI, Chen XS, Ramsay AR, Peeling RW. REASSURED diagnostics to inform disease control strategies, strengthen health systems and improve patient outcomes.

Nat Microbiol. 2019;4:46–54. https://doi.org/10.1038/s41564-018-0295-3
9. Drain PK. Rapid diagnostic testing for SARS-CoV-2. N Engl J Med. 2022;386:264–72. https://doi.org/10.1056/NEJMcp2117115
10. FIND. Monkeypox diagnostic test directory now live [cited 2024 Oct 14]. https://www.finddx.org/publications-and-statements/monkeypox-diagnostic-test-directory-now-live/
11. Lim CK, Roberts J, Moso M, Liew KC, Taouk ML, Williams E, et al. Mpox diagnostics: Review of current and emerging technologies. J Med Virol. 2023;95:e28429. https://doi.org/10.1002/jmv.28429
12. Adler H, Gould S, Hine P, Snell LB, Wong W, Houlihan CF, et al.; NHS England High Consequence Infectious Diseases (Airborne) Network. Clinical features and management of human monkeypox: a retrospective observational study in the UK. Lancet Infect Dis. 2022;22:1153–62. https://doi.org/10.1016/S1473-3099(22)00228-6
13. US Food and Drug Administration. Template for developers of antigen diagnostic tests for monkeypox. Emergency use authorizations for medical devices [cited 2025 Jan 2]. https://www.fda.gov/medical-devices/emergency-use-authorizations-medical-devices/monkeypox-mpox-emergency-use-authorizations-medical-devices#templates
14. Byrne RL, Aljayyoussi G, Kontogianni K, Clerkin K, McIntyre M, Wardale J, et al. Head-to-head comparison of anterior nares and nasopharyngeal swabs for SARS-CoV-2 antigen detection in a community drive-through test centre in the UK. BMJ Open Respir Res. 2025;12:e001747. https://doi.org/10.1136/bmjresp-2023-001747
15. Bunse T, Ziel A, Hagen P, Rigopoulos G, Yasar U, Inan H, et al. Analytical and clinical evaluation of a novel real-time PCR-based detection kit for Mpox virus. Med Microbiol Immunol. 2024;213:18. https://doi.org/10.1007/s00430-024-00800-4
16. Romero-Ramirez A, Somasundaran A, Kontogianni K, Parkes J, Hussain Y, Gould S, et al.; CONDOR steering group; ISARIC 4C Investigators. Evaluation of the diagnostic accuracy of Xpert® Mpox and STANDARD™ M10 MPX/OPX for the detection of monkeypox virus. J Infect. 2025;90:106413. https://doi.org/10.1016/j.jinf.2025.106413
17. International Pandemic Preparedness Secretariat. Mpox day 15: the status of rapid diagnostic tests, Tecovirimat trials and Emergency Use Listings [cited 2024 Oct 9]. https://ippsecretariat.org/news/mpox-day-15
18. Unitaid. Mpox emergency response must prioritize access to diagnostics, clinical care and vaccines [cited 2024 Oct 9]. https://unitaid.org/news-blog/mpox-emergency-response-must-prioritize-access-to-diagnostics-therapeutics-and-vaccines/#en
19. World Health Organization. Target product profiles for tests used for mpox (monkeypox) diagnosis [cited 2025 Jan 4]. https://www.who.int/publications/i/item/9789240076464
20. Townsend MB, MacNeil A, Reynolds MG, Hughes CM, Olson VA, Damon IK, et al. Evaluation of the Tetracore Orthopox BioThreat® antigen detection assay using l aboratory grown orthopoxviruses and rash illness clinical specimens. J Virol Methods. 2013;187:37–42. https://doi.org/10.1016/j.jviromet.2012.08.023
21. Laidlaw SM, Ulaeto D, Lonsdale S, Clark G, Sumner R, Edwards T, et al. Detection of mpox and other orthopoxviruses using a lateral flow device as a point-of-care diagnostic. Microbiol Spectr. 2025;13:e0245624. https://doi.org/10.1128/spectrum.02456-24
22. Mayfield J, Hesse P, Ledden D. The impact of universal transport media and viral transport media liquid samples on a SARS-CoV-2 rapid antigen test. Arch Intern Med Res. 2022;5:481–7. https://doi.org/10.26502/aimr.0137
23. Cubas-Atienzar AI, Kontogianni K, Edwards T, Wooding D, Buist K, Thompson CR, et al. Limit of detection in different matrices of 19 commercially available rapid antigen tests for the detection of SARS-CoV-2. Sci Rep. 2021;11:18313. https://doi.org/10.1038/s41598-021-97489-9
24. Zhou YB. Skin lesion specimens as first choice to detect monkeypox virus. Lancet. 2023;401:1264–5. https://doi.org/10.1016/S0140-6736(23)00283-0
25. Tarín-Vicente EJ, Alemany A, Agud-Dios M, Ubals M, Suñer C, Antón A, et al. Clinical presentation and virological assessment of confirmed human monkeypox virus cases in Spain: a prospective observational cohort study. Lancet. 2022;400:661–9. https://doi.org/10.1016/S0140-6736(22)01436-2
26. Suñer C, Ubals M, Tarín-Vicente EJ, Mendoza A, Alemany A, Hernández-Rodríguez Á, et al.; Movie Group. Viral dynamics in patients with monkeypox infection: a prospective cohort study in Spain. Lancet Infect Dis. 2023;23:445–53. https://doi.org/10.1016/S1473-3099(22)00794-0
27. Mertens P, De Vos N, Martiny D, Jassoy C, Mirazimi A, Cuypers L, et al.; LHUB-ULB SARS-CoV-2 Working Diagnostic Group. Development and potential usefulness of the COVID-19 Ag Respi-Strip Diagnostic Assay in a pandemic context. Front Med (Lausanne). 2020;7:225. https://doi.org/10.3389/fmed.2020.00225
28. Puyskens A, Bayram F, Sesver A, Michel J, Krause E, Bourquain D, et al. Performance of 20 rapid antigen detection tests to detect SARS-CoV-2 B.1.617.2 (Delta) and B.1.1.529 (Omicron) variants using a clinical specimen panel from January 2022, Berlin, Germany. Euro Surveill. 2023;28:2200615. https://doi.org/10.2807/1560-7917.ES.2023.28.16.2200615
29. Gokulan CG, Kiran U, Kuncha SK, Mishra RK. Temporal stability and detection sensitivity of the dry swab-based diagnosis of SARS-CoV-2. J Biosci. 2021;46:1–9. https://doi.org/10.1007/s12038-021-00216-9
30. Milo R, Phillips R. How fast do RNAs and proteins degrade? [cited 2025 Jan 3]. https://book.bionumbers.org/how-fast-do-rnas-and-proteins-degrade
31. Parvu V, Gary DS, Mann J, Lin YC, Mills D, Cooper L, et al. Factors that influence the reported sensitivity of rapid antigen testing for SARS-CoV-2. Front Microbiol. 2021;12:714242. https://doi.org/10.3389/fmicb.2021.714242

Address for correspondence: Ana Isabel Cubas-Atienzar, Centre for Drugs and Diagnostics, Liverpool School of Tropical Medicine, Pembroke Place, Liverpool L3 5QA, UK; email: ana.cubasatienzar@lstmed.ac.uk; Elie Ishara-Nshombo, Institut National de Recherche Biomédicale, 5345, Avenue de la Démocratie, BP1197, Kinshasa, Democratic Republic of the Congo; email: isharaelie@outlook.fr

Force of Infection Model for Estimating Time to Dengue Virus Seropositivity among Expatriate Populations, Thailand

Erica Rapheal, Amornphat Kitro, Hisham Imad, Marco Hamins-Peurtolas, Jutarmas Olanwijitwong, Lapakorn Chatapat, Taweewun Hunsawong, Kathryn Anderson,[1] Watcharapong Piyaphanee[1]

Dengue is a major cause of illness among local populations and travelers in dengue-endemic areas, particularly those who stay for an extended period. However, little is known about dengue risk among expatriates and other long-term travelers. We used catalytic models of force of infection to estimate time to 60% dengue virus (DENV) seropositivity for a cross-section of expatriates living in Bangkok and Pattaya, Thailand. Our model adjusted for daily time spent outside, years not exposed to DENV, sex, living environment, and use of mosquito repellent, nets, long sleeves, and air conditioning. We estimated an adjusted annual force of infection of 0.014 (95% CI 0.003–0.054) per year spent in dengue-endemic areas (67.3 years to 60% seropositivity), below that of local populations. Our findings suggest that expatriates have a DENV exposure profile distinct from locals and short-term travelers and should likely be considered independently when developing vaccine and prevention recommendations.

Dengue virus (DENV) is a mosquitoborne flavivirus that causes an estimated 100 million infections and >50 million febrile illnesses every year (*1*). Although primary DENV infections are typically clinically mild, secondary infection with a different strain can be severe and can result in thrombocytopenia, plasma leakage, pleural effusion, circulatory failure, and death (*2*–*6*). Half of the global population lives in an area suitable for DENV transmission, and changes in climate and human mobility, and the subsequent expansion of mosquito habitats, will continue to increase the global burden of dengue (*7*–*10*).

The development of new dengue vaccines brings with it the need for updated travel recommendations for protection against DENV infection. Four dengue vaccines have passed phase III trials and 2 have been licensed for use in several countries; many more are in earlier phases of development (*11*–*14*). The World Health Organization currently recommends that countries consider incorporating the Qdenga vaccine (Takeda, https://www.takeda.com) into routine immunization programs for populations with ≥60% DENV seropositivity by age 9 but does not make specific recommendations for travelers (*15*–*17*). Travelers to DENV-endemic regions have flavivirus exposure histories and associated immunologic profiles distinct from the local populations, which might necessitate unique vaccine and mosquito bite prevention recommendations for travelers, particularly those who plan to stay for extended periods. The number of travel-associated dengue cases has been steadily increasing since 2007, hitting an all-time high in 2019 (*18*).

Long-term expatriates (persons who have moved from other countries but typically do not seek citizenship and might not plan to stay permanently) might be at higher risk for DENV infection than short-term travelers (*19*). Census estimates in 2010 for Thailand counted 80,000 expatriates from the United States, Europe, and Australia living in the capital city of Bangkok alone, representing almost 1% of the city's total population (*20*). Those persons represent a unique intersection between traditional

Author affiliations: University of Minnesota School of Public Health, Minneapolis, Minnesota, USA (E. Rapheal); Chiang Mai University, Chiang Mai, Thailand (A. Kitro); Mahidol University, Bangkok, Thailand (H. Imad, J. Olanwijitwong, L. Chatapat, W. Piyaphanee); Osaka University, Osaka, Japan (H. Imad); University of California, San Francisco, California, USA (M. Hamins-Peurolas); US Army Medical Directorate of the Armed Force Research Institute of Medical Sciences, Bangkok (T. Hunsawong); SUNY Upstate Medical University, Syracuse, New York, USA (K. Anderson)

DOI: https://doi.org/10.3201/eid3106.241686

[1]These last authors contributed equally to this article.

travelers and native-borne Thai persons because although expatriates (initially) have the naive immunologic profile of a visitor, their daily activities might more closely resemble those of long-term residents (*21*).

An improved understanding of the risks experienced by travelers to dengue-endemic regions is essential to develop safe and effective DENV vaccine usage guidelines for these populations. Although the force of infection (FOI) (the rate at which susceptible persons become infected) among local populations for DENV can be high, risk among travelers might be altered by factors such as increased access to air conditioning and window screens (which might decrease risk), increased immunologic susceptibility to DENV (which might increase risk), or a decreased understanding of local public health threats and mitigation measures for DENV (which might increase risk) (*22*,*23*). Previous studies from this group, including an ongoing cohort study in central Thailand, have indicated that most citizens of Thailand have experienced ≥1 DENV infection by 6–10 years of age (*23*–*26*).

Previously published findings from a cross-sectional study of expatriates living in Bangkok and Pattaya, Thailand, found DENV seroprevalence to be 11%–21% and showed that expatriates who have been in Thailand for a longer duration are more likely to have DENV-neutralizing antibodies (*27*). In this analysis, we continue that work by contrasting the estimated FOI by years of residence in a dengue-endemic area (DEA) (such as Thailand) among expatriates with that experienced by native-born Thai populations. To estimate the time to first DENV infection, we use catalytic models of FOI using age-stratified DENV seroprevalence data. The purpose of this study is to describe how closely the exposure profile of expatriates resembles that of native residents to target public health messaging and inform optimal-use scenarios for DENV countermeasures in this unique population.

Methods

Participant Recruitment

The study population and methods for this study were described previously by Kitro et al. (*27*). In brief, visitors to the Travel Medicine Clinic, Hospital for Tropical Diseases, in Bangkok, Thailand, were actively recruited to participate in this study by a member of the study team staff. Advertisements inviting participants to visit the clinic to enroll in the study were also posted in expatriate groups on social media (i.e., Facebook). Finally, the study team traveled to a meeting of the Pattaya City Expat Club to enroll participants and collect samples on site. Data were collected during December 2017–February 2020. Participants were eligible for inclusion if they were born in a non–flavivirus-endemic region, including the United States/Canada, Europe, the Middle East, Australia/New Zealand, and East Asia (Japan, South Korea, and China); resided in Thailand for >1 year cumulatively over their lifetime; were ≥18 years of age; had no contraindication to blood draw, no history of blood transfusion in the previous 6 months, and no history of dengue vaccination; and provided informed consent.

Data Collection

Study data were collected using a short survey, including information about participant demographics, health behaviors, mosquito bite prevention habits and risk factors, history of flavivirus vaccination and infection, and travel history. Approximately 5 mL of blood was drawn by venipuncture from participants who met the inclusion criteria. Laboratory testing was performed at the Armed Forces Research Institute of Medicine in Bangkok. Specimens were tested for neutralizing antibody titers against all 4 DENV serotypes, as well as Japanese encephalitis (JEV) and Zika virus (ZIKV), using plaque-reduction neutralization test (PRNT). The PRNT assay provides a quantitative measure of the antibody response after arbovirus exposure by measuring the inhibition of virus infection. The in vitro study uses a monolayer of C6/36 cells on agar that are infected with virus, leading to cell death and creation of viral plaques. Viruses used in this study were DENV-1 (16007), DENV-2 (16681), DENV-3 (16562), DENV-4 (C0036/06), JEV 0423 (SA-14-14-2, vaccine strain), and ZIKV (SV127/14, Thai isolated strain). When mixed with serum containing antibodies, the infection is inhibited, and plaque number is reduced. Serum dilutions can be compared with a control with no virus-neutralizing antibodies to determine the serum concentration at which a 50% plaque reduction is observed ($PRNT_{50}$) (*28*).

A $PRNT_{50}$ value of ≥0.5 in any ≥1 of the 4 DENV serotypes qualified a person as seropositive. Participants were defined as DENV naive if they were negative for all 4 DENV strains, monotypic if they were positive for only 1 DENV strain, and multitypic if they were positive for ≥2 DENV strains.

Variables

We calculated time in a DEA by adding cumulative time living in Thailand (in months) and travel of >1 month to dengue-endemic countries. We rounded up time to the nearest year.

We prioritized 6 potential demographic confounders in the analysis for the association between time spent in a DEA and DENV seropositivity: time unexposed (calculated by subtracting time in DEA from age; this covariate was used as a proxy for age to minimize correlation between age and years in DEA), average daily time spent outdoors, sex, marriage to a local of Southeast Asia, employment status, and living environment. Average daily time spent outside was reported in hours. Employment status was categorized into employed or unemployed/retired on the basis of an open-ended survey question. Participants selected urban, suburban, rural, or farm for living environment. Analyses used a binary variable comparing urban to any other response.

We also collected information about how frequently 5 mosquito bite–prevention strategies were used: mosquito repellant, long sleeves, window screens, mosquito netting, and air conditioning. Participants self-reported frequency on a scale of 1 (daily) to 5 (never). We split those measures at the median to create binary variables; we categorized values below the median as more frequent use and values greater than or equal to the median as less frequent use.

Data Analysis

We estimated FOI by fitting serocatalytic models, using seropositivity to ≥1 of the 4 DENV serotypes as the outcome. We fit serostatus by using a binomial model with a *cloglog* link function with log(years in DEA) as an offset. We adapted code from Ribeiro dos Santos et al. (*23*) and implemented it using R-INLA, which is syntactically similar to the lm function in R where linear predictors can be incorporated (*29*). We fit a crude model to estimate overall FOI, as well as univariate models incorporating each of the 6 demographic and 5 mosquito prevention variables described and a saturated model incorporating all 11 variables. We also used a 10% backward selection method to develop a reduced model. In this method, variables are removed from the model sequentially. The variable with the least impact on the model is dropped, provided that removing that variable changes the FOI estimate to <10%. We repeated this process until no variables could be removed without ≥10% change in the FOI. All models included the log(years in DEA) offset term (Appendix, https://wwwnc.cdc.gov/EID/article/31/6/24-1686.App1.pdf). We performed all analyses using R version 4.3.1 (The R Project for Statistical Computing, https://www.r-project.org).

Sensitivity Analysis

To assess the effect of cross-reactivity between flaviviruses, we performed a sensitivity analysis. We assumed all persons with $PRNT_{50}$ >0.5 for JEV or ZIKV were seronegative for DENV.

Ethical Considerations

The study was approved by the Ethics Committee of Mahidol University (FTM ECT-019-06), the Walter Reed Army Institute of Research Institutional Review Board, the oversight body for AFRIMS regulatory approval (WRAIR no. 2500), and the University of Minnesota Institutional Review Board, which was the funding source for this study. All study participants provided informed written consent, and all data were anonymized before analysis.

Results

Participants

Of 235 participants who met the inclusion criteria, 71 (30%) were seropositive for ≥1 DENV strain. Of those, 29 (41%) were monotypic and 42 (59%) were multitypic. Ten (4%) participants were JEV positive and 5 (2%) were ZIKV positive (Table 1). Persons who were DENV negative had spent an average of 9 years in a DEA, compared with 14 years for those who were DENV positive (p = 0.02) (Table 2). Approximately

Table 1. Serostatus of participants in study of force of infection model for estimating time to DENV seropositivity among expatriate populations, Thailand*

Serostatus	No. (%) participants		
	Total, n = 235	DENV-negative, n = 164	DENV-positive, n = 71
Dengue			
DENV-negative	164 (70)		
Monotypic†	29 (12)		
Multitypic‡	42 (18)		
Japanese encephalitis			
JEV-negative	225	160 (71.1)	65 (28.9)
JEV-positive	10	4 (40)	6 (60)
Zika			
ZIKV-negative	230	161 (70)	69 (30)
ZIKV-positive	5	3 (60)	2 (40)

*DENG, dengue virus; JEV, Japanese encephalitis virus; ZIKV, Zika virus.
†Person was previously infected with only 1 DENV serotype.
‡Person was previously infected with ≥2 different DENV serotypes.

Table 2. Descriptive statistics of 235 expatriate participants in study of force of infection model for estimating time to DENV seropositivity among expatriate populations, Thailand*

Characteristic	Total, n = 235	DENV-negative, n = 164	DENV-positive, n = 71	p value
Median time in DEA (range), y	7 (1–53)	7 (1–37)	10 (1–53)	0.02†
Median age (range), y	66 (23–94)	65 (23–88)	68 (27–94)	0.16†
Median time unexposed (range), y	54 (21–78)	53 (21–78)	54 (23–75)	0.94†
Average time outside daily (range), h	5.0 (0.0–24.0)	6.0 (0.0–24.0)	4.5 (0.0–16.0)	0.21†
Sex				0.75‡
M	186 (84)	129 (84)	57 (83)	
F	36 (16)	24 (16)	12 (17)	
Married to person from Southeast Asia				0.91‡
Yes	64 (27)	45 (27)	19 (27)	
No	171 (73)	119 (73)	52 (73)	
Employment status				0.45‡
Employed	50 (25)	36 (26)	14 (21)	
Unemployed/retired	185 (75)	128 (74)	57 (79)	
Living setting				0.084‡
Urban	197 (84)	133 (81)	64 (90)	
Nonurban	38 (16)	31 (19)	7 (10)	
Mosquito repellent				0.68‡
Frequent	56 (24)	38 (23)	18 (26)	
Infrequent	179 (76)	126 (77)	53 (74)	
Long sleeves				0.2‡
Frequent	112 (48)	83 (51)	29 (41)	
Infrequent	123 (52)	81 (49)	42 (59)	
Window screens				0.8‡
Frequent	94 (40)	65 (40)	29 (41)	
Infrequent	141 (60)	99 (60)	42 (59)	
Mosquito nets				0.83‡
Frequent	72 (31)	50 (30)	22 (32)	
Infrequent	163 (69)	114 (70)	49 (68)	
Air conditioning				0.36‡
Frequent	94 (40)	69 (42)	25 (36)	
Infrequent	141 (60)	95 (58)	46 (64)	

*Values are no. (%) except as indicated. DEA, dengue-endemic area; DENV, dengue virus.
†By Wilcoxon rank-sum test.
‡By Pearson χ^2 test.

1% (279 of 25,922 months) of the total months in a DEA were attributed to time spent in dengue-endemic countries outside of Southeast Asia.

Study participants were primarily men (84%) and retired (57%). Participant age ranged from 23 to 94 years; the average age was 61 (median 66) years. Most (60%) participants lived in an urban area, and >1 in 4 (27%) were married to a person from Southeast Asia (Table 2).

FOI Models

Assuming a static FOI for the entirety of time spent in a DEA and incorporating no other risk factors, we estimated an annual FOI of 0.042 (95% CI 0.033–0.053) (≈23.9 years to first DENV infection). Using this model, 60% seroprevalence is reached after 21.9 years in DEA (Figure). Watanabe-Akaike information criterion (WAIC), a Bayesian measure similar to the Akaike information criterion, was 295.0.

No covariates were significantly associated with DENV seropositivity in univariate models (Table 3). The 10% backward selection method retained years unexposed, male, urban living setting, and frequent use of mosquito repellent, mosquito nets, long sleeves, and air conditioning (Table 4). Only urban living setting was significantly associated with DENV seropositivity in the reduced model (OR 2.45 [95% CI 1.09–5.49]). WAIC for that model was 300.8. A difference of 5.8 between WAIC values provides weak but not conclusive evidence that the crude model is a better predictor than the reduced model (*31*).

Using the reduced multivariate model, we estimated an annual FOI of 0.014 (95% CI 0.003–0.054) (73.5 years to first DENV infection, 67.3 years to 60% DENV seropositivity). Using the reduced multivariate model, a person who is at higher risk for all included variables, where higher risk means associated with higher odds of seropositivity in the reduced model regardless of significance (i.e., lived 60 years in a nonendemic region, male sex, urban living setting, frequent use of mosquito repellent and nets, and infrequent use of long sleeves and air conditioning) would have an estimated annual FOI of 0.101 (95% CI 0.046–0.218). Conversely, a person who is at lower risk for those variables (i.e., lived 17 years in a nonendemic region, female sex) would have an estimated annual FOI of 0.007 (95% CI 0.002–0.025).

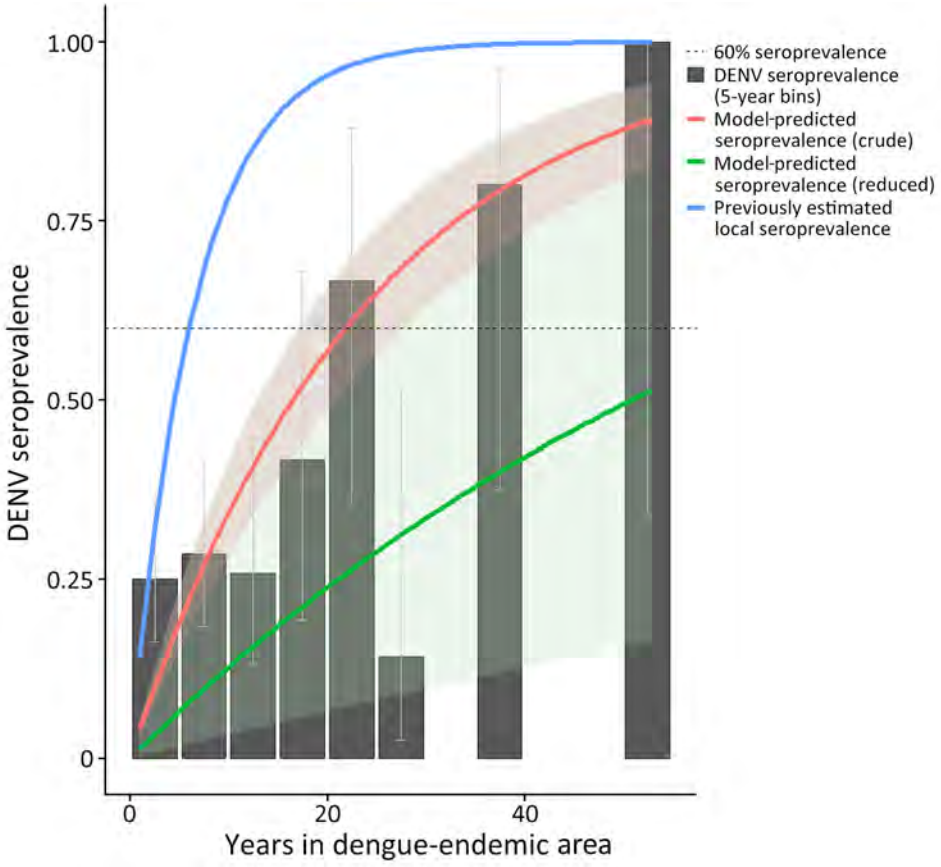

Figure. Crude force of infection by years in dengue-endemic area (DEA) in study of force of infection model for estimating time to DENV seropositivity among expatriate populations, Thailand. A serocatalytic model estimating dengue force of infection was fit using a binomial model with a cloglog link function with log(years in DEA) as an offset. Solid red line represents the crude model; solid green line represents the reduced model. The solid blue line represents approximate seroprevalence among locals of Thailand, as modeled by Hamins Puertolas et al. (*25*). Dotted line indicates 60% DENV seroprevalence. Black bars show the seroprevalence of DENV among all study participants in 5-year bins of years spent in a DEA. Uncertainty in measured seroprevalence was calculated using the Wilson confidence interval for proportions (*30*). DENV, dengue virus.

Sensitivity Analysis

Eight persons who were DENV positive in the original analysis were positive for either ZIKV (n = 2) or JEV (n = 6) and were therefore considered DENV negative for the sensitivity analysis. Using those data, we estimated an average annual FOI of 0.037 (95% CI 0.028–0.046) (26 years to 60% seropositive) in the crude model, representing a 17% decrease, and 0.011 (95% CI 0.003–0.049) (82 years to 60% seropositive) in the adjusted model, representing a 21% decrease.

Discussion

In our study of 235 expatriates living in Bangkok and Pattaya, Thailand, we found a crude DENV FOI of 0.042/year spent in DEA, equating to an estimated 23.9 years to first DENV infection and 21.9 years to 60% DENV seroprevalence. When we adjusted for years unexposed to DENV, sex, living environment, and frequent use of repellent, mosquito nets, long sleeves, and air conditioning, the FOI estimate decreased to 0.014, or 73.5 years to first DENV infection and 67.3 years to 60% DENV seropositivity. Using the

Table 3. Estimates from univariate logistic models of dengue seropositivity by years in a dengue-endemic area in study of force of infection model for estimating time to dengue virus seropositivity among expatriate populations, Thailand*

Covariate in univariate models	Odds ratio (95% CI)
Years unexposed	1.01 (0.9–1.02)
Average daily time outside, h	0.98 (0.92–1.03)
Male sex	1.24 (0.69–2.25)
Married to native of Southeast Asia	0.75 (0.44–1.22)
Employed	0.72 (0.45–1.48)
Urban living setting	2.04 (0.93–4.49)
Frequent use of mosquito repellent	1.11 (0.65–1.91)
Frequent use of mosquito nets	1.02 (0.61–1.71)
Frequent use of window screens	1.02 (0.63–1.65)
Frequent use of long sleeves	0.66 (0.41–1.07)
Frequent use of air conditioning	0.75 (0.46–1.24)

*Force of infection for years in dengue-endemic area (DEA) is 0.04 (95% CI 0.03–0.06). Serocatalytic models estimating dengue force of infection were fit using a binomial model with a cloglog link function with log(years in DEA) as an offset. Crude model contains only log(years in DEA) offset. Univariate models included 1 covariate and the log(years in DEA) offset.

Table 4. Estimates from reduced multivariate model of DENV seropositivity by years in a dengue-endemic area in study of force of infection model for estimating time to seropositivity among expatriate populations, Thailand*

Reduced multivariate model	Odds ratio (95% CI)
Years unexposed	1.01 (0.99–1.02)
Male sex	1.35 (0.74–2.47)
Urban living setting	2.45 (1.09–5.49)
Frequent use of mosquito repellent	1.33 (0.75–2.35)
Frequent use of mosquito nets	1.22 (0.69–2.16)
Frequent use of long sleeves	0.62 (0.36–1.05)
Frequent use of air conditioning	0.77 (0.46–1.30)

*Force of infection (FOI) is 0.01 (95% CI 0.00–0.05). Serocatalytic models estimating dengue force of infection were fit using a binomial model with a cloglog link function with log(years in dengue-endemic area) as an offset. A 10% backward selection method was used to determine which variables were included in the reduced model. Variables were sequentially removed from the model, and the variable with the least impact on the model was dropped. This process was repeated until no variables could be removed without ≥10% change in the FOI.

adjusted model, a person who is at high risk in all our exposure categories has an estimated FOI per year in DEA of 0.101, >8 times higher than that in the low-risk group (0.007).

Our results suggest that expatriates are a unique population who should be considered as such when developing recommendations for DENV control and prevention. Our average time to 60% seroprevalence was more than twice that for Thai locals, suggesting that expatriates and other long-term travelers might experience a much lower risk for DENV exposure relative to native residents. Data from Rayong Province, which is geographically adjacent to Pattaya, found most persons to be infected by age 10; in other areas, that age is as low as 6 years (*26*,*32*,*33*).

The difference in the estimated annual FOI for high (13.5%) versus low (0.4%) risk participants highlights the need to consider risk when recommending vaccination to the expatriate population. For example, short-term travelers who stay in urban areas might benefit from vaccination during periods of epidemic transmission because of possibly high and transient multitypic cross-protection, but they might experience increased risk with subsequent travel (in the months or early years after vaccination) as immunity wanes. This area bears more study and exploration and was not specifically addressed by Takeda or the manufacturers of the Dengvaxia vaccine (Sanofi Pasteur, https://www.sanofi.com), nor was specific guidance provided by the World Health Organization regarding vaccination of short- or long-term travelers.

The use of mosquito repellents such as DEET and picaridin has been shown to be effective in reducing mosquito bite frequency when applied regularly (*34*,*35*). Those and other primary prevention strategies, as well as community mosquito control measures, have been the recommendations for dengue prevention while awaiting more effective countermeasures for DENV (e.g., vaccines and antiviral drugs) (*2*). Although we did not find a significant association between those prevention measures and DENV seropositivity, the difference in FOI between the groups at low risk and high risk (0.007 for low risk and 0.101 for high risk) suggests that those risk factors might still be drivers of infection risk and underscores the continued importance of nonvaccine interventions. Participants also could have overreported repellant usage to more closely align with recommendations, which would introduce bias into those findings.

Of note, our study population was primarily urban (60%) and male (84%), and the average age was 61 years. This group might be slightly older and have a higher representation of men than the overall expatriate population; a 2021 study from Kitro et al. (*36*) found Western expatriates in Bangkok and Chiang Mai to be 75% men and an average of 56 years of age, and the 2010 census reports that expatriates in Bangkok were ≈64% male (*37*). Bangkok and Pattaya are both attractive retirement spots for Westerners and typically attract an older, more male population (*38*). Therefore, we do consider our study population to be representative of the expatriate population in those communities. Lifestyle differences, including working outside during the day and housing- and infrastructure-related risk factors, were expected to play a role in determining time to DENV infection. However, we found no significant association between DENV infection and age (measured as years unexposed to DENV), employment, or time spent outside in univariate or multivariate analyses (Table 2). We did find an association with urban versus nonurban residence (OR 2.45 [95% CI 1.09–5.49]) in the multivariate analysis. Future studies could examine this relationship in more depth by measuring housing and workplace infrastructure more explicitly.

The first limitation of our study is that our model does not directly take multiple infections into account. PRNT results across DENV serotypes are known to be highly cross-reactive, and it is therefore difficult to assess the number and timing of infections associated with multitypic serostatus (*6*). For this reason, the FOI estimated in this model probably slightly underrepresents the actual value, whereas a model incorporating multiple infections would overestimate the true value. In addition, exposure to cross-reacting arboviruses such as JEV and ZIKV might also affect estimates, something we try to account for, making it difficult to address questions about time to postprimary infection.

Dengue has substantial interannual variation, in both number of cases and case serotype (*39*). Major outbreaks occur regularly in Thailand, most recently in 2015, 2019, and 2023 (*40*). This study does not investigate the possibility of cohort effects related to these outbreak years; future studies might use number of outbreaks experienced as a length-of-stay variable, or weight length of stay by annual disease burden. This study lacked the sample size to power a time-varying FOI analysis, but the use of constant FOI to describe DENV serology is common in hyperendemic regions like Thailand, and the models have been shown to fit DENV data well (*25*,*26*). However, more research is necessary to evaluate whether FOI varies over time, which could help identify periods at which expatriates are at higher or lower risk. Finally, the inherent limitations of a cross-sectional study limit capacity to assess the effects of waning immunity and seroreversion. Previous studies have shown seroreversion rates of <4%, but many unknowns remain about the extent to which primary DENV infections provide lasting immunity (*41*–*43*). In addition, we are not able to determine consistency of covariates over time and are therefore only able to draw conclusions about each person's current behaviors. A future prospective study should assess how these characteristics, and their associated outcomes, might change over time.

In conclusion, we found that the DENV infection profile of expatriates living in Bangkok and Pattaya, Thailand, does not closely resemble that of native-born residents. The relatively low rate of DENV infection in expatriates suggests that we should consider them to be a group with a distinct exposure profile compared with both local residents and short-term travelers. Future studies examining longitudinal DENV exposure profiles in other native and expatriate populations, and in other regions, will be key to place these findings in a global context. However, our findings should be considered when developing targeted public health messaging and could help inform recommendations for both vaccine and nonvaccine DENV prevention measures.

Acknowledgments

We thank the staff at the Thai Travel Clinic, as well as the Pattaya City Expat club. We also thank the Armed Forces Research Institute of Medical Sciences staff for their help in collecting specimens, recruiting participants, and analyzing samples.

This work was funded by a seed grant from the Center for Global Health and Social Responsibility, University of Minnesota, Academic Health Center Global Health Seed Grant, and Walter H. Judd International Research Fellowship. Additional funding was provided by the US Department of Health and Human Services, National Institutes of Health, National Institute of Allergy and Infectious Diseases (P01 AI034533/AI/NIAID NIH HHS/United States and R01 AI175941/AI/NIAID NIH HHS/United States).

Material has been reviewed by the Walter Reed Army Institute of Research. There is no objection to its publication. The opinions or assertions contained herein are the private views of the author, and are not to be construed as official, or as reflecting true views of the Department of the Army or the Department of Defense. The investigators have adhered to the policies for protection of human subjects as prescribed in AR 70–25.

About the Author

Ms. Rapheal is a PhD student in the Epidemiology and Community Health program at the University of Minnesota School of Public Health. She is interested in infectious disease, global health, epidemiologic modeling, and spatial epidemiology.

References

1. Cattarino L, Rodriguez-Barraquer I, Imai N, Cummings DAT, Ferguson NM. Mapping global variation in dengue transmission intensity. Sci Transl Med. 2020;12:eaax4144. https://doi.org/10.1126/scitranslmed.aax4144
2. World Health Organization. Dengue and severe dengue [2020 Apr 12]. https://www.who.int/news-room/fact-sheets/detail/dengue-and-severe-dengue
3. Halstead SB, Yamarat C. Recent epidemics of hemorrhagic fever in Thailand: observations related to pathogenesis of a "new" dengue disease. Am J Public Health Nations Health. 1965;55:1386–95. https://doi.org/10.2105/AJPH.55.9.1386
4. Sabin AB. Research on dengue during World War II. Am J Trop Med Hyg. 1952;1:30–50. https://doi.org/10.4269/ajtmh.1952.1.30
5. Centers for Disease Control and Prevention. Dengue shock syndrome (DSS) 2010 case definition [cited 2024 Jan 29]. https://ndc.services.cdc.gov/case-definitions/dengue-shock-syndrome-2010
6. Halstead SB, Rojanasuphot S, Sangkawibha N. Original antigenic sin in dengue. Am J Trop Med Hyg. 1983;32:154–6. https://doi.org/10.4269/ajtmh.1983.32.154
7. Bhatt S, Gething PW, Brady OJ, Messina JP, Farlow AW, Moyes CL, et al. The global distribution and burden of dengue. Nature. 2013;496:504–7. https://doi.org/10.1038/nature12060
8. Naish S, Dale P, Mackenzie JS, McBride J, Mengersen K, Tong S. Climate change and dengue: a critical and systematic review of quantitative modelling approaches. BMC Infect Dis. 2014;14:167. https://doi.org/10.1186/1471-2334-14-167
9. Rocklöv J, Tozan Y. Climate change and the rising infectiousness of dengue. Emerg Top Life Sci. 2019;3:133–42.
10. Gubler DJ. Dengue, urbanization and globalization: the unholy trinity of the 21st century. Trop Med Health. 2011;39(Suppl):3–11. https://doi.org/10.2149/tmh.2011-S05

11. Menon S, Wilder-Smith A. New vaccines on the immediate horizon for travelers: chikungunya and dengue vaccines. Curr Infect Dis Rep. 2023;25:211–24. https://doi.org/10.1007/s11908-023-00811-x
12. Thomas SJ. Is new dengue vaccine efficacy data a relief or cause for concern? NPJ Vaccines. 2023;8:55.
13. Kallás EG, Cintra MAT, Moreira JA, Patiño EG, Braga PE, Tenório JCV, et al. Live, attenuated, tetravalent butantan-dengue vaccine in children and adults. N Engl J Med. 2024;390:397–408. https://doi.org/10.1056/NEJMoa2301790
14. Nogueira ML, Cintra MAT, Moreira JA, Patiño EG, Braga PE, Tenório JCV, et al.; Phase 3 Butantan-DV Working Group. Efficacy and safety of Butantan-DV in participants aged 2–59 years through an extended follow-up: results from a double-blind, randomised, placebo-controlled, phase 3, multicentre trial in Brazil. Lancet Infect Dis. 2024;24:1234–44. https://doi.org/10.1016/S1473-3099(24)00376-1
15. Angelin M, Sjölin J, Kahn F, Ljunghill Hedberg A, Rosdahl A, Skorup P, et al. Qdenga—a promising dengue fever vaccine; can it be recommended to non-immune travelers? Travel Med Infect Dis. 2023;54:102598. https://doi.org/10.1016/j.tmaid.2023.102598
16. Freedman DO. A new dengue vaccine (TAK-003) now WHO recommended in endemic areas; what about travellers? J Travel Med. 2023;30:taad132. https://doi.org/10.1093/jtm/taad132
17. World Health Organization. WHO position paper on dengue vaccines–May 2024 [cited 2024 Sep 4]. https://iris.who.int/bitstream/handle/10665/376641/WER9918-eng-fre.pdf
18. Duvignaud A, Stoney RJ, Angelo KM, Chen LH, Cattaneo P, Motta L, et al.; GeoSentinel Network. Epidemiology of travel-associated dengue from 2007 to 2022: a GeoSentinel analysis. J Travel Med. 2024;31:taae089. https://doi.org/10.1093/jtm/taae089
19. Kitro A, Ngamprasertchai T, Srithanaviboonchai K. Infectious diseases and predominant travel-related syndromes among long-term expatriates living in low-and middle- income countries: a scoping review. Trop Dis Travel Med Vaccines. 2022;8:11. https://doi.org/10.1186/s40794-022-00168-4
20. World Population Review. Bangkok population 2023 [cited 2023 Dec 26]. https://worldpopulationreview.com/world-cities/bangkok-population
21. Shepherd SM, Shoff WH. Vaccination for the expatriate and long-term traveler. Expert Rev Vaccines. 2014;13:775–800. https://doi.org/10.1586/14760584.2014.913485
22. Reiter P, Lathrop S, Bunning M, Biggerstaff B, Singer D, Tiwari T, et al. Texas lifestyle limits transmission of dengue virus. Emerg Infect Dis. 2003;9:86–9. https://doi.org/10.3201/eid0901.020220
23. Ribeiro Dos Santos G, Buddhari D, Iamsirithaworn S, Khampaen D, Ponlawat A, Fansiri T, et al. Individual, household, and community drivers of dengue virus infection risk in Kamphaeng Phet Province, Thailand. J Infect Dis. 2022;226:1348–56. https://doi.org/10.1093/infdis/jiac177
24. Anderson KB, Buddhari D, Srikiatkhachorn A, Gromowski GD, Iamsirithaworn S, Weg AL, et al. An innovative, prospective, hybrid cohort-cluster study design to characterize dengue virus transmission in multigenerational households in Kamphaeng Phet, Thailand. Am J Epidemiol. 2020;189:648–59. https://doi.org/10.1093/aje/kwaa008
25. Hamins-Puértolas M, Buddhari D, Salje H, Cummings DAT, Fernandez S, Farmer A, et al. Household immunity and individual risk of infection with dengue virus in a prospective, longitudinal cohort study. Nat Microbiol. 2024;9:274–83. https://doi.org/10.1038/s41564-023-01543-3
26. Rodríguez-Barraquer I, Buathong R, Iamsirithaworn S, Nisalak A, Lessler J, Jarman RG, et al. Revisiting Rayong: shifting seroprofiles of dengue in Thailand and their implications for transmission and control. Am J Epidemiol. 2014;179:353–60. https://doi.org/10.1093/aje/kwt256
27. Kitro A, Imad HA, Pisutsan P, Matsee W, Sirikul W, Sapbamrer R, et al. Seroprevalence of dengue, Japanese encephalitis and Zika among long-term expatriates in Thailand. J Travel Med. 2024;31:taae022. https://doi.org/10.1093/jtm/taae022
28. Russell PK, Nisalak A. Dengue virus identification by the plaque reduction neutralization test. J Immunol. 1967;99:291–6. https://doi.org/10.4049/jimmunol.99.2.291
29. Rue H, Martino S, Chopin N. Approximate bayesian inference for latent gaussian models by using integrated nested laplace approximations. J R Stat Soc Series B Stat Methodol. 2009;71:319–92. https://doi.org/10.1111/j.1467-9868.2008.00700.x
30. Wilson EB. Probable inference, the law of succession, and statistical inference. J Am Stat Assoc. 1927;22:209–12. https://doi.org/10.1080/01621459.1927.10502953
31. McElreath R. Statistical rethinking: a Bayesian course with examples in R and Stan. New York: CRC Press Taylor & Francis; 2016.
32. Nealon J, Bouckenooghe A, Cortes M, Coudeville L, Frago C, Macina D, et al. Dengue endemicity, force of infection, and variation in transmission intensity in 13 endemic countries. J Infect Dis. 2022;225:75–83. https://doi.org/10.1093/infdis/jiaa132
33. Hamins-Puértolas M, Buddhari D, Salje H, Cummings DAT, Fernandez S, Farmer A, et al. Household immunity and individual risk of infection with dengue virus in a prospective, longitudinal cohort study. Nat Microbiol. 2024;9:274–83. https://doi.org/10.1038/s41564-023-01543-3
34. Patel RV, Shaeer KM, Patel P, Garmaza A, Wiangkham K, Franks RB, et al. EPA-registered repellents for mosquitoes transmitting emerging viral disease. Pharmacotherapy. 2016;36:1272–80. https://doi.org/10.1002/phar.1854
35. Lupi E, Hatz C, Schlagenhauf P. The efficacy of repellents against *Aedes*, *Anopheles*, *Culex* and *Ixodes* spp.—a literature review. Travel Med Infect Dis. 2013;11:374–411. https://doi.org/10.1016/j.tmaid.2013.10.005
36. Kitro A, Sirikul W, Piankusol C, Rirermsoonthorn P, Seesen M, Wangsan K, et al. Acceptance, attitude, and factors affecting the intention to accept COVID-19 vaccine among Thai people and expatriates living in Thailand. Vaccine. 2021;39:7554–61. https://doi.org/10.1016/j.vaccine.2021.11.031
37. NSO. Population and Housing Census [cited 2025 Jan 15]. https://www.nso.go.th/nsoweb/main/summano/aE?year=957&type=3309#data__report
38. Jaisuekun K, Sunanta S. German migrants in Pattaya, Thailand: gendered mobilities and the blurring boundaries between sex tourism, marriage migration, and lifestyle migration. In: Mora C, Piper N, editors. The Palgrave Handbook of Gender and Migration. Cham (Switzerland): Springer International Publishing; 2021. p. 137–149.
39. Kerdpanich P, Kongkiatngam S, Buddhari D, Simasathien S, Klungthong C, Rodpradit P, et al. Comparative analyses of historical trends in confirmed dengue illnesses detected at public hospitals in Bangkok and northern Thailand, 2002–2018. Am J Trop Med Hyg. 2020;104:1058–66. https://doi.org/10.4269/ajtmh.20-0396

40. World Health Organization. Combating dengue outbreak and addressing overlapping challenges with COVID-19 [cited 2024 Jan 5]. https://www.who.int/thailand/news/detail/30-06-2023-combating-dengue-outbreak-and-addressing-overlapping-challenges-with-covid-19
41. Ooi EE, Kalimuddin S. Insights into dengue immunity from vaccine trials. Sci Transl Med. 2023;15:eadh3067. https://doi.org/10.1126/scitranslmed.adh3067
42. Lim JK, Carabali M, Edwards T, Barro A, Lee JS, Dahourou D, et al. Estimating the force of infection for dengue virus using repeated serosurveys, Ouagadougou, Burkina Faso. Emerg Infect Dis. 2021; 27:130–9. https://doi.org/10.3201/eid2701.191650
43. Biggs JR, Sy AK, Sherratt K, Brady OJ, Kucharski AJ, Funk S, et al. Estimating the annual dengue force of infection from the age of reporting primary infections across urban centres in endemic countries. BMC Med. 2021;19:217. https://doi.org/10.1186/s12916-021-02101-6

Address for correspondence: Kathryn Anderson, SUNY Upstate Medical University, 304 Campus West Building (CWB), 750 E Adams St, Syracuse, NY 13210, USA; email: andekath@upstate.edu

etymologia revisited

Haematospirillum jordania

[Hae.ma.to.spi.ril'lum jor.da'ni.ae]

For the sesquipedalian term *Haematospirillum*, *Haema* is derived from the Greek *haima*, meaning blood. *Spirillum* is derived from Medieval Latin in the mid-13th century Latin (*spiralis*), French in the 1550s (*spiral*), and Greek (*speira*). All suggest a winding or coil. A New Latin reference book entry in 1875 implied a little coil.

Isolated from human blood, *Haematospirillum jordaniae* was reported as a novel genus and species in 2016 by Centers for Disease Control and Prevention (CDC) scientist Ben W. Humrighouse and his laboratory team, which included Jean G. Jordan, a microbiologist. This gram-negative bacterium was isolated 14 times in 10 states during 2003–2012 before its identification in 2016.

H. jordaniae was previously considered an environmental bacterium with limited pathogenicity, but increasing numbers of isolates indicated a possible emerging pathogen. All cases occurred in male patients, and the pathogen showed a predilection for infecting lower leg injuries. In 2018, Hovan and Hollinger reported a case of infection in a Delaware man who, in 2016, had sepsis from a lower leg wound. The organism isolated was identified at the CDC Special Bacteriology Reference Laboratory (SBRL) in the Division of High-Consequence Pathogens and Pathology, National Center for Emerging and Zoonotic Infectious Diseases.

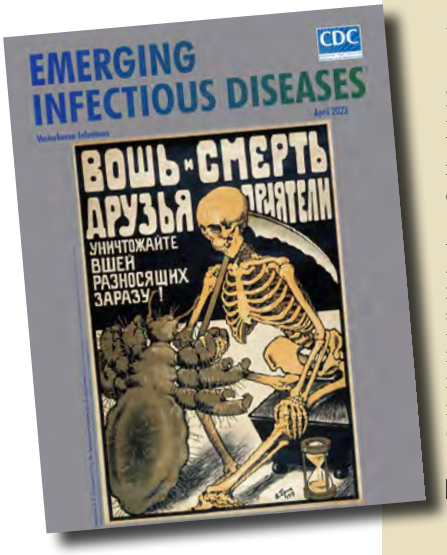

Originally published in April 2023

References

1. Hovan G, Hollinger A. Clinical isolation and identification of *Haematospirillum jordaniae*. Emerg Infect Dis. 2018;24:1955–6.
2. Humrighouse BW, Emery BD, Kelly AJ, Metcalfe MG, Mbizo J, McQuiston JR. *Haematospirillum jordaniae* gen. nov., sp. no v., isolated from human blood samples. Antonie van Leeuwenhoek. 2016;109:493–500.
3. LPSN List of prokaryotic names with standing in nomenclature. Species *Haematospirillum jordaniae* [cited 2022 May 21]. https://lpsn.dsmz.de/species/haematospirillum-jordaniae
4. Jean Jordan obituary. Published by the Atlanta Journal-Constitution on May 28, 2014. [cited 2022 Oct 17]. https://www.legacy.com/us/obituaries/atlanta/name/jean-jordan94
5. Pal E, Štrumbelj I, Kišek TC, Kolenc M, Pirš M, Rus KR, et al. *Haematospirillum jordaniae* cellulitis and bacteremia. Emerg Infect Dis. 2022;28:2116–9.
6. Persiana (1875) (Latin Edition): Heckmanns, Alexius. *Spirillum* (n.) [cited 2022 May 21]. https://www.etymoline.com/word/spirillum
7. Weyant RS, Moss CW, Weaver RE, Hollis, Jordan JG, Cook E, et al.; Centers for Disease Control and Prevention. Identification of unusual pathogenic gram-negative aerobic and facultatively anaerobic bacteria. The Orange Book, 2nd ed. Philadelphia: Lippincott Williams and Wilkins; 1996

https://wwwnc.cdc.gov/eid/article/29/4/22-0831_article

Long-Term Clinical Outcomes of Adults Hospitalized for COVID-19 Pneumonia

Ivan O. Rosas, Alejandra Benitez, James A. McKinnell, Reena Shah, Michael Waters, Bradley D. Hunter, Robert Jeanfreau, Larry Tsai, Margaret Neighbors, Ben Trzaskoma, Rita de Cassia Castro, Fang Cai

We conducted a multicenter, observational, 12-month follow-up study to identify the extended health burden of severe COVID-19 pneumonia by characterizing long-term sequelae of acute infection in participants previously enrolled in clinical trials for severe COVID-19 pneumonia requiring hospitalization. Overall, 134 (77.5%) of 173 participants completed the study. At 12 months, 51 (29.5%) participants reported cough, 60 (34.7%) reported dyspnea, 56 (32.4%) had residual lung texture abnormalities on high-resolution computed tomography scans, 26 (15.0%) had impaired forced vital capacity, 52 (30.1%) had cognitive impairment, and 77 (44.5%) reported fatigue. Disease severity during acute infection and age were associated with persistent lung texture abnormalities; history of hypertension was associated with higher prevalence of fatigue and more frequent dyspnea and cough; and age and obesity were associated with long-term cognitive impairment. Our findings underscore the long-term health burden of severe COVID-19 pneumonia, reinforcing the importance of regular monitoring in older persons and those with underlying illnesses.

COVID-19, attributable to SARS-CoV-2, has been a considerable cause of acute lung injury, multiorgan failure, and death (*1*,*2*). With advances in vaccines and treatments, the incidence of severe outcomes has decreased; however, COVID-19 remains a public health concern (*3*). Some patients have reported prolonged symptoms after recovering from acute COVID-19, including fatigue, respiratory symptoms, cardiovascular symptoms, and abnormalities in cognitive function (*4*–*6*). Early clinical trials during the COVID-19 pandemic provided valuable data on novel therapeutic strategies aimed at reducing the illness and death associated with acute severe COVID-19 pneumonia; however, long-term outcomes are underreported (*7*–*11*).

Long-term respiratory, cardiovascular, and neurologic sequelae develop in some patients who have had severe COVID-19 pneumonia requiring invasive mechanical ventilation or intensive care unit admission (*4*–*6*). Pulmonary complications, such as a reduction in the diffusing capacity of the lungs for carbon monoxide (DLCO) and radiologic abnormalities, might persist for months (*12*). Mechanical ventilation for the treatment of severe COVID-19 pneumonia has been linked to the development of pulmonary fibrosis and worsening of underlying interstitial lung disease (ILD) (*13*). Cardiovascular complications, such as myocarditis, heart failure, and arrhythmias, have also been observed after COVID-19, possibly resulting from viral invasion of myocardial tissue, systemic inflammation, and microvascular damage (*14*). Patients with underlying cardiovascular disease are particularly at risk for severe outcomes and have prolonged recovery periods (*15*). Neurologic sequelae, including cognitive impairment, headaches, and peripheral neuropathy, have been reported in patients recovering from severe COVID-19 (*5*,*16*). Neurotropic properties of the virus and effects of systemic inflammation and hypoxia are thought to contribute to long-term neurologic issues (*17*). To identify the extended health burden of patients hospitalized with severe COVID-19 pneumonia, we conducted the Long-Term Outcomes Post-Acute COVID-19 (LOPAC) study, a multicenter, observational, 12-month follow-up

Author affiliations: Baylor College of Medicine, Houston, Texas, USA (I.O. Rosas); Genentech, South San Francisco, California, USA (A. Benitez, L. Tsai, M. Neighbors, B. Trzaskoma, R. de Cassia Castro, F. Cai); Torrance Memorial Medical Center, Torrance, California, USA (J.A. McKinnell); Aga Khan University Hospital, Nairobi, Kenya (R. Shah); Velocity Clinical Research, Chula Vista, California, USA (M. Waters); Intermountain Healthcare, Salt Lake City, Utah, USA (B.D. Hunter); Velocity Clinical Research, New Orleans, Louisiana, USA (R. Jeanfreau)

DOI: https://doi.org/10.3201/eid3106.241097

study that explored long-term respiratory, cardiac, and neurocognitive sequelae occurring after acute COVID-19 pneumonia.

Methods

Participants and Assessments

Persons ≥18 years of age were eligible for enrollment in the LOPAC study if they had participated in a Genentech/Roche-sponsored parent study while hospitalized for COVID-19 pneumonia. The parent studies were clinical trials (registered with https://www.clinicaltrials.gov) as follows: EMPACTA (study no. NCT04372186), COVACTA (no. NCT04320615), MARIPOSA (no. NCT04363736), COVASTIL (no. NCT04386616), and REMDACTA (no. NCT04409262) (*7*–*11*). The parent studies recruited patients from a total of 15 countries. The LOPAC study was a follow-up to the parent studies that participants could opt into; no investigational drugs were evaluated in the LOPAC study. Participants provided written informed consent, and the study was conducted in accordance with the Declaration of Helsinki and Good Clinical Practice. The protocol was approved by institutional review boards or independent ethics committees at each study site.

We defined baseline as the time of enrollment in the LOPAC study and conducted the baseline study visit after participants completed or discontinued their participation in the parent study; longitudinal study visits occurred every 3 months for 12 months (Figure 1). Key clinical measures were high-resolution computed tomography (HRCT), echocardiogram, and Montreal Cognitive Assessment (MoCA) performed at baseline and month 12; pulmonary function tests performed in a clinic every 3 months; and patient-reported outcomes recorded every 6 months. We assessed patient-reported outcomes by using the Short-Form 36 Question Health Survey version 2 (SF-36v2; Quality Metric, https://www.qualitymetric.com) and the Modified Living with Idiopathic Pulmonary Fibrosis (L-IPF-M) (*18*) symptoms questionnaires. We assessed healthcare resource utilization at each visit. We analyzed blood samples for SARS-CoV-2 antibodies every 6 months and for the *MUC5B* promoter variant rs35705950 (an allele associated with risk for idiopathic pulmonary fibrosis) at 1 visit. WorldCare Clinical, LLC (https://www.voiantclinical.com), conducted and managed independent centralized reads for HRCT scans and echocardiograms, which were also assessed by independent thoracic and cardiology readers. Participants had the option to consent to additional study assessments, including 6-minute walk tests (6MWTs), Borg dyspnea and fatigue scales, home spirometry, and daily monitoring of activity, heart rate, and sleep patterns through a wearable device (Appendix, https://wwwnc.cdc.gov/EID/article/31/6/24-1097-App1.pdf).

Statistical Analyses

We reported categorical variables as counts and percentages. We reported percentages by using the total analysis population (to account for missing data at later visits) and continuous variables by using mean (SD) or median with range (minimum–maximum) or interquartile range. We considered data to be missing if obtained outside the assessment window, the assessment was performed but results were not evaluable, or the assessment was not performed at a study visit. Longitudinal analyses were descriptive and prespecified. We did not apply imputation methods.

To assess associations between lung texture abnormalities and selected pulmonary function tests (forced vital capacity [FVC], forced expiratory volume in 1 second [FEV_1], and DLCO corrected for hemoglobin), we stratified summary statistics (mean [SD] of percent-predicted values) according to HRCT lung texture abnormality status at concurrent visits. We also stratified longitudinal FVC according to baseline FVC status; we defined abnormal FVC at baseline as <80% of the predicted value and normal as ≥80% of predicted value. We performed this analysis in the overall study population and in the subgroup of participants who attended all visits during baseline to month 12. We reported mean FVCs and 95% CIs.

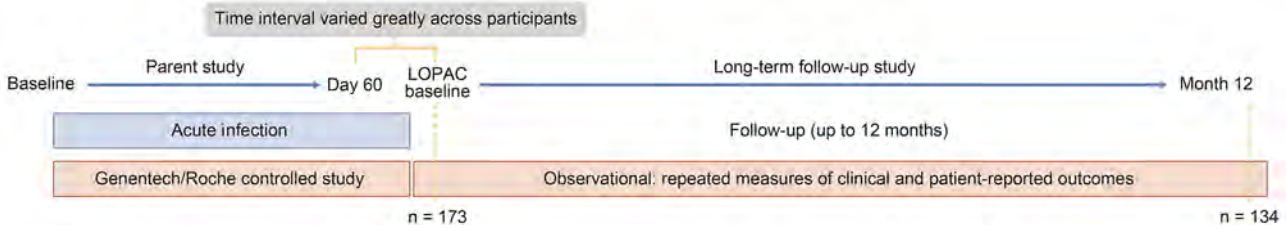

Figure 1. LOPAC study design to determine long-term clinical outcomes of adults hospitalized for COVID-19 pneumonia. Parent studies were sponsored by Genentech (https://www.gene.com) and Roche (https://www.roche.com). LOPAC, Long-Term Outcomes Post Acute COVID-19.

We summarized L-IPF-M questionnaire responses by using mean patient-reported scores for each symptom domain: dyspnea (7 questions), coughing (5 questions), and fatigue (3 questions). Scores ranged from 0 to 3; the lowest score corresponded to no symptoms, and a higher score corresponded to greater symptom severity (*18*). We analyzed the proportion of participants with no symptoms (mean score 0) versus any symptom level (mean score 1–3). We summarized SF-36v2 scores by using the median for each of 8 domains: general health, mental health, physical functioning, bodily pain, role-emotional, role-physical, social functioning, and vitality; we defined normal as a score ≥50 points (range 0–100 points) for each domain (*19*).

We assessed associations between selected endpoints (lung outcomes, cognition, patient-reported outcomes) and selected medical history at LOPAC baseline to supplement the prespecified analyses. We stratified summary statistics according to the presence or absence of each selected medical condition and tested for significance by using a χ^2 test, Student *t*-test, or Welch *t*-test. We also tested those endpoints for associations with age (≥65 years) and disease severity during the COVID-19 acute phase (≥4 on the ordinal scale at baseline of the parent study, requiring high-flow oxygen, invasive ventilation, or additional life support). Those analyses did not adjust for measured confounders, and we did not apply multiple testing adjustment. We used SAS version 9.4 (SAS Institute, Inc., https://www.sas.com) and R version 4.1.0 (The R Project for Statistical Computing, https://www.r-project.org) for analyses.

For descriptive purposes, we further summarized baseline characteristics and a subset of key study endpoints according to the treatment arm that participants were randomly assigned to in the parent studies. That summary resulted in 3 cohorts of LOPAC study participants: those who received tocilizumab as a study drug (including participants randomly assigned to receive tocilizumab and remdesivir), those who received a study drug other than tocilizumab (i.e., remdesivir, astegolimab, or efmarodocokin alfa), and those who received placebo. However, the LOPAC study was not designed to compare the long-term efficacy of tocilizumab versus other study drugs or placebo; therefore, we made no formal comparisons.

Results

We enrolled 173 participants from 29 centers in the United States, Kenya, and Peru who had been previously hospitalized for COVID-19 pneumonia and had participated in 1 of the 5 parent studies. Of the 173 participants, 134 (77.5%) completed and 39 (22.5%) did not complete the LOPAC study (Figure 2). Of the 173 enrolled participants, 94 had been randomly assigned to receive tocilizumab, 41 had been assigned to receive another study drug, and 38 had been assigned to receive placebo in the parent study. Of the 94 participants who had been randomly assigned to receive tocilizumab in the parent study, 58 had been assigned to receive tocilizumab only, and 36 had been assigned to receive tocilizumab plus remdesivir. Overall, the reasons for early discontinuation from the LOPAC study were participant withdrawal (n = 18), loss to follow-up (n = 17), physician decision (n = 2), death (n = 1), and other (n = 1). Early discontinuation occurred in 28.7% (27/94) of participants randomly assigned to receive tocilizumab, 12.2% (5/41) of participants randomly assigned to receive another study drug, and 18.4% (7/38) randomly assigned to receive placebo (Figure 2).

We recorded demographics and clinical characteristics of the study participants (Appendix Table 1). The mean age of participants was 56.3 ± 11.9 years. The most common underlying illnesses were hypertension (63.0%), obesity (46.8%), hyperlipidemia (43.9%), diabetes (35.3%), and asthma (11.0%). At the time of enrollment in the parent studies, 158 (91.3%) participants were not on mechanical ventilation, whereas 15 (8.7%) required mechanical ventilation or extracorporeal membrane oxygenation. At the completion of the parent study, almost all (97.4%) participants were discharged or ready for discharge from the hospital. The median duration of hospital stay during the parent study was 11 (range 3–74) days, and the median time from finishing the parent study to enrolling in LOPAC was 155 (range −1 to 338) days. At the time of enrollment in the LOPAC study, 2 (1.2%) participants required supplemental oxygen.

HRCT Lung Texture Abnormalities and Impaired Pulmonary Function

At least 1 lung texture abnormality on HRCT scan was evident in 91 (52.6%) participants at baseline (i.e., at enrollment into the LOPAC study) and 56 (32.4%) participants at month 12 (Table 1). Groundglass opacification was the most frequently observed abnormality, found in 86 (49.7%) participants at baseline and 51 (29.5%) participants at month 12. Other lung texture abnormalities were reticular pattern in 15 (8.7%) participants at baseline and 10 (5.8%) at month 12, bronchiectasis in 12 (6.9%) participants at baseline and 7 (4.0%) at month 12, and hyperlucency in 2 (1.2%) participants at both time points. No participants had honeycombing at baseline or month 12.

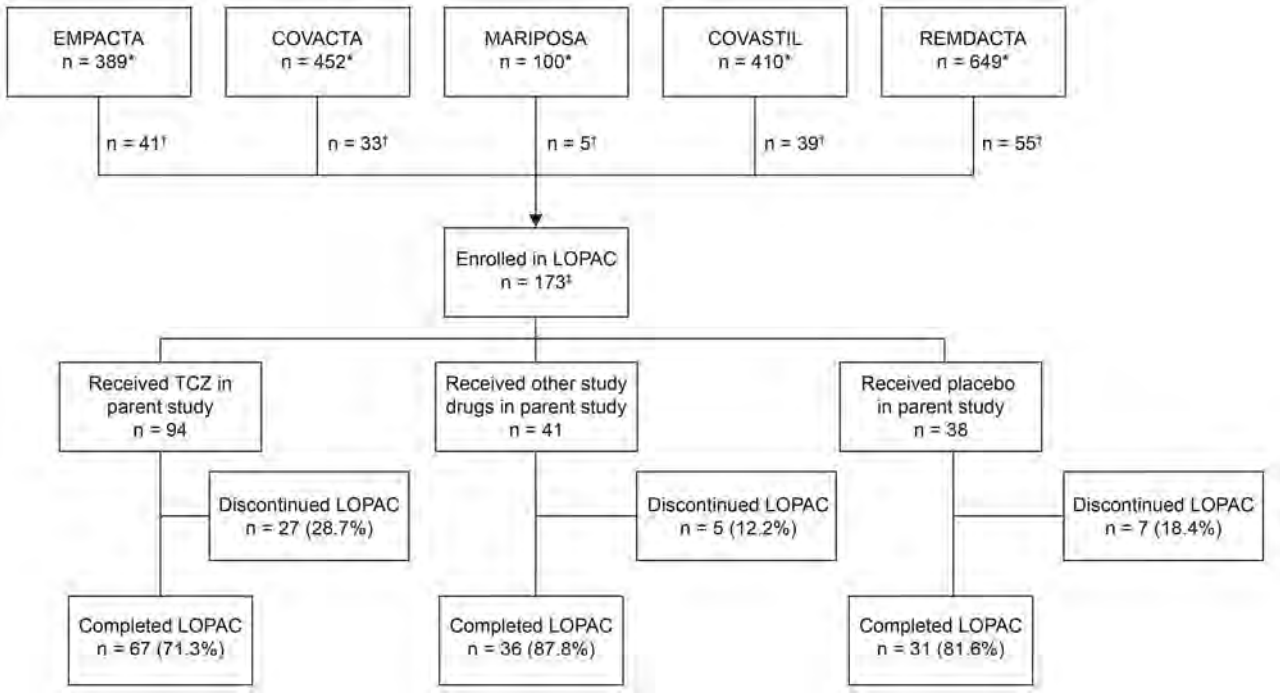

Figure 2. Disposition of LOPAC study participants in study of long-term clinical outcomes of adults hospitalized for COVID-19 pneumonia. The parent studies were clinical trials (registered with https://www.clinicaltrials.gov) as follows: EMPACTA (study no. NCT04372186), COVACTA (no. NCT04320615), MARIPOSA (no. NCT04363736), COVASTIL (no. NCT04386616), and REMDACTA (no. NCT04409262). Participants might have received remdesivir or another antiviral drug as part of the standard of care in the EMPACTA, COVACTA, and MARIPOSA studies. Participants who were randomly assigned to receive placebo, astegolimab, or efmarodocokin alfa might have also received TCZ or remdesivir or both as part of the standard of care in the COVASTIL study. Participants randomly assigned to receive TCZ or placebo in the REMDACTA study also received remdesivir. *Number of participants in each parent study; †number of participants from each parent study who participated in the LOPAC study; ‡1 participant initially enrolled in the LOPAC study did not receive treatment in the parent study and was not included in any analyses for the parent or LOPAC study. LOPAC, Long-Term Outcomes Post Acute COVID-19 study; TCZ, tocilizumab.

Of the 173 participants, 54 (31.2%) had ≥1 lung abnormality at baseline that was still present at month 12, and 55 (31.8%) had no abnormality at either time point (Figure 3). Six (3.5%) participants who had ≥1 lung texture abnormality at baseline showed resolution at month 12, whereas ≥1 lung abnormality had developed at the 12-month follow-up in 2 (1.2%) participants who had no abnormalities at baseline.

At baseline, the mean FVC was 84.5% ± 16.6%, and the mean FEV_1 was 87.8% ± 19.9%. FVC and FEV_1 remained stable across the 12-month follow-up period; the mean change from baseline to month 12 was 2.8% ± 9.1% for FVC and 1.7% ± 10.3% for FEV_1.

Table 1. Proportion of participants with lung texture abnormalities on HRCT scan in LOPAC study of long-term clinical outcomes of adults hospitalized for COVID-19 pneumonia*

HRCT characteristics	No. (%) participants	
	LOPAC study, baseline	LOPAC study, month 12
Participants with ≥1 lung texture abnormality	91 (52.6)	56 (32.4)
Ground-glass opacification	86 (49.7)	51 (29.5)
Reticular pattern	15 (8.7)	10 (5.8)
Bronchiectasis	12 (6.9)	7 (4.0)
Hyperlucency†	2 (1.2)	2 (1.2)
Honeycombing	0	0
Participants with no lung texture abnormality‡	71 (41.0)	62 (35.8)
Participants with missing data	11 (6.4)	55 (31.8)

*Total number of participants enrolled in the LOPAC study was 173. HRCT, high-resolution computed tomography; LOPAC, Long-Term Outcomes Post Acute COVID-19.
†Radiographic evidence of hyperlucency was assessed as unknown in 1 participant's baseline and month 12 HRCT images. This participant was considered to have radiographic evidence of hyperlucency at baseline and month 12.
‡Participants were considered to have no lung texture abnormality if there was no radiologic evidence of ground-glass opacification, reticular pattern, bronchiectasis, hyperlucency, or honeycombing on HRCT scan.

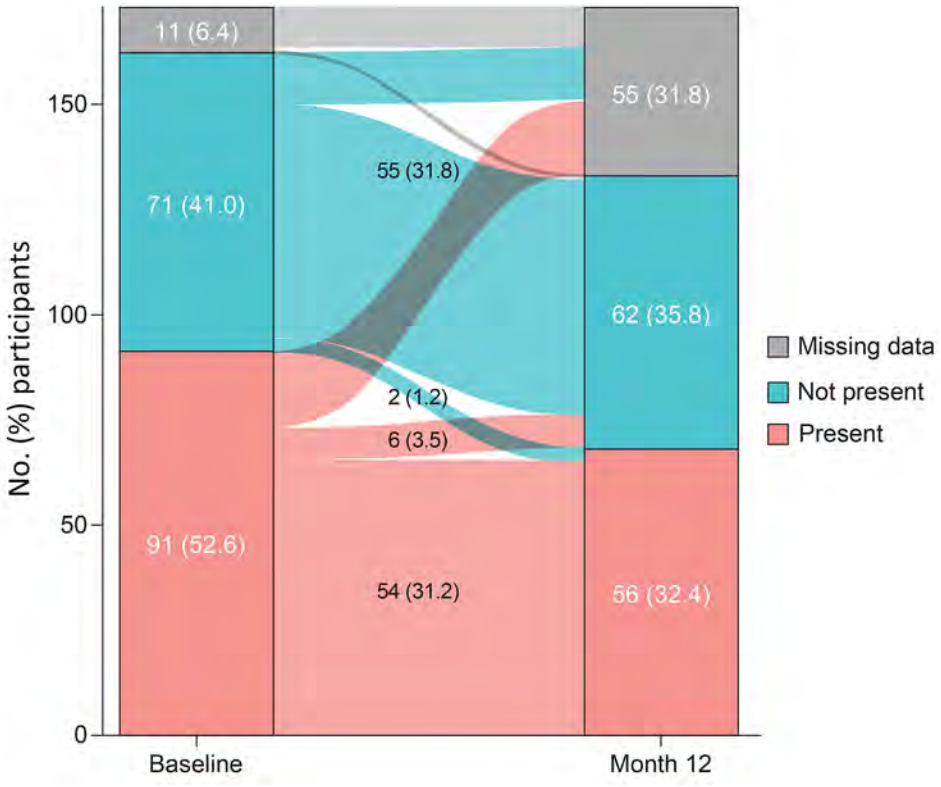

Figure 3. Numbers of participants with ≥1 lung texture abnormality at baseline and at month 12 in study of long-term clinical outcomes of adults hospitalized for COVID-19 pneumonia. Data are shown for a total of 173 participants enrolled in the Long-Term Outcomes Post Acute COVID-19 study. Colors indicate whether the lung texture abnormality was present or absent. Baseline and month 12 columns indicate the no. (%) participants who had ≥1 lung texture abnormality at that time point. Numbers between those columns indicate lung abnormalities that persisted, developed, or resolved by month 12.

Among 90 participants with DLCO measurements available at baseline, the mean was 83.3% ± 21.1%; DLCO remained stable with a mean change from baseline of 1.8% ± 13.8% at month 12.

For most participants who had normal FVC at baseline, FVC appeared to remain stable, and the mean change from baseline appeared to be minimal during the 12-month follow-up (Figure 4, panels A, B). Many participants with abnormal FVC at baseline had an abnormal FVC at the 12-month visit; however, the mean change from baseline to 12 months improved overall. In participants with abnormal baseline FVC who completed the month 12 visit, the mean change from baseline in FVC was 7.3% (Figure 4, panel B). Longitudinal 95% CI of the mean FVC and FVC change from baseline (stratified by baseline FVC) showed consistent results (Appendix, Appendix Figures 1, 2). We observed an inverse association between DLCO and lung texture abnormalities; we did not observe associations between lung texture abnormalities and FVC or FEV_1 (Appendix Table 2).

Participants who had more severe acute infection (ordinal scale score ≥4) at enrollment in the parent study were more likely to have ≥1 lung texture abnormality on HRCT scan (62/101 [61.4%]) than those who had an ordinal scale score of <4 (29/72 [40.3%]); that finding was still apparent at month 12 for participants with scores ≥4 (41/101 [40.6%]) versus those with scores <4 (15/72 [20.8%]) (Appendix Figure 3, panel A). Participants ≥65 years of age were more likely to have lung texture abnormalities through month 12 (Appendix Figure 3, panel B). Participants with a history of hypertension tended to have lower median FVC at LOPAC baseline; however, by month 12, no apparent difference in median FVC between participants with or without a history of hypertension was observed (Appendix Figure 4). No association was detected between *MUC5B* promoter allele status and the presence of ≥1 lung texture abnormality or FVC abnormality at baseline or month 12 (Appendix, Appendix Table 3). Some numeric differences were observed in pulmonary function and lung texture abnormalities between the 3 treatment cohorts (participants who received tocilizumab as a study drug, those who received a study drug other than tocilizumab, and those who received placebo in the parent studies) (Appendix Tables 4, 5).

Cardiac Function

Overall, cardiac function was unremarkable at baseline and did not deteriorate by month 12. Mean left ventricular ejection fraction was 61.8% ± 8.0% at baseline for 156 participants and 63.1% ± 8.6% at month 12 for 115 participants with evaluable results (reference range 52%–72% for male patients, 54%–74% for

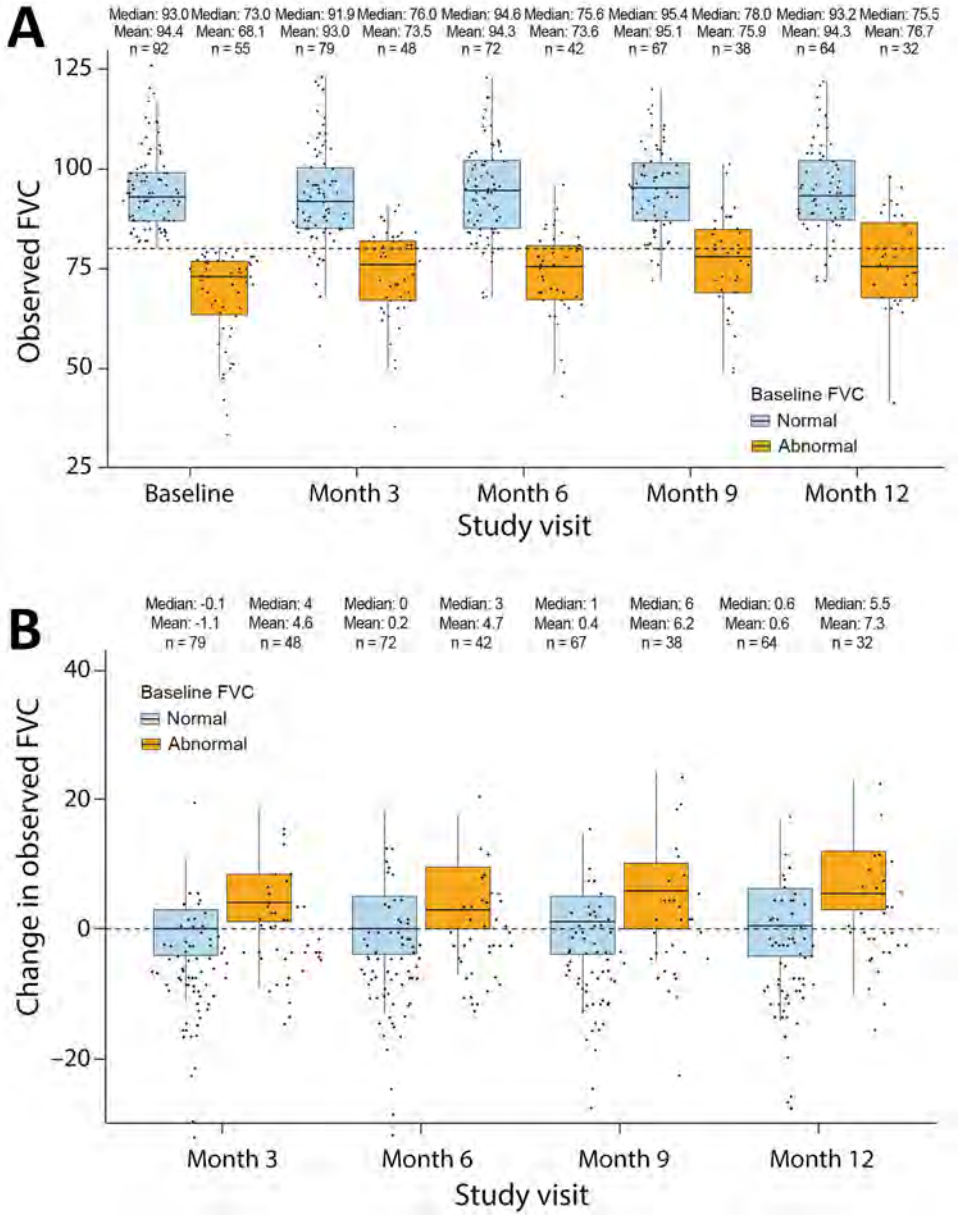

Figure 4. Box plots of longitudinal FVC profiles from the Long-Term Outcomes Post Acute COVID-19 study of adults previously hospitalized for COVID-19 pneumonia. A) Observed percent-predicted FVC at indicated study visits. B) Change in percent-predicted FVC at different study visits according to the baseline FVC. Dashed horizonal lines indicate 80% predicted FVC (A) and no change in percent-predicted FVC (B). Horizontal lines within boxes indicate medians; box tops and bottoms indicate upper (third) and lower (first) quartiles; error bars (whiskers) indicate minimum and maximum values. Dots indicate data points; data points beyond the end of the whiskers are considered outliers. Numbers above the bars indicate mean and median percent-predicted FVC and total number of participants in category. Abnormal is defined as <80% and normal ≥80% predicted FVC. FVC, forced vital capacity.

female patients). Mean pulmonary artery pressure was 13.7 ± 4.5 mm Hg at baseline for 43 participants and 12.5 ± 2.9 mm Hg at month 12 for 36 participants with evaluable results (reference range ≤25 mm Hg). At baseline, 142 (82.0%) participants had unimpaired right ventricular systolic function (RVSF) (evaluated either by endocardial tracing or by medical assessment), 10 (5.8%) had mild impairment, 1 (0.6%) had severe impairment, and 20 (11.6%) had missing results (Table 2). At month 12, a total of 98 (56.6%) participants had unimpaired RVSF, 13 (7.5%) had mild impairment, and 62 (35.8%) had missing results. The participant with severe RVSF impairment at baseline was lost to follow-up at month 12.

Cognitive Impairment

At baseline, the median MoCA score was 25 (range 9–30), and 87 (50.3%) of 173 participants exhibited cognitive impairment, indicated by MoCA scores below the threshold of 26. At month 12, a total of 52 (30.1%) participants had a MoCA score of <26, and 60 (34.7%) participants were missing from the assessment. For 113 participants who had MoCA scores assessed at both baseline and month 12, the median score increased by 1 point (range −9 to 10) by month 12.

Overall, 49 (28.3%) of 173 participants were ≥65 years of age. That age group had a lower mean change (−0.3) in MoCA scores from baseline to month

12 than participants who were <65 years of age (1.1) (p = 0.043). An association was observed between a change in MoCA score and obesity (p = 0.007) (Appendix Figure 5). Mean and median ages were similar between obese and nonobese participants. We also calculated median MoCA scores for the 3 treatment cohorts from the parent studies (Appendix Table 6).

Patient-Reported Outcomes and Respiratory Symptoms

At baseline, the median SF-36v2 questionnaire scores for all 8 domains (general health, mental health, physical functioning, bodily pain, role-emotional, role-physical, social functioning, and vitality) were >50 points (score range 0–100 points) for each domain; a score of 50 is the considered the threshold for a normal SF-36v2 score (*19*) (Figure 5, panel A). Lower median scores were reported for the general health (62.0), role-physical (62.5), vitality (62.5), bodily pain (64.0), and physical functioning (68.3) relative to social functioning (75.0), mental health (80.0), and role-emotional (83.3) domains. For 117 participants who completed the SF-36v2 questionnaire at month 12, median scores consistently increased from baseline to month 12 across all 8 domains. We also calculated mean and median scores for vitality, which denotes the absence of fatigue, for the 3 treatment cohorts from the parent studies (Appendix Table 7).

At baseline, 119 (68.8%) of 173 participants reported fatigue (lack of energy), 87 (50.3%) reported coughing, and 94 (54.3%) reported shortness of breath (dyspnea) on the L-IPF-M questionnaire (Figure 5, panel B). At month 12, a subgroup of participants still reported fatigue (44.5%), coughing (29.5%), or dyspnea (34.7%). Dyspnea, cough, and fatigue symptoms were more likely to be reported for participants who had hypertension at LOPAC baseline than for those who did not (Appendix Figure 6). Among participants who remained in the study at month 12, cough and fatigue were still frequently reported in those with hypertension compared with those without hypertension. We prepared descriptive summaries of healthcare resource utilization, weekly average walking duration, heart rate, and sleep duration (Appendix Table 8; Appendix Figure 7); further analysis is warranted to identify potential trends in those data.

Discussion

We investigated long-term outcomes in the 12-month LOPAC follow-up study conducted with 173 participants who had been hospitalized for COVID-19 pneumonia and had participated in a Genentech/Roche-sponsored intervention parent trial. At baseline in the LOPAC study, >50% of participants had abnormalities on HRCT scans and ≈33% had lung function impairment. The high prevalence of lung abnormalities at baseline, measured at a median of 155 days after participants completed the parent study, aligns with postacute COVID-19 syndrome and meets the definition for long COVID (*20*–*22*).

During the 12-month follow-up, a subgroup of participants continued to exhibit clinical and radiologic abnormalities indicative of long-term COVID-19

Table 2. RVSF at baseline and month 12 of LOPAC study of long-term clinical outcomes of adults hospitalized for COVID-19 pneumonia*

RVSF characteristics	No. participants (%)	
	LOPAC study, baseline	LOPAC study, month 12
Evaluable by endocardial tracing†	74 (42.8)	58 (33.5)
Normal‡	71 (41.0)	56 (32.4)
Mildly impaired	2 (1.2)	2 (1.2)
Severely impaired	1 (0.6)	0§
Not evaluable by endocardial tracing (medical assessment only)¶	84 (48.6)	59 (34.1)
Normal‡	71 (41.0)	42 (24.3)
Mildly impaired	8 (4.6)	11 (6.4)
Severely impaired	0	0
Total evaluable	158 (91.3)	117 (67.6)
Normal‡	142 (82.0)	98 (56.6)
Mildly impaired	10 (5.8)	13 (7.5)
Severely impaired	1 (0.6)	0§
Participants with missing data	20 (11.6)	62 (35.8)
Assessment done, not evaluable by endocardial tracing or medical assessment	5 (2.9)	6 (3.5)
Assessment done, not in window	2 (1.2)	15 (8.7)
Assessment not done	13 (7.5)	41 (23.7)

*Total number of participants enrolled in the LOPAC study was 173. LOPAC, Long-Term Outcomes Post Acute COVID-19; RVSF, right ventricular systolic function.
†RVSF was measured by echocardiogram endocardial tracing, and the impairment level was assessed qualitatively by medical personnel.
‡Right ventricular fractional area change of ≥35% was classified as normal RVSF. Assessment of RVSF for 8 observations with right ventricular fractional area of <35% was obtained by medical personnel in a post hoc assessment.
§Participant who had severely impaired RVSF at baseline was lost to follow-up at month 12.
¶RVSF could not be measured by endocardial tracing and was assessed only qualitatively by medical personnel.

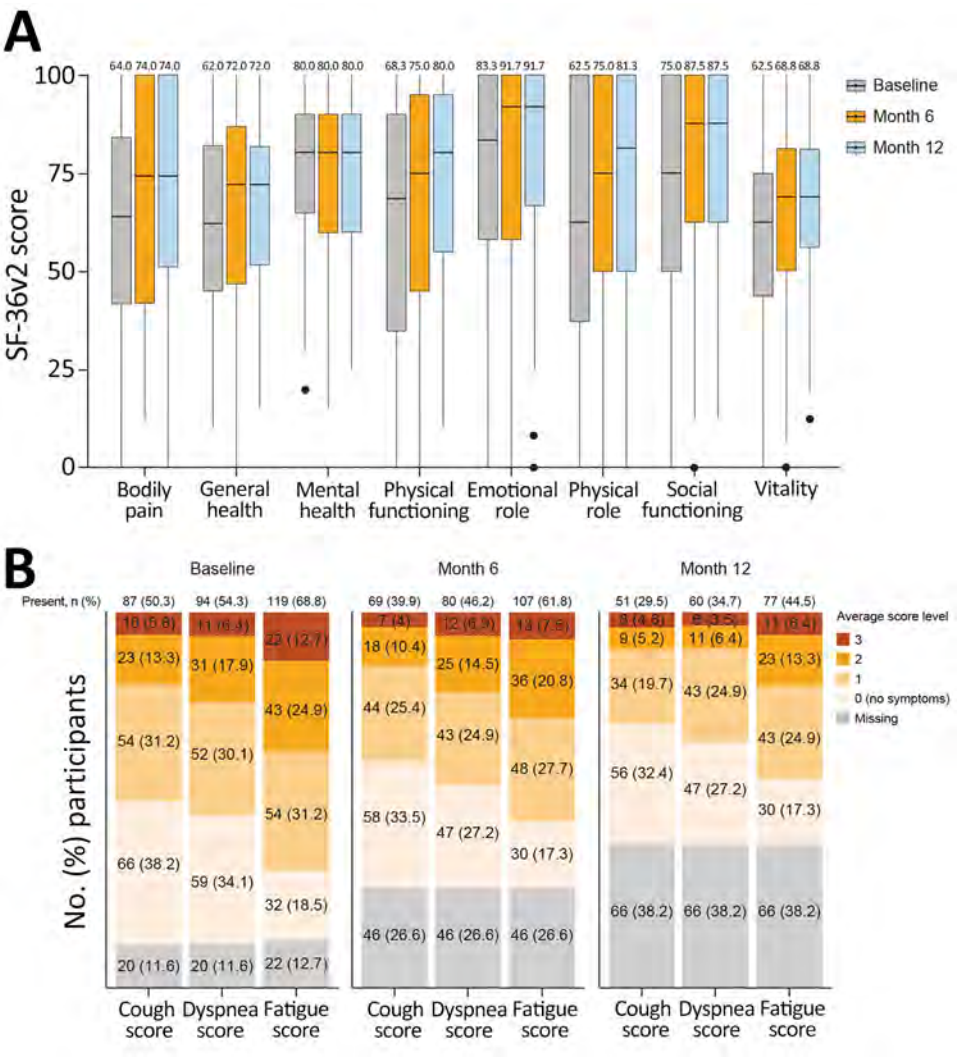

Figure 5. Longitudinal profiles of patient-reported outcomes from the Long-Term Outcomes Post Acute COVID-19 study of adults previously hospitalized for COVID-19 pneumonia. A) Box plots indicate quality of life assessed by SF-36v2 (Quality Metric, https://www.qualitymetric.com). SF-36v2 scores (range 0–100 points) were summarized by using the median for each of the 8 indicated domains. Normal was defined as a score of ≥50 points for each domain. Median percentages of participants within each domain are indicated at the top. Horizontal lines within boxes indicate medians; box tops and bottoms indicate upper (third) and lower (first) quartiles; error bars (whiskers) indicate minimum and maximum values. Closed circles indicate outliers. B) Symptoms of study participants assessed by the Modified Living With Pulmonary Fibrosis Assessment Tool. Data are shown as no. (%) participants experiencing each category of symptoms according to 173 enrolled participants. Baseline refers to study baseline (time of enrollment). Questionnaire responses were summarized by using mean patient-reported scores for each symptom domain: dyspnea (7 questions), coughing (5 questions), and fatigue (3 questions). Scores ranged from 0 to 3; the lowest score corresponds to no symptoms and the higher score corresponds to greater symptom severity. SF-36v2, Short Form 36 Question Health Survey version 2.

sequelae, including abnormal lung texture, impaired pulmonary function, and symptoms of fatigue, coughing, or shortness of breath. The primary lung texture abnormality reported in participants in this study was ground-glass opacification, a nonspecific finding associated with increased lung density and preservation of the bronchopulmonary vasculature (*23*,*24*). Ground-glass opacities might be observed in acute and chronic pulmonary disease and might represent interstitial or alveolar involvement (or both) (*23*,*25*). Ground-glass opacification in COVID-19 characteristically has a bilateral, peripheral distribution, often in the posterior lung segments (*25*). The slow resolution of ground-glass opacities might suggest the development of parenchymal lung disease with ILD features, triggered or exacerbated by COVID-19 (*26*). Those findings contrast with previous reports that suggested ILD-like conditions resolve within a year after SARS-CoV-2 infection (*27*) and necessitate further investigation to prevent parenchymal disease progression and chronicity.

During the acute phase of COVID-19 pneumonia, an ordinal scale score ≥4 was recorded for 101 (58.4%) of 173 LOPAC study participants. That subgroup was at higher risk for prolonged lung texture abnormalities, consistent with previous reports of increased risk for parenchymal lung changes and fibrosis in patients with severe acute COVID-19 pneumonia (*28*) who required mechanical ventilation (*29*–*32*). Fibrotic changes after infection with severe acute respiratory syndrome (*33*) and Middle East respiratory syndrome (*34*) coronaviruses have also been reported.

In this study, participants who had not required mechanical ventilation or extracorporeal membrane oxygenation during acute infection experienced prolonged abnormalities in lung function and texture during follow-up. Older age, a known risk factor for SARS-CoV-2 susceptibility (*35*) and poor COVID-19 clinical outcomes (*36*), was associated with persistent lung abnormalities and cognitive impairment. Older age might compromise the immune system and hinder recovery from COVID-19. Our findings support the hypothesis that age-related factors, such as immune response changes and reduced regenerative capacity, might affect acute and long-term clinical outcomes (*37*).

The prevalence of respiratory and fatigue symptoms was higher in participants with hypertension than in those without hypertension. Hypertension, a key component of metabolic syndrome, is a well-recognized risk factor for severe COVID-19, likely through dysregulation of the renin-angiotensin-aldosterone system, altered immune responses, gastrointestinal disturbances, and increased inflammation; all of which might have prolonged effects on organs, including lungs, heart, and brain, and contribute to persistent symptoms (*38*). Obese participants exhibited persistent cognitive impairment compared with nonobese participants. The association between obesity and cognitive issues suggests potential links between metabolic factors, chronic inflammation, and neurologic consequences of COVID-19 (*17*). Although underlying conditions might influence some aspects of postacute COVID-19 syndrome, their effects vary depending on the specific examined symptom or health aspect. Further research will be required to clarify those associations.

The main contribution of this prospective study is the longitudinal assessment of lung texture; pulmonary, cardiac, and cognitive function; quality of life; and serology that captures detailed and standardized individual-level data. We also investigated baseline clinical characteristics and their associations with key clinical endpoints. However, the first limitation of our study is that we enrolled a small group of participants from each parent study to characterize long-term sequelae of severe COVID-19; we did not design the study to evaluate treatment effects during initial infection on long-term outcomes. In addition to the study drug received in the parent study, all participants received standard-of-care treatment during the acute phase of infection. As the standard-of-care treatments evolved during the COVID-19 pandemic, participants might have received tocilizumab, remdesivir, or both as part of standard care (*7*–*11*). Second, limited information was available on participants before hospitalization for acute COVID-19, and some participants might have been living with undetected underlying conditions. Third, evaluations were limited by baseline imbalances, the 22.5% discontinuation rate, and missing assessments, which are common in long-term follow-up studies. Although some potential confounding factors were identified, we did not adjust for them in this exploratory study. Further investigation adjusting for confounders will be necessary to confirm those findings and further delineate the long-term effects of COVID-19.

In conclusion, a subgroup of participants in this study exhibited persistent lung texture abnormalities, impaired pulmonary function, cognitive impairment, or reported fatigue or respiratory symptoms during the 12-month follow-up period, demonstrating a substantial long-term health burden for persons who have severe COVID-19 pneumonia. The severity of acute infection, age, and certain underlying conditions might influence the long-term sequelae of COVID-19. Our findings underscore the extended health effects of COVID-19 beyond its acute phase and reinforce the importance of regular monitoring of patients with severe COVID-19, particularly in older patients and those with underlying health conditions.

Acknowledgments

Medical writing assistance was provided by Bridget Healy and Sara Duggan (ApotheCom, funded by Hoffmann-La Roche Ltd.).

Qualified researchers can request access to individual participant-level data upon publication through the clinical study data request platform (https://vivli.org). Further details on Roche's criteria for eligible studies are available (https://vivli.org/members/ourmembers). Further details on Roche's Global Policy on the Sharing of Clinical Information and how to request access to related clinical study documents can be obtained at https://www.roche.com/innovation/process/clinical-trials/data-sharing.

This work was supported by F. Hoffmann-La Roche Ltd. (study sponsor). The sponsor was involved in the study design, analysis, and interpretation of data, writing the report, and decision to submit the manuscript for publication. This project was funded in whole or in part with funds from the US Department of Health and Human Services, Office of the Assistant Secretary for Administration for Strategic Preparedness and Response and Biomedical Advanced Research and Development Authority (other transaction agreement no. HHSO100201800036C). The findings and conclusions herein are those of the authors and do not necessarily represent the views of the Department of Health and Human Services or its components.

I.O.R. received funding to Baylor College of Medicine from Genentech/Roche for this work; receives grants from Boehringer Ingelheim, Genentech/Roche, and Tvardi Therapeutics; and participates on advisory boards for Boehringer Ingelheim, Avalyn Pharma, and Structure Therapeutics. A.B. is an employee of Genentech, Inc. J.A.M. receives consulting fees from Thermo Fisher Scientific and promotional speaker fees from AbbVie and Ferring Pharmaceuticals and is president of the Infectious Disease Association of California. B.D.H. receives consulting fees from Genentech, ADC Therapeutics, Kite Pharma, Novartis, Notable Labs, BMS, Janssen/Johnson & Johnson, Genmab, AbbVie, Astellas, Regeneron, and In8 Bio; speakers bureau honoraria from Kite Pharma, AbbVie, and Genmab; manuscript writing support from Novarti and Janssen/Johnson & Johnson; has a leadership or fiduciary role in the American Society of Clinical Oncology, American Society for Transplantation and Cellular Therapy, and other board, society, committee, or advocacy group, paid or unpaid. L.T. is an employee of Genentech, Inc., and stock owner with equity in Roche, and is an author of an unpublished pending patent, Method for Treating Pneumonia, Including COVID-19 Pneumonia, With an IL-6 Antagonist, owned by Genentech/Roche. M.N. is an employee of Genentech, Inc. and has stock options in Roche. B.T. is an employee of Genentech, Inc. with stock/stock options. R.dC.C. is and employee of and owns stock/stock options in Roche/Genentech. F.C. is and employee of Roche/Genentech, holds stock/stock options in Roche, and receives funding from the Biomedical Advanced Research and Development Authority related to this work.

Author contributions: I.O.R., B.T., J.A.M., L.T., and M.N. conceived and designed the study. I.O.R., A.B., J.A.M., R.S., M.W., R.J., L.T., M.N., B.T., R.dC.C., and F.C. acquired, analyzed, and interpreted the data. I.O.R., A.B., J.A.M., R.S., R.J., L.T., M.N., B.T., B.D.H., R.dC.C., and F.C. drafted the manuscript for important intellectual content. All authors critically revised the manuscript, approved the final version to be published, and agreed to be accountable for all aspects of the work.

About the Author

Dr. Rosas is a professor and section chief of the Department of Medicine for Pulmonary, Critical Care, and Sleep Medicine at Baylor College of Medicine. His research interests focus on prevention, diagnosis, and treatment of pulmonary fibrosis; defining populations at risk of developing pulmonary fibrosis; identifying disease biomarkers; and designing and executing clinical trials to test novel treatments for pulmonary fibrosis.

References

1. Synowiec A, Szczepański A, Barreto-Duran E, Lie LK, Pyrc K. Severe acute respiratory syndrome coronavirus 2 (SARS-CoV-2): a systemic infection. Clin Microbiol Rev. 2021;34:e00133-20. https://doi.org/10.1128/CMR.00133-20
2. Elezkurtaj S, Greuel S, Ihlow J, Michaelis EG, Bischoff P, Kunze CA, et al. Causes of death and comorbidities in hospitalized patients with COVID-19. Sci Rep. 2021;11:4263. https://doi.org/10.1038/s41598-021-82862-5
3. Regan JJ, Moulia DL, Link-Gelles R, Godfrey M, Mak J, Najdowski M, et al. Use of updated COVID-19 vaccines 2023–2024 formula for persons aged ≥6 months: recommendations of the Advisory Committee on Immunization Practices—United States, September 2023. MMWR Morb Mortal Wkly Rep. 2023;72:1140–6. https://doi.org/10.15585/mmwr.mm7242e1
4. Jovanoski N, Chen X, Becker U, Zalocusky K, Chawla D, Tsai L, et al. Severity of COVID-19 and adverse long-term outcomes: a retrospective cohort study based on a US electronic health record database. BMJ Open. 2021;11:e056284. https://doi.org/10.1136/bmjopen-2021-056284
5. Mehandru S, Merad M. Pathological sequelae of long-haul COVID. Nat Immunol. 2022;23:194–202. https://doi.org/10.1038/s41590-021-01104-y
6. Nalbandian A, Desai AD, Wan EY. Post-COVID-19 condition. Annu Rev Med. 2023;74:55–64. https://doi.org/10.1146/annurev-med-043021-030635
7. Waters M, McKinnell JA, Kalil AC, Martin GS, Buchman TG, Theess W, et al.; COVID-astegolimab-interleukin (IL) (COVASTIL) Study Group. Astegolimab or efmarodocokin alfa in patients with severe COVID-19 pneumonia: a randomized, phase 2 trial. Crit Care Med. 2023;51:103–16. https://doi.org/10.1097/CCM.0000000000005716
8. Rosas IO, Bräu N, Waters M, Go RC, Hunter BD, Bhagani S, et al. Tocilizumab in hospitalized patients with severe COVID-19 pneumonia. N Engl J Med. 2021;384:1503–16. https://doi.org/10.1056/NEJMoa2028700
9. Rosas IO, Diaz G, Gottlieb RL, Lobo SM, Robinson P, Hunter BD, et al. Tocilizumab and remdesivir in hospitalized patients with severe COVID-19 pneumonia: a randomized clinical trial. Intensive Care Med. 2021;47:1258–70. https://doi.org/10.1007/s00134-021-06507-x
10. Salama C, Han J, Yau L, Reiss WG, Kramer B, Neidhart JD, et al. Tocilizumab in patients hospitalized with COVID-19 pneumonia. N Engl J Med. 2021;384:20–30. https://doi.org/10.1056/NEJMoa2030340
11. Kumar PN, Hernández-Sánchez J, Nagel S, Feng Y, Cai F, Rabin J, et al. Safety and efficacy of tocilizumab 4 or 8 mg/kg in hospitalized patients with moderate to severe coronavirus disease 2019 pneumonia: a randomized clinical trial. Open Forum Infect Dis. 2021;9:ofab608. https://doi.org/10.1093/ofid/ofab608
12. González J, Benítez ID, Carmona P, Santisteve S, Monge A, Moncusí-Moix A, et al.; CIBERESUCICOVID Project (COV20/00110, ISCIII). Pulmonary function and radiologic features in survivors of critical COVID-19: a 3-month prospective cohort. Chest. 2021;160:187–98. https://doi.org/10.1016/j.chest.2021.02.062
13. Fukihara J, Kondoh Y. COVID-19 and interstitial lung diseases: a multifaceted look at the relationship between the two diseases. Respir Investig. 2023;61:601–17. https://doi.org/10.1016/j.resinv.2023.05.007
14. Xie Y, Xu E, Bowe B, Al-Aly Z. Long-term cardiovascular outcomes of COVID-19. Nat Med. 2022;28:583–90. https://doi.org/10.1038/s41591-022-01689-3

15. Ioannou GN, Baraff A, Fox A, Shahoumian T, Hickok A, O'Hare AM, et al. Rates and factors associated with documentation of diagnostic codes for long COVID in the National Veterans Affairs Health Care System. JAMA Netw Open. 2022;5:e2224359. https://doi.org/10.1001/jamanetworkopen.2022.24359
16. Leng A, Shah M, Ahmad SA, Premraj L, Wildi K, Li Bassi G, et al. Pathogenesis underlying neurological manifestations of long COVID syndrome and potential therapeutics. Cells. 2023;12:816. https://doi.org/10.3390/cells12050816
17. Quan M, Wang X, Gong M, Wang Q, Li Y, Jia J. Post-COVID cognitive dysfunction: current status and research recommendations for high risk population. Lancet Reg Health West Pac. 2023;38:100836. https://doi.org/10.1016/j.lanwpc.2023.100836
18. Swigris JJ, Andrae DA, Churney T, Johnson N, Scholand MB, White ES, et al. Development and initial validation analyses of the Living with Idiopathic Pulmonary Fibrosis questionnaire. Am J Respir Crit Care Med. 2020;202:1689–97. https://doi.org/10.1164/rccm.202002-0415OC
19. Maglinte GA, Hays RD, Kaplan RM. US general population norms for telephone administration of the SF-36v2. J Clin Epidemiol. 2012;65:497–502. https://doi.org/10.1016/j.jclinepi.2011.09.008
20. Chippa V, Aleem A, Anjum F. Post-acute coronavirus (COVID-19) syndrome. Treasure Island (FL): StatPearls Publishing; 2023.
21. National Academies of Sciences, Engineering, and Medicine. A long COVID definition: a chronic, systemic disease state with profound consequences. Washington: The National Academies Press; 2024.
22. Zadeh FH, Wilson DR, Agrawal DK. Long COVID: complications, underlying mechanisms, and treatment strategies. Arch Microbiol Immunol. 2023;7:36–61.
23. Lee GM, Carroll MB, Galvin JR, Walker CM. Mosaic attenuation pattern: a guide to analysis with HRCT. Radiol Clin North Am. 2022;60:963–78. https://doi.org/10.1016/j.rcl.2022.06.009
24. Matos MJR, Rosa MEE, Brito VM, Amaral LTW, Beraldo GL, Fonseca EKUN, et al. Differential diagnoses of acute ground-glass opacity in chest computed tomography: pictorial essay. Einstein (Sao Paulo). 2021;19:eRW5772. https://doi.org/10.31744/einstein_journal/2021RW5772
25. Nowers K, Rasband JD, Berges G, Gosselin M. Approach to ground-glass opacification of the lung. Semin Ultrasound CT MR. 2002;23:302–23. https://doi.org/10.1016/S0887-2171(02)90019-3
26. Johnston J, Dorrian D, Linden D, Stanel SC, Rivera-Ortega P, Chaudhuri N. Pulmonary sequelae of COVID-19: focus on interstitial lung disease. Cells. 2023;12:2238. https://doi.org/10.3390/cells12182238
27. Vasarmidi E, Ghanem M, Crestani B. Interstitial lung disease following coronavirus disease 2019. Curr Opin Pulm Med. 2022;28:399–406. https://doi.org/10.1097/MCP.0000000000000900
28. Hama Amin BJ, Kakamad FH, Ahmed GS, Ahmed SF, Abdulla BA, Mohammed SH, et al. Post COVID-19 pulmonary fibrosis; a meta-analysis study. Ann Med Surg (Lond). 2022;77:103590. https://doi.org/10.1016/j.amsu.2022.103590
29. Touman A, Kahyat M, Bulkhi A, Khairo M, Alyamani W, Aldobyany AM, et al. Post COVID-19 chronic parenchymal lung changes. Cureus. 2022;14:e25197. https://doi.org/10.7759/cureus.25197
30. Duong-Quy S, Vo-Pham-Minh T, Tran-Xuan Q, Huynh-Anh T, Vo-Van T, Vu-Tran-Thien Q, et al. Post-COVID-19 pulmonary fibrosis: facts-challenges and futures: a narrative review. Pulm Ther. 2023;9:295–307. https://doi.org/10.1007/s41030-023-00226-y
31. McAuley HJC, Evans RA, Bolton CE, Brightling CE, Chalmers JD, Docherty AB, et al.; PHOSP-COVID Study Collaborative Group. Prevalence of physical frailty, including risk factors, up to 1 year after hospitalisation for COVID-19 in the UK: a multicentre, longitudinal cohort study. EClinicalMedicine. 2023;57:101896. https://doi.org/10.1016/j.eclinm.2023.101896
32. Bamps L, Armenti JP, Bojan M, Grandbastien B, von Garnier C, Du Pasquier R, et al.; The RegCOVID Study Group. Long-term consequences of COVID-19: a 1-year analysis. J Clin Med. 2023;12:2673. https://doi.org/10.3390/jcm12072673
33. Zuo W, Zhao X, Chen YG. SARS coronavirus and lung fibrosis. In: Lal SK, editor. Molecular biology of the SARS-coronavirus. Berlin, Heidelberg: Springer Berlin, Heidelberg; 2010. p. 247–58.
34. Das KM, Lee EY, Singh R, Enani MA, Al Dossari K, Van Gorkom K, et al. Follow-up chest radiographic findings in patients with MERS-CoV after recovery. Indian J Radiol Imaging. 2017;27:342–9. https://doi.org/10.4103/ijri.IJRI_469_16
35. Farshbafnadi M, Kamali Zonouzi S, Sabahi M, Dolatshahi M, Aarabi MH. Aging & COVID-19 susceptibility, disease severity, and clinical outcomes: the role of entangled risk factors. Exp Gerontol. 2021;154:111507. https://doi.org/10.1016/j.exger.2021.111507
36. Molani S, Hernandez PV, Roper RT, Duvvuri VR, Baumgartner AM, Goldman JD, et al. Risk factors for severe COVID-19 differ by age for hospitalized adults. Sci Rep. 2022;12:6568. https://doi.org/10.1038/s41598-022-10344-3
37. Bajaj V, Gadi N, Spihlman AP, Wu SC, Choi CH, Moulton VR. Aging, immunity, and COVID-19: how age influences the host immune response to coronavirus infections? Front Physiol. 2021;11:571416. https://doi.org/10.3389/fphys.2020.571416
38. Peng M, He J, Xue Y, Yang X, Liu S, Gong Z. Role of hypertension on the severity of COVID-19: a review. J Cardiovasc Pharmacol. 2021;78:e648–55. https://doi.org/10.1097/FJC.0000000000001116

Address for correspondence: Ivan O. Rosas, Department of Medicine, Pulmonary, Critical Care and Sleep Medicine, Baylor College of Medicine, One Baylor Plaza, Houston, TX 77030, USA; email: ivan.rosas@bcm.edu

High Genetic Diversity of Histoplasma in the Amazon Basin, 2006–2017

Tani Ly,[1] Marcus de Melo Teixeira,[1] Gaston I. Jofre,[1] Denis Blanchet, Sigrid MacDonald, Primavera Alvarado, Silvia Helena Marques da Silva, Victoria E. Sepúlveda, Qandeel Zeb, Stephen Vreden, Antoine Adenis, Francisco Yegres, Magalie Demar, Maria José Serna Buitrago, Bridget M. Barker, Mathieu Nacher, Daniel R. Matute

Histoplasmosis is one of the most common pulmonary mycosis diseases in the world. Genome sequencing has revealed that *Histoplasma*, the cause of histoplasmosis, is composed of several phylogenetic species. The genetic diversity of the pathogen remains largely unknown, especially in the tropics. We sequenced the genomes of 91 *Histoplasma* isolates from the Amazon basin of South America and used phylogenomics and population genetic evidence to measure the genetic variation of the genus in South America. We report a previously unidentified clade of *Histoplasma* endemic to the Amazon basin. The lineage is widespread across the continent and contains 5 lineages that are sufficiently differentiated to be considered phylogenetic species. We found the geographic range of those lineages is largely but not completely overlapping. Finally, we found that the patient median age and sex ratio differs among species, suggesting differences in the epidemiology of histoplasmosis caused by each *Histoplasma* lineage.

Fungal diseases have a large and negative effect on human well-being (*1*). Histoplasmosis is one of the most common pulmonary mycosis diseases in the world (*2*). In immunocompetent hosts, cases of histoplasmosis are mildly symptomatic and self resolutive. In those patients, mandatory reporting is not needed, and the disease is often undiagnosed or misdiagnosed. In contrast, histoplasmosis is critical in immunosuppressed patients. In some areas, histoplasmosis will affect up to 25% of the HIV-positive population, and infections frequently are fatal (*3*). Histoplasmosis is diagnosed in ≈500,000 persons each year, and nearly 100,000 persons develop a progressive disseminated disease (*4*). Among persons with advanced HIV (CD4 cell count <200 cells/mm^4), the disease has a case-fatality rate of <5%–50% when treated (*5*,*6*) and close to 100% if not treated (*6*).

The etiologic agent of histoplasmosis, *Histoplasma*, is a cosmopolitan fungus detected in all continents (*7*) including Antarctica (*8*). Histoplasmin, the main *Histoplasma* antigen, skin testing has revealed the fungus has a large geographic range (*9*). Nuclear gene genealogies and a global sample of *Histoplasma* strains from 8 countries revealed the existence of ≥7 phylogenetic species (*7*,*10*), monophyletic groups that are reciprocally monophyletic and isolated from each other. Genome sequencing has confirmed the existence of differentiated phylogenetic species within *Histoplasma* (*11*,*12*). Those assessments are limited because the sampling for *Histoplasma* has been heavily biased toward North America and because few samples from other locations have been fully sequenced.

Nonetheless, histoplasmosis is rampant throughout the Americas. Patients in South America suffer

Author affiliations: Université de la Guyane, Cayenne, French Guiana (T. Ly); Universidade de Brasilia, Brasilia, Brazil (M. de Melo Teixeira); Northern Arizona University, Flagstaff, Arizona, USA (M. de Melo Teixeira, B.M. Barker); Virginia Commonwealth University, Richmond, Virginia, USA (G.I. Jofre); Centre Hospitalier de Cayenne, Cayenne (D. Blanchet, A. Adenis); University of Amsterdam, Amsterdam, Netherlands (S. MacDonald); Instituto de Biomedicina, Caracas, Venezuela (P. Alvarado); Evandro Chagas Institute, Ananindeua, Brazil (S.H. Marques da Silva); University of North Carolina, Chapel Hill, North Carolina, USA (V.E. Sepúlveda, Q. Zeb, F. Yegres, D.R. Matute); Foundation of Scientific Research Suriname, Paramaribo, Suriname (S. Vreden); Centre hospitalier Andree Rosemon, Cayenne (M. Demar); Instituto de Salud Carlos III, Madrid, Spain (M.J.S. Buitrago); Centre d'Investigation Clinique Antilles Guyane, Cayenne (M. Nacher).

DOI: https://doi.org/10.3201/eid3106.241386

[1]These first authors contributed equally to this article.

from disseminated histoplasmosis at one of the highest incidences in the world (1.5 cases/100 person-years in persons living with HIV) (*13*). Histoplasmin surveys have detected multiple localized foci of high skin reactivity to *Histoplasma* (*14*). Preliminary genetic analysis suggests isolates from South America are genetically diverse (*10*,*15*). More recent approaches have used genomic data and revealed the existence of a phylogenetic species endemic to Rio de Janeiro, Brazil (*16*). Yet, the *Histoplasma* isolates from South America, a continent that is hypothesized as a reservoir of diversity for the genus (*7*,*10*), remain largely uncharacterized genetically. A systematic study of the genome-wide diversity of *Histoplasma* across the Americas is sorely needed.

In this report, we used whole-genome sequences to measure the genetic diversity of *Histoplasma* across the Americas. We sequenced 91 genomes of isolates from South and Central America, used data from previous sequencing efforts, generated the largest phylogenetic assessment for this pathogen to date (187 genomes), and studied the extent of divergence within *Histoplasma* spp. from the Americas. We identified 5 lineages that meet the classification criteria as phylogenetic species and compared the epidemiology of histoplasmosis caused by each lineage.

Materials and Methods

Fungal Isolates

We obtained pure mycelial cultures from patients in Central and South America who had clinically defined histoplasmosis diagnosed during 2006–2017 and compiled the collection site, sex, age, and the type of sampling and disease for each patient (Appendix Table 1, https://wwwnc.cdc.gov/EID/article/31/6/24-1386-App1.pdf). We subcultured samples on Sabouraud agar with chloramphenicol, gentamycin, and actidione (Bio-Rad Laboratories, https://www.bio-rad.com) to obtain enough fungal biomass for DNA extraction (≥500 mg). We then conducted DNA extraction (Appendix).

Reference Genome for *Histoplasma* mz5-like

We assembled a de novo genome for the *H. suramericanum* strain mz5, an isolate originally collected in Colombia, by using Oxford Nanopore (https://nanoporetech.com) long-reads. We obtained a total of 231,650 reads, with an average length of 4,681.3 bp (National Center for Biotechnology Information Sequence Read Archive accession no. PRJNA1263433). The mean coverage from our reads was 31.13. We used Flye (*17*) to assemble the reads and 3 runs of Racon (*18*) and Medaka (version 1.11.3, https://github.com/nanoporetech/medaka; *19*) to polish the assembly. We used Pilon (*20*) for insertion/deletion corrections 4 times by using the FASTQs files. To assess the quality and completeness of our resulting assembly, we used Quast (*21*) and BUSCO (*22*) with the fungi and Eurotiomycetes OrthoDB V10 databases (*23*). The assembly had 26 contigs; 95.92% of the genome was assembled in the 10 largest contigs, and we focused on those for the phylogenetic analysis.

Isolate Resequencing

To prepare genomic libraries, we used KAPA library preparation kits (Kapa Biosystems, https://kapabiosystems.com) for Illumina (Illumina, https://www.illumina.com) next-generation sequencing and 1 μg of purified DNA per isolate. Next, we indexed the libraries by using unique 8-bp nucleotide identifiers. We evaluated the concentration of each library with a Kapa library quantification kit (Kapa Biosystems) on a 7900HT Instrument (Thermo Fisher Scientific, https://www.thermofisher.com). We sequenced the libraries to a read length of 100 bp by using v3 or v4 chemistries on an Illumina HiSeq 2500 instrument (Illumina) or to 150 bp by using v2 chemistry on an Illumina NextSeq platform (Illumina), both on a high output mode (paired-end). We recorded the coverage and accession numbers for each isolate (Appendix Table 2).

Previously Published Data

To compare the *Histoplasma* isolates from Central and South America with isolates from other locations, we used 30 previously sequenced genomes (*12*). We also used 16 genomes from a *Histoplasma* lineage endemic to India (*24*) and 50 genomes from Rio de Janeiro (*16*). To root the phylogenetic trees (Figure 1), we used *Paracoccidioides* genomes from 2 different species (*P. restrepiensis,* n = 3; *P. brasiliensis* sensu stricto, n = 2) (*25*), *Blastomyces* (n = 5) (*26*), *Emmonsia crescens* (n = 2) (*27*), and *Emergomyces pasteurianus* (n = 1) (*27*). The genomes all have available Sequence Read Archive accession numbers (Appendix Table 3).

Read Mapping

We used 1 of the samples from the newly identified Latin America lineage to produce a new reference genome for the group (strain mz5). This reference genome has a total length of 34,827,701 bp, with 26 contigs, an N50 of 5,161,774 bp, and a benchmarking universal single-copy orthologs (BUSCO) completeness assessment of 98.6% complete Eurotiomycetes orthologs and 98.5% complete fungi

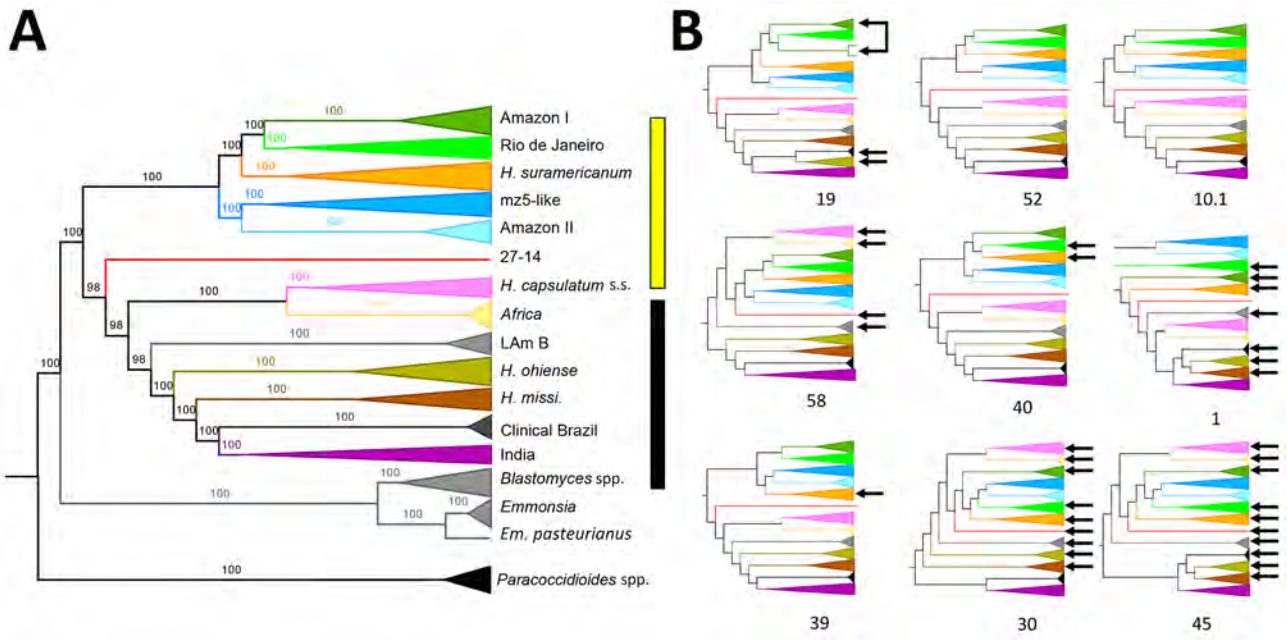

Figure 1. Phylogenetic analyses showing a high genetic diversity of *Histoplasma* in the Amazon basin, 2006–2017. A) Whole-genome concatenated phylogenetic tree with markers shows the existence of ≥12 monophyletic groups. Yellow bar, the Latin American clade; black bar, the global clade. The numbers above each bar represent the concordance value. B) The 9 largest supercontigs showing largely consistent topologies. Arrows show lineages with positions that differ from the inferred species tree. The identification numbers of each supercontig are below each graph.

orthologs (*22*). We mapped 200 short-read sequenced samples (91 newly sequenced genomes) to the reference. The total number of *Histoplasma* genomes from the Americas is 113. We used specific protocols to call variants (Appendix).

Phylogenetic Analysis

To study the genealogical relationships among *Histoplasma* isolates, we converted our multisample variant call format (VCF) file into a concatenated genome-wide alignment in Phylip format by using a Python script (vcf2phylip, https://zenodo.org/records/2540861). We then extracted the 10 largest contigs from our multisample VCF by using bcftools (*28*). Then, we built maximum likelihood trees from the 10 largest contigs and the genome-wide alignment by using IQ-TREE 2 (*29*). ModelFinder (*30*) determined that the transversion with equal base frequences plus R3 model was the best-fitting model of nucleotide substitution for the genomewide alignment (Appendix Table 4). To estimate branch support, we generated 1,000 tree replicates with an ultrafast bootstrap approximation (*31*). We used a similar approach to generate genealogies for the largest 10 supercontigs in the nuclear genome. We compared those trees by using a Robertson-Foulds distance (*32*) as implemented in the R function treedist (library phangorn) (*33*).

Next, we estimated the extent of genealogical concordance for the nuclear genome in 2 ways. First, we studied whether different genomic windows showed the same genealogy. We split into 325 nonoverlapping windows, each 100 kb, and used IQ-TREE 2 (*29*) to generate a genealogy from each partition (325 genome-window trees; different partitions gave similar results). We calculated the concordance factors (CF) (*34,35*) as the fraction of genealogies concordant with each branch from the species trees. Second, we used gene trees from 3,494 complete Eurotiomycetes orthologs (*22,23*). Our approach to generate the gene trees is identical to previously described gene genealogies (*12,24*). Lineages that showed reciprocal monophyly and had high levels of concordance among supercontigs were treated as potential phylogenetic species for further analyses (*36*).

Genetic Diversity and Differentiation

We used population genetics approaches to study the partition of genetic variation in *Histoplasma*. We estimated the magnitude of genetic variation (π) within each lineage of *Histoplasma* (as identified by the concatenated phylogenetic tree and the concordance analysis, see immediately above) and compared these values to the magnitude of pairwise divergence between species (Dxy). Instances of advanced speciation show a much higher Dxy between the 2 focal

groups than the π value of either group (*37*). We used Pixy (*38*) for all calculations. To compare the values of π in each lineage with the pairwise Dxy, we used an approximative 2-sample Fisher-Pitman permutation test (*39*).

Patient Characteristics for Each *Histoplasma* Lineage

We studied general epidemiologic patterns of histoplasmosis caused by each lineage identified in this study. For clinical isolates, we collected patient age, sex, and HIV status and a description of the disease (Appendix Table 1). We conducted 3 analyses by using this dataset. First, we compared whether the 4 countries with the largest number of cases (French Guyana, Brazil, Suriname, and Venezuela) had similar proportional representation of the 6 resident *Histoplasma* phylogenetic species by using a 2-sample test for equality of proportions with continuity correction (prop.test function, R library stats) (*40*). We did 6 pairwise comparisons and adjusted the p values by using a Bonferroni correction (The R Project for Statistical Computing, https://www.r-project.org). We calculated the power of the proportion tests by using the function pwr.2p2n.test (R library pwr).

Second, we studied whether reports of histoplasmosis were equally common in males and females across lineages. We used a χ^2 test by using the R function chisq.test. We calculated the power of each χ^2 test by using the function power.chisq.test (R library DescTools). We only report the comparisons for the 2 lineages that had a χ^2 power $\geq$0.5. We also compared whether the patient sex proportional representation differed among lineages by using a linear model.

Finally, we compared the age of the histoplasmosis patients affected by the 5 lineages. We used a type-III analysis of variance (R library car) (*40*), followed with Tukey honestly significant difference post-hoc pairwise comparisons (R library multcomp) h (*41*) to identify whether lineages differed from each other.

Ethics Considerations

Ethics approval was obtained by the Comité de Protection des Personnes (approval no. CPP2012-47) and the Commission Nationale Informatique et Libertés (approval no. CNIL913511). Biological collection for samples was approved (approval no. DC-2013-1902).

Results

We used *Histoplasma* samples collected for 11 years (2006–2017) in French Guiana, Suriname, Brazil, Venezuela, Guyana, Martinique, Nicaragua, and Spain to conduct a phylogenetics and population genetics analysis to understand the epidemiologic patterns of histoplasmosis in the Amazon basin and adjacent areas. First, we used the genomewide data to resolve the phylogenetic relationships between *Histoplasma* lineages. We created a maximum-likelihood phylogenetic tree for all samples of *Histoplasma* by using concatenated markers to reveal the existence of a monophyletic group composed of *Histoplasma* from South and Central America (Figure 1, panel A). The clade includes *H. suramericanum*. We refer to this clade as the Latin American *Histoplasma* clade, but the group may contain unsampled lineages from outside Latin America. Most previously sequenced samples from North America, South America, and India (*14*,*24*) form a second monophyletic group, which we refer to as the global *Histoplasma* species complex. The global species complex includes 8 lineages (7 with $\geq$1 isolate), 1 from Africa, 1 from India, and 6 from the Americas: *H. ohiense*, *H. mississippiense*, Latin American group B, *H. capsulatum* subspecies (originally thought to be restricted to Central America), and 2 poorly sampled lineages of clinical origin (1 isolate, 27_14, forming the first lineage and 2 clinical isolates from Brazil forming the second lineage). The 2 clinical isolates were not previously described, but all other lineages have been reported previously (*14*,*24*).

The Latin American lineage only includes samples from South and Central America and is highly diverged from most of the previously sequenced samples of *Histoplasma* from around the world. This lineage contains 5 clades (*H. suramericanum* [*11*], Amazon I, Amazon II, RJ [*16*], and mz5-like). Because this lineage has a mutation rate similar to that of other ascomycetes (*42*), we believe the Latin American lineage is 3.2 million years old (CI 2.3–4.1 million years).

We evaluated whether the 5 monophyletic groups revealed by the concatenated tree fulfilled the requirements to be considered different phylogenetic species. We tested 2 additional criteria to assess whether the groups were differentiated enough in the speciation continuum. In cases of advanced speciation, different genome sections show consistent evolutionary trajectories. The 5 groups appear as monophyletic in the concatenated analyses, which is consistent with the possibility of each lineage being a phylogenetic species. All the clades, apart from the RJ lineage, co-occur in the Amazon basin. We evaluated whether the signal from the concatenated genome was also consistent at a more granular level (Figure 1, panel B). Local ancestry analyses are consistent with the genomewide results. Concordance between supercontigs was high, but not perfect, and some supercontigs revealed variations in the inferred phylogenetic relationships (Figure 1, panel B; Appendix Figures 1, 2).

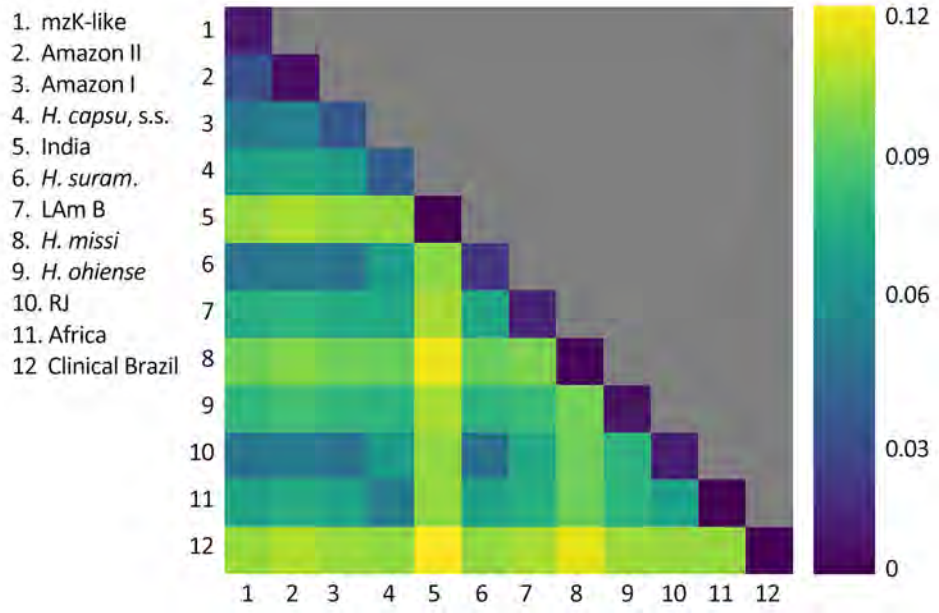

Figure 2. Genetic variation within and between lineages of *Histoplasma* found in the Amazon Basin, 2006–2017. Interspecific genetic distance is larger than the intraspecific variation in most pairwise comparisons. The upper diagonal shows intraspecific variation; all other squares show the pairwise distance between interspecific genetic distance. Unit on right side of graph is pairwise genetic distance.

CF at the genome window level showed that 4 of the 5 lineages had moderately high CF (CF >50%) (Appendix Figure 1), but 1 group, the lineage Amazon I, showed a low CF of 17%, which suggests diverse genetic trajectories along the genome. Of note, this lineage also showed nonmonophyly in supercontig 19 (Figure 1, panel B). We found the Robertson-Foulds distance between pairs of supercontigs and with the tree inferred from a concatenated alignment (Figure 1, panel A; Appendix Figure 2). In general, recent divergences have high bootstrap support and concordance factors, but older splits had lower support (Figure 1; Appendix Figures 1, 2). Despite those genealogical differences, the genome and local ancestry results indicate a high level of phylogenetic concordance among different genomic regions.

Second, the genetic distance between isolates of different species tends to be larger than the extent of polymorphism within species (*36*,*43*). We evaluated whether the extent of Dxy between the monophyletic lineages was larger than the magnitude of π. We found in almost all pairwise assessments (74 of 78) (Appendix Table 5) that Dxy was larger than the variation in any of the lineages, suggesting increased divergence in Latin America (Figure 2). The 4 pairs of lineages that were not major involved only 2 isolates. Isolate 27_14 was detected in 3 pairs and the clinical isolate from Brazil was detected in 2 pairs, including once in combination with isolate 27_14 (Appendix Table 5). Of note, we found a weak association between heterozygosity and geographic range size (Spearman rank correlation $\rho = 0.685$, $p = 0.035$), indicating the larger ranges might serve as large reservoirs of genetic variation in *Histoplasma* (Figure 3).The extent of genetic differentiation as revealed by both phylogenetic and population genetics approaches suggests that speciation is considerable among the lineages from the Latin American clade and that these lineages fulfill the criteria to be considered phylogenetic species.

We then compared some epidemiologic aspects of histoplasmosis caused by each phylogenetic species. Of the 4 countries that had ≥10 samples, 3 (Suriname, French Guiana, and Brazil) had a high prevalence of

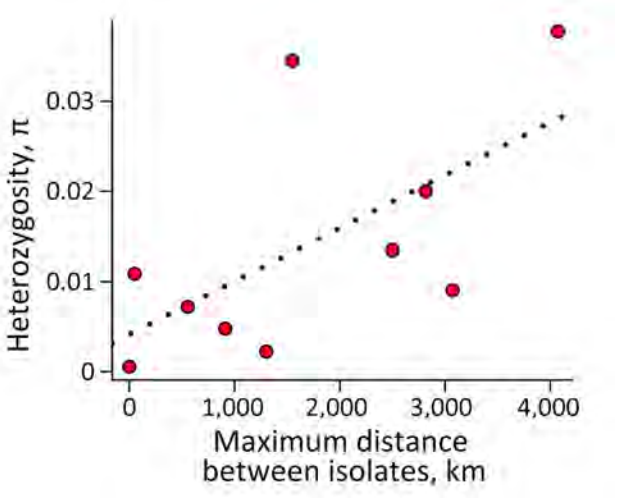

Figure 3. Genetic variation within and between lineages of *Histoplasma* found in the Amazon Basin, 2006–2017. The red dots are the values of nucleotide diversity in each lineage. Dotted line is the predicted linear regression. π is correlated with the geographic range size of each lineage, measured as the distance between the most distant isolates in a lineage. π, within-species genetic variation.

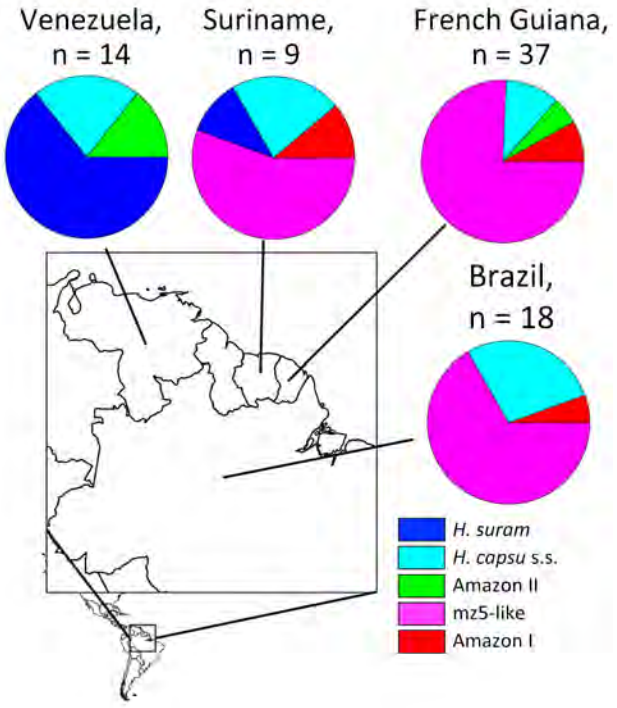

Figure 4. Proportional representation of the *Histoplasma* phylogenetic species identified in 4 countries of the Amazon basin, 2006–2017. s.s., sensu stricto.

the mz5-like lineage (Figure 4). Venezuela demonstrated a high prevalence of *H. suramericanum* and no mz5-like isolates. Of consequence, the species composition of the Venezuela *Histoplasma* sample is the only sample that differs from other countries (χ^2 >6.941, degrees of freedom = 1; p<0.008, $p_{adjusted}$<0.034). Of note, the isolates collected from Spain (n = 4) were collected from patients that migrated from South and Central America, and all belong to *H. suramericanum* (Appendix Table 1).

We studied whether the species composition of the sample changed between years. We evaluated the proportional representation of each lineage per year (Figure 5, panel A). The year with the highest numbers of cases was 2015 with 13 cases, whereas the lowest were 2005 and 2011 with 2 cases. The mz5-like lineage accounted for >50% of the cases reported in this study in all years except for 2009, when it accounted for 42.9% of the samples. None of those proportions differed significantly from each other (2-sample test for equality of proportions with continuity correction: χ^2 = 1.641d.f. = 1, p = 0.200).

Third, we compared the mean patient age for each of the lineages identified. We detected significant differences among the age of patients affected by the 5 lineages (1-way analysis of variance: $F_{5,62}$ = 2.621, p = 0.032). Patients with histoplasmosis caused by 4 lineages had a median age of ≈40 years (Figure 5, panel B). Two lineages were significantly different from the others. Amazon I lineage patients had a younger median age (17.0 ± 10.05 years). The mz5-like lineage patients had an older median age (38.0 ± 16.24 years). Amazon II lineage also has a high median age (41.5 years) but a low sample size (n = 2). We performed Tukey pairwise comparisons among lineages (Appendix Table 6).

Finally, we compared the histoplasmosis sex ratio for each of the 6 phylogenetic species. Previous studies have noted that histoplasmosis is more common in men (*44*). All lineages show a higher proportional representation of male than female patients (Table). The mz5-like and *H. capsulatum* s.s. lineages show sufficient power for the comparison (Table). The mz5-like lineage shows no significant differences in the frequency of male and female patients. The *H. capsulatum* subspecies was almost exclusively isolated

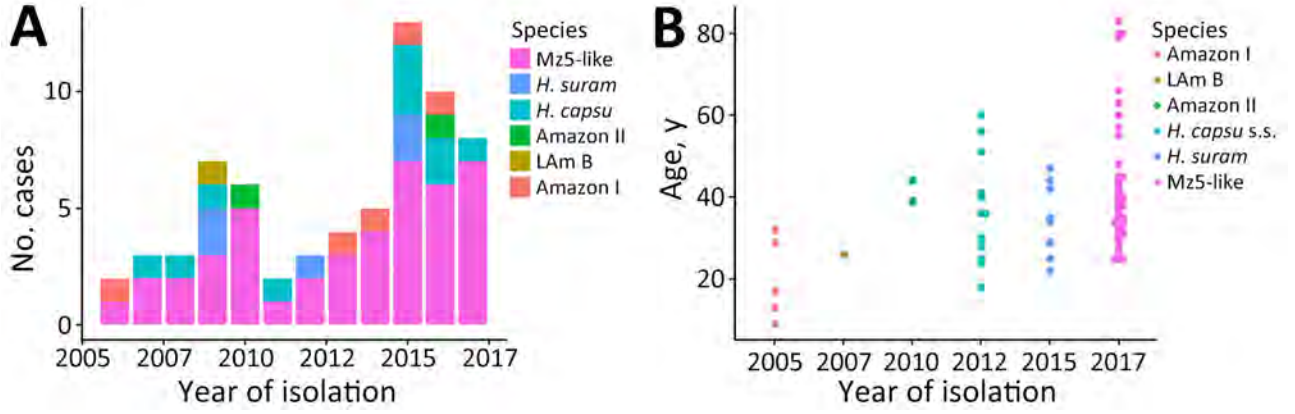

Figure 5. Epidemiologic characteristics of the 6 *Histoplasma* phylogenetic species detected in the Amazon basin, 2006–2017. A) Yearly proportions of each phylogenetic species in the samples collected. B) Age distribution of the patients with histoplasmosis caused by each of the 6 phylogenetic species. LAm B, Latin American group B; s.s., sensu stricto.

Table. Numbers of cases of histoplasmosis caused by each lineage of *Histoplasma*, number of patients who are HIV positive, number of patients with disseminated disease, and sex ratio of patients, Amazon basin, 2006–2017*

Lineage	No. cases	HIV positive	Disseminated disease	Sex			χ^2 power	p value†
				M	F	Ratio		
mz5-like	45	40	25	30	15	2.00	0.918	χ^2 = 1.931, d.f. = 1, p = 0.165
H. capsulatum subspecies	15	11	8	14	1	14.00	0.491	χ^2 = 4.9658, d.f. = 1, p = 0.026
Amazon I	8	4	3	5	3	1.67	0.293	NA
Amazon II	4	4	2	2	2	2.00	0.232	NA
H. suramericanum	15	3	2	6	2	3.00	0.293	NA
Latin American group B	1	1	0	0	1	NA	NA	NA

*d.f., degrees of freedom; NA, not applicable.
†By χ^2 test.

from male patients (Table). *H. capsulatum* subspecies seems to have a higher male:female patient sex ratio than the other species found in the Amazon basin (Appendix Table 7).

Discussion

Histoplasma is one of the most crucial fungal pathogens in the world, and the disease burden of histoplasmosis is a major concern for public health. Genome sequencing has revealed the existence of multiple cryptic species within the genus (*11*,*14*,*24*). The high incidence of histoplasmosis and the high rates of histoplasmin skin reactivity in South America have led to the hypothesis that *Histoplasma* harbors a high level of genetic diversity in this continent. A potential corollary is this genetic diversity also has clinical implications for patients with histoplasmosis. In this article, we identify a monophyletic group that contains 4 previously unidentified and highly differentiated phylogenetic species endemic to South and Central America, all related to *H. suramericanum*, and demonstrate that South America is a biodiversity hotspot for *Histoplasma* and houses ≥7 phylogenetic species. The second most diverse continent, to date, is North America with 3 phylogenetic species (*45*).

Our sampling also enabled us to show that the epidemiologic trends of histoplasmosis differ depending on the causal lineage. We report 2 potentially epidemiologic differences of note between lineages of *Histoplasma* spp., the age and sex ratio of the affected patients. Histoplasmosis patients are more frequently male, and the ratio is reported to be close to 3:1 (*14*,*46*). Our findings suggest differences between the *Histoplasma* spp. in the Amazon basin and the sex ratio varies from 3:2 (Amazon I) to 14:1 (*H. capsulatum* s.s.). Nonetheless, those assessments should be considered carefully. The drivers of the HIV epidemic may vary between territories leading to different age distributions and sex ratios. Furthermore, women are usually tested earlier for HIV and are more likely to seek medical care than men. In contrast, outdoor physical labor and exposure to *H. capsulatum* may be more frequent among men. Controlled animal infections will be the ultimate test of whether different lineages of *Histoplasma* represent a different health risk to different sexes.

The identification of phylogenetic species is the first step to understanding the genetic diversity of *Histoplasma* spp. Perhaps the most crucial question is whether different species are associated with differences in virulence and clinical manifestations of histoplasmosis, which remains largely understudied. We report epidemiologic differences among lineages in South America, but only a comparative assessment from multiple isolates from each *Histoplasma* lineage will demonstrate whether genetic differences among lineages also lead to phenotypic differences in clinical traits. Future research should address whether different clades differ in virulence, which in turn will address whether the epidemiologic patterns observed in our study are caused by genetic changes in each of the *Histoplasma* lineages.

Even though South America harbors the highest number of phylogenetic species known in *Histoplasma* to date, our sampling does not enable us to definitively affirm that South America is the most diverse hotspot of *Histoplasma* because sampling on other continents has been limited. We did not name additional species in this study because it is likely there are other groups around the world needing study, and taxonomy should not be revisited until a more global portrait emerges.

Clinical and epidemiologic comparisons between the different lineages of *Histoplasma* remain rare (*14*) (Appendix Table 8) but are a study frontier that can reveal the tempo and mode of evolution of virulence strategies in fungal pathogens. Overall, our results suggest South America is a geographic reservoir of genetic diversity of *Histoplasma* and underscore the need for systematic collection of the agents of endemic mycoses across tropical regions to better understand their evolutionary history. Now that genome

sequencing is available for most species, it should be fully deployed to clarify the evolutionary history and epidemiologic patterns of histoplasmosis and other endemic mycoses.

Acknowledgments

We would like to thank our reviewers and members of the Matute laboratory for helpful comments on earlier versions of the manuscript. We thank Anastasia Litvintseva and Lalitha Gade for donating strains. This project used isolates from the Evaluation de la prévalence chez les patients infectés par le VIH à l'aide d'une méthode ELISA de détection d'antigènes sérique et urinaire d'*Histoplasma* study and the Technical Cooperation Among Countries project, "Control of Histoplasmosis on HIV infected patients in the Guiana Shield" granted in French Guiana and Suriname by the European Regional Development Fund (Presage no. 31362) and the Pan American Health Organization and World Health Organization through the Agence Nationale de Recherche sur le Sida et les hépatites virales, Agence autonome de l'Inserm (project no. 12260).

All sequenced *Histoplasma* genomes were deposited within the National Center for Biotechnology Information Sequence Read Archive.

This study was funded in part by the Ministère des Outre Mers (convention no. 2014-324-0008). M.M.T. is supported through funding from Fundação de Apoio à Pesquisa do Distrito Federal (award no. 00193-00001871/2023-99). V.E.S., Q.Z., and D.R.M. are supported by the National Institute of Allergy and Infectious Disease of the National Institutes of Health (award no. R01AI153523).

About the Author

Dr. Ly recently completed her PhD from the Université de Guyane. Her research interests include genomics and epidemiology of neglected tropical diseases.

References

1. Vallabhaneni S, Mody RK, Walker T, Chiller T. The global burden of fungal diseases. Infect Dis Clin North Am. 2016;30:1–11. https://doi.org/10.1016/j.idc.2015.10.004
2. Scully MC, Baddley JW. Epidemiology of histoplasmosis. Curr Fungal Infect Rep. 2018;12:51–8. https://doi.org/10.1007/s12281-018-0309-x
3. Pasqualotto AC, Quieroz-Telles F. Histoplasmosis dethrones tuberculosis in Latin America. Lancet Infect Dis. 2018; 18:1058–60. https://doi.org/10.1016/S1473-3099(18)30373-6
4. Bongomin F, Kwizera R, Denning DW. Getting histoplasmosis on the map of international recommendations for patients with advanced HIV disease. J Fungi (Basel). 2019;5:80. https://doi.org/10.3390/jof5030080
5. Rakislova N, Hurtado JC, Palhares AEM, Ferreira L, Freire M, Lacerda M, et al. High prevalence and mortality due to *Histoplasma capsulatum* in the Brazilian Amazon: an autopsy study. PLoS Negl Trop Dis. 2021;15:e0009286. https://doi.org/10.1371/journal.pntd.0009286
6. Caceres DH, Knuth M, Derado G, Lindsley MD. Diagnosis of progressive disseminated histoplasmosis in advanced HIV: a meta-analysis of assay analytical performance. J Fungi (Basel). 2019;5:76. https://doi.org/10.3390/jof5030076
7. Kasuga T, White TJ, Koenig G, McEwen J, Restrepo A, Castañeda E, et al. Phylogeography of the fungal pathogen *Histoplasma capsulatum*. Mol Ecol. 2003;12:3383–401. https://doi.org/10.1046/j.1365-294X.2003.01995.x
8. Moreira LM, Meyer W, Chame M, Brandão ML, Vivoni AM, Portugal J, et al. Molecular detection of *Histoplasma capsulatum* in Antarctica. Emerg Infect Dis. 2022;28:2100–4. https://doi.org/10.3201/eid2810.220046
9. Ashraf N, Kubat RC, Poplin V, Adenis AA, Denning DW, Wright L, et al. Re-drawing the maps for endemic mycoses. Mycopathologia. 2020;185:843–65. https://doi.org/10.1007/s11046-020-00431-2
10. Teixeira MM, Patané JSL, Taylor ML, Gómez BL, Theodoro RC, de Hoog S, et al. Worldwide phylogenetic distributions and population dynamics of the genus *Histoplasma*. PLoS Negl Trop Dis. 2016;10:e0004732. https://doi.org/10.1371/journal.pntd.0004732
11. Sepúlveda VE, Márquez R, Turissini DA, Goldman WE, Matute DR. Genome sequences reveal cryptic speciation in the human pathogen *Histoplasma capsulatum*. MBio. 2017;8:e01339–17. https://doi.org/10.1128/mBio.01339-17
12. Sepúlveda VE, Rader JA, Li J, Goldman WE, Matute DR. Phenotypic characterization of cryptic species in the fungal pathogen *Histoplasma*. MSphere. 2024;9:e0000924. https://doi.org/10.1128/msphere.00009-24
13. Adenis AA, Valdes A, Cropet C, McCotter OZ, Derado G, Couppie P, et al. Burden of HIV-associated histoplasmosis compared with tuberculosis in Latin America: a modelling study. Lancet Infect Dis. 2018;18:1150–9. https://doi.org/10.1016/S1473-3099(18)30354-2
14. Almeida MA, Almeida-Silva F, Guimarães AJ, Almeida-Paes R, Zancopé-Oliveira RM. The occurrence of histoplasmosis in Brazil: a systematic review. Int J Infect Dis. 2019;86:147–56. https://doi.org/10.1016/j.ijid.2019.07.009
15. Zancopé-Oliveira RM, Morais e Silva Tavares P, Muniz MM. Genetic diversity of *Histoplasma capsulatum* strains in Brazil. FEMS Immunol Med Microbiol. 2005;45:443–9. https://doi.org/10.1016/j.femsim.2005.05.018
16. Almeida-Silva F, de Melo Teixeira M, Matute DR, de Faria Ferreira M, Barker BM, Almeida-Paes R, et al. Genomic diversity analysis reveals a strong population structure in *Histoplasma capsulatum* LAmA (*Histoplasma suramericanum*). J Fungi (Basel). 2021;7:865. https://doi.org/10.3390/jof7100865
17. Kolmogorov M, Yuan J, Lin Y, Pevzner PA. Assembly of long, error-prone reads using repeat graphs. Nat Biotechnol. 2019;37:540–6. https://doi.org/10.1038/s41587-019-0072-8
18. Vaser R, Sović I, Nagarajan N, Šikić M. Fast and accurate de novo genome assembly from long uncorrected reads. Genome Res. 2017;27:737–46. https://doi.org/10.1101/gr.214270.116
19. Zhang X, Liu CG, Yang SH, Wang X, Bai FW, Wang Z. Benchmarking of long-read sequencing, assemblers and polishers for yeast genome. Brief Bioinform. 2022;23:bbac146. https://doi.org/10.1093/bib/bbac146
20. Walker BJ, Abeel T, Shea T, Priest M, Abouelliel A, Sakthikumar S, et al. Pilon: an integrated tool for comprehensive microbial variant detection and genome

assembly improvement. PLoS One. 2014;9:e112963. https://doi.org/10.1371/journal.pone.0112963
21. Gurevich A, Saveliev V, Vyahhi N, Tesler G. QUAST: quality assessment tool for genome assemblies. Bioinformatics. 2013;29:1072–5. https://doi.org/10.1093/bioinformatics/btt086
22. Waterhouse RM, Seppey M, Simão FA, Manni M, Ioannidis P, Klioutchnikov G, et al. BUSCO applications from quality assessments to gene prediction and phylogenomics. Mol Biol Evol. 2018;35:543–8. https://doi.org/10.1093/molbev/msx319
23. Kriventseva EV, Kuznetsov D, Tegenfeldt F, Manni M, Dias R, Simão FA, et al. OrthoDB v10: sampling the diversity of animal, plant, fungal, protist, bacterial and viral genomes for evolutionary and functional annotations of orthologs. Nucleic Acids Res. 2019;47(D1):D807–11. https://doi.org/10.1093/nar/gky1053
24. Jofre GI, Singh A, Mavengere H, Sundar G, D'Agostino E, Chowdhary A, et al. An Indian lineage of *Histoplasma* with strong signatures of differentiation and selection. Fungal Genet Biol. 2022;158:103654. https://doi.org/10.1016/j.fgb.2021.103654
25. Mavengere H, Mattox K, Teixeira MM, Sepúlveda VE, Gomez OM, Hernandez O, et al. *Paracoccidioides* genomes reflect high levels of species divergence and little interspecific gene flow. MBio. 2020;11:e01999–20. https://doi.org/10.1128/mBio.01999-20
26. Chowdhary A, Jofre GI, Singh A, Dagilis AJ, Sepúlveda VE, McClure AT, et al. Autochthonous *Blastomyces dermatitidis*, India. Emerg Infect Dis. 2024;30:2577–82. https://doi.org/10.3201/eid3012.240830
27. Muñoz JF, McEwen JG, Clay OK, Cuomo CA. Genome analysis reveals evolutionary mechanisms of adaptation in systemic dimorphic fungi. Sci Rep. 2018;8:4473. https://doi.org/10.1038/s41598-018-22816-6
28. Li H. A statistical framework for SNP calling, mutation discovery, association mapping and population genetical parameter estimation from sequencing data. Bioinformatics. 2011;27:2987–93. https://doi.org/10.1093/bioinformatics/btr509
29. Nguyen L-T, Schmidt HA, von Haeseler A, Minh BQ. IQ-TREE: a fast and effective stochastic algorithm for estimating maximum-likelihood phylogenies. Mol Biol Evol. 2015;32:268–74. https://doi.org/10.1093/molbev/msu300
30. Kalyaanamoorthy S, Minh BQ, Wong TKF, von Haeseler A, Jermiin LS. ModelFinder: fast model selection for accurate phylogenetic estimates. Nat Methods. 2017;14:587–9. https://doi.org/10.1038/nmeth.4285
31. Minh BQ, Nguyen MAT, von Haeseler A. Ultrafast approximation for phylogenetic bootstrap. Mol Biol Evol. 2013;30:1188–95. https://doi.org/10.1093/molbev/mst024
32. Bryant D, Steel M. Computing the distribution of a tree metric. IEEE/ACM Trans Comput Biol Bioinform. 2009;6:420–6. https://doi.org/10.1109/TCBB.2009.32
33. Schliep KP. phangorn: phylogenetic analysis in R. Bioinformatics. 2011;27:592–3. https://doi.org/10.1093/bioinformatics/btq706
34. Baum DA. Concordance trees, concordance factors, and the exploration of reticulate genealogy. Taxon. 2007;56:417–26. https://doi.org/10.1002/tax.562013
35. Lanfear R, Hahn MW. The meaning and measure of concordance factors in phylogenomics. Mol Biol Evol. 2024;41:msae214. https://doi.org/10.1093/molbev/msae214
36. Matute DR, Sepúlveda VE. Fungal species boundaries in the genomics era. Fungal Genet Biol. 2019;131:103249. https://doi.org/10.1016/j.fgb.2019.103249
37. Birky CW Jr, Adams J, Gemmel M, Perry J. Using population genetic theory and DNA sequences for species detection and identification in asexual organisms. PLoS One. 2010;5:e10609. https://doi.org/10.1371/journal.pone.0010609
38. Korunes KL, Samuk K. pixy: Unbiased estimation of nucleotide diversity and divergence in the presence of missing data. Mol Ecol Resour. 2021;21:1359–68. https://doi.org/10.1111/1755-0998.13326
39. Hothorn T, Hornik K, Van De Wiel MA, Zeileis A. Implementing a class of permutation tests: the coin package. J Stat Softw. 2008;28:1–23. https://doi.org/10.18637/jss.v028.i08
40. Fox J, Weisberg S. An R companion to applied regression, 3rd ed. Thousand Oaks (CA): Sage Publications; 2019.
41. Hothorn T, Bretz F, Westfall P. Simultaneous inference in general parametric models. Biom J. 2008;50:346–63. https://doi.org/10.1002/bimj.200810425
42. Farlow A, Long H, Arnoux S, Sung W, Doak TG, Nordborg M, et al. The spontaneous mutation rate in the fission yeast *Schizosaccharomyces pombe*. Genetics. 2015;201:737–44. https://doi.org/10.1534/genetics.115.177329
43. Birky CW Jr. Species detection and identification in sexual organisms using population genetic theory and DNA sequences. PLoS One. 2013;8:e52544. https://doi.org/10.1371/journal.pone.0052544
44. Egger M, Hoenigl M, Thompson GR III, Carvalho A, Jenks JD. Let's talk about sex characteristics—as a risk factor for invasive fungal diseases. Mycoses. 2022;65:599–612. https://doi.org/10.1111/myc.13449
45. Tenório BG, Kollath DR, Gade L, Litvintseva AP, Chiller T, Jenness JS, et al. Tracing histoplasmosis genomic epidemiology and species occurrence across the USA. Emerg Microbes Infect. 2024;13:2315960. https://doi.org/10.1080/22221751.2024.2315960
46. Develoux M, Amona FM, Hennequin C. Histoplasmosis caused by *Histoplasma capsulatum* var. *duboisii*: a comprehensive review of cases from 1993 to 2019. Clin Infect Dis. 2021;73:e543–9. https://doi.org/10.1093/cid/ciaa1304

Address for correspondence: Daniel R. Matute, University of North Carolina, Chapel Hill, 250 Bell Tower Rd, Ste 3161, Chapel Hill, NC 27516, USA; email: dmatute@email.unc.edu

Emergence of Oropouche Virus in Espírito Santo State, Brazil, 2024

Edson Delatorre, Gabriela Colombo de Mendonça, Felipe Donateli Gatti, Anna Clara Gregório Có, Julia del Piero Pereira, Eric Arrivabene Tavares, Joana Zorzal Nodari, Agata Rossi, Suwellen Sardinha Dias de Azevedo, Cláudio Tavares Sacchi, Karoline Rodrigues Campos, Adriana Bugno, Lyvia Neves Rebello Alves, Lucas André Silva Bonela, Jaqueline Pegoretti Goulart, Thiago de Jesus Sousa, Felipe Gomes Naveca, Rodrigo Ribeiro-Rodrigues

Oropouche virus (OROV), historically endemic to the Amazon, had spread to nearly all Brazil states by 2024; Espírito Santo emerged as a transmission hotspot in the Atlantic Forest biome. We characterized the epidemiologic factors driving OROV spread in nonendemic southeast Brazil, analyzing environmental and agricultural conditions contributing to viral transmission. We tested samples from 29,080 suspected arbovirus-infected patients quantitative reverse transcription PCR for OROV and dengue, chikungunya, Zika, and Mayaro viruses. During March–June 2024, the state had 339 confirmed OROV cases, demonstrating successful local transmission. Spatial analysis revealed that most cases clustered in municipalities with tropical climates and intensive cacao, robusta coffee, coconut, and pepper cultivation. Phylogenetic analysis identified the Espírito Santo OROV strains as part of the 2022–2024 Amazon lineage. The rapid spread of OROV outside the Amazon highlights its adaptive potential and public health threat, emphasizing the need for enhanced surveillance and targeted control measures.

Oropouche virus (OROV), classified as *Orthobunyavirus oropoucheense*, family *Peribunyaviridae*, is an arthropodborne virus with a negative-sense RNA genome consisting of 3 segments, large (L), medium (M), and small (S) (*1*). A neglected arbovirus, OROV causes Oropouche fever and circulates primarily in Central America, South America, and the Caribbean (*2*–*4*). In Brazil, OROV was historically confined to the Amazon basin, where several vector species and a range of reservoirs maintain its sylvatic transmission cycle (*2*,*3*,*5*). In urban areas in the Amazon, *Culicoides paraensis*, a midge commonly found in tropical, humid environments rich in organic matter, such as forests and plantations, is the primary vector responsible for OROV transmission to humans (*3*,*4*). Humans might acquire OROV infection in forested regions and subsequently introduce it to urban settings. The widespread distribution of the vector, coupled with increased human mobility and the influence of climate change, might enable the virus's gradual expansion beyond its historical range in Brazil, raising concerns about the potential for broader geographic spread (*6*,*7*).

Since the 1960s, occasional OROV spillovers to humans have led to >30 documented localized outbreaks or large-scale epidemics in the Amazon basin, underscoring the virus's epidemic potential (*8*–*12*). Although incidence is highest in the Amazon, sporadic cases have been reported in other states in Brazil without leading to widespread outbreaks (*13*).

During August 2022–March 2024, a new outbreak triggered by a reassortant OROV lineage emerged in Brazil's western Amazon region, causing ≈6,000 reported cases (*14*). In 2024, that reassortant lineage led to the largest recorded outbreak outside the virus's endemic zone; OROV was detected in all regions of Brazil (*15*,*16*). Outside the Amazon, high incidence rates were observed in the Atlantic Forest region, particularly in municipalities with low population densities and agricultural activities favoring the establishment of *C. paraensis* vector populations, such as cocoa and banana cultivation (*17*).

Author affiliations: Universidade Federal do Espírito Santo Centro de Ciências da Saúde, Vitória, Brazil (E. Delatorre, A. Rossi, R. Ribeiro-Rodrigues); Laboratório Central de Saúde Pública do Estado do Espírito Santo, Vitória (G.C. de Mendonça, F.D. Gatti, A.C.G. Có, J.P. Pereira, E.A. Tavares, J.Z. Nodari, S.S.D. de Azevedo, L.N.R. Alves, L.A.S. Bonela, J.P. Goulart, T.J. Sousa); Instituto Adolfo Lutz, São Paulo, Brazil (C.T. Sacchi, K.R. Campos, A. Bugno); Instituto Oswaldo Cruz, Fiocruz, Rio de Janeiro, Brazil (F.G. Naveca); Instituto Leônidas e Maria Deane, Fiocruz, Manaus, Brazil (F.G. Naveca)

DOI: https://doi.org/10.3201/eid3106.241946

OROV infections typically manifest as an acute febrile illness characterized by headache, myalgia, and arthralgia (*14*). Those symptoms overlap with those of infection with other endemic arboviruses, such as dengue virus (DENV), Zika virus (ZIKV), and chikungunya virus (CHIKV) (*2*,*3*). However, emerging evidence has linked OROV to fatal cases (*18*). Unprecedented vertical transmission was also reported, and some cases resulted in congenital anomalies or fetal death (*19*,*20*). Therefore, the significant shift in OROV's pathogenicity marks a new epidemiologic paradigm for Oropouche fever.

Espírito Santo state, located in southeastern Brazil and entirely within the Atlantic Forest biome, has emerged as a major hotspot for OROV transmission outside the Amazon region, recording the highest state-level incidence rate among non-Amazon states in 2024 (*21*). The state's extensive agricultural activities, particularly in coffee, cocoa, and banana cultivation (*22*), combined with high rural worker mobility and environmental conditions favorable for *C. paraensis* midge establishment, may have contributed to viral spread. The first case of Oropouche infection in Espírito Santo was detected on March 24, 2024. We used epidemiologic and genomic approaches to analyze the emergence and dissemination of the new OROV variant in Espírito Santo state. We also examined the regional characteristics that enable its transmission and contribute to its establishment in this previously unaffected area.

Materials and Methods

Study Population

Our study analyzed samples from patients who visited public health units in Espírito Santo state with arboviral-like symptoms (ZDC: Zika, dengue, and chikungunya) during February 25–June 15, 2024. All suspected cases of acute arboviral infections in Espírito Santo are centralized at the state's central laboratory, Laboratório Central de Saúde Pública do Espírito Santo (LACEN-ES, Vitória, Brazil), which receives samples from all 78 municipalities for diagnostic testing. During the study period, a total of 29,080 samples were tested, corresponding to ≈0.76% of the state's population (3,833,712 inhabitants). The serum or plasma samples were subsequently sent to the LACEN-ES for viral molecular diagnosis. The Human Research Ethics Committee at the University of Vila Velha (Vila Velha, Brazil) approved this study (Certificate of Presentation for Ethical Assessment no. 84698324.7.0000.5064) and waived the need for written informed consent. The committee is registered with Brazil's National Research Ethics Commission and oversees studies involving public health institutions in Espírito Santo, including the state's Central Laboratory where this investigation was conducted.

Sample Processing and Quantitative Reverse Transcription PCR

We processed samples for nucleic acid extraction using magnetic bead-based systems TANBead Maelstrom 9600 (Taiwan Advanced Nanotech Inc., https://www.tanbead.com), EXTRACTA 96 (Loccus, https://www.loccus.com.br) and TechStar YC-702 (Wuxi Techstar Technology Co., http://www.techstarbio.com), following manufacturers' instructions. Subsequently, for molecular testing, we used 3 different quantitative reverse transcription (qRT-PCR) kits: Molecular ZCD Tipagem Bio-Manguinhos (https://www.bio.fiocruz.br), Biomol ZDC (IBMP, https://www.ibmp.org.br), and VIASURE Zika, Dengue & Chikungunya (ThermoFisher, https://www.thermofisher.com), following the manufacturers' protocols. For the samples not detectable for ZDC, we performed a multiplex qRT-PCR to investigate for OROV and Mayaro virus (MAYV), as described by Naveca et al. (*23*). To extend testing, we adapted the laboratory diagnosis to carry out the procedure on a pool of 8 samples. After detecting the target, we conducted another q RT-PCR with the 8 samples individually to confirm the test.

Epidemiologic Data and Environmental Context

We retrieved individual-level of OROV-positive case data from the eSUS Brazil Ministry of Health (https://sisaps.saude.gov.br/sistemas/esusaps) and Gerenciador de Ambiente Laboratorial (GAL; http://gal.datasus.gov.br) systems at the municipal level for the state of Espírito Santo, covering cases reported through June 15, 2024. We linked each case to anonymized metadata, including demographics, location, symptoms (fever, headache, myalgia, retroorbital pain, back pain, arthritis, petechiae, rash, arthralgia, nausea, conjunctivitis, vomiting, and leukopenia), and hospitalization and notification/symptom dates.

We calculated the municipal incidence of OROV on the basis of the 2022 census data from the Brazilian Institute of Geography and Statistics (IBGE) (*24*). Estimated incidence mapping used the geoBR package in RStudio (http://www.rstudio.com) with IBGE municipal boundary shapefiles (*25*). We obtained data about the agricultural establishments at the municipal level from the 2017 IBGE census of agriculture (*26*). We estimated the Spearman correlation for all municipalities reporting cases to explore the

relationship between the planted area of the top 10 crops in Espírito Santo and the number of OROV cases. In addition, we analyzed between-group differences in cycle threshold (Ct) values (viral load proxy) for each symptom using 2-tailed Mann-Whitney U tests ($\alpha = 0.05$).

Generation Time and Instantaneous Reproduction Number Estimation

The generation time represents the interval between successive rounds of infection. Although that interval has been estimated for other arboviruses, no such estimates exist for OROV. We estimated the generation time using a combination of human viral clearance data (*27*), mosquito mortality rates (*28*), and data from experimental studies involving vector competence (*29*), using a framework applied previously for ZIKV (*30*) and MAYV (*31*). We conducted parameter inference using a Bayesian framework implemented with Markov chain Monte Carlo methods (Appendix Figures 1, 2, https://wwwnc.cdc.gov/EID/article/31/6/24-1946-App1.pdf). We then used the posterior distributions of the generation time parameters (Appendix Tables 1, 2) to inform the calculation of the reproduction number. We estimated the instantaneous reproduction number (R_t) for OROV using the R package EpiEstim (*32*). We reconstructed the R_t for the April–June period using a Bayesian inference model with a sliding time window of $\tau = 7$ days (Appendix).

Sample Selection and Next-Generation Sequencing

We selected 7 samples with Ct <27 for whole-genome sequencing from a pool of all OROV-positive samples identified through RT-PCR during the study. To ensure geographic representativeness, we chose samples from the municipalities of Colatina, Rio Bananal, and Laranja da Terra, which were among the most affected regions in the state. We sequenced 6 samples at Instituto Adolfo Lutz (IAL), yielding complete S and M segments (Appendix Table 3). We sequenced 1 sample at LACEN/ES using Illumina RNA Prep with Enrichment Tagmentation protocol (https://www.illumina.com) with the Respiratory Pathogen ID/AMR Enrichment Panel Kit (Illumina); we extracted OROV reads from the nontarget portion of the kit. We conducted genome assembly using a custom version of the ViralFlow pipeline version 1.0.1 (*33*), referencing GenBank sequences NC_005776.1 (L segment), NC_005775.1 (M segment), and NC_005777.1 (S segment).

Bioinformatics and Phylogenetic Inference

For the phylogenetic analysis, we aligned 7 new sequences from Espírito Santo with 145 OROV strains sampled in the Americas (1955–2023) and available in GenBank as of August 2024. The alignment, performed in MAFFT version 7 (https://mafft.cbrc.jp) (*34*), included the prototypical viruses Iquitos, Madre de Dios, and Perdões as outgroups. We selected the generalized time-reversible discrete gamma substitution model in jModelTest2 (https://github.com/ddarriba/jmodeltest2). We used phylogenetic inference in MrBayes version 3.2.7a (*35*) to sample trees until parameter convergence (effective sample size >200), with node support determined by posterior probabilities from the majority-rule consensus topology.

Results

Approximately 29,100 patients in Espírito Santo experiencing arbovirus-like illness were tested by real-time RT-PCR for the presence of DENV-1, DENV-2, CHIKV, ZIKV, OROV, and MAYV during March–June 2024. Until epidemiologic week 13, DENV-1 represented ≈50% of the positive cases, followed by CHIKV and DENV-2 (Figure 1). However, from epidemiologic week 13 onward, OROV cases were detected, marking a pronounced shift in the epidemiologic landscape. OROV cases increased rapidly, reaching 339 cases within 10 weeks. By epidemiologic week 24, the frequency of OROV infections approached the levels of DENV-1, DENV-2, and CHIKV, indicating a comparable circulation of these viruses at the outbreak's peak. After the emergence of OROV, the proportion of CHIKV cases also rose, eventually surpassing that of DENV. Initially, OROV cases were primarily classified as imported; however, community spread became evident as local transmission was established. During epidemiologic weeks 18–27, the time-varying R_t for OROV remained ≈2.5 (95% credible interval ≈1.5–3.0), we observed a peak value of ≈3.0 in epidemiologic week 26. After this peak, a marked reduction in R_t occurred, and it was below 1.0 by epidemiologic week 28, indicating a decline in transmission and a shift toward containment of the outbreak (Figure 1).

We observed a marked predominance of male patients in OROV cases (Figure 2, panel A); male-to-female ratio was 1.5:1. Most cases occurred in persons >20 years of age, suggesting that adult men may be disproportionately affected by this outbreak. The most frequently reported symptoms were fever (307/339 [90.56%]), headache (275/339 [81.12%]), myalgia (232/339 [68.44%]), and retroorbital pain (113/339 [33.33%]) (Figure 2, panel B). We observed no significant differences in symptoms between male and female patients. We used real-time RT-PCR Ct values as a proxy for the patient's plasmatic viral load

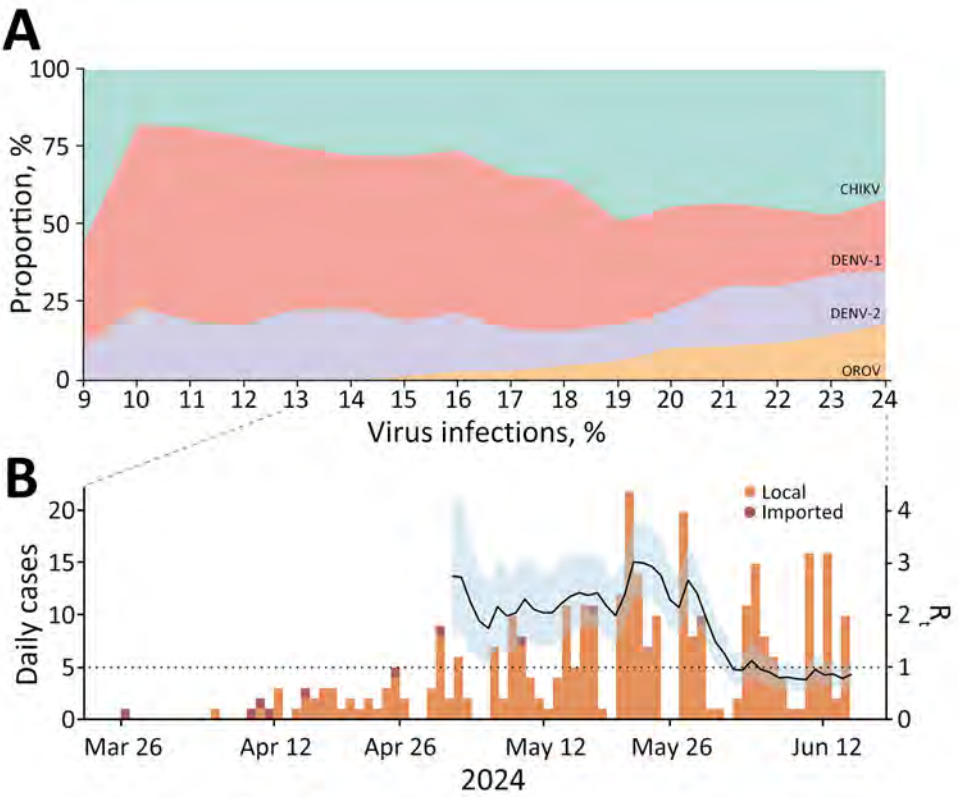

Figure 1. Temporal distribution and reproduction number of Oropouche virus in Espírito Santo, Brazil. A) Weekly percentages of CHIKV, DENV-1, DENV-2, and OROV infections for epidemiologic weeks 9–24, 2024. B) Estimates of R_t during the OROV outbreak. Solid black curve represents the median R_t; shaded area indicates 95% credible interval, based on daily incidence data including local and imported cases. Dotted line indicates $R_t = 1$. R_t was estimated using sliding windows of $\tau = 7$ days. CHIKV, chikungunya virus; DENV, dengue virus; OROV, Oropouche virus; R_t, instantaneous reproduction number.

to investigate its relationship to symptomatology. Patients with fever exhibited significantly lower median Ct values than those without fever ($p = 0.017$), suggesting a higher viral load in febrile patients. We observed a similar trend for headache ($p = 0.043$), myalgia ($p = 0.025$), and retroorbital pain ($p = 0.017$) (Figure 2, panel C). Comparisons for other symptoms did not yield statistically significant differences (Appendix Figure 1).

During the OROV outbreak in Espírito Santo, the virus spread across 17 municipalities, culminating in 8.84 cases/100,000 inhabitants statewide. Most cases were concentrated in 2 distinct hotspots: the regions surrounding the municipalities of Colatina/Rio Bananal and Laranja da Terra (Figure 3, panel A). In total, 332/339 (98%) of the diagnosed cases were associated with tropical climates, in accordance with Köppen-Geiger climate classification; 308 (≈91%) occurred in municipalities classified as having a tropical savanna climate (Köppen-Geiger classification Aw), and 24 (7%) were linked to tropical monsoon climate (Köppen-Geiger classification Am) (Figure 3, panel B). In contrast, only 7/339 cases (≈2%) were distributed across municipalities with temperate climates, such as humid subtropical (Köppen-Geiger classification Cfa) and temperate oceanic (Köppen-Geiger classification Cfb). No cases were reported in areas classified as subtropical highland climate (Köppen-Geiger classification Cwb).

The initial spread of OROV in Espírito Santo followed a clear spatial pattern, predominantly affecting municipalities within the tropical savanna climate (Figure 4). This dissemination phase, epidemiologic weeks 17–18, marked the entry of the virus into areas with different climatic conditions. The peak incidence, exceeding 200 cases/100,000 inhabitants, was recorded at the municipality level during epidemiologic weeks 21–24, particularly in the epicentral municipalities of Colatina and Laranja da Terra. Those areas, situated within the tropical savanna climate zone, appear to have served as primary foci for transmitting OROV throughout the state. To characterize the ecologic niches contributing to the introduction and spread of OROV in Espírito Santo, we examined the association between OROV prevalence and the cultivated areas for the 10 most widely grown crops in the state. We found significant associations between specific crops and OROV incidence (Table 1); robusta coffee (Spearman correlation coefficient [ρ] = 0.55, $p = 0.004$), cacao ($\rho = 0.54$, $p = 0.005$), coconut ($\rho = 0.43$, $p = 0.003$), and pepper ($\rho = 0.43$, $p = 0.034$) displayed moderate positive correlations with the number of OROV cases.

Phylogenetic analysis of each genomic segment individually showed that all cases detected within

Espírito Santo belong to the novel reassortant $M_1L_2S_2$ ($OROV_{BR2015–2024}$) lineage (*15*) with high branch support (posterior probability ≥0.98). That lineage circulated in the Amazon Basin during 2023–2024, causing a major outbreak (Figure 5). Of interest, in the S and M trees, the Espírito Santo samples do not form a monophyletic clade, which indicated multiple introductions of OROV into the state.

Discussion

The emergence and rapid spread of arboviruses beyond their traditional endemic regions is driven by changing climate patterns and human land use (*7*). Our study used high-resolution data to document the unprecedented establishment of OROV in Brazil's Atlantic Forest, showing its adaptations and spread beyond the Amazon Basin. The expansion mirrors patterns observed for other arboviruses, such as ZIKV (*36*), CHIKV (*37*), and West Nile virus (*38*), in which changes in vector ecology, human mobility, and environmental conditions have led to emergence of those viruses in previously unaffected regions (*6*). OROV's successful establishment in southeast Brazil underscores both an immediate public health concern and the complex ecologic and epidemiologic factors enabling arboviral adaptation to novel environments.

Our findings revealed a marked epidemiologic shift with the emergence and rapid establishment of OROV transmission in the state amidst the ongoing endemic circulation of DENV and CHIKV. Within ≈11 weeks from its initial detection, OROV reached infection levels comparable to those of endemic arboviruses in Espírito Santo, suggesting robust viral transmission. The concurrent presence of OROV alongside DENV and CHIKV, without evident competitive interference, could reflect vector-specific ecologic differences: although DENV and CHIKV are transmitted predominantly by *Aedes* spp. mosquitoes in urban areas (*39*), OROV transmission is driven mainly by *C. paraensis* midges (*3*,*27*). The estimated transmissibility, with R_t peaking at ≈3.0, parallels the

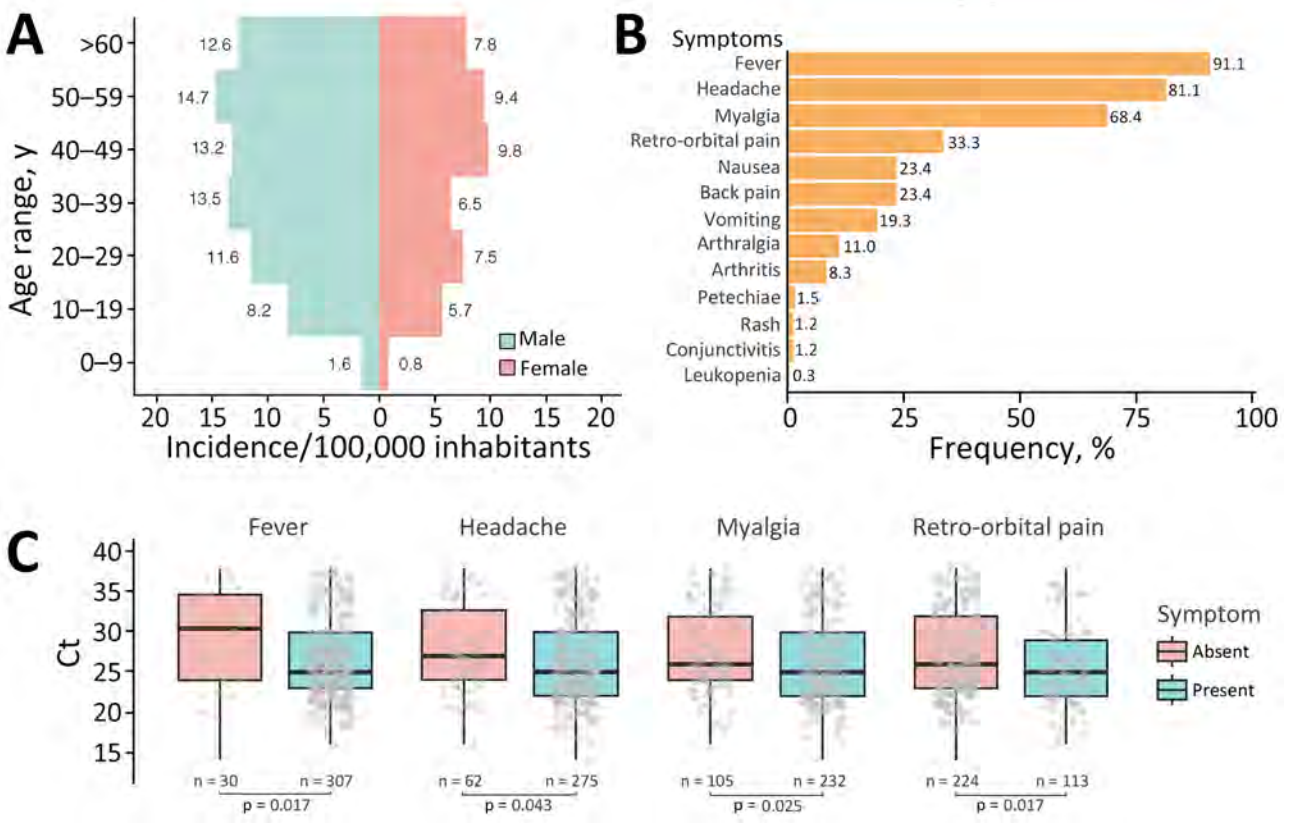

Figure 2. Demographics, symptoms, and Ct value comparison in OROV-positive patients from Espírito Santo, Brazil. A) Age-sex pyramid of the OROV incidence rate (per 100,000 inhabitants). Incidence rates are shown for each age group. B) Frequency of symptoms reported in OROV-positive patients. C) Boxplots of Ct values from OROV reverse transcription PCR in patients with or without fever, headache, myalgia, and retroorbital pain. Black horizontal bars indicate medians, tops and bottoms of boxes indicate interquartile ranges, vertical whiskers indicate ranges. Gray dots represent individual Ct values. p values determined by 2-sided Mann–Whitney U test for each comparison.

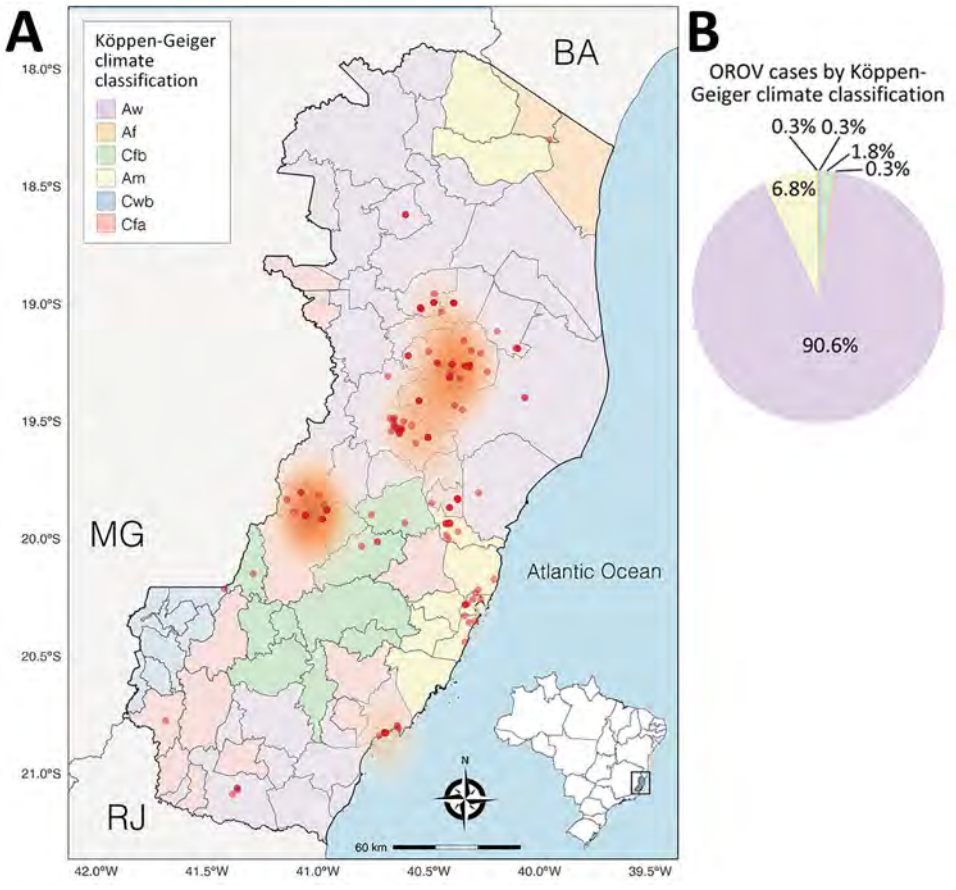

Figure 3. Spatial distribution of Oropouche virus cases and climate classification in Espírito Santo, Brazil. A) Espírito Santo, with municipalities colored according to the Köppen-Geiger climate classification. Red dots indicate cases. Orange shading represents case density. Inset shows location of Espírito Santo state in Brazil. B) Pie chart showing the percentage of cases in each Köppen-Geiger climate category.

dynamics seen in both urban and sylvatic arboviruses within immunologically naive or mixed populations. Similar patterns were reported for ZIKV; R_t values were 2.6–4.8 in French Polynesia (*40*), 3.0–6.6 in Colombia (*41*), and as high as 2.5 in Brazil (*30*). Likewise, MAYV, endemic to the Amazon region, showed R_t values of 2.1–2.9 within its primary range, decreasing to 1.1–1.3 in non-Amazon regions (*31*). The high transmissibility of OROV observed in Espírito Santo could be attributed to multiple factors, including the predominantly mild or asymptomatic nature of OROV infections (*3*,*27*) and favorable local conditions for *C. paraensis* midge proliferation (*28*). Our R_t estimates might underestimate transmissibility by excluding unreported asymptomatic and mild cases. However, if underreporting remains stable, the inferred trends should still reliably reflect epidemic dynamics (*32*).

The demographic profile of affected persons in this outbreak showed predominance of adult male case-patients, which contrasts with previous OROV outbreaks (*12*,*14*). The male predominance may reflect occupational exposure in rural agricultural activities, increasing contact with *C. paraensis* vectors, as seen in previous Brazil outbreaks where farming was a major risk factor (*42*). Clinical manifestations aligned with previous OROV cases across diverse regions, including recent Amazon outbreaks (*12*,*14*,*43*). The association between key symptoms and lower Ct values suggested that higher viral loads may drive the intensity of clinical manifestations, as documented for other arboviruses, such as DENV (*44*,*45*), yet remains largely unexplored for OROV. Of note, recent fatal OROV cases in nonendemic regions of Brazil, characterized by low Ct values and rapid progression to severe hemorrhagic symptoms within days, underscored the potential link between viral load and disease severity (*18*).

Phylogenetic analysis of OROV genomic sequences from Espírito Santo revealed a complex pattern of viral spread, with multiple independent introductions of the virus into the state. The samples clustered within the $OROV_{Brazil2015-2024}$ clade, specifically within the $M_1L_2S_2$ reassortant lineage that caused the recent outbreak in the Amazon region (*14*). The absence of monophyly in the S and M segment trees suggests that multiple introduction events occurred followed by local spread through different routes, as described in Gräf et al. (*17*). That molecular pattern corroborates the epidemiologic data showing the initial emergence of imported cases

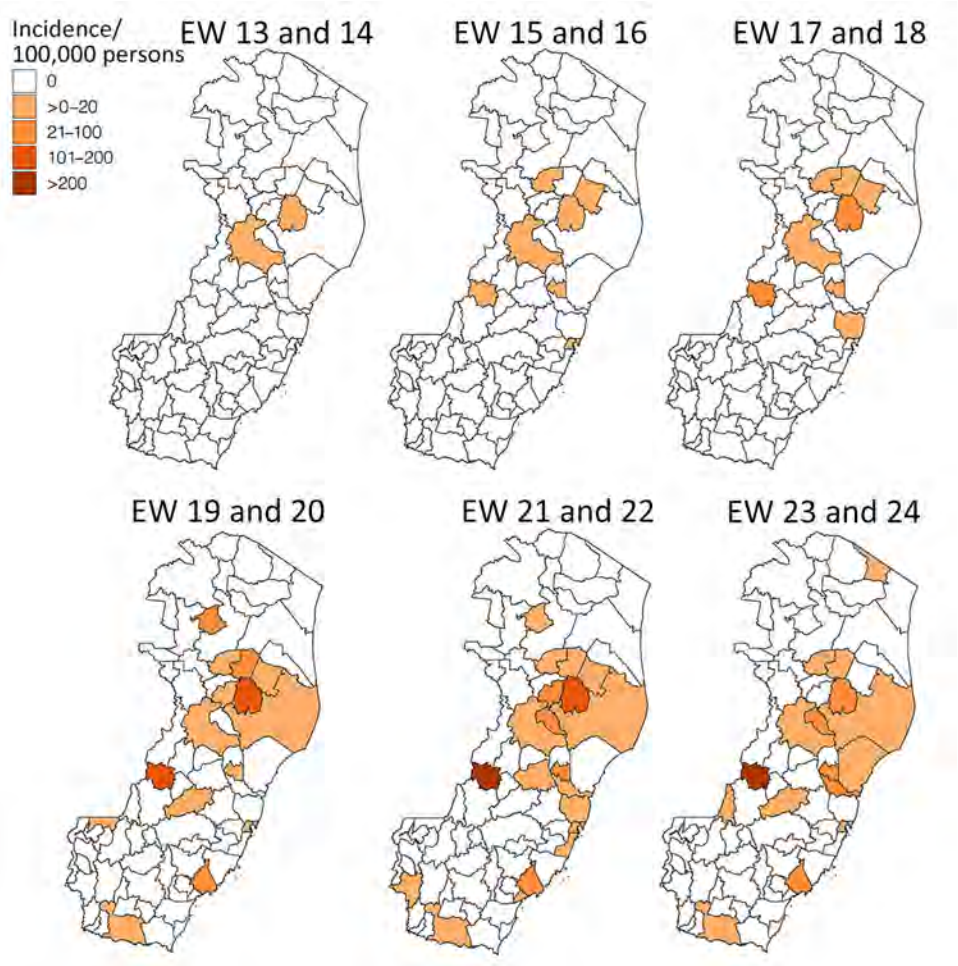

Figure 4. Oropouche virus case incidence by municipality and 2-week epidemiologic period, Espírito Santo state, Brazil. EW, epidemiologic week.

followed by rapid establishment of autochthonous transmission in different municipalities. Further genomic surveillance is needed to fully understand the dispersal patterns and the state's role in the virus's spread to other regions, highlighting the need for comprehensive and continuous surveillance throughout the region.

The predominance of OROV transmission in regions with tropical climates (Köppen-Geiger classifications Aw and Am) highlights the critical role of environmental conditions that favor a high prevalence of potential vectors, particularly *C. paraensis* midges. Although comprehensive studies on *Culicoides* spp. distribution across climate zones of Brazil are lacking, studies in Europe have documented strong associations between Köppen climate classifications and *Culicoides* spp. diversity (*46*). The tropical climates of Espírito Santo outbreak zones have high temperatures and seasonal rainfall, likely creating optimal conditions for *C. paraensis* breeding. Those environments provide abundant organic matter for larval development; decomposing vegetation, fruit waste, banana tree stumps, and cacao husks, common agricultural byproducts in the region, are ideal breeding sites (*3*,*4*,*27*). Indeed, studies report peak *C. paraensis* midge populations during the rainy season; temperatures are 30°C–32°C and relative humidity 75%–85% (*47*), favorable macroclimatic and microclimatic conditions for vector proliferation. In contrast, temperate and subtropical highland climates, characterized by lower temperatures, more evenly distributed rainfall, and distinct vegetation, present less favorable conditions

Table. Association between agricultural crop cultivation and Oropouche virus cases, Espírito Santo, Brazil*

Crop	Spearman ρ (95% CI)	p value
Robusta coffee	0.549 (0.185–0.781)	**0.004**
Cocoa	0.530 (0.159–0.770)	**0.006**
Coconut	0.434 (0.035–0.714)	**0.030**
Pepper	0.426 (0.024–0.709)	**0.034**
Banana	0.345 (−0.070 to 0.658)	0.091
Orange	0.037 (−0.374 to 0.436)	0.861
Cassava	0.026 (−0.384 to 0.427)	0.902
Corn	−0.086 (−0.475 to 0.331)	0.684
Bean	−0.213 (−0.569 to 0.211)	0.307
Arabica coffee	−0.259 (−0.601 to 0.164)	0.212

*Bold text indicates statistically significant correlation (p<0.05).

for vector establishment. Despite the widespread distribution of *Culicoides* spp. midges across the Americas (*28*), no cases of OROV had been reported in Espírito Santo state until 2024. The introduction of OROV into Espírito Santo is estimated to have occurred multiple times during February–March 2024 (*17*), and its establishment may reflect ecologic shifts that have amplified vector density or increased human–vector contact, particularly among susceptible populations in Espírito Santo and other regions of Brazil. Espírito Santo's recent biting midge infestation in 2019 (*48*) likely supported conditions for OROV emergence by increasing vector populations in previously unaffected areas. Climate change projections in Europe suggest a shift toward warmer and wetter conditions that may transform humid subtropical climates into subtropical climates with hot summers, further promoting *Culicoides* spp. establishment (*46*). Modeling studies indicate that climate-driven increases in temperature and extreme weather events could expand arboviral transmission in tropical regions like Espírito Santo, as observed for DENV (*49*). These ecologic changes likely interact with agricultural and land-use patterns, shaping OROV transmission and creating corridors that intensify

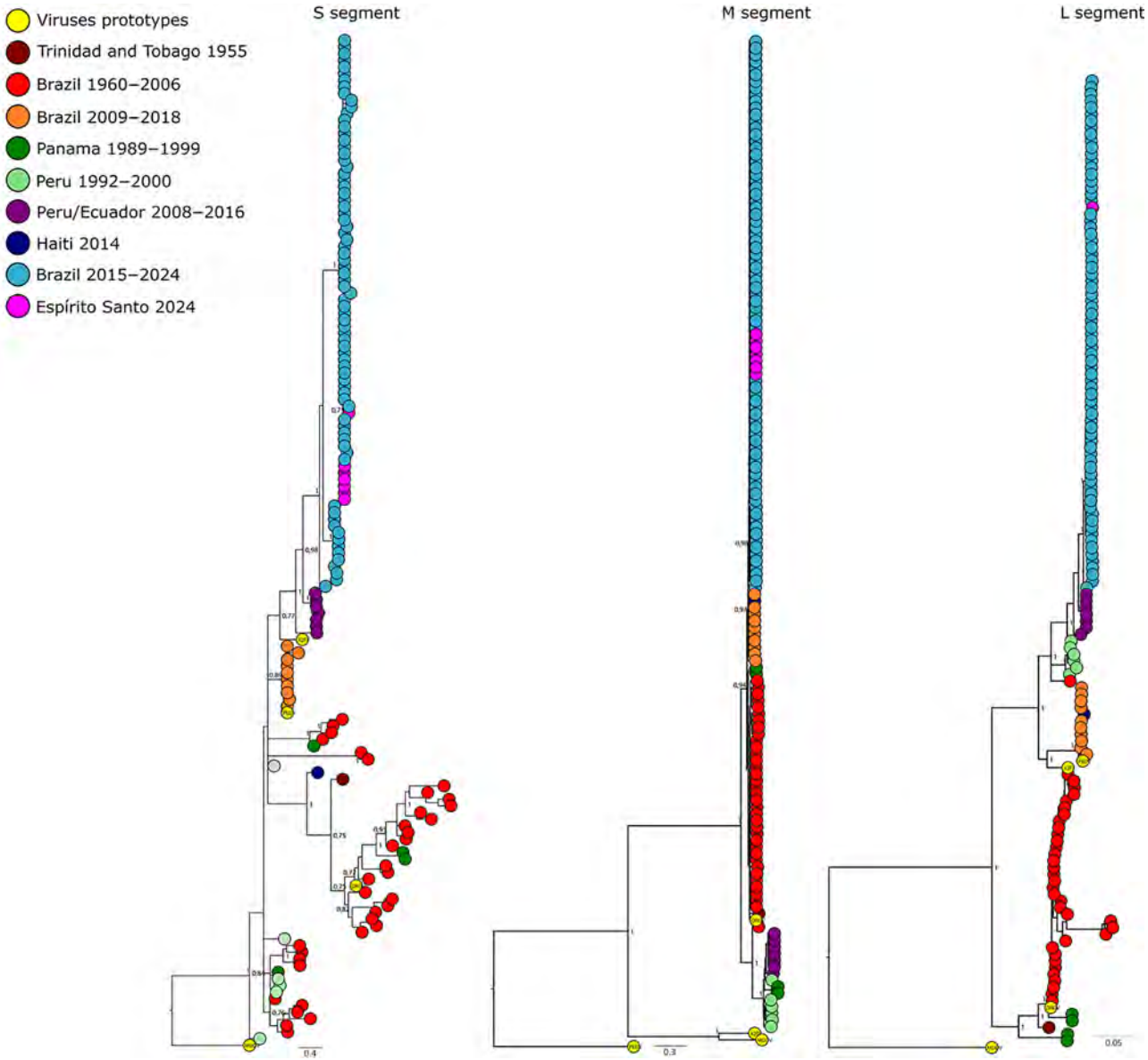

Figure 5. Bayesian phylogenetic trees created from analysis of Oropouche virus segments associated with the reassortant lineage $M_1L_2S_2$ in Espírito Santo, Brazil, and reference sequences. Each tree includes a representative subsample of genomes from the epidemic clade (highlighted); tip colors indicate sampling locations. Branch support values are shown for the main clades. Scale bars indicate the number of nucleotide substitutions per site. S, small; M, medium; L, long.

virus-vector-host interactions. Further research is warranted to quantify the relationships between climatic variables, *C. paraensis* species dynamics, and OROV transmission in Espírito Santo and other countries.

The significant correlations between OROV incidence and specific crops in Espírito Santo underscore the complex interactions between agricultural landscapes and arboviral transmission dynamics. Outside the Amazon region, OROV transmission has been predominantly associated with rural settings, where *C. paraensis* midges find optimal breeding conditions. *C. paraensis* larvae develop effectively in microhabitats created by decaying organic matter from banana and cacao plantations (*3*,*4*,*27*); of note, recent outbreaks outside the Amazon have occurred along the Atlantic Forest biome where these crops are prevalent (*17*). The emergence of OROV in Espírito Santo's regions with high densities of robusta coffee, pepper, and coconut cultivation represents a novel association that warrants further investigation, because it would broaden our understanding of potential agricultural landscapes that may support *C. paraensis* populations. That pattern aligns with the vector's documented ability to occupy both sylvatic and anthropic environments (*28*) and suggests that agricultural expansion may create ecologic pathways that encourage viral spread. The fragmentation of forest landscapes by agricultural activities likely intensifies human–vector contact, particularly in areas where multiple crops create diverse microhabitats suitable for vector breeding. The strong presence of OROV in Espírito Santo's major agricultural regions, especially where coffee and cacao cultivation predominate, emphasizes the need for detailed ecologic studies of *C. paraensis* midges in those settings to identify and predict potential outbreak hotspots.

Our study provides valuable insights into environmental and ecologic factors influencing OROV emergence in Espírito Santo. A limitation is that inferences about spatial dissemination relied on assumptions regarding the primary vector, *C. paraensis* midges, without directly assessing its competence, density, or dispersal potential, which may affect estimates of transmission dynamics. In addition, reliance on secondary epidemiologic data, rather than targeted field sampling, limits the granularity and completeness of information on transmission patterns and hotspots. Observed correlations between OROV cases and crops might also reflect geographic clustering effects, potentially introducing spatial biases. Future research with fine-scale spatial modeling and systematic vector surveillance is essential to clarify interactions among environmental variables, vector ecology, and OROV transmission dynamics.

In conclusion, our study reveals a substantial epidemiologic shift marked by the emergence and establishment of OROV in Espírito Santo, underscoring the virus's capacity to adapt to new ecologic landscapes outside its Amazon origins. The rapid rise in OROV cases to levels comparable with established arboviruses like DENV and CHIKV, without apparent competitive inhibition, highlights the distinct ecologic niches exploited by *Culicoides* spp. vectors in periurban and rural areas. The interplay between tropical climate, expanding agricultural landscapes, and favorable breeding sites for *C. paraensis* midges likely enabled this outbreak, positioning Espírito Santo as a potential hotspot for arboviral transmission amid environmental and climatic changes. As such, our findings call for heightened surveillance of both human cases and vector populations along with further investigation into the eco-epidemiologic drivers of OROV in Atlantic Forest regions. Understanding those dynamics will be crucial to predict, prevent, and respond to future outbreaks of OROV and other emerging arboviruses in similar environments.

This article was preprinted at https://www.medrxiv.org/content/10.1101/2024.12.11.24318883v1.full.pdf.

Acknowledgments

We thank the staff at Laboratório Central de Saúde Pública do Espírito Santo and the Adolfo Lutz Institute for their invaluable contributions to this study. Their dedication to public health was instrumental in the successful completion of our research and in advancing scientific knowledge in this field. We also thank Gabriel Lessa Lavagnoli for his assistance in implementing the framework for generation time estimation.

All viral sequence data generated in this study are available in GenBank (accession nos. PQ197397–405).

This study was partially funded by a grant from the State of Espírito Santo Government through the Fundação de Amparo à Pesquisa e Inovação do Espírito Santo (FAPES) (grant no. 2025-25N6P-DI 006/2025-SESA/SEAG/FAPES). This study also received institutional support from the Brazilian Ministry of Health and the Espírito Santo State Government. A.R. is a doctoral fellow funded by FAPES under the PROCAP 2025 program (grant no. 2025-0Z48T, DI 106/2025). F.G.N. is supported by FAPEAM call 04/2022/FIOCRUZ/FAPEAM/FAPERO–Inovação na Amazônia; FAPEAM–call 023/2022–Iniciativa Amazônia+10; and Conselho Nacional de Desenvolvimento Científico e Tecnológico–CNPq–Chamada CNPq/MCTI 10/2023– Faixa B–Grupos Consolidados–Universal 2023 (421620/2023-4). The authors declare no conflicts of interest.

About the Author

Dr. Delatorre is a professor and researcher at the Federal University of Espírito Santo, specializing in viral genomics and infectious disease epidemiology. His research focuses on the evolutionary dynamics and spatial-temporal dispersion of emerging viruses, with an emphasis on genomic surveillance and public health responses.

References

1. de Souza WM, Calisher CH, Carrera JP, Hughes HR, Nunes MRT, Russell B, et al. ICTV virus taxonomy profile: *Peribunyaviridae* 2024. J Gen Virol. 2024;105:002034. https://doi.org/10.1099/jgv.0.002034
2. Sakkas H, Bozidis P, Franks A, Papadopoulou C. Oropouche fever: a review. Viruses. 2018;10:175. https://doi.org/10.3390/v10040175
3. Travassos da Rosa JF, de Souza WM, Pinheiro FP, Figueiredo ML, Cardoso JF, Acrani GO, et al. Oropouche virus: clinical, epidemiological, and molecular aspects of a neglected orthobunyavirus. Am J Trop Med Hyg. 2017;96:1019–30. https://doi.org/10.4269/ajtmh.16-0672
4. Wesselmann KM, Postigo-Hidalgo I, Pezzi L, de Oliveira-Filho EF, Fischer C, de Lamballerie X, et al. Emergence of Oropouche fever in Latin America: a narrative review. Lancet Infect Dis. 2024;24:e439–52. https://doi.org/10.1016/S1473-3099(23)00740-5
5. Pereira-Silva JW, Ríos-Velásquez CM, Lima GRD, Marialva Dos Santos EF, Belchior HCM, Luz SLB, et al. Distribution and diversity of mosquitoes and Oropouche-like virus infection rates in an Amazonian rural settlement. PLoS One. 2021;16:e0246932. https://doi.org/10.1371/journal.pone.0246932
6. de Thoisy B, Gräf T, Mansur DS, Delfraro A, Dos Santos CND. The risk of virus emergence in South America: a subtle balance between increasingly favorable conditions and a protective environment. Annu Rev Virol. 2024;11:43–65. https://doi.org/10.1146/annurev-virology-100422-024648
7. Baker RE, Mahmud AS, Miller IF, Rajeev M, Rasambainarivo F, Rice BL, et al. Infectious disease in an era of global change. Nat Rev Microbiol. 2022;20:193–205. https://doi.org/10.1038/s41579-021-00639-z
8. Naveca FG, Nascimento VA, Souza VC, Figueiredo RMPD. Human Orthobunyavirus Infections, Tefé, Amazonas, Brazil. PLoS Curr. 2018. https://doi.org/10.1371/currents.outbreaks.7d65e5eb6ef75664da68905c5582f7f7
9. Vasconcelos HB, Azevedo RSS, Casseb SM, Nunes-Neto JP, Chiang JO, Cantuária PC, et al. Oropouche fever epidemic in northern Brazil: epidemiology and molecular characterization of isolates. J Clin Virol. 2009;44:129–33. https://doi.org/10.1016/j.jcv.2008.11.006
10. Terzian ACB, Bronzoni RVM, Drumond BP, Da Silva-Nunes M, Santos da Silva N, Ferreira MU, et al. Sporadic Oropouche virus infection, acre, Brazil. Emerg Infect Dis. 2009;15:348–50. https://doi.org/10.3201/eid1502.080401
11. Mourão MPG, Bastos MS, Gimaqu JBL, Mota BR, Souza GS, Grimmer GHN, et al. Oropouche fever outbreak, Manaus, Brazil, 2007–2008. Emerg Infect Dis. 2009;15:2063–4. https://doi.org/10.3201/eid1512.090917
12. Azevedo RS, Nunes MRT, Chiang JO, Bensabath G, Vasconcelos HB, Pinto AYDN, et al. Reemergence of Oropouche fever, northern Brazil. Emerg Infect Dis. 2007;13:912–5. https://doi.org/10.3201/eid1306.061114
13. Pan American Health Organization, World Health Organization. Epidemiological alert. Oropouche in the Region of the Americas: vertical transmission event under investigation in Brazil—July 17, 2024. 2024 [cited 2025 Apr 17]. https://www.paho.org/pt/documentos/alerta-epidemiologico-oropouche-na-regiao-das-americas-evento-transmissao-vertical-sob
14. Naveca FG, Almeida TAP, Souza V, Nascimento V, Silva D, Nascimento F, et al. Human outbreaks of a novel reassortant Oropouche virus in the Brazilian Amazon region. Nat Med. 2024;30:3509–21. https://doi.org/10.1038/s41591-024-03300-3
15. Scachetti GC, Forato J, Claro IM, Hua X, Salgado BB, Vieira A, et al. Re-emergence of Oropouche virus between 2023 and 2024 in Brazil: an observational epidemiological study. Lancet Infect Dis. 2025;25:166–75. https://doi.org/10.1016/S1473-3099(24)00619-4
16. Moreira FRR, Dutra JVR, de Carvalho AHB, Reis CR, Rios JSH, Ribeiro MO, et al. Oropouche virus genomic surveillance in Brazil. Lancet Infect Dis. 2024;24:e664–6. https://doi.org/10.1016/S1473-3099(24)00558-9
17. Gräf T, Delatorre E, do Nascimento Ferreira C, Rossi A, Santos HGG, Pizzato BR, et al.; OROV Study Group. Expansion of Oropouche virus in non-endemic Brazilian regions: analysis of genomic characterisation and ecological drivers. Lancet Infect Dis. 2025;25:379–89. https://doi.org/10.1016/S1473-3099(24)00687-X
18. Bandeira AC, Pereira FM, Leal A, Santos SPO, Barbosa AC, Souza MSPL, et al. Fatal Oropouche virus infections in nonendemic region, Brazil, 2024. Emerg Infect Dis. 2024;30:2370–4. https://doi.org/10.3201/eid3011.241132
19. das Neves Martins FE, Chiang JO, Nunes BTD, Ribeiro BFR, Martins LC, Casseb LMN, et al. Newborns with microcephaly in Brazil and potential vertical transmission of Oropouche virus: a case series. Lancet Infect Dis. 2025; 25:155–65. https://doi.org/10.1016/S1473-3099(24)00617-0
20. Garcia Filho C, Lima Neto AS, Maia AMPC, da Silva LOR, Cavalcante RDC, Monteiro HDS, et al. A case of vertical transmission of Oropouche virus in Brazil. N Engl J Med. 2024;391:2055–7. https://doi.org/10.1056/NEJMc2412812
21. Secretaria de Vigilância em Saúde e Ambiente, Ministério da Saúde. Monitoring of arboviruses and closing balance of the Emergency Operations Committee (COE) dengue and other arboviruses 2024 [in Portuguese]. Boletim Epidemiológico vol. 55, no. 11. 2024 [cited 2025 Apr 17]. https://www.gov.br/saude/pt-br/centrais-de-conteudo/publicacoes/boletins/epidemiologicos/edicoes/2024/boletim-epidemiologico-volume-55-no-11.pdf/view
22. Galeano EAV, Padovan MP, de Figueiredo MRP, Takemoto ACK, Maioli HRO. Performance of agricultural production in Espírito Santo from 2010 to 2022 [in Portuguese]. Vitoria, Brazil: Incaper (Instituto Capixaba de Pesquisa, Assistência Técnica e Extensão Rural); 2024 [cited 2025 Apr 17]. https://biblioteca.incaper.es.gov.br/digital/bitstream/item/4703/1/Doc311-DesempenhodaProducadoES-Incaper.pdf
23. Naveca FG, Nascimento VAD, Souza VC, Nunes BTD, Rodrigues DSG, Vasconcelos PFDC. Multiplexed reverse transcription real-time polymerase chain reaction for simultaneous detection of Mayaro, Oropouche, and Oropouche-like viruses. Mem Inst Oswaldo Cruz. 2017;112:510–3. https://doi.org/10.1590/0074-02760160062
24. Instituto Brasileiro de Geografia e Estatística. 2022 Census. 2025 [cited 2025 Apr 17]. https://www.ibge.gov.br/en/statistics/social/labor/22836-2022-census-3.html

25. Instituto Brasileiro de Geografia e Estatística. Geosciences downloads. 2025 [cited 2025 Apr 17]. https://www.ibge.gov.br/en/geosciences/downloads-geosciences.html
26. Instituto Brasileiro de Geografia e Estatística. Census of agriculture 2017. 2025 [cited 2025 Apr 17]. https://censoagro2017.ibge.gov.br
27. Pinheiro FP, Travassos da Rosa AP, Travassos da Rosa JF, Ishak R, Freitas RB, Gomes ML, et al. Oropouche virus. Am J Trop Med Hyg. 1981;30:149–60. https://doi.org/10.4269/ajtmh.1981.30.149
28. Mellor PS, Boorman J, Baylis M. *Culicoides* biting midges: their role as arbovirus vectors. Annu Rev Entomol. 2000;45:307–40. https://doi.org/10.1146/annurev.ento.45.1.307
29. McGregor BL, Connelly CR, Kenney JL. Infection, dissemination, and transmission potential of North American *Culex quinquefasciatus*, *Culex tarsalis*, and *Culicoides sonorensis* for Oropouche virus. Viruses. 2021;13:226. https://doi.org/10.3390/v13020226
30. Ferguson NM, Cucunubá ZM, Dorigatti I, Nedjati-Gilani GL, Donnelly CA, Basáñez MG, et al. Countering the Zika epidemic in Latin America. Science. 2016;353:353–4. https://doi.org/10.1126/science.aag0219
31. Caicedo EY, Charniga K, Rueda A, Dorigatti I, Mendez Y, Hamlet A, et al. The epidemiology of Mayaro virus in the Americas: A systematic review and key parameter estimates for outbreak modelling. PLoS Negl Trop Dis. 2021;15:e0009418. https://doi.org/10.1371/journal.pntd.0009418
32. Cori A, Ferguson NM, Fraser C, Cauchemez S. A new framework and software to estimate time-varying reproduction numbers during epidemics. Am J Epidemiol. 2013;178:1505–12. https://doi.org/10.1093/aje/kwt133
33. da Silva AF, da Silva Neto AM, Aksenen CF, Jeronimo PMC, Dezordi FZ, Almeida SP, et al. ViralFlow v1.0-a computational workflow for streamlining viral genomic surveillance. NAR Genom Bioinform. 2024;6:lqae056. https://doi.org/10.1093/nargab/lqae056
34. Katoh K, Standley DM. MAFFT multiple sequence alignment software version 7: improvements in performance and usability. Mol Biol Evol. 2013;30:772–80. https://doi.org/10.1093/molbev/mst010
35. Ronquist F, Teslenko M, van der Mark P, Ayres DL, Darling A, Höhna S, et al. MrBayes 3.2: efficient Bayesian phylogenetic inference and model choice across a large model space. Syst Biol. 2012;61:539–42. https://doi.org/10.1093/sysbio/sys029
36. Metsky HC, Matranga CB, Wohl S, Schaffner SF, Freije CA, Winnicki SM, et al. Zika virus evolution and spread in the Americas. Nature. 2017;546:411–5. https://doi.org/10.1038/nature22402
37. Souza TML, Vieira YR, Delatorre E, Barbosa-Lima G, Luiz RLF, Vizzoni A, et al. Emergence of the East-Central-South-African genotype of Chikungunya virus in Brazil and the city of Rio de Janeiro may have occurred years before surveillance detection. Sci Rep. 2019;9:2760. https://doi.org/10.1038/s41598-019-39406-9
38. Kramer LD, Ciota AT, Kilpatrick AM. Introduction, Spread, and Establishment of West Nile Virus in the Americas. J Med Entomol. 2019;56:1448–55. https://doi.org/10.1093/jme/tjz151
39. Segura NA, Muñoz AL, Losada-Barragán M, Torres O, Rodríguez AK, Rangel H, et al. Minireview: epidemiological impact of arboviral diseases in Latin American countries, arbovirus-vector interactions and control strategies. Pathog Dis. 2021;79:ftab043. https://doi.org/10.1093/femspd/ftab043
40. Kucharski AJ, Funk S, Eggo RM, Mallet HP, Edmunds WJ, Nilles EJ. Transmission dynamics of Zika virus in island populations: a modelling analysis of the 2013–14 French Polynesia outbreak. PLoS Negl Trop Dis. 2016;10:e0004726. https://doi.org/10.1371/journal.pntd.0004726
41. Nishiura H, Mizumoto K, Villamil-Gómez WE, Rodríguez-Morales AJ. Preliminary estimation of the basic reproduction number of Zika virus infection during Colombia epidemic, 2015–2016. Travel Med Infect Dis. 2016;14:274–6. https://doi.org/10.1016/j.tmaid.2016.03.016
42. Carvalho VL, Azevedo RSS, Carvalho VL, Azevedo RS, Henriques DF, Cruz ACR, et al. Arbovirus outbreak in a rural region of the Brazilian Amazon. J Clin Virol. 2022; 150-151:105155. https://doi.org/10.1016/j.jcv.2022.105155
43. Silva-Caso W, Aguilar-Luis MA, Palomares-Reyes C, Mazulis F, Weilg C, Del Valle LJ, et al. First outbreak of Oropouche fever reported in a non-endemic western region of the Peruvian Amazon: molecular diagnosis and clinical characteristics. Int J Infect Dis. 2019;83:139–44. https://doi.org/10.1016/j.ijid.2019.04.011
44. Vaughn DW, Green S, Kalayanarooj S, Innis BL, Nimmannitya S, Suntayakorn S, et al. Dengue viremia titer, antibody response pattern, and virus serotype correlate with disease severity. J Infect Dis. 2000;181:2–9. https://doi.org/10.1086/315215
45. Bhatt P, Jayaram A, Varma M, Mukhopadhyay C. Kinetics of dengue viremia and its association with disease severity: an ambispective study. Virusdisease. 2024;35:250–9. https://doi.org/10.1007/s13337-024-00872-z
46. Brugger K, Rubel F. Characterizing the species composition of European *Culicoides* vectors by means of the Köppen-Geiger climate classification. Parasit Vectors. 2013;6:333. https://doi.org/10.1186/1756-3305-6-333
47. Feitoza LHM, de Carvalho LPC, da Silva LR, Meireles ACA, Rios FGF, Silva GS, et al. Influence of meteorological and seasonal parameters on the activity of *Culicoides paraensis* (Diptera: Ceratopogonidae), an annoying anthropophilic biting midge and putative vector of Oropouche virus in Rondônia, Brazilian Amazon. Acta Trop. 2023;243:106928. https://doi.org/10.1016/j.actatropica.2023.106928
48. Prefeitura de Marechal Floriano. Anchieta, Alfredo Chaves and Marechal unite to try to fight the advance of the maruim. 2024 [cited 2025 Apr 17]. https://www.marechalfloriano.es.gov.br/anchieta-alfredo-chaves-e-marechal-se-unem-para-tentar-combater-avanco-do-maruim
49. Barcellos Madeira Rosa Y, Tamanini Silva Moschen H, Loss AC, Cardoso da Silva TC, Brioschi Dos Santos AP, Caetano Pimenta B, et al. Climate change impacts on dengue transmission areas in Espírito Santo state, Brazil. Oxf Open Immunol. 2024;5:iqae011. https://doi.org/10.1093/oxfimm/iqae011

Address for correspondence: Edson Delatorre, Laboratório de Genômica e Ecologia Viral, Centro de Ciências da Saúde, Universidade Federal do Espírito Santo, Av. Marechal Campos, 1468–Maruípe, 29.040-090, Vitória, ES, Brazil; email: edson.delatorre@ufes.br

Cadaveric Human Growth Hormone–Associated Creutzfeldt-Jakob Disease with Long Latency Period, United States

Anatevka S. Ribeiro, Andrew B. Wolf, Ellen W. Leschek, Lawrence B. Schonberger, Joseph Y. Abrams, Ryan A. Maddox, Brian S. Appleby, Katie Glisic, Aaron Carlson, Elizabeth Matthews

We report a case of iatrogenic Creutzfeldt-Jakob disease (iCJD) after a 48.3-year incubation period in a patient treated with cadaveric human growth hormone. iCJD was pathologically confirmed; genetic analysis was negative for pathogenic mutations. Clinicians should consider iCJD in patients with progressive neurologic signs who had received cadaveric human growth hormone treatment.

Prion diseases are fatal neurodegenerative disorders caused by pathogenic misfolded prion protein (PrP^{Sc}). PrP^{Sc} induces surrounding normal proteins to misfold, leading to a pathologic misfolding cascade that results in widespread neuronal cell death. Creutzfeldt-Jakob disease (CJD) is a prion disease that is considered transmissible because iatrogenic PrP^{Sc} exposure in specific circumstances can trigger the disease.

The 3 forms of CJD are defined according to the mechanism by which PrP^{Sc} is acquired: sporadic (sCJD), iatrogenic (iCJD), and genetic (gCJD) (*1*,*2*). sCJD generally has a slower primarily cognitive nonfocal onset, but iCJD progresses rapidly with focal symptoms such as ataxia and jerky movements (*1*). iCJD has been a particular public health concern because of the potential for outbreaks. A well-described cause of iCJD is cadaveric human growth hormone (chGH), which was used to treat growth failure in ≈7,700 US patients during the 1960s through the 1980s through the National Hormone Pituitary Program (NHPP) (*3*). We report a case of iCJD after a long latency period in a patient treated with chGH in the 1970s.

The Study

A 58-year-old woman was evaluated for a 2-week history of gait imbalance and tremors. Her medical history was notable for depression, cervical spine fusion, and idiopathic panhypopituitarism. She received chGH treatment for 9.3 years through NHPP, starting in late 1971 at 7 years of age.

Initial neurologic examination revealed frequent lateral movements of the head and trunk and hand movements that were irregular in amplitude and frequency without a null point that resolved with distraction. The examination was otherwise unremarkable, including gait evaluation, despite subjective gait impairment. The attending physician favored a diagnosis of functional neurologic disorder.

Brain and cervical spine contrast magnetic resonance imaging (MRI) at initial examination was unremarkable (Figure 1, panels A, B). Mayo Clinic Autoimmune Movement Disorders Panel and HIV screening results were negative, and copper, vitamin E, and vitamin B12 levels were within reference ranges. The patient was referred to the movement disorders clinic and advised to start physical therapy and continue psychological treatment.

Over the next 4 weeks, urinary incontinence, worsening tremors, decreased speech output, and gait disturbance developed. She returned to the hospital

Author affiliations: University of California, Irvine, Orange, California, USA (A.S. Ribeiro); University of Colorado School of Medicine, Aurora, Colorado, USA (A.S. Ribeiro, A.B. Wolf); National Institutes of Health, National Institute of Diabetes, Digestive and Kidney Diseases, Bethesda, Maryland, USA (E.W. Leschek); Centers for Disease Control and Prevention, Atlanta, Georgia, USA (L.B. Schonberger, J.Y. Abrams, R.A. Maddox); Case Western Reserve University, National Prion Disease Pathology Surveillance Center, Cleveland, Ohio, USA (B.S Appleby, K. Glisic); University Hospitals Cleveland Medical Center, Cleveland (B.S. Appleby, K. Glisic); University of Colorado Anschutz Medical Campus, Aurora (A. Carlson, E. Matthews)

DOI: https://doi.org/10.3201/eid3106.241519

with tachypnea, hyperekplexia, and appendicular rigidity. Her respiratory status and alertness rapidly declined, and she required intubation. Over several days, both stimulus-induced and spontaneous myoclonus developed, and she remained comatose.

A repeat brain MRI 2 months after the initial MRI demonstrated subtle areas of symmetric T2 hyperintensity in the insulae and frontotemporal lobes and deep gray structures with diffusion restriction along the bilateral insulae and caudate heads without gadolinium enhancement (Figure 1, panels C, D). Continuous electroencephalogram showed frequent 1–2.5 Hz generalized periodic discharges lasting 3–9 seconds. Antinuclear antibody level was mildly positive at 1:160; all other serum test results, including autoantibody evaluations, were unremarkable. Cerebrospinal fluid viral and autoantibody results were negative. Oligoclonal bands were absent. Prion testing, performed at the National Prion Disease Pathology Surveillance Center (NPDPSC), Case Western Reserve University (Cleveland, Ohio), revealed elevated total τ of 9,104 pg/mL (reference <1,149 pg/mL) and elevated 14-3-3 protein level of 30,868 AU/mL (reference <1,999 AU/mL); real-time quaking-induced conversion assay was positive for prions. In accordance with her predetermined wishes, the patient was palliatively extubated and died.

Autopsy performed at NPDPSC confirmed CJD by Western blot and immunohistochemistry analysis on brain tissue. *PRNP* genetic analysis was negative for pathogenic mutations, supporting a diagnosis of iCJD in the context of prior chGH treatment. The patient had a methionine/valine (M/V) polymorphism at codon 129 of the *PRNP* gene, which has been associated with longer latency periods in acquired human prion disease (*1*,*4*).

Cases of iCJD linked to chGH were first recognized in the United States in 1985 (*1*,*4*,*5*). Those reported iCJD cases led to the immediate cessation of chGH production and administration by the NHPP. Shortly thereafter, chGH was replaced with recombinant (biosynthetic) human growth hormone. Nevertheless, the iCJD outbreak linked to chGH continued because the latency period could be long among some previous chGH recipients. Latency or incubation periods for prion diseases have been shown to be variable and depend upon multiple factors, including the infectious particle dose, because higher doses are associated with shorter latency; route of infection, because central nervous system exposures are generally associated with shorter latency than peripheral exposures; and recipient genetics, particularly the codon 129 polymorphism in the *PRNP* gene (*6*). This patient was the 36th identified iCJD case among US NHPP chGH recipients and the 254th chGH-associated iCJD case reported worldwide as of January 2024 (*3*).

Determining the precise latency period for chGH-associated iCJD cases is often impossible because chGH exposure typically occurred over many years. Thus, latency must be estimated using one of several methods. First, latency can be calculated from the first dose of chGH to the onset of iCJD symptoms, which provides the maximum possible latency period. Second, latency can be estimated by calculating time from the midpoint of chGH treatment to iCJD symptom onset and is a standard estimate method used in other studies (*7*). Third, latency can be calculated as the time between the last dose of chGH and the onset of symptoms, which provides the minimum possible latency period. A final way to estimate latency is to use the midpoint of chGH treatment calculated from the first chGH dose to the end of 1977; then, latency is calculated between that midpoint and symptom onset. The reason for considering that method of calculation involves the epidemiology of the US outbreak, which suggests that

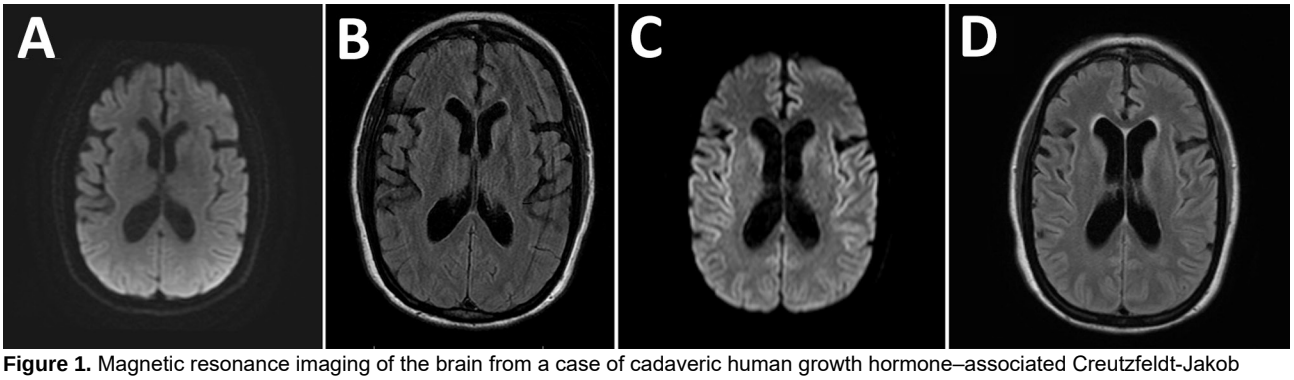

Figure 1. Magnetic resonance imaging of the brain from a case of cadaveric human growth hormone–associated Creutzfeldt-Jakob disease with long latency period, United States. A, B) Images obtained at initial clinical examination were unremarkable. C, D) Images obtained 3 months later demonstrated subtle areas of symmetric T2 hyperintensity in the insulae and frontotemporal lobes (C) and deep gray structures with diffusion restriction along the bilateral insulae and caudate heads without gadolinium enhancement (D).

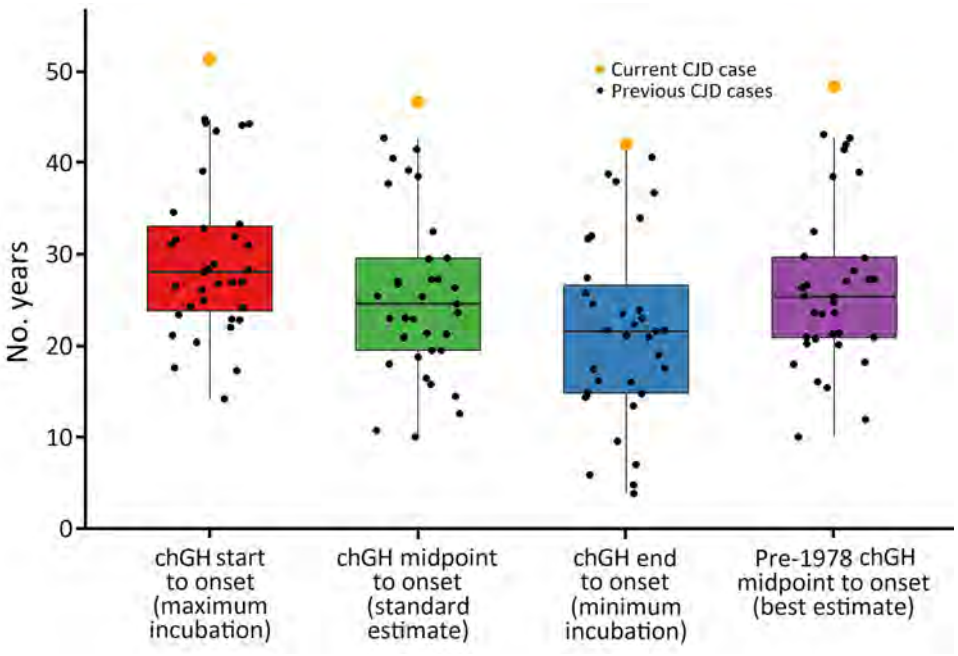

Figure 2. Comparison of latency estimates among US cases in a study of chGH-associated CJD with long latency period, United States. The patient in this report (current CJD case) was treated with chGH for 9.3 years starting in late 1971 at 7 years of age, and neurologic symptoms developed when she was 58 years of age. We used data from all 36 US cases of chGH-associated CJD to compare estimates of CJD latency periods via 4 methods: first dose of chGH to symptom onset (red), midpoint of chGH treatment to symptom onset (green), last dose of chGH to symptom (blue), and midpoint of pre-1978 chGH to symptom onset (purple). Using those 4 methods, we believe the last (purple box plot) to be the most accurate, giving a best estimate of 48.3 years for our patient's latency period. Black dots indicate other CJD cases, box top and bottoms indicate 25th and 75th percentiles, horizontal lines inside boxes indicate medians, and whiskers extend to the furthest observed points within 1.5 times the interquartile range from the 25th and 75th percentiles. chGH, cadaveric human growth hormone; CJD, Creutzfeldt-Jakob disease.

the most likely source of iCJD infection came from chGH administered before or during 1977, even though most of the ≈7,700 NHPP recipients started chGH treatment after 1977 (*8*). Of note, none of the 36 US iCJD cases exclusively received post-1977 chGH, likely because the NHPP developed a new laboratory method to extract chGH from pituitary glands in 1977. That method included column purification to separate and collect multiple hormones from the glands, a procedure now known to have greatly reduced prion contamination (*3*,*8*).

We performed all 4 latency estimate calculations for our patient. First dose of chGH to symptom onset was 51.3 years, midpoint of chGH treatment to symptom onset was 46.7 years, last dose of chGH to symptom onset was 42.1 years, and midpoint of pre-1978 chGH to symptom onset was 48.3 years. We compared our patient's latency estimate calculation to all US chGH-associated iCJD cases (Figure 2), and given the evidence implicating pre-1978 chGH, we considered the final method to provide the most accurate estimate of 48.3 years latency.

Conclusions

In the ongoing US iCJD outbreak resulting from chGH, the shortest estimated latency was 10 years, whereas among the first 226 cases reported internationally, the shortest latency was 5 years, suggesting a lower level of prion contamination in the US NHPP-distributed chGH (*9*). In addition, experimental transmission studies in nonhuman primates using samples from all 76 lots of chGH retained on file at the US NHPP demonstrated that prion contamination was rare, random, and at a low level (*10*). That low level of contamination, the purification step introduced in the United States in 1977, and the peripheral route of administration created an environment that would be expected to result in longer latency periods.

Although the US iCJD outbreak has slowed substantially, the potential for new cases remains, particularly among persons who are heterozygous M/V at codon 129 of the *PRNP* gene. Clinicians should recognize the continued possibility of chGH-associated CJD cases and include iCJD in the differential diagnosis for anyone with new neurologic symptoms and prior chGH exposure, particularly patients exposed to chGH before the 1977 updated purification process.

Acknowledgments

We extend our deepest gratitude to the patients and families affected by the NHPP. We acknowledge Centers for Disease Control and Prevention and the National Institutes of Health for their collaboration, guidance, and commitment to public health. In addition, we thank Natalie Marzec, who served as a liaison with the state during the investigation into this case.

Historical and cohort data were derived from the National Hormone Pituitary Program database. Management of this database is performed by Westat, which is funded by National Institutes of Health contract no. GS00F009DA.

About the Author

Dr. Ribeiro is a neuro-oncology fellow at the University of California, Irvine. Her primary research interests include medical education and low-grade gliomas.

References

1. Watson N, Brandel JP, Green A, Hermann P, Ladogana A, Lindsay T, et al. The importance of ongoing international surveillance for Creutzfeldt-Jakob disease. Nat Rev Neurol. 2021;17:362–79. https://doi.org/10.1038/s41582-021-00488-7
2. Appleby BS, Shetty S, Elkasaby M. Genetic aspects of human prion diseases. Front Neurol. 2022;13:1003056. https://doi.org/10.3389/fneur.2022.1003056
3. National Institutes of Health, National Institute of Diabetes and Digestive and Kidney Diseases. National Hormone & Pituitary Program (NHPP): information for people treated with pituitary human growth hormone [cited 2024 Jul 28]. https://www.niddk.nih.gov/health-information/endocrine-diseases/national-hormone-pituitary-program
4. Brandel JP, Preece M, Brown P, Croes E, Laplanche JL, Agid Y, et al. Distribution of codon 129 genotype in human growth hormone-treated CJD patients in France and the UK. Lancet. 2003;362:128–30. https://doi.org/10.1016/S0140-6736(03)13867-6
5. Douet JY, Huor A, Cassard H, Lugan S, Aron N, Mesic C, et al. Prion strains associated with iatrogenic CJD in French and UK human growth hormone recipients. Acta Neuropathol Commun. 2021;9:145. https://doi.org/10.1186/s40478-021-01247-x
6. Collinge J, Whitfield J, McKintosh E, Beck J, Mead S, Thomas DJ, et al. Kuru in the 21st century—an acquired human prion disease with very long incubation periods. Lancet. 2006;367:2068–74. https://doi.org/10.1016/S0140-6736(06)68930-7
7. Brown P, Brandel JP, Sato T, Nakamura Y, MacKenzie J, Will RG, et al. Iatrogenic Creutzfeldt-Jakob disease, final assessment. Emerg Infect Dis. 2012;18:901–7. https://doi.org/10.3201/eid1806.120116
8. Abrams JY, Schonberger LB, Belay ED, Maddox RA, Leschek EW, Mills JL, et al. Lower risk of Creutzfeldt-Jakob disease in pituitary growth hormone recipients initiating treatment after 1977. J Clin Endocrinol Metab. 2011;96:E1666–9. https://doi.org/10.1210/jc.2011-1357
9. Bonda DJ, Manjila S, Mehndiratta P, Khan F, Miller BR, Onwuzulike K, et al. Human prion diseases: surgical lessons learned from iatrogenic prion transmission. Neurosurg Focus. 2016;41:E10. https://doi.org/10.3171/2016.5.FOCUS15126
10. Gibbs CJ Jr, Asher DM, Brown PW, Fradkin JE, Gajdusek DC. Creutzfeldt-Jakob disease infectivity of growth hormone derived from human pituitary glands. N Engl J Med. 1993; 328:358–9. https://doi.org/10.1056/NEJM199302043280520

Address for correspondence: Anatevka S. Ribeiro, University of California Irvine, 200 S Manchester Ave, Ste 206, Orange, CA 92868, USA; email: anatevkr@hs.uci.edu

Oral Flea Preventive to Control *Rickettsia typhi*–Infected Fleas on Reservoir Opossums, Galveston, Texas, USA, 2023–2024

Lucas S. Blanton, Alejandro Villasante-Tezanos

Murine typhus, a fleaborne bacterial disease caused by *Rickettsia typhi*, has reemerged and spread in the United States. We tested spinosad, an oral flea preventive, in opossum flea reservoirs. Spinosad killed 98% of fleas infesting opossums. Oral preventives could control fleas in host species and curb murine typhus spread to humans.

Rickettsia typhi is a fleaborne bacterium that causes murine typhus, an acute undifferentiated febrile illness, in humans (*1*). The organism is classically maintained by rats and transmitted by their fleas (*Xenopsylla cheopis*). In the United States, the incidence of murine typhus drastically fell after campaigns to control rat fleas with DDT (*2*). In the past decade, murine typhus has reemerged in the United States and alarmingly increased in incidence and geographic distribution (*3*). In endemic areas of North America, murine typhus has been associated with a transmission cycle involving opossums (*Didelphis virginiana*) and cat fleas (*Ctenocephalides felis*) (*1*).

One way to reduce murine typhus is field-based control of fleas that transmit *R. typhi* to humans. Spinosad (Comfortis; Elanco, https://farmanimal.elanco.com) is an orally ingested medication (comprising spinosyn A and spinosyn D) approved for use in dogs and cats. A single monthly dose is highly effective in killing fleas by activating nicotinic acetylcholine receptors, leading to flea paralysis and death (*4*). We tested effectiveness of spinosad for killing fleas on opossums in a murine typhus–endemic area. The study was approved by the University of Texas Medical Branch Institutional Animal Care and Use Committee (protocol no. 2104030) and Texas Parks and Wildlife (scientific permit no. SPR-1020154).

Authors affiliation: University of Texas Medical Branch, Galveston, Texas, USA

DOI: https://doi.org/10.3201/eid3106.241817

The Study

To capture opossums, we deployed Havahart 1-door cage traps (81 cm × 31 cm × 25 cm) (Woodstream Corporation, https://www.woodstream.com) in Galveston, Texas, USA, during evening hours. We conducted 2 arms, comprising an experimental group and a control group. In the experimental group, we baited traps with canned cat food mixed with a crushed 270-mg spinosad tablet. In the control group, we trapped opossums using cat food without spinosad in the bait.

Spinosad starts to kill fleas within 30 minutes, and studies show it can kill 100% of fleas within 4 hours of ingestion in dogs and within 24 hours in cats (*4*). To collect dead fleas fallen from opossums, we placed a white terrycloth towel (160 cm × 84 cm) under the trap (Figure, panel A; Video, https://wwwnc.cdc.gov/EID/article/31/6/24-1817-V1.htm). To ensure trapped opossums ingested bait at least 2 hours before flea collection, we checked traps between 4 AM and 6 AM the morning after setting.

We used intramuscular ketamine (30 mg/kg) to anesthetize trapped opossums. After adequate sedation, we collected fleas by combing through the fur with a flea comb (Hartz, https://www.hartz.com) for 15 minutes, then placed fleas on masking tape and secured in sealable plastic storage bags (Figure, panels B–D). After we collected fleas from the anesthetized opossum, we collected fleas from the towel. During collections, we observed flea activity and considered moving fleas to be alive and fleas without movement to be dead. All opossums recovered uneventfully from anesthesia and were released at a distant site to avoid subsequent trapping of the same animal. We

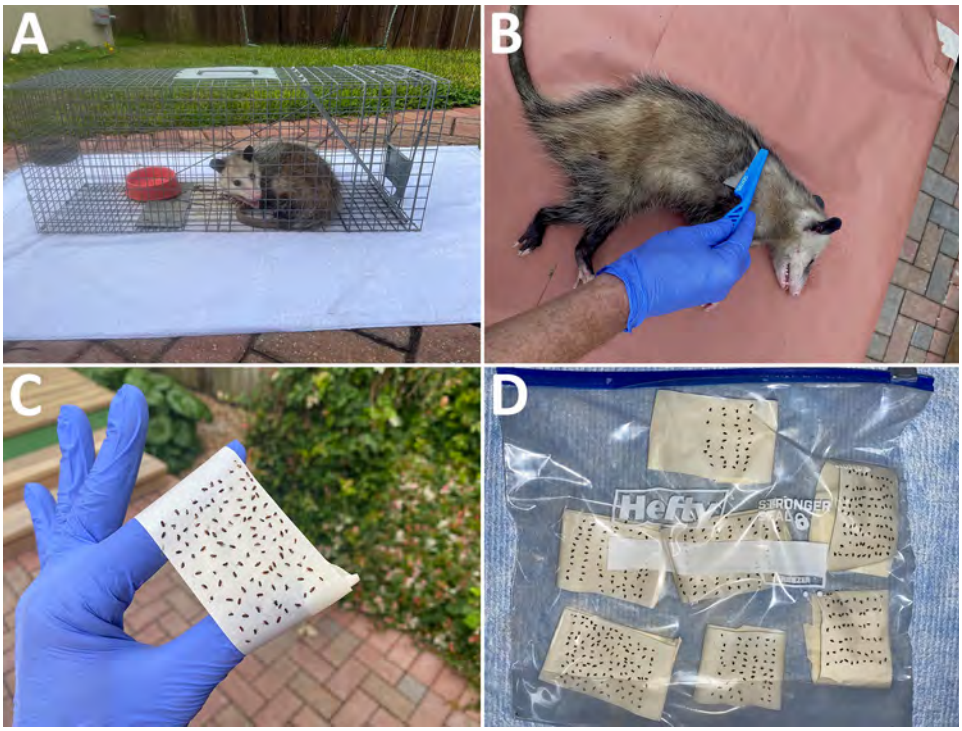

Figure. Trapping and flea collection in a study of use of oral flea preventive to control *Rickettsia typhi*–infected fleas on reservoir opossums, Galveston, Texas, USA, 2023–2024. A) Trapped opossum; B) anesthetized opossum being combed for fleas; C) masking tape displaying collected fleas; D) sealable plastic bag containing fleas from a single opossum. To determine the effectiveness of spinosad (Elanco, https://farmanimal.elanco.com) as a flea-killing agent on opossums, cage traps were baited with canned cat food mixed with a crushed 270-mg spinosad flea control tablet for the experimental group and cat food without flea control for opossums in the control group. Fleas collected from opossums ingesting spinosad were almost uniformly dead; thus, they were straightforward to collect, easy to organize when placed on tape, and remained affixed to the tape (panels C, D). On the contrary, fleas in the control group were uniformly alive when collected, moved vigorously, and could not be affixed to the tape in an organized row-by-row manner, as seen for fleas in the experimental group.

caught 3 off-target species (1 raccoon and 2 cats) and released those animals on-site without intervening procedures.

We captured 9 opossums over 19 trap nights: 5 in the experimental group and 4 in control group (Table 1). Six (66.7%) were female and 3 (33.3%) were male. The mean weight was 2.1 kg. All opossums completely ingested food within the trap. We observed fleas on all 9 opossums. Among the opossums that ingested spinosad, fleas were largely immobile and easily combed from fur; fleas were also numerous on the towel and were easily collected and bagged (Figure, panels C, D). In contrast, fleas in the control group moved rapidly within the opossums' fur; were difficult to comb off, often jumping off the comb; and would frequently escape from the tape after being bagged.

We examined collected fleas with a dissecting microscope and identified flea species by taxonomic key (*5*). We pooled fleas (dead and alive) in groups of 5–20 fleas based on the animal from which they were collected. We homogenized a subset of pools from each opossum and extracted DNA, as previously described (*6*). We used a multiplex real-time PCR to amplify and identify *R. typhi* and *R. felis* from flea homogenates (*7*).

We compared the proportion of dead fleas from the experimental and control groups. Because those

Table 1. Summary of fleas collected from opossums in a study of use of oral flea preventive to control *Rickettsia typhi*–infected fleas on reservoir opossums, Galveston, Texas, USA, 2023–2024*

Opossum no.	Group	Total no. fleas	No. live fleas	No. dead fleas	Proportion dead fleas
1	Experimental	87	7	80	0.920
3	Experimental	8	0	8	1
5	Experimental	715	1	714	0.999
6	Experimental	595	3	592	0.995
8	Experimental	247	2	245	0.992
2	Control	5	5	0	0
4	Control	54	54	0	0
7	Control	89	89	0	0
9	Control	247	247	0	0
Total		2,047	408	1,639	

*Opossums in the experimental group were captured by using traps baited with canned cat food mixed with a crushed 270-mg spinosad flea control tablet (Elanco, https://farmanimal.elanco.com); opossums in the control group were trapped in the same manner but did not receive spinosad. For both groups, opossums were sedated and combed for fleas, which we determined to be alive (moving) or dead (no movement).

Table 2. Summary of pooled fleas tested in a study of use of oral flea preventive to control *Rickettsia typhi*–infected fleas on reservoir opossums, Galveston, Texas, USA, 2023–2024*

Opossum no.	Total no. fleas	No. pools tested	No. positive pools		Infection rate, % (95% CI)	
			R. typhi	*R. felis*	*R. typhi*	*R. felis*
1	50	10	0	2	0 (0–6.3)	4.2 (0.8–13.3)
2	0†	0	NA	NA	NA	NA
3	8	3	0	0	0 (0–25.3)	0 (0–25.3)
4	54	12	9	3	24.2 (12.9–42.7)	6.1 (1.6–16.0)
5	150	10	1	6	0.7 (0–3.3)	5.5 (2.3–12.0)
6	100	10	1	2	1.0 (0.1–4.9)	2.1 (0.4–6.9)
7	89	7	0	2	0 (0–3.3)	2.4 (0.5–7.8)
8	150	10	0	4	0 (0–2.1)	3.2 (1.1–7.8)
9	143	9	0	4	0 (0–2.2)	3.2 (1.1–7.9)
Total	744	71	11	23	1.3 (0.7–2.2)	3.2 (2.2–4.6)

*Flea pools consisted of 5–20 fleas and were tested by duplex real-time PCR for *Rickettsia typhi* and *Rickettsia felis*. NA, not applicable
†Five fleas were found within the fur of opossum 2, but fleas escaped and were not collected.

proportions were bounded by 0 and 1, we transformed proportions by taking the arcsine of their square root (*8*). We needed sample sizes of at least 3 opossums in the experimental and 2 in the control groups to achieve 82% power to reject the null hypothesis with a significance level (α) of 0.05 using a 2-sided 2-sample equal-variance *t*-test. We determined rates of *R. typhi* and *R. felis* flea infection by using previously described methods (*9*) (Appendix, https://wwwnc.cdc.gov/EID/article/31/6/24-1817-App1.pdf).

We collected a total of 2,047 fleas and identified all as *Ct. felis*. The proportion of dead fleas from opossums in the experimental group was 0.98 (range 0.92–1) compared with 0 ($p<0.001$) in the control group (Table 1).

We tested 71 pools (comprising 744 fleas) by PCR; 11 pools demonstrated *R. typhi* DNA, and 23 pools demonstrated *R. felis* DNA (Table 2). Those findings correspond to an infection rate of 1.3% (95% CI 0.7–2.2) for *R. typhi* and 3.2% (95% CI 2.2–7.9) for *R. felis*. Sequenced PCR products of portions of rickettsial *htrA* (GenBank accession no. PQ625781) and *sca5* (GenBank accession no. PQ625780) of an *R. typhi*–infected flea pool detected by real-time PCR confirmed 100% homology with *R. typhi* Wilmington type strain.

Conclusions

In this study, we showed that commercially available spinosad (approximately $20 per tablet) effectively kills fleas infesting opossums. The observed animals readily fed on bait laced with the medication, and almost 100% of collected fleas were found dead at least 2 hours after opossums ingested the preventive. Although spinosad caused mild side effects (e.g., vomiting) in dogs and cats in controlled studies (*4*), little data on adverse effects in other species are available. Although we noticed no ill effects in opossums in this study, the sample size was small.

Consistent with other areas of the United States where murine typhus is endemic, we detected *R. typhi* in cat fleas collected from opossums (*6*,*10*). In contrast, other reports show few fleas collected from domestic cats are infected with *R. typhi (11*,*12)*.

Targeted efforts to control rat fleas via application of DDT on rat runs and harborages during the 1940s and 1950s exemplify how vector control can break the cycle of vectorborne disease transmission. In 1944, murine typhus peaked at 5,401 reported cases, but that number fell to <100 reported cases annually by the mid-1950s after introduction of DDT (*2*,*3*). However, the effects of DDT seemed to have little spillover into opossums (*13*), and the lingering low-level endemicity of murine typhus in the United States was eventually attributed to an alternate *R. typhi* transmission cycle involving opossums and cat fleas (*1*,*3*). Those findings support the need to focus flea control efforts on opossums in murine typhus endemic areas of the United States. More research is required to investigate the proposed methods' feasibility, effectiveness in nonexperimental conditions, logistics and toxicity among nontarget species, and effects on disease transmission in murine typhus endemic areas. For instance, in high-burden disease locations, field-deployable methods could include manual dispersion of spinosad-impregnated food pellets or timed-release dispenser stations placed at strategic distances.

In conclusion, the growing distribution and incidence of murine typhus in the United States are a call to develop and implement integrated pest control strategies to aid public health prevention (*14*,*15*). We found that oral flea preventive effectively controlled *R. typhi* flea vectors in reservoir opossums. The proposed method could be used to control vector fleas among reservoir hosts and reduce risk for murine typhus in humans.

Acknowledgments

We thank Matthew Dacso and Susan McLellan for allowing trappings on their properties. We also thank David Walker for his mentorship and review of the manuscript.

About the Authors

Dr. Blanton is an infectious disease physician at the University of Texas Medical Branch in Galveston, Texas. His research interests are focused on the study of rickettsial diseases.

Dr. Villasante-Tezanos is a biostatistician at the University of Texas Medical Branch. His research interests include clinical trials and nonparametric statistics.

References

1. Civen R, Ngo V. Murine typhus: an unrecognized suburban vectorborne disease. Clin Infect Dis. 2008;46:913–8. https://doi.org/10.1086/527443
2. Pratt HD. The changing picture of murine typhus in the United States. Ann N Y Acad Sci. 1958;70:516–27. https://doi.org/10.1111/j.1749-6632.1958.tb35408.x
3. Anstead GM. History, rats, fleas, and opossums. II. The decline and resurgence of flea-borne typhus in the United States, 1945–2019. Trop Med Infect Dis. 2020;6:2. https://doi.org/10.3390/tropicalmed6010002
4. Elanco Animal Health. Comfortis (spinosad) package insert [cited 2025 March 7]. https://assets-eu-01.kc-usercontent.com/ad0f862a-9fb6-0162-80e8-2abe0fae68af/c1680843-25ec-4a2a-a152-2a1dacbcf4d2/Comfortis_Pack_Insert.pdf
5. Communicable Diseases Center. Pictorial keys to arthropods, reptiles, birds, and mammals of public health significance, 1966 [cited 2025 Mar 7]. https://stacks.cdc.gov/view/cdc/13428
6. Blanton LS, Idowu BM, Tatsch TN, Henderson JM, Bouyer DH, Walker DH. Opossums and cat fleas: new insights in the ecology of murine typhus in Galveston, Texas. Am J Trop Med Hyg. 2016;95:457–61. https://doi.org/10.4269/ajtmh.16-0197
7. Karpathy SE, Hayes EK, Williams AM, Hu R, Krueger L, Bennett S, et al. Detection of *Rickettsia felis* and *Rickettsia typhi* in an area of California endemic for murine typhus. Clin Microbiol Infect. 2009;15(Suppl 2):218–9. https://doi.org/10.1111/j.1469-0691.2008.02140.x
8. Sokal RR, Rohlf FJ. Biometry: the principles and practice of statistics in biological research. Third edition. New York: W.H. Freeman and Co; 1995.
9. Biggerstaff BJ. Confidence intervals for the difference of two proportions estimated from pooled samples. J Agric Biol Environ Stat. 2008;13:478–96. https://doi.org/10.1198/108571108X379055
10. Maina AN, Fogarty C, Krueger L, Macaluso KR, Odhiambo A, Nguyen K, et al. Rickettsial infections among *Ctenocephalides felis* and host animals during a flea-borne rickettsioses outbreak in Orange County, California. PLoS One. 2016;11:e0160604. https://doi.org/10.1371/journal.pone.0160604
11. Mullins KE, Maina AN, Krueger L, Jiang J, Cummings R, Drusys A, et al. Rickettsial infections among cats and cat fleas in Riverside County, California. Am J Trop Med Hyg. 2018;99:291–6. https://doi.org/10.4269/ajtmh.17-0706
12. Nelson K, Maina AN, Brisco A, Foo C, Croker C, Ngo V, et al. A 2015 outbreak of flea-borne rickettsiosis in San Gabriel Valley, Los Angeles County, California. PLoS Negl Trop Dis. 2018;12:e0006385. https://doi.org/10.1371/journal.pntd.0006385
13. Mohr CO, Morlan HB. The nature of parasitism of the opossum by fleas in southwestern Georgia. J Parasitol. 1959;45:233–7. https://doi.org/10.2307/3286539
14. Yomogida K, Kjemtrup A, Martínez-López B, Ibrahim M, Contreras Z, Ngo V, et al. Surveillance of flea-borne typhus in California, 2011–2019. Am J Trop Med Hyg. 2024;110:142–9. https://doi.org/10.4269/ajtmh.23-0272
15. Murray KO, Evert N, Mayes B, Fonken E, Erickson T, Garcia MN, et al. Typhus group rickettsiosis, Texas, USA, 2003–2013. Emerg Infect Dis. 2017;23:645–8. https://doi.org/10.3201/eid2304.160958

Address for correspondence: Lucas S. Blanton, University of Texas Medical Branch, 301 University Blvd, Galveston, TX 77555-0435, USA; email: lsblanto@utmb.edu

OXA-204 Carbapenemase in Clinical Isolate of *Pseudomonas guariconensis*, Tunisia

Nadia Jaidane, Wejdene Mansour, Lamia Tilouche, Pierre Châtre, Pauline François, Agnese Lupo, Saoussen Oueslati, Aymeric Jacquemin, Ali Lazzem, Sonia Karaborni, Laetitia Du Fraysseix, Yomna Ben Lamine, Nidhal Mahdhi, Abdelhalim Trabelsi, Jean-Yves Madec, Marisa Haenni,[1] Thierry Naas[1]

We report an OXA-204–producing *Pseudomonas guariconensis* clinical isolate in Tunisia, proving the spread of OXA-48 variants beyond Enterobacterales. The $bla_{OXA-204}$ gene was carried on a 119-kb chromosomally integrated plasmid fragment, along with multiple additional resistance genes. Surveillance, diagnostic tools, and antimicrobial drug access are needed to mitigate spread of carbapenem-resistant pathogens.

Multidrug-resistant (MDR) *Pseudomonas* spp. are major contributors to life-threatening infections, especially in severe burn patients. *Pseudomonas guariconensis* was initially isolated from rhizospheric soils in 2013 (*1*) but has since been described in various clinical contexts, underscoring its pathogenic potential. Clinical manifestations of *P. guariconensis* infections include infective endocarditis (*2*), necrotizing fasciitis (*3*), and asymptomatic bacteriuria with a VIM-2 metallo-β-lactamase–producing isolate (*4*). We characterized the molecular mechanism sustaining carbapenem resistance in a clinical *P. guariconensis* isolate from Tunisia.

The Study

On May 28, 2023, an 8-year-old child with severe high-voltage electric shock burns on 64% of his body was admitted to the Center for Traumatology and Major Burns, Ben Arous (Tunis, Tunisia). Multiple complications developed, including sepsis, urinary tract infection, and wound infections, which required the administration of broad-spectrum antimicrobial drugs (cefotaxime, imipenem, gentamicin, colistin, teicoplanin, and fosfomycin). On August 25, 2023, we transferred the patient to the burn unit of Sahloul Hospital (Sousse, Tunisia), where he received nutritional support with a high-protein high-calorie diet, transfusions for anemia, and extensive wound care and surgical skin grafting procedures. On September 20, 2023, after we isolated *Morganella morganii*, *Proteus mirabilis*, methicillin-susceptible *Staphylococcus aureus*, and glycopeptide-resistant *Enterococcus faecium* from bone fragments, the patient received piperacillin/tazobactam and cotrimoxazole for 21 days. On October 12, 2023, positive blood cultures revealed an extremely drug-resistant gram-negative bacillus we identified as *Pseudomonas aeruginosa* by Vitek 2.0 (bioMerieux, https://www.biomerieux.com). We conducted matrix-assisted laser desorption/ionization time-of-flight mass spectrometry (Bruker Daltonics, https://www.bruker.com) and identified the isolate as *P. guariconensis* with a score of 1.84.

We determined the MICs of the *P. guariconensis* isolate (65411) by using broth microdilution (Sensititre; ThermoFisher, https://www.thermofisher.com) and interpreted according to clinical breakpoints of the Comité de l'Antibiogramme de la Société Française de Microbiologie/European Committee on Antimicrobial Susceptibility Testing referential (version 2024; https://www.sfm-microbiologie.org/wp-content/uploads/2024/06/CASFM2024_V1.0.pdf).

Author affiliations: Université de Sousse Faculté de Médecine, Sousse, Tunisia (N. Jaidane, W. Mansour); Sahloul Hospital, Sousse (L. Tilouche); Anses Laboratoire de Lyon, Lyon, France (P. Châtre, P. François, A. Lupo, L. Du Fraysseix, J.-Y. Madec, M. Haenni); Inserm U1184, Le Kremlin-Bicêtre, France (S. Oueslati, A. Jacquemin, T. Naas); Sahloul University Hospital, Sousse (A. Lazzem, S. Karaborni, Y. Ben Lamine, N. Mahdhi, A. Trabelsi); Université Paris-Saclay BU Kremlin-Bicêtre, Le Kremlin-Bicêtre, France (T. Naas)

DOI: https://doi.org/10.3201/eid3106.250131

[1]These senior authors contributed equally to this article.

MIC testing revealed resistance to nearly all antimicrobial drugs tested, including ceftolozane/tazobactam (MIC >16 mg/L), imipenem and meropenem (MIC >32 mg/L), imipenem/relebactam (MIC >16 mg/L), meropenem/vaborbactam (MIC >32 mg/L), and aztrenoam/avibactam (MIC >16 mg/L), but susceptibility to ceftazidime/avibactam (MIC ≤0.5 mg/L), cefiderocol (MIC ≤1 mg/L), and colistin (MIC ≤0.5 mg/L). We adjusted the treatment regimen on the basis of antimicrobial drug susceptibility results and the availability of medications in Tunisia, where cefiderocol and ceftazidime/avibactam are not yet available. We administered colistin (150,000 units/kg; 1 million units 3×/d intravenously for 25 days), along with rifampicin (20 mg/kg/d; 450 mg 1×/d intravenously for 15 days), resulting in clinical stabilization and improvement.

We reported a negative result when testing *P. guariconensis* 65411 by using a homemade carbaNP assay (*5*) and a positive result for OXA-48–like enzymes by using the lateral flow immunoassay NG-Test Carba 5 assay (NG-Biotech, https://www.ngbiotech.com) (*6*). We conducted short-read (Illumina, https://www.illumina.com) and long-read (Oxford Nanopore, https://nanoporetech.com) whole-genome sequencing to consolidate bacterial identification (we confirmed *P. guariconensis*-like-3 by using Centrifuge [*7*]), identify resistance genes (Center for Genomic Epidemiology, https://www.genomicepidemiology.org), and determine the $bla_{\text{OXA-48-like}}$ genetic environment. We generated 1 contig of 5.6 Mbp with a guanine-cytosine content of 64.1% from a hybrid assembly by using Unicycler 0.5.0 (*8*), which agreed with the characteristics of reference *P. guariconensis* isolate ASM4082203v1 (GenBank accession no. GCF_040822035.1). We submitted the genome of isolate 65411 to the National Center for Biotechnology Information Nucleotide database (https://www.ncbi.nlm.nih.gov/nuccore; Bioproject no. PRJNA1150136).

The resistome of *P. guariconensis* 65411 contained acquired genes conferring resistance to β-lactams ($bla_{\text{CMY-16}}$, $bla_{\text{DHA-1}}$, $bla_{\text{OXA-1}}$, $bla_{\text{OXA-10}}$, and $bla_{\text{OXA-204}}$), aminoglycosides [*aac(6′)Ib-cr, ant(2′′)-Ia, aph(3′′)-Ib, aph(3′)-Via, aph(3′)-VIb, aph(6′)-Id*], fosfomycin (*fosA*), fluoroquinolones [*aac(6′)Ib-cr*], and additional antimicrobial drugs and biocides *(catB3, ARR-3, sul1/2, qacE*). High-level resistance to fluoroquinolones was because of a T83I substitution in the quinolone resistance-determining regions of GyrA. The RAST annotation identified an additional chromosome-encoded class A β-lactamase gene, named $bla_{\text{GUA-1}}$, displayed 100% sequence identity with a β-lactamase encoded in the genome of a *P. guariconensis* from the Czech Republic (GenBank accession no. UQM99659.1); 72% with that of *P. fulva* (accession no. MBF8778391.1), *P. mosselii* (accession no. WP_345894069.1), and *P. soli* (accession no. UXZ44560.1); and 57% with the extended-spectrum β-lactamase $bla_{\textit{LUT-1}}$ from *P. luteola* (*9*). All conserved motifs essential for β-lactamase activity were preserved, including the serine active site motif (S_{70}XXK), the hydrolytic water-binding site (S_{130}DN), and the catalytic triad component (K_{234}TG) (*10*). Those findings suggest the $bla_{\text{GUA-1}}$ gene likely encodes an intrinsic class A β-lactamase (Appendix Figure, https://wwwnc.cdc.gov/EID/article/31/6/25-0131-App1.pdf). We cloned $bla_{\text{GUA-1}}$ into an expression vector. The overexpression revealed crude protein extracts with strong nitrocefin hydrolytic activity. We confirmed the presence of a β-lactamase capable of hydrolyzing first-and third-generation cephalosporins (Appendix reference *1*) by using β-lactamase testing (Bio-Rad Laboratories, https://www.bio-rad.com).

The $bla_{\text{OXA-204}}$ carbapenemase gene is mostly detected in Tunisia (*11*) and in France from patients with previous travel to Tunisia. The gene is mostly found in *Klebsiella pneumoniae* and *Escherichia coli* isolates (*11*; Appendix reference *2*), but also rarely in *P. mirabilis*, *Citrobacter freundii*, *Serratia marcescens* (*12*), *Enterobacter cloacae* (*13*), and *Shewanella xiamenensis* (*14*). The $bla_{\textit{OXA-204}}$ gene is described as part of a Tn*2016* transposon located on IncA/C plasmids (Appendix reference *1*). In *P. guariconensis* 65411, the comprehensive analysis of the genetic environment of the $bla_{\text{OXA-204}}$ gene revealed the integration of a 119-kb plasmid fragment into the chromosome (Figure 1). This fragment displayed multiple resistance genes, including the β-lactamases $bla_{\textit{DHA-1}}$, $bla_{\textit{CMY-16}}$, $bla_{\textit{OXA-1}}$, and $bla_{\textit{OXA-204}}$, alongside genes conferring resistance to chloramphenicol (*catB3*) and aminoglycosides [*aph(6′)-Ic, aph(6′)-Id, aph(3′′)-I, aph(3′)-III, aph(3′)-IV, aph(3′)-VI, aph(3′)-VII,* and *aac(6′)-Ib-cr*]. The inserted fragment was bound by 2 IS*26* elements and an 8-bp target site duplication, suggesting an IS*26*-mediated insertion into the chromosome. The inserted plasmid shared homology (100% homology over an 88% coverage of the 119-kbp fragment) with part of a 189,866-bp IncC plasmid originating from a *K. pneumoniae* isolate (GenBank accession no. CP086448) coproducing OXA-10, CMY-16, and NDM-1 (*15*) (Figure 2). The $bla_{\textit{OXA-204}}$ gene was embedded within a 3,958 bp IS*Ecp1*-based Tn*2016*-like transposon (*11*; Appendix reference *1*) bracketed by a 5-bp target site duplication (Figure 3). In the prototypical Tn*2016*, IS*Ecp1* was disrupted by an IS*Kpn15* (*11*; Appendix reference *1*), whereas in *P. guariconensis* 65411, it was disrupted by an IS*903B* generating a 9-bp

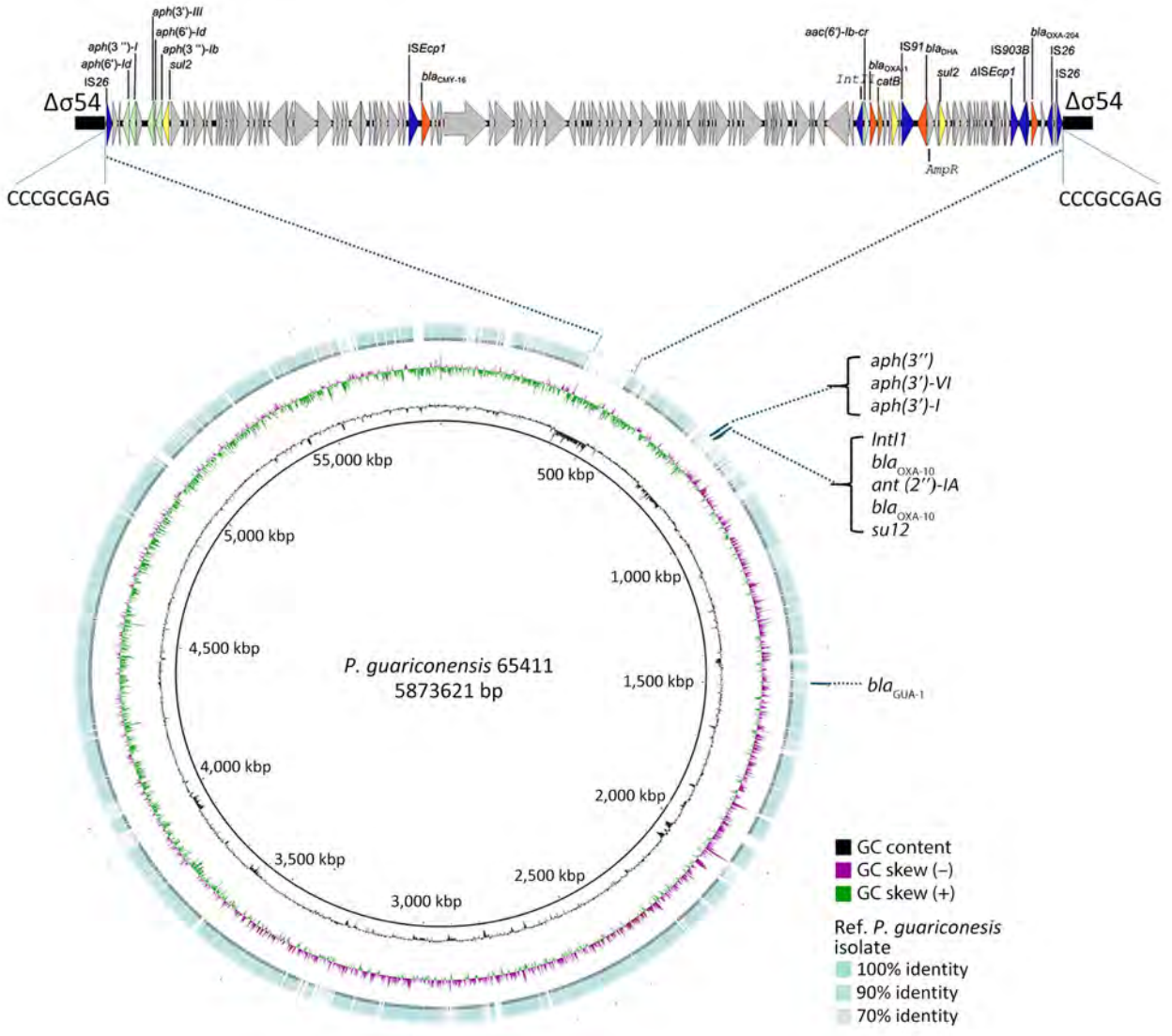

Figure 1. Comparative genomic analysis of OXA-204 carbapenemase-positive *Pseudomonas guariconensis* isolated from a child in Tunisia, 2023, using *P. guariconensis* GenBank accession no. GCF_040822035 as the reference genome. The concentric ring represents the BLAST (https://blast.ncbi.nlm.nih.gov) results of the *P. guariconensis* isolate from this study, 65411, with the reference genome. The color intensity of the outer ring indicates the level of sequence similarity, with darker shades representing higher sequence identity percentages. Gaps in the outer ring indicate very low identity or absence of the region. The magnified segment is the site of the IS*26*-mediated insertion of a 119-kbp plasmid fragment in the chromosome of *P. guariconensis* 65411. In the magnified portion, resistance genes and the associated mobile elements likely involved in their mobility are indicated in blue. Genes involved in resistance to β-lactams are indicated in orange (β-lactamases), to aminoglycosides in light green, to chloramphenicol in orange, and to sulfonamides in yellow. GC, guanine-cytosine. Figure created using BRIG software, https://sourceforge.net/projects/brig.

target site duplication in the Tn*2016*-like transposon. As suggested for IS*Kpn15* insertion, the IS*903B* insertion should not interfere with the strong outward oriented promoter of IS*Ecp1* (*11*; Appendix reference *1*), enabling high-level expression of $bla_{\text{OXA-204}}$.

Conclusions

We describe an OXA-48-like carbapenemase in *Pseudomonas* clinical isolate, demonstrating the dissemination of $bla_{\text{OXA-48-like}}$ genes beyond Enterobacterales. OXA-204–producing *P. guariconensis* was initially identified as *P. aeruginosa* by using biochemical methods, suggesting the real occurrence of *P. guariconensis* might be underestimated in clinical settings. The $bla_{\text{OXA-204}}$ gene was carried by an IS*Ecp1*-based Tn*2016*-like element present on a 119-kb plasmid fragment inserted into the chromosome by a large IS*26*-mediated composite transposon. The integrated DNA carried additional resistance determinants, including 2 cephalosporinases (CMY-16 and DHA-1)

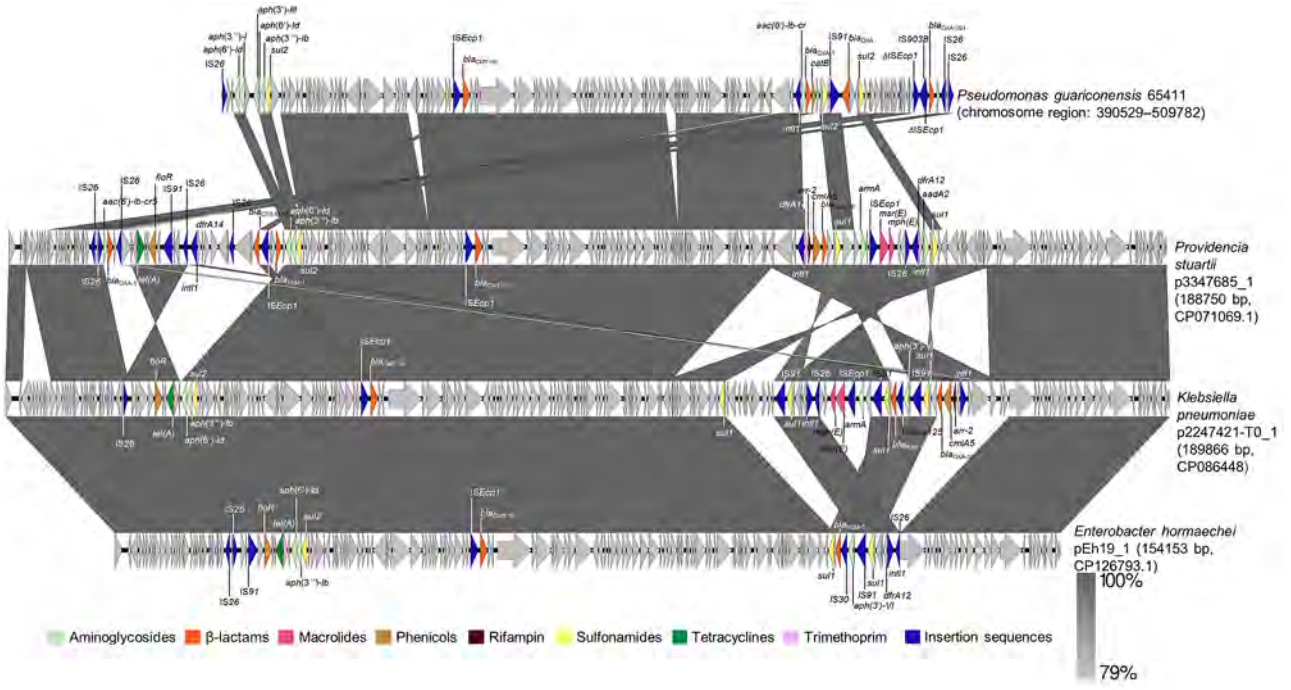

Figure 2. Representation of nucleotide alignment between the IS*26*-mediated transposon in the OXA-204 carbapenemase positive *Pseudomonas guariconensis* isolated from a child in Tunisia, 2023 (65411), and reference plasmids characterized in Enterobacterales (GenBank accession numbers provided). The matches ranged from 85% to 89% coverage, with 100% nucleotide identity. Arrows indicate genes and their transcription orientations. Open reading frames are colored according to antimicrobial drug family. Image created using Easyfig v.2.2.5 (https://mjsull.github.io/Easyfig).

and multiple associated resistance genes, resulting in an extremely drug-resistant phenotype. At first, the $bla_{\text{OXA-204}}$ gene was characterized on a 150-kb IncA/C broad host range carrying $bla_{\text{CMY-4}}$ that could be transferred to *P. aeruginosa* and lead to MICs for imipenem of 8 mg/L and meropenem of 32 mg/L (*11*). The high level carbapenem resistance in *P. guariconenesis* 65411 is likely the result of the expression of OXA-204 carbapenemase together with CMY-16 and DHA-1, which are 2 cephalosporinases known to weakly hydrolyze carbapenems (Appendix reference *3*).

Our findings reinforce the critical need for ongoing surveillance, advanced diagnostic tools, antimicrobial drug stewardship, and access to novel antimicrobial drugs in low- to middle-income countries to mitigate the spread of carbapenem-resistant pathogens. Carbapenemase detection should not rely exclusively on carbapenem-hydrolytic activity such as Carba NP but also on lateral flow immunoassays for

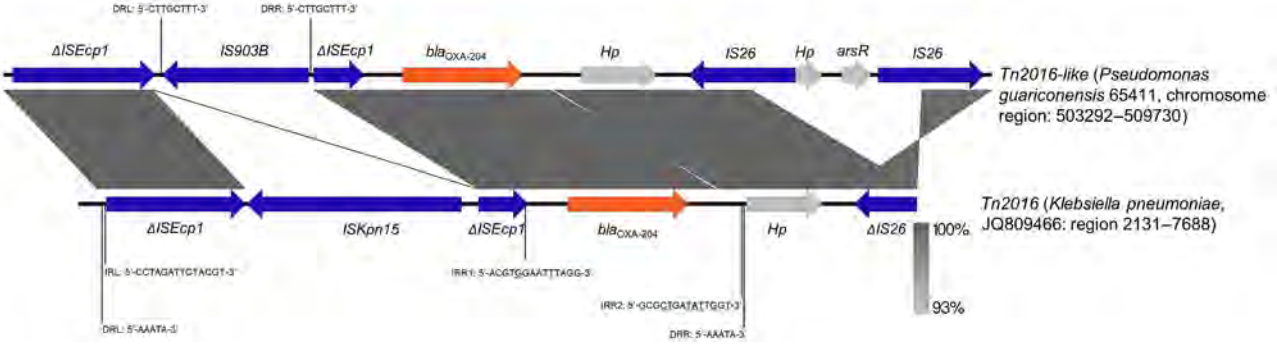

Figure 3. Representation of the nucleotide alignment between the Tn*2016*-like transposon carrying the $bla_{\text{OXA-204}}$ gene in the OXA-204 carbapenemase positive *Pseudomonas guariconensis* isolated from a child in Tunisia, 2023 (65411), chromosome region 503292–509730, and the Tn*2016* characterized in *Klebsiella pneumoniae* plasmid p204B (GenBank accession no. JQ809466). Arrows indicate genes and their transcription orientations. DRL, direct repeats left; DRR, direct repeats right; Hp, hypothetical protein; IRL, inverted repeat left; IRR, inverted repeat right. Image created using Easyfig v.2.2.5 (https://mjsull.github.io/Easyfig).

confirming the presence of carbapenemases, including OXA-48–like enzymes in nonfermenting gram-negative pathogens.

Acknowledgments

We thank Sameh Boussetta, Houda Youssef, and the dedicated laboratory staff who helped with data collection and technical issues.

This work was funded by the French Agency for Food, Environmental and Occupational Health Safety and by the Tunisian Ministry of Higher Education (project cofund no. JPI-AMR- PAIRWISE).

This study was reviewed and approved by the Ethics Committee of the University Hospital of Sahloul (reference no. HS09-2024).

About the Author

Dr. Jaidane is a postdoctoral researcher at the Laboratory of Metabolic Biophysics and Applied Pharmacology at the University of Sousse. Her research interests include epidemiology, genetics, and biochemistry of β-lactamases in gram-negative bacteria.

References

1. Toro M, Ramírez-Bahena MH, Cuesta MJ, Velázquez E, Peix A. *Pseudomonas guariconensis* sp. nov., isolated from rhizospheric soil. Int J Syst Evol Microbiol. 2013;63:4413–20. https://doi.org/10.1099/ijs.0.051193-0
2. Okano H, Okado R, Ito H, Asakawa H, Nose K, Tsuruga S, et al. Ischemic hepatitis with infectious endocarditis: a case report. Biomed Rep. 2021;15:97. https://doi.org/10.3892/br.2021.1473
3. Moseley EJ, Zhang JC, Williams OM. *Pseudomonas guariconensis* necrotizing fasciitis, United Kingdom. Emerg Infect Dis. 2024;30:185–7. https://doi.org/10.3201/eid3001.231192
4. Yoon C, Lee Y. Emerging of multidrug-resistant *Pseudomonas guariconensis* with blaVIM-2 in an asymptomatic bacteriuria patient: a rare clinical presentation. Diagn Microbiol Infect Dis. 2024;108:116182. https://doi.org/10.1016/j.diagmicrobio.2024.116182
5. Dortet L, Agathine A, Naas T, Cuzon G, Poirel L, Nordmann P. Evaluation of the RAPIDEC® CARBA NP, the Rapid CARB Screen® and the Carba NP test for biochemical detection of carbapenemase-producing Enterobacteriaceae. J Antimicrob Chemother. 2015;70:3014–22. https://doi.org/10.1093/jac/dkv213
6. Boutal H, Vogel A, Bernabeu S, Devilliers K, Creton E, Cotellon G, et al. A multiplex lateral flow immunoassay for the rapid identification of NDM-, KPC-, IMP- and VIM-type and OXA-48-like carbapenemase-producing Enterobacteriaceae. J Antimicrob Chemother. 2018;73:909–15. https://doi.org/10.1093/jac/dkx521
7. Kim D, Song L, Breitwieser FP, Salzberg SL. Centrifuge: rapid and sensitive classification of metagenomic sequences. Genome Res. 2016;26:1721–9. https://doi.org/10.1101/gr.210641.116
8. Wick RR, Judd LM, Gorrie CL, Holt KE. Unicycler: resolving bacterial genome assemblies from short and long sequencing reads. PLOS Comput Biol. 2017;13:e1005595. https://doi.org/10.1371/journal.pcbi.1005595
9. Doublet B, Robin F, Casin I, Fabre L, Le Fleche A, Bonnet R, et al. Molecular and biochemical characterization of the natural chromosome-encoded class A beta-lactamase from *Pseudomonas luteola*. Antimicrob Agents Chemother. 2010;54:45–51. https://doi.org/10.1128/AAC.00427-09
10. Philippon A, Slama P, Dény P, Labia R. A structure-based classification of class A β-lactamases, a broadly diverse family of enzymes. Clin Microbiol Rev. 2016;29:29–57. https://doi.org/10.1128/CMR.00019-15
11. Potron A, Nordmann P, Poirel L. Characterization of OXA-204, a carbapenem-hydrolyzing class D β-lactamase from *Klebsiella pneumoniae*. Antimicrob Agents Chemother. 2013;57:633–6. https://doi.org/10.1128/AAC.01034-12
12. Potron A, Bernabeu S, Cuzon G, Pontiès V, Blanchard H, Seringe E, et al. Analysis of OXA-204 carbapenemase-producing Enterobacteriaceae reveals possible endoscopy-associated transmission, France, 2012 to 2014. Euro Surveill. 2017;22(49):17–00048 https://doi.org/10.2807/1560-7917.ES.2017.22.49.17-00048
13. Messaoudi A, Saras E, Grami R, Bouallègue O, Boujâafar N, Madec JY, et al. Emergence of OXA-204 carbapenemase in *Enterobacter cloacae*. Int J Antimicrob Agents. 2019;54:829–30. https://doi.org/10.1016/j.ijantimicag.2019.09.001
14. Ncir S, Lupo A, Drapeau A, Châtre P, Souguir M, Azaiez S, et al. Back to the origin: *bla*OXA-204 and *bla*NDM-1 genes in *Shewanella* spp. from a Tunisian river. Tyne DV, éditeur. Microbiol Spectr. 2022;10(5):e01605-22.
15. Moser AI, Campos-Madueno EI, Perreten V, Endimiani A. Genome stability during serial subculturing in hyperepidemic multidrug-resistant *Klebsiella pneumoniae* and *Escherichia coli*. J Glob Antimicrob Resist. 2022;31:152–61. https://doi.org/10.1016/j.jgar.2022.08.014

Address for correspondence: Nadia Jaidane, Faculty of Medicine of Sousse, Rue Mohamed Karoui Sousse, 4002, Sousse, Tunisia; email: nadia_jaidane@famso.u-sousse.tn

Investigation of Influenza A(H5N1) Virus Neutralization by Quadrivalent Seasonal Vaccines, United Kingdom, 2021–2024

Phoebe Stevenson-Leggett,[1] Lorin Adams,[1] David Greenwood,[1] Abi Lofts, Vincenzo Libri, Bryan Williams, Sonia Gandhi, Charles Swanton, Steve Gamblin, Edward J. Carr,[1] Ruth Harvey,[1] Nicola S. Lewis,[1] Mary Y. Wu, Emma C. Wall[1]; Crick Neutralization Consortium[2]; Legacy Investigators[3]

We tested cross-neutralization against highly pathogenic avian influenza A(H5N1) virus in adults vaccinated with 2021–2023 seasonal quadrivalent influenza vaccine in the United Kingdom. Seasonal quadrivalent influenza vaccines are unlikely to protect vulnerable persons against severe H5N1 disease during widespread transmission. Enhanced measures are needed to protect vulnerable people from H5N1 virus infection.

Highly pathogenic avian influenza (HPAI) A(H5N1) clade 2.3.4.4b viruses have been spreading worldwide among wild birds and poultry since 2020 (*1*). Officials in multiple US states confirmed spillover mammal infections in dairy cattle and detection in commercial milk samples in early 2024, enabled by uninterrupted cattle movement (*2*). Reports following documented human transmission in 2024 show evidence of H5N1 seroconversion in 7% of sampled dairy workers and that >30% of dairy herds in California are affected (*3*,*4*). Cow–human zoonotic transmission causing symptomatic but nonsevere infections have been reported in dairy workers, and 1 case was reported in September 2024 in a hospitalized person without exposure to animals and subsequent mild infection among healthcare workers caring for that patient (https://www.cdc.gov/bird-flu/spotlights/h5n1-response-09272024.html). However, a lack of widespread surveillance in cows and dairy and healthcare workers risks substantial underascertainment of bovine–human transmission events (*5*), which are further suggested by detection of H5N1 clade 2.3.4.4b viruses in Texas wastewater in March–July 2024 (*6*). In addition, fomite transmission through commercial milking equipment has been proposed as the primary route of cow–human transmission (N.J. Halwe et al., unpub. data, https://doi.org/10.1101/2024.08.09.607272).

Although pasteurization renders HPAI H5N1 clade 2.3.4.4b viruses nonviable, viable virions have been detected in unpasteurized milk and caused fatal disease in cats that ingested the milk (*4*,*7*). Ongoing limited surveillance, detection, and containment of H5N1 clade 2.3.4.4b virus in the United States in both animal and human populations has led to mounting concern that this virus is gaining adaptions that could lead to effective human–human transmission, which could be catastrophic for clinically vulnerable people, particularly those who are immunocompromised and at the extremes of age (*2*).

Candidate vaccine viruses for pandemic preparedness have been recommended since the reemergence

Author affiliations: The Francis Crick Institute, London, UK (P. Stevenson-Leggett, L. Adams, D. Greenwood, A. Lofts, S. Gandhi, C. Swanton, S. Gamblin, E.J. Carr, R. Harvey, N.S. Lewis, M.Y. Wu, E.C. Wall); Royal Veterinary College, London (L. Adams, N.S. Lewis); University College London Hospitals National Institute for Health Research Biomedical Research Unit, London (V. Libri, B. Williams, E.C. Wall); University College London, London (V. Libri, B. Williams, S. Gandhi, C. Swanton); University College London Centre for Kidney and Bladder Health, London (E.J. Carr); University College London Division of Infection and Immunity, London (E.C. Wall)

DOI: https://doi.org/10.3201/eid3106.241796

[1]These authors contributed equally to this article.

[2]Members of the Crick Neutralization Consortium are listed at the end of this article.

[3]Members of the Legacy Investigators are listed at the end of this article.

of A/goose/Guangdong/1/1996 lineage influenza A(H5) viruses in 2003. Vaccines against H5 clades, including clade 2.3.4.4b, have been in development, and some countries have small stockpiles. Whether those vaccines protect against severe disease is unknown, and current supplies to combat epidemic or pandemic spread of H5 virus are limited (*8*).

Adults vaccinated with licensed H5N1 vaccines generate cross-reactive neutralizing antibodies against clade 2.3.4.4b viruses (*9*), but less is known about cross-protection against H5N1 viruses from quadrivalent influenza vaccines (QIVs). Antigen-specific B-cell monoclonal neutralizing antibodies (nAbs) against H5N1 virus can be found after QIV in humans (*10*), and studies in ferrets show further nAbs generated by seasonal influenza exposure might offer some protection against HPAI H5 challenge (S. Lakdawala et al., unpub. data, https://doi.org/10.21203/rs.3.rs-4935162/v1); however, QIV vaccination did not protect against H5N1 virus in mice (*11*). We investigated whether vaccine-induced immunity generated by seasonal QIVs would partially boost cross-reactive immunity against HPAI H5N1 virus in humans.

The Study

We compared humoral neutralization of 2 H5N1 viruses, A/dairy_cattle/Texas/24-008749-002/2024 (2.3.4.4b) and A/Cambodia/NPH230776/2023 (2.3.2.1c), in serum samples alongside a seasonal influenza A(H1N1) virus isolate, A/Wisconsin/67/2022, before and after QIV in participants from the University College London Hospitals–Francis Crick Institute Legacy study cohort (https://clinicaltrials.gov/study/NCT04750356) (Appendix Figure, https://wwwnc.cdc.gov/EID/article/31/6/24-1796-App1.pdf). The study included 61 adults (median age 49 [range 38–58] years); 44 (72%) were women, and 17 (28%) were men. Thirty (49%) adults were vaccinated in only the 2021–22 season, but all 61 were vaccinated in ≥1 study season (2021–22, 2022–23, and 2023–24). Median sampling duration after vaccine dose for 2021–22 was 81 (interquartile range [IQR] 61–81) days, for 2022–23 was 67 (IQR 38–68) days, and for 2023–24 was 77 (IQR 44–77) days. Twenty-seven (44%) participants reported a single underlying condition (Table).

In line with their effectiveness against seasonal influenza, each QIV generated a statistically significant boost in serum neutralization of A/Wisconsin/67/2022 in each season tested ($p = 0.003–0.007$ by χ^2 test) (Figure). In contrast, HPAI H5 virus neutralization in our cohort of healthy adults was blunted or absent. In prevaccine serum samples, we detected neutralization above background against A/Cambodia/NPH230776/2023 in a few samples but did not detect any neutralization against A/dairy_cattle/

Table. Characteristics of patients in investigation of influenza A(H5N1) virus neutralization by quadrivalent seasonal vaccines, United Kingdom, 2021–2024*

Characteristic	Sampling season		
	2021–22, n = 30	2022–23, n = 54	2023–24, n = 59
Sex			
F	21 (70)	40 (74)	43 (73)
M	9 (30)	14 (26)	16 (27)
Median age, y (IQR)	56 (40–62)	49 (38–58)	49 (38–58)
Sampling site			
Crick	19 (63)	31 (57)	34 (58)
NHS sites UCLH or CNWL	11 (37)	23 (42)	25 (42)
Underlying conditions, any	16 (53)	24 (44)	25 (42)
Type 1 diabetes	1 (3.3)	1 (1.9)	1 (1.7)
Type 2 diabetes	2 (6.7)	2 (3.7)	2 (3.4)
Cancer, stroke, or heart problems	2 (6.7)	3 (5.6)	4 (6.8)
High blood pressure	5 (17)	5 (9.3)	6 (10)
Asthma or COPD	3 (10)	6 (11)	7 (12)
Alcohol consumption			
Never	0 (0)	4 (10)	5 (11)
Monthly or less	6 (26)	12 (30)	13 (30)
2–4 times/mo	0 (0)	0 (0)	0 (0)
2 or 3 times/wk	11 (48)	19 (48)	21 (48)
≥4 times/wk	6 (26)	5 (13)	5 (11)
Unknown	7	14	15
Smoking status			
Never smoker	25 (83)	41 (76)	47 (80)
Ex-smoker	5 (17)	10 (19)	9 (15)
Current smoker	0 (0)	3 (5.6)	3 (5.1)
Median days from vaccine to sample collection (IQR)	82 (61–81.5)	67 (33.75–67)	61 (26–61)

*Values are no. (%) except as indicated. CNWL, Central Northwest London; COPD, chronic obstructive pulmonary disease; IQR, interquartile range; NHS, National Health Service; UCLH, University College London Hospitals.

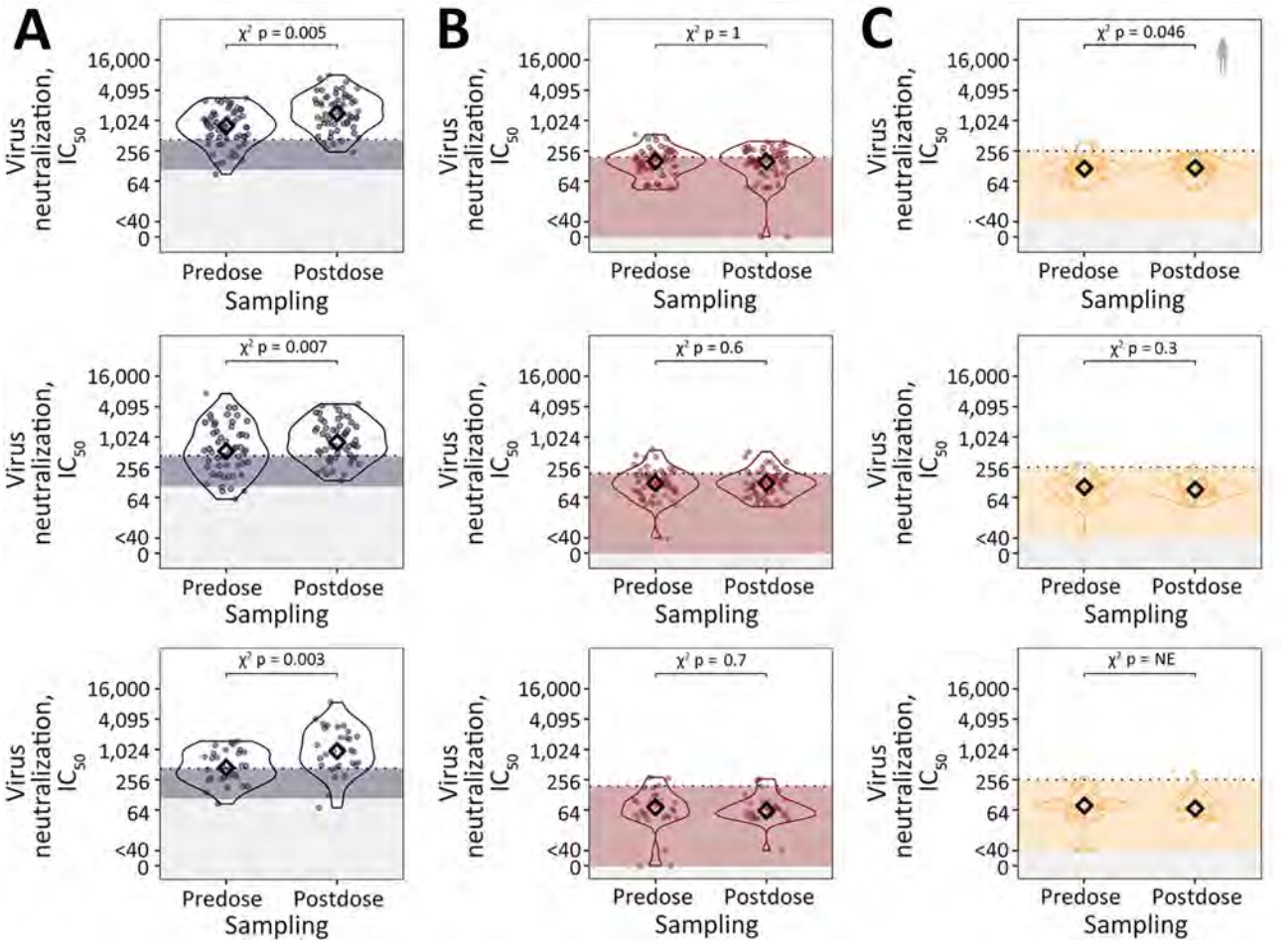

Figure. Live-virus neutralization of preseasonal and postseasonal quadrivalent influenza vaccination in a study of influenza A(H5N1) virus neutralization by quadrivalent seasonal vaccines, United Kingdom, 2021–2024. Violin plots show paired serum samples before and after each seasonal vaccine (top row, 2023–24, n = 59; middle row, 2022–23, n = 54; bottom row, 2021–22, n = 30) tested against pandemic H1 and 2 highly pathogenic avian influenza H5 strains: H1N1 strain (A), H5N1 Cambodia strain (B), and H5H1 Texas dairy strain (C). Virus neutralization reported as $\log_2$-transformed IC_{50}. Black diamonds indicate median IC_{50}. Nonspecific cross-reactivity levels are shown as shaded areas. p values from McNemar tests are shown, comparing the number of persons above background (dashed line) before and after quadrivalent influenza vaccination. IC_{50}, reciprocal titer at which 50% of viral infection is inhibited; NE, not estimated.

Texas/24-008749-002/2024 isolate (Figure). No seasonal QIV resulted in a cross-neutralization boost against either HPAI H5 virus (Figure).

Ongoing adaptation of HPAI H5N1 clade 2.3.4.4b virus in cows and other mammal hosts found on dairy farms, including rodents and cats, substantially increases the risk for a major HPAI H5N1 virus epidemic or pandemic in humans (*2*,*4*). The paucity of human serologic memory against either H5N1 virus strain raises the potential for widespread vulnerability to infection within the adult population. We observed a predictable boost to neutralizing titers against the contemporary seasonal influenza A(H1N1) virus (A/Wisconsin/67/2022) that was absent for the 2 clinically relevant H5N1 viruses tested in our high-throughput neutralization assay (Appendix). Neutralizing antibody titers have long been used as a correlate of protection against seasonal influenza (*12*); thus, our observations suggest seasonal QIVs are unlikely to offer adequate serologic protection against H5N1 virus.

Immunity against influenza evolves throughout the lifespan, and early infection exposures influence subsequent antibody responses after infection and vaccination (*13*). Few participants in our study had detectable neutralizing titers above background to the 2.3.2.1c A/Cambodia/NPH230776/2023 virus and none to the 2.3.4.4b A/dairy_cattle/Texas/24-008749-002/2024 virus. Together with our observed lack of QIV boosting, our results suggest that strategies reliant on existing population-level or QIV-based immunity against H5N1 virus infection must be approached with caution.

One limitation of this study is the lack of in vivo challenge to test for cross-protection. Some studies have reported transient protection against H5N1 challenge after transferring QIV-vaccinated human serum to mice, which was not accurately predicted by in vitro assays, including virus neutralization assays (*14,15*). Cross-neutralization might also occur in the absence of nAbs, but without in vivo testing, we cannot conclusively determine the extent to which the QIV might provide protection against H5N1 virus. A second limitation is that our cohort, predominately working age, healthy adults receiving occupational QIV, do not represent a population at high risk for severe influenza disease and death. However, they represent an immunocompetent population and would be expected to have the most robust detectable immunity. Third, although we tested 2 H5N1 viruses associated with recent human disease, despite extensive efforts, we could not eliminate background signal in our assay. Thus, we were unable to fully quantify neutralization at lower titers and opted to describe the range within which we detected background signal. As of 2025, no neutralization titers were available from postinfection serum samples in dairy farm workers to further refine that cutoff (*6*). Further investigation is required to address the issue of background signal. However, other studies suggest nonspecific inhibition by human serum as a possible explanation for low-level readouts for protection (*15*). Finally, our use of whole virus to assess nAb titers did not allow determination of the extent to which hemagglutinin- or neuraminidase-specific antibodies might have contributed to overall neutralization. However, the high-throughput live-virus neutralization we describe (Appendix) is a highly valuable tool for pandemic preparedness, offering a method for near real-time analysis of serum-based immunity to emerging viruses in large cohorts.

Conclusions

The effectiveness of QIV against influenza A(H5N1) virus remains uncertain, and clarification on the extent of cross-protection in humans is urgently needed. Considering that uncertainty, timely and effective deployment of targeted vaccines would be crucial during widespread influenza A(H5N1) outbreaks. To reduce risks for severe illness and death requires enhanced measures that mitigate the spread of HPAI H5N1 viruses to humans, accelerated pipelines for H5-directed influenza vaccines, and systems that rapidly and equitably reach clinically vulnerable persons worldwide (*2*).

Additional members of the Crick Neutralization Consortium: A. Hobbs, G. Dowgier, R. Penn, T. Sanderson, J. Bazire, A.S. Fowler, M. Miah, C. Smith, M. Miranda, P. Bawumia, N. O'Reilly, S. Warcha, K. Ambrose, A. Strange, G. Kelly, and S. Kjar.

Additional members of the Legacy Investigators: P. Papineni, T. Corrah, R. Gilson, R. Beale, and D.L.V. Bauer.

Acknowledgments

We thank all the study participants and the staff of the National Institute for Health Research Clinical Research Facility at University College London Hospitals, including Miguel Alvarez and Marivic Ricamara, for participant recruitment and management. We also thank the staff of the Worldwide Influenza Centre, the Scientific Technology Platforms, and the COVID-19 testing pipeline at the Francis Crick Institute for access to the virus isolates used in this study, providing participant sample and data management, and supporting assay development and analysis.

Anonymized data and R code are available at https://github.com/FrancisCrickInstitute/Crick-UCLH-Legacy-live-virus-microneutralization-for-H5N1.

The Legacy study was approved by London Camden and Kings Cross Health Research Authority Research and Ethics committee (reference no. 20/HRA/4717) Integrated Research Application System (IRAS) no. 286469 and sponsored by University College London Hospitals.

This work was undertaken at University College London Hospitals/University College London, which received a proportion of funding from the National Institute for Health Research University College London Hospitals Department of Health's National Institute for Health Research Biomedical Research Centre. E.C.W., V.L., and B.W. are supported by the Centre's funding scheme. E.J.C. is supported by a Medical Research Council clinician scientist fellowship.

This work was jointly supported by the National Institute for Health Research that funds the University College London Hospitals Department of Health's National Institute for Health Research Biomedical Research Centre and core funding from the Francis Crick Institute from Cancer Research UK (grant nos. CC2166, CC1283, CC1114, CC2230, CC2060, and CC2041), the UK Medical Research Council (grant nos. CC2166, CC1283, CC1114, CC2230, CC2060, and CC2041), and the Wellcome Trust (grant nos. CC2166, CC1283, CC1114, CC2230, CC2060, and CC2041). This project was funded in part with federal funds from the National Institute of Allergy and Infectious Diseases, National Institutes of

Health, Department of Health and Human Services (contract no. 75N93021C00015). Additional funding for this study was from UKRI (grant nos. MR/W005611/1, MR/Y004205/1, and MR/X006751/1 to E.J.C.). The funders of the study had no role in study design, data collection, data analysis, data interpretation, or writing of the report.

About the Author

Dr. Stevenson-Leggett is a specialist COVID Unit postdoctoral researcher at the Francis Crick Institute. Her research interests include high-throughput, live virus neutralization. Mr. Adams is a PhD student within the World Health Organization's Worldwide Influenza Centre. His research interests include in vitro pathogenicity assessment of influenza viruses, including H5N1 strains.

References

1. Peacock T, Moncla L, Dudas G, VanInsberghe D, Sukhova K, Lloyd-Smith JO, et al. The global H5N1 influenza panzootic in mammals. Nature. 2025;637:304–13. https://doi.org/10.1038/s41586-024-08054-z
2. Lewis N, Beer M. Stop H5N1 influenza in US cattle now. Science. 2024;385:123. https://doi.org/10.1126/science.adr5866
3. Mellis AM, Coyle J, Marshall KE, Frutos AM, Singleton J, Drehoff C, et al. Serologic evidence of recent infection with highly pathogenic avian influenza A(H5) virus among dairy workers—Michigan and Colorado, June–August 2024. MMWR Morb Mortal Wkly Rep. 2024;73:1004–9. https://doi.org/10.15585/mmwr.mm7344a3
4. Burrough ER, Magstadt DR, Petersen B, Timmermans SJ, Gauger PC, Zhang J, et al. Highly pathogenic avian influenza A(H5N1) clade 2.3.4.4b virus infection in domestic dairy cattle and cats, United States, 2024. Emerg Infect Dis. 2024;30:1335–43. https://doi.org/10.3201/eid3007.240508
5. Shittu I, Silva D, Oguzie JU, Marushchak V, Olinger GG, Lednicky JA, et al. A One Health investigation into H5N1 avian influenza virus epizootics on two dairy farms. Clin Infect Dis. 2025;80:331–8. https://doi.org/10.1093/cid/ciae576
6. Tisza MJ, Hanson BM, Clark JR, Wang L, Payne K, Ross MC, et al. Sequencing-based detection of avian influenza A(H5N1) virus in wastewater in ten cities. N Engl J Med. 2024;391:1157–9. https://doi.org/10.1056/NEJMc2405937
7. Guan L, Eisfeld AJ, Pattinson D, Gu C, Biswas A, Maemura T, et al. Cow's milk containing avian influenza A(H5N1) virus—heat inactivation and infectivity in mice. N Engl J Med. 2024;391:87–90. https://doi.org/10.1056/NEJMc2405495
8. World Health Organization. Zoonotic influenza: candidate vaccine viruses and potency testing reagents [cited 2024 Oct 5]. https://www.who.int/teams/global-influenza-programme/vaccines/who-recommendations/zoonotic-influenza-viruses-and-candidate-vaccine-viruses
9. Khurana S, King LR, Manischewitz J, Posadas O, Mishra AK, Liu D, et al. Licensed H5N1 vaccines generate cross-neutralizing antibodies against highly pathogenic H5N1 clade 2.3.4.4b influenza virus. Nat Med. 2024;30:2771–6. https://doi.org/10.1038/s41591-024-03189-y
10. Throsby M, van den Brink E, Jongeneelen M, Poon LL, Alard P, Cornelissen L, et al. Heterosubtypic neutralizing monoclonal antibodies cross-protective against H5N1 and H1N1 recovered from human IgM+ memory B cells. PLoS One. 2008;3:e3942. https://doi.org/10.1371/journal.pone.0003942
11. Beukenhorst AL, Frallicciardi J, Rice KL, Koldijk MH, Moreira de Mello JC, Klap JM, et al. A pan-influenza monoclonal antibody neutralizes H5 strains and prophylactically protects through intranasal administration. Sci Rep. 2024;14:3818. https://doi.org/10.1038/s41598-024-53049-5
12. Verschoor CP, Singh P, Russell ML, Bowdish DM, Brewer A, Cyr L, et al. Microneutralization assay titres correlate with protection against seasonal influenza H1N1 and H3N2 in children. PLoS One. 2015;10:e0131531. https://doi.org/10.1371/journal.pone.0131531
13. Edler P, Schwab LSU, Aban M, Wille M, Spirason N, Deng YM, et al. Immune imprinting in early life shapes cross-reactivity to influenza B virus haemagglutinin. Nat Microbiol. 2024;9:2073–83. https://doi.org/10.1038/s41564-024-01732-8
14. Roos A, Roozendaal R, Theeuwsen J, Riahi S, Vaneman J, Tolboom J, et al. Protection against H5N1 by multiple immunizations with seasonal influenza vaccine in mice is correlated with H5 cross-reactive antibodies. Vaccine. 2015;33:1739–47. https://doi.org/10.1016/j.vaccine.2015.01.070
15. Roozendaal R, Tolboom J, Roos A, Riahi S, Theeuwsen J, Bujny MV, et al. Transient humoral protection against H5N1 challenge after seasonal influenza vaccination of humans. PLoS One. 2014;9:e103550. https://doi.org/10.1371/journal.pone.0103550

Address for correspondence: Emma Wall, The Francis Crick Institute, NW409, 1 Midland Rd, London NW1 1AT, UK; email: emma.wall@crick.ac.uk

Mycoplasma arginini Cellulitis, Tenosynovitis, and Arthritis in Kidney Transplant Recipient, Slovenia, 2024

Tjaša Vivoda, Tereza Rojko, Barbara Kokošar Ulčar, Katja Strašek Smrdel, Andraž Celar Šturm, Darja Keše, Tina Triglav, Željka Večerić Haler

Mycoplasma arginini is a bacterium primarily found in animals and is seldom reported in human infections. We identified *M. arginini* infection in a severely immunocompromised kidney transplant recipient in Slovenia. Clinicians should be aware of *M. arginini*'s potential as a pathogen in immunocompromised persons with animal contact.

Mycoplasma species belong to the class Mollicutes, a group of bacteria characterized by lack of a cell wall. Those organisms are among the smallest organisms capable of autonomous replication and measure ≈0.3–0.8 μm.

M. arginini is a common colonizer in respiratory and urogenital tracts of various animals, including cats, dogs, cattle, and sheep, and is generally considered to be of low pathogenicity (*1*). However, in immunocompromised persons, *M. arginini* infection can lead to severe complications (*2*–*4*; M.A. May et al., unpub. data, https://www.preprints.org/manuscript/201809.0533/v1). We report a case of *M. arginini* infection in a kidney transplant recipient in Slovenia.

The Study

A 56-year-old woman was seen for a 3-week history of swelling, redness, and pain in her left forearm. She had a 17-year history of IgG kappa plasmacytoma and C3 glomerulonephritis, which led to end-stage renal failure and 2 kidney transplants. She underwent her first kidney transplant in 2011 and then a second transplant in 2022 after failure of the first graft. Both transplants were complicated by C3 glomerulonephritis recurrence. Approximately 6 months after the second kidney transplant, she started treatment with high-dose intravenous methylprednisolone, rituximab (chimeric monoclonal antibody targeting CD20 on B cells), and plasmapheresis, in addition to standard immunosuppressive therapy (tacrolimus, mycophenolate mofetil, and methylprednisolone). During that intensive immunosuppression, opportunistic infections developed, including cutaneous *Alternaria alternata* fungi infection of the left shin and cytomegalovirus reactivation, which necessitated adjustments to her immunosuppressive regimen. Over the next 2 years, declining graft function caused by C3 glomerulonephritis was managed with ravulizumab (a monoclonal antibody targeting complement component 5) and plasmapheresis. Granulocyte colony-stimulating factors were intermittently administered to treat episodes of neutropenia.

Approximately 2 years after her second kidney transplant, she noticed a small lump in the left mid-forearm with redness that progressively spread toward her wrist and elbow. Her doctors prescribed oral amoxicillin/clavulanic acid. After 5 days, that treatment failed to resolve her worsening symptoms, which prompted hospitalization. At admission, she exhibited swelling, redness, and restricted joint mobility in the left wrist. The patient had frequent contact with household cats and a dog and reported having sustained a cat bite at the site of small lump in the mid-forearm a week before admission.

Laboratory findings showed elevated C-reactive protein and β-D-glucan levels, normal procalcitonin level, and normal leukocyte count. Immune status

Author affiliations: University Medical Center Ljubljana, Ljubljana, Slovenia (T. Vivoda, T. Rojko, B. Kokošar Ulčar, Ž. Večerić Haler); Faculty of Medicine, University of Ljubljana, Ljubljana (T. Vivoda, T. Rojko, K. Strašek Smrdel, D. Keše, T. Triglav, Ž. Večerić Haler); Institute of Microbiology and Immunology, Ljubljana (K. Strašek Smrdel, A. Celar Šturm, D. Keše, T. Triglav)

DOI: https://doi.org/10.3201/eid3106.250149

Table. Laboratory values for *Mycoplasma arginini* cellulitis, tenosynovitis, and arthritis in kidney transplant recipient, Slovenia, 2024*

Variable	Sample collection				Reference range
	At clinic†	At admission	At discharge	After treatment‡	
White blood count, cells × 10^9/L	5.5	4.2	5.5	6.8	4.0–10.0
C-reactive protein, mg/L	5	40	13	<5	<5
Procalcitonin, μg/L	0.6	0.10	0.05	NA	<0.24
IgG, g/L	NA	2.7	14.7§	6.1	7.67–15.90
IgA, g/L	NA	<0.24	<0.24	NA	0.61–3.56
IgM, g/L	NA	<0.17	0.24	NA	0.37–2.86
β-D-glucan, pg/mL	189.3	207.2	170.2	192	<59.9
GM antigen, ELISA index	0.06	0.12	NA	NA	<0.5
Cryptococcal antigen, ELISA titer	1:0.03	1:0.04	NA	NA	<1:1
Blood cultures¶	NA	Negative	NA	NA	Negative

*IgG values were adjusted on the basis of presence of known IgG/κ spike. GM, galactomannan; NA, not available.
†The patient's clinic at symptom onset.
‡Treatment included a completed 6-week course of doxycycline.
§Higher IgG concentration after administration of intravenous immunoglobulin.
¶Bactec FX Blood Culture System (Becton, Dickinson and Company, https://www.bd.com).

evaluation using QuantiFERON Monitor (QIAGEN, https://www.qiagen.com) showed a moderate cell-mediated immune response, elevated plasma Torque Teno virus DNA (167,000 copies/mL), substantially decreased B-lymphocyte counts (likely caused by rituximab), and severe hypogammaglobulinemia (Table; Appendix, https://wwwnc.cdc.gov/EID/article/31/6/25-0149-App1.pdf). An ultrasound confirmed cellulitis, tenosynovitis of carpal extensor tendons, and arthritis of the radiocarpal joint (Appendix Figure 1).

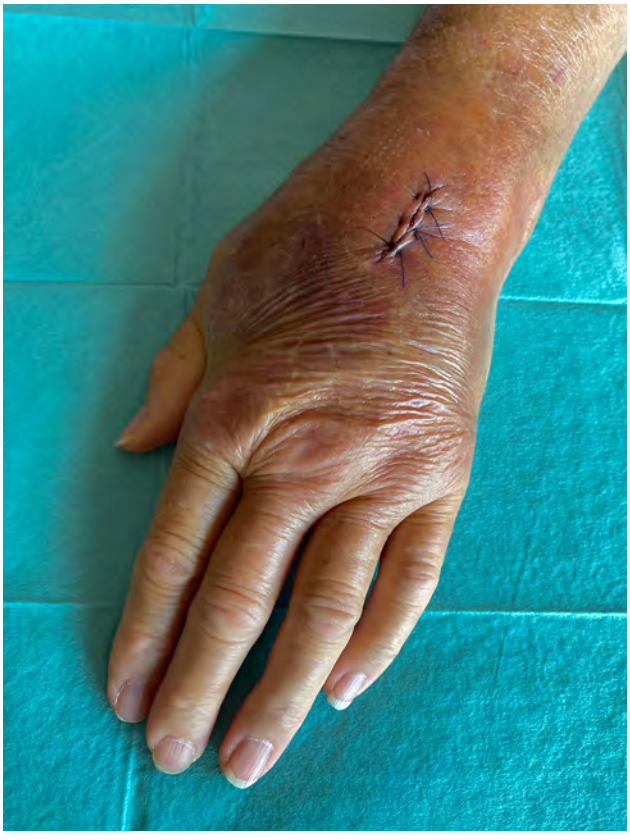

Figure 1. Surgical site after treatment for *Mycoplasma arginini* cellulitis, tenosynovitis, and arthritis in kidney transplant recipient, Slovenia, 2024. We observed swelling, redness, and restricted joint mobility in the left wrist before surgery.

At admission, doctors initiated intravenous flucloxacillin therapy. The next day, doctors added doxycycline after an atypical infection was suspected. Surgical intervention on the radiocarpal joint included irrigation and the collection of synovial fluid and a biopsy specimen for microbiological analysis (Figure 1). Broad-range bacterial PCR with sequencing from synovial fluid identified *M. arginini* with 99.5% sequence identity; therefore, the sample was plated on arginine-enriched A8 agar. After 4 days, stereomicroscopy showed small colonies with a characteristic fried egg appearance (Figure 2).

After identification of *Mycoplasma* spp. from synovial fluid, we discontinued flucloxacillin and added moxifloxacin. The combination of doxycycline and moxifloxacin led to clinical improvement that allowed de-escalation to doxycycline monotherapy after 8 days. We treated severe hypogammaglobulinemia (IgG 2.7 g/L) with intravenous immunoglobulin on day 10 after admission. We discontinued mycophenolate on day 6 after confirmation of *M. arginini* infection. Ravulizumab, last administered 6 weeks before hospitalization, was postponed because of ongoing infection. Redness, swelling, and pain in the wrist and elbow resolved, and we discharged the patient on a 10-week course of doxycycline with outpatient follow-up.

After discharge and 3 weeks of doxycycline treatment, we excised a painless subcutaneous nodular lesion below the left elbow (Figure 3). Broad-range PCR performed on a sample from lesion confirmed *M. arginini* with 100% sequence identity. *Mycoplasma* spp. culture was negative. Histopathology showed mild inflammatory changes consistent with bacterial infection. Four months after ending the 10-week

course of doxycycline treatment, the patient was doing well, without any local or systemic signs of *M. arginini* infection.

We tested oropharyngeal swab specimens from the patient's 3 cats and 1 dog using a genus-specific mycoplasma PCR (*5*) and confirmed colonization with *M. gateae* and *M. maculosum*. We found that 1 cat had a mixed *Mycoplasma* infection, but we could not definitively confirm or rule out *M. arginini* in that cat. We gave a 2-week doxycycline course to the pets to treat *Mycoplasma*, although reinfection remained possible because they moved indoors and outdoors.

Only a few documented published cases support zoonotic potential of *M. arginini*, particularly in immunocompromised patients. Those cases include reports of disseminated infection in a slaughterhouse worker with advanced non-Hodgkin lymphoma (*2*), septicemia with polyarthritis in another therapy-resistant non-Hodgkin lymphoma patient who had close contact with several cats (*3*), a disseminated infection in a young bodybuilder with a history of use of nutritional supplements derived from animal materials of uncontrolled origin (*6*), and a deep tissue infection in a hunter with an open femur fracture from a lion attack (*7*). Common among those cases were profound immunosuppression and consumption of animal products or close contact with animals, as seen in our patient.

Research indicates that *M. arginini* poses little risk to persons with healthy immune systems. A study of 22 persons at occupational risk for *Mycoplasma* infections (e.g., veterinarians, farmers, and slaughterhouse workers) found no substantial infection risk in those with normal immune function, suggesting that human exposure to *M. arginini* is generally not a clinical concern for immunocompetent persons (*8*). Most documented cases, including the patient we report, involve immunocompromised persons, often with hypogammaglobulinemia, which is a known risk factor for infections caused by *Mycoplasma* spp. (*4*).

The optimal treatment for *M. arginini* infection remains uncertain because of its rarity in humans. Reported cases are typically managed with long-term courses of antimycoplasmal antibiotic drugs, such as macrolides, quinolones, and tetracyclines (*3*,*6*,*7*). In 1 instance, a patient treated with erythromycin ultimately died from the infection, and postmortem testing showed erythromycin-resistant *M. arginini* (*2*). That testing suggests that broader-spectrum antibiotic drugs may be more effective as initial treatment, particularly because erythromycin resistance is well documented in several *Mycoplasma* species (*9*,*10*).

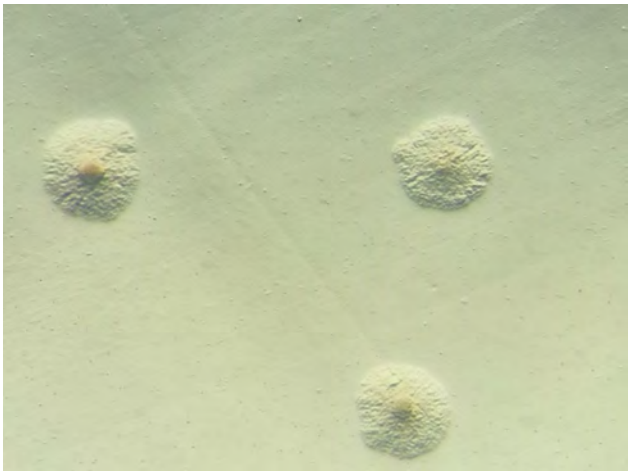

Figure 2. Stereomicroscopy of *Mycoplasma arginini* culture from the patient's synovial fluid sample, showing small colonies with a characteristic fried egg appearance, with dense central core surrounded by a lighter peripheral zone. Original magnification ×40.

Because *Mycoplasma* bacteria lack a cell wall, infections are best addressed with intracellular-acting antibiotic drugs such as tetracyclines or macrolides. Dual antibiotic drug therapy has been applied in

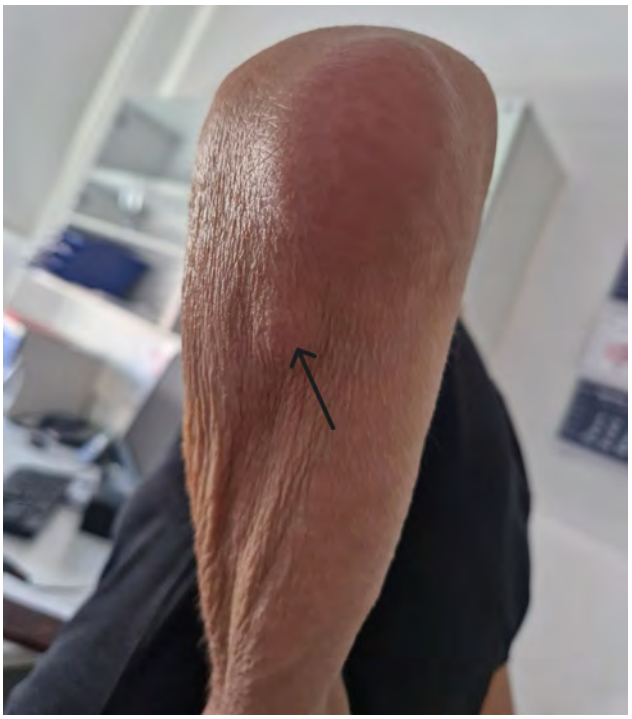

Figure 3. Subcutaneous nodular lesion (arrow) measuring 3 cm × 2.5 cm below elbow of patient in a case of *Mycoplasma arginini* cellulitis, tenosynovitis, and arthritis in kidney transplant recipient, Slovenia, 2024. The patient reported no pain in this nodule, and it was excised after discharge and 3 weeks of doxycycline treatment. Broad-range PCR confirmed *M. arginini* with 100% sequence identity, but *Mycoplasma* spp. culture was negative. Histopathology showed mild inflammatory changes consistent with bacterial infection.

specific cases to improve treatment outcomes, especially in immunocompromised persons or patients with disseminated infections (*11*). Treatment duration remains unclear. A meta-analysis of septic arthritis caused by *Mycoplasma* spp. reported therapy durations ranging from 2 weeks to >2 years. Clinical improvement, normalization of inflammatory markers, and negative reculture results should guide discontinuation (*11*).

The case we report also raises questions about persistently elevated β-D-glucan levels, which decreased but did not normalize after treatment. Although *Mycoplasma* species are not commonly associated with β-D-glucan production, studies suggest some species, such as *M. agalactiae*, might produce it (*12*). The zoonotic aspect is also notable, considering the well-documented colonization of domestic animals by *M. arginini* and the patient's history of cat bites, likely making her pets the source of infection.

Conclusions

This case underscores the limitations of conventional microbiology for detecting fastidious pathogens and highlights the value of molecular diagnostics for ensuring rapid and accurate diagnoses and effective treatment. Early recognition and appropriate therapy are crucial for improving outcomes in rare but serious *Mycoplasma* infections. Clinicians should consider *M. arginini* in the differential diagnosis of indolent infections in immunocompromised patients, particularly those with hypogammaglobulinemia and close animal contact.

The data associated with the project are accessible in the European Nucleotide Archive database (https://www.ebi.ac.uk/ena/browser/home) under accession no. PRJEB84416.

Written informed consent was obtained from the patient for the publication of this case report, including the use of accompanying photographs.

This study was supported by the Ministry of Higher Education, Science and Innovation, Republic of Slovenia (grant nos. P3-0083 and P3-0323).

About the Author

Dr. Vivoda is a nephrology resident at the Department of Nephrology, University Medical Centre Ljubljana, Slovenia. Her research primarily focuses on the nutritional management of patients with end-stage kidney disease.

References

1. Chalker VJ. Canine mycoplasmas. Res Vet Sci. 2005;79:1–8. https://doi.org/10.1016/j.rvsc.2004.10.002
2. Yechouron A, Lefebvre J, Robson HG, Rose DL, Tully JG. Fatal septicemia due to *Mycoplasma arginini*: a new human zoonosis. Clin Infect Dis. 1992;15:434–8. https://doi.org/10.1093/clind/15.3.434
3. Watanabe M, Hitomi S, Goto M, Hasegawa Y. Bloodstream infection due to *Mycoplasma arginini* in an immunocompromised patient. J Clin Microbiol. 2012;50:3133–5. https://doi.org/10.1128/JCM.00736-12
4. Roifman CM, Rao CP, Lederman HM, Lavi S, Quinn P, Gelfand EW. Increased susceptibility to *Mycoplasma* infection in patients with hypogammaglobulinemia. Am J Med. 1986;80:590–4. https://doi.org/10.1016/0002-9343(86)90812-0
5. Lierz M, Hagen N, Harcourt-Brown N, Hernandez-Divers SJ, Lüschow D, Hafez HM. Prevalence of mycoplasmas in eggs from birds of prey using culture and a genus-specific mycoplasma polymerase chain reaction. Avian Pathol. 2007;36:145–50. https://doi.org/10.1080/03079450701213347
6. Silló P, Pintér D, Ostorházi E, Mazán M, Wikonkál N, Pónyai K, et al. Eosinophilic fasciitis associated with *Mycoplasma arginini* infection. J Clin Microbiol. 2012;50:1113–7. https://doi.org/10.1128/JCM.05568-11
7. Prayson MJ, Venkatarayappa I, Srivastava M, Northern I, Burdette SD. Deep infection with *Mycoplasma arginini* in an open femur fracture secondary to an African lion bite: a case report. Inj Extra. 2008;39:243–6. https://doi.org/10.1016/j.injury.2007.12.009
8. Sillis M. *Mycoplasma arginini*—a new human zoonosis? Clin Infect Dis. 1994;18:488–488. https://doi.org/10.1093/clinids/18.3.488
9. Hannan PCT. Guidelines and recommendations for antimicrobial minimum inhibitory concentration (MIC) testing against veterinary mycoplasma species. International Research Programme on Comparative Mycoplasmology. Vet Res. 2000;31:373–95. https://doi.org/10.1051/vetres:2000100
10. Okazaki N, Narita M, Yamada S, Izumikawa K, Umetsu M, Kenri T, et al. Characteristics of macrolide-resistant *Mycoplasma pneumoniae* strains isolated from patients and induced with erythromycin in vitro. Microbiol Immunol. 2001;45:617–20. https://doi.org/10.1111/j.1348-0421.2001.tb01293.x
11. Chen Y, Huang Z, Fang X, Li W, Yang B, Zhang W. Diagnosis and treatment of mycoplasmal septic arthritis: a systematic review. Int Orthop. 2020;44:199–213. https://doi.org/10.1007/s00264-019-04451-6
12. Gaurivaud P, Baranowski E, Pau-Roblot C, Sagné E, Citti C, Tardy F. *Mycoplasma agalactiae* secretion of β-(1→6)-glucan, a rare polysaccharide in prokaryotes, is governed by high-frequency phase variation. Appl Environ Microbiol. 2016;82:3370–83.https://doi.org/10.1128/AEM.00274-16

Address for correspondence: Željka Večerić Haler, University Medical Center Ljubljana, Zaloška 2, 1000 Ljubljana, Slovenia; email: zeljka.vecerichaler@kclj.si

High Prevalence of Artemisinin-Resistant *Plasmodium falciparum*, Southeastern Sudan

Mariangela L'Episcopia, Albadawi A. Talha, Bakri Y.M. Nour, Ibrahim Mohamed Ahmed Sana, Emmanuelle Caspar, Lucas Thiebaut, Lucien Platon, Buze Chala, Laurence Ma, Lemu Golassa, Edvige Perrotti, Carlo Severini, Didier Menard

We conducted a hospital-based cross-sectional study of *Plasmodium falciparum* in 2017 in southeastern Sudan. Among 257 *P. falciparum* samples, we found 22% harbored the *pfkelch13* R622I mutation and 10.7% showed *hrp2/3* gene deletions. Our findings highlight the urgent need for enhanced surveillance of drug- and diagnostic-resistant parasites in the Horn of Africa.

Malaria challenges global public health, especially in high-transmission areas of sub-Saharan Africa (*1*). Artemisinin-based drug combination therapy (ACT) has greatly reduced malaria illness and death, but the emergence and spread of partial resistance to artemisinin drug derivatives (ART-R) in *Plasmodium falciparum* threatens those gains. ART-R, which delays parasite clearance after 3 days of ACT, is associated with specific nonsynonymous polymorphisms in the propeller domain of the *P. falciparum kelch13* (*Pfkelch13*) gene (*2*–*4*). Although ACTs remain effective in Africa, recent reports have identified *Pfkelch13* mutations (R561H, C469Y, A675V, and R622I) linked to ART-R in several countries, particularly Rwanda, Uganda, Tanzania, and Eritrea (*5*–*9*). In addition, *P. falciparum* isolates with *hrp2/3* gene deletions, which evade detection by HRP2-based rapid diagnostic tests (RDTs), have emerged in the Horn of Africa, highlighting the need for vigilant monitoring of resistance and gene deletions (*8*,*10*).

Sudan, a major contributor to malaria cases in the World Health Organization Eastern Mediterranean Region (*1*), has struggled to meet the 2030 Global Technical Strategy targets. During 2015–2020, malaria incidence rose by >40%, leading to the adoption of the high burden to high impact strategy in 2022 (*11*). *P. falciparum* drug resistance, particularly to artesunate/sulfadoxine and pyrimethamine drugs, complicates those efforts, prompting a shift to artemether/lumefantrine drugs as first-line treatment. In addition, *hrp2* gene deletions were recently identified in >10% of *P. falciparum* isolates (*12*) (Appendix, https://wwwnc.cdc.gov/EID/article/31/6/24-1810-App1.pdf). In this study, we analyzed *P. falciparum* blood sample isolates from southeastern Sudan for molecular markers associated with antimalarial drug resistance and *hrp2* and *hrp3* gene deletions.

The Study

We conducted a hospital-based cross-sectional observational study during August–December 2017 in Al Jazirah and Al Qadarif states, located in the east-central region of Sudan. Those sites are characterized by a subequatorial climate with a rainy season typically occurring during June–early November (*13*) (Appendix). All patients exhibiting clinical symptoms suggestive of malaria were eligible for blood sampling, after informed consent was obtained from the patient or parents. We confirmed *P. falciparum* malaria diagnosis through microscopy by using thick and thin blood films. Patients received treatment with AL drugs in accordance with the national drug policy.

Author affiliations: Istituto superiore di sanità, Rome, Italy (M. L'Episcopia, E. Perrotti, C. Severini); Jouf University, Sakaka, Saudi Arabia (A.A. Talha); University of Gezira, Wad Medani, Sudan (B.Y.M. Nour, I.M.A. Sana); University of Strasbourg, Strasbourg, France (E. Caspar, L. Thiebaut, L. Platon, D. Menard); Addis Ababa University, Addis Ababa, Ethiopia (B. Chala, L. Golassa); Institut Pasteur, Paris, France (L. Ma, D. Menard); Centre Hospitalier Universitaire de Strasbourg, Strasbourg, France (D. Menard); Institut Universitaire de France, Paris (D. Menard)

DOI: https://doi.org/10.3201/eid3106.241810

We spotted finger-prick blood onto Whatman 3MM filter papers (Whatman International, https://www.cytivalifesciences.com) to make dried blood spots for molecular analysis. The study received ethical approval from the Ministry of Health in Gezira State (approval no. MU/2019).

We extracted genomic DNA from three 3-mm punches of dried blood spots, as previously described (*14*). We conducted Illumina paired-end sequencing (Illumina, https://www.illumina.com) and selective amplification of parasite DNA to identify single-nucleotide polymorphisms in the *Pfkelch13*, *Pfcrt*,

Table 1. Frequency of the *Pfkelch13*, *Pfcrt*, *Pfmdr-1*, *dhfr*, and *dhps* genotypes in blood samples collected in patients with *Plasmodium falciparum* malaria before artemisinin-based combination therapy from Al Jazirah and Al Qadarif, Sudan, 2017*

Gene	Codon	Amino acid	No. (%) samples			p value
			Al Jazirah	Al Qadarif	Total	
No. samples	NA	NA	170	87	257	NA
Pfkelch13†	Wilms tumor	NA	123 (72.4)	69 (79.3)	192 (74.7)	0.01
	494	Valine → Isoleucine	1 (0.6)	0	1 (0.4)	
	622	Arginine → Isoleucine	42 (24.7)	10 (11.5)	52 (20.2)	
	625	Glycine → Arginine	1 (0.6)	6 (6.9)	7 (2.7)	
	622/625	Arginine → Isoleucine / Glycine → Arginine	1 (0.6)	2 (2.3)	3 (1.2)	
	622/494	Arginine → Isoleucine / Valine → Isoleucine	1 (0.6)	0	1 (0.4)	
	494/658	Valine → Isoleucine / Lysine → Threonine	1 (0.6)	0	1 (0.4)	
Pfcrt	72	Cysteine	170 (100)	87 (100)	257 (100)	NA
		Serine	NA	NA	NA	
	74	Methionine	124 (73)	44 (51)	168 (65)	0.0004
		Isoleucine	46 (27)	43 (49)	89 (35)	
	75	Asparagine	124 (73)	44 (51)	168 (65)	0.0004
		Glutamic acid	46 (27)	43 (49)	89 (35)	
	76	Lysine	124 (73)	44 (51)	168 (65)	0.0004
		Threonine	46 (27)	43 (49)	89 (35)	
	93	Threonine	170 (100)	86 (99)	256 (99.6)	0.2
		Serine	0	1 (1)	1 (0.4)	
	356	Isoleucine	169 (99)	85 (98)	254 (98.8)	0.2
		Threonine	1 (1)	2 (2)	3 (1.2)	
Pfmdr-1	86	Asparagine	145 (85)	75 (86)	220 (86)	0.8
		Tyrosine	25 (15)	12 (14)	37 (14)	
	184	Tyrosine	20 (12)	14 (16)	34 (13)	0.3
		Phenylalanine	150 (88)	73 (84)	223 (87)	
	1034	Serine	139 (82)	70 (80)	209 (81)	0.8
		Cysteine	31 (18)	17 (20)	48 (19)	
	1042	Asparagine	170 (100)	87 (100)	257 (100)	NA
		Aspartic acid	NA	NA	NA	
	1246	Aspartic acid	170 (100)	87 (100)	257 (100)	NA
		Tyrosine	NA	NA	NA	
dhfr	51	Asparagine	79 (46)	16 (18)	95 (37)	<0.0001
		Isoleucine	91 (54)	71 (82)	162 (63)	
	59	Cysteine	151 (90)	76 (87)	227 (89)	0.4
		Arginine	16 (10)	11 (13)	27 (11)	
	108	Serine	72 (42)	22 (25)	94 (37)	0.007
		Asparagine	98 (58)	65 (75)	163 (63)	
	164	Isoleucine	170 (100)	87 (100)	257 (100)	NA
		Leucine	NA	NA	NA	
dhps	431	Isoleucine	170 (100)	87 (100)	257 (100)	NA
		Valine	NA	NA	NA	
	436	Serine	167 (98)	83 (95)	250 (97)	0.2
		Alanine	3 (2)	4 (5)	7 (3)	
	437	Alanine	30 (18)	35 (40)	65 (25)	0.0001
		Glycine	140 (82)	52 (60)	192 (75)	
	540	Lysine	162 (95)	72 (83)	234 (91)	0.0009
		Glutamic acid	8 (5)	15 (17)	23 (9)	
	581	Alanine	170 (100)	87 (100)	257 (100)	NA
		Glycine	NA	NA	NA	
	613	Alanine	169 (99)	86 (99)	255 (99)	0.6
		Serine	1 (1)	1 (1)	2 (1)	

*p values indicate the difference in percentages between sites. NA, not available.
†*Pfkelch13* 622I/625R, 1 sample from Al Jazirah and 2 samples from Al Qadarif; *Pfkelch13* 494I/622I, 1 sample from Al Jazirah; *Pfkelch13* 494I/658T, 1 sample from Al Jazirah.

Table 2. Genetic backgrounds associated with antimalarial drug resistance and polymorphisms of *hrp2/3* genes of *Pfkelch13 R622* and *622I* isolates collected from patients with *Plasmodium falciparum* malaria before treatment from Al Jazirah and Al Qadarif, Sudan, 2017*

			Al Jazirah			Al Qadarif			Total		
Gene	Allele		R622	622I	p value	R622	622I	p value	R622	622I	p value
No. samples	NA		126	44	NA	75	12	NA	201	56	NA
Pfcrt	CVMNKTHFIMCGI	NA	93 (74)	31 (71)	0.2	39 (52)	5 (42)	0.005	132 (65.7)	36 (64.3)	0.01
	CVIETTHFIMCGI	74I/75E/76T	33 (26)	12 (27)		35 (47)	5 (42)		68 (33.8)	17 (30.4)	
	CVIETSHFIMCGI	74I/75E/76T/93S	0	0		1 (1)	0		1 (0.5)	0	
	CVIETTHFIMCGT	74I/75E/76T/356T	0	1 (2)		0	2 (17)		0	3 (5.4)	
Pfmdr-1	NYSND	NA	11 (9)	3 (7)	0.3	10 (13)	1 (8)	0.6	21 (10.4)	4 (7.1)	0.2
	YYSND	86Y	0	1 (2)		0	0		0	1 (1.8)	
	NFSND	184F	73 (58)	31 (70)		41(55)	9 (75)		114 (56.7)	40 (71.4)	
	NYCND	1034C	5 (4)	0		3 (4)	0		8 (4.0)	0	
	YFSND	86Y/184F	15 (12)	5 (11)		9 (12)	0		24 (11.9)	5 (8.9)	
	NFCND	184F/1034C	19 (15)	3 (7)		9 (12)	2 (17)		28 (13.9)	5 (8.9)	
	YFCND	86Y/184F/1034C	3 (2)	1 (2)		3 (4)	0		6 (3.0)	1 (1.8)	
dhfr	ACNCSI	NA	28 (22)	21 (48)	0.06	10 (13)	2 (17)	0.6	38 (18.9)	23 (41.1)	0.01
	ACICSI	51I	15 (12)	4 (9)		8 (11)	1 (8)		23 (14.4)	5 (8.9)	
	ACNCNI	108N	21 (17)	7 (16)		2 (3)	2 (17)		23 (14.4)	9 (16.1)	
	ACICNI	51I/108N	48 (38)	10 (23)		44 (59)	7 (58)		92 (45.8)	17 (30.4)	
	ACIRSI	51I/59R	4 (3)	0		1 (1)	0		5 (2.5)	0	
	ACNRNI	59R/108N	2 (2)	0		0	0		2 (1.0)	0	
	ACIRNI	51I/59R/108N	8 (6)	2 (5)		10 (13)	0		18 (9.0)	2 (3.6)	
dhps	SAKAA	NA	99 (79)	32 (73)	0.8	30 (40)	6 (50)	0.7	129 (64.2)	38 (67.9)	0.8
	SGKAA	437G	18 (14)	9 (20)		28 (37)	4 (33)		46 (22.9)	13 (23.2)	
	SAEAA	540E	6 (5)	2 (5)		14 (19)	1 (8)		20 (10.0)	3 (5.4)	
	SAKAS	613S	1 (1)	0		0	0		1 (0.5)	0	
	AGKAA	436A/437G	2 (2)	1 (2)		2 (3)	1 (8)		4 (2.0)	2 (3.6)	
	AAKAS	436A/613S	0	0		1 (1)	0		1 (0.5)	0	
hrp	no deletion	NA	112 (89)	35 (80)	0.1	56 (75)	7 (58)	0.3	168 (83.6)	42 (75.0)	0.09
	hrp2 deletion	NA	1 (1)	0		0	0		1 (0.5)	0	
	hrp3 deletion	NA	11 (9)	5 (11)		15 (20)	3 (25)		26 (12.9)	8 (14.3)	
	hrp2/3 deletion	NA	2 (2)	4 (9)		4 (5)	2		6 (3.0)	6 (10.7)	

*Values are no. (%) except as indicated. p values are the differences in proportions between *Pfkelch13 R622* and *Pfkelch13 622I* parasites. NA, not available.

Pfmdr-1, *dhfr*, and *dhps* genes, as previously described (*8*). In addition, we assessed deletions of the *hrp2* or *hrp3* genes, which can lead to false-negative results in HRP2-based RDTs. We used laboratory reference parasite strains (Dd2, 7G8, HB3, and Cambodia culture-adapted strains) with known alleles and the presence or absence of *hrp2* and *hrp3* deletions as controls (Appendix).

We collected a total of 257 blood samples from 2 study sites: 170 from Al Jazirah and 87 from Al Qadarif. Demographic data were missing for 2 samples, resulting in a study population of 255 participants, 128 female and 127 male, ages 1–44 years. Most enrolled patients were febrile (95.6%), and their clinical manifestations were common to malaria, such as headache and vomiting (58.6%). After we examined the thick and thin blood films, we found all the patients were positive for *P. falciparum*.

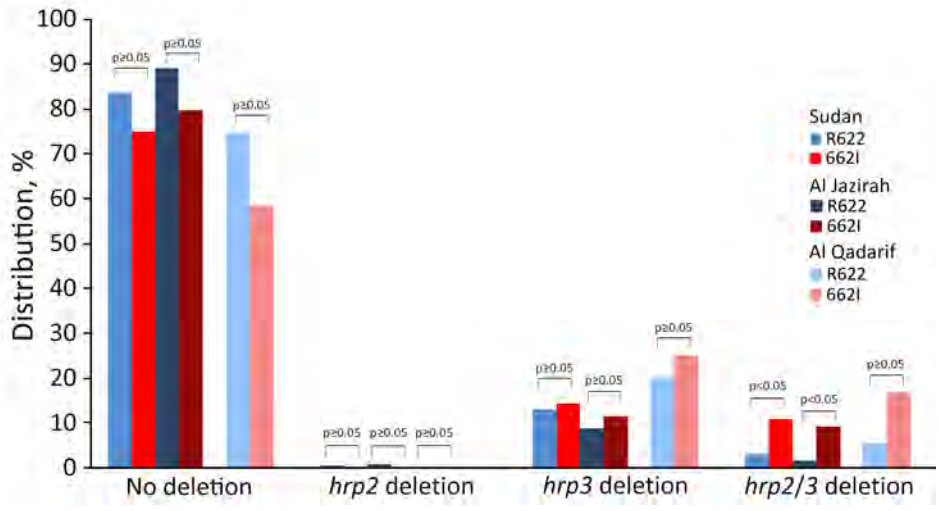

Figure. Distribution of artemisinin-resistant *Plasmodium falciparum*, southeastern Sudan, 2017. Percentages of *Pfkelch13* R622 and *Pfkelch13* 622I *P. falciparum* parasites with no *hrp2/3* deletion, *hrp2* deletion, *hrp3* deletion, and *hrp2/3* deletion are shown for Sudan and the 2 study sites, Al Jazirah and Al Qadarif.

Molecular analysis of the 257 samples revealed a high prevalence of the *Pfkelch13* 622I mutant parasites (21.8%, n = 56), a mutation validated by the World Health Organization as associated with ART-R. Among them, we identified 192 *Pfkelch13* wild-type, 52 *Pfkelch13* 622I single mutants, 1 *Pfkelch13* 494I single mutant, 7 *Pfkelch13* 625R single mutants, and 5 isolates with polyclonal infections (3 *Pfkelch13* 622I/625R, 1 *Pfkelch13* 622I/494I, and 1 *Pfkelch13* 494I/658T) (Table 1).

We further explored the genetic profile of the *Pfkelch13* R622 wild-type parasites from Sudan and 622I mutants at known antimalarial drug–resistance loci and the frequency of *hrp2* and *hrp3* deletions, a genomic feature previously observed in *Pfkelch13* 622I mutants in Eritrea and Ethiopia (*8*,*10*). We examined 201 *Pfkelch13* R622 wild-type and 56 *Pfkelch13* 622I mutant parasites for mutations across 4 genes (Table 2). Differences in allele frequencies were noted in the *Pfcrt* gene, associated with resistance to chloroquine, and the *dhfr* gene, associated with resistance to pyrimethamine. We conducted a stratified analysis that revealed a higher difference in *Pfcrt* allele frequencies in the Al Qadarif site compared with Al Jazirah. High proportions of *Pfkelch13* 622I parasites exhibited *Pfcrt* 74I/75E/76T/356T mutations (5.4% vs. 0% for *Pfkelch13* R622 wild-type parasites; p = 0.01) as well as the *dhfr* wild-type allele (41.1% vs. 18.9% for *Pfkelch13* R622 wild-type parasites; p = 0.001).

We also analyzed *hrp2* and *hrp3* deletions. We found a higher proportion of *Pfkelch13* 622I parasites with both *hrp2* and *hrp3* deletions compared with *Pfkelch13* R622 wild-type parasites (10.7% vs. 3.0%; p = 0.02) (Table 2; Figure). This difference was significant in samples from Al Jazirah (p = 0.04).

Conclusions

The spread of the *Pfkelch13* 622I mutant in the Horn of Africa is alarming because it raises the potential for ART-R to take hold in this region. Data from this study show parallels with findings from Eritrea (*8*) and possibly Ethiopia (*10*). With confirmed cases in Eritrea and possible cases in Ethiopia (*8*,*10*), the presence of this mutant in Sudan suggests a possible cross-border spread that could threaten malaria treatment in several countries. If left uncontained, *Pfkelch13* 622I mutant parasites could undermine the efficacy of ACTs, threatening progress in malaria control in East Africa. Rapid regional surveillance and coordinated response efforts are urgently needed to contain this threat before it escalates further. In addition, the presence of *hrp2/hrp3* gene deletions in 10.7% of the *Pfkelch13* 622I mutants reported in this study is an additional concern, because it affects the results of HRP2-based RDTs in detecting *P. falciparum* parasites. Because of the presence of those gene deletions, the variants could spread more easily because they are not detected by the HRP2-based RDT, complicating malaria control efforts in affected regions.

The first limitation of this study is that we could not confirm the association between the presence of *Pfkelch13* 622I and the persistence of parasitemia on day 3, because clinical data were not available. Second, our data came from only 2 health facilities with limited catchment areas. Third, the samples were collected in 2017, but the findings remain highly relevant in 2025 because they provide critical baseline data on the early spread of resistance markers in Sudan. Although clinical reports of treatment failures in Sudan remain limited, our data are essential for understanding the persistence and regional transmission dynamics

of ART-R *P. falciparum* parasites, which is crucial for guiding current malaria control strategies.

Our findings increase the need for further studies to determine whether the *Pfkelch13* 622I mutants observed in Sudan represent a local emergence or are directly linked to the *P. falciparum* parasite population from Eritrea or Ethiopia, as well as to clarify the flow of the *Pfkelch13* 622I mutant parasite population in this region. With ART-R now confirmed in *P. falciparum* and *hrp2* and *hrp3* deletions in parasite populations in Sudan, additional strategies must be implemented to contain the spread of these lineages across the Horn of Africa. Otherwise, the emergence of partner drug resistance could lead to higher rates of treatment failure and uncontrolled spread of potentially resistant *P. falciparum* parasites beyond this region.

Acknowledgments

We thank the patients who contributed samples, their guardians in the communities of Al Jazirah and Al Qadarif, all team members in the health centers, and the personnel at the Biomics Platform at the Institut Pasteur for their help with this work.

This work was supported by Fondation Recherche Médicale (grant no. EQU202403018026), by the Institut Universitaire de France, and by France Génomique (grant no. ANR-10-INBS-09) and Infrastructures en Biologie Santé et Agronomie.

About the Author

Dr. L'Episcopia is a researcher with the Department of Infectious Diseases, Istituto Superiore di Sanità, specializing in the molecular epidemiology of infectious diseases, particularly malaria. Her research interests include the identification and surveillance of drug-resistant *P. falciparum* parasites.

References

1. World Health Organization. World malarial report 2024: addressing inequity in the global malaria response. [cited 2025 Feb 4]. https://www.who.int/teams/global-malaria-programme/reports/world-malaria-report-2024
2. Ariey F, Witkowski B, Amaratunga C, Beghain J, Langlois AC, Khim N, et al. A molecular marker of artemisinin-resistant *Plasmodium falciparum* malaria. Nature. 2014;505:50–5. https://doi.org/10.1038/nature12876
3. Ashley EA, Dhorda M, Fairhurst RM, Amaratunga C, Lim P, Suon S, et al.; Tracking Resistance to Artemisinin Collaboration (TRAC). Spread of artemisinin resistance in *Plasmodium falciparum* malaria. N Engl J Med. 2014;371:411–23. https://doi.org/10.1056/NEJMoa1314981
4. Dondorp AM, Nosten F, Yi P, Das D, Phyo AP, Tarning J, et al. Artemisinin resistance in *Plasmodium falciparum* malaria. N Engl J Med. 2009;361:455–67. https://doi.org/10.1056/NEJMoa0808859
5. Conrad MD, Asua V, Garg S, Giesbrecht D, Niaré K, Smith S, et al. Evolution of partial resistance to artemisinins in malaria parasites in Uganda. N Engl J Med. 2023;389:722–32. https://doi.org/10.1056/NEJMoa2211803
6. Ishengoma DS, Mandara CI, Bakari C, Fola AA, Madebe RA, Seth MD, et al. Evidence of artemisinin partial resistance in northwestern Tanzania: clinical and molecular markers of resistance. Lancet Infect Dis. 2024;24:1225–33. https://doi.org/10.1016/S1473-3099(24)00362-1
7. Juliano JJ, Giesbrecht DJ, Simkin A, Fola AA, Lyimo BM, Pereus D, et al. Prevalence of mutations associated with artemisinin partial resistance and sulfadoxine-pyrimethamine resistance in 13 regions in Tanzania in 2021: a cross-sectional survey. Lancet Microbe. 2024;5:100920. https://doi.org/10.1016/S2666-5247(24)00160-5
8. Mihreteab S, Platon L, Berhane A, Stokes BH, Warsame M, Campagne P, et al. Increasing prevalence of artemisinin-resistant HRP2-negative malaria in Eritrea. N Engl J Med. 2023;389:1191–202. https://doi.org/10.1056/NEJMoa2210956
9. Uwimana A, Legrand E, Stokes BH, Ndikumana JM, Warsame M, Umulisa N, et al. Emergence and clonal expansion of in vitro artemisinin-resistant *Plasmodium falciparum* kelch13 R561H mutant parasites in Rwanda. Nat Med. 2020;26:1602–8. https://doi.org/10.1038/s41591-020-1005-2
10. Fola AA, Feleke SM, Mohammed H, Brhane BG, Hennelly CM, Assefa A, et al. *Plasmodium falciparum* resistant to artemisinin and diagnostics have emerged in Ethiopia. Nat Microbiol. 2023;8:1911–9. https://doi.org/10.1038/s41564-023-01461-4
11. World Health Organization Eastern Mediterranean Region. Sudan's adoption of "high burden to high impact" approach to boost malaria control efforts. 2022 [cited 2025 Feb 4]. https://www.emro.who.int/malaria/rbm-news/sudans-adoption-of-high-burden-to-high-impact-approach-to-boost-malaria-control-efforts.html
12. Prosser C, Gresty K, Ellis J, Meyer W, Anderson K, Lee R, et al. *Plasmodium falciparum* histidine-rich protein 2 and 3 gene deletions in strains from Nigeria, Sudan, and South Sudan. Emerg Infect Dis. 2021;27:471–9. https://doi.org/10.3201/eid2702.191410
13. Elagali A, Ahmed A, Makki N, Ismail H, Ajak M, Alene KA, et al. Spatiotemporal mapping of malaria incidence in Sudan using routine surveillance data. Sci Rep. 2022;12:14114. https://doi.org/10.1038/s41598-022-16706-1
14. Zainabadi K, Adams M, Han ZY, Lwin HW, Han KT, Ouattara A, et al. A novel method for extracting nucleic acids from dried blood spots for ultrasensitive detection of low-density *Plasmodium falciparum* and *Plasmodium vivax* infections. Malar J. 2017;16:377. https://doi.org/10.1186/s12936-017-2025-3

Address for correspondence: Didier Ménard, University of Strasbourg, 3 rue Koéberlé, F-67000 Strasbourg, France; email: dmenard@unistra.fr

Highly Pathogenic Avian Influenza A(H5N1) in Wild Birds and a Human, British Columbia, Canada, 2024

Chelsea G. Himsworth, Jessica M. Caleta, Agatha N. Jassem, Kevin C. Yang, James E.A. Zlosnik, John R. Tyson, Laurie Wilson, Kevin S. Kuchinski, Jolene Giacinti, Megan Willie, Tony D. Redford, Maeve Winchester, Caeley Thacker, Yohannes Berhane, Theresa Burns, Natalie Prystajecky, Shannon L. Russell

We characterized highly pathogenic avian influenza A(H5N1) clade 2.3.4.4b genotype D1.1 in wild birds and a human in British Columbia, Canada, during 2024. D1.1, the predominant genotype circulating in fall 2024, is a reassortment between Eurasian A3 lineage viruses, introduced to North America in 2022, and North American lineage viruses.

In fall 2021, highly pathogenic avian influenza (HPAI) A(H5N1) virus clade 2.3.4.4b was introduced into wild birds and domestic poultry in eastern Canada via the East Atlantic Flyway (*1*). It subsequently spread throughout North America before arriving in British Columbia, Canada, in April 2022 (*1*). A second incursion of HPAI H5N1 virus, clade 2.3.4.4b, brought in by the Pacific Flyway (genotype A3) (*2*), occurred in February 2022, resulting in both viruses circulating among wild birds in the province and causing numerous spillover events into poultry (*3*). The virus affected more poultry flocks in British Columbia than in any other province in Canada (*4*), likely because high-density poultry farming is co-located with optimal habitat for overwintering waterfowl in the Fraser Valley (*3*).

As of the end of 2024, British Columbia had endured 4 distinct waves of HPAI H5N1 clade 2.3.4.4b virus; each wave was characterized by increased detections in wildlife and poultry, the emergence of new genotypes (Table), and shifts in the dominant genotype (Figure 1). Most circulating HPAI H5N1 clade 2.3.4.4b viruses in the first 3 waves were reassortant descendants of the virus introduced via the East Atlantic Flyway (*3*); however, in fall 2024, a new wave of infections occurred in British Columbia wild bird populations associated primarily with a novel genotype (D1.1, 3) that was a descendant of the A3 genotype. We used whole-genome sequencing and phylogenetic analysis of HPAI H5N1 clade 2.3.4.4b viruses detected in wild birds in British Columbia during October and November 2024 to describe the features, ecology, and possible origins of this genotype.

The Study

As part of initiatives driven by the British Columbia Wildlife Avian Influenza Surveillance Program, we screened oropharyngeal and cloacal swab specimens collected from wild bird carcasses using quantitative reverse transcription PCR targeting a conserved region in the matrix gene and subjected positive samples (cycle threshold <36) to whole-genome sequencing (*3*). Sequences underwent subtyping, genotyping, and phylogenetic analysis as previously described (*3*).

Author affiliations: British Columbia Ministry of Agriculture and Food, Abbotsford, British Columbia, Canada (C.G. Himsworth, T.D. Redford, T. Burns); British Columbia Centre for Disease Control, Vancouver, British Columbia, Canada (J.M. Caleta, A.N. Jassem, K.C. Yang, J.E.A. Zlosnik, J.R. Tyson, K.S. Kuchinski, N. Prystajecky, S.L. Russell); Canadian Wildlife Service–Environment and Climate Change Canada, Delta, British Columbia, Canada (L. Wilson, M. Willie); Environment and Climate Change Canada, Ottawa, Ontario, Canada (J. Giacinti); British Columbia Ministry of Water, Land and Resource Stewardship, Nanaimo, British Columbia, Canada (M. Winchester, C. Thacker); Canadian Food Inspection Agency, Winnipeg, Manitoba, Canada (Y. Berhane)

DOI: http://doi.org/10.3201/eid3106.241862

Table. Reassortant classification and genotypic characterization of clade 2.3.4.4b viruses in a study of highly pathogenic avian influenza A(H5N1) in wild birds and a human, British Columbia, Canada, 2024*

GenoFLU genotype†	Genotype assignment by influenza A segment								Outbreak wave‡
	HA	NA	M	NP	NS	PA	PB1	PB2	
B2.1	EA1	EA1	EA1	Am1.1	EA1	EA1	EA1	Am1.2	Wave 1
B3.2	EA1	EA1	EA1	Am1.4.1	Am1.1	EA1	Am1.2	Am2.1	Waves 1–3
B3.6	EA1	EA1	EA1	Am1.4.1	Am1.1	EA1	Am4	Am5	Wave 3
B3.10	EA1	EA1	EA1	Am4	Am1.1	EA1	Am4	Am5	Wave 3
B3.1	EA1	EA1	EA1	Am1.4.1	EA1	EA1	EA1	Am2.1	Wave 1
B4.1	EA1	EA1	EA1	Am1.3	EA1	EA1	EA1	Am2.2	Waves 1–3
A3	EA3	EA3	EA3	EA3	EA3	EA3	EA3	EA3	Waves 1–4
D1.1	EA3	Am4N1	EA3	Am13	EA3	Am4	EA3	Am24	Wave 4
B3.13	EA1	EA1	EA1	Am8	Am1.1	EA1	Am4	Am2.2	US cattle genotype (for context only)

*Data show viruses detected in British Columbia, Canada, during September 2021–November 2024 contextualized by the US cattle virus genotype B3.13 identified in 2024. Am, North American lineage; EA, Eurasian lineage; HA, hemagglutinin; M, matrix; NA, neuaminidase; NP, nucleoprotein; NS, nonstructural; PA, polymerase acidic; PB, polymerase basic.
†Genotype assignment from GenoFlu pipeline (*2*).
‡Wave 1, April–Sept 2022; wave 2, Sept 2022–Aug 2023; wave 3, Sept 2023–Aug 2024; wave 4, Sept 2024–November 2024.

During October 3, 2024–November 8, 2024, there were 57 detections of HPAI H5N1clade 2.3.4.4b virus in wild birds in British Columbia, including 6 detections of genotype A3 and 51 detections of genotype D1.1 (Figure 1, panel A). Of note, A3 viruses identified in BC in 2024 were more closely related to A3 viruses from Japan (2024) than A3 viruses from British Columbia in 2023, suggesting that they represent a new HPAI incursion from East Asia (Appendix Figure, https://wwwnc.cdc.gov/EID/article/31/6/24-1862-App1.pdf). Most (68.6%, 35/51) detections occurred in the Fraser Valley. Across the province, detections occurred predominantly in cackling geese (*Branta hutchinsii*; 35.3%, 18/51), followed by Canada geese (*Branta canadensis*; 17.6%, 9/51) and snow geese (*Anser caerulenscens*; 15.7%, 8/51); 1–3 detections each occurred in American wigeons (*Mareca americana*), bald eagles (*Haliaeetus leucocephalus*), barred owls (*Strix varia*), great blue herons (*Ardea herodias*), great horned owls (*Bubo virginianus*), green-winged teals (*Anas carolinensis*), northern pintails (*Anas acuta*), peregrine falcons (*Falco peregrinus*), and red-tailed hawks (*Buteo jamaicensis*).

On November 8, 2024, we confirmed a diagnosis of influenza caused by HPAI H5N1 clade 2.3.4.4b genotype D1.1 in a teenager from the Fraser Valley (*5*). The sequence we obtained from this patient was most closely related to viruses detected in wild birds (Figure 2). The D1.1 lineage strain of the virus has also been associated with all but one of the 60 poultry outbreaks that occurred in British Columbia during October 21–November 30, 2024 (*4*).

The D1.1 genotype contained 4 Eurasian lineage segments (hemagglutinin, matrix, nonstructural, and polymerase basic 1) that were related to the 2023 BC A3 lineage viruses and 4 segments from North American lineage viruses (neuraminidase [NA], nucleoprotein, polymerase acidic, and polymerase basic 2), including an NA segment not previously associated with HPAI H5N1 clade 2.3.4.4b viruses in British Columbia (Table). Although the 2024 D1.1 lineage viruses and the 2023 A3 lineage viruses shared a recent common ancestor, the 2024 D1.1 lineage viruses displayed less genetic divergence than expected over that intervening time (Figure 1, panel B). Phylodynamic analysis using BEAST (https://beast.community) and sequences from National Center for Biotechnology Information and GISAID (https://www.gisaid.org) databases revealed that the closest relative to the D1.1 Am4N1 NA segment was an H1N1 virus detected in a mallard (A/mallard/BC/AIV-PHL-2360/2024) from the British Columbia interior on August 20, 2024, and that the reassortment event involving that segment may have occurred in fall 2023 (Figure 3) (*6*). That H1N1 virus belongs to a lineage of earlier H1N1 viruses also detected in mallards and was distantly related to another H1N1 detected in Alberta (A/Mallard/AB/539/2023). Of note, several Am4N1 segments from D1.1 viruses in poultry from the same British Columbia outbreak (A/chicken/BC/FAV-0289-002/2024, A/chicken/BC/FAV-0284-001/2024, A/turkey/BC/FAV-0306-1/2024) had a mutation associated with antiviral resistance, NA-H275Y (*7*); however, that mutation was not detected in any of the wild bird sequences.

Conclusions

The once dominant B genotypes associated with the HPAI H5N1 clade 2.3.4.4b virus incursion via the Eastern Atlantic Flyway do not appear to be circulating in wild birds within the Pacific Flyway as of fall 2024 (despite the continuing presence of genotype B3.13 in cattle in the western United States [*8*]) (Table). Instead, a novel genotype, D1.1, has emerged that is the result of a reassortment among the A3 genotypes originally introduced via the Pacific Flyway and ≥1 North American lineage avian influenza viruses. This virus spilled

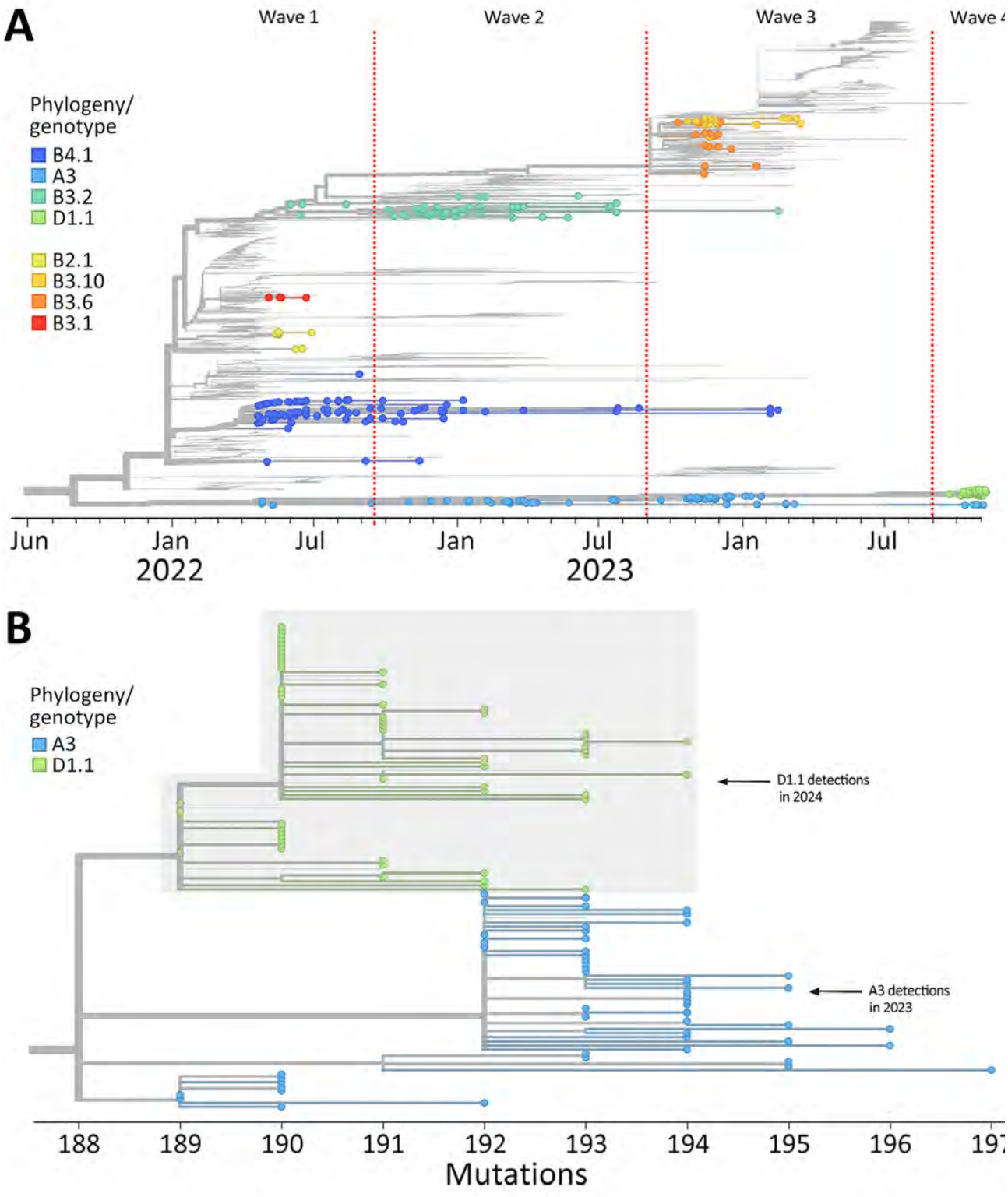

Figure 1. Hemagglutinin-specific phylogenetic analysis of clade 2.3.4.4b detections from a study of highly pathogenic avian influenza A(H5N1) in wild birds and a human, British Columbia, Canada, 2024. Data based on detections during September 2021–November 2024 contextualized by sequences from other parts of North and South America. Trees are rooted on the A/goose/Guangdong/1/96 (H5) reference sequence. A) Detections of all genotypes plotted on the basis of specimen collection date. B) Genotype A3 and D1.1 detections plotted on the basis of divergence.

over into poultry in British Columbia and infected 1 human and has also been detected in parts of the United States south of British Columbia (Figure 2).

Compared with A3 viruses detected a year earlier, the hemagglutinin segment of the D1.1 viruses had acquired fewer net substitutions than expected, despite sharing a relatively recent common ancestor (Figure 1, panel B). This finding could suggest that the D1.1 genotype or its ancestors may have been preserved in an environmental reservoir—e.g., in frozen wetlands in the high arctic (*9*)—in the summer of 2024 before being reintroduced into migratory birds in the fall. Alternatively, this viral lineage may be particularly well adapted to certain wild bird species or populations, resulting in circulation with minimal evolutionary pressure. This finding has implications for the use of molecular clock theory in phylodynamic modeling of HPAI viruses.

We note that D1.1 appears to be unique among the HPAI H5N1 clade 2.3.4.4b genotypes due to the acquisition of a North American lineage NA segment. The Am4N1 NA segment likely originated from a reassortment event involving waterfowl in western Canada, potentially within British Columbia. Further studies are needed to determine where and when the other reassorted segments were acquired.

Of interest, the prevalence of environmental HPAI H5N1 virus clade 2.3.4.4b detections based on genomic analysis of wetland sediment was far greater in fall 2024 than for data from fall 2023 (*10*). This phenomenon could suggest that a great number of birds were infected with D1.1 compared with other genotypes in previous years, that the genotype is associated with greater viral shedding, or both. The NA segment encodes the enzyme required for viral release from infected cells (*11*). Certain NA lineages, therefore, might increase viral shedding in wild birds. Considering the explosive wave of poultry outbreaks observed in British Columbia in late 2024, it would be prudent to investigate whether the Am4N1 NA segment has a functional impact on host-virus interactions. In addition, it will be important to determine the implications of D1.1 for host range and infectivity, given that the virus detected in the human case was most closely related to those found in wild birds, suggesting the potential for direct or indirect transmission from wild birds to humans.

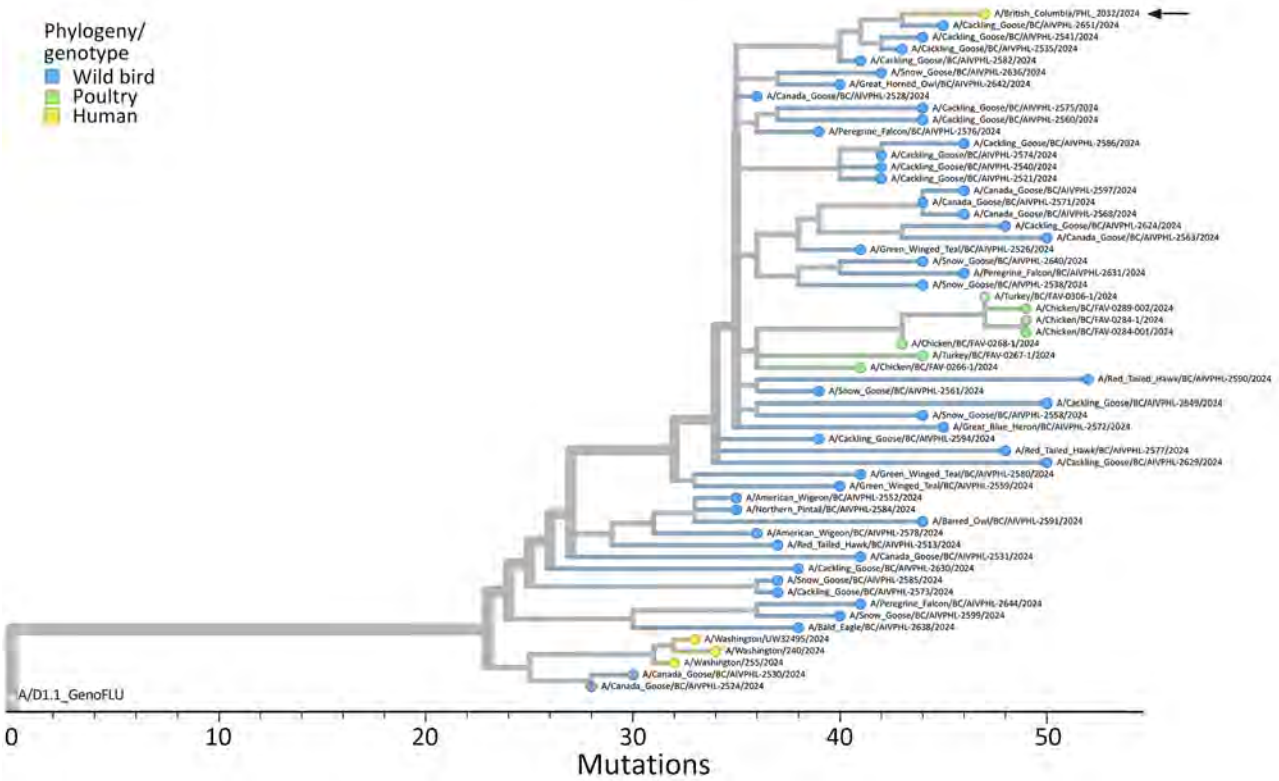

Figure 2. Phylogenetic analysis of concatenated full genome sequences of clade 2.3.4.4b genotype D1.1 detections in wild birds, poultry, and a human from a study of highly pathogenic avian influenza A(H5N1) in wild birds and a human (arrow), British Columbia, Canada, 2024. Data drawn from detections during October 3–November 8, 2024. Tree is plotted based on divergence and rooted to a composite D1.1 reference sequence assembled from D1.1 segments obtained from the GenoFLU Version 1.0.5 database (https://github.com/USDA-VS/GenoFLU/).

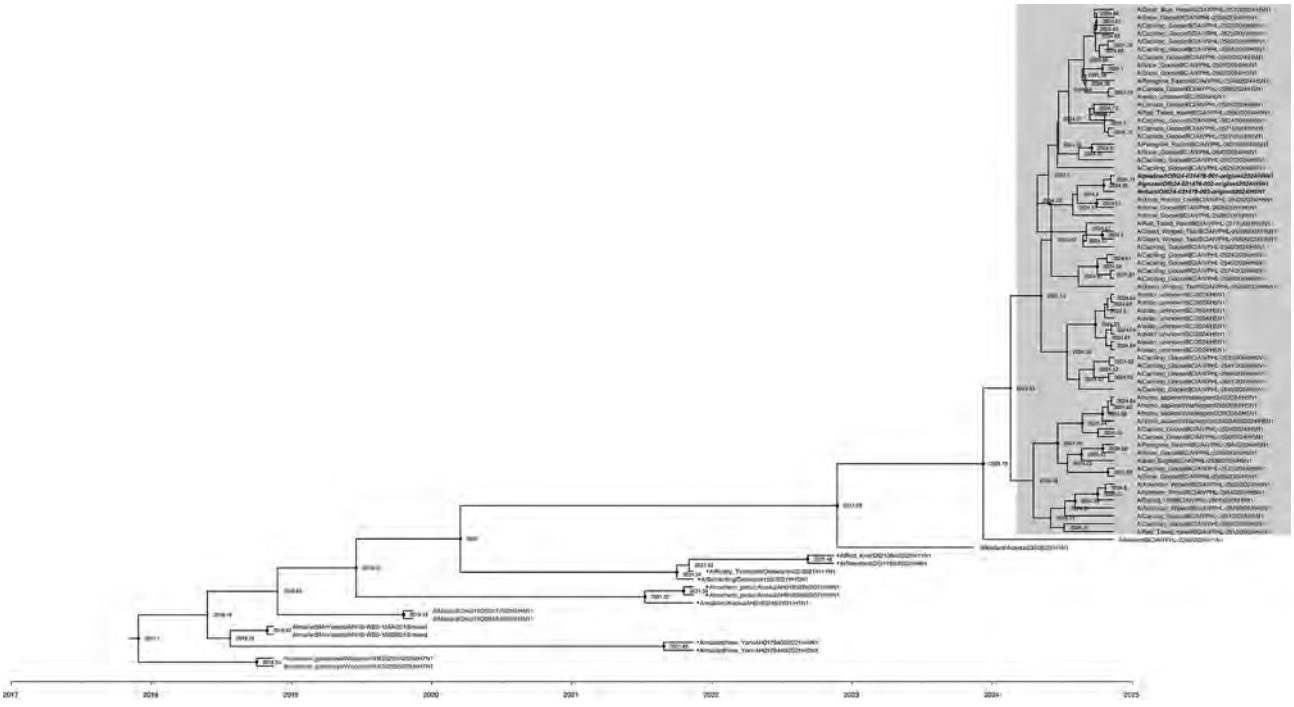

Figure 3. Phylogenetic relationships and possible origins of the neuraminidase (NA) segment (Am4N1) of the clade 2.3.4.4b D1.1 genotype detected in fall 2024 as part of a study of highly pathogenic avian influenza A(H5N1) in wild birds and a human, British Columbia, Canada, 2024. The maximum clade credibility tree was inferred by using BEAST v2.7.7 (*6*), incorporating NA gene sequences from D1.1 viruses and closely related sequences from wild birds detected in British Columbia and National Center for Biotechnology Information databases; the full tree is available online (https://wwwnc.cdc.gov/EID/article/31/6/24-1862-F3.htm). Analysis used an uncorrelated relaxed log-normal clock, the Hasegawa-Kishino-Yano substitution model without gamma rate heterogeneity, and a coalescent Bayesian skyline tree prior. The posterior distribution was approximated using 100 million Markov chain Monte Carlo steps, sampled every 10,000 steps, with a 10% burn-in. All NA segments were identified as Am4N1 by GenoFLU except those indicated with a black dot on the tree tip label; non-Am4N1 sequences were classified as unassigned. D1.2 samples are bolded and italicized. Node support values and branch lengths indicate the evolutionary divergence and probable reassortment timeframes leading to the emergence of the Am4N1 NA segment in the D1.1 genotype.

This study was supported by the Sustainable Canadian Agricultural Partnership program.

About the Author

Dr. Himsworth is a veterinary pathologist and epidemiologist who is the Deputy Chief Veterinarian for the Province of British Columbia, Canada, the British Columbia Regional Director for the Canadian Wildlife Health Cooperative, and an Associate Clinical Professor in the School of Population and Public Health at the University of British Columbia. Her research and practice centers around One Health–based transdisciplinary approaches to the surveillance and management of health issues associated with wild and domestic animals.

References

1. Alkie TN, Lopes S, Hisanaga T, Xu W, Suderman M, Koziuk J, et al. A threat from both sides: multiple introductions of genetically distinct H5 HPAI viruses into Canada via both East Asia-Australasia/Pacific and Atlantic flyways. Virus Evol. 2022;8:veac077. https://doi.org/10.1093/ve/veac077
2. Youk S, Torchetti MK, Lantz K, Lenoch JB, Killian ML, Leyson C, et al. H5N1 highly pathogenic avian influenza clade 2.3.4.4b in wild and domestic birds: introductions into the United States and reassortments, December 2021–April 2022. Virology. 2023;587:109860. https://doi.org/10.1016/j.virol.2023.109860
3. Russell SL, Andrew CL, Yang KC, Coombe M, McGregor G, Redford T, et al. Descriptive epidemiology and phylogenetic analysis of highly pathogenic avian influenza H5N1 clade 2.3.4.4b in British Columbia (B.C.) and the Yukon, Canada, September 2022 to June 2023. Emerg Microbes Infect. 2024;13:2392667. https://doi.org/10.1080/22221751.2024.2392667
4. Canadian Food Inspection Agency. Flocks in Canada where HPAI has been detected. 2024 November 28 [cited 2024 Nov 29]. https://inspection.canada.ca/en/animal-health/terrestrial-animals/diseases/reportable/avian-influenza/latest-bird-flu-situation/status-ongoing-response.
5. Jassem AN, Roberts A, Tyson J, Zlosnik JE, Russell SL, Caleta JM, et al. Critical illness in an adolescent with influenza A(H5N1) virus infection. N Engl J Med. 2025;392:927-929. https://doi.org/10.1056/NEJMc2415890
6. Bouckaert R, Vaughan TG, Barido-Sottani J, Duchêne S, Fourment M, Gavryushkina A, et al. BEAST 2.5: an advanced

software platform for Bayesian evolutionary analysis. PLOS Comput Biol. 2019;15:e1006650. https://doi.org/10.1371/journal.pcbi.1006650
7. Signore AV, Joseph T, Ranadheera C, Erdelyan CNG, Alkie T, Raj S, et al. Neuraminidase reassortment and oseltamivir resistance in clade 2.3.4.4b A(H5N1) viruses circulating among Canadian poultry, 2024. Emerg Microbes Infect. 2025;14:2469643. https://doi.org/10.1080/22221751.2025.2469643
8. Animal and Plant Health Inspection Service, US Department of Agriculture. HPAI confirmed cases in livestock [cited 2025 Feb 13]. https://www.aphis.usda.gov/livestock-poultry-disease/avian/avian-influenza/hpai-detections/hpai-confirmed-cases-livestock
9. Ramey AM, Reeves AB, Lagassé BJ, Patil V, Hubbard LE, Kolpin DW, et al. Evidence for interannual persistence of infectious influenza A viruses in Alaska wetlands. Sci Total Environ. 2022;803:150078. https://doi.org/10.1016/j.scitotenv.2021.150078
10. British Columbia Ministry of Agriculture. HPAI detections in BC: wildlife and environmental surveillance. [cited 2024 Dec 2]. https://governmentofbc.maps.arcgis.com/apps/dashboards/8c6c84718e5748179102a0be2368029a
11. Aoki FY, Boivin G. Influenza virus shedding: excretion patterns and effects of antiviral treatment. J Clin Virol. 2009;44:255–61. https://doi.org/10.1016/j.jcv.2009.01.010

Address for correspondence: Chelsea G. Himsworth, British Columbia Ministry of Agriculture and Food, 1767 Angus Campbell Rd, Abbotsford, BC V3G 2M3, Canada; email: chelsea.himsworth@gov.bc.ca

Dual-Genotype *Orientia tsutsugamushi* Infections, Hainan Island, China, 2023

Yi Niu,[1] Siqi Chen,[1] Gaoyu Wang, Yijia Guo, Nan Ge, Xiaoyuan Hu, Chuanning Tang, Ruoyan Peng, Xiuji Cui, Biao Wu, Bo Wang, Yueping Wang, Dachuan Lin, Yongguo Du, Jasper Fuk-Woo Chan, Long Sun, Kwok-Yung Yuen,[2] Liyuan Zhang,[2] Feifei Yin[2]

We report 3 cases of dual-genotype *Orientia tsutsugamushi* infection in Hainan Island, China. Patients exhibited diverse clinical manifestations, including afebrile illness and multiorgan involvement, highlighting the complexity associated with genetic diversity in scrub typhus. Clinicians should maintain heightened suspicion for atypical scrub typhus manifestations in endemic regions

Scrub typhus, caused by the obligate intracellular bacterium *Orientia tsutsugamushi*, is a significant but underrecognized tropical disease endemic found mainly throughout the Asia-Pacific region (*1*). Scrub typhus places approximately 1 billion persons at risk and causes illness in 1 million persons each year (*2*). Extensive genetic diversity is a hallmark of *O. tsutsugamushi*, influencing disease severity and complicating vaccine development and diagnostic accuracy (*3*). We describe 3 cases from Hainan Island, China, that illustrate the clinical variability and diagnostic challenges associated with dual-genotype infections and underscore the need for further investigation into their clinical implications.

The Study

Patient 1 was a 55-year-old male farmer from Lingao County in Hainan Province, China (Table), who sought treatment for symptoms that included a 5-day history of fever peaking at 39.8°C, along with chills, headache, and fatigue. On September 12, 2023, he was admitted to the Infectious Diseases Department, Second Affiliated Hospital of Hainan Medical University (Haikou, China). At admission, laboratory test results showed markedly elevated inflammatory markers and liver enzymes: high-sensitivity C-reactive protein 122.70 mg/L (reference range <10 mg/L), neutrophil percentage 84.1% (reference range 40%–70%), alanine aminotransferase 301 U/L (reference range <40 U/L), aspartate transaminase 384 U/L (reference range <40 U/L), and direct bilirubin 7.0 μmol/L (reference range <5 μmol/L). In addition, interleukin 6 was markedly elevated at 156.00 pg/mL (reference range <7 pg/mL) and D-dimer was 100.39 μg/mL (reference range <0.5 μg/mL).

We determined the illness to be scrub typhus based on clinical manifestations and results from real-time PCR testing targeting the *O. tsutsugamushi* 47-kDa and 56-kDa type-specific antigen genes (Zybio Inc., https://www.zybio.com) and serologic testing for IgM and IgG using a Gold-immuno-chromatographic assay kit (Beijing Wantai, https://www.ystwt.cn). We promptly administered intravenous doxycycline (0.2 g in 250 mL normal saline daily) plus supportive care, and the patient's condition gradually improved. He was discharged 6 days after admission.

Patient 2 was a 49-year-old male farmer from Wanning City, Hainan Province, whose symptoms included a 10-day history of high-grade fever (up to 40°C), cough with yellow sputum, and chest tightness (Table). His symptoms worsened 2 days before admission, with recurrence of those symptoms plus shortness of breath and urinary frequency. Admitted to the emergency intensive care unit (ICU), First Affiliated Hospital of Hainan Medical University (Haikou, China), on June 14, 2023, the patient received an

Author affiliations: Hainan Medical University, Haikou, China (Y. Niu, S. Chen, G. Wang, Y. Guo, N. Ge, X. Hu, C. Tang, R. Peng, X. Cui, B. Wu, B. Wang, Y. Wang, D. Lin, Y. Du, L. Sun, L. Zhang, F. Yin); University of Hong Kong, Hong Kong, China (J. F.-W. Chan, K.-Y. Yuen)

DOI: http://doi.org/10.3201/eid3106.241967

[1]These authors contributed equally to this article.

[2]These authors contributed equally to this article and are co–senior authors.

Table. Clinical and laboratory features of patients in study of dual-genotype *Orientia tsutsugamushi* infections, Hainan, China, 2023*

Patient	Age, y/sex	Clinical status at admission	Site of eschar	Disease severity	Genotypes (ratio)	Hospital stay, d
1	55/M	5-day history of fever, headache, fatigue	NA	Moderate	Karp_B + JG_C (1:2)	6
2	49/M	10-day history of fever, cough, dyspnea	Below clavicle	Severe (ICU)	Karp_A + JG_C (17:2)	16
3	64/M	5-day history of ataxia, weakness (afebrile)	Hip	Severe (shock)	Karp_B + Kato_B (1:1)	6

*ICU, intensive care unit; NA, not applicable.

initial diagnosis of severe pneumonia. Laboratory tests revealed severe inflammation and multiorgan involvement: high-sensitivity C-reactive protein 183.74 mg/L, neutrophil percentage 75.6%, leukocyte count 17.94 × 10^9 cells/L (reference range 4–10 × 10^9 cells/L), alanine aminotransferase 77 U/L, aspartate transaminase 150 U/L, D-dimer 11.81 μg/mL, albumin 19.6 g/L (reference range 35–50 g/L), arterial oxygen partial pressure/fractional inspired oxygen ratio 284 mm Hg (reference range >300 mm Hg), and platelet count 67 × 10^9/L (reference range 150–400 × 10^9/L). Imaging revealed bilateral pulmonary infiltrates, mild pleural effusion, enlarged axillary lymph nodes, and splenomegaly. Investigation revealed a 0.3 cm × 0.5 cm eschar below the right clavicle, strongly suggesting scrub typhus as the underlying cause. We

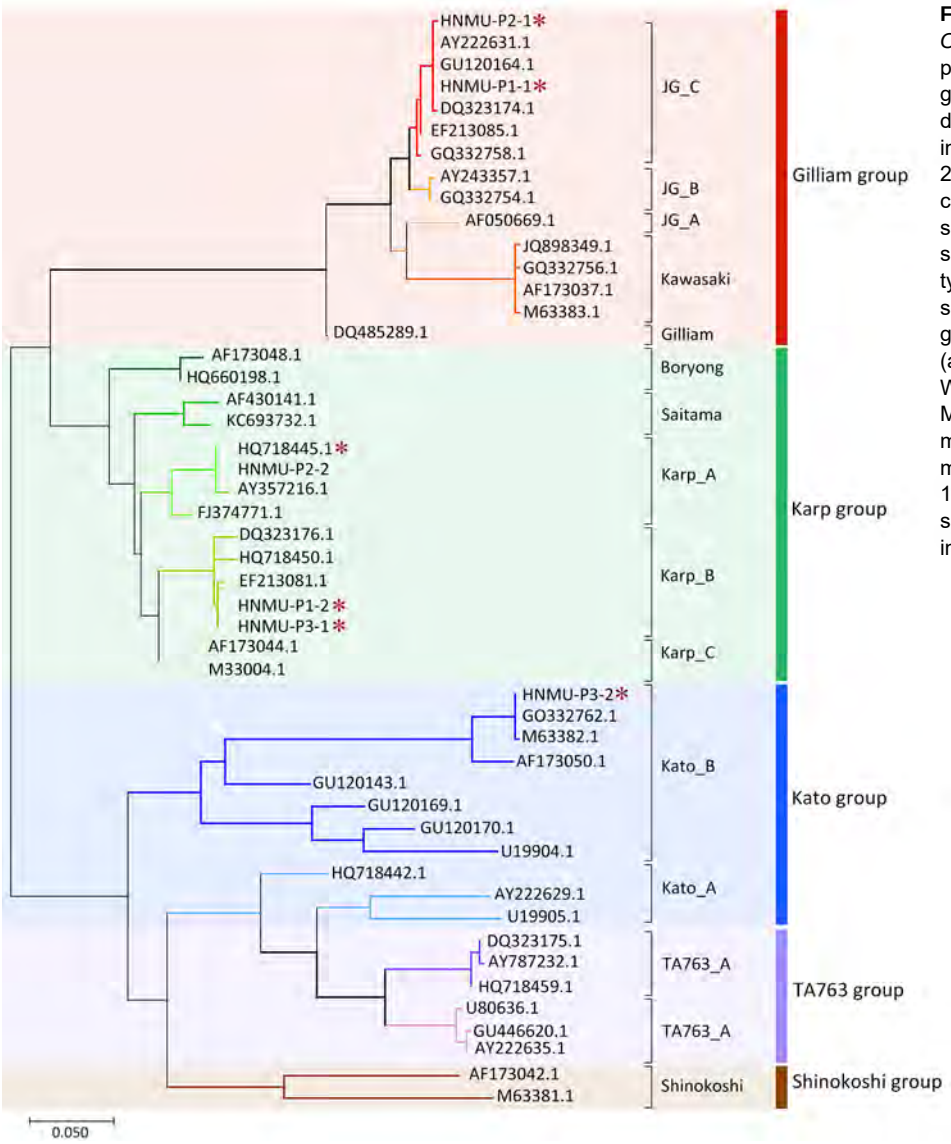

Figure. Phylogenetic analysis of *Orientia tsutsugamushi* based on partial 56-kDa type-specific antigen gene sequences from a study of dual-genotype *O. tsutsugamushi* infections, Hainan Island, China, 2023. Phylogenetic tree was constructed using partial gene sequences from whole blood samples of 3 patients with scrub typhus (red asterisks) and reference sequences representing dominant genotypes retrieved from GenBank (accession numbers indicated). We performed the analysis with MEGA X software (https://www.megasoftware.net) using the maximum-likelihood method and 1,000 bootstrap replicates. Color shading and vertical bars at right indicate genotypes.

later confirmed *O. tsutsugamushi* infection by real-time PCR and serologic testing. Oral doxycycline (0.2 g/d) and supportive treatment led to improvement by the third day of treatment. The patient was discharged 16 days after admission.

Patient 3 was a 64-year-old male farmer from Chengmai County, Hainan Province, who sought treatment for a 5-day history of unsteady gait, limb weakness, and fatigue (Table). He had a 40-year history of epilepsy, managed with valproic acid and oxcarbazepine. The patient was admitted to the Neurology Department, Second Affiliated Hospital of Hainan Medical University, on November 23, 2023. Examination showed impaired articulation and a positive Romberg sign, but no fever (36.8°C). Laboratory tests indicated elevated inflammatory markers and mild hepatic injury: high-sensitivity C-reactive protein 71.06 mg/L, alanine aminotransferase 54 U/L, aspartate transaminase 86 U/L, interleukin 6 127.00 pg/mL, D-dimer 5.47 μg/mL, and platelet count 62 × 10^9/L. Computed tomography of the patient's chest revealed mild, ground glass opacities in multiple lung segments, bilateral pleural thickening, mild pleural effusion, and enlarged axillary lymph nodes. Given the initial signs and symptoms of thrombocytopenia, liver dysfunction, and pneumonitis, we treated the patient with antiepileptic drugs and ceftriaxone, which imparted minimal effect. On the third hospital day, attending staff noted a 0.3 cm × 0.4 cm eschar on the patient's hip. Subsequent real-time PCR analysis and IgM/IgG serologic testing for *O. tsutsugamushi* yielded positive results, thereby confirming a diagnosis of scrub typhus. We then treated the patient with intravenous doxycycline (0.2 g in 250 mL normal saline daily), along with supportive treatments that included inotropic support and antiepileptic therapy. His condition improved within 3 days, and he was discharged 6 days after admission.

All 3 patients with scrub typhus tested positive by real-time PCR, IgM and IgG serology, and nested PCR targeting the 483-bp fragment of the 56-kDa type-specific antigen gene (*4*). Sanger sequencing showed overlapping nucleotide peaks, indicating mixed infection. Cloning and subsequent sequencing of individual amplicons confirmed dual-genotype *O. tsutsugamushi* infections. Patient 1 was co-infected with Karp B (Karp group) and JG_C (Gilliam group) genotypes at a 1:2 ratio (Karp B: 5/15 clones; JG_C: 10/15 clones), with 74.43% nucleotide sequence identity between them (Figure). Patient 2 carried Karp A (Karp group) and JG_C genotypes in a 17:2 ratio (Karp A: 17/19 clones, JG_C: 2/19 clones) at 74.25% identity. Patient 3 was co-infected with Karp B and Kato_B (Kato group) genotypes in a 1:1 ratio (Karp B: 9/18 clones, Kato_B: 9/18 clones) at 72.87% identity.

All 3 patients were middle-aged, male farmers (mean age 56 ± 7.55 years) with recent outdoor exposure, consistent with typical risk factors for scrub typhus. We discovered an eschar on 2 of the patients, a characteristic clinical feature of the disease. The severity of illness varied widely among the 3 case patients: 1 patient developed severe scrub typhus requiring ICU care; another had a relatively mild, afebrile course. Despite differences in severity, all 3 case patients shared common features, including pulmonary involvement and liver dysfunction, markedly elevated inflammatory markers, and thrombocytopenia. Among the 3 patients, patient 2 exhibited the highest proportion of the Karp_A genotype and required ICU admission, indicating greater disease severity (Table). Previous studies have associated the Karp genotype with more severe clinical manifestations and higher bacterial loads (*5*–*7*). Although limited by sample size, our preliminary observations suggest that genotype dominance in dual-genotype infections may influence disease severity, warranting larger-scale studies.

Conclusions

Dual-genotype *O. tsutsugamushi* infections represent a complex and underexplored aspect of scrub typhus epidemiology (*8*–*13*). Our study highlights dual-genotype *O. tsutsugamushi* infections in 3 patients from Hainan Island, China, and emphasizes the genetic complexity and clinical variability associated with scrub typhus. We observed Karp-group strains consistently present alongside Gilliam and Kato strains, reflecting dominant regional circulation patterns (*5*). Despite varied clinical severities, all patients exhibited common features, namely pulmonary involvement, hepatic dysfunction, elevated inflammatory markers, and thrombocytopenia. The presence of multiple genotypes within individual infections, confirmed through sequencing and cloning, underscores the diagnostic and therapeutic challenges associated with scrub typhus. Our findings necessitate further studies to elucidate the influence of dual-genotype infections on disease progression, clinical outcomes, and treatment efficacy. Clinicians should maintain heightened suspicion for atypical scrub typhus manifestations in endemic regions.

Acknowledgments

The authors thank all patients for participating in this study and the support from Emerging Tropical Infectious

Diseases Science Innovation Group of Hainan Medical University and the Hainan Tropical Infectious Diseases Biobank.

This study was approved by the Ethics Committee of the Hainan Medical University (ethics approval no. HYLL-2020-061). Written informed consent to participate in this study was obtained from all patients.

All sequences analyzed during this study are available from GenBank (accession nos. PQ788284–9).

This study was funded by the Key Research and Development Plan of Hainan Province (ZDYF2022SHFZ098), Hainan Provincial International Science and Technology Cooperation Research and Development Project (GHYF2024021), Hainan Provincial Natural Science Foundation of China (824MS067, 821QN0896, 821QN262, and G20230324004Y), the National Natural Science Foundation of China (82060378 and 82160387, 2022YFC2305005), and Major Project of Guangzhou National Laboratory (GZNL2023A01001). The funding sources had no role in the study design, data collection, analysis, interpretation, or writing of this report.

About the Author

Ms. Niu is a doctoral candidate at Hainan Medical University, specializing in the clinical manifestations, comparative genomics, and pathogenesis of scrub typhus. Her research focuses on elucidating the genetic factors that influence disease severity and developing improved diagnostic and therapeutic strategies for this tropical disease.

References

1. Walker DH. Scrub typhus—scientific neglect, ever-widening impact. N Engl J Med. 2016;375:913–5. https://doi.org/10.1056/NEJMp1608499
2. Xu G, Walker DH, Jupiter D, Melby PC, Arcari CM. A review of the global epidemiology of scrub typhus. PLoS Negl Trop Dis. 2017;11:e0006062. https://doi.org/10.1371/journal.pntd.0006062
3. Kim G, Ha NY, Min CK, Kim HI, Yen NT, Lee KH, et al. Diversification of *Orientia tsutsugamushi* genotypes by intragenic recombination and their potential expansion in endemic areas. PLoS Negl Trop Dis. 2017;11:e0005408. https://doi.org/10.1371/journal.pntd.0005408
4. Mahajan SK, Rolain J-M, Kashyap R, Bakshi D, Sharma V, Prasher B, et al. Scrub typhus in Himalayas. Emerg Infect Dis. 2006;12:1590–2. https://doi.org/10.3201/eid1210.051697
5. Wang G, Fu R, Zhang L, Xue L, Al-Mahdi AY, Xie X, et al. Genomic bacterial load associated with bacterial genotypes and clinical characteristics in patients with scrub typhus in Hainan Island, Southern China. PLoS Negl Trop Dis. 2023;17:e0011243. https://doi.org/10.1371/journal.pntd.0011243
6. Mika-Gospodorz B, Giengkam S, Westermann AJ, Wongsantichon J, Kion-Crosby W, Chuenklin S, et al. Dual RNA-seq of *Orientia tsutsugamushi* informs on host-pathogen interactions for this neglected intracellular human pathogen. Nat Commun. 2020;11:3363. https://doi.org/10.1038/s41467-020-17094-8
7. Kim DM, Yun NR, Neupane GP, Shin SH, Ryu SY, Yoon HJ, et al. Differences in clinical features according to Boryoung and Karp genotypes of *Orientia tsutsugamushi.* PLoS One. 2011;6:e22731. https://doi.org/10.1371/journal.pone.0022731
8. Zhang M, Zhao ZT, Wang XJ, Li Z, Ding L, Ding SJ, et al. Mixed scrub typhus genotype, Shandong, China, 2011. Emerg Infect Dis. 2014;20:484–5. https://doi.org/10.3201/eid2003.121349
9. Le-Viet N, Phan DT, Le-Viet N, Trinh S, To M, Raoult D, et al. Dual genotype *Orientia tsutsugamushi* infection in patient with rash and eschar, Vietnam, 2016. Emerg Infect Dis. 2018;24:1520–3. https://doi.org/10.3201/eid2408.171622
10. Nanaware N, Desai D, Banerjee A, Zaman K, Mittal M, Mittal M, et al. Genotypic characterization of *Orientia tsutsugamushi* isolated from acute encephalitis syndrome and acute febrile illness cases in the Gorakhpur area, Uttar Pradesh, India. Front Microbiol. 2022;13:910757. https://doi.org/10.3389/fmicb.2022.910757
11. Usha K, Kumar E, Kalawat U, Kumar BS, Chaudhury A, Gopal DVRS. Molecular characterization of *Orientia tsutsugamushi* serotypes causing scrub typhus outbreak in southern region of Andhra Pradesh, India. Indian J Med Res. 2016;144:597–603. https://doi.org/10.4103/0971-5916.200886
12. Sonthayanon P, Peacock SJ, Chierakul W, Wuthiekanun V, Blacksell SD, Holden MT, et al. High rates of homologous recombination in the mite endosymbiont and opportunistic human pathogen *Orientia tsutsugamushi.* PLoS Negl Trop Dis. 2010;4:e752. https://doi.org/10.1371/journal.pntd.0000752
13. Tang C, Zhang L, Huang Y, Mai W, Xue L, Wang G, et al. Mixed genotypes of *Orientia tsutsugamushi* in conserved genes and a single immune-dominant tsa56 genotype discovered from a patient with scrub typhus in Hainan Island, China: a case report. BMC Infect Dis. 2022;22:698. https://doi.org/10.1186/s12879-022-07682-y

Address for correspondence: Feifei Yin, Xueyuan Rd No. 3#, Hainan Medical University, Haikou, 571199, China; email: yinfeifeiff@163.com

Eschar

[es'kahr, es'kər]

Neha Srivastava, Kamran Zaman, Mahima Mittal

Eschars, distinctive skin lesions from rickettsial infection induced by feeding ticks or mites, play a crucial role in diagnosing scrub typhus and spotted fever rickettsioses. Eschars occur at the sites where rickettsial pathogens are inoculated into the skin by an arthropod vector and typically emerge within a few (median 5) days after tick or mite bites, during the incubation period before symptom onset.

Rickettsia-associated eschar is caused by rickettsial growth in endothelial cells, leading to thrombosis, ischemia, and necrosis of dermal tissue. The lesion initially resembles a small papule or pustule, then evolves into a central 0.5–3.0-cm ulcer covered by brown-black crust and encircled by a red halo (Figure), which can take several weeks to heal and can leave a small, depressed scar. Rickettsial eschars are typically painless, nonitchy, and frequently overlooked in patients with dark complexions, resulting in delayed diagnosis and treatment. PCR detection of pathogen DNA from eschar tissue or swab samples serves as a rapid diagnostic tool in early stages of eschar-associated rickettsial infection.

Sometimes, atypical eschars resembling acne may be observed. In mite-associated rickettsioses, eschars appear in areas where skin surfaces meet or clothes bind, such as the axilla, groin, neck, and waist, but occasionally occur at uncommon sites, such as wrist or elbow joints. However, tick-associated rickettsioses often manifest eschars on the extremities and trunk. Cutaneous manifestations of other infectious diseases, including tularemia, leishmaniasis, anthrax, and certain mycobacterial and fungal infections, can also produce eschars.

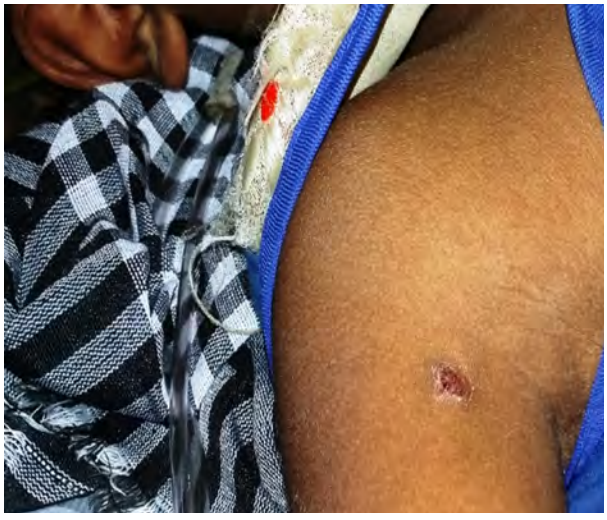

Figure. An eschar in the axillary area in the stage of healing in a patient with diagnosed scrub typhus.

The term eschar finds its root from the Ancient Greek *eskhára*, meaning hearth, brazier, or scab, from which Middle French *eschare* and Late Latin *eschara*, both signifying scar or scab, evolved. That linguistic journey reflects the lesion's historical association with healing and scarring of burnt skin.

Acknowledgments

We extend our sincere thanks to Rohit Beniwal and Asif Kavathekar for their support.

Sources

1. Bechah Y, Socolovschi C, Raoult D. Identification of rickettsial infections by using cutaneous swab specimens and PCR. Emerg Infect Dis. 2011;17:83–6. https://doi.org/10.3201/eid1701.100854
2. Jensenius M, Fournier PE, Kelly P, Myrvang B, Raoult D. African tick bite fever. Lancet Infect Dis. 2003;3:557–64. https://doi.org/10.1016/S1473-3099(03)00739-4
3. Kim DM, Won KJ, Park CY, Yu KD, Kim HS, Yang TY, et al. Distribution of eschars on the body of scrub typhus patients: a prospective study. Am J Trop Med Hyg. 2007;76:806–9. https://doi.org/10.4269/ajtmh.2007.76.806
4. Merriam Webster.com Dictionary. Eschar [cited 2024 Feb 8]. https://www.merriam-webster.com/dictionary/eschar
5. Paddock CD, Finley RW, Wright CS, Robinson HN, Schrodt BJ, Lane CC, et al. *Rickettsia parkeri* rickettsiosis and its clinical distinction from Rocky Mountain spotted fever. Clin Infect Dis. 2008;47:1188–96. https://doi.org/10.1086/592254

Author affiliations: ICMR-Regional Medical Research Centre, Gorakhpur, India (N. Srivastava, K. Zaman); ICMR-National Institute of Traditional Medicine, Belagavi, India (K. Zaman); All India Institute of Medical Sciences, Gorakhpur (M. Mittal)

Address for correspondence: Mahima Mittal, Department of Pediatrics, All India Institute of Medical Sciences, Kaysa Rd, Gorakhpur, Uttar Pradesh 273008, India; email: drmahimamittal@gmail.com

DOI: https://doi.org/10.3201/eid3106.240223

Skin Infections Caused by Panton-Valentine Leukocidin and Methicillin-Susceptible *Staphylococcus aureus* in Child, Japan

Kensuke Shoji, Kazue Yoshida, Marie Takenouchi, Junzo Hisatsune, Shoko Kutsuno, Chika Arai, Kanako Masuda, Motoyuki Sugai, Takashi Ishikawa, Toshinao Kawai, Kazuhiro Uda, Isao Miyairi

We describe a pediatric case of recurrent skin infections caused by a Panton-Valentine leukocidin and exfoliative toxin E double-positive methicillin-susceptible *Staphylococcus aureus* clonal complex 188 clone. Most of the patient's family members were infected with the same strain, and intrafamilial transmission was strongly suspected. Decolonization procedures were not effective.

Recurrent skin and soft tissue infections (SSTIs) caused by Panton-Valentine leukocidin (PVL)–positive methicillin-resistant *Staphylococcus aureus* (MRSA) have been reported worldwide (*1*,*2*). Recurrence may be attributed to intrafamilial transmission; in such cases, decolonization by nasal mupirocin ointment and topical skin application of 4% chlorhexidine are treatments for family members (*3*). Methicillin-susceptible *S. aureus* (MSSA) strains that possess virulence factors similar to those of MRSA have been reported (*4*,*5*); however, the clinical significance of such bacterial strains and the efficacy of decolonization are still unclear. We report a case of a child in Japan with recurrent SSTIs caused by PVL and exfoliative toxin E (ETE) double-positive MSSA refractory to decolonization, with evidence of intrafamilial transmission.

Author affiliations: National Center for Child Health and Development, Tokyo, Japan (K. Shoji, K. Yoshida, M. Takenouchi, T. Ishikawa, T. Kawai, K. Uda, I. Miyairi); National Institute of Infectious Diseases, Japan Institute for Health Security, Tokyo (J. Hisatsune, S. Kutsuno, C. Arai, M. Sugai); Project Research Center for Nosocomial Infectious Diseases, Hiroshima University, Hiroshima, Japan (J. Hisatsune, S. Kutsuno, C. Arai, K. Masuda, M. Sugai); Okayama University Hospital, Okayama, Japan (K. Uda); Hamamatsu University School of Medicine, Hamamatsu, Japan (I. Miyairi)

DOI: https://doi.org/10.3201/eid3106.241955

The Study

A 7-year-old girl with atopic dermatitis was referred to the National Center for Child Health and Development (Tokyo, Japan) for impetigo and recurrent multiple furuncles (furunculosis) (Figure 1). The child had no history of serious infections and no suspected immunodeficiencies. We instructed the patient to maintain skin cleanliness by showering and using moisturizers and to repeatedly treat with oral antimicrobial agents when furuncles manifested. However, the skin lesions relapsed 2–4 weeks after discontinuing the antimicrobial therapy. Culture of the pus from a furuncle identified MSSA (strain name JH62PP1) (Appendix Table, https://wwwnc.cdc.gov/EID/article/27/11/21-1265-App1.pdf).

The patient's father, older brother (12 years of age), and younger brother (3 years of age) also had similar skin lesions; we suspected intrafamilial infection of MSSA. In addition to lifestyle guidance (hand hygiene; keeping fingernails short; changing underwear, towels, and sleepwear each day; washing sheets and pillowcases weekly; washing the body with soap daily; and avoiding sharing personal items), all family members underwent decolonization using mupirocin ointment (applied to each nostril 3×/d for 3 days) and 4% chlorhexidine (applied to all skin areas below the neck 3×/wk for 4 weeks). Although the time interval between relapse of skin lesions increased temporarily, the frequency returned to the same level ≈4 months after the first decolonization (Figure 2).

We then attempted decolonization for the patient and each family member with a bleach bath in water

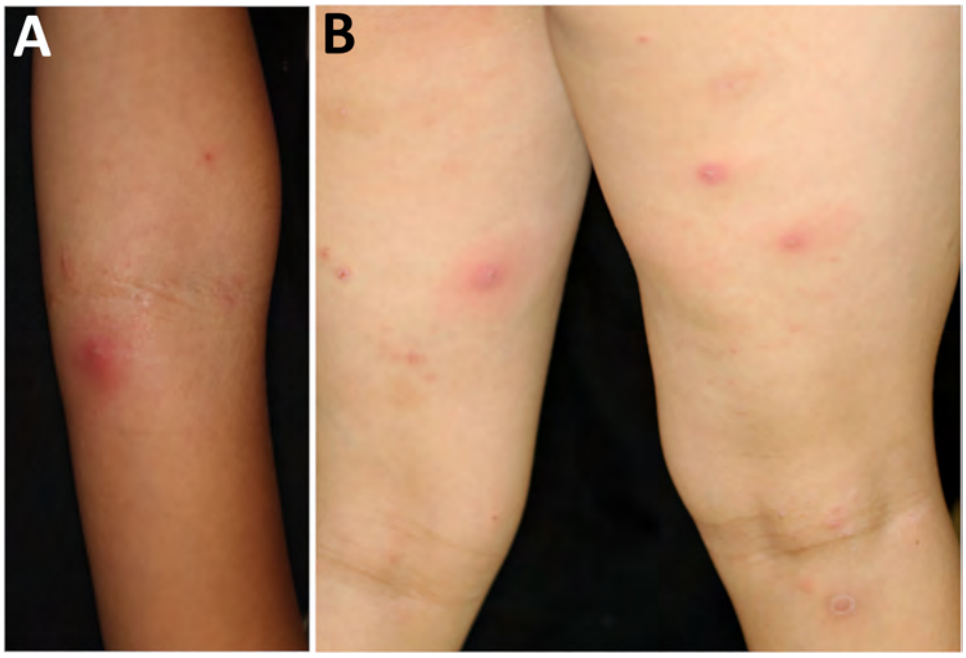

Figure 1. Multiple furuncles (furunculosis) on forearm (A) and thigh (B) of child experiencing recurrent skin infections caused by Panton-Valentine leukocidin and exfoliative toxin E double-positive methicillin-susceptible *Staphylococcus aureus* clonal complex 188 clone, Japan.

containing 0.005% hypochlorous acid as approved by the institutional ethics committee (NCCHD-1912). We instructed the patient and family to first wash their bodies with soap, then soak in the bathtub for 5–10 minutes, and finally rinse thoroughly in the shower. They performed the procedure twice a week. However, recurrences occurred within ≈2 weeks, indicating that the bath was not effective.

We assessed the patient's immune condition by blood tests, including a complete blood count with differential, immunoglobulin and complement levels, lymphocyte proliferation assay, superoxide production, and flow cytometry. The results of those tests were within reference ranges; we considered known primary immunodeficiencies, including chronic granulomatous disease and hyper-IgE syndrome, unlikely. Thereafter, we abandoned attempts at decolonization and gave the patient oral antimicrobial medication when a skin lesion formed. The frequency of skin lesions improved when the patient was 10 years of age; we observed no relapses after the patient turned 11, with no additional interventions. Outpatient follow-up ended.

In this case, we strongly suspected familial transmission of *S. aureus*. Therefore, we conducted a phylogenetic analysis using whole-genome sequencing on a total of 7 MSSA strains: 2 strains (JH62PP1 and JH62PP2) isolated from swab specimens of the patient's pus at the initial and follow-up visits and 5 strains (JH62PN, JH62F, JH62M, JH62B1, and JH62B2) isolated from nasal swab specimens of the patient and 4 other family members before decolonization treatment. We performed purification of genomic DNA, preparation of sequencing libraries, whole-genome sequencing, and core-genome–based phylogenetic analyses in this study as previously described (*6*). We deposited raw read sequences obtained in this study in GenBank/DDBJ/EMBL (BioProject no. PRJDB19081).

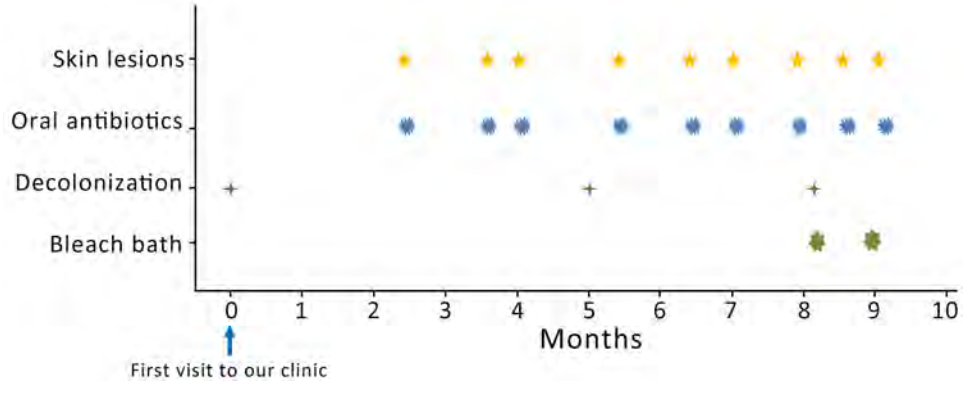

Figure 2. Timeline of symptoms and treatment of child experiencing recurrent skin infections caused by Panton-Valentine leukocidin and exfoliative toxin E double-positive methicillin-susceptible *Staphylococcus aureus* clonal complex 188 clone, Japan.

MLST analysis revealed that the JH62PP1 and JH62PN strains isolated from the patient's pus and nasal swab specimens at the initial visit, as well as those (JH62F, JH62M, and JH62B1) from nasal swab specimens of the father, mother, and older brother, were identified as MSSA sequence type (ST) 2233 (Appendix Figure 1). ST2233 belongs to clonal complex (CC) 188, as determined by eBURST analysis of PHYLoViZ version 2.0 web tool (https://www.phyloviz.net). JH62PP2, isolated from the patient's pus at the follow-up visit, belonged to ST1, and JH62B2, isolated from the younger brother's nasal swab, ST188; their STs were distinct from ST2233, which was the ST of the suspected strain of household transmission. In the case of *S. aureus*, the single-nucleotide polymorphism cutoff value for excluding patient-to-patient transmission in an outbreak setting is considered to be <15 within the previous 6 months (*7*). Therefore, all ST2233 isolates from the 4 family members were found to be very closely related, confirming that the causative clone was transmitted within the family.

We also investigated the virulence, antimicrobial-resistance, and disinfectant-resistance genes by whole-genome sequencing analysis (Table 1). Five ST2233 isolates possessed multiple virulence genes: Panton-Valentine leukocidin genes *lukS-PV* and *lukF-PV*; staphylococcal enterotoxin genes *seg*, *seh*, *sei*, *sem*, *sen*, *seo*, *ses*, and *seu*; exfoliative toxin gene *ete*; and some antimicrobial-resistance genes, including β-lactam resistance gene *blaZ* and quinolone resistance–determining region mutations GrlA S80Y and GyrA S84L. However, we did not detect the mupirocin-resistance gene *mup* or any *qac* homologs, such as *qacA*, *qacB*, *qacE*, *qacG*, and *qacH*, which are known as disinfectant-resistance genes and known to reduce efficacy (*8*,*9*). We also investigated biofilm formation, which is associated with bacterial colonization and drug resistance. However, the biofilm-forming ability of these ST2233 strains was only slightly higher than that of the negative control FK300 ($p<0.05$) and not particularly strong (Appendix Figure 2).

ETE is a recently identified toxin that specifically degrades desmoglein-1 in the epidermis of many mammal species, including humans (*10*). A PVL and ETE double-positive strain is very rare; only 1 case has been reported, from necrotizing fasciitis (*11*). We have not found other reports of PVL and ETE double-positive *S. aureus* belonging to CC188, the most frequently isolated clone from healthy adult skin in Japan.

Conclusions

SSTIs caused by *S. aureus* are known to recur. A large multicenter cohort study of 959 staphylococcal SSTI cases revealed that 16.4%–19.0% of patients experienced ≥1 recurrence within a 12-month follow-up period (*1*). Intrafamilial transmission of *S. aureus* in patients with SSTIs is also known; Rodriguez et al. reported that among 163 pediatric patients with community-associated *S. aureus* SSTIs, intrafamilial strain relationships were observed in 105 (64%) families (*12*). Decolonization is occasionally attempted for all family members of patients with relapsing staphylococcal SSTIs; well-known decolonization techniques are nasal decolonization by mupirocin ointment and topical body decolonization by chlorhexidine (*3*) and

Table. Genetic characteristics of strains isolated in study of skin infections caused by Panton-Valentine leukocidin and methicillin-susceptible *Staphylococcus aureus* in child, Japan*

ID	Source	ST	Relevant molecular characteristics
JH62M	Mother	ST2233	TGs: *pvl*, *ete*, *seg*, *seh*, *sei*, *sem*, *sen*, *seo*, *ses*, *seu* ARGs: *blaZ*, GrlA/S80Y, GyrA/S84L DRGs: none
JH62PP1	Patient	ST2233	TGs: *pvl*, *ete*, *seg*, *seh*, *sei*, *sem*, *sen*, *seo*, *ses*, *seu* ARGs: *blaZ*, GrlA/S80Y, GyrA/S84L DRGs: none
JH62PN	Patient	ST2233	TGs: *pvl*, *ete*, *seg*, *seh*, *sei*, *sem*, *sen*, *seo*, *ses*, *seu* ARGs: *blaZ*, GrlA/S80Y, GyrA/S84L DRGs: none
JH62B1	Older brother	ST2233	TGs: *pvl*, *ete*, *seg*, *seh*, *sei*, *sem*, *sen*, *seo*, *ses*, *seu* ARGs: *blaZ*, GrlA/S80Y, GyrA/S84L DRGs: none
JH62F	Father	ST2233	TGs: *pvl*, *ete*, *seg*, *she*, *sei*, *sem*, *sen*, *seo*, *ses*, *seu* ARGs: *blaZ*, GrlA/S80Y, GyrA/S84L DRGs: none
JH62B2	Younger brother	ST188	TGs: none ARGs: none DRGs: none
JH62PP2	Patient (second time)	ST1	TGs: *sea*, *seh*, *sek*, *seq*, *ses* ARGs: *blaZ*, *ant(9)-Ia*, *erm*(A) DRGs: none

*ARG, antimicrobial-resistance gene; DRG; disinfectant-resistance gene; ID, identification; ST, sequence type; TG, toxin gene.

sometimes bleach baths, in which the patient bathes in a bathtub filled with diluted hypochlorous acid water (*13*). Although we applied all 3 techniques to our patient and her family members, they were ineffective. Detailed strain analysis showed that the strains did not harbor resistance genes to mupirocin or disinfectants, and resistance to them was not the cause of their insufficient efficacy. Further strategies to control relapsing staphylococcal SSTI are required.

In summary, we encountered a child with relapsing SSTI caused by a PVL and ETE double-positive MSSA ST2233 strain that was refractory to decolonization procedures. Further investigation will reveal the clinical significance of the ST2233 strain and effective techniques for decolonization. Clinicians should be aware of the possibility of disinfectant resistance in SSTIs caused by MSSA infections.

We obtained written permission for publication from the patient's parents.

This study was supported by a grant (no. NCCHD 30E-1) from the National Center for Child Health and Development to I.M. and partly supported by the Japan Agency for Medical Research and Development under the Research Program on Emerging and Re-emerging Infectious Diseases (grant no. JP21fk0108604 to M.S.).

We used an artificial intelligence tool for grammatical correction of the manuscript.

All authors declare that they do not have any potential, perceived, or real conflicts of interest relevant to this study. All authors meet ICMJE criteria for authorship.

Author contributions: J.H., C.A., and K.M. assisted with and provided advice on experiments regarding the genomic analysis of *S. aureus*. K.S. and I.M. wrote the first draft of the manuscript and J.H., S.K., C.A., K.M., and M.S. performed the analysis of the MSSA strain. T.I. and T.K. performed the immunologic assessment of the patient. T.I., T.K., K.Y., M.T., and K.U. revised the manuscript.

About the Author

Dr. Shoji is a staff physician in the Division of Infectious Disease at the National Center for Child Health and Development, Japan. His research interests focus on pediatric pharmacology and infections in immunocompromised children.

References

1. Vella V, Galgani I, Polito L, Arora AK, Creech CB, David MZ, et al. *Staphylococcus aureus* skin and soft tissue infection recurrence rates in outpatients: a retrospective database study at 3 US medical centers. Clin Infect Dis. 2021;73:e1045–53. https://doi.org/10.1093/cid/ciaa1717
2. McNeil JC, Fritz SA. Prevention strategies for recurrent community-associated *Staphylococcus aureus* skin and soft tissue infections. Curr Infect Dis Rep. 2019;21:12. https://doi.org/10.1007/s11908-019-0670-0
3. Liu C, Bayer A, Cosgrove SE, Daum RS, Fridkin SK, Gorwitz RJ, et al.; Infectious Diseases Society of America. Clinical practice guidelines by the Infectious Diseases Society of America for the treatment of methicillin-resistant *Staphylococcus aureus* infections in adults and children. Clin Infect Dis. 2011;52:e18–55. https://doi.org/10.1093/cid/ciq146
4. Bourigault C, Corvec S, Brulet V, Robert PY, Mounoury O, Goubin C, et al. Outbreak of skin infections due to Panton-Valentine leukocidin-positive methicillin-susceptible *Staphylococcus aureus* in a French prison in 2010–2011. PLoS Curr. 2014;6:ecurrents.outbreaks.e4df88f057fc49e2560a235e0f8f9fea
5. Gopal Rao G, Batura R, Nicholl R, Coogan F, Patel B, Bassett P, et al. Outbreak report of investigation and control of an outbreak of Panton-Valentine leukocidin-positive methicillin-sensitive *Staphylococcus aureus* (PVL-MSSA) infection in neonates and mothers. BMC Infect Dis. 2019;19:178. https://doi.org/10.1186/s12879-019-3802-0
6. Inagawa T, Hisatsune J, Kutsuno S, Iwao Y, Koba Y, Kashiyama S, et al. Genomic characterization of *Staphylococcus aureus* isolated from patients admitted to intensive care units of a tertiary care hospital: epidemiological risk of nasal carriage of virulent clone during admission. Microbiol Spectr. 2024;12:e0295023. https://doi.org/10.1128/spectrum.02950-23
7. Coll F, Raven KE, Knight GM, Blane B, Harrison EM, Leek D, et al. Definition of a genetic relatedness cutoff to exclude recent transmission of meticillin-resistant *Staphylococcus aureus*: a genomic epidemiology analysis. Lancet Microbe. 2020;1:e328–35. https://doi.org/10.1016/S2666-5247(20)30149-X
8. Hetem DJ, Bonten MJ. Clinical relevance of mupirocin resistance in *Staphylococcus aureus*. J Hosp Infect. 2013;85:249–56. https://doi.org/10.1016/j.jhin.2013.09.006
9. Furi L, Ciusa ML, Knight D, Di Lorenzo V, Tocci N, Cirasola D, et al. Evaluation of reduced susceptibility to quaternary ammonium compounds and bisbiguanides in clinical isolates and laboratory-generated mutants of *Staphylococcus aureus*. Antimicrob Agents Chemother. 2013;57:3488–97. https://doi.org/10.1128/AAC.00498-13
10. Imanishi I, Nicolas A, Caetano AB, Castro TLP, Tartaglia NR, Mariutti R, et al. Exfoliative toxin E, a new *Staphylococcus aureus* virulence factor with host-specific activity. Sci Rep. 2019;9:16336. https://doi.org/10.1038/s41598-019-52777-3
11. Sabat AJ, Wouthuyzen-Bakker M, Rondags A, Hughes L, Akkerboom V, Koutsopetra O, et al. Case report: necrotizing fasciitis caused by *Staphylococcus aureus* positive for a new sequence variant of exfoliative toxin E. Front Genet. 2022;13:964358. https://doi.org/10.3389/fgene.2022.964358
12. Rodriguez M, Hogan PG, Burnham CA, Fritz SA. Molecular epidemiology of *Staphylococcus aureus* in households of children with community-associated *S aureus* skin and soft tissue infections. J Pediatr. 2014;164:105–11. https://doi.org/10.1016/j.jpeds.2013.08.072
13. Hogan PG, Parrish KL, Mork RL, Boyle MG, Muenks CE, Thompson RM, et al. HOME$_2$ study: household versus personalized decolonization in households of children with methicillin-resistant *Staphylococcus aureus* skin and soft tissue infection—a randomized clinical trial. Clin Infect Dis. 2021;73:e4568–77. https://doi.org/10.1093/cid/ciaa752

Address for correspondence: Kensuke Shoji, National Center for Child Health and Development, 2-10-1 Okura, Setagaya-ku, Tokyo 157-8535, Japan; email: shoji-k@ncchd.go.jp

A One Health Approach to Investigating Cache Valley Virus, Arkansas, USA, July 2023[1]

Ann Carpenter, Noah Kojima, Theresa M. Dulski, Amanda E. Calvert, Kristen L. Burkhalter, Jennifer R. Ballard, Keith Blount, Anna Fagre, Elisa Thrasher, Katelyn Lazenby, Stephen Hedges, Audrey Long, Kerri Miazgowicz, Erin Wood, Phillip Owens, C. Roxanne Connelly, Carolyn V. Gould, J. Erin Staples, Laura Rothfeldt, Stacey W. Martin, Joan Burke

Cache Valley virus (CVV), a mosquitoborne virus, can cause neuroinvasive disease in humans and adverse reproductive outcomes in sheep and goats. In 2023, CVV RNA was detected in an aborted lamb from a flock in Arkansas, USA. We conducted a One Health investigation to explore the potential effects of CVV in Arkansas.

Cache Valley virus (CVV), a mosquitoborne virus in the family *Peribunyaviridae*, genus *Orthobunyavirus*, and serogroup Bunyamwera, circulates among several vertebrate species, including sheep, deer, horses, and cattle (*1*–*3*). CVV has been isolated from multiple mosquito genera, but the primary vector species likely varies by geographic location (*1*–*6*).

Humans are susceptible to CVV and can develop asymptomatic infection or clinical disease ranging from febrile illness to meningitis and encephalitis. Although most CVV infections in animals are subclinical, infection in sheep and goats during pregnancy can cause abortions, malformed fetuses, and congenital abnormalities (*1*). Fetal deformities involve musculoskeletal and central nervous system malformations such as scoliosis, hydrocephalus, and arthrogryposis (*7*). Adverse fetal impact depends on the timing of infection during gestation (*8*).

The geographic distribution and burden of CVV disease among humans and animals is not well characterized (*2*,*4*,*9*). Since the initial identification of CVV in mosquitoes in Utah, USA, in 1956, the virus has been detected across North America, including the United States, Canada, and Mexico (*1*,*3*). Eight human disease cases have been reported in the United States, with likely exposures in North Carolina, Missouri, Wisconsin, Michigan, and New York (*10*–*12*); an additional case was associated with blood transfusion from an asymptomatic infected blood donor in Illinois (*13*). Seroprevalence studies have demonstrated widespread exposure to CVV in humans and animals (*2*,*3*).

In February 2023, CVV RNA was detected in tissues from an aborted lamb at a farm in central Arkansas, USA (farm A). The farmer reported an abortion storm with an attack rate of ≈30%. Previously, there had been 1 other report of CVV in Arkansas in 2020, a seropositive sheep from a flock in northwest Arkansas (farm B), located ≈60 miles northwest of farm A (Figure). The identification of an abortion storm in a flock potentially related to CVV raised concern about the potential risk for CVV to human and animal health. We investigated the occurrence and health risk for CVV among humans and animals in Arkansas.

The Study

To investigate the effect of CVV on livestock, we acquired archived serum samples collected at breeding

Author affiliations: Centers for Disease Control and Prevention, Atlanta, Georgia, USA (A. Carpenter, N. Kojima, T.M. Dulski, A. Fagre); Arkansas Department of Health, Little Rock, Arkansas, USA (T.M. Dulski, K. Blount, K. Lazenby, S. Hedges, L. Rothfeldt); Centers for Disease Control and Prevention, Fort Collins, Colorado, USA (A.E. Calvert, K.L. Burkhalter, A. Fagre, E. Thrasher, A. Long, K. Miazgowicz, C.R. Connelly, C.V. Gould, J.E. Staples, S.W. Martin); Arkansas Game and Fish Commission, Little Rock (J.R. Ballard); US Department of Agriculture Agricultural Research Service, Booneville, Arkansas, USA (E. Wood, P. Owens, J. Burke)

DOI: https://doi.org/10.3201/eid3106.250052

[1]Preliminary results from this investigation were presented at the Southern Section American Society of Animal Science, January 28–30, 2024, Louisville, Kentucky, USA.

in August 2022 and 2 months' gestation from sheep bred at farm B. Most of the flock were lambing for the first time, and the others did not have a history of fertility issues. Husbandry records included reproductive outcomes. To confirm the presence of CVV-specific antibodies in wild ungulates, we obtained archived serum samples from white-tailed deer culled in 2017 and 2020 during herd health assessments conducted in 3 counties in Arkansas (Figure).

We performed plaque reduction neutralization tests on sheep and deer serum diluted 2-fold from 1:10 to 1:1,280. We calculated maximal effective concentrations in which the serum dilution resulted in a 50% reduction in viral plaques (EC_{50}) using virus neutralization curves with a 4-parameter logistic model. We defined seropositivity as $EC_{50} \geq 20$. We also screened deer serum for neutralizing antibodies against Potosi and Jamestown Canyon viruses, 2 related orthobunyaviruses known to infect white-tailed deer in North America, including Arkansas (*1*).

To identify potential CVV vectors in Arkansas, we conducted dusk-to-dawn mosquito trapping using CO_2-baited CDC miniature light traps, with and without light over 9 trap nights around farms A and B during the 2023 arboviral season (epidemiologic weeks 25–46). We homogenized captured female mosquitoes in cell culture medium/bovine albumin and extracted RNA for real-time reverse transcription PCR (*14*).

Meningitis and encephalitis are reportable conditions in Arkansas. To identify patients with meningitis and encephalitis of unknown etiology among cases reported to the Arkansas Department of Health (ADH) during January 1, 2022–July 9, 2023, we reviewed case data and applied standardized case definitions. Inclusion criteria were acute onset of fever and cerebrospinal fluid pleocytosis, defined as leukocytes (leukocyte) $\geq$5 cells/mm^3. Patients classified as having encephalitis had $\geq$1 of the following: altered mental status, neurologic deficits, abnormal neuroimaging, abnormal electroencephalogram, or seizure. Patients classified as having meningitis had none of the characteristics of encephalitis and reported headache, stiff neck, or photophobia. To avoid capturing infections acquired at birth or in the hospital, we excluded patients <2 months of age and those whose initial CSF specimen was obtained on or after the third day of admission.

The Centers for Disease Control and Prevention deemed our investigation to be public health surveillance. We obtained archived serum samples from ewes under material transfer agreements with US Department of Agriculture and samples from deer from the Arkansas Game and Fish Commission. All specimens were collected under Institutional Animal Care and Use Committee–approved protocols held by the respective agencies.

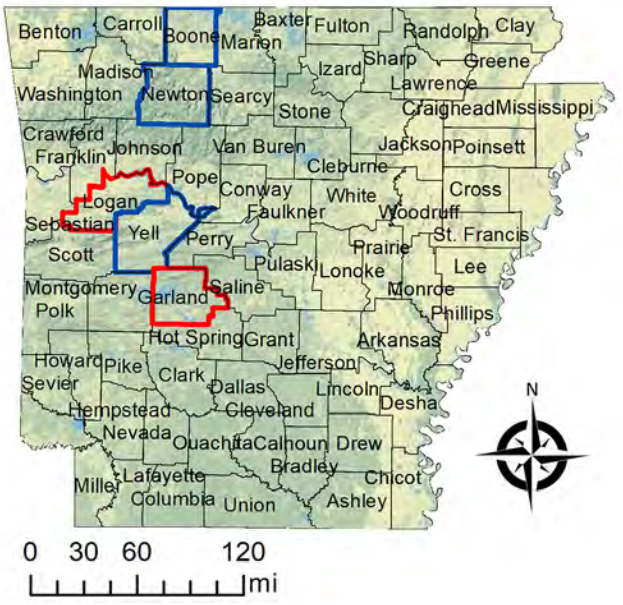

Figure. County locations for 2 farms with evidence of Cache Valley virus in sheep (red outline) and counties with specimens available from culled white-tailed deer (outlined in blue) for study of Cache Valley virus, Arkansas, USA, 2023.

We identified 39 ewes bred in August 2022 and lambed in mid-January to early February of 2023 with paired specimens at farm B. Of the 39 ewes, 8 (21%) were seropositive for CVV at breeding and 31 (79%) were seronegative. Of the seronegative ewes, 3 (10%) seroconverted during pregnancy; of those, 2 (66%) had adverse reproductive outcomes. The first ewe gave birth to a stillborn lamb with angular limb deformities and CVV detected in kidney tissue by PCR performed at Texas A&M Veterinary Medical Diagnostic Laboratory (College Station, Texas, USA) and a seropositive liveborn lamb reported to have weak legs. The second ewe had a stillborn lamb and a healthy-appearing liveborn lamb; no additional testing was performed. Of the 36 ewes that did not seroconvert during pregnancy, including the 8 seropositive at breeding, 6 (17%) had no pregnancy detected. Of the 30 with confirmed pregnancies, 10 (33%) had adverse reproductive outcomes: 3 embryo losses, 3 abortions, 3 stillbirths, and 1 congenital deformity.

Of 13 specimens obtained from deer culled in Yell, Boone, and Newton Counties (Figure), 11 (85%) were seropositive for CVV, including 1 that was seropositive only for CVV and 10 that were also seropositive for Jamestown Canyon or Potosi viruses (Table 1). One deer was seropositive for only Potosi virus. None of the 204 mosquito pools, representing 641 mosquitoes, tested positive for CVV (Table 2).

Table 1. Information on orthobunyavirus infections in white-tailed deer culled in 3 counties included as part of investigation of Cache Valley virus, Arkansas, USA, 2023*

County	CVV only	POTV only	CVV and JCV	CVV, JCV, and POTV
Yell, n = 5†	1 (20)	1 (20)	0	2 (40)
Boone, n = 1	0	0	0	1 (100)
Newton, n = 7	0	0	1 (14)	6 (85)
All, n = 13	1 (8)	1 (15)	1 (15)	9 (30)

*Values are no. (%) specimens with EC_{50} neutralizing antibodies ≥20. CVV, Cache Valley virus; EC_{50}, effective concentration in which serum dilution resulted in a 50% reduction in viral plaques; JCV, Jamestown Canyon virus; POTV, Potosi virus.
†One deer in Yell County tested negative for antibodies against all 3 viruses.

We excluded 83 (40%) of 206 human patients reported with suspected meningitis and encephalitis from our study. Of the 123 remaining, 82 (67%) had complete records available and met case definition. Of those 82 cases, 4 (5%) had an unknown etiology, and none had a record of arboviral testing.

Conclusions

This One Health investigation identified the presence of CVV and its likely effect on livestock health in Arkansas (*15*). Testing data for arboviral infections, including CVV infections, among human patients with meningitis and encephalitis were limited, suggesting human cases may be underdiagnosed.

We documented seroconversion during gestation in sheep, including those with adverse reproductive outcomes. Seropositivity among culled white-tailed deer provided further evidence of CVV transmission. We also detected antibodies to 2 related viruses in deer. More work is needed to understand the circulation and implications of CVV and other related orthobunyaviruses in domesticated and wild ungulates.

Vector surveillance activities did not identify CVV in collected mosquitoes. However, more extensive and sustained surveillance efforts over time are likely needed to detect virus in mosquitoes. Identifying reservoirs and local vectors of CVV will clarify opportunities for control measures to help prevent human and animal cases.

Table 2. Aggregated count of female mosquitoes trapped and tested as part of investigation of Cache Valley virus, Arkansas, USA, 2023*

Species	No. collected
Aedes albopictus	32
Ae. atlanticus	5
Ae. cinereus	1
Ae. dupreei	10
Ae. infirmatus	2
Ae. triseriatus	22
Ae. vexans	264
Aedex spp.	10
Anopheles crucians complex	3
An. perplexens	2
An. punctipennis	77
An. quadrimaculatus	5
An. spp.	3
Culex erraticus	113
Cx. nigripalpus	5
Cx. quinquefasciatus	13
Cx. salinarius	13
Cx. tarsalis	14
Cx. territans	1
Culex spp.	9
Culiseta inornata	3
Psorophora columbiae	9
Uranotaenia sapphirina	17
Unknown	8
Total	641

*All mosquito pools tested were negative for Cache Valley virus by real-time reverse transcription PCR.

Acknowledgments

We thank Lisa Lewis and the Southeastern Cooperative Wildlife Disease Study, as well as Reagan Taylor, Madisyn Doddridge, and Morgan Hulbert, for their support of this project.

This research was funded in part by the State of Arkansas and US Fish and Wildlife Service Zoonotic Disease Initiative (grant no. F23AP00161-00).

The findings and conclusions in this report are those of the authors and do not necessarily represent the official position of the Centers for Disease Control and Prevention or Arkansas Department of Health, nor do they necessarily reflect the views or policies of the Arkansas Game and Fish Commission. Product references do not constitute endorsements.

About the Author

Dr. Carpenter completed this work as an Epidemic Intelligence Service Officer in the Division of Vector-Borne Diseases, National Center for Emerging and Zoonotic Infectious Diseases, Centers for Disease Control and Prevention. She previously worked with the Centers for Disease Control and Prevention One Health Office. Her professional interests include infectious disease epidemiology, emerging rickettsial diseases, and the human–animal bond.

References

1. Hughes HR, Kenney JL, Calvert AE. Cache Valley virus: an emerging arbovirus of public and veterinary health importance. J Med Entomol. 2023;60:1230–41. https://doi.org/10.1093/jme/tjad058
2. Waddell L, Pachal N, Mascarenhas M, Greig J, Harding S, Young I, et al. Cache Valley virus: a scoping review of the

global evidence. Zoonoses Public Health. 2019;66:739–58. https://doi.org/10.1111/zph.12621
3. Bergevin MD, Ng V, Sadeghieh T, Menzies P, Ludwig A, Mubareka S, et al. A scoping review on the epidemiology of orthobunyaviruses in Canada, in the context of human, wildlife, and domestic animal host species. Vector Borne Zoonotic Dis. 2024;24:249–64. https://doi.org/10.1089/vbz.2023.0109
4. Andreadis TG, Armstrong PM, Anderson JF, Main AJ. Spatial-temporal analysis of Cache Valley virus (Bunyaviridae: Orthobunyavirus) infection in anopheline and culicine mosquitoes (Diptera: Culicidae) in the northeastern United States, 1997–2012. Vector Borne Zoonotic Dis. 2014;14:763–73. https://doi.org/10.1089/vbz.2014.1669
5. Corner LC, Robertson AK, Hayles LB, Lversen JO. Cache Valley virus: experimental infection in *Culiseta inornata.* Can J Microbiol. 1980;26:287–90. https://doi.org/10.1139/m80-048
6. Ayers VB, Huang YS, Lyons AC, Park SL, Higgs S, Dunlop JI, et al. *Culex tarsalis* is a competent vector species for Cache Valley virus. Parasit Vectors. 2018;11:519. https://doi.org/10.1186/s13071-018-3103-2
7. Chung SI, Livingston CW Jr, Edwards JF, Crandell RW, Shope RE, Shelton MJ, et al. Evidence that Cache Valley virus induces congenital malformations in sheep. Vet Microbiol. 1990;21:297–307. https://doi.org/10.1016/0378-1135(90)90001-C
8. Chung SI, Livingston CW Jr, Edwards JF, Gauer BB, Collisson EW. Congenital malformations in sheep resulting from in utero inoculation of Cache Valley virus. Am J Vet Res. 1990;51:1645–8. https://doi.org/10.2460/ajvr.1990.51.10.1645
9. McLean RG, Calisher CH, Parham GL. Isolation of Cache Valley virus and detection of antibody for selected arboviruses in Michigan horses in 1980. Am J Vet Res. 1987;48:1039–41. https://doi.org/10.2460/ajvr.1987.48.07.1039
10. Sexton DJ, Rollin PE, Breitschwerdt EB, Corey GR, Myers SA, Dumais MR, et al. Life-threatening Cache Valley virus infection. N Engl J Med. 1997;336:547–9. https://doi.org/10.1056/NEJM199702203360804
11. Campbell GL, Mataczynski JD, Reisdorf ES, Powell JW, Martin DA, Lambert AJ, et al. Second human case of Cache Valley virus disease. Emerg Infect Dis. 2006;12:854–6. https://doi.org/10.3201/eid1205.051625
12. Nguyen NL, Zhao G, Hull R, Shelly MA, Wong SJ, Wu G, et al. Cache Valley virus in a patient diagnosed with aseptic meningitis. J Clin Microbiol. 2013;51:1966–9. https://doi.org/10.1128/JCM.00252-13
13. Al-Heeti O, Wu EL, Ison MG, Saluja RK, Ramsey G, Matkovic E, et al. Transfusion-transmitted Cache Valley virus infection in a kidney transplant recipient with meningoencephalitis. Clin Infect Dis. 2023;76:e1320–7. https://doi.org/10.1093/cid/ciac566
14. Baker M, Hughes HR, Naqvi SH, Yates K, Velez JO, McGuirk S, et al. Reassortant Cache Valley virus associated with acute febrile, nonneurologic illness, Missouri. Clin Infect Dis. 2021;73:1700–2. https://doi.org/10.1093/cid/ciab175
15. Food and Agriculture Organization of the United Nations, United Nations Environment Programme, World Health Organization, World Organisation for Animal Health. One Health Joint Plan of Action (2022–2026). Working together for the health of humans, animals, plants and the environment. Rome: The Organizations; 2022.

Address for correspondence: Laura Rothfeldt, Arkansas Department of Health, 4815 W Markham St, Slot 62, Little Rock, AR 72205-5432 USA; email: laura.rothfeldt@arkansas.gov

Prevalence of Nitroimidazole-Refractory Giardiasis Acquired in Different World Regions, Sweden, 2008–2020

Karin A. Ydsten, Joanna Nederby Öhd, Urban Hellgren, Hilmir Asgeirsson

Treatment-refractory giardiasis is an emerging clinical problem. Of 4,285 giardiasis cases identified during 2008–2020 in Stockholm, Sweden, 102 (2.4%) were nitroimidazole refractory. Among cases acquired in India, the percentage was high (64/545 [12%]) and increased over time. The region of acquisition needs to be taken into consideration when managing patients.

Giardia intestinalis (*G. lamblia, G. duodenalis*) is an intestinal protozoal pathogen found worldwide; the highest incidence occurs in developing countries. For decades, the first-line treatment for giardiasis has been the 5-nitroimidazoles, such as metronidazole and tinidazole (*1*). Since the early 2000s, reports of giardiasis refractory (resistant) to 5-nitroimidazoles have increased, posing a clinical challenge. The reports are mostly from travelers returning from the Indian subcontinent (*2*–*6*). Information on the prevalence of giardiasis refractory to 5-nitroimidazoles in India and global epidemiology is scarce. To examine global prevalence, we assessed the percentage of nitroimidazole-refractory disease among giardiasis cases acquired in different geographic world regions.

The Study

In Sweden, giardiasis is a notifiable disease. We retrospectively extracted cases reported during January 2008–December 2020 from Stockholm County with information on age, sex, and country of infection from the national electronic notification system (SmiNet). In Stockholm, giardiasis patients not responding to treatment (repeat fecal sample testing is generally only done if symptoms continue) are referred to specialized adult and pediatric centers at Karolinska University Hospital, which are the only clinics providing second-line treatment alternatives because those require special prescribing licenses. We retrospectively evaluated medical records of all giardiasis cases seen at the centers during the study period. We defined a case as nitroimidazole refractory if the case had a positive fecal sample for giardiasis by microscopy (whole study period) or PCR (from 2016) after a full 5-nitroimidazole treatment course (metronidazole 400 mg 3×/d for 5–7 days or a single dose of tinidazole 2 g) and no indication of reinfection. The treating clinician determined whether the case was related to travel. The Regional Ethical Review Board in Stockholm (approval nos. 2018/2309-31 and 2020-06183) approved the study.

During the 13-year study period, Stockholm had 4,285 notified giardiasis cases, of which 3,172 (74%) were acquired abroad and 881 (21%) were acquired domestically; 232 had unknown acquisition (Table). The mean incidence of all cases was 15.2/100,000 population/year and incidence among domestic cases was 3.2/100,000 population/year.

The number of cases identified as nitroimidazole refractory was 102 (2.4%), and 97/102 (95%) were related to travel. Of 102 treatment-refractory cases, 96 had received ≥2 courses of 5-nitroimidazoles. In the first half of the study period (January 2008–June 2014), the percentage of nitroimidazole-refractory cases was 2.0% (46/2,255), compared with 2.8% (56/2,030) in the second half (July 2014–December 2020; p = 0.12). For cases acquired specifically in India, the percentage rose from 8.5% (29/341) to 17.2% (35/204) between the 2 periods (p = 0.002 by χ^2 test).

Author affiliations Capio St. Görans Hospital, Stockholm, Sweden (K.A. Ydsten); Karolinska University Hospital, Stockholm (K.A. Ydsten, U. Hellgren, H. Asgeirsson); Region Stockholm, Stockholm (J.N. Öhd); Karolinska Institutet, Stockholm (U. Hellgren, H. Asgeirsson)

DOI: https://doi.org/10.3201/eid3106.250076

The median patient age was 30 (range 0–89) years in the total study population and 35 (range 1–78) years in patients with refractory disease. Among 4,285 cases, 55% were in male patients and 45% were in female patients; slightly more (55/102) male patients had nitroimidazole-refractory infections than female patients (47/102). Only 2 of the nitroimidazole-refractory cases were identified with immunosuppressive conditions, 1 receiving rituximab and methotrexate and 1 prednisolone; none had other immunoglobulin deficiencies or HIV. The treatment and outcome of the patients are described elsewhere (*6*).

The percentage of patients with nitroimidazole-refractory disease varied by countries visited (Table). A high prevalence of 12% (64/545) was seen in persons returning from India, compared with 1.1% (9/792) from the rest of Asia (excluding India; p<0.0001) and 1.0% (38/3,740) from the rest of the world (p<0.0001): Asia (1.1%; 9/792), Africa (1.5%; 17/1,115), Europe (0.9%; 11/1,247), and the Americas (0.3%; 1/349). The highest (29%; 2/7) prevalence was noted in patients infected in Nepal. Among 881 cases acquired domestically in Sweden, 5 (0.6%) were nitroimidazole refractory. Only 1 of those 5 case-patients had known contact with a travel-related case. Among the 97 travel-related nitroimidazole-refractory giardiasis cases (all symptomatic ≤28 days of returning from travel), tourism was the most common reason for travel (75%; 73/97), followed by work or studies (11%; 11/97), immigration (9%; 9/97), and visiting friends or relatives (4%; 4/97).

This study conducted in a low-endemic population-based setting showed that the proportion of nitroimidazole-refractory giardiasis was >10 times higher in persons who had acquired the infection in India (12%) compared with other parts of the world (1.0%). Of note, the proportion of nitroimidazole-refractory disease among cases acquired in India rose over the study period (from 8.5% to 17%). The percentage of nitroimidazole-refractory cases acquired in India (12%) was similar to that found in a previous small study from India (10%; 8/82) (*7*). Other studies from specialized centers in Europe have reported substantially higher percentages from India, up to 50% (*2*,*3*,*6*). However, those studies were small and might have been biased because they mostly included referred patients, whereas this study is based on all giardiasis cases identified in a large well-defined geographic area. Data from countries outside Asia are sparse in the literature. Studies from Cuba have reported a metronidazole refractory rate of 46% (248/456) in 2017–2018 and 15% (11/75) in 2009 (*8*,*9*). That rate is much higher than the 0.3% (1/349) noted from the Americas in this study, but that total included only 14 cases from Cuba (none treatment refractory).

The reason for the higher, and increasing, prevalence of nitroimidazole-refractory disease in India compared with other countries is not known. High drug pressure (frequent use of 5-nitroimidazoles) could perhaps be an explanation. That pressure is seen with bacterial drug resistance, also common in India (*4*,*10*). The lower prevalence found in neighboring Pakistan (1%), which has similar living conditions, is at the same time difficult to explain. To

Table. Giardiasis by country of acquisition and rate of nitroimidazole-refractory cases, Stockholm, Sweden, 2008–2020

Origin of infection*	Total no. cases	No. (%) nitroimidazole-refractory cases
Asia	1,337	73 (5.5)
India	545	64 (11.7)†
Thailand	168	4 (2.4)
Pakistan	94	1 (1.1)
Iraq	71	0
Turkey	65	0
Afghanistan	58	0
Syria	45	0
China	36	0
Sri Lanka	33	0
Cambodia	25	0
Indonesia	25	0
Bangladesh	23	2 (8.7)
Nepal	7	2 (28.6)
Africa	1,115	17‡ (1.5)
Tanzania	136	3 (2.2)
Somalia	133	1 (0.8)
Ethiopia	105	1 (0.9)
Kenya	94	0
Eritrea	93	0
Uganda	65	2 (3.1)
Egypt	57	0
Gambia	45	0
Sudan	37	0
South Africa	26	1 (3.8)
Morocco	23	0
Americas	349	1 (0.3)
Colombia	67	1 (1.5)
Brazil	55	0
Peru	36	0
Mexico	28	0
United States	23	0
Europe	1,247	11§ (0.9)
Sweden	881	5 (0.6)
Spain	107	2 (1.9)
Greece	36	0
France	29	1 (3.4)
Oceania	5	0
Unknown	232	0
Total	4,285	102 (2.4)

*Countries with ≥20 giardiasis cases in total are shown, as well as countries with ≥2 treatment refractory cases.
†p<0.0001 for India compared with rest of Asia and for India compared with the rest of the world (by χ^2 test).
‡In addition, the following countries had 1 case: Angola, Benin, Central African Republic, Democratic Republic of the Congo, Ghana, Madagascar, Sudan, Chad, and Zimbabwe.
§In addition, the following countries had 1 case: Belgium, Italy, and Switzerland.

understand those geographic and temporal variations, better knowledge on the mechanisms behind nitroimidazole-refractory giardiasis is needed.

Treatment-refractory disease with persistence of protozoa in fecal samples may result from parasite drug resistance, but host-related factors, such as immunoglobulin deficiencies and HIV, can also play a role (*11*). Drug resistance is difficult to evaluate in clinical settings because antimicrobial drug susceptibility testing for *Giardia* is lacking (*12*,*13*), and the underlying molecular resistance mechanisms are not well understood (*1*,*14*). In our cohort, only a small percentage (2%) of patients with nitroimidazole-refractory diseases had known immunosuppressive conditions. Furthermore, all patients (n = 56) who were treated with quinacrine improved (*6*). Although quinacrine has been reported to have good efficacy against nitroimidazole-refractory giardiasis (clinical cure rates of 98% and parasitologic cure rates of 89% from pooled studies) (*5*,*6*,*15*), increased use might pose a risk for further resistance. Without reliable diagnostic assays on antimicrobial drug resistance, the management of treatment-refractory giardiasis will remain a clinical challenge.

A limitation of the study is that some treatment-refractory cases might not have been referred to our center and thereby missed. Missing cases would lead to an underestimation of nitroimidazole-refractory disease, but the underestimation would most likely be similar for different regions. Similarly, the study focused on clinically refractory disease, and asymptomatic carriage after nitroimidazole treatment could go unnoticed. Another limitation is that, despite a large total number of cases, the numbers from specific countries were often low, which makes drawing conclusions on a country level difficult. Strengths of the study are its population-based approach, the low likelihood of missed cases because in Sweden giardiasis is notifiable, the low-endemic setting with small risk for reinfections, and that all nitroimidazole-refractory cases were well defined with a thorough follow-up.

Conclusions

The results of this study show that nitroimidazole-refractory giardiasis is prevalent on the Indian subcontinent but is substantially less common in the rest of the world. Further studies on the epidemiology of treatment-refractory giardiasis and possible underlying resistance mechanisms are needed. Clinicians should take into consideration the region where infection was acquired when managing and treating giardiasis patients.

Acknowledgments

We thank Olof Hertting for evaluating the pediatric patients.

About the Author

Mrs. Ydsten is a specialist at Capio Saint Goran's Hospital, Stockholm, Sweden. Her research interests include tropical infections and giardiasis.

References

1. Mørch K, Hanevik K. Giardiasis treatment: an update with a focus on refractory disease. Curr Opin Infect Dis. 2020; 33:355–64. https://doi.org/10.1097/QCO.0000000000000668
2. Muñoz Gutiérrez J, Aldasoro E, Requena A, Comin AM, Pinazo MJ, Bardají A, et al. Refractory giardiasis in Spanish travellers. Travel Med Infect Dis. 2013;11:126–9. https://doi.org/10.1016/j.tmaid.2012.10.004
3. Nabarro LE, Lever RA, Armstrong M, Chiodini PL. Increased incidence of nitroimidazole-refractory giardiasis at the Hospital for Tropical Diseases, London: 2008–2013. Clin Microbiol Infect. 2015;21:791–6. https://doi.org/10.1016/j.cmi.2015.04.019
4. Requena-Méndez A, Goñi P, Rubio E, Pou D, Fumadó V, Lóbez S, et al. The use of quinacrine in nitroimidazole-resistant *Giardia duodenalis*: an old drug for an emerging problem. J Infect Dis. 2017;215:946–53. https://doi.org/10.1093/infdis/jix066
5. Neumayr A, Schunk M, Theunissen C, Van Esbroeck M, Mechain M, Hatz C, et al. Efficacy and tolerability of quinacrine monotherapy and albendazole plus chloroquine combination therapy in nitroimidazole-refractory giardiasis: a TropNet study. Clin Infect Dis. 2021;73:1517–23. https://doi.org/10.1093/cid/ciab513
6. Ydsten KA, Hellgren U, Asgeirsson H. Quinacrine treatment of nitroimidazole-refractory giardiasis. J Infect Dis. 2022;225:1773–6. https://doi.org/10.1093/infdis/jiab287
7. Yadav P, Tak V, Mirdha BR, Makharia GK. Refractory giardiasis: a molecular appraisal from a tertiary care centre in India. Indian J Med Microbiol. 2014;32:378–82. https://doi.org/10.4103/0255-0857.142236
8. Cañete R, Noda AL, Rodríguez M, Brito K, Herrera E, Kofoed PE, et al. 5-nitroimidazole refractory giardiasis is common in Matanzas, Cuba and effectively treated by secnidazole plus high-dose mebendazole or quinacrine: a prospective observational cohort study. Clin Microbiol Infect. 2020;26:1092. https://doi.org/10.1016/j.cmi.2019.12.017
9. Cañete R, Rodríguez P, Mesa L, Brito K, Prior A, Guilhem D, et al. Albendazole versus metronidazole in the treatment of adult giardiasis: a randomized, double-blind, clinical trial. Curr Med Res Opin. 2012;28:149–54. https://doi.org/10.1185/03007995.2011.637915
10. Antimicrobial Resistance Collaborators. Global burden of bacterial antimicrobial resistance in 2019: a systematic analysis. Lancet. 2022;399:629–55. https://doi.org/10.1016/S0140-6736(21)02724-0
11. Faubert G. Immune response to *Giardia duodenalis*. Clin Microbiol Rev. 2000;13:35–54. https://doi.org/10.1128/CMR.13.1.35
12. Lemée V, Zaharia I, Nevez G, Rabodonirina M, Brasseur P, Ballet JJ, et al. Metronidazole and albendazole susceptibility of 11 clinical isolates of *Giardia duodenalis* from France.

J Antimicrob Chemother. 2000;46:819–21. https://doi.org/10.1093/jac/46.5.819
13. Farbey MD, Reynoldson JA, Thompson RC. In vitro drug susceptibility of 29 isolates of *Giardia duodenalis* from humans as assessed by an adhesion assay. Int J Parasitol. 1995;25:593–9. https://doi.org/10.1016/0020-7519(94)00174-M
14. Loderstädt U, Frickmann H. Antimicrobial resistance of the enteric protozoon *Giardia duodenalis* – a narrative review. Eur J Microbiol Immunol (Bp). 2021;11:29–43. https://doi.org/10.1556/1886.2021.00009
15. Bourque DL, Neumayr A, Libman M, Chen LH. Treatment strategies for nitroimidazole-refractory giardiasis: a systematic review. J Travel Med. 2022;29:taab120. https://doi.org/10.1093/jtm/taab120

Address for correspondence: Karin A. Ydsten, Department of Infectious Diseases, Capio Saint Goran´s Hospital, Sankt Göransplan 1, 112 19 Stockholm, Sweden; email: karin.ydsten@capiostgoran.se

Three Cases of Human Babesiosis, Italy, 2017–2020

Chiara Sepulcri,[1] Rachele Pincino,[1] Federico Baldi,[1] Giovanni Cenderello, Stefania Zanet, Daniela Boccolini, Anna Rosa Sannella, Mariangela L'Episcopia, Carlo Severini, Matteo Bassetti, Chiara Dentone, Ezio Ferroglio

We report 3 cases of babesiosis in Italy caused by *Babesia* species that are rarely reported in humans. The circulation of *Babesia* spp. among vectors, animals, and humans might be more common than previously thought, and babesiosis might be an underdiagnosed and emerging disease in Italy and Europe.

Babesiosis is a tickborne disease caused by apicomplexan hemoprotozoan parasites of the genus *Babesia*. The biologic cycle of *Babesia* spp. involves species-specific interactions among the pathogen, host, and reservoir (*1*). More than 100 *Babesia* spp. have been described as cause of disease in animals, but only a few are involved in human infections.

Most human babesiosis cases have been reported in North America, where *B. microti* is the main pathogen (*1*). In Europe, where most infections are caused by either *B. divergens* or *B. venatorum* (*2*), only ≈50 human cases have been reported since 1957 (*3*). In Italy, only 1 case has been reported, in 2004 (*4*). In contrast to the paucity of clinically relevant cases, results from a seroprevalence study in Spain suggest that human infection might be more common; seroreactivity up to 39.2% in tick-exposed persons has been reported (*5*).

The growing use of molecular techniques is enabling new insights into the epidemiology of *Babesia* spp. in wildlife and domestic animals (*6*), as well as enabling identification of species that were previously unreported in humans, such as *B. bovis* and *B. canis* (*7*). We describe 3 clinical cases of human babesiosis that occurred in a northern region of Italy. All patients provided written consent for the use of their medical records for scientific research purposes at the time of hospital admission according to local legislation.

The Study

To molecularly identify *Babesia* and *Theileria* spp. parasites, we extracted total genomic DNA from 200 μL of whole blood in EDTA by using the GenElute Mammalian Genomic DNA Miniprep Kit (Sigma-Aldrich, https://www.sigmaaldrich.com) according to the manufacturer's instructions. We performed direct molecular detection of *Babesia* and *Theileria* spp. DNA by using a seminested PCR protocol targeting a 400-bp fragment of the V4 hypervariable region of the 18S ribosomal RNA gene, as previously described (*6*). We purified PCR positive samples by using the QIAquick PCR Purification Kit (QIAGEN, https://www.qiagen.com). Macrogen (http://www.macrogen.com) directly sequenced both DNA strands. We compared the sequences with those in Genbank by using BLAST (https://blast.ncbi.nlm.nih.gov) and used ClustalX software (http://www.clustal.org) to construct multiple sequence alignments. We analyzed the phylogenetic relationships of *Babesia* spp. isolates by using the maximum-likelihood method and the Jukes-Cantor model with 1,000 bootstrap replicates. We performed nested PCR for *Plasmodium* spp. detection, as previously described (*8*).

Patient 1 was a woman in her 20s with a history of Raynaud syndrome. In 2017, she was admitted to a hospital in the western part of northern Italy

Author affiliations: University of Genoa, Genoa, Italy (C. Sepulcri, M. Bassetti); Ospedale Sanremo, Sanremo, Italy (R. Pincino, G. Cenderello); AON SS Antonio e Biagio e Cesare Arrigo University Hospital, Alessandria, Italy (F. Baldi); University of Turin, Turin, Italy (S. Zanet, E. Ferroglio); Istituto Superiore di Sanità, Rome, Italy (D. Boccolini, A.R. Sannella, M. L'Episcopia, C. Severini); IRCCS Ospedale Policlinico San Martino, Genoa (M. Bassetti, C. Dentone)

DOI: https://doi.org/10.3201/eid3106.241776

[1]These first authors contributed equally to this article.

for arthralgia, myalgia, asthenia, fever, and weight loss, all occurring during the previous 2 weeks. She lived with 2 dogs and had no history of recent travel or transfusions with any blood components. Her clinical evaluation and bloodwork were unremarkable. She had negative results for HIV, hepatitis C virus, *Borrelia* and *Bartonella* spp. antibodies, autoimmunity tests, and blood and urine cultures. To rule out hematologic disorders, we prepared blood smears and found evidence of trophozoite forms. A malaria rapid test was negative for all *Plasmodium* spp. The National Reference Laboratory in Rome, Italy, performed microscopic examination of the smears, which showed both extraerythrocytic and intraerythrocytic trophozoites, suggesting *Babesia* spp. (Figure 1, panels A, B). The local Zooprofilactic Institute confirmed that finding by performing *Babesia* spp. PCR 40 days after the patient's hospital admission. Further molecular analysis identified the species as *B. canis canis* (Genbank accession no. PQ049251; 100% query coverage and maximum identity) (Figure 2). Treatment consisted of a 10-day course of oral atovaquone (750 mg 2×/d) and azithromycin (500 mg 1×/d), which led to symptom remission and a negative blood smear. One of the patient's 2 dogs was positive for *B. canis canis* by species-specific seminested PCR, conducted as previously described (*9*).

Patient 2 was a child <10 years of age admitted in 2018 to the same hospital as patient 1 for headache, arthralgia, myalgia, pharyngitis with tonsillitis, and fever that began 8 days before admittance. The patient had no travel history or history of transfusions with blood components. Blood exams revealed hypereosinophilia (24,200 cells/μL). Blood microscopy showed the presence of scant trophozoites; a malaria rapid diagnostic test and PCR were negative for all *Plasmodium* spp. Suspecting babesiosis, we sent a blood sample to the local Zooprofilactic Institute to test for *Babesia* spp. by PCR 2 days after admission; results were positive for babesiosis, and *B. microti*–like species was identified (Genbank accession no. PQ049252; 100% query coverage, 95.36% maximum identity) (Figure 2). Treatment consisted of a 7-day course of intravenous azithromycin (10 mg/kg 1×/d) and atovaquone (20 mg/kg 2×/d). Symptoms resolved (afebrile, resolution of arthralgia and myalgia) after 3 days of treatment, and a negative blood smear was observed.

Patient 3 was a man in his 20s born in West Africa admitted in 2020 for fever, night sweats, and productive cough that began 1 month before admittance. The patient had been admitted the year before to the same pulmonary tuberculosis (TB) unit but was subsequently lost to follow-up. At admission, he was stably residing in Italy and had not traveled abroad

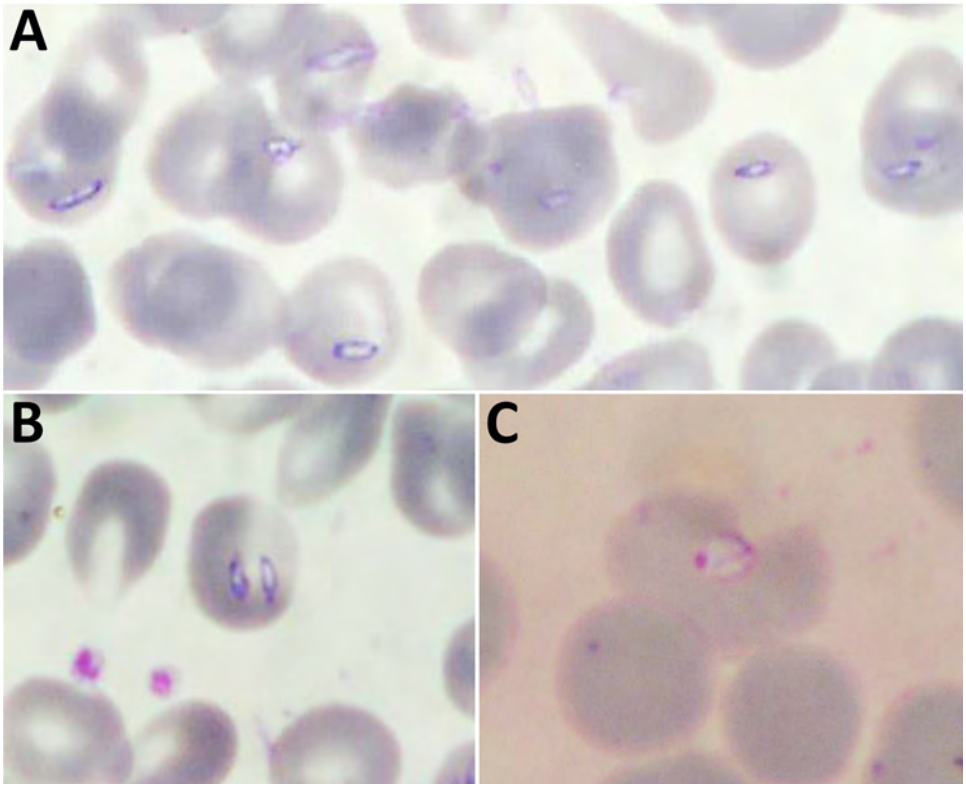

Figure 1. Blood smears showing *Babesia* spp. trophozoites in study of 3 cases of human babesiosis, Italy, 2017–2020. Smears were stained with Giemsa stain. A, B) *B. canis canis* identified in patient 1. Original magnification ×630. C) *B. vulpes* identified in patient 3. Original magnification ×1,000 (oil immersion).

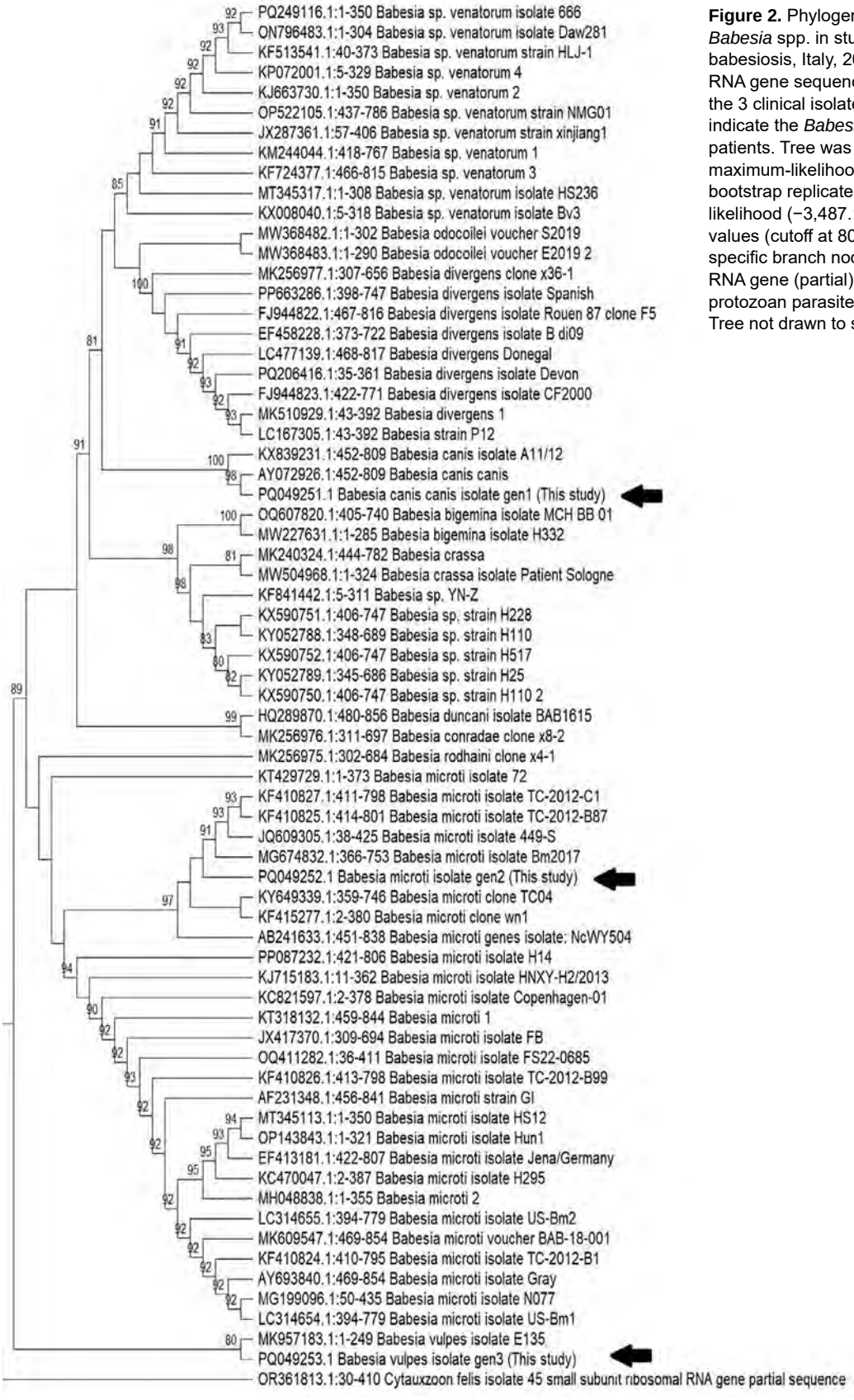

Figure 2. Phylogenetic analysis of the *Babesia* spp. in study of 3 cases of human babesiosis, Italy, 2017–2020. 18S ribosomal RNA gene sequences were amplified from the 3 clinical isolates from Italy. Arrows indicate the *Babesia* isolates from the 3 patients. Tree was inferred by using the maximum-likelihood method with 1,000 bootstrap replicates. Tree with the highest log likelihood (−3,487.14) is shown. Bootstrap values (cutoff at 80%) are indicated at specific branch nodes. 18S ribosomal RNA gene (partial) from *Cytauxzoon felis* protozoan parasite was used as the outlier. Tree not drawn to scale.

in the previous 5 years. We diagnosed pulmonary TB and started treatment with rifampin, isoniazid, ethambutol, and pyrazinamide. At the time of admission, he had fever, anemia (hemoglobin level 6.6 g/dL), hemoglobinuria, and elevated inflammatory markers. Three weeks after admission, he had persistent fever and anemia despite TB treatment and blood transfusions. We suspected malaria reactivation and prepared thick and thin blood smears, which showed intraerythrocytic trophozoites. The National Reference Laboratory performed a rapid malaria test and nested PCR, which were negative for all *Plasmodium* spp. We suspected babesiosis, which we confirmed by microscopy of a blood smear (Figure 1, panel C). Parasitemia was 0.2%. Further molecular testing identified the species as *B. vulpes* (Genbank accession no. PQ049253; 71% query coverage, 97.29% maximum identity) (Figure 2). We treated the patient with oral quinine and intravenous clindamycin. After 10 days of therapy, he was still symptomatic with persistent parasitemia observed in blood smears. We extended the treatment duration to 21 days, resulting in symptoms resolution and repeated negative blood smears.

Conclusions

The 3 human babesiosis cases described here were sustained by *Babesia* spp. rarely reported as a cause of human disease. Although none of the patients specifically reported a history of tick bites, all had potential environmental exposure to ticks. The circulation of *Babesia* spp. in Italy has been increasingly recognized both in its vector (mainly *Ixodes ricinus* ticks) (*10*) and in wild and domestic animals (*11*). In particular, *B. vulpes* was recently isolated from wild boars (*Sus scrofa*) in southern Italy (*12*). The population of wild boars in Italy is expanding and, in Genoa, where the case of *B. vulpes* was reported, the presence of wild boars within an urban space is an increasingly critical phenomenon (*13*). Furthermore, as shown by a seroprevalence study conducted in central and northern Italy, seroreactivity to *Babesia* spp. was detected in 24.4% of persons with high tick exposure (i.e., foresters, hunters) and 7% in persons with a lower exposure risk (*14*), suggesting a high rate of infection in the population. Current ecologic changes are likely to influence the emergence and prevalence of zoonotic diseases worldwide; the complex interactions among climate, pathogens, vectors, and hosts are dynamically changing and warrant the implementation of a One Health approach (*15*). Babesiosis is an example of those complex interactions and might be an underdiagnosed and emerging disease in Italy and Europe.

Acknowledgments

We thank Luigi Gradoni, Michela Menegon, and Simone Cacciò for their support in the malaria and babesiosis investigations and Bruno Barbara for her contribution in the initial microscopic assessment.

None of the authors has conflicts of interest to disclose related to this work. Outside the submitted work, M.B. has received funding for scientific advisory boards and travel and speaker honoraria from Angelini Pharma, Astellas, BioMérieux, Cidara, Gilead, Menarini, MSD, Pfizer, Shionogi, Tetraphase, and Nabriva. C.D. has received personal advisor/consultant or speaker/chairman fees from Angelini Pharma, Novartis, Gilead, ViiV, MSD, Shinogi, MSD, and Astrazeneca.

About the Author

Dr. Sepulcri is a medical doctor specialized in infectious and tropical diseases and a PhD candidate at the University of Genoa, Italy. Her primary research interests are tuberculosis and nontuberculous mycobacteria and emerging infectious diseases.

References

1. Vannier E, Krause PJ. Human babesiosis. N Engl J Med. 2012;366:2397–407. https://doi.org/10.1056/NEJMra1202018
2. Gray J, Zintl A, Hildebrandt A, Hunfeld KP, Weiss L. Zoonotic babesiosis: overview of the disease and novel aspects of pathogen identity. Ticks Tick Borne Dis. 2010;1:3–10. https://doi.org/10.1016/j.ttbdis.2009.11.003
3. Hildebrandt A, Zintl A, Montero E, Hunfeld KP, Gray J. Human babesiosis in Europe. Pathogens. 2021;10:1165. https://doi.org/10.3390/pathogens10091165
4. Piccaluga PP, Poletti G, Martinelli G, Gherlinzoni F. Babesia infection in Italy. Lancet Infect Dis. 2004;4:212. https://doi.org/10.1016/S1473-3099(04)00970-3
5. Montero E, Folgueras M, Rodriguez-Pérez M, Pérez-Ls L, Díaz-Arias J, Meana M, et al. Retrospective study of the epidemiological risk and serological diagnosis of human babesiosis in Asturias, northwestern Spain. Parasit Vectors. 2023;16:195. https://doi.org/10.1186/s13071-023-05817-x
6. Zanet S, Trisciuoglio A, Bottero E, de Mera IGF, Gortazar C, Carpignano MG, et al. Piroplasmosis in wildlife: *Babesia* and *Theileria* affecting free-ranging ungulates and carnivores in the Italian Alps. Parasit Vectors. 2014;7:70. https://doi.org/10.1186/1756-3305-7-70
7. Homer MJ, Aguilar-Delfin I, Telford SR 3rd, Krause PJ, Persing DH. Babesiosis. Clin Microbiol Rev. 2000;13:451–69. https://doi.org/10.1128/CMR.13.3.451
8. Snounou G, Viriyakosol S, Zhu XP, Jarra W, Pinheiro L, do Rosario VE, et al. High sensitivity of detection of human malaria parasites by the use of nested polymerase chain reaction. Mol Biochem Parasitol. 1993;61:315–20. https://doi.org/10.1016/0166-6851(93)90077-B
9. Birkenheuer AJ, Levy MG, Breitschwerdt EB. Development and evaluation of a seminested PCR for detection and differentiation of *Babesia gibsoni* (Asian genotype) and *B. canis* DNA in canine blood samples.

J Clin Microbiol. 2003;41:4172–7. https://doi.org/10.1128/JCM.41.9.4172-4177.2003
10. Melis S, Batisti Biffignandi G, Olivieri E, Galon C, Vicari N, Prati P, et al. High-throughput screening of pathogens in *Ixodes ricinus* removed from hosts in Lombardy, northern Italy. Ticks Tick Borne Dis. 2024;15:102285. https://doi.org/10.1016/j.ttbdis.2023.102285
11. Battisti E, Zanet S, Khalili S, Trisciuoglio A, Hertel B, Ferroglio E. Molecular survey on vector-borne pathogens in alpine wild carnivorans. Front Vet Sci. 2020;7:1. https://doi.org/10.3389/fvets.2020.00001
12. Sgroi G, D'Alessio N, Auriemma C, Salant H, Gallo A, Riccardi MG, et al. First molecular detection of *Babesia vulpes* and *Babesia capreoli* in wild boars from southern Italy. Front Vet Sci. 2023;10:1201476. https://doi.org/10.3389/fvets.2023.1201476
13. Piana P, Brocada L, Hearn R, Mangano S. Urban rewilding: human–wildlife relations in Genoa, NW Italy.Cities. 2024;144:104660. https://doi.org/10.1016/j.cities.2023.104660
14. Gabrielli S, Calderini P, Cassini R, Galuppi R, Tampieri MP, Pietrobelli M, et al. Human exposure to piroplasms in central and northern Italy. Vet Ital. 2014;50:41–7. https://doi.org/10.12834/VetIt.1302.13
15. Ostfeld RS, Levi T, Keesing F, Oggenfuss K, Canham CD. Tick-borne disease risk in a forest food web. Ecology. 2018;99:1562–73. https://doi.org/10.1002/ecy.2386

Address for correspondence: Chiara Sepulcri, Division of Infectious Diseases, Department of Health Sciences (DISSAL), University of Genoa, Via Pastore 1, 16132 Genoa, Italy; email: chiara.sepulcri@gmail.com

Usutu Virus Antibody Dynamics in Naturally Infected Blackbirds, the Netherlands, 2016–2018

Erwin de Bruin,[1] Jurrian van Irsel, Felicity Chandler, Robert Kohl,[2] Tess van de Voorde, Anne van der Linden, Fred de Boer, Marion Koopmans, Henk van der Jeugd,[3] Chantal Reusken[2,3]

Author affiliations: ErasmusMC, Rotterdam, the Netherlands (E. de Bruin, F. Chandler, R. Kohl, A. van der Linden, M. Koopmans, C. Reusken); Nederlands Instituut voor Ecologie, Dutch Centre for Avian Migration and Demography, Wageningen, the Netherlands (J. van Irsel, T. van de Voorde, H. van der Jeugd); Wildlife Ecology and Conservation Group, Wageningen University and Research, Wageningen (W.F. de Boer)

DOI: http://doi.org/10.3201/eid3106.241744

Usutu virus is a zoonotic arbovirus that causes massive mortality in blackbirds. Using a unique longitudinal dataset on the kinetics of virus-specific antibodies in naturally infected wild blackbirds (*Turdus merula*), we found that individual birds may remain seropositive for >1 year and that reinfection can occur despite low-level virus neutralizing antibodies.

[1]Current affiliation: Faculty of Veterinary Medicine, Utrecht University, Utrecht, the Netherlands.

[2]Current affiliation: Centre for Infectious Disease Control, National Institute for Public Health and the Environment, Bilthoven, the Netherlands.

[3]These authors contributed equally to this article.

Usutu virus (USUV), a mosquitoborne zoonotic virus of the genus *Orthoflavivirus*, was first detected in the Netherlands in 2016 (*1*). Eurasian blackbirds (*Turdus merula*) are remarkably susceptible to USUV disease; exceptional die-off among blackbirds is a hallmark of the (re)-emergence of virus circulation in a region (*2*,*3*). Information on survival of blackbirds after USUV infection and the resulting prevalence of USUV antibodies in such populations is limited, and knowledge of the longitudinal dynamics in USUV antibody responses in individual naturally infected blackbirds is lacking. We studied the presence of USUV-specific antibodies in blackbirds during the first 3 years after the initial detection of the virus in the Netherlands.

During March 2016–October 2018, as part of a broader study of zoonoses in songbirds in the Netherlands, we registered 1,181 blackbird captures; 969 unique birds were captured 1–9 times (*1*,*4*). Sampling locations were biased; of 77 sampling locations, just 4 contributed nearly 50% of all samples (Overdinkel, 52°14′N, 7°01′E; Wageningen, 51°59′N, 5°39′E; Haarzuilens, 52°08′N, 5°00′E; Eastermar, 53°11′N, 6°03′E).

We sampled healthy birds by wing vein puncture. Overall, a total of 667 serum samples from 534 unique blackbirds were tested. The samples were screened in a 2-tier system of protein microarray testing including the nonstructural 1 proteins of USUV and West Nile virus (WNV), followed by confirmation of positive IgG results based on comparative USUV and WNV neutralization (*5*). USUV and WNV belong to the same serogroup, causing probable cross-reactivity in serologic assays (*6*). Therefore, we only considered serum samples confirmed for antibodies when microarray reactivity was confirmed by comparative virus neutralization test (VNT) results showing USUV antibody titers ≥4-fold

Table. Summary of serologic results for USUV and WNV in a study of antibody dynamics in naturally infected blackbirds, the Netherlands, 2016–2018*

	USUV			No. samples			
Serologic result	Protein microarray	VNT	WNV VNT	2016	2017	2018	Total
USUV negative	<6,000	NT	NT	59	249	192	500
USUV positive	>6,000	≥16†	4-fold <USUV VNT	3	21	26	50
WNVpositive	<6,000	<16	≥16	0	0	1	1
Subtotal				62	270	219	551
Orthoflavivirus positive	>6,000	≥16	NT	0	7	9	16
	>6,000	≥16 equal to WNV VNT	≥16 equal to USUV VNT	0	0	3	3
	<6,000	NT	≥16	0	0	2	2
Subtotal				0	7	14	21
Possible orthoflavivirus	>6,000	NT	NT	1	3	4	8
Subtotal				1	3	4	8
Total				63	280	237	580

*Serum samples were screened in a 2-tier system of protein microarray testing, followed by confirmation of positive IgG results based on VNT. Strains used for virus neutralization were WNV strain B956 and USUV isolate Africa-3 collected from a blackbird in the Netherlands in 2016. Serum was only considered confirmed for USUV antibodies when VNT USUV antibody titer was ≥4-fold the WNV antibody titer, and vice versa for WNV. Serum samples with a positive USUV microarray result but no conclusive confirmation by VNT were considered orthoflavivirus positive. Negative indicates absence of detectable level of specific antibodies, positive indicated presence of detectable level of specific antibodies. NT, not tested; USUV, Usutu virus; VNT, virus neutralization test; WNV, West Nile virus.
†Reciprocal titers ranged from 1:16 to ≥1:1,024.

higher than a WNV antibody titer, or vice versa. Serum samples with a positive USUV microarray result but no conclusive confirmation by VNT were considered orthoflavivirus positive (Table). To determine the USUV seroprevalence by calendar year, we only included birds that were repeatedly sampled within the same year once, and in cases of seroconversion within a year (n = 4), we only included the positive outcome.

According to the stated criteria for confirmed infection, 3 (4.8%) of 63 unique birds were positive for USUV-specific antibodies in 2016; in 2017, the total was 21 (7.5%) of 280; and in 2018, the total was 26 (10.0%) of 237 (Table). Results showed a significant increase in seroprevalence over those years [$\chi^2(1) = 6.01$, p = 0.01; Hosmer-Lemeshow goodness-of-fit $\chi^2(8) = 3.24$, p = 0.92], with a peak in autumn 2017 (data not shown) (*7*). That increase is in line with observations in Austria, where seropositivity of 9.1% in blackbirds was found 2 years after the virus was first detected, and 9.6% 3 years after (*8*). However, in Germany, seropositivity remained low (≤3.9%) in the 5 years after a massive blackbird die-off (*9*).

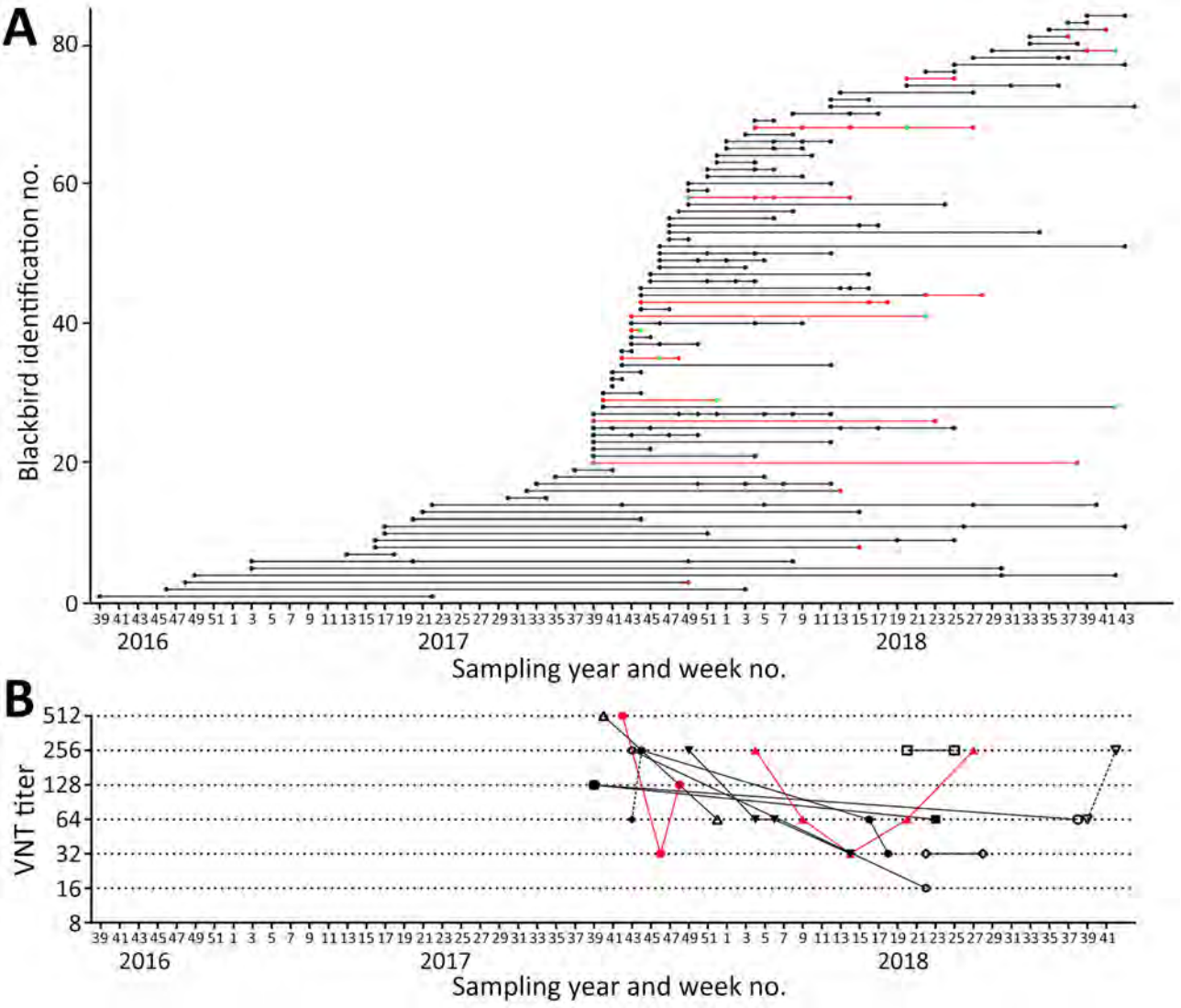

Figure. Longitudinal results for Usutu virus (USUV) serologic testing of serum samples from naturally study of USUV antibody dynamics in naturally infected blackbirds, the Netherlands, 2016–2018. Birds were recaptured and sampled >1 time. A) USUV seropositivity status for recaptured blackbirds that were sampled 2–9 times (n = 84). Left axis indicates individual blackbird identification numbers (1–84); dots represent moment of actual sampling; lines connecting sampling moments of each individual bird are supportive to figure interpretation and have no meaning. Black dots indicate seronegative by microarray; red dots, confirmed positive for USUV antibodies by microarray and comparative VNT USUV versus West Nile virus; green dots, confirmed positive for orthoflavivirus antibodies. B) Trends in USUV virus neutralization test titers in time for recaptured blackbirds that were seropositive >1 time (n = 11). Reciprocal antibody titers are shown. Red lines indicate birds that showed an increase in titer after an initial decline; black lines indicate birds that showed no kinetics or a decline in titer over time. VNT, virus neutralization test.

Starting in September 2016, the Netherlands study captured 124 blackbirds >1 time (range 2–9 times); 84 birds had serum samples taken at >1 capture. Of those birds, 17 were confirmed seropositive >1 time; 7 seroconverted during the study period, and 10 were positive at all time points (Figure, panel A). Of the remaining 67 recaptured birds, 66 remained seronegative throughout the study, whereas 1 bird seroconverted for USUV, based on microarray and USUV VNT only. No seroreversion was observed.

The longest period of seropositivity recorded was ≥361 days. That bird was already seropositive at first sampling and was not followed beyond 361 days. To gain insight into functional neutralizing antibody kinetics, we plotted over time the VNT titers of the 12 birds that were positive at multiple sampling points (Figure, panel B). Six birds showed waning neutralizing antibody titers in time with variable kinetics. Two birds showed no changes in titers in samples taken 33 and 42 days apart, whereas 2 other birds showed an increase in titers taken 5 and 21 days apart. Two birds showed an initial decline in VNT titers, then an increase within 41 and 113 days; corresponding cloaca swab specimens showed a similar trend (positive-negative-positive) for the presence of USUV RNA (no sequence information available). That finding might be indicative for the occurrence of reinfection in the presence of low USUV-neutralizing antibodies, whether or not by different USUV lineages; Africa-3 is the most common infecting lineage in the Netherlands, followed by Europe-3 lineage (*4*). Alternatively, such observations might be the result of exacerbation of a persistent infection (*10*). Conclusive evidence is needed from additional longitudinal studies, including experimental infections. Further insight into the longevity of USUV-specific antibodies in different bird species, the occurrence of reinfections, and the relationship between variations in the immune-status of a specific bird population and variations in the level of virus circulation will contribute to a better understanding of the added value of the assessment of public health risks based on seroecologic surveillance.

In conclusion, our study provides a unique longitudinal dataset on the kinetics of USUV-specific antibodies in naturally infected wild blackbirds. We show seropositivity in individual blackbirds for >1 year and the possible occurrence of reinfection in the presence of low-level virus neutralizing antibodies.

Blackbird captures were performed under ethical permit no. AVD801002015342 to the Netherlands Institute of Ecology.

This project was executed as part of Eco-Alert and funded by ZonMw grant no. 50-52200-98-026.

References

1. Rijks JM, Kik ML, Slaterus R, Foppen R, Stroo A, IJzer J, et al. Widespread Usutu virus outbreak in birds in the Netherlands, 2016. Euro Surveill. 2016;21:21. https://doi.org/10.2807/1560-7917.ES.2016.21.45.30391
2. Gaibani P, Rossini G. An overview of Usutu virus. Microbes Infect. 2017;19:382–7. https://doi.org/10.1016/j.micinf.2017.05.003
3. Weissenböck H, Kolodziejek J, Url A, Lussy H, Rebel-Bauder B, Nowotny N. Emergence of Usutu virus, an African mosquito-borne flavivirus of the Japanese encephalitis virus group, central Europe. Emerg Infect Dis. 2002;8:652–6. https://doi.org/10.3201/eid0807.020094
4. Oude Munnink BB, Münger E, Nieuwenhuijse DF, Kohl R, van der Linden A, Schapendonk CME, et al. Genomic monitoring to understand the emergence and spread of Usutu virus in the Netherlands, 2016–2018. Sci Rep. 2020;10:2798. https://doi.org/10.1038/s41598-020-59692-y
5. Cleton NB, Godeke GJ, Reimerink J, Beersma MF, Doorn HR, Franco L, et al. Spot the difference—development of a syndrome based protein microarray for specific serological detection of multiple flavivirus infections in travelers. PLoS Negl Trop Dis. 2015;9:e0003580. https://doi.org/10.1371/journal.pntd.0003580
6. Kasbergen LMR, Nieuwenhuijse DF, de Bruin E, Sikkema RS, Koopmans MPG. The increasing complexity of arbovirus serology: an in-depth systematic review on cross-reactivity. PLoS Negl Trop Dis. 2023;17:e0011651. https://doi.org/10.1371/journal.pntd.0011651
7. Hosmer DW, Hjort NL. Goodness-of-fit processes for logistic regression: simulation results. Stat Med. 2002;21:2723–38. https://doi.org/10.1002/sim.1200
8. Meister T, Lussy H, Bakonyi T, Sikutová S, Rudolf I, Vogl W, et al. Serological evidence of continuing high Usutu virus (Flaviviridae) activity and establishment of herd immunity in wild birds in Austria. Vet Microbiol. 2008;127:237–48. https://doi.org/10.1016/j.vetmic.2007.08.023
9. Michel F, Fischer D, Eiden M, Fast C, Reuschel M, Müller K, et al. West Nile virus and Usutu virus monitoring of wild birds in Germany. Int J Environ Res Public Health. 2018;15:171. https://doi.org/10.3390/ijerph15010171
10. Streng K, Atama N, Chandler F, Blom R, van der Jeugd H, Schrama M, et al. Sentinel chicken surveillance reveals previously undetected circulation of West Nile virus in the Netherlands. Emerg Microbes Infect. 2024;13:2406278. https://doi.org/10.1080/22221751.2024.2406278

Address for correspondence: Chantal Reusken, Centre for Infectious Disease Control, National Institute for Public Health and the Environment, PO Box 1, 3720 BA Bilthoven, the Netherlands; email: chantal.reusken@rivm.nl

Francisella tularensis Subspecies *holarctica* in Stranded Beluga Whales, Cook Inlet, Alaska, USA

Natalie Rouse, Jeremy Buttler, Kristy Pabilonia, Christina Weller, Laurel Respicio-Kingry, Elizabeth Dietrich, Jeannine Petersen, Ganna Kovalenko, Eric Bortz, Kathy Burek Huntington

Author affiliations: Alaska Veterinary Pathology Services, Eagle River, Alaska, USA (N. Rouse, K. Burek Huntington); University of Alaska Anchorage, Anchorage, Alaska, USA (N. Rouse, J. Buttler, G. Kovalenko, E. Bortz); Colorado State University, Fort Collins, Colorado, USA (K. Pabilonia, C. Weller); Centers for Disease Control and Prevention, Fort Collins (L. Respicio-Kingry, E. Dietrich, J. Petersen)

DOI: http://doi.org/10.3201/eid2806.250033

We report fatal tularemia in stranded beluga whales in Cook Inlet, Alaska, USA. *Francisella tularensis* was detected by nanopore metagenomics, confirmed by quantitative PCR and immunohistochemistry, and characterized as *F. tularensis* subspecies *holarctica* by multilocus sequence typing. Our findings should be considered when assessing biosecurity and marine mammal health in the North Pacific.

Francisella tularensis is a highly pathogenic gram-negative bacterium that infects a large range of animals and humans, primarily in the Northern Hemisphere, causing the clinical disease tularemia. Human disease manifests with influenza-like symptoms (lymphadenopathy, conjunctivitis, pneumonia, septicemia) and other specific symptoms corresponding to the route of exposure. Two subspecies, *F. tularensis* subsp. *tularensis* and *holarctica*, are known pathogens and can be acquired via multiple routes, including arthropod vector, cutaneous, ingestion, or inhalation (*1*).

F. tularensis was first documented in Alaska, USA, in 1938 (*2*) and has been isolated infrequently in ticks, lagomorphs, and rodents. Serologic studies have confirmed exposure in humans, avian species, terrestrial mammals, and polar bears in multiple areas of the state (*2*). In October 2023, tularemia was diagnosed in a pinniped in Washington, USA, when a biologist was infected during necropsy (*3*). The same fall, dead stranded beluga whales (*Delphinapterus leucas*) in Cook Inlet, Alaska, were found to have gross lesions consistent with tularemia. We report the results of an investigation of those deaths.

Necropsies were performed and tissues collected and stored following standard procedures. Samples for histopathology were fixed in 10% neutral buffered formalin (Table). We submitted varied tissues from 2 sufficiently fresh animals (no. 2023279: fetal spleen, mediastinal lymph node, spleen, blowhole swab, heart, liver; and no. 2023288: brain, liver, mammary gland, mediastinal lymph node, spleen) for aerobic culture and testing for known cetacean pathogens, including influenza and *Erysipelothrix* sp. by PCR, and for harmful algal bloom toxins by ELISA (Table). We analyzed blowhole swab, lung, mediastinal lymph node, and rectal swab samples from animal 2023279 by metagenomic sequencing. In brief, we extracted and amplified total nucleic acids (I.M. Claro et al., unpub. data, https://doi.org/10.12688/wellcomeopenres.17170.2) and sequenced cDNA and metagenomics libraries by SMART9N using an Oxford Nanopore Rapid PCR barcoding and MinION device (https://nanoporetech.com) (Table; Appendix Figure 1, https://wwwnc.cdc.gov/EID/article/31/6/25-0033-App1.pdf) (*4*). We classified sequence reads by using wf-metagenomics and wf-alignment in epi2melabs v.5.1.3 (Oxford Nanopore), mapped to the *F. tularensis* genome (GenBank accession no. NC_007880.1) by reference-based assembly using minimap2, and annotated using tbCon and ggplot in RStudio (Posit, https://posit.co) (Table). Subsequently, we tested lung and liver tissue from both animals for *F. tularensis* by immunohistochemistry and by culture and PCR using Centers for Disease Control and Prevention Laboratory Response Network proprietary protocols (Table). We then typed samples from positive animals by multilocus type sequencing of 6 genes (*fabH, tpiA, sdhA, rpoA, groEL,* and *pgm*) (*5*–*7*) and sequenced multiplexed amplicon libraries on the MiSeq platform (Illumina, https://www.illumina.com) (Table). We mapped amplicon sequence reads to reference genes from *F. tularensis* subsp. *holarctica* live vaccine strain, concatenated, and aligned with corresponding sequences from *F. tularensis* and other *Francisella* spp. to construct phylogenetic trees.

Both animals were pregnant adult females with markedly enlarged mediastinal lymph nodes, pleuritis, and pneumonia (Figure, panel A). One animal had severe multifocal random ecchymotic hemorrhage in the blubber (Figure, panel B). Histologic findings included necrosuppurative and histiocytic bronchopneumonia, lymphadenitis, and hepatitis (Appendix Figure 2, panels A–C). Immunohistochemistry demonstrated positive staining in areas of inflammation (Appendix Figure 2, panel D). Domoic acid and saxitoxin

Table. Tests performed on dead stranded beluga whales infected with *Francisella tularensis*, Cook Inlet, Alaska, USA*

Procedure	Method	Method detail	Laboratory	Manufacturer† or reference
Gross necropsy	NA	Tissues stored in whirl paks and swabs in cryovials with VTM or TSB with 15% glycerol and frozen at −80°C within 6 hours of sampling.	AVPS	Remel (VTM), Hardy Diagnostics (TSB)
Nanopore metagenomics	QiAMP DNA/RNA kit	Eluted in 50 µL elution buffer	UAA	QIAGEN
Nanopore metagenomics	Rapid SMART9N	Superscript IV TR-ase (Thermo Fisher Scientific†); primers RLB RT-9N, TTTTTCGTGCGCCGCTTCAACNNNNNNNNN and RLB TSO-RNA (r-hybrid oligo), GCTAATCATTGCTTTTTCGTGCGCCGCTTCA ACATrGrGrG without DNase treatment. Cycling conditions: 42°C for 90 min; 70°C for 10 min; 4°C hold.	UAA	‡
Nanopore metagenomics	ONT† SQK-RPB114.96 kit (V14)	LongAmp Taq (2X; New England BioLabs†) PCR (95°C for 45 min, then 30 cycles at 95°C for 15 s; 56°C for 15 s; 65°C for 5 min; and 10 min final extension) with Rapid PCR barcoding using ONT SQK-RPB114.96 kit V14 on an ONT MinION Mk1B device running MinKNOW v.24.06.8 with high-accuracy basecalling.	UAA	(*4*)
Nanopore metagenomics: bioinformatics sequence read classification	wf-metagenomics and wf-alignment in Epi2me Labs v.5.1.3	NA	UAA	Epi2me Labs
Nanopore metagenomics: *F. tularensis* genome mapping	Reference-based assembly	Minimap2	UAA	NA
Nanopore metagenomics: sequence allignment and annotation	tbCon and ggplot in RStudio v. 2024.04.0+735	NA	UAA	NA
MLST: amplification	Amplification of 6 genes: *fabH, tpiA, sdhA, rpoA, groEL*, and *pgm*	Primers described in references	CDC	(*5*–*7*)
MLST: sequencing of amplicon libraries	Multiplexed amplicon sequencing on MiSeq platform	Nextera XT and V2 300 cycle reagent kit	CDC	Illumina
MLST: *F. tularensis* genome mapping	Reads were mapped to reference genes from *F. tularensis* subsp. *holarctica* LVS	CLC Genomics Workbench	CDC	QIAGEN
MLST: phylogenetic tree construction	Maximum-likelihood analysis	Generalized time-reversible nucleotide substitution model with gamma distribution (4 categories) plus invariant sites and 1,000 bootstrap replications	CDC	MEGAX
F. tularensis culture	LRN protocol	NA	CDC	CDC LRN
F. tularensis PCR	LRN protocol	NA	CSU VDL	CDC LRN
Erysipelothrix sp. PCR	NA	Primers ERy4423F and Ery4587R only	AVDL	(*8*)
Influenza A virus PCR	NA	Primers described in reference	Tufts and UAA	(*9*)
Histopathology	Hematoxylin and eosin staining	NA	HCS and AVPS	NA
Immunohistochemistry for *F. tularensis*	NA	NA	KSU	NA
Saxitoxin	ELISA	NA	WARRN West	Abraxis
Domoic acid	ELISA	NA	WARRN West	Abraxis

*AVDL, University of Georgia Athens Veterinary Diagnostic Laboratory; AVPS, Alaska Veterinary Pathology Services; CDC, Centers for Disease Control and Prevention; CSU VDL, Colorado State University Veterinary Diagnostic Laboratory; HCS, Histological Consulting Services; KSU, Kansas State University Veterinary Diagnostic Laboratory; LRN, CDC Laboratory Response Network; LVS, live vaccine strain; MLST, multilocus sequence typing; NA, not applicable; ONT, Oxford Nanopore Technologies; TSB, tryptic soy broth; Tufts, Tufts University; UAA, University of Alaska; VTM, viral transport medium; WARRN West, National Oceanic and Atmospheric Administration Wildlife Algal-toxin Research and Response Network West.
†Manufacturers and products: Abraxis, https://www.bms.com; Epi2me Labs, https://epi2me.nanoporetech.com; Hardy Diagnostics, https://hardydiagnostics.com; MEGAX, https://www.megasoftware.net; Minimap2, https://github.com/lh3/minimap2; New England BioIabs, https://www.neb.com; Oxford Nanopore Technologies, https://nanoporetech.com; QIAGEN, https://www.qiagen.com; Remel, https://www.thermofisher.com; RStudio, https://posit.co; tbCon, https://github.com/jeremyButtler/bioTools; Thermo Fisher Scientific; https://www.thermofisher.com.
‡I.M. Claro et al., unpub. data, https://doi.org/10.12688/wellcomeopenres.17170.2.

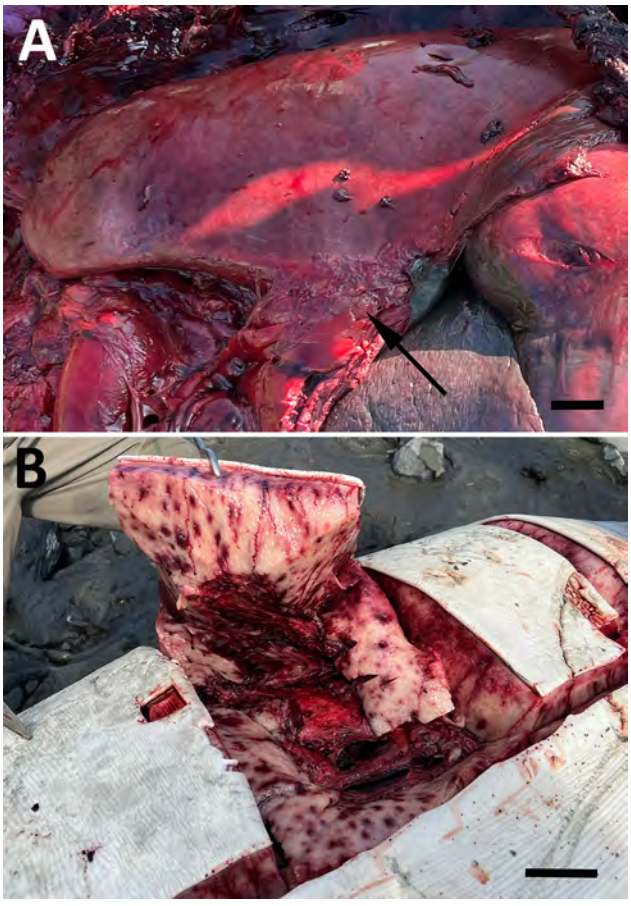

Figure. Gross examination of a beluga whale infected with *Francisella tularensis* subspecies *holarctica*, Cook Inlet, Alaska, USA. A) Lung and enlarged mediastinal lymph node (arrow). Scale bar = 6 cm. B) Ecchymoses in the blubber, showing extensive positive staining primarily in areas of inflammation. Scale bar = 5 cm.

were not found, and PCRs and bacterial cultures yielded negative results or mixed organisms believed to be postmortem overgrowth (Appendix Table).

We identified the causative organism by using metagenomics. We mapped sequence reads from animal 2023279 by reference-based assembly and found those reads to be distributed at low read depth (2–21×; 1,181 sequence reads; N50 = 275 nt, quality score = 9) across the 1.89-Mbp *F. tularensis* genome. We detected *F. tularensis* DNA in all samples by quantitative PCR with cycle threshold values <25. By multilocus sequence typing, we identified a concatenated sequence of 4,107 bp as *F. tularensis* subsp. *holarctica*. Phylogenetic analysis placed this strain in a clade identical to the 2023 pinniped case from Washington, as well as other isolates from the Northern Hemisphere (Appendix Figure 3).

Although Cook Inlet belugas are known to be susceptible to a variety of bacterial pathogens (*10*), *F. tularensis* has not been previously detected in this population, or in other cetaceans. The pattern of pathology represents the pulmonary form of tularemia, and the route of exposure was likely inhalation of contaminated water. *F. tularensis* is primarily a disease associated with freshwater, but the brackish nature of Cook Inlet and nearshore residence of belugas expose them to potentially contaminated freshwater runoff as well as to other reservoirs typically associated with freshwater (e.g., aquatic rodents, mosquito larvae) (*1*,*2*). The cause of the infections in a previously unreported host is unknown; however, host factors such as immunosuppression or environmental changes, such as increased runoff, could be considered.

One human case of tularemia was reported in Cook Inlet's largest adjacent city in 2023 (https://epi.alaska.gov/bulletins/docs/b2024_14.pdf); however, the circumstances of exposure were not reported. The propensity of whales to travel long distances could further disseminate this pathogen, increasing exposure to humans and wildlife. Our findings highlight a new risk to persons working in the marine environment and should be considered when assessing biosecurity and marine mammal health in the North Pacific.

Acknowledgments

We thank the Alaska Marine Mammal Stranding network, Melanie Iverson, and the National Marine Fisheries Service Protected Species Division for assistance with field sampling, and Hailei Nystuen, Soren George-Nichol, and Bryce Inman for assistance with molecular analysis.

All samples were collected under National Oceanic and Atmospheric Administration permit no. 24359. Diagnostics not related to these findings were run at University of California Davis and University of Georgia Veterinary Diagnostic lab (aerobic culture), Tufts Puyear lab (viral PCRs), and WARRN West (harmful algal bloom toxin testing). We deposited sequences from this study into GenBank (accession nos. PQ724310–21) and the National Center for Biotechnology Information Sequence Read Archive (accession nos. SRR31713860 and SRR31713861) (Appendix).

Funding for stranding response, molecular analyses, and manuscript preparation was provided by the John H. Prescott grant program (grant nos. NA22NMF4390247 and NA23NMF4390303) and National Marine Fisheries Service contract no. 1333MF22PNFFS0225. Funding for pathogen genomics analysis was provided by the National Institutes of Health National Institute of General Medical Sciences IDeA Networks of Biomedical

Research Excellence grant no. P20GM103395 (Alaska INBRE), US Department of Agriculture American Rescue Plan SPASAK project subaward to U.A.A. (Animal Research Service grant no. AP23OA000000C014), and the National Institutes of Health National Institute of Allergy and Infectious Diseases Centers of Excellence for Influenza Research and Response (contract no. 75N93021C00014).

About the Author

Ms. Rouse is a necropsy biologist at Alaska Veterinary Pathology Services, Eagle River, Alaska. Her main interests are wildlife health and disease ecology.

References

1. Hennebique A, Boisset S, Maurin M. Tularemia as a waterborne disease: a review. Emerg Microbes Infect. 2019;8:1027–42. https://doi.org/10.1080/22221751.2019.1638734
2. Smith MM, Van Hemert C, Atwood TC, Sinnett DR, Hupp JW, Meixell BW, et al. A serologic survey of *Francisella tularensis* exposure in wildlife on the Arctic Coastal Plain of Alaska, USA. J Wildl Dis. 2022;58:746–55. https://doi.org/10.7589/JWD-D-21-00162
3. Inouye W, Oltean HN, McMillan M, Schnitzler H, Lipton B, Peterson JM, et al. Notes from the field: tularemia associated with harbor seal necropsy—Kitsap County, Washington, October 2023. MMWR Morb Mortal Wkly Rep. 2024;73:731–2. https://doi.org/10.15585/mmwr.mm73333a3
4. Buttler J, Drown DM. Accuracy and completeness of long read metagenomic assemblies. Microorganisms. 2022;11:96. https://doi.org/10.3390/microorganisms11010096
5. Ahlinder J, Öhrman C, Svensson K, Lindgren P, Johansson A, Forsman M, et al. Increased knowledge of *Francisella* genus diversity highlights the benefits of optimised DNA-based assays. BMC Microbiol. 2012;12:220. https://doi.org/10.1186/1471-2180-12-220
6. Mikalsen J, Olsen AB, Tengs T, Colquhoun DJ. *Francisella philomiragia* subsp. *noatunensis* subsp. nov., isolated from farmed Atlantic cod (*Gadus morhua L.*). Int J Syst Evol Microbiol. 2007;57:1960–5. https://doi.org/10.1099/ijs.0.64765-0
7. Brett M, Doppalapudi A, Respicio-Kingry LB, Myers D, Husband B, Pollard K, et al. *Francisella novicida* bacteremia after a near-drowning accident. J Clin Microbiol. 2012;50:2826–9. https://doi.org/10.1128/JCM.00995-12
8. Pal N, Bender JS, Opriessnig T. Rapid detection and differentiation of *Erysipelothrix* spp. by a novel multiplex real-time PCR assay. J Appl Microbiol. 2010;108:1083–93. https://doi.org/10.1111/j.1365-2672.2009.04560.x
9. Puryear WB, Keogh M, Hill N, Moxley J, Josephson E, Davis KR, et al. Prevalence of influenza A virus in live-captured North Atlantic gray seals: a possible wild reservoir. Emerg Microbes Infect. 2016;5:e81. https://doi.org/10.1038/emi.2016.77
10. Rouse NM, Burek-Huntington K. Cook Inlet beluga whale *Delphinapterus leucas* with valvular endocarditis, encephalitis, rhabdomyolysis, heavy parasitism and fungal dermatitis. Dis Aquat Organ. 2023;155:1–6. https://doi.org/10.3354/dao03736

Address for correspondence: Natalie Rouse, University of Alaska Anchorage, 3211 Providence Dr, Anchorage, AK 99508, USA; email: avps.natalierouse@gmail.com

Nosocomial Transmission of *Plasmodium falciparum* Malaria, Spain, 2024

Manuel F. Liroa Romero, Maite Ruiz Pérez de Pipaón, Maria D. Navarro Amuedo, Jose M. Rubio Muñoz, Jose M. Jiménez-Hoyuela, Jose M. Cisneros

Author affiliations: University of Seville, Seville, Spain (M.F. Liroa Romero, M. Ruiz Pérez de Pipaón, M.D. Navarro Amuedo, J.M. Jiménez-Hoyuela, J.M. Cisneros); Hospital Universitario Virgen del Rocío/IBis, Seville (M.F. Liroa Romero, M. Ruiz Pérez de Pipaón, M.D. Navarro Amuedo, J.M. Cisneros); CIBERINFEC, Instituto de Salud Carlos III, Madrid, Spain (J.M. Rubio Muñoz, J.M. Cisneros)

DOI: https://doi.org/10.3201/eid3106.241932

We report nosocomial *Plasmodium falciparum* malaria in Spain, which was confirmed microbiologically and genomically. Transmission occurred through insufficiently disinfected reusable syringe lead shielding during thyroid scintigraphy. Genomic analysis showed high similarity between isolates from index and source cases. Strict biosafety measures are needed in healthcare settings to prevent malaria transmission.

Malaria is an infectious disease caused by *Plasmodium* protozoa and is primarily transmitted to humans through the bite of an *Anopheles* mosquito (*1*). Countries without malaria report cases of infection through blood product transfusions (1 case/4 million inhabitants) (*2*) and solid organ transplants (1 case/1 million inhabitants) (*3*). Cases were also reported for which transmission mechanism was not established and a parenteral route was suspected (0.006 cases/1 million inhabitants) (*4*).

In 2022, a total of 6,131 cases of malaria were confirmed in Europe. Fourteen autochthonous cases were caused by *P. falciparum*: 9 cases related to airports, 3 cryptogenic cases (epidemiologic investigations failed to identify an apparent mode of acquisition), and 2 cases acquired in a hospital in Spain (*5*).

In Spain, autochthonous malaria was eradicated in 1964 (*4*). Since then, *P. vivax* malaria was found in 2 autochthonous cases (*6*) and was explained by the presence the *P. vivax* vector *An. atroparvus* mosquito in Spain (*6*). Conversely, *P. falciparum* vectors *An. algeriensis* and *An. plumbeus* mosquitoes are not found in Spain (*7*). In 2024, the annual number of imported malaria cases in Spain was 600 (*4*,*8*); 2 cases of airport transmission and 5 cases of

nosocomial acquisition also occurred (*6*). Of the 5 nosocomial acquisition cases, 1 case was linked to a blood product transfusion (*6*), 1 case was linked to organ transplantation (*6*), and 3 cases had no identified nosocomial transmission mechanism (*6*). None of the 5 nosocomial malaria cases had parasite identification in the source patient, and thus, transmission was not confirmed through genomic comparison (*4*). We describe a case of nosocomial malaria acquired in Spain in 2024, with microbiological and genomic confirmation and transmission mechanism identification.

A 60-year-old woman from Gilena, southern Spain, who had arterial hypertension and was under study for a thyroid nodule sought care at an emergency department with fever (38°C), general malaise, night sweats, and arthralgia lasting 5 days. She had thrombocytopenia (47,000 platelets/μL) and elevated total bilirubin level (2.18 mg/dL, reference range 0.3–1.2 mg/dL). Peripheral blood smear showed abundant erythrocytes infected with *Plasmodium* spp. PCR in blood and thick smear confirmed *P. falciparum* infection with blood parasitemia index of 7%. Intravenous artesunate treatment was initiated, followed by combination oral dihydroartemisinin/piperaquine treatment for 3 days, which resulted in rapid recovery.

We initiated an exhaustive epidemiologic investigation after diagnosing presumably autochthonous *P. falciparum* malaria. The patient confirmed she had never traveled outside Spain, visited airports, been hospitalized, or received blood transfusions or organ transplants. However, 15 days before fever onset, she underwent thyroid scintigraphy with radioactive iodine. The patient who had been tested before her was from Equatorial Guinea; he was asymptomatic, afebrile, had no signs of infection, and had not traveled to his home country in >2 years. However, he reported a history of malaria in childhood. PCR and thick blood smear testing was conducted and identified asymptomatic *P. falciparum* infection with low-grade parasitemia. Genetic analysis comparing *P. falciparum* isolates from both patients, focusing on *PfMSP-1* and *PfMSP-2* (merozoite surface proteins), showed substantial genetic similarity (Figure 1). Of the remaining patients who underwent scintigraphy the same day, none had fever or infection signs within 30 days of the procedure.

We reviewed the scintigraphy procedure and confirmed that the syringe was discarded after intravenous administration of radioactive iodine. A lead protector shielded the syringe and needle (Figure 2). Single-dose vials had traceability labels. For thyroid scintigraphy, intravenous administration of the radiopharmaceutical is required. Although blood aspiration is generally avoided, minimal aspiration may occur during venous access. Slight blood aspiration during venous access is the most probable explanation of the nosocomial transmission (https://youtu.be/2OW9g2tiBjc). After administration, the syringe and needle are discarded as radioactive waste, and lead shields are cleaned with 70% isopropyl alcohol and immersed in peroxide-based disinfectants for reuse. Contamination of the new syringe with blood from the previous patient by placing it in the inadequately cleaned sheath was the likely mechanism of *P. falciparum* transmission. However, the lead shield was also reused, after cleaning with antiseptic solution.

This study clinically and microbiologically confirms a case of *P. falciparum* acquisition in Spain and describes a nosocomial transmission mechanism through intravenous administration of radioactive iodine during thyroid scintigraphy caused by inadequate

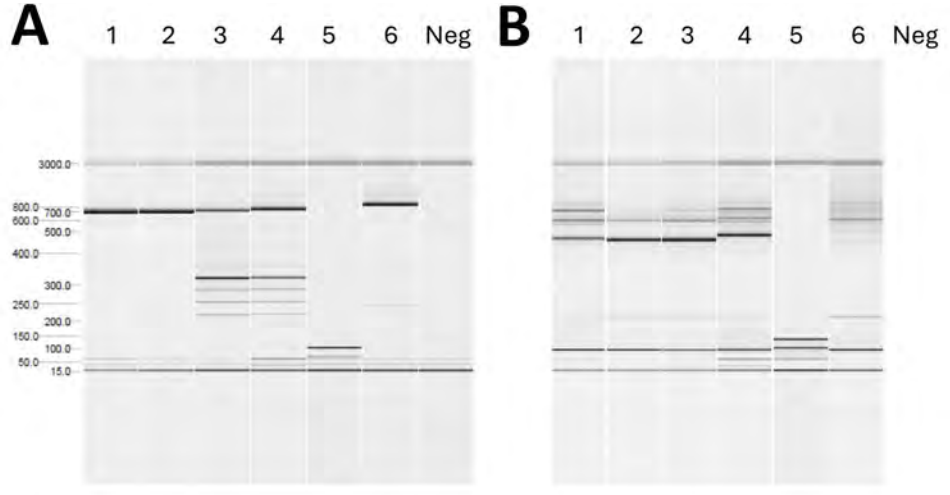

Figure 1. Genotyping study of *Plasmodium falciparum* isolated from 2 patients involved in nosocomial transmission of *P. falciparum* malaria, Spain, 2024. The genes analyzed were *PfMSP-1* and *PfMSP-2*. Results for genotypes FC27 (A) and IC (B) for the MSP-2 families are shown. The findings indicate that the fragments detected in the index case are also present in the source case. MSP, merozoite surface protein; neg, negative.

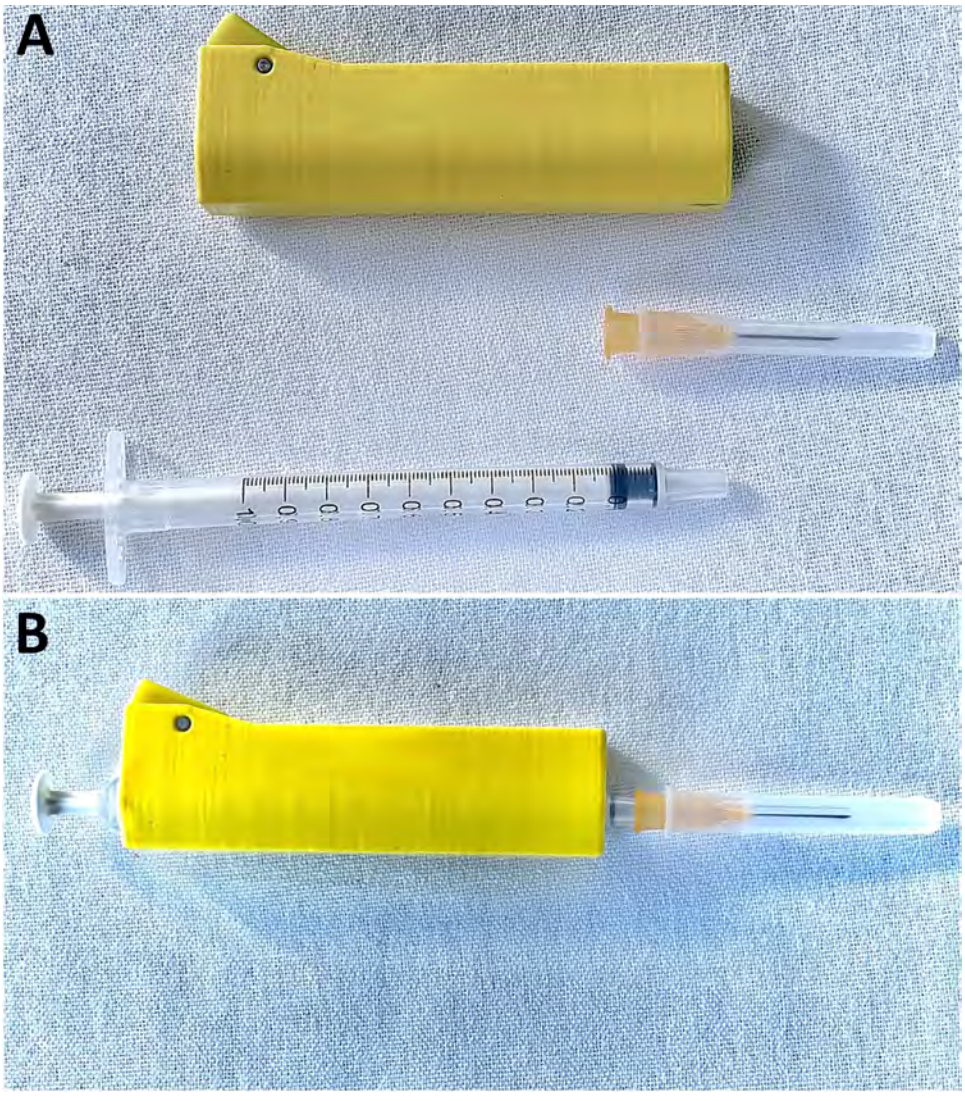

Figure 2. Syringe covered with a lead shield used during nosocomial transmission of *Plasmodium falciparum* Malaria, Spain, 2024. A) Yellow lead shield with removable disposable syringe and needle. B) Syringe assembled with the lead shield.

disinfection of the reusable lead shield. The sequence of events—scintigraphy performed on the source case followed by the index case, identification of *P. falciparum* in blood of both patients, and genetic concordance of the isolates—shows the transmission mechanism. Our findings helped identify and correct a safety issue in the diagnostic procedure. Each lead cover is now used only 1 time per day and then autoclave sterilized before use another day.

This case underscores the importance of asymptomatic carriers as reservoirs for malaria transmission, which is a well-known issue in endemic regions (*9*,*10*). Asymptomatic carriers should be considered in nonendemic areas because of globalization and increased healthcare interactions. Malaria should be included in the differential diagnosis for patients with fever and unexplained thrombocytopenia in nonendemic countries. Clinicians must recognize the critical need for stringent biosafety measures and safe practices in health-care settings.

About the Author

Dr. Liroa Romero is an infectious disease physician at the Virgen del Rocío University Hospital in Seville, a reference center for tropical infectious diseases. He primarily focuses on the care of urgent and rapidly resolved infectious diseases.

References

1. Muñoz J, Rojo-Marcos G, Ramírez-Olivencia G, Salas-Coronas J, Treviño B, Perez Arellano JL, et al. Diagnosis and treatment of imported malaria in Spain: recommendations from the Malaria Working Group of the Spanish Society of Tropical Medicine and International Health (SEMTSI) [in Spanish]. Enferm Infecc Microbiol Clin. 2015;33:e1–13. https://doi.org/10.1016/j.eimc.2013.12.014

2. Batista-Dos-Santos SA, Freitas DRC, Raiol M, Cabral GF, Feio AC, Póvoa MM, et al. Strategy to improve malaria surveillance system preventing transfusion-transmitted malaria in blood banks using molecular diagnostic. Malar J. 2018;17:344. https://doi.org/10.1186/s12936-018-2486-z
3. Schwartz BS, Mawhorter SD; AST Infectious Diseases Community of Practice. Parasitic infections in solid organ transplantation. Am J Transplant. 2013;13:280–303. https://doi.org/10.1111/ajt.12120
4. Instituto de Salud Carlos III. ISCIII portal web [cited 2024 Nov 3]. https://www.isciii.es
5. European Centre for Disease Prevention and Control. Annual epidemiological report for 2022: malaria [cited 2024 Dec 26]. https://www.ecdc.europa.eu/en/publications-data/annual-epidemiological-report-2022-malaria
6. ISCIII-Vigilancia en Salud Pública-RENAVE. ISCIII portal web [cited 2024 Nov 3]. https://www.isciii.es/servicios/vigilancia-salud-publica-renave
7. Ministerio de Sanidad. Informes de situación y evaluación del riesgo publicados por el CCAES [cited 2024 Nov 3]. https://www.sanidad.gob.es/areas/alertasEmergenciasSanitarias/situacionRiesgo/informes.htm
8. National Institute of Allergy and Infectious Diseases (NIAID). Malaria [cited 2024 Nov 3]. https://www.niaid.nih.gov/diseases-conditions/malaria
9. Bottius E, Guanzirolli A, Trape JF, Rogier C, Konate L, Druilhe P. Malaria: even more chronic in nature than previously thought: evidence for subpatent parasitaemia detectable by the polymerase chain reaction. Trans R Soc Trop Med Hyg. 1996;90:15–9. https://doi.org/10.1016/S0035-9203(96)90463-0
10. Aguas R, Maude RJ, Gomes MGM, White LJ, White NJ, Dondorp AM. Infectivity of chronic malaria infections and its consequences for control and elimination. Clin Infect Dis. 2018;67:295–302. https://doi.org/10.1093/cid/ciy055

Address for correspondence: Jose M. Cisneros, Hospital Virgen del Rocío, Manuel Siurot Ave, s/n. 41013 Sevilla, Spain; email: jmcisnerosh@gmail.com

Avian Influenza A(H5N1) Isolated from Dairy Farm Worker, Michigan, USA

Nicole Brock, Joanna A. Pulit-Penaloza, Jessica A. Belser, Claudia Pappas, Xiangjie Sun, Troy J. Kieran, Hui Zeng, Juan A. De La Cruz, Yasuko Hatta, Han Di, C. Todd Davis, Terrence M. Tumpey, Taronna R. Maines

Author affiliation: Centers for Disease Control and Prevention, Atlanta, Georgia, USA

DOI: https://doi.org/10.3201/eid3106.250386

Influenza A(H5N1) viruses have been detected in US dairy cow herds since 2024. We assessed the pathogenesis, transmission, and airborne release of A/Michigan/90/2024, an H5N1 isolate from a dairy farm worker in Michigan, in the ferret model. Results show this virus caused airborne transmission with moderate pathogenicity, including limited extrapulmonary spread, without lethality.

Highly pathogenic avian influenza A(H5N1) clade 2.3.4.4b viruses have displayed unprecedented global spread among wild birds leading to numerous spillover infections in mammalian species. Of note, outbreaks in dairy cattle and gallinaceous birds have resulted in human infections in the United States during 2024–2025 (*1*). Increased frequency of H5N1 viruses crossing species barriers has caused concern that the avian influenza viruses are adapting to mammals. A critical component of influenza pandemic preparedness is early identification of emerging novel influenza viruses that cause disease and transmit efficiently in humans. A clade 2.3.4.4b H5N1 virus, A/Michigan/90/2024 (MI90), genotype B3.13, was isolated from a conjunctival swab specimen collected from a human patient in Michigan with conjunctivitis after exposure to infected cattle (*2*,*3*). In this article, we report the pathogenesis, transmission, and airborne exhalation of MI90 virus in ferrets, the standard animal model for influenza virus risk assessments (*4*).

We inoculated 18 ferrets with MI90 virus as previously described (*5*,*6*). We euthanized 3 ferrets on 3 and 5 days postinoculation (dpi) to assess virus spread in tissues. We used 6 ferrets to assess transmission in a cohoused, direct contact setting as a direct contact transmission model and through the air in the absence of direct or indirect contact as a respiratory droplet transmission model. We paired each ferret with a naive contact, as previously described (*4*). We observed clinical manifestations daily and collected

Table. Clinical signs and virus titers in ferrets infected with avian influenza A(H5N1) isolated from dairy farm worker in Michigan, 2024*

Clinical signs and tissues sampled	Inoculated ferrets		Transmission models		
	Euthanized at 3 dpi	Euthanized at 5 dpi	Inoculated	DCT	RDT
Weight loss, %†	4.5 (3/3)	11.8 (3/3)	9.8 (12/12)	5.5 (6/6)	6.6 (3/6)
Fever, °C above baseline‡	0.9 (3/3)	1.3 (2/3)	1.8 (11/12)	1.8 (6/6)	2.0 (3/6)
Nasal wash	6.1 (3/3)	5.4 (3/3)	5.1 (1–5 d)	4.6 (5–7 d)	4.5 (9–11 d)
Conjunctival wash§	1.4 (3/3)	NT	3.2 (3 d)	ND	ND
Rectal swab¶	1.4 (3/3)	NT	2.6 (3–5 d)	1.0 (3 d)	1.4 (3 d)
Tissues					
Nasal turbinate	6.6 (3/3)	5.3 (3/3)	NT	NT	NT
Ethmoid turbinate	7.4 (3/3)	6.5 (3/3)	NT	NT	NT
Soft palate	3.5 (1/3)	NT	NT	NT	NT
Lung#	3.5 (2/3)	4.3 (3/3)	NT	NT	NT
Trachea#	5.9 (3/3)	5.8 (2/3)	NT	NT	NT
Intestine#	1.8 (1/3)	ND (0/3)	NT	NT	NT
Brain#	2.4 (3/3)	2.4 (2/3)	NT	NT	NT
Olfactory bulb	3.1 (2/3)	4.2 (3/3)	NT	NT	NT

*Values are $\log_{10}$ PFU/mL (no. ferrets affected/total no. in group) except as indicated. DCT, direct contact transmission model; ND, not detected; NT, not tested; RDT, respiratory droplet transmission model.
†Mean maximum weight loss after inoculation with 10^6 PFU A/Michigan/90/2024 A(H5N1) virus in a 1-mL volume.
‡Mean maximum rise in body temperature from baseline (37.4°C–39.0°C).
§Conjunctival washes collected from 6 of 12 inoculated animals and 3 each of DCT and RDT contact ferrets in the transmission experiment; number of ferrets with detectable virus or day of mean peak shown parenthetically.
¶Virus in rectal swab samples detected in 8 of 12 inoculated and 1 each of DCT and RDT contact ferrets in the transmission experiment; number of ferrets with detectable virus or day of mean peak shown parenthetically.
#Values are $\log_{10}$ PFU/g.

nasal wash (NW), conjunctival, and rectal swab samples every 2 days postinoculation or postcontact. We confirmed transmission by testing for seroconversion to homologous virus in the contact animals.

Although all MI90-infected ferrets survived the 21-day study, we noted moderate disease. In inoculated ferrets, the mean maximum weight loss was 9.8%, fever (1.8°C above baseline) and lethargy were transient, and nasal and ocular discharge and sneezing were evident at 4–9 dpi (Table). We detected virus 3 dpi primarily in respiratory tract tissues; titers were highest in ethmoid turbinate samples (7.4 $\log_{10}$ PFU/mL) and at low levels in brain and gastrointestinal tissues. We observed similar results in tissues collected 5 dpi.

During the direct contact transmission experiment, inoculated ferrets shed virus in NW that peaked at 4.7–5.4 $\log_{10}$ PFU/mL at 1–5 dpi (Figure, panel A). Four of 6 cohoused contact animals had virus in NW (peak 2.5–4.9 $\log_{10}$ PFU/mL) at 5–7 days postcontact, whereas all 6 contact animals had viral RNA detected (3.6–7.7 $\log_{10}$ copies/mL) in NW (*7*) and seroconverted to MI90 virus, indicating that transmission was 100% (6/6 animals). In the respiratory droplet transmission experiment, NW collected from inoculated animals peaked 2.6–4.8 $\log_{10}$

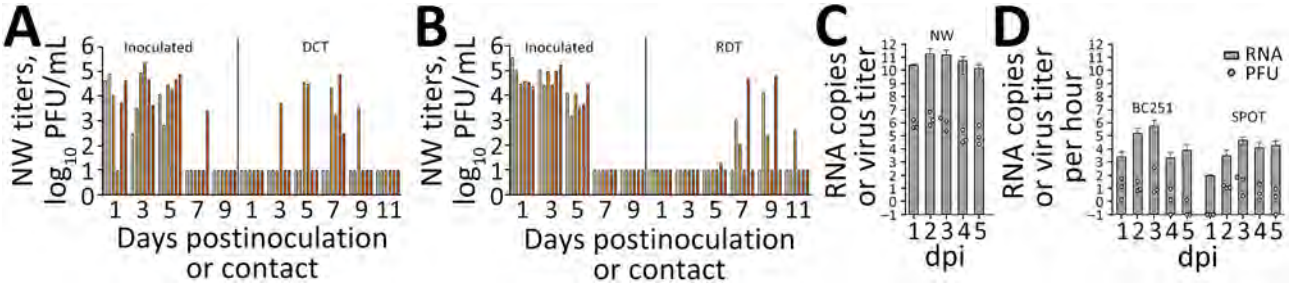

Figure. Transmission and measurement of airborne avian influenza A(H5N1) virus isolated from dairy farm worker, Michigan. A, B) For DCT and RDT testing, ferrets (n = 12) were intranasally inoculated with 10^6 PFU A/Michigan/90/2024 virus, isolated from the dairy worker, in 1 mL phosphate-buffered saline and were cohoused with naive ferrets in a DCT model (A) or in adjacent cages with perforated sidewalls permitting airborne virus spread but restricting contact in an RDT model (B). Each bar represents a single animal. C, D) For aerosol testing, ferrets (n = 3) were inoculated intranasally with 10^6 PFU of MI90 virus and tested daily (C). Orange dots represent viral titers from NW in log10 PFU/mL; limit of detection 10 PFU/mL. Gray bars show average viral M gene RNA load. Error bars indicate SD. Limit of detection was 2.9 log10 RNA copies/mL. D) Aerosol samples were collected daily for 5 dpi by using a BC251 cyclone-based sampler (kindly provided by Dr. William Lindsley, National Institute for Occupational Safety and Health) and the SPOT water condensation sampler (Aerosol Devices, https://aerosoldevices.com), as described previously (8). Orange dots represent log10 PFU/mL per hour. Gray bars show average viral M gene RNA. Error bars indicate SD. Limit of detection was 2.5 log10 RNA copies/h. Ferrets were used for tissue collection on day 5. DCT, direct contact transmission; dpi, days postinoculation; NW, nasal washes; RDT, respiratory droplet transmission.

PFU/mL at 1–3 dpi, whereas 3/6 contact ferrets had detectable virus in NW by day 7 postcontact (peak 2.6–4.8 $\log_{10}$ PFU/mL; days 9–11 postcontact) (Figure, panel B) as well as viral RNA (6.7–8.2 $\log_{10}$ copies/mL), and seroconverted, confirming transmission through the air in 50% of ferrets (3/6). We also detected infectious virus in conjunctival and rectal samples from inoculated animals, but only from 2 contact animals (Table).

To further evaluate the level of virus exhaled by MI90-inoculated ferrets and the potential for airborne transmission, we collected aerosol samples 1 time each day at 1–5 dpi for 1 hour from the 3 ferrets that were euthanized at 5 dpi. Air samples were analyzed for infectious virus and viral RNA by using the BC251 cyclone-based sampler (kindly provided by Dr. William Lindsley, National Institute for Occupational Safety and Health) and the SPOT water condensation sampler (Aerosol Devices, https://aerosoldevices.com), as described previously (*8*) (Figure, panel D). The highest mean titer of virus was detected at 2 dpi in NW collected from all 3 inoculated ferrets (6.5 $\log_{10}$ PFU/mL) (Figure, panel C). Airborne virus was highest at 3 dpi as measured in both samplers, up to 133 and 41 PFU/hour, supporting transmission observed in both contact models within 3–5 days after exposure.

Overall, MI90 virus displayed reduced virulence in ferrets compared with another H5N1 virus isolated from a dairy farm worker in Texas (*8*,*9*); the Texas virus possesses a genetic marker in the polymerase basic 2 protein (E627K), known for enhanced replication and pathogenesis in mammals. At this position, MI90 encodes 627E, like most other viruses isolated from cattle, and contains polymerase basic 2 M631L, which is associated with mammal adaptation (*3*,*9*). In addition, polymerase acidic 142N/E has been linked to increased virulence in mice (*10*); the Texas virus has an E and MI90 virus has a K at this position. Both viruses have identical hemagglutinin sequences associated with receptor binding and the multi-basic cleavage site. Despite differences in virulence, both viruses transmitted in the ferret model with similar proficiency and levels of airborne virus.

Because avian H5N1 viruses cross the species barrier and adapt to dairy cattle, each associated human infection presents further opportunity for mammal adaption. This potential poses an ongoing threat to public health and requires continual surveillance and risk assessment of emerging viruses to improve our ability to predict and prepare for the next influenza pandemic.

Acknowledgments

We thank the Centers for Disease Control and Prevention's Comparative Medicine Branch (Division of Scientific Resources, National Center for Emerging and Zoonotic Infectious Diseases) for providing excellent animal care and the Mid-Michigan District Health Department and the Michigan Department of Health and Human Services for access to the human samples for virus isolation. We thank William Lindsley for his extensive contributions in developing and generously providing access to BC251 cyclone samplers, which have led to risk assessments of airborne pathogens worldwide.

All animal procedures were approved by the Institutional Animal Care and Use Committee of the Centers for Disease Control and Prevention and were conducted in an AAALAC-accredited facility.

About the Author

Dr. Brock is a microbiologist in the Influenza Division, National Center for Immunization and Respiratory Diseases, at the Centers for Disease Control and Prevention. Her research interests include the pathogenicity, transmissibility, and host response associated with emerging strains of influenza virus.

References

1. Webby RJ, Uyeki TM. An update on highly pathogenic avian influenza A(H5N1) virus, clade 2.3.4.4b. J Infect Dis. 2024;230:533–42. https://doi.org/10.1093/infdis/jiae379
2. Garg S, Reed C, Davis CT, Uyeki TM, Behravesh CB, Kniss K, et al. Outbreak of highly pathogenic avian influenza a(h5n1) viruses in U.S. dairy cattle and detection of two human cases—United States, 2024. MMWR Morb Mortal Wkly Rep. 2024;73:501–5. https://doi.org/10.15585/mmwr.mm7321e1
3. Morse J, Coyle J, Mikesell L, Stoddard B, Eckel S, Weinberg M, et al. Influenza A(H5N1) virus infection in two dairy farm workers in Michigan. N Engl J Med. 2024;391:963–4. https://doi.org/10.1056/NEJMc2407264
4. Maines TR, Chen LM, Matsuoka Y, Chen H, Rowe T, Ortin J, et al. Lack of transmission of H5N1 avian-human reassortant influenza viruses in a ferret model. Proc Natl Acad Sci U S A. 2006;103:12121–6. https://doi.org/10.1073/pnas.0605134103
5. Maines TR, Lu XH, Erb SM, Edwards L, Guarner J, Greer PW, et al. Avian influenza (H5N1) viruses isolated from humans in Asia in 2004 exhibit increased virulence in mammals. J Virol. 2005;79:11788–800. https://doi.org/10.1128/JVI.79.18.11788-11800.2005
6. Belser JA, Gustin KM, Maines TR, Pantin-Jackwood MJ, Katz JM, Tumpey TM. Influenza virus respiratory infection and transmission following ocular inoculation in ferrets. PLoS Pathog. 2012;8:e1002569. https://doi.org/10.1371/journal.ppat.1002569
7. Pulit-Penaloza JA, Brock N, Belser JA, Sun X, Pappas C, Tumpey TM, et al. Kinetics and magnitude of viral RNA shedding as indicators for influenza A virus transmissibility in ferrets. Commun Biol. 2023;6:90. https://doi.org/10.1038/s42003-023-04459-0

8. Pulit-Penaloza JA, Belser JA, Brock N, Kieran TJ, Sun X, Pappas C, et al. Transmission of a human isolate of clade 2.3.4.4b A(H5N1) virus in ferrets. Nature. 2024;636:705–10. https://doi.org/10.1038/s41586-024-08246-7
9. Gu C, Maemura T, Guan L, Eisfeld AJ, Biswas A, Kiso M, et al. A human isolate of bovine H5N1 is transmissible and lethal in animal models. Nature. 2024;636:711–8. https://doi.org/10.1038/s41586-024-08254-7
10. Kim JH, Hatta M, Watanabe S, Neumann G, Watanabe T, Kawaoka Y. Role of host-specific amino acids in the pathogenicity of avian H5N1 influenza viruses in mice. J Gen Virol. 2010;91:1284–9. https://doi.org/10.1099/vir.0.018143-0

Address for correspondence: Taronna R. Maines, Centers for Disease Control and Prevention, 1600 Clifton Rd NE, Mailstop H17-5, Atlanta, GA 30329-4018, USA; email: tmaines@cdc.gov

Aedes aegypti Mosquito Detection at Bus Stations, Bogota, Colombia, 2023–2024

Andrea Villamizar Gomez, Sandra Patricia Pérez Español, Marco Alexander Figueroa Caicedo, Andrea Camila Márquez Nossa

Author affiliations: Subred Integrada de Servicios de Salud Sur Occidente E.S.E., Bogota, Colombia (A. Villamizar Gomez, M.A. Figueroa Caicedo); Secretaría Distrital de Salud de Bogota, Bogota (S.P. Pérez Español, A.C. Márquez Nossa)

DOI: https://doi.org/10.3201/eid3106.241052

We monitored mosquitoes in 3 bus stations in Bogota, Colombia, located at 2,625 m above sea level. During December 2023–January 2024, we collected 27 larvae and 1 adult female *Aedes aegypti* mosquitoes at 1 station. Detection of *Ae. aegypti* mosquitoes in Bogota is a call to continue monitoring mosquitoes at stations.

Aedes spp. mosquitoes can feed on many species, including humans (*1*,*2*). *Ae. aegypti* mosquitoes are a public health concern because they can transmit pathogens that cause some of the most common arboviral diseases, such as dengue fever, Zika, chikungunya, and yellow fever (*2*–*4*). Among the *Aedes* mosquito species, *Ae. aegypti* is the most widely studied because of its broad distribution range and widespread association with arboviral transmission, especially dengue virus (*2*,*4*). *Ae. aegypti* mosquitoes are found in tropical climates where temperatures range from 15°C to 30°C, and the altitude is generally ≤1,700 meters above sea level (masl). Some countries, such as Mexico, Peru, and Bolivia, have reported *Ae. aegypti* mosquitoes at >2,000 masl (*1*,*4*–*6*). However, some reports in Colombia note *Ae. aegypti* mosquitoes at altitudes as high as 2,100 masl (*7*,*8*). *Ae. aegypti* mosquitoes are found in most urban and peri-urban areas of Colombia, according to a survey published by the National Health Institute (*7*).

In Colombia, dengue fever is the most common arbovirus disease. In 2024, the country registered 27,649 cases: 15,926 (57.6%) persons showed mild symptoms, 11,419 (41.3%) showed moderate symptoms, and 304 (1.1%) had severe symptoms (*8*). A group of 10 states, Valle del Cauca, Cali, Tolima, Huila, Santander, Norte de Santander, Antioquia, Bolívar, Cundinamarca, and Meta, had 21,392 (77.4%) of those cases. Cundinamarca, the state in which Bogota is located, had 867 reports. Only 36 cases of Zika virus infection were recorded in Colombia in 2024, 12 (33.3%) of which occurred in Cundinamarca. Furthermore, 15 cases of chikungunya virus were documented; of those, 1 (6.6%) case was reported in Cundinamarca in the area around Bogota (*8*). Of note, Bogota is the only place in Cundinamarca with no reports of arboviruses, but notifications have been made in most neighboring municipalities at lower altitudes (200–1,700 masl). Bogota is at 2,600 masl and is considered outside the distribution range of the vectors.

Climate change has increased global temperatures, leading to new arboviral outbreaks. Recent studies have shown that *Ae. aegypti* mosquitoes now inhabit areas that were once outside their distribution range (*1*,*2*,*5*,*6*,*8*). The temperature in Bogota has consistently risen since the 1990s. In the mid-1960s, the average temperature per year was 12.6°C. In 2022, the average temperature reached 13.8°C; the highest temperature recorded was 25.1°C (*9*). That temperature increase suggests that Bogota may no longer be outside the distribution range of *Aedes* spp. mosquitoes. Herein, we report detection of *Ae. aegypti* mosquitoes in the city of Bogota, Colombia.

The possibility of an expansion in the distribution range of *Ae. aegypti* mosquitoes created the need for weekly monitoring and sample collection by the Secretaría Distrital de Salud (https://www.saludcapital.gov.co) of Bogota beginning in May 2023. The sampling efforts focused on the 3 bus stations of the city

that have heavy traffic to and from areas of *Ae. aegypti* mosquito endemicity.

We set up a total of 5 traps per bus station. We designed 3 traps to attract mosquitoes to lay eggs. We made the traps from dark plastic containers half filled with water; inside the containers, we put a flat wooden stick with rough surfaces designed to support the adhesion of eggs to the surface. We placed those traps in bathrooms and security guard booths. We also filled 2 larvae traps, made of discarded car tires containing water to allow egg development, and put them in green areas around each bus station. We also caught adults by using mosquito nets in the green areas and in surrounding buildings, such as bathrooms, offices, and security guard booths at each station.

We took all samples to the Secretaría Distrital de Salud for identification. During 1 year of surveillance, we identified 318 larval and 3,527 adult (1,862 females and 1,665 males) *Culex quinquefasciatus* mosquitoes, which is a species commonly reported in Bogota (*10*). In addition, in 1 bus station, during December 2023–January 2024, we caught 27 *Ae. aegypti* mosquito larvae in a larval trap and 1 adult female *Ae. aegypti* mosquito near the same trap; that species has never been reported in Bogota (*2*).

The bus stations are in urban areas that experience heavy travel of persons from other cities and towns in Colombia. Some of those urban areas are endemic for *Aedes* spp. mosquitoes (*7*). Mosquitoes might have arrived by bus and were likely caught in set traps or nets in an isolated event. However, those isolated events might lead to *Ae. aegypti* mosquito populations becoming established in Bogota. Therefore, we advise reinforcing hospital surveillance and notification systems to help identify local outbreaks of arbovirus infections. Detection of *Ae. aegypti* mosquitoes in Bogota is a call to set up a permanent monitoring program for mosquito species at bus stations in the city.

Acknowledgments

We thank the Subsecretaría de Salud Pública for supporting the implementation of entomologic surveillance activities in the city of Bogota.

The Subred Integrada de Servicios de Salud Sur Occidente provided logistic support that allowed the activities to be conducted at the bus stations. Terminal S.A. and co-ownership of Terminal Salitre facilitated the sampling at the city's bus stations. The entomology group of the Instituto Nacional de Salud confirmed the identification of the captured specimens as *Aedes aegypti*.

About the Author

Dr. Villamizar Gomez is a veterinarian at the Subred Integrada de Servicios de Salud Sur Occidente E.S.E. Her research interests include detection and surveillance of zoonotic diseases in the animal population.

References

1. Laporta GZ, Potter AM, Oliveira JFA, Bourke BP, Pecor DB, Linton YM. Global distribution of *Aedes aegypti* and *Aedes albopictus* in a climate change scenario of regional rivalry. Insects. 2023;14:2–18. https://doi.org/10.3390/insects14010049
2. Conway MJ, Colpitts TM, Fikrig E. Role of the vector in arbovirus transmission. Annu Rev Virol. 2014;1:71–88. https://doi.org/10.1146/annurev-virology-031413-085513
3. Bugher JC, Boshell-Manrique J, Roca-Garcia M, Osorno-Mesa E. Epidemiology of jungle yellow fever in eastern Colombia. Am J Hyg. 1944;39:16–51. https://doi.org/10.1093/oxfordjournals.aje.a118895
4. Freire de Melo Ximenes MF, De Araújo Galvão JM, Cássio Lázaro SI, Macêdo e Silva VP, Pereira RLdN, Gomes Pinheiro MP, et al. Arbovirus expansion: new species of culicids infected by the chikungunya virus in an urban park of Brazil. Acta Trop. 2020;209:105538. https://doi.org/10.1016/j.actatropica.2020.105538
5. Lippi CA, Mundis SJ, Sippy R, Flenniken JM, Chaudhary A, Hecht G, et al. Trends in mosquito species distribution modeling: insights for vector surveillance and disease control. Parasit Vectors. 2023;16:302. https://doi.org/10.1186/s13071-023-05912-z
6. Piovezan R, Acorinthe JPO, Souza JHTD, Visockas A, Azevedo TSD, Zuben CJV. Spatial distribution of Culicidae (Diptera) larvae, and its implications for public health, in five areas of the Atlantic Forest biome, State of São Paulo, Brazil. Rev Bras Entomol. 2017;61:123–35. https://doi.org/10.1016/j.rbe.2016.12.007
7. Instituto Nacional de Salud. Weekly epidemiological bulletin: epidemiological week 33 August 13–19, 2023 [in Spanish] [cited 2025 Feb 20]. https://www.ins.gov.co/buscador-eventos/BoletinEpidemiologico/2023_Bolet%C3%ADn_epidemiologico_semana_33.pdf
8. Instituto Nacional de Salud. Weekly epidemiological bulletin: epidemiological week 05 January 28–February 03, 2024 [in Spanish] [cited 2025 Feb 20]. https://www.ins.gov.co/buscador-eventos/BoletinEpidemiologico/2024_Bolet%C3%ADn_epidemiologico_semana_5.pdf
9. Ruiz Murcia JF, Escobar García OF. Changes in precipitation and temperature due to climate variability and change in the city of Bogotá [in Spanish] [cited 2024 Aug 16]. http://www.cpc.ncep.noaa.gov/data/indices/
10. Rivera Pineda MG, Garzón Lozano SP, Villarreal Salazar LI. The *Culex quinquefasciatus* mosquito, an urban pest [in Spanish]. Rev Clepsidra. 2008;4:74–8. https://doi.org/10.26564/19001355.287

Address for correspondence: Andrea Villamizar Gomez, Subred Integrada de Servicios de Salud Sur Occidente E.S.E., Carrera no. 32 12-81, Puente Aranda, Bogota 111600, Colombia; email: lidercaracterizacionzoonosis@subredsuroccidente.gov.co

Rapid Subcutaneous Migration of *Dirofilaria repens* Nematode in Facial Tissue, Italy

Mariaelisa Carbonara, Simona Gabrielli, Alessia Ricci, Roberta Iatta, Riccardo Paolo Lia, Maria Virginia Tomassi, Andrea Mariano, Jairo Alfonso Mendoza-Roldan, Domenico Otranto

Author affiliations: University of Bari Aldo Moro, Bari, Italy (M. Carbonara, A. Ricci, R. Iatta, R.P. Lia, J.A. Mendoza-Roldan, D. Otranto); University of Rome Sapienza, Rome, Italy (S. Gabrielli); National Institute for Infectious Diseases Lazzaro Spallanzani, Rome (M.V. Tomassi, A. Mariano); City University of Hong Kong, Kowloon, Hong Kong, China (D. Otranto)

DOI: https://doi.org/10.3201/eid3106.241915

We report a *Dirofilaria repens* nematode infection in a woman in Italy who sought care for a fast-creeping lesion within her subcutaneous facial tissue. Dirofilariosis should be included in differential diagnosis of subcutaneous nodules or creeping lesions. This case highlights the need for controlling canine dirofilarioses to mitigate zoonotic risk.

Dirofilarioses are mosquitoborne zoonotic diseases caused by filarial nematodes, which affect domestic and wild carnivores in tropical, subtropical, and temperate areas worldwide (*1*). Humans act as dead-end hosts because the third stage larvae, which are transmitted by mosquitoes during the blood meal, do not usually reach sexual maturity. Human cases of dirofilariosis have been documented worldwide; *Dirofilaria immitis* and *D. repens* nematodes have been reported from both the New and Old World (*2*). In humans, subcutaneous lesions caused by *D. repens* nematode infection can occur in several anatomic areas (e.g., forehead, arms, and periorbital and perioral areas) and, rarely, in deeper tissues (e.g., lymph nodes, lungs, muscles, and dura) (*3*). In addition, pulmonary localization of *Dirofilaria* spp. is characterized by the presence of solitary, well-circumscribed, noncalcified peripheral subpleural pulmonary nodules (coin lesions), which mimic lung cancer (*4*). In the Mediterranean Basin, ideal climatic conditions for the development of mosquito vectors, as well as the high prevalence of microfilaremic dogs, are risk factors for human infections, as observed in areas highly endemic for canine dirofilariosis, such as southern Italy (*5*,*6*). Specifically, in Europe, *D. repens* is considered an emerging pathogen, because it presents an expanding distribution linked to an increasing number of human cases (*4*). We report a case of human dirofilariosis in a woman in her forties, living in Rome, Italy, with 3 cats as pets.

The patient first underwent ophthalmologic consultation because of visual impairment; her condition was initially misdiagnosed as an allergic reaction of the right upper eyelid. Five days later, the patient was referred to the National Institute for Infectious Diseases Lazzaro Spallanzani after she reported a worm-like organism creeping within the subcutaneous tissue of the right lower periorbital region (Video, https://wwwnc.cdc.gov/EID/article/31/6/24-1915-V; Appendix Figure, https://wwwnc.cdc.gov/EID/article/31/6/24-1915-App1.pdf). No other clinical signs (e.g., dermo-epidermal eruptive patches) were recorded besides retroauricular lymphadenomegaly and low-grade fever (up to 38.0°C). The patient had not recently traveled abroad.

After signing informed consent, the patient was hospitalized but surgery was not performed because the suspected parasite (likely *Dirofilaria* spp.) had migrated to the right parietal area of the head (i.e., the subcutaneous tissue at the parietal bone of the skull), preventing its removal. During her 5-day hospitalization, the patient was in good clinical condition; hematological and serologic biochemical parameters were within reference ranges; eosinophilia was not present. Infections by *Strongyloides stercoralis* and zoonotic filarial worms (i.e., *Brugia* spp., *Wuchereria bancrofti*, *Mansonella* spp., and *Oncocherca* spp.) were excluded by serologic assays (i.e., commercial ELISA kits). Chest radiography was performed to exclude the presence of coin lesions typical of *Dirofilaria* spp. infection.

We tested a serum sample at the Department of Public Health and Infectious Diseases Sapienza, University of Rome, to assess exposure to *Dirofilaria*

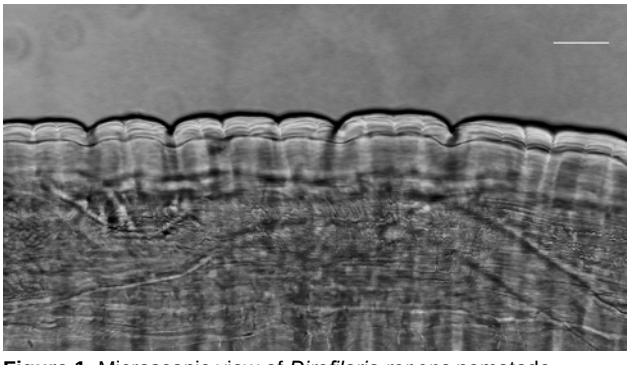

Figure 1. Microscopic view of *Dirofilaria repens* nematode extracted from subcutaneous facial tissue of a patient, Italy. Microscopic analysis revealed a thick laminated cuticle with characteristic longitudinal ridges and cross-striations, leading to the identification of the parasite. Scale bar indicates 100 μm.

Figure 2. Phylogeny of *Dirofilaria repens* based on *cox*1 gene sequences in study of rapid subcutaneous migration of *D. repens* nematode in facial tissue, Italy. The sequence from this study is shown in bold. *Wuchereria bancrofti* was used as outgroup. Bootstrap confidence values (1,000 replicates) are shown at the nodes only for values >60%.

spp. by using an in-house ELISA based on somatic antigens of adult *D. repens* (*6*,*7*), which yielded positive results (i.e., optical density 1.56; optical density cut off 1.03 for *D. repens*). The woman was discharged from the hospital with the recommendation to return on observation of parasite reemergence to the facial subcutaneous tissue.

Two weeks later, the nematode migrated in the frontal area, and a surgical excision was performed under local anesthesia. The specimen was shipped to the University of Bari (Italy) for further morphological and molecular analysis. The fragmented nematode was morphologically identified as a mature female, cylindrical, ≈2.96 cm in length, and 0.480 mm thick (Figure 1). Microscopic analysis revealed a thick laminated cuticle with characteristic longitudinal ridges and cross-striations (Figure 1), leading to the identification of the parasite as *D. repens* (*8*).

Genomic DNA was extracted from the nematode and tested by conventional PCR targeting *cox*1 gene (*9*) to obtain a reference sequence. BLAST (https://blast.ncbi.nlm.nih.gov) analysis revealed 100% nucleotide identity with reference sequence of *D. repens* in the GenBank database (accession no. MW675692), which further confirmed by phylogenetic analyses (Figure 2). At the 5-month follow-up, the patient's only residual symptom was a persisting uncomfortable feeling, likely associated with parasite migration. We also performed specific tests to detect *Dirofilaria* spp. on her pets, yielding negative results.

The increasing incidence of human cases of dirofilariosis in Europe (*10*) underscores the need for including this emerging zoonotic disease in the differential diagnosis of pulmonary or subcutaneous nodules in absence of eosinophilia. The rapid migration of the nematode in this case was unusual, highlighting the variability of clinical signs in patients infected by *D. repens* nematodes, which range from stationary nodules to fast-migrating lesions in subcutaneous tissues. Human dirofilariosis is typically an abortive infection because humans are accidental hosts, and microfilaremia is absent (*1*). Consequently, traditional diagnostic methods applied in veterinary medicine (e.g., Knott's test) are unsuitable. Definitive diagnosis in human patients is challenging, and often only achievable after surgical removal of the parasite.

In summary, we identified *D. repens* nematode infection in a woman with a creeping lesion in her subcutaneous facial tissue. This case highlights the need for a One Health approach in implementing vector control strategies and regular monitoring of reservoir hosts in endemic areas to mitigate the risk for human *D. repens* infection.

Acknowledgments

We are grateful to the patient involved in the study and to Livia Perles for assistance with the phylogenetic analysis.

No funding has been employed for the present work. D.O., J.A.M.R., and R.I. were partially supported by European Union funding within the NextGeneration EU-MUR PNRR Extended Partnership initiative on Emerging Infectious Diseases (project no. PE00000007, INF-ACT).

About the Author

Dr. Carbonara is a research fellow at the Department of Veterinary Medicine, University of Bari. Her main research interest is in vectorborne pathogens of zoonotic concern in both animals and humans.

References

1. Perles L, Dantas-Torres F, Krücken J, Morchón R, Walochnik J, Otranto D. Zoonotic dirofilariases: one, no one, or more than one parasite. Trends Parasitol. 2024;40:257–70. https://doi.org/10.1016/j.pt.2023.12.007
2. Dantas-Torres F, Otranto D. Dirofilariosis in the Americas: a more virulent *Dirofilaria immitis?* Parasit Vectors. 2013;6:288. https://doi.org/10.1186/1756-3305-6-288

3. Grapatsas K, Kayser G, Passlick B, Wiesemann S. Pulmonary coin lesion mimicking lung cancer reveals an unexpected finding: *Dirofilaria immitis*. J Thorac Dis. 2018;10:3879–82. https://doi.org/10.21037/jtd.2018.05.137
4. Capelli G, Genchi C, Baneth G, Bourdeau P, Brianti E, Cardoso L, et al. Recent advances on *Dirofilaria repens* in dogs and humans in Europe. Parasit Vectors. 2018;11:663. https://doi.org/10.1186/s13071-018-3205-x
5. Otranto D, Brianti E, Gaglio G, Dantas-Torres F, Azzaro S, Giannetto S. Human ocular infection with *Dirofilaria repens* (Railliet and Henry, 1911) in an area endemic for canine dirofilariasis. Am J Trop Med Hyg. 2011;84:1002–4. https://doi.org/10.4269/ajtmh.2011.10-0719
6. Mendoza-Roldan JA, Gabrielli S, Cascio A, Manoj RRS, Bezerra-Santos MA, Benelli G, et al. Zoonotic *Dirofilaria immitis* and *Dirofilaria repens* infection in humans and an integrative approach to the diagnosis. Acta Trop. 2021;223:106083. https://doi.org/10.1016/j.actatropica.2021.106083
7. Potters I, Vanfraechem G, Bottieau E. *Dirofilaria repens* nematode infection with microfilaremia in traveler returning to Belgium from Senegal. Emerg Infect Dis. 2018;24:1761–3. https://doi.org/10.3201/eid2409.180462
8. Otranto D, Eberhard ML. Zoonotic helminths affecting the human eye. Parasit Vectors. 2011;4:41. https://doi.org/10.1186/1756-3305-4-41
9. Casiraghi M, Anderson TJC, Bandi C, Bazzocchi C, Genchi C. A phylogenetic analysis of filarial nematodes: comparison with the phylogeny of *Wolbachia* endosymbionts. Parasitology. 2001;122:93–103. https://doi.org/10.1017/S0031182000007149
10. Simón F, Diosdado A, Siles-Lucas M, Kartashev V, González-Miguel J. Human dirofilariosis in the 21st century: a scoping review of clinical cases reported in the literature. Transbound Emerg Dis. 2022;69:2424–39. https://doi.org/10.1111/tbed.14210

Address for correspondence: Domenico Otranto, University of Bari Aldo Moro, Str. prov. per Casamassima km 3, 70010 Valenzano (Bari), Italy; email: domenico.otranto@uniba.it

Ehrlichia chaffeensis DNA in *Haemaphysalis longicornis* Ticks, Connecticut, USA

Goudarz Molaei, Amrita Ray Mohapatra, Noelle Khalil, Duncan Cozens, Denise Bonilla

Author affiliations: The Connecticut Agricultural Experiment Station, New Haven, Connecticut, USA (G. Molaei, A.R. Mohapatra, N. Khalil, D. Cozens); US Department of Agriculture Animal and Plant Health Inspection Service, Fort Collins, Colorado, USA (D. Bonilla)

DOI: http://doi.org/10.3201/eid3106.250034

Informed by passive tick surveillance, we collected questing *Haemaphysalis longicornis* ticks from southwestern Connecticut, USA. Of 445 ticks tested by PCR, 3 nymphs were positive: 1 for *Ehrlichia chaffeensis* and 2 for *Borrelia burgdorferi*. This finding highlights the enduring public health challenges of invasive ticks and associated pathogens.

Ehrlichia chaffeensis is the most common causative agent of human monocytic ehrlichiosis (HME) and is transmitted primarily by the lone star tick (*Amblyomma americanum*) (*1*). Frequently reported from the southeast and south central United States, HME cases increased nearly 15-fold during 2001–2019 (from 142 to 2,093 cases), and then decreased substantially in 2020 (n = 1,178 cases), likely due to the COVID-19 pandemic. In subsequent years, disease cases remained lower than prepandemic levels. In Connecticut, reported HME cases totaled just 2 during 2008–2018; however, since 2019, reports from Connecticut indicated an annual recurrence of the disease, and cases increased to a total of 28 during 2019–2023. As with other tickborne diseases, convincing evidence indicates the number of HME cases is underreported and because of the recent range expansion of *A. americanum*, particularly in northeast sections of the United States, investigators anticipate an increase in disease cases (*2*).

Native to eastern Asia and invasive to Australia, New Zealand, and several Pacific Islands, the first report of *Haemaphysalis longicornis* in the United States came from New Jersey in 2017 (*3*), and the species subsequently spread into at least 21 mostly eastern and northeastern states (Figure, panel A) (*4*). Because of its wide host range and ability to survive in an expansive breadth of climatic conditions, *H. longicornis* will likely spread to and establish populations across a large portion of the United States (*5*). This tick is a

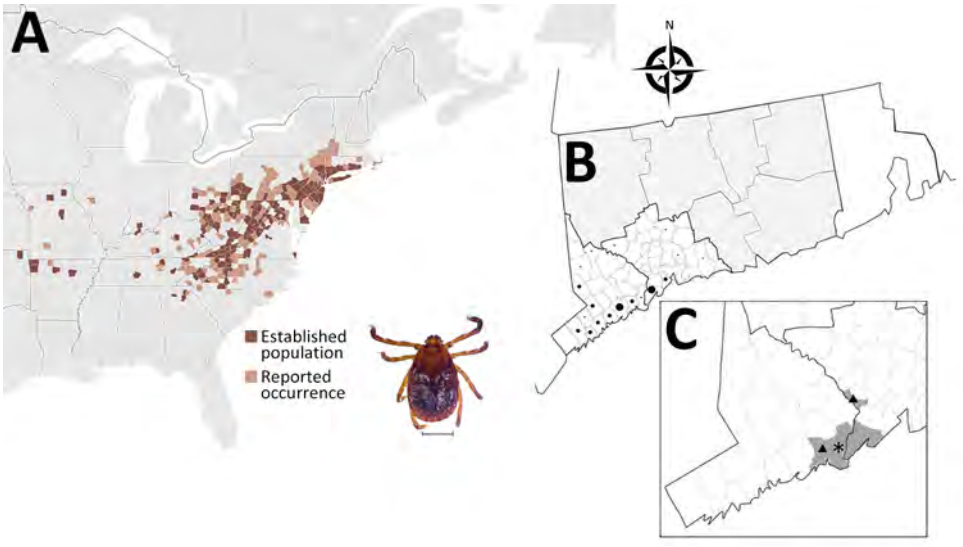

Figure. Maps showing range and locations of ticks in a study of *Ehrlichia chaffeensis* DNA in *Haemaphysalis longicornis* ticks, Connecticut, USA. A) Map of eastern United States showing states with established populations or reported occurrence of *H. longicornis*. B) For comparison, map of Connecticut showing locations (dots) where residents reported removing *H. longicornis* ticks that they submitted to the Connecticut Agricultural Experiment Station Tick Testing Laboratory. This area overlaps with area in which *E. chaffeensis*–positive *H. longicornis* ticks were collected for this study (C); dot size indicates number of ticks collected per area, either 1, 2–5, or >5 ticks. C) Map of southwestern part of the state showing areas of known established *H. longicornis* tick populations (shaded in gray), location of tick specimen found to be positive for *E. chaffeensis* (asterisk), and location of specimens found to be positive for *Borrelia burgdorferi* (triangles). Inset shows adult female *H. longicornis* tick; scale bar indicates 1 mm.

known vector of a wide array of pathogens in its native and invasive ranges, and researchers have detected genetic materials from *Anaplasma phagocytophilum*, *Babesia microti*, *Borrelia burgdorferi*, Bourbon virus, and *Theileria orientalis* Ikeda in environmentally collected specimens in the United States; however, its vector potential for many of these pathogens remains unclear (*6*–*9*). We screened ticks collected in Connecticut to assess potential human pathogens.

Of 8,700 *H. longicornis* larvae (n = 8,120), nymphs (n = 412), and adult female ticks (n = 168) we collected from 4 towns in southwestern Connecticut during 2021–2024, we tested 88 females and 357 nymphs for evidence of infection. Of those ticks, 2 (0.6%) nymphs tested positive for *B. burgdorferi*, 1 collected in April 2021 from Bridgeport (41.159°N, 73.202°W) and 1 collected in August 2023 from Derby (41.336°N, 73.1006°W) (Appendix, https://wwwnc.cdc.gov/EID/article/31/6/25-0034-App1.pdf). In screening a subset of *H. longicornis* nymphs (n = 126), 1 (0.8%) nymph collected in May 2021 from Stratford (41.1526°N, 73.1471°W) tested positive for *E. chaffeensis* (Appendix Table). The 16S rRNA gene fragment for *E. chaffeensis* (GenBank accession no. PQ569094) from this assay showed 99.9% identity to several sequences of the same gene in the GenBank database. The cytochrome *c* oxidase subunit 1 gene fragment of the *H. longicornis* specimen (GenBank accession no. PQ561597) showed 99.7% identity to similar gene sequences in GenBank, confirming the species identity.

The overall 0.8% *E. chaffeensis* infection rate in *H. longicornis* is similar to that in the principal vector of this pathogen, *A. americanum*, in Connecticut (1%) and substantially lower than that in the United States (5%–15%). The detection of *B. burgdorferi* in 2 *H. longicornis* nymphs with an infection rate of 0.6% is slightly higher than that reported in a study of field collections of this tick in Pennsylvania (0.4%) (*8*).

The Stratford site where the *E. chaffeensis*–positive specimen was collected is frequented by white-tailed deer, and repeated surveys have revealed that the area is heavily infested with *H. longicornis* and *A. americanum*. Both tick species are 3-host ticks (*2*,*9*), and all life stages readily feed on white-tailed deer. White-tailed deer are known reservoir hosts for *E. chaffeensis* (*1*), and have an infection rate ranging 7%–54% (*10*). Records of human *H. longicornis* bites exist in the United States (*9*), but how frequently this species will infest humans remains unclear. Evidence has also been reported on partial blood feeding in host-seeking *H. longicornis*, which could lead to pathogen transmission as the tick attempts to complete a blood meal after partially feeding on an infected host in the same life stage (*8*). *H. longicornis* could thus conceivably acquire *E. chaffeensis* directly from an infected white-tailed deer or during cofeeding with an infected *A. americanum* and transmit to humans during an initial blood meal or a secondary partial blood meal.

Aided by frequent intercontinental movement of humans and importation of animals and agricultural products, the United States has recently witnessed

an increase in the introduction of invasive ticks capable of transmitting a diverse group of pathogens of public health concern. Those nonnative tick species have the potential to establish populations and expand their range under conducive climatic conditions. Thus, mitigating public and animal health risks depends on increasing public awareness of the risks associated with invasive ticks and pathogens, expanding passive and active surveillance programs, and continued diligent inspection of animals and plants. Improving the capacity to accurately identify tick species and test for native and nonnative pathogens should be an integral part of any comprehensive program designed to expand our understanding of the distribution and prevalence of tickborne infections.

Acknowledgments

We are grateful to Stacy Gardner of Animal and Plant Health Inspection Service for the distribution map of *H. longicornis* in the United States. We also thank Katherine Dugas of the Connecticut Agricultural Experiment Station for the distribution map of Connecticut.

Funding for this study was provided, in part, by the US Congressionally Directed Spending administered by the United States Department of Agriculture/Animal and Plant Health Inspection Service/Veterinary Services (agreement no. AP23VSSP0000G001) to the Connecticut Agricultural Experiment Station-Tick Testing Laboratory.

About the Author

Dr. Molaei is a research scientist and Director of the Tick and Tick-borne Pathogen Surveillance Program at the Center for Vector Biology & Zoonotic Diseases and the Northeast Regional Center for Excellence in Vector-Borne Diseases of the Connecticut Agricultural Experiment Station and an associate professor adjunct at the Yale School of Public Health. His current research interests include the ecology and epidemiology of tickborne and mosquitoborne pathogens of human health concern.

References

1. Paddock CD, Childs JE. *Ehrlichia chaffeensis*: a prototypical emerging pathogen. Clin Microbiol Rev. 2003;16:37–64. https://doi.org/10.1128/CMR.16.1.37-64.2003
2. Molaei G, Little EAH, Williams SC, Stafford KC. Bracing for the worst—range expansion of the lone star tick in the Northeastern United States. N Engl J Med. 2019;381:2189–92. https://doi.org/10.1056/NEJMp1911661
3. Rainey T, Occi JL, Robbins RG, Egizi A. Discovery of *Haemaphysalis longicornis* (Ixodida: Ixodidae) parasitizing a sheep in New Jersey, United States. J Med Entomol. 2018;55:757–9. https://doi.org/10.1093/jme/tjy006
4. Myers SA, Scimeca RC. First report of *Haemaphysalis longicornis* (Neumann) in Oklahoma, USA. Pathogens. 2024;13:861. https://doi.org/10.3390/pathogens13100861
5. Rochlin I, Egizi A, Narvaez Z, Bonilla DL, Gallagher M, Williams GM, et al. Microhabitat modeling of the invasive Asian longhorned tick (*Haemaphysalis longicornis*) in New Jersey, USA. Ticks Tick Borne Dis. 2023;14:102126. https://doi.org/10.1016/j.ttbdis.2023.102126
6. Beard CB, Occi J, Bonilla DL, Egizi AM, Fonseca DM, Mertins JW, et al. Multistate infestation with the exotic disease–vector tick *Haemaphysalis longicornis*—United States, August 2017–September 2018. MMWR Morb Mortal Wkly Rep. 2018;67:1310–3. https://doi.org/10.15585/mmwr.mm6747a3
7. Oakes VJ, Yabsley MJ, Schwartz D, LeRoith T, Bissett C, Broaddus C, et al. *Theileria orientalis* Ikeda genotype in cattle, Virginia, USA. Emerg Infect Dis. 2019;25:1653–9. https://doi.org/10.3201/eid2509.190088
8. Price KJ, Khalil N, Witmier BJ, Coder BL, Boyer CN, Foster E, et al. Evidence of protozoan and bacterial infection and co-infection and partial blood feeding in the invasive tick *Haemaphysalis longicornis* in Pennsylvania. J Parasitol. 2023;109:265–73. https://doi.org/10.1645/22-122
9. Molaei G, Little EAH, Williams SC, Stafford KC III. First record of established populations of the invasive pathogen vector and ectoparasite *Haemaphysalis longicornis* (Acari: Ixodidae) in Connecticut, United States. J Med Entomol. 2021;58:2508–13. https://doi.org/10.1093/jme/tjab117
10. Paddock CD, Yabsley MJ. Ecological havoc, the rise of white-tailed deer, and the emergence of *Amblyomma americanum*-associated zoonoses in the United States. Curr Top Microbiol Immunol. 2007;315:289–324. https://doi.org/10.1007/978-3-540-70962-6_12

Address for correspondence: Goudarz Molaei, The Connecticut Agricultural Experiment Station, 123 Huntington St, New Haven, CT 06511, USA; email: goudarz.molaei@ct.gov

Molecular Detection of Wesselsbron Virus in Dromedary Camels, Borana Zone, Ethiopia, 2024

Hassan Ishag, El Tigani El Tigani-Asil, Wubishet Zawde, Abdelmalik I. Khalafalla, Mohammed Albreiki, Noura Al Zarooni, Abde Mohammed, Hagos Asgedom, Getnet Abei, Tesfaye Riufael, Golo Dabasa, Derara Birasa, Jarso Debano, Ghada Abdelwahab, Shameem Habeeba, Mokonin Belexe, Gerade Abduljami, Kassaw Amssalu, Mohd Farouk Yusof, Fikru Ragassa, Asma Mohamed

Author affiliations: Abu Dhabi Agriculture and Food Safety Authority, Abu Dhabi, United Arab Emirates (H. Ishag, E.T. El Tigani-Asil, A.I. Khalafalla, M. Albreiki, N. Al Zarooni, G. Abdelwahab, S. Habeeba, M.F. Yusof, A. Mohamed); Ministry of Agriculture, Addis Ababa, Ethiopia (W. Zawde, D. Birasa, K. Amssalu, F. Ragassa); Animal Health Institute, Sebeta, Ethiopia (A. Mohammed, H. Asgedom, G. Abei, T. Riufael); Yabello Regional Veterinary, Yabello, Ethiopia (G. Dabasa, J. Debano, M. Belexe, G. Abduljami)

DOI: https://doi.org/10.3201/eid3106.250130

We used PCR, Sanger sequencing, and phylogenetic analysis to identify Wesselsbron virus (WSLV) clade 1 in sick camels from Borana Zone, Ethiopia. Although WSLV primarily infects sheep and cattle, its pathogenicity in camels remains unclear. Camel farmers in the region should be aware of WSLV and its health effects in camels.

Camel husbandry is crucial for the pastoral communities in East Africa; however, rising death rates among camels remain poorly understood. During 1995–2004, various pathogens, including *Mannheimia hemolytica* (*1*), morbillivirus (*2*), and *Streptococcus equi* (*3*), were associated with epidemics in camels. Since 2005, unexplained camel deaths were reported in Ethiopia, and later in Somalia and Kenya, and death rates reached 6.6% (*4*). A new disease outbreak in 2020–2021 further threatened camels in Kenya, Ethiopia, and Somalia (*5*).

On May 7, 2024, outbreaks of an unidentified camel disease were first reported in the Dubluk district of the Borana Zone of Ethiopia. The outbreak continued until July and affected 8 districts: Gomole, Arero, Dubluk, Miyo, Yabello, Dilo, Wacile, and Dhas (Appendix Figure 1, https://wwwnc.cdc.gov/EID/article/31/6/25-0130-App1.pdf). A total of 147 camels died, a case fatality rate of 70% (147/209).

In July 2024, a joint investigation team from the World Organisation for Animal Health Collaborating Centre for Camel Diseases at the Abu Dhabi Agriculture and Food Safety Authority in the United Arab Emirates and the Animal Health Institute (AHI) in Ethiopia investigated camel deaths in the Arero and Gomole districts (Appendix Figure 1). The AHI Animal Research Scientific and Ethics Review Committee granted ethics approval (approval no. ARSERC APP/002/2025). During the investigation, we examined 24 camels (16 sick and 8 recovered) <3 years of age. We observed clinical signs such as lethargy, dullness, shivering, and bilateral lacrimation that resulted in vision impairment. Other signs involved labored breathing, yawning, and nervous signs such as tremors that often progressed to recumbency (Figure 1, panel A). Some camels experienced oliguria, constipation, and death within an average of 2–3 days.

We collected 34 nasal, oral, or ocular swab samples and 16 blood samples from sick and recovered camels. We performed necropsies on 2 euthanized camels and 1 recently dead calf. We took tissue and fluid samples (n = 35) from various organs, including

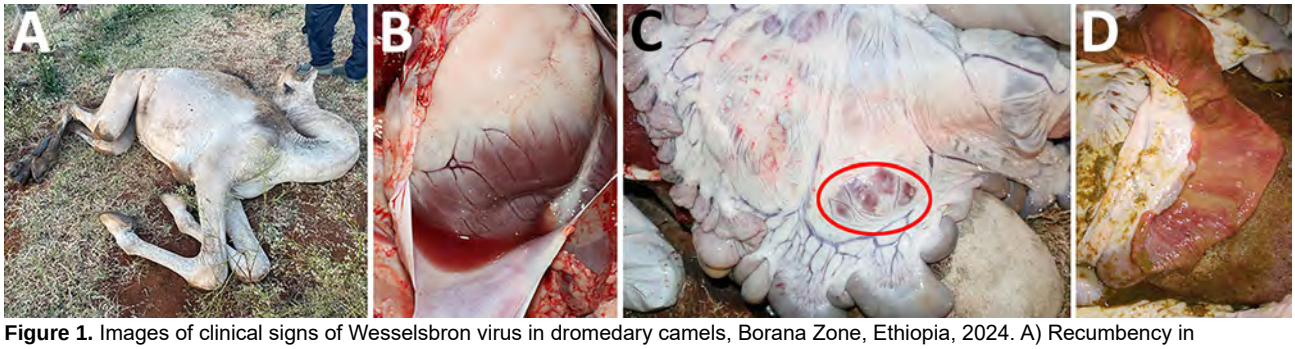

Figure 1. Images of clinical signs of Wesselsbron virus in dromedary camels, Borana Zone, Ethiopia, 2024. A) Recumbency in a calf that died. B–D) Necropsy images of from 2 other camels that died: B) pericardium demonstrating fluid around to the heart (hydropericardium); C) enlarged and congested myenteric lymph nodes (circled in red) in the abdomen; and D) intestine showing edema and congested mucosa.

the lung, spleen, liver, heart, kidney, cerebrum, cerebellum, mesenteric lymph node, intestine, mediastinal lymph node, prescapular lymph node, and pericardial fluids. We stored all samples at −20°C and fixed some tissue samples in 10% formalin at Yabello Sub-National Veterinary Laboratory, Yabello, Ethiopia. We sent the samples through the AHI laboratory to the Abu Dhabi Agriculture and Food Safety Authority laboratory. The main postmortem findings included hydropericardium (Figure 1, panel B), myenteric lymph node enlargement with congestion (Figure 1, panel C), and intestinal edema with congested mucosa (Figure 1, panel D).

A bacteriologic analysis of 19 swab samples and tissue specimens identified *Escherichia coli*, *Enterococcus* spp., *Staphylococcus* spp., *Rothia* spp., *Bacillus cereus*, *Moellerella wisconsensis*, *Corynebacterium* spp., and *Curtobacterium citreum*, which were likely environmental contaminants. Parasitologic examination of 13 fecal samples detected *Eimeria cameli* oocysts, Trichostrongylidae ova, and *Trichuris* ova.

We used genus-wide panvirus PCR assays to screen for several viruses, including bluetongue virus, bovine viral diarrhea virus, coronaviruses, peste des petits ruminants virus, paramyxovirinae, parapoxviruses, and orthoflavivirus. We also conducted targeted assays for Rift Valley fever, foot and mouth disease, enzootic bovine leukosis, Crimean Congo hemorrhagic fever, and camelpox viruses (Appendix Table).

All assays returned negative results, except for the panflavivirus reverse transcription PCR targeting the *NS5* gene (*6*), which detected orthoflavivirus in 18 (51.4%) of 35 necropsy samples and 3 (8.8%) of 34 swab samples (Appendix Figure 2); we found no positive results in blood samples. A Wesselsbron virus (WSLV)–specific real-time PCR (*7*) considerably improved detection, identifying WSLV in 25 (71.4%) of 35 tissue samples, and 3 (18.8%) of 16 blood samples, whereas swab samples had the same results as the panflavivirus assay. Detection of the virus in all 3 necropsied camels and multiple tissue samples suggests viremia and systemic infection.

We selected 15 (83.3%) of 18 panflavivirus-positive tissue samples for Sanger sequencing on the basis of the quality of the PCR bands. The National Center for Biotechnology Information BLAST (https://blast.ncbi.

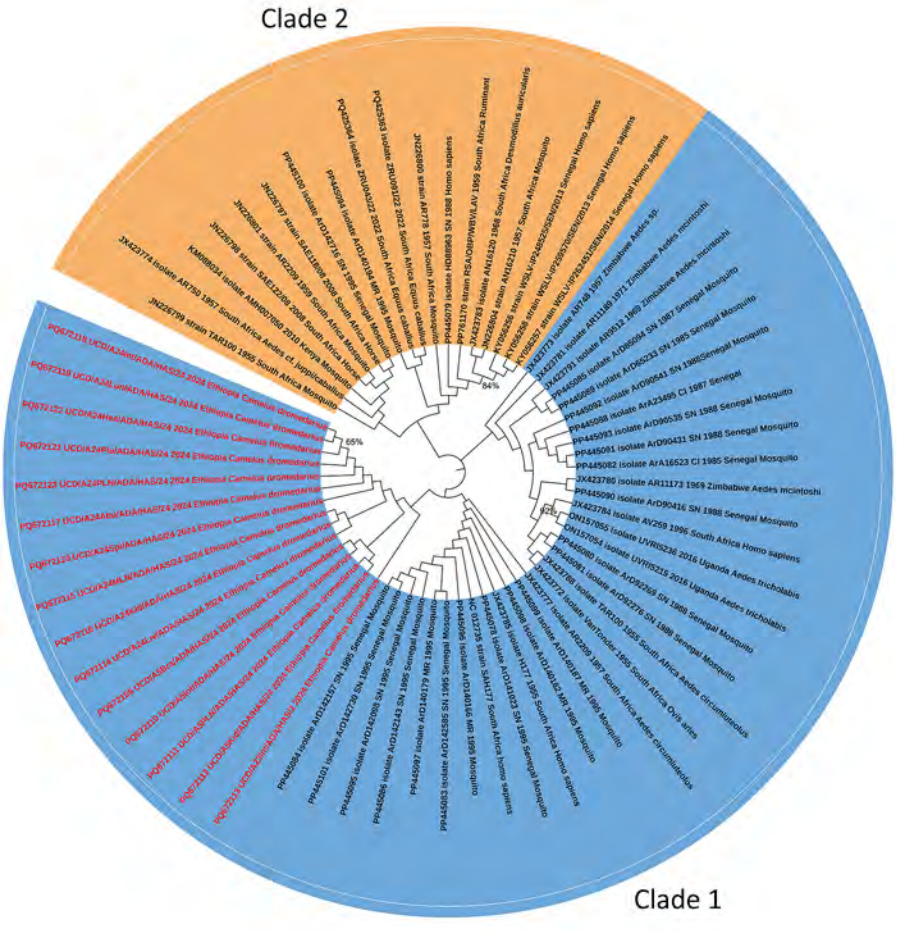

Figure 2. Phylogenetic analysis of Wesselsbron virus (WSLV) in dromedary camels, Borana Zone, Ethiopia, 2024. The maximum-likelihood phylogenetic tree was constructed with 1,000 bootstrap replicates based on 65 partial *NS5* gene sequences of WSLV, including the camel-derived WSLV sequences (maximum length 252 bp). The newly identified camel WSLV strains from this study are in red within clade 1.

nlm.nih.gov) analysis showed that the sequences had 97%–98% identity with existing WSLV sequences. We deposited the sequences in GenBank (accession nos. PQ672109–PQ672123). The sequences aligned with National Center for Biotechnology Information data and previously published WSLV sequences. A phylogenetic analysis using the maximum-likelihood method indicated sequences were in WSLV clade 1 (Figure 2).

This study comprehensively analyzed WSLV in various tissue, swab, and blood samples from affected camels. The identified virus strain belongs to clade 1, which is recognized for its pathogenicity and neurotropism (*8*). WSLV is associated with Wesselsbron disease, which can cause reproductive, neurologic, and systemic effects in various hosts, including humans, livestock, and rodents (*9*,*10*).

In conclusion, we identified WSLV in sick camels, and provided a WSLV partial gene sequence derived from camels. Whole-genome sequencing, virus isolation, and experimental infection testing in healthy camels are needed to understand the pathogenicity and to address existing knowledge gaps of this virus. Nonetheless, this detection expanded the known geographic range of WSLV to Ethiopia and farmers should be aware of this virus and its effects in camels.

Acknowledgments

We thank the technical staff at Abu Dhabi Agriculture and Food Safety Authority and Animal Health Institute, the farmers, and workers at Yabello Veterinary Hospital for their contribution to the investigation.

This work was funded by the Abu Dhabi Agriculture and Food Safety Authority, Abu Dhabi, United Arab Emirates.

About the Author

Dr. Ishag is a molecular biology expert at the World Health Organization Collaborating Centre for Camel Diseases in the United Arab Emirates. His research interests include the use of genomics to explore and characterize the full diversity of viruses and bacteria in camels through metagenomics.

References

1. Bekele T. Studies on the respiratory disease 'sonbobe' in camels in the eastern lowlands of Ethiopia. Trop Anim Health Prod. 1999;31:333–45. https://doi.org/10.1023/A:1005290523034
2. Roger F, Yigezu LM, Hurard C, Libeau G, Mebratu G, Diallo A, et al. Investigations on a new pathological condition of camels in Ethiopia. J Camel Pract Res. 2000;7:163–6.
3. Yigezu LM, Roger F, Kiredjian M, Tariku S. Isolation of *Streptococcus equi* subspecies *equi* (strangles agent) from an Ethiopian camel. Vet Rec. 1997;140:608. https://doi.org/10.1136/vr.140.23.608
4. Gluecks I, Suisse VSF, Younan M. ELMT technical brief: technical report on camel sudden death syndrome: outbreak of unknown camel disease in the Horn of Africa. Washington (DC): USAID; 2010.
5. Intergovernmental Authority on Development. Regional consultative meeting on the outbreak of unknown camel disease in border areas [cited 2021 Jul 19]. https://icpald.org/unknown-camel-disease
6. Moureau G, Temmam S, Gonzalez JP, Charrel RN, Grard G, de Lamballerie X. A real-time RT-PCR method for the universal detection and identification of flaviviruses. Vector Borne Zoonotic Dis. 2007;7:467–77. https://doi.org/10.1089/vbz.2007.0206
7. Faye M, Seye T, Patel P, Diagne CT, Diagne MM, Dia M, et al. Development of real-time molecular assays for the detection of Wesselsbron virus in Africa. Microorganisms. 2022;10:550. https://doi.org/10.3390/microorganisms10030550
8. Oymans J, van Keulen L, Wichgers Schreur PJ, Kortekaas J. Early pathogenesis of Wesselsbron disease in pregnant ewes. Pathogens. 2020;9:373. https://doi.org/10.3390/pathogens9050373
9. Weiss K, Haig D, Alexander R. Wesselsbron virus—a virus not previously described, associated with abortion in domestic animals. Onderstepoort J Vet Res. 1956;27.
10. Venter MM, Human S, Eeden C, Niekerk S, Williams J, Steyl J, et al. The role of zoonotic vector borne viruses as neurological pathogens in horses and wildlife in South Africa. In: Proceedings of the 9th Annual Congress of the Southern African Society for Veterinary Epidemiology and Preventive Medicine; Pretoria, South Africa; 2010 Aug 18–20. Pretoria: Southern African Society for Veterinary Epidemiology and Preventive Medicine; p. 85–9.

Address for correspondence: Hassan Ishag, Biosecurity Affairs Division, Development and Innovation Sector, Abu Dhabi Agriculture and Food Safety Authority, PO Box 52150, Abu Dhabi, United Arab Emirates; email: hassan.ishag@adafsa.gov.ae

Baylisascaris procyonis Roundworm in Common Raccoon (*Procyon lotor*), Mexico

Ana Luisa Gómez-Sánchez, Carlos Daniel Pinacho-Pinacho, Juan José Barrios-Gutierrez, Ismael Guzmán-Valdivieso, Alberto Gonzalez-Romero, Tania Fonseca-Leal, Andrés M. López-Pérez

Author affiliation: Instituto de Ecología-INECOL A.C., Xalapa, Mexico

We found the zoonotic nematode, *Baylisascaris procyonis*, in a common raccoon (*Procyon lotor*) in Mexico. Expansion of raccoons into human-dominated regions might increase the risk of *B. procyonis* infections in humans. Increased surveillance and healthcare provider awareness of baylisascariasis in Mexico will be needed to prevent those infections in humans.

DOI: https://doi.org/10.3201/eid3106.241672

Baylisascaris procyonis, also known as the raccoon roundworm, is a zoonotic ascarid nematode that parasitizes the small intestine of its definitive host, the common raccoon (*Procyon lotor*). *B. procyonis* worms are commonly found in the United States and Canada (*1*). The *B. procyonis* life cycle involves direct transmission via the fecal–oral route between raccoons, but raccoons can also acquire the parasite indirectly by ingesting infected paratenic (transport) hosts (*1*,*2*). In the definitive host, the parasite life cycle occurs in the small intestine, where larvae hatch from infective eggs and develop into adults; male and female adult worms then mate and eggs are oviposited. However, larvae do not develop to adult stages in humans and other paratenic hosts. Instead, once the larvae hatch, they rapidly penetrate the intestinal mucosa and migrate through blood to the liver, lungs, or other tissues, causing visceral, ocular, or neural larval migrans, which can result in fatal disease or neurologic disease with severe outcomes (*1*,*2*). Exposure risk is highest for young children, who are more likely to accidentally ingest animal feces (*1*,*3*).

B. procyonis roundworms are considered a rare cause of human disease; ≈40 cases have been reported worldwide (*3*). However, human infection is increasingly recognized as an emerging public health concern in North America and in some countries in Europe and Asia, where raccoons have been introduced (*1*,*2*).

In January 2024, we captured a juvenile (<1 year of age), male raccoon in a patch of cloud forest in Veracruz, Mexico (latitude 19°30′47′′N, longitude 96°56′33′′W) that showed clinical signs consistent with distemper virus infection. Because of illness severity, we euthanized the raccoon and subsequently performed a necropsy. We conducted all handling procedures according to the Universidad Veracruzana Institutional Animal Care and Use Committee protocol (no. 003/2024-UV-IACUC) and the collection permit issued by the Mexico Secretary of Environment (permit no. SPARN/DGVS/06330/23). During necropsy, we collected 4 roundworms from the small intestine. We preserved 2 worms in 96% ethanol for molecular testing and fixed the other 2 worms in 4% formalin for morphologic identification. We did not detect eggs in the feces by using sedimentation or flotation tests.

All 4 roundworms were initially identified as *Baylisascaris* sp. by using a Leica DM750 light microscope (Leica, https://www.leica-microsystems.com) (*4*). To better characterize morphology, we processed 1 female specimen for scanning electron microscopy using standard methods, including washing, rinsing, and dehydrating steps, followed by a critical point drying step and mounting on aluminum stubs with a carbon adhesive before sputter coating with gold in a Quorum Q150RS instrument (Quorum Technologies, https://www.quorumtech.com). We produced scanning electron micrographs of the female specimen (Figure 1). We deposited 1 male *B. procyonis* roundworm specimen into the Colección Nacional de Helmintos del Instituto de Biología at the Universidad Nacional Autonoma de Mexico in México City (accession no. CNHE 8585).

We extracted genomic DNA from 2 worms by using DNAzol (Molecular Research Center, https://www.mrcgene.com) (*5*). To confirm morphologic identification of *Baylisascaris* sp., we amplified partial segments of the domains D2–D3 of the 28S rDNA gene (785 bp) by using 502 and 536 primers and conditions, as previously described (*6*). Macrogen Inc. (https://dna.macrogen.com) purified and sequenced the PCR samples. We assembled contigs and resolved base-calling differences by using Geneious version 8.1.8 (https://www.geneious.com). We generated consensus sequences and compared them with sequences in GenBank. Using MEGA11 (*7*), we aligned sequences by using the ClustalW algorithm and constructed phylogenetic trees by using the maximum-likelihood method. Phylogenetic analysis of the 28S rRNA sequences showed 100% identity with *B. procyonis* worms collected from raccoons in the United

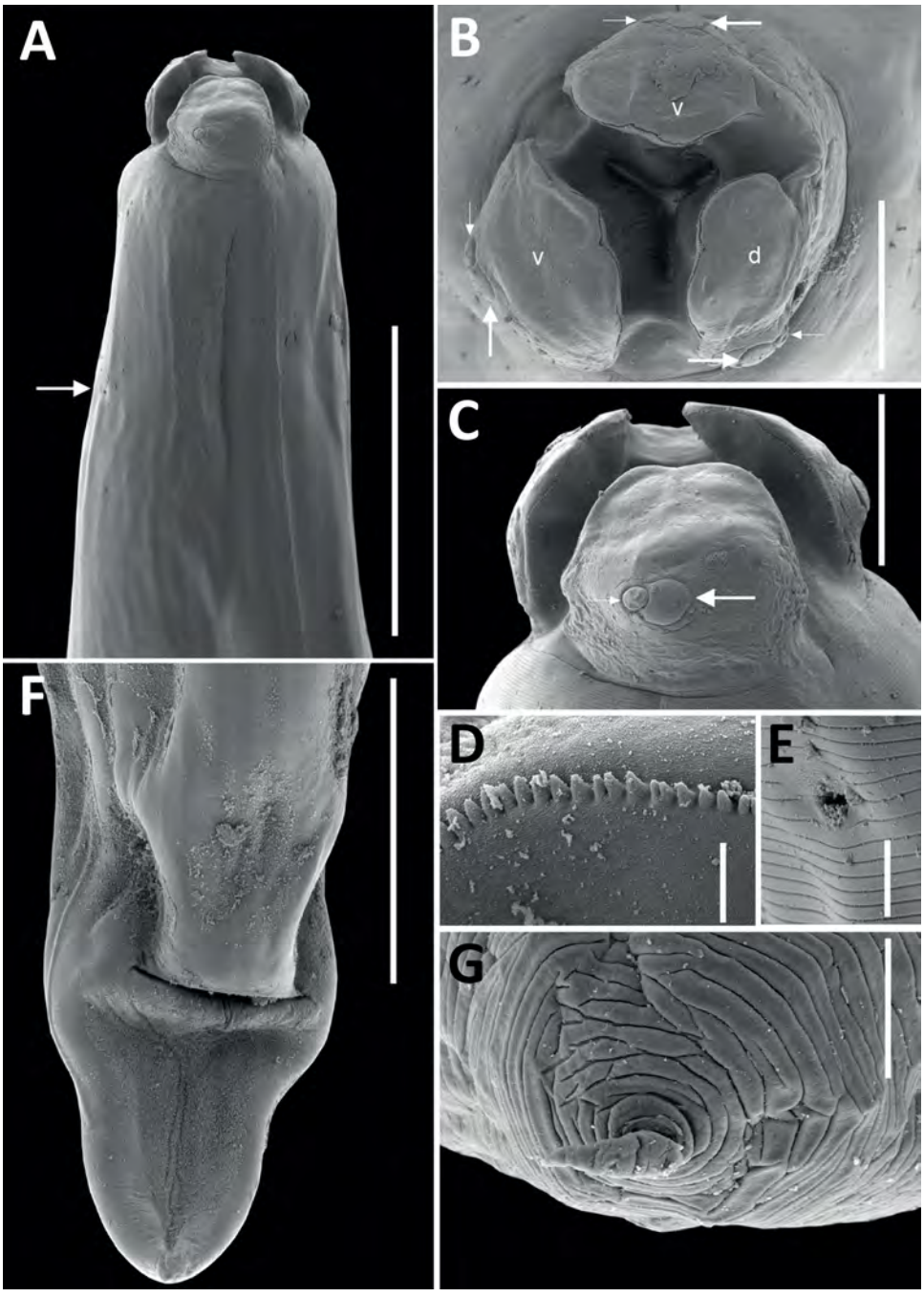

Figure 1. Scanning electron micrographs of female *Baylisascaris procyonis* roundworm detected in common raccoon (*Procyon lotor*), Mexico. A) Anterior end of worm body. Arrow indicates the excretory pore. Scale bar indicates 400 μm. B) Cephalic end, apical view of worm. Lowercase letters indicate dorsal (d) and ventral (v) lips, each having 1 large double papillae instead of a dorsal lip with 2 large double papillae, as reported previously (*4*). Small and large arrows indicate the double papillae. Scale bar indicates 100 μm. C) Cephalic end of worm. Small and large arrows indicate the double papillae. Scale bar indicates 100 μm. D) Magnified image of labial denticles. Scale bar indicates 5 μm. E) Magnified image of the excretory pore. Scale bar indicates 10 μm. F) Posterior end of the worm body. Scale bar indicates 300 μm. G) Magnified image of the tail tip. Scale bar indicates 10 μm.

States (GenBank accession no. KP843605), China (accession no. OR457646) and Norway (accession no. KC543470) (Figure 2). We submitted sequences from this study to GenBank (accession nos. PQ471568 and PQ471569).

Finding *B. procyonis* roundworms in a raccoon in Mexico extends the geographic distribution of this zoonotic nematode in the Americas, which has been described throughout Canada and the United States and, in 1 report, from Costa Rica (*1*,*8*). Despite the relatively low number of human cases reported worldwide and previous absence of *B. procyonis* worms in Mexico, the ecoepidemiology of *B. procyonis* roundworms suggests that the number of infection cases are underestimated. Infection prevalence is high in raccoons across their known distribution range; infected animals can carry several adult worms, which can excrete millions of eggs into the environment (*1*). A high infection prevalence likely also applies to Mexico because raccoons

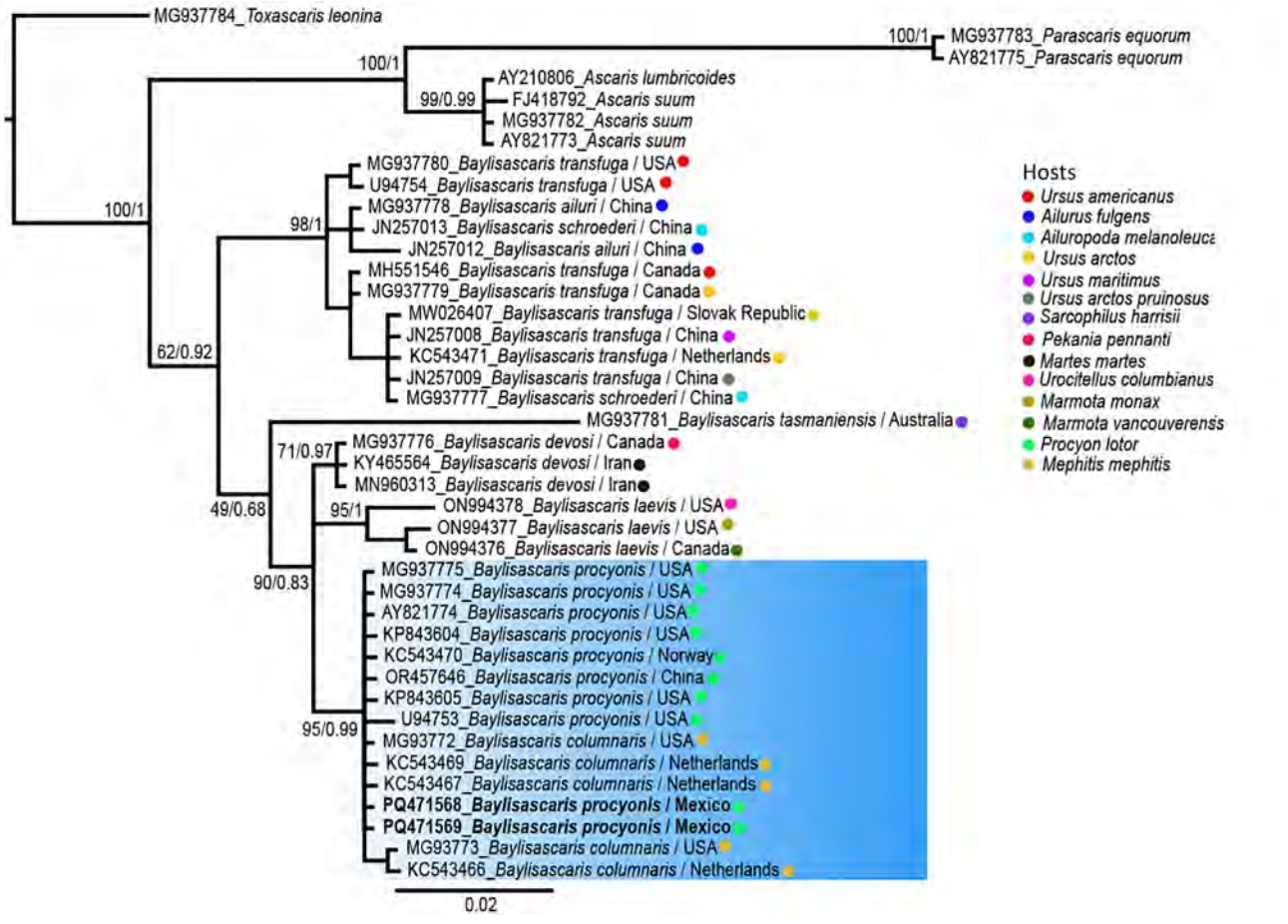

Figure 2. Phylogenetic analysis of *Baylisascaris procyonis* roundworms obtained from common raccoon (*Procyon lotor*), Mexico. Maximum-likelihood and Bayesian inference tree of *Baylisascaris* spp. according to the general time-reversible model with gamma distribution. Blue shading indicates GenBank sequences with greatest identity to sequences from Mexico (bold font). Numbers near internal nodes indicate bootstrap values/posterior probability of clade frequencies. Colored dots indicate host species. Scale bar indicates nucleotide substitutions per site.

are distributed throughout all the states within the country, and they have increasingly become synanthropic, living close to human settlements, where they are also occasionally kept as pets (*9*,*10*). In addition, domestic dogs could also play a key role in the epidemiology of *B. procyonis* roundworms, and other zoonotic ascarids such as *Toxocara canis*, which raises the risk for human exposure and infection (*1*,*2*). Our findings highlight the importance of increasing epidemiologic surveillance and healthcare provider awareness of baylisascariasis in Mexico to effectively prevent infections, particularly in areas where humans (especially children) and dogs might come into contact with raccoons or *B. procyonis* eggs in the environment.

Acknowledgments

We thank Greta Hanako, Rosas Saito, and Eva López Tello for technical support.

This work was funded by the Government of Mexico Ministry of Science, Humanities, Technology and Innovation (SECIHTI grant no. CF-2023-G-95) and by the Institute of Ecology, A.C. (INECOL grant no. 20030-11909).

About the Author

Dr. Gómez-Sánchez is a veterinarian and Master's candidate at the Institute of Ecology, A.C. Her research interests focus on the eco-epidemiology of endoparasites using a One Health approach.

References

1. US Geological Survey, National Wildlife Health Center. *Baylisascaris* larva migrans. Circular 1412. 2016 [cited 2024 Apr 25]. https://pubs.usgs.gov/circ/1412/cir1412.pdf
2. Bauer C. Baylisascariosis—infections of animals and humans with 'unusual' roundworms. Vet Parasitol. 2013;193:404–12. https://doi.org/10.1016/j.vetpar.2012.12.036

3. Lipton BA, Oltean HN, Capron RB, Hamlet A, Montgomery SP, Chancey RJ, et al. *Baylisascaris procyonis* roundworm infection in child with autism spectrum disorder, Washington, USA, 2022. Emerg Infect Dis. 2023;29:1232–5. https://doi.org/10.3201/eid2906.230290
4. Gu XH, Chen HX, Hu JJ, Li L. Morphology and ASAP analysis of the important zoonotic nematode parasite *Baylisascaris procyonis* (Stefahski and Zarnowski, 1951), with molecular phylogenetic relationships of *Baylisascaris* species (Nematoda: Ascaridida). Parasitology. 2024;151:200–12. https://doi.org/10.1017/S0031182023001312
5. Pinacho-Pinacho CD, Calixto-Rojas M, García-Vásquez A, Guzmán-Valdivieso I, Barrios-Gutiérrez JJ, Rubio-Godoy M. Species delimitation of *Gyrodactylus* (Monogenea: Gyrodactylidae) infecting the southernmost cyprinids (Actinopterygii: Cyprinidae) in the New World. Parasitol Res. 2021;120:831–48. https://doi.org/10.1007/s00436-020-06987-8
6. García-Varela M, Nadler SA. Phylogenetic relationships of Palaeacanthocephala (Acanthocephala) inferred from SSU and LSU rDNA gene sequences. J Parasitol. 2005;91:1401–9. https://doi.org/10.1645/GE-523R.1
7. Tamura K, Stecher G, Kumar S. MEGA11: molecular evolutionary genetics analysis version 11. Mol Biol Evol. 2021;38:3022–7. https://doi.org/10.1093/molbev/msab120
8. Baldi M, Alvarado G, Smith S, Santoro M, Bolaños N, Jiménez C, et al. *Baylisascaris procyonis* parasites in raccoons, Costa Rica, 2014. Emerg Infect Dis. 2016;22:1502–3. https://doi.org/10.3201/eid2208.151627
9. Mezhua-Velázquez MJ, Serna-Lagunes R, Torres-Cantú GB, Pérez-Gracida LD, Salazar-Ortiz J, Mora-Collado N. Diversity of medium and large mammals from the Ejido Zomajapa Zongolica, Veracruz, Mexico: management implications [in Spanish.]. Ecosist Recur Agropecu. 2022;9:e3316. https://doi.org/10.19136/era.a9n2.3316
10. García-Padilla BF, Zalapa SS, Guerrero-Vázquez S, Pérez-Arteaga A, Camacho-Rodríguez A. Abundance and activity of domestic and wild medium-sized mammals in a protected mangrove remnant, Puerto Vallarta, Mexico. West N Am Nat. 2021;81:285–92. https://doi.org/10.3398/064.081.0214

Address for correspondence: Andrés M. López-Pérez, Red de Biología y Conservación de Vertebrados, Instituto de Ecología A.C., Xalapa, Veracruz 91073, Mexico; email: andres.lopez@inecol.mx

etymologia revisited

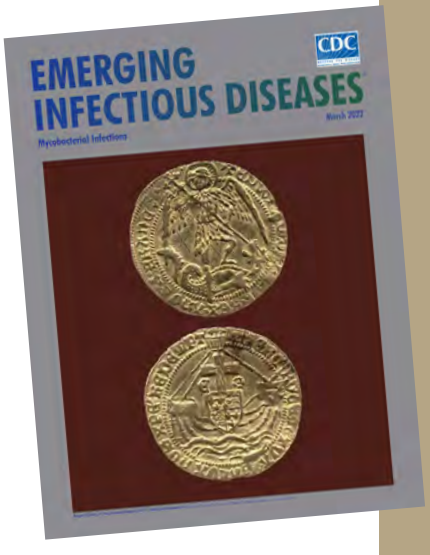

Originally published in March 2022

Schizophyllum commune

[skiz-of′-ĭ-ləm kom′-yoon]

Schizophyllum commune, or split-gill mushroom, is an environmental, wood-rotting basidiomycetous fungus. *Schizophyllum* is derived from "*Schíza*" meaning split because of the appearance of radial, centrally split, gill like folds; "*commune*" means common or shared ownership or ubiquitous. Swedish mycologist, Elias Magnus Fries (1794–1878), the Linnaeus of Mycology, assigned the scientific name in 1815. German mycologist Hans Kniep in 1930 discovered its sexual reproduction by consorting and recombining genomes with any one of numerous compatible mates (currently >2,800).

References

1. Chowdhary A, Kathuria S, Agarwal K, Meis JF. Recognizing filamentous basidiomycetes as agents of human disease: a review. Med Mycol. 2014;52: 782–97. https://doi.org/10.1093/mmy/myu047
2. Cooke WB. The genus *Schizophyllum*. Mycologia. 1961;53:575–99. https://doi.org/10.1080/00275514.1961.12017987
3. Greer DL. Basidiomycetes as agents of human infections: a review. Mycopathologia. 1978;65:133–9. https://doi.org/10.1007/BF00447184
4. O'Reilly P. *Schizophyllum commune*, split gill fungus, 2016 [cited 2021 Aug 23]. https://www.first-nature.com/fungi/schizophyllum-commune.php
5. Raper CA, Fowler TJ. Why study *Schizophyllum*? Fungal Genet Rep. 2004;51:30–6. https://doi.org/10.4148/1941-4765.1142

https//wwwnc.cdc.gov/eid/article/28/3/et-2803_article

A Pictorial Human Case of "Furious Rabies"

Charles E. Rupprecht, Alan C. Jackson

Author affiliations: Auburn University College of Veterinary Medicine, Auburn, Alabama, USA (C.E. Rupprecht); University of Calgary Cumming School of Medicine, Calgary, Alberta, Canada (A.C. Jackson)

DOI: https://doi.org/10.3201/eid3106.250167

To the Editor: We congratulate Perciaccante et al. (*1*) on their article about a Paczka painting showing doctors looking for evidence of a dog bite on a presumed encephalitic rabies patient. However, the story incorrectly references "Émile Roux's first inoculation of a human with rabies vaccine in July 1885."

Émile Roux (1853–1933) was a brilliant physician and scientist who began work with Louis Pasteur during 1878. Roux was noted for rabies research and standardized techniques for intracerebral inoculation of animals. In fact, Roux designed the well-known technique of using a flask to inactivate suspended rabies virus–infected rabbit cord through desiccation (an idea Pasteur borrowed). Roux was nominated for the Nobel Prize in 1888 for his research on diphtheria and later became director of the Pasteur Institute (1904–1933). Clinician, researcher, and scholar, Roux was renowned for multiple accomplishments but not his involvement with Joseph Meister's vaccination.

Roux and Pasteur had many disagreements, including the ethics of human experimentation. After only 5 weeks of animal research, Roux was unconvinced the experimental biologic made from dried spinal cords of infected rabbits was safe for human administration and did not support its use for Meister (*2*). His objection was problematic, because Pasteur, not a physician, could not administer the vaccine. Rather, vaccination proceeded under the supervision of E.F.A. Vulpian and Joseph Grancher. Dr. Grancher, professor, tuberculosis specialist, and Pasteur collaborator, administered the first vaccination, and fortunately, Meister survived (*3*,*4*). That news was shared only after vaccination of Jean-Baptiste Jupille, a 15-year-old shepherd, who was bitten in October and also survived (*5*). "… Roux, who would normally have administered inoculations for Pasteur, was notably absent..." (*6*). Only once evidence had accumulated did Roux relax his stance. Thereafter, he became an adherent of the "Pasteurian method" (*6*). This occurrence demonstrates that success is not without controversy or risk, and experts often disagree, given differing backgrounds, training, philosophy, and ethics.

References

1. Perciaccante A, DeLuca M, Dechelette C, Sebille N, Charlier P. A pictorial human case of "furious rabies." Emerg Infect Dis. 2025;31:410–2. https://doi.org/10.3201/eid3102.AC3102
2. Geison GL. The private science of Louis Pasteur. Princeton (NJ): Princeton University Press; 1995.
3. Pasteur Institute. Paris France [cited 2025 Jan 28]. https://www.pasteur.fr/en/institut-pasteur/history/troisieme-epoque-1877-1887
4. Geison GL. Pasteur, Roux, and rabies: scientific versus clinical mentalities. J Hist Med Allied Sci. 1990;45:341–65. https://doi.org/10.1093/jhmas/45.3.341
5. Pasteur L. Method to prevent rabies after a bite [in French]. Comptes Rendus des Séances de l'Académie des Sciences. October 26, 1885.
6. Conniff R. Ending epidemics: a history of escape from contagion. Cambridge (MA): MIT Press; 2023.

Address for correspondence: Charles E. Rupprecht, Auburn University College of Veterinary Medicine, Scott-Ritchey Research Center, 1265 H C Morgan, Auburn, AL 36849, USA; email: charles_rupprecht@yahoo.com

Sarah Hunter (1883–1967), *Jar-shaped Basket*, 1910. Willow, bulrush; coiled (3 rods), 4 15/16 in × 7 5/16 in/12.5 cm × 18.5 cm. Open access image from Cleveland Museum of Art, Cleveland, Ohio, USA.

Art of the Interwoven

Byron Breedlove

In an article from the Gilcrease Museum website, anthropologist Jason Baird Jackson notes, "From the enormous diversity of American Indian peoples, speaking thousands of different languages and possessing distinct cultural traditions, inhabiting a great variety of natural settings, flowed a remarkable number of different basketry forms and techniques." The Panamint Shoshone Tribe, today identified as the Timbisha Shoshone Tribe, "is historically known for some of the finest, tightly-coiled Native basketry on the continent," according to the Portland Art Museum.

Author affiliation: Centers for Disease Control and Prevention, Atlanta, Georgia, USA

DOI: https://doi.org/10.3201/eid3106.AC3106

Appearing on this month's cover is a jar-shaped basket created by Sara Hunter, who belonged to the Panamint Shoshone Tribe and was, according to the Cleveland Museum of Art, the last American Indian basket weaver to live in the Saline Valley on the edge of what is now Death Valley National Park in California. Eva Slater, an art historian and artist, notes in her book *Panamint Shoshone Basketry*, that "Sarah Hunter lived most of her life in the isolation of Hunter Canyon, the largest and most ancient of three camps in the valley."

The Panamint Shoshones, a small branch of the Shoshone, have inhabited the Death Valley area for perhaps a thousand years and for centuries before Europeans ventured into the area. The US National Park service notes, "They hunted and followed sea-

sonal migrations for harvesting of pinyon pine nuts and mesquite beans with their families. To them, the land provided everything they needed and many areas were, and are, considered to be sacred places."

Initially, the Panamint created baskets for utilitarian purposes such as transporting and storing food, water, and possessions or for trapping birds and small game. Later, as settlers, silver miners, and others moved into the region, the Portland Art Museum explains that "the fine quality of Panamint baskets created a collectors' market, which lasted well into the mid-twentieth century. For Panamint and other American Indian weavers, adapting utilitarian baskets to saleable ones preserved Native basket-making techniques and provided much needed income for many families still trying to live a traditional life."

Slater writes that in the 1930s, Hunter "became known for her large oval vessels with zoomorphic design elements scattered playfully over the basket surface in petroglyph fashion revealing a relationship to Maggie Juaquin of Darwin, who was her sister." Hunter, along with other basket makers in that region, would have gathered and prepared plants such as bulrush, bunchgrass, devil's claw sumac, willow, and yucca for making baskets. The Cleveland Museum of Art, where this basket may be viewed, notes that "If stages of the process are not done properly and at the right time, color will be uneven and stitches will twist and split."

The Cleveland Museum of Art recounts that "Hunter's basketry is noted for geometricized motifs reminiscent of the animals depicted in petroglyphs on canyon walls in the Death Valley region. Here they include pronghorn mountain sheep, deer, and birds, along with humans, all created in light-brown bulrush against a honey-colored willow ground." Animals adapted to living in this harsh ecosystem, like the plants found there, would have been essential resources for the Panamint tribe.

Living in proximity with nature also potentially increases human exposure to pathogens that could cause infection. In Death Valley, for example, zoonotic pathogens such as hantaviruses carried by rodents pose health threats to humans. The harsh, arid climate of this region confers, for now, protection from some vectorborne illnesses. The first recorded human-to-human transmission of plague in the United States was in San Francisco, California, in 1900. After fleas infected sylvatic rodents with plague, the disease spread across California, eventually reaching the Death Valley region. Western blacklegged ticks (*Ixodes pacificus*) that can transmit Lyme disease have been found in this region. Environmental changes and human encroachment may increase the prevalence of vectorborne diseases in Death Valley and similar areas.

Perhaps this jar-shaped basket showing the interconnection of animals, humans, and the environment in Death Valley and, created from weaving together various plants found in that harsh environment, may serve as a metaphor for One Health. One Health, as explained by the One Health High-Level Expert Panel, is globally recognized as "an integrated, unifying approach that aims to sustainably balance and optimize the health of people, animals, and ecosystems. It recognizes the health of humans, domestic and wild animals, plants, and the wider environment (including ecosystems) are closely linked and interdependent." One Health is often described by words such as "integrated," "intertwined," and "interwoven." From her work as basket maker and her knowledge of the land and its resources, Hunter would have intrinsically understood that underlying unity.

Bibliography

1. Burns JE, Metzger ME, Messenger S, Fritz CL, Vilcins IE, Enge B, et al. Novel focus of Sin Nombre virus in *Peromyscus eremicus* mice, Death Valley National Park, California, USA. Emerg Infect Dis. 2018;24:1112–5. https://doi.org/10.3201/eid2406.180089
2. California Department of Public Health. California compendium of plague control [cited 2025 May 12]. https://www.cdph.ca.gov/Programs/CID/DCDC/CDPH%20Document%20Library/CAPlagueCompendium.pdf
3. California Department of Public Health. Lyme disease in California [cited 2025 May 5]. https://storymaps.arcgis.com/stories/f64d0c19a3ab42cf90e8ce38397e96e0
4. Centers for Disease Control and Prevention. One Health basics [cited 2023 Oct 23]. https://www.cdc.gov/onehealth/basics/index.html
5. Cleveland Museum of Art. Jar-shaped basket [cited 2023 Oct 2] https://www.clevelandart.org/art/1917.454
6. Jackson JB. Article: Containers of tradition: Southeastern Indian basketry. Gilcrease Museum [cited 2023 Oct 19]. https://collections.gilcrease.org/articles/article-containers-tradition-southeastern-indian-basketry
7. National Park Service. Death Valley. Land of a thousand stories: Native Americans [cited 2023 Oct 25] https://www.nps.gov/deva/learn/historyculture/people.htm
8. One Health High-Level Expert Panel (OHHLEP); Adisasmito WB, Almuhairi S, Behravesh CB, Bilivogui P, Bukachi SA, Casas N, et al. One Health: A new definition for a sustainable and healthy future. PLoS Pathog. 2022;18:e1010537. https://doi.org/10.1371/journal.ppat.1010537
9. Portland Art Museum. Panamint Coiled Baskets [cited 2023 Oct 19]. http://portlandartmuseum.us/mwebcgi/mweb.exe?request=record;id=261496;type=801
10. Slater E. Panamint Shoshone Basketry. Morongo Valley (CA): Sagebrush Press; 2000. p. 15–16, 19–20, 55–61.

Address for correspondence: Byron Breedlove, EID Journal, Centers for Disease Control and Prevention, 1600 Clifton Rd NE, Mailstop H16-2, Atlanta, GA 30329-4018, USA; email: eideditor@cdc.gov

EMERGING INFECTIOUS DISEASES®

Upcoming Issue • Bacterial Infections

- Retrospective Analysis of Human *Streptococcus suis* Infections, South America, 1995–2024
- Systematic Review of Contact Investigation Costs for Tuberculosis, United States
- Estimation of Incubation Period for Oropouche Virus Disease among Travel-Associated Cases, 2024–2025
- Outbreak of Sexually Transmitted *S. sonnei* $bla_{ctx\text{-}m\text{-}15}$ in England—an Epidemiological and Genomic Investigation
- Persistence of the SARS-CoV-2 Alpha Variant in White-Tailed Deer in Northeast Ohio
- Incidence and Predictive Factors of Disseminated Histoplasmosis in Persons Living with HIV in France and Its Overseas Territories, 1992–2021
- Emergence of Flucytosine-Resistant Non–Wild-Type *Candida tropicalis* Clade, the Netherlands
- Emergence of Distinct *Salmonella* Enteritidis Lineage since 2020, South Korea
- *Peromyscus* Species Deer Mice as Rodent Model of Acute Leptospirosis
- Role of Nonpharmaceutical Interventions during 1918–20 Influenza Pandemic, Alaska, USA
- Human Infections with Novel Zoonotic Species *Corynebacterium silvaticum*, Germany
- Multisystemic Disease and Septicemia Caused by Presumptive *Burkholderia pseudomallei* in American Quarter Horse
- Lyme Disease Testing in High-Incidence Region, United States, 2016–2019
- *Borrelia* Lineages Adjacent to Zoonotic Clades in Black Flying Foxes (*Pteropus alecto*), Australia, 2018–2020
- Emergence and Prevalence of *Vibrio cholerae* O1 Sequence Type 75 Clonal Complex Strains, Fujian Province, China, 2009–2023
- Detection of Novel Orthobunyavirus Reassortants in Fatal Neurologic Case in Horse and *Culicoides* Biting Midges, South Africa
- Community Infections Linked with Parvovirus B19 Genomic DNA in Wastewater, Texas, USA, 2023–2024
- Fatal Acute Hypoxemic Respiratory Failure Caused by *Burkholderia thailandensis*, China
- Genomic Deletion of PfHRP2/PfHRP3 Antigens in *Plasmodium falciparum* Strains, Ethiopia, 2009
- *Plasmodium knowlesi* Malaria in Persons Returning to Israel from Thailand, 2023

Complete list of articles in the July issue at https://wwwnc.cdc.gov/eid/#issue-323

Earning CME Credit

To obtain credit, you should first read the journal article. After reading the article, you should be able to answer the following, related, multiple-choice questions. To complete the questions (with a minimum 75% passing score) and earn continuing medical education (CME) credit, please go to http://www.medscape.org/journal/eid. Credit cannot be obtained for tests completed on paper, although you may use the worksheet below to keep a record of your answers.

You must be a registered user on http://www.medscape.org. If you are not registered on http://www.medscape.org, please click on the "Register" link on the right hand side of the website.

Only one answer is correct for each question. Once you successfully answer all post-test questions, you will be able to view and/or print your certificate. For questions regarding this activity, contact the accredited provider, CME@medscape.net. For technical assistance, contact CME@medscape.net. American Medical Association's Physician's Recognition Award (AMA PRA) credits are accepted in the US as evidence of participation in CME activities. For further information on this award, please go to https://www.ama-assn.org. The AMA has determined that physicians not licensed in the US who participate in this CME activity are eligible for AMA PRA Category 1 Credits™. Through agreements that the AMA has made with agencies in some countries, AMA PRA credit may be acceptable as evidence of participation in CME activities. If you are not licensed in the US, please complete the questions online, print the AMA PRA CME credit certificate, and present it to your national medical association for review.

Article Title

Clinical Manifestations, Risk Factors, and Disease Burden of Rickettsiosis, Cambodia, 2007–2020

CME Questions

1. Approximately what percentage of patients with acute undifferentiated febrile illness (AUFI) were found to have an acute rickettsial infection in the current study?

A. 3%
B. 8%
C. 19%
D. 31%

2. Which of the following organisms was responsible for the greatest proportion of rickettsial infection in the current study?

A. *Rickettsia typhi*
B. *Rickettsia rickettsii*
C. *Rickettsia conorii*
D. *Orientia tsutsugamushi*

3. Which of the following variables was most associated with rickettsial infection among patients with AUFI in the current study?

A. Age <15 years
B. Case presentation during the wet season
C. Travel to the forest specifically
D. Antibiotic use during the past 30 days

4. Which of the following symptoms was most specifically associated with rickettsial infection in the current study of patients with AUFI?

A. Joint pain
B. Nausea
C. Headache
D. Abdominal cramping

Earning CME Credit

To obtain credit, you should first read the journal article. After reading the article, you should be able to answer the following, related, multiple-choice questions. To complete the questions (with a minimum 75% passing score) and earn continuing medical education (CME) credit, please go to http://www.medscape.org/journal/eid. Credit cannot be obtained for tests completed on paper, although you may use the worksheet below to keep a record of your answers.

You must be a registered user on http://www.medscape.org. If you are not registered on http://www.medscape.org, please click on the "Register" link on the right hand side of the website.

Only one answer is correct for each question. Once you successfully answer all post-test questions, you will be able to view and/or print your certificate. For questions regarding this activity, contact the accredited provider, CME@medscape.net. For technical assistance, contact CME@medscape.net. American Medical Association's Physician's Recognition Award (AMA PRA) credits are accepted in the US as evidence of participation in CME activities. For further information on this award, please go to https://www.ama-assn.org. The AMA has determined that physicians not licensed in the US who participate in this CME activity are eligible for AMA PRA Category 1 Credits™. Through agreements that the AMA has made with agencies in some countries, AMA PRA credit may be acceptable as evidence of participation in CME activities. If you are not licensed in the US, please complete the questions online, print the AMA PRA CME credit certificate, and present it to your national medical association for review.

Article Title

Multicenter Retrospective Study of *Spiroplasma ixodetis* Infantile Cataract in 8 Countries in Europe

CME Questions

1. Which of the following statements regarding *Spiroplasma* sp. is most accurate?

A. The main vector of infection is mosquitoes
B. *Spiroplasma* has been established as a human pathogen for three decades
C. There are a small number of reports of systemic infection with *Spiroplasma*
D. Nearly all cases in the current study were caused by an arthropod bite during pregnancy

2. What percentage of eyes infected with *Spiroplasma* a in the current study showed evidence of anterior uveitis?

A. 12%
B. 39%
C. 62%
D. 100%

3. Which of the following statements regarding other ocular findings in the current study of infants with *Spiroplasma* infections is most accurate?

A. Approximately half of infants with uveitis had posterior synechiae
B. Nearly all infants had a pupillary membrane
C. Nearly half of all infants had unilateral cataracts
D. Intraocular pressure fell in all infants after cataract surgery

4. Which of the following tests to detect *Spiroplasma* in the current study was superior in producing a positive sample?

A. 16S-rRNA PCR
B. Transmission electron microscopy (TEM)
C. Culture of lens material
D. All of the above methods were similar in producing positive results for Spiroplasma

Emerging Infectious Diseases
Photo Quiz Articles

Volume 14, Number 9
September 2008

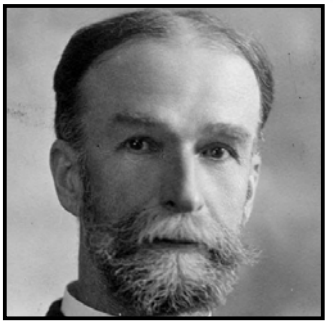

Volume 14, Number 12
December 2008

Volume 15, Number 9
September 2009

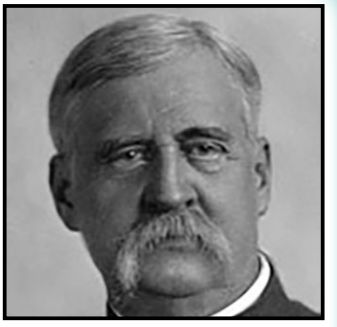

Volume 15, Number 10
October 2009

Volume 16, Number 6
June 2010

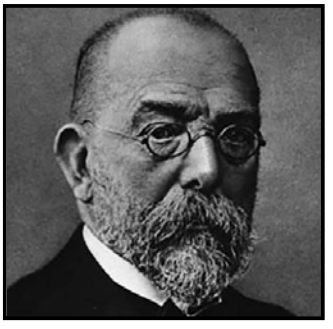

Volume 17, Number 3
March 2011

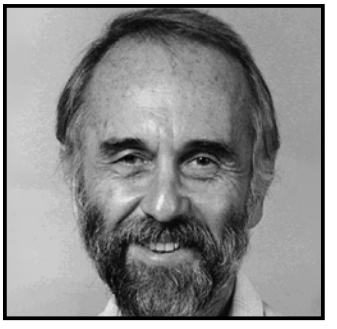

Volume 17, Number 12
December 2011

Volume 19, Number 4
April 2013

Volume 20, Number 5
May 2014

Volume 21, Number 9
September 2015

Volume 22, Number 8
August 2016

Volume 28, Number 3
March 2022

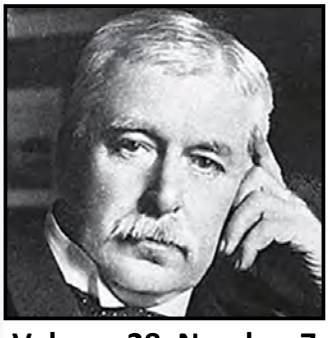

Volume 28, Number 7
July 2022

Click on the link below to read about the people behind the science.

https://bit.ly/3LN02tr

See requirements for submitting a photo quiz to EID.

https://bit.ly/3VUPqfj

EID Journal